GLOBAL EXCELLENCE IN FOOD CHEMISTRY

EDITED BY: A. M. Abd El-Aty, Jesus Simal-Gandara and
Alaa El-Din Ahmed Bekhit
PUBLISHED IN: Frontiers in Nutrition

frontiers Research Topics

About Frontiers

Frontiers is more than just an open-access publisher of scholarly articles: it is a pioneering approach to the world of academia, radically improving the way scholarly research is managed. The grand vision of Frontiers is a world where all people have an equal opportunity to seek, share and generate knowledge. Frontiers provides immediate and permanent online open access to all its publications, but this alone is not enough to realize our grand goals.

Frontiers Journal Series

The Frontiers Journal Series is a multi-tier and interdisciplinary set of open-access, online journals, promising a paradigm shift from the current review, selection and dissemination processes in academic publishing. All Frontiers journals are driven by researchers for researchers; therefore, they constitute a service to the scholarly community. At the same time, the Frontiers Journal Series operates on a revolutionary invention, the tiered publishing system, initially addressing specific communities of scholars, and gradually climbing up to broader public understanding, thus serving the interests of the lay society, too.

Dedication to Quality

Each Frontiers article is a landmark of the highest quality, thanks to genuinely collaborative interactions between authors and review editors, who include some of the world's best academicians. Research must be certified by peers before entering a stream of knowledge that may eventually reach the public - and shape society; therefore, Frontiers only applies the most rigorous and unbiased reviews.
Frontiers revolutionizes research publishing by freely delivering the most outstanding research, evaluated with no bias from both the academic and social point of view. By applying the most advanced information technologies, Frontiers is catapulting scholarly publishing into a new generation.

What are Frontiers Research Topics?

Frontiers Research Topics are very popular trademarks of the Frontiers Journals Series: they are collections of at least ten articles, all centered on a particular subject. With their unique mix of varied contributions from Original Research to Review Articles, Frontiers Research Topics unify the most influential researchers, the latest key findings and historical advances in a hot research area! Find out more on how to host your own Frontiers Research Topic or contribute to one as an author by contacting the Frontiers Editorial Office: frontiersin.org/about/contact

GLOBAL EXCELLENCE IN FOOD CHEMISTRY

Topic Editors:
A. M. Abd El-Aty, Cairo University, Egypt
Jesus Simal-Gandara, University of Vigo, Spain
Alaa El-Din Ahmed Bekhit, University of Otago, New Zealand

Table of Contents

frontiers | Frontiers in Nutrition

Editorial: Global excellence in food chemistry

Alaa El-Din A. Bekhit[1]*, Jesus Simal-Gandara[2] and
A. M. Abd El-Aty[3,4]

[1]Department of Food Science, University of Otago, Dunedin, New Zealand, [2]Nutrition and
Bromatology Group, Analytical and Food Chemistry Department, Faculty of Food Science and
Technology, University of Vigo, Ourense, Spain, [3]Department of Pharmacology, Faculty of Veterinary
Medicine, Cairo University, Giza, Egypt, [4]Department of Medical Pharmacology, Medical Faculty,
Ataturk University, Erzurum, Turkey

Editorial on the Research Topic
Global excellence in food chemistry

The current global changes in economic, social, and technological production systems of food necessitate developing innovative solutions and strategies that ensure maximum utilization of food resources to produce desirable and wholesome food products. Food chemistry and related research activities are arguably the core of research activities that ensure the achievement of the above goals. This Research Topic is aimed at capturing prominent food chemistry research activities to provide recent insights and current research activities to meet the above goals. This Research Topic provides a balanced collection of original research, reviews, and new methods contributions, authored by experts in the field. The studies reported in the present Research Topic can be generally categorized into the following themes: food safety research that was concerned with the detection and quantification of pesticides and antimicrobial agents; studies on bioactive compounds, their stability and biofunctionalities; fractionation of pea protein, and others.

Food safety

Given the obvious importance of food safety, this theme area has been a major topic of interest in this Research Topic. The use of pesticides to protect crops is crucial for financial and food security reasons. However, pesticide residue in agricultural produce is known to have harmful effects on human health, especially those that are consumed fresh without any effective pre-processing treatments (e.g., peeling, sanding, other surface treatment, or thermal treatments). Considering these aspects, Park et al. investigated common food preparations (washing and blanching) on residual cyantraniliprole contents in spinach using ultrahigh-performance liquid chromatography-tandem mass spectrometry (UHPLC–MS/MS). A synergistic effect for washing with a neutral detergent and blanching for 5 min in boiling water led to a 93.5%

reduction in cyantraniliprole content. Furthermore, Zhai R. et al. investigated the content of imidacloprid in Chinese chives using a quick, easy, cheap, effective, rugged, and safe (QuEChERS) method combined with liquid chromatography-tandem mass spectrometry (LC–MS/MS). The authors reported good linearity ($R^2 = 0.9988$), a limit of quantification of $\leq 8.07 \times 10^4$ mg/kg, and a recovery range of 78.34–91.17%. The dissipation dynamics of imidacloprid in Chinese chives followed first-order kinetics, and the pesticide had a half-life of 2.92 days. Applying the method to commercial samples revealed that the imidacloprid contents in Chinese chives (0.00923–0.166 mg/kg) were below the maximum residue limit (MRL) of 1 mg/kg. Similar research that investigated dissipation and contents of fenpyroximate acaricide in/on guava, orange, and eggplant under open field conditions is reported by Malhat et al. The authors reported the kinetics of the pesticide in all crops to follow a first-order kinetics model with half-lives of 1.7, 2.2, and 1.9 days for eggplants, guavas, and oranges, respectively. An important finding of the study was that 3 and 7 days of the postharvest interval were proposed for oranges and eggplant to reach a level that complies with MRLs in these agricultural products. For guava, no postharvest interval time was proposed due to the absence of MRL.

Concerns over the translocation of phthalates from food packaging to beef were investigated by Baranenko et al. The contents of dimethyl terephthalate (DMTP), di-n-butyl phthalate (DnBP), and diisooctyl phthalate (DiOP) were determined in commercial beef samples. The authors found that mince beef had a higher phthalate content than sliced beef due to the larger contact area and the presence of distributed fat on the surface of the minced meat in direct contact with the packaging material.

Interest in rapid methods for the detection and quantification of pesticides is also reported in this Research Topic. A colloidal gold immunochromatographic strip was developed for the rapid detection of aldicarb in vegetables (leeks and cabbages) (Shen et al.). The strips were accurately capable of identifying positive samples but detected false positives for negative samples.

A fast method for simultaneous quantification of chloramphenicol, thiamphenicol, florfenicol, and florfenicol amine in meat and seafood was reported by Jung et al. The authors employed a QuEChERS extraction method coupled with a liquid chromatography-tandem mass spectrometry (LC–MS/MS) method that offers several advantages. The developed method had limits of detection of 0.005–3.1 μg/kg and limits of quantification of 0.02–10.4 μg/kg. The method was verified using various animal-derived products. The authors concluded that the developed method was versatile, sensitive, and suitable for the quantification of antimicrobials in animal products.

A competitive assay combining aptamer (DNA)-specific recognition and bimetallic nanozyme gold@platinum (Au@Pt) catalysis was developed by Chen et al. to quantify carbendazim,

a fungicide used in agricultural products. The developed method had a limit of detection of 0.038 ng/mg, and a good correlation was established between the developed method and parallel analysis carried out using liquid chromatography coupled with mass spectrometry analysis. The authors concluded that the competitive assay based on dual-mode Au@Pt-DNA biosensors has a high potential for detecting fungicides in agroproducts. A similar approach was used by Zhang et al. to determine fenvalerate contents in vegetables using the immunocompetition method that employed an electrospun fiber membrane containing a fenvalerate hapten-mouse IgG-Eu fluorescent probe.

Bioactives

The effect of terpinen-4-ol (the major component in tea tree oil) on inflammatory bowel disease (IBD) was evaluated using a cell model [lipopolysaccharide (LPS)-induced intestinal epithelial cell barrier function impairment in intestinal porcine epithelial cell lines] and an animal model [dextran sulfate sodium (DSS)-induced IBD in mice] (Yong et al.). Terpinen-4-ol was successful in protecting intestinal porcine epithelial cell lines against LPS-induced damage and attenuated DSS-induced colitis in mice. The authors demonstrated that terpinen-4-ol activity was due to the promotion of tight junction (TJ) proteins. Additionally, Zhai X. et al. investigated the use of ultrasound-assisted extraction techniques to accelerate the extraction of cold coffee brewing. The authors compared the physicochemical characteristics and non-volatile and volatile compounds of ultrasound-extracted coffee extracts with hot brewing and conventional static cold brewing methods. The ultrasound technique resulted in a faster extraction time (1 h compared to 12 h in the traditional cold extraction process) and higher total dissolved solids (6–26%), total lipids (10–21%), proteins (26–31%), and titrated acids (12–15%) than the static cold brews. A "pour-over" extraction with hot water (92°C, 3 min, 3 stages) resulted in higher caffeine, chlorogenic acid, and trigonelline contents compared to boiling (95°C, 5 min), cold brewing for 12 h, and ultrasound-assisted extraction for 1 h. The volatile profiles of the ultrasound-assisted cold brew extracts were similar to static cold ones, but both of these samples were different from the hot brewed samples. Overall, the research showed the usefulness of ultrasound in enhancing the extraction process without compromising the coffee flavor.

A Q Exactive Hybrid Quadrupole-Orbitrap Mass Spectrometer was used for the identification of flaxseed cyclolinopeptides, cyclic peptides that have been reported to have a wide range of bioactivities, such as inhibition of osteoclast differentiation and antimalarial, immunosuppressive, and antitumor activities (Fojnica et al.). The study identified twelve cyclolinopeptides, and the stability and degradation of the cyclolinopeptides in flaxseed oil were studied over 60 days

at room temperature and 90°C. The majority of the peptides were rapidly degraded at 90°C and slowly degraded at room temperature with significant degradation profiles and rates among the various peptides.

Microencapsulation of plant (red beet, broccoli, and spinach leaf) phenolic extracts was carried out using a complex coacervation method to improve their stability (Soliman et al.). The microcapsules were tested for their physicochemical properties, sensory attributes, and bioactivities in a rat model. Overall, these microcapsules were found to support brain health, improve metabolic strategies and neurobehavioral systems and enhance protein biosynthesis in AlCl3 (100 mg/kg body weight/d)-treated rats. A similar study investigated the protective effects of D-cycloserine and L-serine in the AlCl3-induced experimental rat model of Alzheimer's disease and reported positive results (Tozlu et al.).

Bioactives and their health benefits have received comprehensive reviews that summarize up-to-date information on bioactive peptides from food and byproducts (Zaky et al.; Mitra et al.), polysaccharides in *Cordyceps militaris* (Miao et al.), and protein-phenolic interactions (Yilmaz et al.).

Fractionation of pea protein

Asen and Aluko investigated the aggregation of pea proteins as affected by pH (3.0, 5.0, 7.0, or 9.0), heat treatment (100°C for 30 min), and fractionation (<30, 30–50, and >50 kDa fractions). The >50 kDa fractions had higher protein content than the other fractions. Within this fraction, different protein aggregation temperatures were found (124.30, 190.66, 206.33, and 203.17°C for pH 3.0, 5.0, 7.0, and 9.0, respectively), which were higher than that of the pea protein concentrate (74.45°C). The >50 kDa fractions obtained at pH 3.0, 7.0, and 9.0 had better solubility, oil holding capacity, protein content, foam capacity, foam stability, water holding capacity, and surface hydrophobicity. Overall, the study demonstrated the ability to manipulate the techno-functionality of the pea protein isolate through the manipulation of pH and fraction.

Miscellaneous

A meta-analysis for autoclaving-cooling conditions that result in an increased resistant starch content in starchy foods was reported by Faridah et al., and technologies used for rice wine production were reviewed by Pei et al.

Author contributions

All authors listed have made a substantial, direct, and intellectual contribution to the work and approved it for publication.

Acknowledgments

The editors would like to thank the authors, the reviewers, the editors, and the editorial office for their support and time that enabled rapid handling and ensured the publishing of high-quality work.

Conflict of interest

The authors declare that the research was conducted in the absence of any commercial or financial relationships that could be construed as a potential conflict of interest.

Publisher's note

All claims expressed in this article are solely those of the authors and do not necessarily represent those of their affiliated organizations, or those of the publisher, the editors and the reviewers. Any product that may be evaluated in this article, or claim that may be made by its manufacturer, is not guaranteed or endorsed by the publisher.

Simultaneous Quantification of Chloramphenicol, Thiamphenicol, Florfenicol, and Florfenicol Amine in Animal and Aquaculture Products Using Liquid Chromatography-Tandem Mass Spectrometry

Hae-Ni Jung[1], Da-Hee Park[1], Yeon-Jae Choi[1], Se-Hyeong Kang[1], Hee-Jung Cho[1], Jeong-Min Choi[1], Jae-Han Shim[2], Ahmed A. Zaky[3], A. M. Abd El-Aty[4,5*] and Ho-Chul Shin[1*]

[1] Department of Veterinary Pharmacology and Toxicology, College of Veterinary Medicine, Konkuk University, Seoul, South Korea, [2] Natural Products Chemistry Laboratory, College of Agriculture and Life Sciences, Chonnam National University, Gwangju, South Korea, [3] Department of Food Technology, National Research Centre, Cairo, Egypt, [4] Department of Pharmacology, Faculty of Veterinary Medicine, Cairo University, Giza, Egypt, [5] Department of Medical Pharmacology, Medical Faculty, Ataturk University, Erzurum, Turkey

The accumulation of antimicrobial residues in edible animal products and aquaculture products could pose health concerns to unsuspecting consumers. Hence, this study aimed to develop a validated method for simultaneous quantification of chloramphenicol (CAP), thiamphenicol (TAP), florfenicol (FF), and florfenicol amine (FFA) in beef, pork, chicken, shrimp, eel, and flatfish using a quick, easy, cheap, effective, rugged, and safe (QuEChERS) extraction method coupled with liquid chromatography-tandem mass spectrometry (LC-MS/MS). Primary-secondary amine (PSA) and $MgSO_4$ were used for sample purification. The analytes were separated on a reversed-phase analytical column. The coefficients of determination for the linear matrix-matched calibration curves were ≥ 0.9941. Recovery rates ranged between 64.26 and 116.51% for the four analytes with relative standard deviations (RSDs) $\leq 18.05\%$. The calculated limits of detection (LODs) and limits of quantification (LOQs) were 0.005–3.1 and 0.02–10.4 µg/kg, respectively. The developed method was successfully applied for monitoring samples obtained from local markets in Seoul, Republic of Korea. The target residues were not detected in any tested matrix. The designed method was versatile, sensitive, and proved suitable for quantifying residues in animal-derived products.

Keywords: chloramphenicol, thiamphenicol, florfenicol, florfenicol amine, residue analysis, LC-MS/MS, method development

INTRODUCTION

The increasing demand for meat products has led to an expansion in intensive animal farming. In 2018, global meat production reached 342 million tons, and fishery and aquaculture production reached 179 million tons (1). Factory farming exposes animals to higher levels of stress and a broader spectrum of diseases (2); thus, the use of antibiotics in animal farming has been steadily increasing (3). Worldwide, 73% of all antimicrobials (mainly antibiotics) are consumed by animals farmed for food (4). Hence, the accumulation of drug residues in edible tissues of animal and fish products is highly likely, which would pose a public health hazard, particularly for the consumers of those products (5). Previous studies have shown that approximately 4% of antimicrobial resistance formed in the human body has been transferred from animals (6). Amphenicols (chloramphenicol (CAP), thiamphenicol (TAP), florfenicol (FF), and florfenicol amine (FFA)) are among the antibiotics that cause resistance. Despite usage regulations, amphenicol antibiotics are widely used illegally by farmers of various animals due to their broad range of effects and low cost (7, 8). Therefore, the quantification of amphenicol antibiotic residual levels in meat and fish products is necessary.

CAP, TAP, FF, and FFA (**Supplementary Figure 1**) antibiotics belong to the family of amphenicols and are extensively administered to livestock to prevent and treat various infections due to their ability to inhibit the growth of both gram-positive and negative bacteria (9, 10). CAP, the first antibiotic isolated from *Streptomyces venezuelae* in 1947, binds to the 50S subunit of bacterial ribosomes and inhibits intra-bacterial protein synthesis (10, 11). This drug is highly effective in treating animal diseases; however, it exhibits many toxic effects. Its use is thus restricted in many countries, including the United States, the Republic of Korea, and those in the European Union (EU) (12–14). TAP and FF are structural analogs of CAP (15). FF is widely used to prevent and treat bacterial infections in livestock because its bioavailability in many species is considerably higher than tetracycline antibiotics (16, 17). Furthermore, it is used in the aquaculture industry to treat bacterial diseases (18). Following animal administration, FF is partially converted to FFA and florfenicol oxamic acid (19). FFA is a major metabolite of FF in beef, pork, and chicken (20). Therefore, in many countries, FFA has been designated as one of the marker residues indicative of FF presence (21).

Various analytical methods entailing LC-MS/MS have been reported for determining amphenicols in animal tissues following various extraction techniques, either single (22, 23) or multiple analytes (24–27). For example, CAP was extracted from seafood products, honey, and royal jelly using methanol by Kikuchi et al. (22). CAP, TAP, FF, and FFA were extracted from poultry, swine, bovine, and fish muscle using liquid-liquid extraction (LLE) (24). Fedeniuk et al. (27) quantified CAP, CAP 3-O-β-d-glucuronide (CAP-GLUC), TAP, FF, and FFA in the bovine, equine, and porcine liver following a modified quick, easy, cheap, effective, rugged, and safe (QuEChERS) extraction method combined with SPE cleanup. However, to the best of our knowledge, few studies have reported the use of the "QuEChERS" method for the

simultaneous determination of CAP, TAP, FF, and FFA in a variety of food products (beef, pork, chicken, shrimp, eel, and flatfish).

Hence, the purpose of this study was to establish an accurate and sensitive method using modified QuEChERS extraction methods and LC-MS/MS for the quantification of CAP, TAP, FF, and FFA in commonly consumed products, including beef, pork, chicken, shrimp, eel, and flatfish in a single chromatographic run. This study was conducted based on the maximum residue limits (MRL) established by the Korean Ministry of Food and Drug Safety (KMFDS) and others (28–32) (**Table 1**). The MRL of FF in eel and flatfish (100 μg/kg) is higher than the quantifiable concentration range of the analytical device. Therefore, the reference concentration was lowered to 50 μg/kg. Analytes without a specified MRL were set at 10 μg/kg. The KMFDS has banned the use of CAP in animal products. Thus, it was analyzed based on the minimum required performance limit (MRPL) (0.5 μg/kg) of the KMFDS. The study adhered to the guidelines established by the Codex Alimentarius Commission (33).

MATERIALS AND METHODS

Chemicals, Reagents, and Samples

CAP (99.8% purity, CAS No.: 56-75-7), TAP (99.9% purity, CAS No.: 15318-45-3), FF (99% purity, CAS No.: 73231-34-2), FFA (99.3% purity, CAS No.: 76639-93-5), acetic acid (99.5% purity), ammonium hydroxide solution (NH_4OH), and ethylenediaminetetraacetic acid disodium salt (EDTA) solution (0.5 M in H_2O) were acquired from Sigma-Aldrich Corporation (St. Louis, MO, USA). HPLC-grade methanol (MeOH; 99.9% purity) and acetonitrile (ACN; 100% purity) were purchased from Pharmaco-Aaper (Brookfield, CT, USA) and JT Baker (Phillipsburg, NJ, USA). QuEChERS dSPE kits (containing 150 mg of primary-secondary amine (PSA) and 900 mg of $MgSO_4$) were obtained from Phenomenex (Torrance, CA, USA). Cellulose acetate membrane filters (0.45 μm) were supplied by MILLEX (Merck Millipore Ltd, Co. Cork, Ireland), and 0.2 μm PTFE syringe filters were sourced from Pall Corporation (Michigan, USA). The polypropylene conical tubes (15 and 50 mL) used throughout the entire experiment were acquired from FALCON (Tamaulipas, Mexico). Ultrapure water (resistivity of 18.2 MΩ.cm at 25°C) was supplied by a Milli-Q water purification system (Millipore, Bedford, MA, USA). All matrices (beef, pork, chicken, shrimp, eel, and flatfish) were procured from local markets in Seoul, Republic of Korea.

Preparation of the Standard Solutions

The primary stock standard solutions of CAP, TAP, and FF (1,000 μg/mL) in MeOH were prepared by reconstituting each drug standard according to its respective purity. The FFA stock solution (200 μg/mL) was prepared by accurately dissolving 2.0 mg of FFA in 1 mL double-distilled water (DDW) and 9 mL of ACN using an AG 285 analytical balance (Mettler Toledo, Seoul, Republic of Korea). The stock solutions were stored in the dark at −20°C and diluted accordingly before analysis. Depending on the levels of validation, the concentrations of the analyte working solutions differed. The mixed working solutions at specific CAP, TAP, FF, and FFA concentrations were

TABLE 1 | Maximum residue limit (MRL) and minimum required performance limit (MRPL) criteria for six animal-derived food products set by various regulatory authorities.

Analytes	Matrix	KMFDS[1] (µg/kg)	Codex[2] (µg/kg)	JAP[3] (µg/kg)	AUS[4] (µg/kg)	EU[5] (µg/kg)	USA[6] (µg/kg)
Chloramphenicol	Beef	0.5[a]	–	–	–	–	–
	Pork	0.5[a]	–	–	–	–	–
	Chicken	0.5[a]	–	–	–	–	–
	Shrimp	0.5[a]	–	–	–	–	–
	Eel	0.5[a]	–	–	–	–	–
	Flatfish	0.5[a]	–	–	–	–	–
Thiamphenicol	Beef	50	–	20	–	50	–
	Pork	50	–	–	–	50	–
	Chicken	50	–	50	–	50	–
	Shrimp	–[b]	–	–	–	50	–
	Eel	–[b]	–	–	–	50	–
	Flatfish	50	–	–	–	50	–
Florfenicol	Beef	100[c]	–	150	150	100	150
	Pork	150[c]	–	150	250	50	–
	Chicken	50[c]	–	100	–	50	–
	Shrimp	50[c]	–	–	–	50	–
	Eel	100[c]	–	4000	–	500	–
	Flatfish	100[c]	–	500	-	500	-
Florfenicol amine	Beef	100	–	150	150	100	150
	Pork	150	–	150	250	50	–
	Chicken	50	–	100	–	50	–
	Shrimp	50	–	–	–	50	–
	Eel	100[d]	–	4000	–	500	–
	Flatfish	100[d]	–	500	–	500	–

– No MRL.

[a] The KMFDS has banned chloramphenicol use in farmed animals. It was tested based on MRPL (0.5 µg/kg).

[b] Set to 10 µg/kg for analytes without a specified MRL.

[c] Set to 10 µg/kg for analytes with higher than the quantifiable concentration range of the device.

[d] This value is specified as 50 µg/kg, lower than the established MRL (100 µg/kg).

[1] Korean Ministry of Food and Drug Safety (2019) (14).

[2] Codex Alimentarius Commission (2018) (29).

[3] The Japan Food Chemical Research Foundation (2021) (31).

[4] Australian Pesticides and Veterinary Medicines Authority (2019) (28).

[5] European Commission (2010) (30).

[6] US Food and Drug Administration (2021) (32).

TABLE 2 | Multiple reaction monitoring (MRM) transitions of the tested drugs.

Analytes	CAS No.	Molecular Weight	Precursor ion (m/z)	Identity	Product ion (m/z)	Q1 Pre Bias (V)	Collision Energy (eV)	Q3 Pre Bias (V)
Chloramphenicol	56-75-7	323.1	321.1	[M-H]⁻	152.1*	12	17	15
					257.05	22	11	28
Thiamphenicol	15318-45-3	356.2	354.1	[M-H]⁻	185.1*	13	19	11
					290	13	12	12
Florfenicol	73231-34-2	358.2	356.1	[M-H]⁻	335.95*	13	9	10
					185.1	13	19	10
Florfenicol amine	76639-93-5	247.3	248.0	[M+H]⁺	230.1*	−15	−13	−25
					130.05	−14	−22	−22

*Quantification ion.

prepared by diluting the stock solutions with ACN. All working standard solutions were stored at −20°C and analyzed within a week.

Extraction Procedures

Homogenized beef, pork, chicken, shrimp, eel, and flatfish matrices (2.0 g) were weighed in 50 mL conical tubes. The

TABLE 3 | Method performance for chloramphenicol, thiamphenicol, florfenicol, and florfenicol amine analysis in spiked beef, pork, chicken, shrimp, eel, and flatfish samples.

Analytes	Matrix	Spiking level (μg/kg)	Intra-day (n = 3)	Inter-day (n = 9)	R²	LOD (μg/kg)	LOQ (μg/kg)
			Recovery (RSD) (%)	Recovery (RSD) (%)			
Chloramphenicol	Beef	0.5	83.61 (7.80)	97.90 (1.05)	0.9980	0.01	0.04
		1	94.66 (5.03)	115.49 (3.26)			
		5	101.12 (1.20)	107.17 (4.36)			
	Pork	0.5	94.66 (4.24)	95.07 (7.69)	0.9994	0.01	0.04
		1	106.76 (7.77)	102.14 (4.93)			
		5	99.73 (6.53)	87.46 (4.38)			
	Chicken	0.5	92.30 (14.23)	106.01 (12.79)	0.9971	0.02	0.07
		1	109.32 (5.21)	116.51 (3.05)			
		5	108.82 (4.90)	94.31 (7.24)			
	Shrimp	0.5	84.34 (11.53)	77.85 (6.70)	0.9989	0.01	0.05
		1	92.14 (5.33)	75.02 (3.14)			
		5	74.54 (15.73)	64.26 (7.78)			
	Eel	0.5	95.48 (9.71)	84.18 (4.41)	0.9990	0.01	0.04
		1	92.41 (11.33)	98.78 (1.12)			
		5	79.66 (8.29)	82.73 (1.03)			
	Flatfish	0.5	92.50 (4.53)	91.24 (7.03)	0.9976	0.01	0.02
		1	99.18 (2.52)	86.91 (4.63)			
		5	81.90 (9.45)	81.95 (2.92)			
Thiamphenicol	Beef	25	71.66 (3.11)	86.86 (2.86)	0.9993	0.1	0.3
		50	93.69 (8.28)	99.68 (3.92)			
		100	97.06 (5.14)	96.65 (1.48)			
	Pork	25	73.20 (3.57)	74.37 (2.28)	0.9994	0.09	0.3
		50	100.36 (7.19)	83.59 (4.23)			
		100	95.22 (3.30)	78.48 (6.04)			
	Chicken	25	96.62 (3.38)	87.38 (3.53)	0.9996	0.1	0.3
		50	100.74 (6.46)	92.79 (7.89)			
		100	91.57 (8.27)	91.30 (2.34)			
	Shrimp	5	91.20 (1.37)	88.85 (4.68)	0.9990	0.09	0.3
		10	86.66 (7.92)	84.69 (6.88)			
		20	80.32 (10.35)	83.34 (4.87)			
	Eel	5	96.51 (7.03)	96.92 (4.45)	0.9996	0.05	0.2
		10	86.25 (6.79)	99.59 (6.47)			
		20	81.19 (9.46)	83.36 (4.47)			
	Flatfish	25	90.92 (7.46)	92.22 (4.19)	0.9989	0.05	0.2
		50	106.91 (6.51)	96.67 (4.47)			
		100	106.41 (9.51)	104.39 (5.13)			
Florfenicol	Beef	5	93.91 (5.05)	76.12 (5.21)	0.9989	0.01	0.04
		10	100.50 (4.21)	87.20 (1.68)			
		20	102.47 (1.90)	86.82 (2.40)			
	Pork	5	104.43 (2.40)	102.82 (4.49)	0.9995	0.02	0.06
		10	100.88 (6.15)	104.03 (2.43)			
		20	90.89 (2.80)	97.08 (1.96)			
	Chicken	5	93.60 (11.08)	96.25 (8.38)	0.9995	0.01	0.02
		10	90.77 (10.92)	105.49 (6.71)			
		20	96.50 (2.11)	109.57 (0.81)			
	Shrimp	5	84.75 (11.31)	81.54 (8.35)	0.9976	0.01	0.04
		10	101.92 (3.05)	92.98 (3.84)			

(Continued)

TABLE 3 | Continued

Analytes	Matrix	Spiking level (µg/kg)	Intra-day (n = 3)	Inter-day (n = 9)	R²	LOD (µg/kg)	LOQ (µg/kg)
			Recovery (RSD) (%)	Recovery (RSD) (%)			
		20	91.17 (6.15)	88.30 (11.49)			
	Eel	5	85.54 (7.90)	90.96 (3.53)	0.9992	0.01	0.02
		10	90.93 (5.26)	99.04 (2.12)			
		20	86.94 (5.17)	86.06 (2.26)			
	Flatfish	5	85.30 (6.34)	85.05 (6.13)	0.9980	0.005	0.02
		10	101.17 (4.79)	90.05 (5.56)			
		20	100.13 (5.59)	96.36 (6.35)			
Florfenicol amine	Beef	50	93.11 (6.38)	80.72 (5.52)	0.9941	3.1	10.4
		100	88.46 (5.87)	85.34 (3.44)			
		200	86.46 (4.35)	81.29 (2.65)			
	Pork	75	88.66 (1.78)	82.95 (1.50)	0.9998	1.5	5.1
		150	82.12 (13.16)	74.70 (1.19)			
		300	94.28 (9.65)	84.43 (1.19)			
	Chicken	25	78.08 (2.58)	85.37 (2.27)	0.9964	0.6	1.8
		50	88.16 (18.05)	91.58 (14.39)			
		100	87.45 (1.47)	83.01 (1.50)			
	Shrimp	25	93.72 (6.32)	100.57 (2.62)	0.9991	1.3	4.3
		50	101.23 (1.34)	91.71 (4.76)			
		100	91.05 (4.46)	85.49 (5.83)			
	Eel	25	89.39 (1.94)	91.22 (0.69)	0.9979	2.1	7.1
		50	92.72 (4.31)	107.36 (2.47)			
		100	76.29 (12.65)	82.41 (3.57)			
	Flatfish	25	92.64 (5.65)	91.86 (3.47)	0.9979	1	3.3
		50	89.06 (10.50)	82.97 (9.23)			
		100	86.64 (5.38)	86.45 (2.93)			

samples were spiked with 0.2 mL of the working solution and equilibrated for 5 min. Next, a mixture of 1 mL of 0.1M EDTA in DDW and 1 mL of ammonium hydroxide: DDW (2:98, *v/v*) was added, and the mixture was vortex-mixed for 5 min. Then, 1% acetic acid in a 10 mL ACN was added to beef, pork, and chicken samples, while 10 mL ACN was added to shrimp, eel, and flatfish samples. After vortex-mixing for 10 min, the mixtures were sonicated in an ultrasonic bath (Bransonic 8210 ultrasonic cleaner, Branson Ultrasonics Corporation, Danbury, CT, USA) at 25 °C (40 k*Hz*: 5 min). The samples were centrifuged at 1392 rcf for 15 min at 4°C (Allegra X-15R, Beckman Coulter Inc., Brea, CA, USA), and the supernatants were transferred to tubes containing 150 mg PSA and 900 mg MgSO₄. These mixtures were vortexed for 10 min and centrifuged at 1392 rcf for 15 min at 4 °C. The obtained supernatant was transferred to a clean 15 mL conical tube and dried under nitrogen gas at 40 °C using a TurboVap®RV device (Caliper Life Sciences, Hopkinton, USA) to remove all the moisture. Before analysis, the residues were reconstituted in 1 mL ACN: DDW (90:10, *v/v*), sonicated at 25 °C (40 k*Hz*: 5 min) and centrifuged at 12525 rcf at 4 °C for 15 min. Before LC-MS/MS analysis, the concentrated solutions were filtered through a 0.2 µm PTFE syringe filter and passed through a 0.22-µm filter before LC-MS/MS analysis.

LC-MS/MS Instrumentation and Conditions
Chromatography Conditions
LC-MS/MS analysis was conducted using a Shimadzu high-performance liquid chromatography system (Columbia, MD, USA) equipped with two pumps (LC-30 AD), an autosampler (SIL-30AC), a degasser (DGU-20A5R), and a column oven (CTO-30A). Mass spectrometric detection was performed on a Shimadzu 8060 LC-MS/MS system (Shimadzu Scientific, Inc., MD, USA). Chromatographic separation was achieved on a Phenomenex Luna omega polar C18 100 Å (100 × 2.1 mm, 3 µm) at a column oven temperature of 40 °C and an injection volume of 3 µL. The mobile phases used for separating analytes were (A) DDW and (B) 0.1% acetic acid in ACN. The flow rate was 0.2 mL/min with a linear mobile phase gradient (time (min), % mobile phase B) at the following conditions: (0–1, 10% B); (1–2.5 min, 10%−100% B); (2.5–3.5 min, 100% B); (3.5–3.6 min, 100–10% B); (3.6–6 min, 10% B).

Mass Spectrometry Conditions
An electrospray ionization (ESI) in both positive (ESI+) and negative (ESI−) ion-switching modes were used for the triple quadrupole mass spectrometer (MS/MS). FFA was analyzed in positive ion mode, whereas CAP, TAP, and FF were analyzed in

negative ion mode. Multiple reaction monitoring (MRM) mode and LabSolutions (version 5.89, Shimadzu) analyst software was implemented for data collection. The operating conditions of the mass spectrometer were as follows: an interface temperature of 300°C, heat block temperature of 400°C, dwell time of 17 ms, and ion spray voltage of ±3 kV. Individual working standard solutions (0.1 μg/mL) were employed for optimizing the precursor ion, product ion, and collision energy. The fragment $[M+H]^+$ of the precursor ion was employed to identify FFA, whereas the $[M-H]^-$ ion was selected for CAP, TAP, and FF. The MRM transitions and parameters are presented in **Table 2**.

Method Validation

The following parameters were validated according to KMFDS, 2019: linearity, precision (relative standard deviation, RSD), accuracy (recovery), limits of detection (LODs), and limits of quantification (LOQs). Four drugs were tested according to the specified MRL set by the KMFDS. Matrix-fortified calibration curves achieved linearity at six concentration levels based on **Table 3**. The calibration curves were constructed by plotting the response factor as a function of drug concentration. The calculated LOD and LOQ were obtained as signal-to-noise ratios of (S/N) $\geq$3 and S/N $\geq$10. Accuracies of intra-day (single day, $n = 3$) and inter-day (three days, $n = 9$) recovery values were estimated at three spiking levels (CAP: 0.5, 1, and 5 μg/kg; TAP, FF, and FFA: ×1/2, ×1, ×2 of the MRL values). The intra- and inter-day RSD were calculated at the above-listed concentrations. Additionally, matrix effects at a spiking level of 0.5 μg/kg (CAP) and 1MRL values (TAP, FF, and FFA) were calculated for all four amphenicols.

Statistical Analyses

IBM SPSS Statistics, v25 (NY, USA) was used to compare the various extraction methods. Statistical analysis was performed using one-way ANOVA. Differences were considered significant when $P \leq 0.05$.

RESULTS AND DISCUSSION

Optimization of Sample Preparation

Various extraction methods were conducted to optimize the sample preparation protocol and achieve the maximum extraction efficiency (recovery rate). As a representative of all the samples, pork was fortified at a concentration rate based on the MRL (CAP: MRPL). The extraction of chopped samples was evaluated in ACN containing acid or base and in MeOH (common extraction solvents used for protein precipitation. The eight extraction conditions were: (a) MeOH, (b) ACN, (c) 1% acetic acid in ACN, (d) 1% formic acid in ACN, (e) ammonium hydroxide: ACN (2:98, v/v), (f) 1 mL of 0.1M EDTA in DDW + 1% acetic acid in ACN, (g) 1 mL of 0.1M EDTA in DDW + ammonium hydroxide: ACN (2:98, v/v), (h) 1 mL of 0.1 M EDTA in DDW + 1 mL of ammonium hydroxide: DDW (2:98, v/v) + 1% acetic acid in CAN (26, 27, 34–37). The recovery rates for each condition are shown in **Figure 1**. The recovery rate of FFA using (h) (79.13%) was 10%−60% higher than achieved under other conditions, which were: (a) 42.82%, (b) 40.21%, (c) 51.86%,

(d) 20.56%, (e) 41.95%, (f) 70.99%, and (g) 31.23%. Furthermore, employing (h), the recovery rates of CAP, TAP, and FF were 82.76, 74.16, and 87.99 %, respectively. However, conditions (h) did not provide a satisfactory recovery rate of FFA from fishery products (shrimp: 59.26%, eel: 58.79%, and flatfish: 43.93%). The use of ACN (without acetic acid) as an extraction solvent increased the recovery rate of shrimp (85.81%), eel (96.55%), and flatfish (86.42%) (**Figure 2**). Therefore, the selected extraction solvent for beef, pork, and chicken was 0.1 M EDTA in DDW + ammonium hydroxide: DDW (2:98, v/v) + 1% acetic acid in ACN and 0.1 M EDTA in DDW + ammonium hydroxide: DDW (2:98, v/v) + ACN for shrimp, eel, and flatfish.

Livestock products contain a higher proportion of endogenous interferences, such as lipids, phospholipids, and fatty acids, than vegetables and fruits; a purification process is necessary (35, 37). Therefore, four purification protocols were compared, namely: (A) 10 mL of *n*-hexane saturated with ACN, (B) C18 150 mg, (C) PSA 150 mg, C18 150 mg, and $MgSO_4$ 900 mg, and (D) PSA 150 mg and $MgSO_4$ 900 mg. Recoveries ranging from 71.91 to 89.49% (RSD: 4.80–9.18%), 60.96–82.08% (RSD: 6.52–9.25%), 68.40–88.97% (RSD: 1.64–8.92%), and 79.08–97.52% (RSD: 0.57–3.57%) were obtained under the conditions of (A), (B), (C), and (D), respectively. The recovery rate of condition (D) was the highest with the lowest RSD; thus, it was chosen as the purification method. Then, a high-speed centrifuge was used to remove low-layer impurities and obtain a clearer solution. Additionally, a syringe filter was used for further purification and instrument protection.

LC-MS/MS Conditions

The amphenicol drugs were analyzed using ESI turbo-positive and negative ion modes (positive ion mode: FFA; negative ion mode: CAP, TAP, and FF). All parameters used for quantification in MRM mode are shown in **Table 2**. For LC-MS/MS analysis, several combinations of mobile phases (A) and (B) were tested due to the significant effect of mobile phase composition on ionization efficiency. The solvents tested in the mobile phase (A) were: DDW, 0.1% acetic acid, 0.2% acetic acid, 0.1% formic acid, 1 mM ammonium formate, and 1 mM ammonium acetate. When acid and ammonium were not added to DDW, the peak intensities were satisfactory, and the peak of FFA was sharp. For solvent (B), ACN, 0.1% acetic acid in ACN, 0.1% formic acid in ACN, and MeOH were compared. When ACN or MeOH was used, peak tailing and peak splitting were observed for CAP, and a messy baseline and weak peak sensitivity were noted for all the drug analytes. ACN with 0.1% acetic acid was chosen as solvent (B) as it provided the sharpest peak shape and high-intensity peaks. Various C18 columns based on a silica hydride support, including basic (such as Phenomenex Luna C18 and Phenomenex Kinetex C18), high-strength silica (such as Waters X-Select HSS C18), extensive pH (such as Phenomenex Kinetex EVO C18), consistent performance in both volatile and non-volatile buffers (such as Phenomenex Gemini-NX C18), and polarity (such as Phenomenex Luna omega polar C18) were compared to obtain optimal peak parameters for the four tested drugs. The use of columns with basic, high-intensity silica, and extensive pH characteristics led to peak
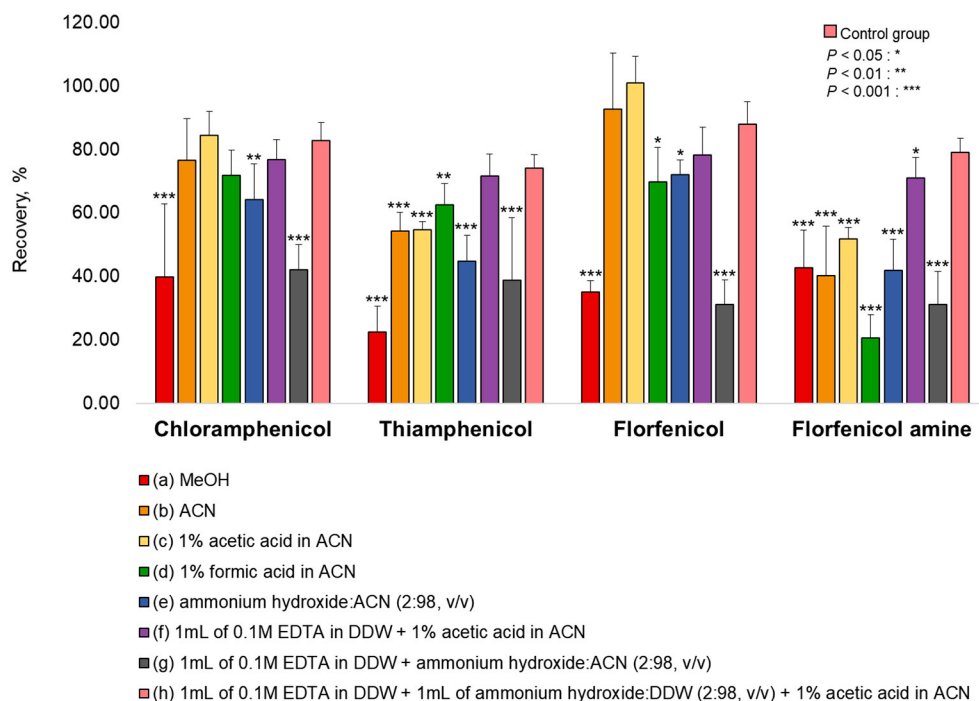
FIGURE 1 | Extraction efficiencies of various solvents for the tested analytes in pork. The pork was fortified at a concentration rate of CAP: 1 μg/kg, TAP: 50 μg/kg, FF: 10 μg/kg, and FFA: 150 μg/kg for each extraction protocol. (h) was used as a control group. Statistical analysis (IBM SPSS Statistics, v25, NY, USA) was conducted using one-way ANOVA analysis. $*P < 0.05$; $**P < 0.01$; and $***P < 0.001$ were considered statically significant.
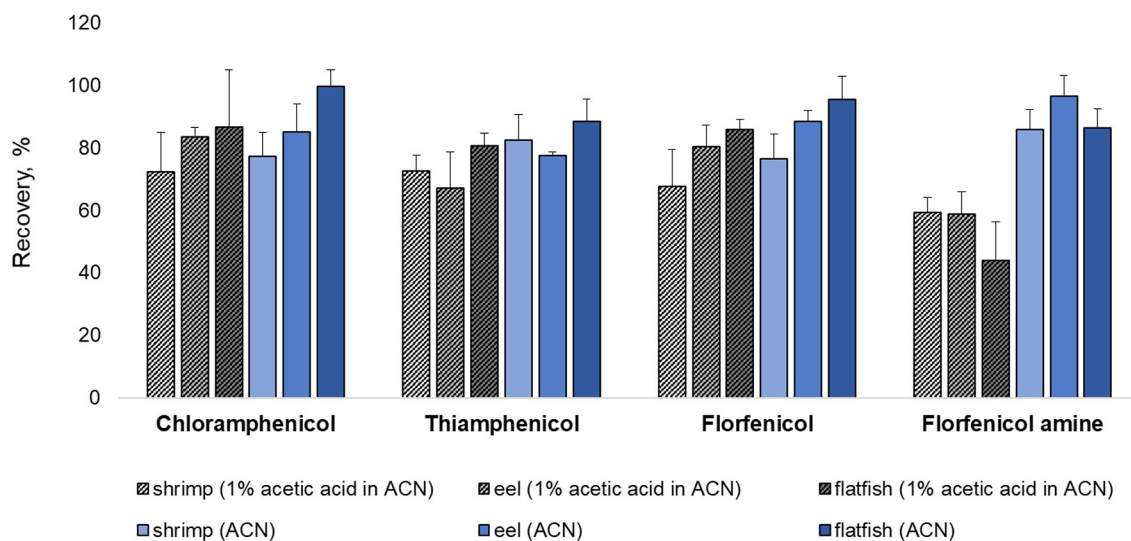
FIGURE 2 | Comparison of extraction methods with or without 1% acetic acid addition for shrimp, eel, and flatfish. Three samples were fortified at their respective MRL (CAP: MRPL) concentrations.

broadening/splitting. The Phenomenex Gemini-NX C18 column with consistent performance in volatile and non-volatile buffers gave poor signals and peak tailing for TA and FFA. Hence, the Phenomenex Luna omega polar C18 column (100 × 2.0 mm, 3 μm particle size) with unique polar selectivity was chosen to achieve optimal chromatographic separation.

Method Performance
Specificity and Linearity
Specificity was determined by analyzing blank beef, pork, chicken, shrimp, eel, and flatfish samples ($n = 3$) spiked with each analyte at a concentration of the MRL values. As shown in **Supplementary Figures 2, 3**,

TABLE 4 | Comparison with other studies. Matrices, extraction methods, analytical devices, recovery rates, LODs, and LOQs were compared for the tested drugs.

No.	Analytes	Matrix	Extraction method	Analytical device	Recovery (RSD) %	LOD (μg/kg)	LOQ (μg/kg)	Reference
1	Chloramphenicol, chloramphenicol 3-O-β-d-glucuronide, florfenicol, florfenicol amine and thiamphenicol	Bovine, equine, and porcine liver	Modified QuEChERS	LC-MS/MS	50–105 (7.6–45)	0.03–0.84	0.11–2.75	Fedeniuk et al. (27)
2	Chloramphenicol, thiamphenicol, florfenicol and florfenicol amine	Poultry, swine, bovine, and fish	LLE	LC-MS/MS	82–111 (1.1–18.1)	0.06–252.10	0.11–304.20	Barreto et al. (24)
3	Chloramphenicol, thiamphenicol, florfenicol, and florfenicol amine	Poultry eggs	LLE	UPLC-MS/MS	90.31–107.79 (1.42–6.65)	0.03–0.4	0.08–1.2	Wang et al. (25)
4	Chloramphenicol, thiamphenicol, florfenicol and florfenicol amine	Chicken muscle	LLE and SPE	LC-MS/MS	95.1–107.3 (4.4–10.9)	0.1–1	0.3–3	Zhang et al. (26)
5	Chloramphenicol, thiamphenicol, and florfenicol	Fish muscle	MSPD	UPLC-MS/MS	84.2–99.8 (<12)	-	-	Pan et al. (40)
6	Chloramphenicol, thiamphenicol, and florfenicol	Bovine muscle	tetrahydrofuran (THF)–water	LC-MS/MS	90–112 (5–15)	-	0.141–12.9	Sichilongo et al. (41)
7	Chloramphenicol, thiamphenicol, florfenicol, and florfenicol amine	Beef, pork, chicken, shrimp, eel, and flatfish	Modified QuEChERS	LC-MS/MS	64.26–116.51 (≤ 18.05)	0.005–3.1	0.02–10.4	This study

SPE, solid-phase extraction; MSPD, Matrix Solid-Phase Dispersion Extraction; UPLC-MS/MS, ultra-performance liquid chromatography-tandem mass spectrometry.

no interference from endogenous materials was observed.

According to MFDS guidelines (14), matrix-matched calibration curves from the responses of the four drugs were constructed by plotting the peak area of each tested analyte *vs.* the concentration (CAP: ×1, ×2–×6 the MRPL values; TAP, FF, and FFA: ×1/2, ×1, and ×2 to ×5 the MRL values, $n = 3$). The linearity was satisfactory, with coefficients of determination (R^2) being ≥0.9941 for all matrices.

LODs, LOQs, and Matrix Effects

As shown in **Table 3**, the LOD ranges were 0.01–0.02, 0.05–0.1, 0.005–0.02, and 0.6–3.1 μg/kg, and the LOQ ranges were 0.02–0.07, 0.2–0.3, 0.02–0.06, and 1.8–10.4 μg/kg for CAP, TAP, FF, and FFA, respectively. Furthermore, the LODs and LOQs were lower than the MRLs established for each drug. The LOQ of FFA was similar or higher than that in other studies (25, 27); however, the values for the other tested analytes were generally lower.

The matrix effects (MEs) gave rise to either ion suppression or enhancement depending on the matrix. MEs were determined at a spiking level of 0.5 μg/kg (CAP) and 1MRL values (TAP, FF, and FFA) as follows:

$$\text{MEs}(\%) = (A - B)/B \times 100$$

where A denotes the peak area of the standard in the matrix and B denotes the peak area of the standard in pure solvent. ME ranges were: −70.17 – 11.97% (beef), −67.60 – −7.20% (pork), −68.74 – 9.22% (chicken), −89.20 – 18.92% (shrimp), −84.68 – 3.88% (eel), and −69.76 – 5.59% (flatfish). In general, matrices containing proteins and lipids exhibit significant matrix-specific effects (38). As livestock products contain numerous proteins and fat, matrix-specific effects could not be completely ruled out (39).

Accuracy and Precision

The accuracy (expressed as recovery %) and precision (expressed as RSD%) were evaluated based on the criteria set by the Codex Alimentarius Commission (spiking concentrations: ≤1, 1–10, 10–100 and 100–1,000 μg/kg; recoveries: 50–120%, 60–120%, 70–120%, and 70–110%; RSDs: ≤35%, ≤30%, ≤20%, and ≤15% for CAP, TAP, FF, and FFA, respectively) (33). Blank samples spiked at three concentration levels (CAP: ×1, ×2, and ×6 the MRPL values; TAP, FF, and FFA: ×1/2, ×1, and ×2 the MRL values) were analyzed ($n = 3$) on a single day (intra-day) or for three consecutive days (inter-day) ($n = 9$). As shown in **Table 3**, the intra-day recovery values and RSDs were 71.66–109.32% and ≤ 18.05%, while the inter-day recovery values and RSDs were 64.26–116.51% and ≤14.39% for the four tested drugs in various matrices.

These results show that the developed method satisfies the Codex guidelines.

Comparison With Other Methods

As shown in **Table 4**, most of the studies employed LLE methods for extracting CAP, TAP, FF, and FFA. It has to be noted that only one study used the QuEChERS method; however, the recovery rate was lower than the present study. In addition, none of the studies monitored the analytes in various livestock and fishery products (beef, pork, chicken, shrimp, eel, and flatfish).

Method Application

Commercial samples of beef, pork, chicken, shrimp, eel, and flatfish were obtained from local markets in Seoul, Republic of Korea. The samples were handled according to the method described in Section 2.3. As shown in **Supplementary Figures 2, 3**, none of the samples tested positive for the target analytes.

CONCLUSIONS

An analytical protocol based on LC-MS/MS was developed and validated to simultaneously determine CAP, TAP, FF, and FFA. The four analytes were extracted from six samples (beef, pork, chicken, shrimp, eel, and flatfish) using LLE and modified QuEChERS methods for LC-MS/MS analysis. Recovery rate ranges of 64.26–116.51%, 71.66–106.91%, 76.12–109.57%, and 74.70–107.36% were obtained for CAP, TAP, FF, and FFA, respectively, in all matrices. The developed protocol offers a rapid and straightforward method for the simultaneous determination of these four analytes. Regulatory authorities can evaluate it as a reference method for establishing amphenicol MRLs in various livestock products.

DATA AVAILABILITY STATEMENT

The original contributions presented in the study are included in the article/**Supplementary Material**, further inquiries can be directed to the corresponding authors.

AUTHOR CONTRIBUTIONS

H-NJ and D-HP: formal analysis, investigation, validation, and writing-original draft. Y-JC and S-HK: methodology. H-JC: methodology and visualization. J-MC: methodology. J-HS and AZ: writing-review and editing. AA: data curation, formal analysis, and writing-review and editing. H-CS: conceptualization, resources, writing-review and editing, funding acquisition, project administration, and supervision. All authors contributed to the article and approved the submitted version.

FUNDING

SUPPLEMENTARY MATERIAL

The Supplementary Material for this article can be found online at: https://www.frontiersin.org/articles/10.3389/fnut.2021.812803/full#supplementary-material

REFERENCES

1. FAO, World Food Agric. - Stat. Yearb 2020. (2020). Available online at: http://www.fao.org/documents/card/en/c/cb1329en (accessed July 1, 2021).

2. Moberg GP. Biological response to stress: implications for animal welfare, Biol Anim Stress Basic Princ Implic Anim Welf. 1 (2000) 21.

3. WHO. *Antibiotic Resist.* (2020). Available online at: https://www.who.int/en/news-room/fact-sheets/detail/antibiotic-resistance (accessed July 1, 2021).

4. Van Boeckel TP, Pires J, Silvester R, Zhao C, Song J, Criscuolo NG, et al. Global trends in antimicrobial resistance in animals in low-and middle-income countries. *Science.* (2019) 365:eaaw1944. doi: 10.1126/science.aaw1944

5. Boison JO. Drug residues in foods. *J AOAC Int.* (2004) 87:261–9. doi: 10.1093/jaoac/87.1.261

6. Bywater RJ. Veterinary use of antimicrobials and emergence of resistance in zoonotic and sentinel bacteria in the EU. *J Vet Med Ser B.* (2004) 51:361–3. doi: 10.1111/j.1439-0450.2004.00791.x

7. Xie X, Wang B, Pang M, Zhao X, Xie K, Zhang Y, et al. Quantitative analysis of chloramphenicol, thiamphenicol, florfenicol and florfenicol amine in eggs via liquid chromatography-electrospray ionization tandem mass spectrometry. *Food Chem.* (2018) 269:542–8. doi: 10.1016/j.foodchem.2018.07.045

8. Ory EM, Yow EM. The use and abuse of the broad spectrum antibiotics. *JAMA.* (1963) 185:273–9. doi: 10.1001/jama.1963.03060040057022

9. Graziani C, Busani L, Dionisi AM, Lucarelli C, Owczarek S, Ricci A, et al. Antimicrobial resistance in Salmonella enterica serovar Typhimurium from human and animal sources in Italy. *Vet Microbiol.* (2008) 128:414–8. doi: 10.1016/j.vetmic.2007.10.017

10. Pongs O. Antibiotics: mechanism of action of antibacterial agents. (1979) 26. doi: 10.1007/978-3-642-46403-4_3

11. Shaw WV. Chloramphenicol acetyltransferase: enzymology and molecular biology. *Crit Rev Biochem.* (1983) 14:1–46. doi: 10.3109/10409238309102789

12. Balizs G, Hewitt A. Determination of veterinary drug residues by liquid chromatography and tandem mass spectrometry. *Anal Chim Acta.* (2003) 492:105–1. doi: 10.1016/S0003-2670(03)00890-0

13. EC, Commission Decision (2003/181/EC) of 13 March 2003. *Off J Eur Union.* (2003) L71:17–8.

14. Korean Ministry of Food and Drug Safety, MRLs Vet. Drugs, Repub. Korea (2019).Available online at: https//Www.Foodsafetykorea.Go.Kr/Residue/vd/Mrls/List.Do?MenuKey=2&subMenuKey=83. (accessed June 6, 2021).

15. Shen J, Hu D, Wu X, Coats JR. Bioavailability and pharmacokinetics of florfenicol in broiler chickens. *J Vet Pharmacol Ther.* (2003) 26:337–41. doi: 10.1046/j.1365-2885.2003.00495.x

16. Fukui H, Fujihara Y, Kano T. *In vitro* and *in vivo* antibacterial activities of florfenicol, a new fluorinated analog of thiamphenicol, against fish pathogens. *Fish Pathol.* (1987) 22:201–7. doi: 10.3147/jsfp.22.201

17. Park B, Lim J, Kim M, Yun H. Pharmacokinetics of florfenicol and its metabolite, florfenicol amine, in the Korean catfish (Silurus asotus). *J Vet Pharmacol Ther.* (2006) 29:37–40. doi: 10.1111/j.1365-2885.2006.00709.x

18. Hayes JM, Determination of florfenicol in fish feed by liquid chromatography. *J AOAC Int.* (2005) 88:1777–83. doi: 10.1093/jaoac/88.6.1777

19. Hormazabal V, Steffenak I, Yndestad M. Simultaneous determination of residues of florfenicol and the metabolite florfenicol amine in fish tissues by high-performance liquid chromatography. *J Chromatogr B Biomed Sci Appl.* (1993) 616:161–5. doi: 10.1016/0378-4347(93)80484-L

20. Committee for Proprietary Medicinal Products (CVMP). Florfeniciol (Extension to pigs) Summary Report (4) EMEA/MRL/591/99-FINAL. (1999) 7–10.

21. Wrzesinski CL, Crouch LS, Endris R. Determination of florfenicol amine in channel catfish muscle by liquid chromatography. *J AOAC Int.* (2003) 86:515–520.

22. Kikuchi H, Sakai T, Teshima R, Nemoto S, Akiyama H. Total determination of chloramphenicol residues in foods by liquid chromatography-tandem mass spectrometry, *Food Chem.* (2017) 230:589–93. doi: 10.1016/j.foodchem.2017.03.071

23. Chughtai MI, Maqbool U, Iqbal M, Shah MS, Fodey T. Development of in-house ELISA for detection of chloramphenicol in bovine milk with subsequent confirmatory analysis by LC-MS/MS. *J Environ Sci Heal B.* (2017) 52:871–9. doi: 10.1080/03601234.2017.1361771

24. Barreto F, Ribeiro C, Barcellos Hoff R, Dalla Costa T. Determination of chloramphenicol, thiamphenicol, florfenicol and florfenicol amine in poultry, swine, bovine and fish by liquid chromatography-tandem mass spectrometry. *J Chromatogr A.* (2016) 1449:48–53. doi: 10.1016/j.chroma.2016.04.024

25. Wang B, Pang M, Zhao X, Xie K, Zhang P, Zhang G, et al. Development and comparison of liquid–liquid extraction and accelerated solvent extraction methods for quantitative analysis of chloramphenicol, thiamphenicol, florfenicol, and florfenicol amine in poultry eggs. *J Mass Spectrom.* (2019) 54:488–94. doi: 10.1002/jms.4355

26. Zhang S, Liu Z, Guo X, Cheng L, Wang Z, Shen J. Simultaneous determination and confirmation of chloramphenicol, thiamphenicol, florfenicol and florfenicol amine in chicken muscle by liquid chromatography–tandem mass spectrometry. *J Chromatogr B.* (2008) 875:399–404. doi: 10.1016/j.jchromb.2008.09.035

27. Fedeniuk RW, Mizuno M, Neiser C, O'Byrne C. Development of LC–MS/MS methodology for the detection/determination and confirmation of chloramphenicol, chloramphenicol 3-O-β-d-glucuronide, florfenicol, florfenicol amine and thiamphenicol residues in bovine, equine and porcine liver. *J Chromatogr B.* (2015) 991:68–78. doi: 10.1016/j.jchromb.2015.04.009

28. Australian Pesticides and Veterinary Medicines Authority. Agric. Vet. Chem. Code (MRL Stand. Instrum. 2019. (2019). Available online at: https://www.legislation.gov.au/Search/Agricultural and Veterinary Chemicals Code (accessed July 1, 2021).

29. Codex Alimentarius, Maximum Residue Limits Risk Manag. Recomm. Residues Vet. Drugs Foods. (2018). Available online at: http://www.fao.org/fao-who-codexalimentarius/codex-texts/maximum-residue-limits/en/ (accessed July 1, 2021).

30. EU Commission, Comm. Regul. No 37/2010 22 December 2009 Pharmacol. Act. Subst. Their Classif. Regarding Maximum Residue Limits Foodst. *Anim Orig Off J Eur Union* (2010).

31. The Japan Food Chemical Research Foundation, Maximum Residue Limits List Agric. Chem. Foods (2021). Available online at: http://db.ffcr.or.jp/front/ (accessed July 1, 2021).

32. US Food and Drug Administration, United States Dep. Agric. Maximum Residue Limits Database. (2021). Available online at: https://www.fas.usda.gov/maximum-residue-limits-mrl-database (accessed July 1, 2021).

33. Codex Alimentarius Commission, Guidel. Des. Implement. Natl. Regul. Food Saf. Assur. Program. Assoc. With Use Vet. Drugs Food Prod. Anim. CAC/GL 71-2009 (2012).

34. Imran M, Habib FE, Majeed S, Tawab A, Rauf W, Rahman M, et al. LC-MS/MS-based determination of chloramphenicol, thiamphenicol, florfenicol and florfenicol amine in poultry meat from the Punjab-Pakistan. *Food Addit Contam Part A Chem Anal Control. Expo Risk Assess.* (2018) 35:1530–42. doi: 10.1080/19440049.2018.1463569

35. Jung HN, Park DH, Yoo KH, Cho HJ, Shim JH, Shin HC, et al. Simultaneous quantification of 12 veterinary drug residues in fishery products using liquid chromatography-tandem mass spectrometry. *Food Chem.* (2021) 348:129105. doi: 10.1016/j.foodchem.2021.129105

36. Yoo KH, Park DH, Abd El-Aty AM, Kim SK, Jung HN, Jeong DH, et al. Development of an analytical method for multi-residue quantification of 18 anthelmintics in various animal-based food products using liquid chromatography-tandem mass spectrometry. *J Pharm Anal.* (2021) 11:68–76. doi: 10.1016/j.jpha.2020.03.008

37. Zheng W, Yoo KH, Choi JM, Park DH, Kim SK, Kang YS, et al. A modified QuEChERS method coupled with liquid chromatography-tandem mass spectrometry for the simultaneous detection and quantification of scopolamine, L-hyoscyamine, and sparteine residues in animal-derived food products. *J Adv Res.* (2019) 15:95–102. doi: 10.1016/j.jare.2018.09.004

38. Park J, Abd El-Aty AM, Zheng W, Kim S, Choi J, Hacimüftüoglu A, et al. Determination of metoserpate, buquinolate, and diclofenac in pork, eggs, and milk using liquid chromatography–tandem mass spectrometry. *Biomed Chromatogr.* (2018) 32:e4215. doi: 10.1002/bmc.4215

39. Van Eeckhaut A, Lanckmans K, Sarre S, Smolders I, Michotte Y. Validation of bioanalytical LC–MS/MS assays: evaluation of matrix effects. *J Chromatogr B.* (2009) 877:2198–207. doi: 10.1016/j.jchromb.2009.01.003

40. Pan XD, Wu PG, Jiang W, Ma BJ. Determination of chloramphenicol, thiamphenicol, and florfenicol in fish muscle by matrix solid-phase dispersion extraction (mspd) and ultra-high pressure liquid chromatography tandem mass spectrometry. *Food Control.* (2015) 52:34–8. doi: 10.1016/j.foodcont.2014.12.019

41. Sichilongo KF, Kolanyane P, Masesane IB. A sensitive LC-MS/MS method employing a THF–water solvent system for the determination of chloramphenicol, thiamphenicol and florfenicol in bovine muscle. *Anal Methods.* (2014) 6:7015–21. doi: 10.1039/C4AY01135J

Conflict of Interest: The authors declare that the research was conducted in the absence of any commercial or financial relationships that could be construed as a potential conflict of interest.

Publisher's Note: All claims expressed in this article are solely those of the authors and do not necessarily represent those of their affiliated organizations, or those of the publisher, the editors and the reviewers. Any product that may be evaluated in this article, or claim that may be made by its manufacturer, is not guaranteed or endorsed by the publisher.

Bioactivities, Applications, Safety, and Health Benefits of Bioactive Peptides From Food and By-Products: A Review

Ahmed A. Zaky[1]*, Jesus Simal-Gandara[2], Jong-Bang Eun[3], Jae-Han Shim[4]* and A. M. Abd El-Aty[5,6]*

[1] National Research Centre, Department of Food Technology, Food Industries and Nutrition Research Institute, Cairo, Egypt, [2] Nutrition and Bromatology Group, Department of Analytical Chemistry and Food Science, Faculty of Science, Universidade de Vigo, Ourense, Spain, [3] Department of Food Science and Technology, Chonnam National University, Gwangju, South Korea, [4] Natural Products Chemistry Laboratory, Biotechnology Research Institute, Chonnam National University, Gwangju, South Korea, [5] Department of Pharmacology, Faculty of Veterinary Medicine, Cairo University, Giza, Egypt, [6] Department of Medical Pharmacology, Medical Faculty, Ataturk University, Erzurum, Turkey

Bioactive peptides generated from food proteins have great potential as functional foods and nutraceuticals. Bioactive peptides possess several significant functions, such as antioxidative, anti-inflammatory, anticancer, antimicrobial, immunomodulatory, and antihypertensive effects in the living body. In recent years, numerous reports have been published describing bioactive peptides/hydrolysates produced from various food sources. Herein, we reviewed the bioactive peptides or protein hydrolysates found in the plant, animal, marine, and dairy products, as well as their by-products. This review also emphasizes the health benefits, bioactivities, and utilization of active peptides obtained from the mentioned sources. Their possible application in functional product development, feed, wound healing, pharmaceutical and cosmetic industries, and their use as food additives have all been investigated alongside considerations on their safety.

Keywords: bioactive peptides, health benefits, bioactivities, applications, safety

INTRODUCTION

Nowadays, food is recognized as a source of dietary substances and biologically active compounds that improve human health and the general conditions of the organism. The consumers' increasing awareness of the influence of diet on health is reflected in their selection of natural products, abundant in vitamins, minerals, and other bioactive compounds like carotenoids (1), anthocyanins (2), polyphenols (3), or peptides (4, 5).

Bioactive peptides are protein fragments that benefit the body systems and overall human health. Most bioactive peptides range between two (dipeptides) and 20 amino acid residues and have a molecular mass of 0.4–2 kDa (6). Longer peptides have also been reported in rare cases. Lunasin, for example, is a peptide formed by 43 amino acids produced from soy, which demonstrates anti-cancer and hypocholesterolemic properties (7).

Bioactive peptides generated from food possess an excellent potential for creating functional foods and/or nutraceuticals to prevent or treat some chronic diseases (8). Many articles on the generation and characterization of bioactive peptides with antimicrobial, anti-inflammatory, antihypertensive, anti-obesity, and antioxidant attributes have been published (9). Herein, we

focused on bioactive peptides from different foods and their by-products, their effects on health, and possible applications.

In this investigation, eligible studies (in English) were acknowledged during an electronic search of the PubMed database (1991–2021) (https://www.nlm.nih.gov/) and Google. We employed the chief search word "bioactive peptides" along with the words "sources," "by-products," "extraction," "purification," "identification," "bioactivities," "health effects," "pharmaceutical applications," "food applications," "cosmeceutical applications," "feed applications," and "safety" to find the relevant articles. We selected the titles, keywords, and abstracts of the articles collected from the database. Several review articles were omitted in favor of the primary sources cited.

THE SOURCES OF BIOACTIVE PEPTIDES

Peptides and proteins are critical macronutrients as they provide the necessary raw materials for protein production and serve as a source of energy. Bioactive peptides have been isolated or produced from various plant and animal sources (**Tables 1–4**). Food proteins are chosen as a reference for bioactive peptides based on two factors: (i) a desire to add value to abundant underused proteins or protein-rich industrial food waste, and (ii) the use of proteins with particular peptide sequences or amino acid residues with specific pharmacological benefits (87).

Extraction of Bioactive Peptides

Bioactive peptides are conventionally isolated by chemical or enzymatic hydrolysis and fermentation. To enhance the degree of hydrolysis in the generation of bioactive peptides, new approaches, such as microwave, ultrasound-assisted extraction, ohmic heating, pulsed electric fields, and subcritical water hydrolysis, have been investigated (88). Physical processes are at the core of these techniques (**Figure 1**).

Chemical Methods

Chemical techniques using alkalis, such as sodium hydroxide, are the most typical and conventional method for protein extraction from plant sources (89, 90). It can effectively break hydrogen and amide bonds to solubilize rice bran proteins. Although this process is highly effective in obtaining most proteins in a soluble form, it creates specific structural changes that cause a protein to lose its original function (91).

Enzymatic Methods

Enzymatic hydrolysis is another common approach for separating proteins and hydrolysates/peptides from various food sources (92). Enzymes are employed in diverse ways to facilitate protein extraction from food, such as cell wall degradation, starch-bond protein release, and protein solubility improvement (93). In this regard, Wang et al. (94) utilized phytase and xylanase to isolate protein from rice bran and noticed that the use of carbohydrates could be helpful to improve the yield of soluble protein.

Physical Methods

Physical methods are often favored over chemical or enzymatic treatments for food production because they have fewer changes (95). These techniques are more economical and easy to adapt and use in the industry. Conventional physical procedures, such as colloidal milling, homogenization, high-speed blending, freeze-thaw, and high pressure, have been utilized for protein extraction (90).

Microwave-Assisted Extraction

Microwave heating is a novel technology based on electromagnetic waves with wavelengths and frequencies ranging from 1 mm to 1 m and 300 MHz to 300 GHz, respectively. It has gained popularity in the food processing industry because of its uniform heating, high heating rates, safety, simple, quick, and clean operation, and low maintenance. Furthermore, this kind of heating has a lower impact on food products' flavor and nutritional quality than conventional heating. By shattering disulfide and hydrogen bonds (non-covalent bonds), this approach can cause protein unfolding, which affects the secondary and tertiary structures of proteins (96, 97). In this respect, the microwave process was shown to assist the chia seed protein enzymatic hydrolysis with enhanced bioactivity (antioxidant activity), and functionality (emulsification and foaming properties) gained in a shorter time in comparison to traditional hydrolysis techniques (98).

Ultrasound-Assisted Extraction

Sonication is a green, novel, innovative and sustainable strategy based on high sound waves of frequencies (>16 kHz) undetectable by the human ear. This approach has several benefits compared with traditional thermal processes, including higher efficiency, higher rate, more accessible and cheaper application and operation, lower equipment contamination, and higher quality and functionality of processed foods (98, 99). In this context, Zhao et al. (100) demonstrated that sonication with power levels of 200, 400, or 600 W for 15 or 30 min altered the secondary and tertiary structure of walnut protein isolate without any impact on its primary structure since the process could not break the covalent bonds. Further, Vanga et al. (101) indicated that ultrasonic treatment (25 kHz, 400 W, 1–16 min) reduced soymilk protein trypsin inhibitor activity by 52% and enhanced its digestibility.

Ohmic Heating

Ohmic heating is a thermal processing technology that applies alternating electric currents directly into a semi-conductive media. It was initially employed for milk pasteurization in 1920. According to Joule's law, direct or volumetric heat is generated in products by passing a moderate and alternating electric current through them, which functions as resistance in an electrical circuit (102, 103). In this way, Li et al. (104) evaluated the structure and techno-functionality of proteins in soybean milk when using ohmic heating against traditional heating. Their findings revealed that ohmic heating effectively reduced heating time and enhanced the protein's emulsifying capacity.

TABLE 1 | Peptides from milk and by-products and their bioactivity.

Source	Peptide sequence	Bioactivity	References
Bovine milk	Lys-Val-Leu-Pro-Val-P(Glu)	Antihypertensive activity	(10)
	N/A	Antimicrobial activity	(11)
Cheddar cheeses	N/A	Antimicrobial, antioxidant, and antihypertensive activity	(12)
	N/A	Phosphopeptides	(13)
Casein hydrolysates	Arg-Tyr-Lue-Gly-Tyr	Antihypertensive activity	(14)
Comte cheese	N/A	Phosphopeptides	(15)
Feta, Swiss cheeses	N/A	Antiamnesic	(16)
Mik fermented	Ile-Pro-Pro Val-Pro-Pro	ACE-inhibitory activity	(17)
Enzyme modified cheese	N/A	Opioid activity and ACE-inhibitory activity	(18)
Yogurt	N/A	Antihypertensive and antimicrobial activity	(19)
	κ-casein: Met-Ala-Ile	Antithrombotic activity	(20)
	N/A	Immunomodulatory	(13)
	N/A	Antithrombotic	(21)
β- lactoglobulin	β-lactosin B	Antihypertensive activity	(22)
		Antithrombotic activity	(23)
Fermented milk	Val-Pro-Pro,Ile-Pro-Pro	Antihypertensive activity	(24)
Sour milk	N/A	Phosphopeptides	(25)
	N/A	Antihypertensive properties	(16)
By-products			
Whey protein hydrolysate	Lactoferricin	Antimicrobial activity, anti-cancer	(24)
	N/A	Opioid activity	(26)
	TTFHTSGY GYDTQAIVQ	Antihypertensive properties	(13)
Whey proteins	N/A	Anticancer	(15)

N/A, Not available.

The protein's foaming ability, on the other hand, reduced as its surface hydrophobicity dropped.

The Pulsed-Electric Field (PEF)

The pulsed-electric field (PEF) technique has been employed as a non-thermal process for microorganisms and enzymes inactivation. In this technology, the food sample is subjected to short high-power electrical pulses (μs or ms) between electrodes (105). A PEF system consists of a chamber, electrodes, a high-voltage pulse generator, and a computer for monitoring and controlling devices. A strong electric field is formed between two electrodes because of their electrical potential difference. During the PEF process, the generated electrical energy might cause protein unfolding and enhanced interactions with the solute. This can impact the peptides/protein's functional characteristics by increasing its solubility (106). In this regard, PEF treatment of canola seeds enhanced the extracted protein's solubility, emulsifying, and foaming capabilities, according to Zhang et al. (107). Nevertheless, depending on the strength and duration of the PEF process, it can result in denaturation and aggregation, resulting in decreased solubility. The PEF method can change plant-derived peptides and proteins' secondary and tertiary structures. Changes in the secondary structure of peptides derived from pine nut protein were also informed, along with their antioxidant effect (108).

Purification and Identification of Bioactive Compounds

All the methods for purifying and identifying bioactive peptides are very similar. Purification of active peptides is required to produce a commercially viable product. Ultrafiltration, RP-HPLC, size exclusion chromatography, and ion-exchange chromatography, can all be used to purify bioactive peptides. Additionally, for protein identification, analytical techniques such as mass spectrometry (MS), electrospray ionization MS, matrix-assisted laser desorption ionization time-of-flight MS, liquid chromatography-MS/MS, and hydrophilic interaction liquid chromatography (HILIC) are widely utilized (109).

BIOACTIVITIES OF BIOACTIVE PEPTIDES AND THEIR IMPACT ON HEALTH

Proteins are necessary for the growth and the preservation of many biological processes. The awareness regarding physiologically active peptides is growing quickly, as they may serve as possible modifiers for several regulative functions in the body. Bioactive peptides have different biological actions depending on the amino acid class, net charge, secondary structures, sequence, and molecular mass (110). Multiple studies have determined the bioactivities of peptides, which were linked

TABLE 2 | Peptides from meat and by-products and their bioactivity.

Source	Peptide sequence	Bioactivity	References
Duck breast meat	LQAEVEELRAALE IEDPFDQDDWGAWKK	Antioxidant activity	(27)
Beef muscle	DFHING	Antihypertensive activity	(28)
Bovine brain	MPPPLPARVDFSLAGALN	Phosphoenolpyruvate inhibitory activity	(29)
Venison muscle	MQIFVKTLTG DLSDGEQGVL	Antioxidant activity	(30)
Beef muscle	GFHI, DFHING, FHG, GLSDGEWQ	Antimicrobial activity	(28)
Fermented meat sauce	GYP	Antioxidant activity	(31)
Chicken breast protein	Breast protein hydrolysate	Antioxidant activity	(32)
Bovine muscle	YEDCTDCGN	Anti-opioid activity and ACE-inhibitory activity	(29)
By-products			
Duck skin	N/A	Antioxidant activity	(33)
Bovine myoglobin	AKHPSDFGADAQA		(34)
Bovine blood	YPWT	Opioid activity	(29)
Bovine blood	TKAVEHLDDLPGALSELSDLHAHKLR VDPVNFKLLSHSLL	Antihypertensive activity	(35)
Bovine tendon	AKGANGAPGIAGAPGFPG ARGPSGPQGPSGPP		(36)
Bovine blood	STVLTSKYR	Antimicrobial activity	(37)
Buffalo horn	AADNANELFPPN	Antioxidant activity	(38)
Bovine skin	N/A		(39)
Bovine brain	N/A		(40)
Buffalo horn	AADNANELFPPN		(38)
Yak skin	<3 kDa		(41)
Sheep abomasum protein	LEDGLK		(42)
Bovine liver	<10 kDa		(43)
Dry-cured ham bones	N/A		(44)
Chicken liver	N/A		(45)
Chicken bone collagen hydrolysates	N/A	Lipid-lowering activity	(46)

N/A, Not available.

to improved overall health and a lower risk of specific chronic diseases, such as cancer, diabetes, and heart diseases (**Figure 2**).

Antioxidant Activity

Reactive oxygen species cause cell damage, leading to cancer, diabetes, cardiovascular disease, and hypertension (111). The antioxidative characteristics of bioactive peptides are associated with their composition, formation, and hydrophobicity. Histidine, glutamic acid, proline, tyrosine, cysteine, methionine, and phenylalanine are all amino acids with antioxidant properties (112). Amino acids bind pro-oxidant metal ions to perform their activity, scavenge the OH radical and/or inhibit lipid peroxidation. As a result, each amino acid contributes as an antioxidant uniquely, depending on its type (67). Most antioxidant peptides include 4–16 amino acid residues and have a molecular mass of 0.4–2 kDa. Peptide molecular size influences both the pathways to target locations and the gastrointestinal digesting process, potentially increasing antioxidant activity *in vivo* (113). Tyrosine-containing peptides work primarily through hydrogen atom transfer, whereas cysteine, tryptophan, and histidine-containing peptides work mainly through single electron transfer (114). Aromatic amino acids like Tyr and Phe are excellent at donating protons to electron-deficient radicals. This characteristic enhances the bioactive peptides' radical-scavenging abilities. The antioxidant capacity of His-containing peptides is confirmed to be linked to hydrogen donating and lipid peroxyl radical trapping (115). The sulfhydryl group in cysteines, on the other hand, is endowed with an antioxidant effect because of its primary reaction with radicals (116). Plant-based proteins derived from industrial food and its by-products, such as soybean, wheat germ, hemp seeds, rice bran, sesame bran, wheat bran, and rapeseed, possess bioactive peptides with antioxidant characteristics (117).

Antimicrobial Activity

Antimicrobial peptides possess an antimicrobial activity that protects mammals from various bacteria, fungi, and viruses. Antimicrobial activity is also a coveted feature in prepared foods since it directly impacts the product's shelf life. Antimicrobial peptides are divided into three categories: short (20–46 amino acid residues), basic (rich in Lys or Are), and amphipathic. They are commonly abundant in hydrophobic residues, such

TABLE 3 | Peptides from plants and by-products and their bioactivity.

Source	Peptide sequence	Bioactivity	References
Maize	RSGRGECRRQCLRRHEGQPWET QECMRRC RRR/ YA, LMCH (zein)/ LPP (zein)	Antimicrobial, antioxidant, and antihypertensive activities	(24)
Soybean	1–3 kDa	Antimicrobial activity	(47)
Oat and wheat grains	N/A	Antihypertensive, antioxidant, antithrombotic, and opioid activities	(48)
Sweet potato	N/A	Antioxidant activity	(49)
Corn protein	Pro-Phe and Leu-Pro-Phe		(50)
Amaranth	VW, GQ/PYY, RWY, WY, RW PWW, PWR, PW, PWY WYS/VGECVRGRCPSGMCCSQF GYCGKGPKYCG	Anticancer, antioxidant and antimicrobial activities	(24, 51)
Rice protein	Thr-Gln-Val-Tyr	ACE-inhibitory, antimicrobial, and antioxidant activities	(48, 52)
Lentils	N/A	Antioxidant activity	(53)
Zein hydrolysate	N/A	Antioxidant activity	(54)
Quinoa flour	5 peptides; <1.1 kDa		(55)
Moringa seed	Peptied fractions < 10 kDa	Antidiabetic, antioxidant, and antidiabetic activities	(56)
By-products			
Plum by-product	N/A	Antioxidant and ACE inhibiting activities	(57)
Rice bran protein hydrolysates	N/A	Antioxidant activity	(4, 58)
Soybean meal	Peptied fractions: < 5 kDa, 3–5 kDa, 1–3 kDa, >1 kDa	Antioxidant, antimicrobial, and antitumor activities	(59, 60)
Palm kernel oil cake	YLLLK YGIKVGYAIP GGIF GIFE GVQEGAGHYALL LPWRPATNVF	Antihypertensive activity	(61)
Wheat bran protein hydrolysates	Gluten	Antihypertensive and antioxidant activities	(62)
Sunflower seed meal	FVNPQAGS	Antihypertensive activity	(63)
Watermelon seed	Hydrophobic amino acids (Gly,Ala, Val, Met, Ile) Aromatic amino acids (Tyr, Phe, His)	Antioxidant activity	(64)
Tomato seed cake	10 peptides; <1 kDa	ACE inhibitory and antioxidant activities	(65)
Cottonseed meal	<1 kDa	Antioxidant activity	(66)
Corn gluten meal	Peptides fraction of 500–1,500 Da		(67)
Sesame meal	N/A		(68)

N/A, Not available.

as Leu, Ile, Val, Phe, and Try (118). Multicellular organisms create antimicrobial peptides as defensive strategies against pathogenic microorganisms. Antimicrobial peptides can alter the cell membrane and biological processes, including cell division (119). Their action is assumed to create channels or pores within bacterial membranes, inhibiting anabolic activities, changes in gene expression and signaling transduction, and promoting angiogenesis. For example, the antimicrobial action of milk is demonstrated by extensive research. Lactoferrin, which is hydrolyzed into lactoferricin in the gastrointestinal tract, is an essential contributor to the synthesis of various other bioactive peptides and has antimicrobial ability in and of itself (120). Antimicrobial peptides have also been discovered in marine products. Many microorganisms, like *Staphylococcus aureus, Escherichia coli, Bacillus subtilis, Shigella*

dysenteriae, Pseudomonas aeruginosa, Salmonella typhimurium, and *Streptococcus pneumoniae,* were inhibited by the peptide GLSRLFTALK, isolated from anchovy cooking wastewater (121). Moreover, Aguilar-Toalá et al. (122) found that adding chia protein hydrolysate (<3 kDa) possessed higher antimicrobial activity than both chia peptide fraction 3–10 kDa. Furthermore, the <3 kDa fraction demonstrated a notable increase in membrane permeability of *E. coli* (71.49% crystal violet uptake) and *L. monocytogenes* (80.10% crystal violet uptake).

Mineral Binding

At intestinal pH, peptides with specific sequences create compounds by binding in solution with minerals, such as calcium (Ca) and phosphorus (P). As these peptides have a higher anionic character, they form soluble complexes

Source		Bioactivity	References
Shrimp proteins	N/A	Antihypertensive activity	(69)
Tuna proteins	N/A		(70)
Sea cucumber hydrolysate			(71)
Conger eel protein	LGLNGDDVN	Antioxidant activity	(72)
Sardine protein	LQPGQGQQ		(73)
Mackerel filet protein hydrolysate	N/A		(74)
Royal jelly protein	AL, FK, FR, IR, KF, KL, KY, RY, YD, YY, LDR, KNYP		(75)
Mollusks (*Conus magus*)	N/A	Analgesic	(24)
Seaweed (*Eucheuma serra*)	Lectins	Anticancer	(76)
Sponges (*Jaspis* spp.)	Jaspamide		(77)
Geodia corticostylifera	N/A	Antiproliferative	(78)
By-products			
Tilapia (*O. niloticus*) skin	Leu-Ser-Gly-Tyr-Gly-Pro	Antihypertensive activity	Chen et al. (79)
Pacific cod skin gelatin	N/A		(80)
Tuna backbone	VKAGFAWTANQQLS	Antioxidant activity	(81)
Hoki skin gelatin	HGPLGPL		(82)
Salmon (Protamine, derived from fish milt)	Pro-Arg (271.3 Da)		(83)
Horse mackerel viscera	Ala-Cys-Phe-Leu		(84)
Olive flounder (*P. olivaceus*) surimi	N/A	Antihypertensive activity	(85)
Bluefin leatherjacket heads	Trp-Glu-Gly-ProLys; Gly-Pro-Pro; Gly-Val-Pro-Leu-Thr	Antioxidant activity	(86)

N/A, Not available.

FIGURE 1 | Scheme for extracting bioactive peptides.
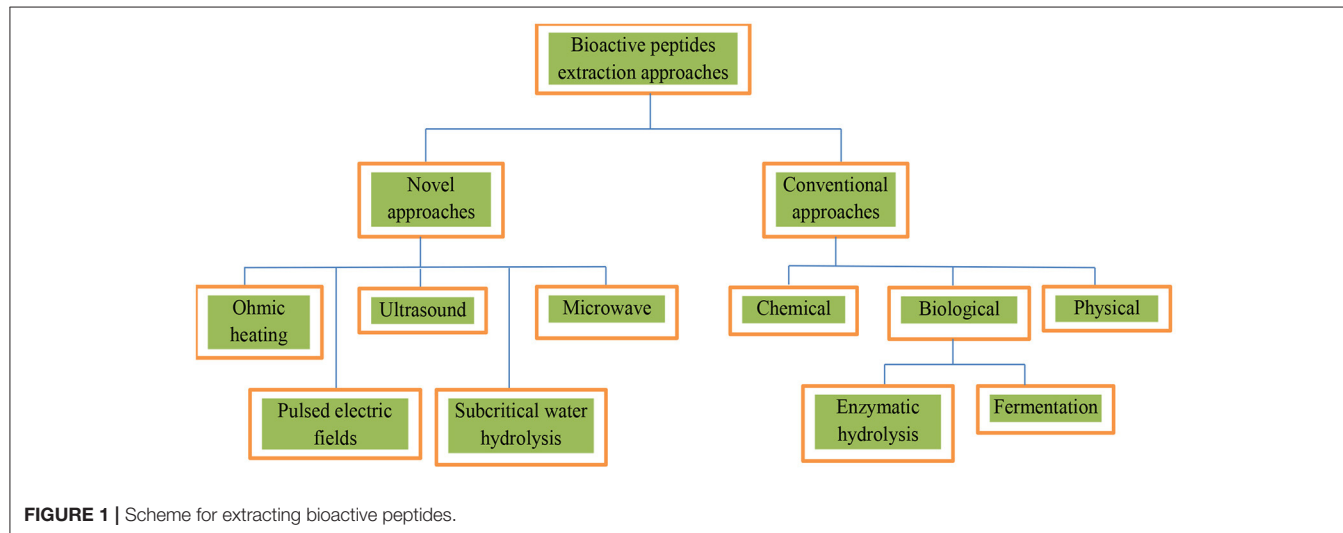
immune to additional proteolytic attacks, blocking the creation of insoluble mineral compounds (24). Flaxseed proteins contain hydrophobic and positively charged amino acids that might aid enzymatic hydrolysis in generating calmodulin (CaM)-binding peptides. Flaxseed proteins were digested with alcalase to produce low-MW peptides (123). Milk caseins are also known to bind Ca and P ions, increasing their bioavailability (24).

Opioid Activity

Opioid peptides are naturally synthesized and have analgesic properties (124). They bind to the opiate receptor and exhibit opiate-like actions suppressed by naloxone (125), with a specific impact on the neurological system (126). Prodynorphin (dynorphins), proopiomelanocortin (endorphins), and proenkephalin (enkephalin) are the three types of precursor proteins found in typical opioid peptides (127). The N-terminal

FIGURE 2 | Bioactivities of bioactive peptides.
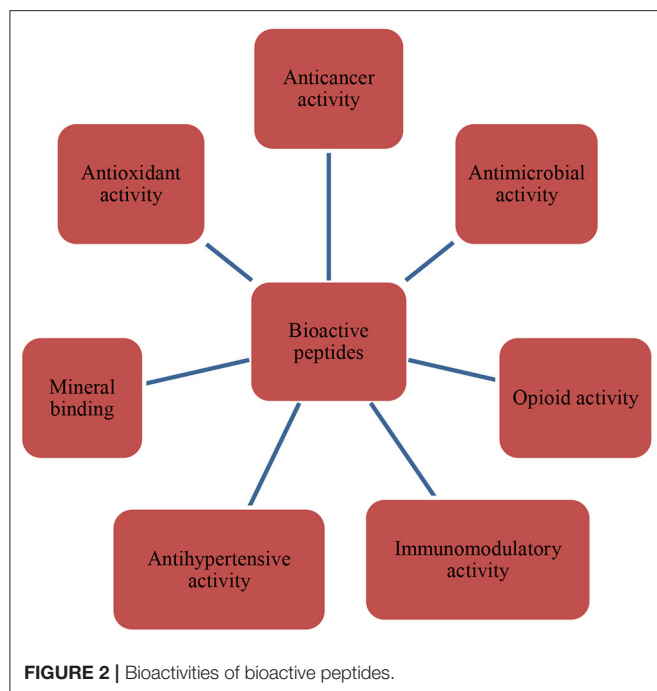
sequences Tyr-Gly-Gly-Phe and Tyr-Pro are prevalent in these peptides (113). Opioid peptides can be found in milk and dairy products (18) and various plant sources, including oats, wheat, rye, barley, and maize (128). Pihlanto-Leppälä (129) found that opioid peptides interact with particular receptors on target cells.

Anticancer Activity

Cancer has become one of the world's most feared and deadly diseases. Pharmaceutical companies are developing anticancer and antitumor medications at a rapid pace. Further, oncology research is well-progressed and has improved our understanding of tumors over time (130). Food protein hydrolysate is an excellent foundation for the generation of anticancer peptides. The anticancer effect of rice and soy protein hydrolysates has been previously demonstrated. In rice, anticancer peptides are produced by alcalase digestion of rice bran proteins (131). Another anticancer peptide (Ala-Phe-Asn-Ile-His-Asn-Arg-Asn-Leu-Leu) was separated from shellfish proteins, which successfully killed breast, prostate, and lung cancer cells while leaving normal liver cells unharmed (132). Most anticancer investigations on peptides are conducted on lunasin; a peptide derived from soy or wheat grains (24). The anticancer properties of lunasin are linked to its particular amino acid sequences, which contain Arg-Gly-Asp for cell adhesion and a polyaspartic acid chain with nine aspartic acid residues (133). Fermented soybean extracts impact the proliferation of MCF7 breast cancer cells and downregulate gene expression, according to Hwang et al. (134). The investigators found that, through stimulating the TGF pathway, fermented soybean extracts may effectively prevent breast cancer. According to Badger et al. (135), soy peptide concentrates reduce the incidence of breast, prostate, and gastrointestinal cancers. They claimed that soy peptide

concentrates could reduce cancer incidence by 80%. Further, peptides from black soybean, mung bean meal, and adzuki bean were found to suppress cancer cells at 200–600 g/mL concentrations (136). These anticancer peptides were only studied *in vitro*; further investigation on their bioavailability is needed.

Antihypertensive Activity

Owing to the changes in lifestyle in modern society, there is a growing need for functional foods with blood-pressure-lowering benefits in the therapy of hypertension. Hypertension can cause multiple disorders, including heart and renal diseases, arteriosclerosis, and stroke (137). Antihypertensive peptides (also known as angiotensin-converting enzyme (ACE) inhibitors) generated by protein hydrolysates are the most studied peptides (138). In this respect, ACE has a crucial effect since it catalyzes the transformation of angiotensin I to angiotensin II, which leads to a rise in blood pressure. Aromatic amino acid residues at the C-terminus and hydrophobic amino acid residues at the N-terminus help peptides block ACE function more effectively (139). Various plant sources, including pea (Ile-Arg, Lys-Phe, and Glu-Phe), soybean (Asp-Leu-Pro and Asp-Gly), and rice (Ile-His-Arg-Phe), have been shown to possess active peptides with antihypertensive capacity (117). Marambe et al. (140) found that defatted flaxseed protein hydrolysate reduced the ACE activity, lowering the risk of cardiovascular disorders. Many tripeptides that restrain ACE have been separated from foods. In this context, Wang et al. (141) confirmed that an active peptide (Tyr-Ser-Lys) derived from rice bran had a potent ACE inhibitory effect. Another work by Tuomilehto et al. (17) found that the milk-obtained bioactive tripeptides (Val-Pro-Pro and Ile-Pro-Pro) lowered blood pressure in moderately hypertensive patients. Bioactive peptides, particularly those with low molecular weight, inhibited ACE, decreased blood pressure and prevented hypertension.

Immunomodulatory Activity

Immunomodulatory activity is essential for the human immune system to function correctly. The immunomodulatory effect of bioactive peptides depends on cytokine regulation, antibody formation, immune system stimulation *via* reactive oxygen species, conformational changes in tubulin, and inhibition of protein synthesis (87). Furthermore, the amino acid content, sequence, length, charge, hydrophobicity, and peptide structure are linked to the immunomodulatory function. In this regard, soy protein hydrolysates with low molecular weight and many positively charged peptides have been proven to stimulate immunomodulation (142). Numerous plant-generated bioactive peptides with immunomodulatory action, including Leu-Asp-Ala-Val-Asn-Arg and Met-Met-Leu-Asp-Phe, possess low molecular weights (686 and 655 Da, respectively) and hydrophobic characteristics (143). According to Ngo et al. (144), marine products are a significant source of bioactive peptides that have been used as a treatment for a variety of disorders.

Anti-inflammatory Activity

Anti-inflammatory effects have been found in proteins/peptides derived from eggs, milk, and plants (145). The anti-inflammatory characteristics of new active peptides from sponges, bacteria, and microalgae have been documented, along with the molecular diversity of marine peptides and data regarding their anti-inflammatory impact and modes of action (146). Zhao et al. (147) reported that anti-inflammatory peptides generated from velvet antler simulated gastrointestinal digests were purified and identified using LC-MS/MS. Four anti-inflammatory peptides were identified, namely VH, LAN, AL, and IA. These findings proposed that peptides obtained from velvet antler protein might be a viable anti-inflammatory agent in functional ingredients. Bioactive peptides promoted diet-induced hepatic fat deposition and hepatocyte pro-inflammatory response when evaluated on SAMP8 aging rats (148). *In vitro* and *in vivo* investigations have revealed that corn, whey, and soybean protein hydrolysates have a powerful anti-inflammatory effect (149, 150).

APPLICATIONS OF BIOACTIVE PEPTIDES

Food Applications

Bioactive peptides have shown to be extremely useful in developing numerous health-oriented functional diets. These peptides are used as sweeteners, color stabilizers, thickeners, anti-caking factors, emulsifiers, flavor enhancers, emulsifiers in food preparation, and acidity control. Bioactive peptides may also improve food quality by affecting the water and oil retention capacity, colloidal stability, viscosity, and foam generation in the finished product (151). Peptide isolates used in the formulation of functional products aid in creating certain required technical qualities. Numerous studies have been conducted on proteins/peptides of different origins to produce functional foods. Emulsification is a necessary procedure that is frequently utilized to assess protein-rich products. Due to their amphiphilic character, bioactive peptides derived from food by-products are important for emulsifying attributes (152). Active peptides derived from plant sources like potato (153), flaxseed (154), and soybean (155) have been found to exhibit emulsifying capabilities. As reported by Álvarez et al. (156), adding rice bran protein concentrate to beef products increased its emulsion stability and rheological qualities. Due to the increased levels of bioactive peptides, Talukder and Sharma (157) found that using oat bran concentrate in the formulation of chicken meat patties resulted in better emulsion activity than that obtained using wheat bran concentrate. Likewise, Kamani et al. (158) observed that soy protein concentrate and gluten in sausage recipes increased emulsion stability and gel-forming capabilities by producing a robust structural network.

Foam formation can generate acceptable textural and sensory characteristics in food such as pastries and sauces (159). Their capacity to reduce surface tension facilitates the use of active peptides as foam stabilizers. Rice bran protein isolates had a comparable foaming potential to egg white but much lower foaming stability (114). Similarly, Elsohemy et al. (160) reported that the foaming capacity of the quinoa seed protein concentrate was much higher than that of soybean cake protein concentrate.

According to Kamani et al. (158), soy protein concentrate minimizes the cooking/frying loss and shrinkage and enhances foaming stability in chicken sausages.

Various trials have evaluated plant protein concentrates in food applications to reduce the oil ratio and improve the end product's industrial attributes. Plant-based protein hydrolysates have been given significant attention, particularly for enhancing the water-holding ability of meat products (161), which plays a critical role in defining their juiciness, an expression that also refers to the flavor, texture, and color required throughout technological operations (162). In this regard, Carvalho et al. (163) stated that soy protein concentrate employed in beef burger formulation significantly improved the patties' water-holding capacity. Additionally, Hidayat et al. (162) found that this capacity ranged from 86 to 89% in beef sausage and was enhanced by replacing beef with texturized vegetable protein (0–40%). This might be attributed to the existence of more water-soluble components than in animal proteins. According to Karami and Akbariadergani (164), canola protein hydrolysates improved the cooking yield by raising the water-retaining capability of the meat product.

Consumers and the food industry are concerned about lipid oxidation, creating unwanted off-flavors, odors, and possibly serious reaction products (165). Suppressing lipid peroxidation in foodstuffs is critical to prevent food deterioration and protect consumers against hazardous diseases. In this regard, antioxidants are utilized to keep food safe by preventing discoloration and the decay caused by oxidation (166, 167). Despite the extensive use of synthetic antioxidants in food production, the consumers' concern around food safety prompted the food industry to seek natural alternatives (168, 169). Antioxidant proteins and peptides can replace artificial antioxidants since they have an equivalent or higher ability to suppress lipid oxidation (170). Carnosine (β-alanyl-L-histidine) and glutathione (γ-Glu-Cys-Gly) are natural antioxidants in muscle tissue. It has been discovered that they can scavenge hydroxyl radicals, quench singlet oxygen, and restrain lipid oxidation (171). The peptide Pro—Ala—Gly—Tyr separated from Amur sturgeon skin gelatin has scavenging abilities against DPPH, ABTS, and hydroxyl radicals, according to Nikoo et al. (172). The peptide reduced lipid oxidation in minced fish at a concentration of 25 ppm, but it was ineffective at greater concentrations. According to Shahidi et al. (173), incorporation of capelin protein hydrolysate at 0.5–3.0% in a beef model decreased the generation of TBARS by 17.7–60.4%. Over 14 days of storage at 4°C, Kittiphattanabawon et al. (174) assessed lipid peroxidation in treated pork containing gelatin hydrolysate of 40% DH, at concentrations of 100, 500, and 1,000 ppm, and BHA (100 ppm). In both the carotene linoleate and treated pork model systems, they found that gelatin hydrolysate at 500 and 1,000 ppm inhibited lipid peroxidation. Bougatef et al. (175) isolated and purified antioxidant peptides from *Sardinella aurita* proteins by enzymatic hydrolysis. These peptides were found to have a high antioxidant potential in meat-based products. Furthermore, the antioxidant activity of peptides isolated from the mushroom *Ganoderma lucidum* was discovered to reduce lipid oxidation without altering the

products' consumer desirability qualities. The antioxidant activity of *G. lucidum* was attributed to the polysaccharide–peptide complex, polysaccharides, and phenolics. Nevertheless, the study found that *G. lucidum* peptide (GLP) is the main antioxidant in *G. lucidum*, which may effectively reduce lipid peroxidation in meat goods by scavenging free radicals, chelating metals, and acting as an antioxidant (176). In a linoleic acid model system, gelatin hydrolysates from cobia (*Rachycentron canadum*) skin delayed lipid oxidation. Cobia gelatin hydrolysate at 8 and 10 mg/mL exhibited a higher inhibitory effect on lipid peroxidation than BHA at 10 mg/L (177). In addition, according to Cai et al. (178), peptides gained from grass carp (*Ctenopharyngodon idella*) skin protein hydrolysate significantly prevented peroxidation in a linoleic acid model system. Sivaraman et al. (179) reported that the squid protein hydrolysate generated by papain has a comparable lipid peroxidation inhibitory capacity as ascorbic acid in the sardine ground meat model system. Similarly, zein hydrolysate has been shown to suppress lipid oxidation, diminish hydrogen peroxide and TBARS generation, and considerably increase the oxidative stability of model oils (180). Furthermore, this hydrolysate shows no adverse effects on emulsion quality and could be used as an effective antioxidant in food emulsion (181). Cuttlefish skin gelatin hydrolysates (0.5 mg/g) prevented turkey sausage lipid peroxidation for up to 10 days at 4°C (182).

Proteins derived from dairy sources are, likewise, high in antioxidant peptides, which could be helpful in the preservation of meat. In this respect, casein calcium peptide (2.0%) combined with beef paste homogenate can suppress around 70% of lipid peroxidation of the homogenate, preventing the formation of odors in meat products and thus, extending their shelf life (183). Additionally, whey protein peptides have also demonstrated their ability to be utilized as functional components in meat goods. Peña-Ramos and Xiong (184) found that adding 2% whey protein hydrolysates to pig meat in cold storage decreased oxidative deterioration and loss during cooking. From the experience of the authors, there are numerous bioactive peptides available. Nevertheless, adaptability with different foods, gastrointestinal stability, bioavailability, and long-term stability must be investigated before application as functional food additives.

Pharmaceutical Applications

The use of bioactive peptides for pharmaceutical applications is as interesting as that for food purposes. In this context, bioactive peptides and their by-products have been applied as antidiabetic, anticancer, and anti-inflammatory agents, to name a few. Anti-diabetic hydrolysates, for example, can be added to sausages to fortify the sausages with anti-diabetic peptides to reduce the probability of developing diabetes (185). The identity of 24, 30, and 38 bioactive peptides were established in each of three infant milk formulas after separating and identifying bioactive peptides in three hypoallergenic formulas. A large number of these peptides has been identified as ACE inhibitors. The presence of sequences with antihypertensive, hypocholesterolemic, immunomodulation, antibacterial, cytotoxicity, antigenic, antioxidant, and antigenic activities was also established (186).

Chou et al. (45) investigated the impact of antioxidant peptides from the chicken liver after enzyme digestion by pepsin and the induction of CAT, GPx, and SOD in D-galactose-induced rats. Comparing the control and the D-galactose-induced groups of rats, the doses of chicken liver hydrolysate administered (0.25 and 0.5 g/kg) resulted in equal or enhanced antioxidant capacity in the liver, heart, kidney, and brain. The researchers discovered that dosages of 0.25 and 0.5 g/kg inhibited the same rate of lipid oxidation in serum and liver as in the control group. Similar findings were also observed by other scientists in terms of the antioxidant potential (*in vivo*) of loach meat hydrolysates (187), chicken breast hydrolysates (32), rice proteins (188), and tilapia collagen (189). Fazhi et al. (68) reported that three peptides (tri-, tetra-, and hexapeptide) were isolated from fermented sesame meal. They found that MDA buildup in serum and liver was decreased by supplementation with any peptide at 0.1, 0.2, or 0.4 g/kg. In addition, all treated mice had higher levels of SOD and GPx.

Numerous bioactive peptides from food have been shown to possess cytomodulatory properties. In particular, peptides recovered from waste whey of mozzarella cheese exhibited an antiproliferative action when evaluated in a human colorectal cancer cell line (190). Similarly, cytomodulatory peptides decreased the growth of cancer cells while also increasing the activity of immune and neonatal intestinal cells (191). The cytotoxic effects of several black cumin extracts as an additional remedy to doxorubicin treatment in human MCF-7 breast cancer cells were also investigated in terms of their anticancer activity. The LC50 of black cumin lipid extract was 2.720 0.2 mg/mL, indicating cytotoxicity. The cytotoxicity of the aqueous extract was evident when the level was as high as 50 mg/mL (192). Furthermore, Saisavoey et al. (193) studied rice bran protein hydrolysate antioxidant and anti-inflammatory properties on the RAW264.7 macrophage cell line, where LPS and rmIFN-g were found to co-stimulate the target protein's inhibitory effect against nitric oxide production. In addition, casein has been discovered to be an abundant source of active opioid peptides. Different casein fragments are hydrolyzed by distinct digestive enzymes, resulting in the formation of peptides with opioid activity (194). These opioid casein fractions were solely discovered in the plasma of newborns, which was surprising. In both animal and human trials, a marketable, valuable 1-casein-derived peptide frequently utilized in confections and soft beverages were shown to have anxiolytic-like stress-relieving characteristics (194).

Plant-based proteins have proven to be a precious source of innovative and effective antihypertensive peptides (113). In this respect, four angiotensin-converting enzyme inhibitory peptides (Val- Trp, Val-Trp-Ile-Ser, Ile-Tyr, and Arg-Ile-Tyr) were identified from rapeseed proteins digested with subtilisin. When orally administered, these peptides were reported to reduce blood pressure in hypertensive rats, with the most significant effect occurring between 2 and 4 h from administration (195). Incorporating these and other antihypertensive peptides into pharmaceutical medicines and functional diets may effectively prevent and treat hypertension. In mammals, antihypertensive peptides also aid in regulating salt balance and fluids (196). Milk-based bioactive peptides might be used to reduce the risk

of metabolic syndrome by modulating blood pressure, food consumption, and free radical absorption (197).

Cosmeceutical Applications

Since a scientific demonstration of the stated bioactivity of novel cosmeceutical substances is frequently required, research in the cosmeceutical sector, which combines cosmetics and pharmaceuticals, is continuously growing. Indeed, one feature that distinguishes cosmeceuticals from traditional cosmetics is the discovery and characterization of active substances and the demonstration of their efficacy in the stated activity (198). Peptides are an important collection of bioactive cosmeceutical components that, due to their unique qualities, suit the majority of the cosmeceutical industry's needs when creating new compositions. In this respect, in addition to bioactivity, two other features of peptides as cosmeceutical components have lately been considered: bioavailability and stability. Moreover, peptides are recognized as valuable cosmetic materials, as they are light and air-stable, present low toxicity, show a powerful affinity for water, and possess moisturizing capabilities (199, 200). Peptides are frequently employed as ingredients in functional cosmetics to treat skin conditions, promoting collagen synthesis and antioxidant, anti-inflammatory, anti-wrinkle, whitening, and wound healing properties (201, 202). Developing new natural peptides and more stable and effective synthetic peptides has sparked renewed interest in peptide-based skincare products (203). Peptides are used as anti-aging skincare due to their ability to synthesize extracellular matrix (ECM) tissue, the disruption of which is key to skin aging (204). Signal, carrier, neurotransmitter inhibitor, and enzyme inhibitor peptides can be categorized as topical cosmeceuticals. Larger molecules can penetrate the skin barrier, particularly in dry and aged skin (205). Synthetic peptides are made up of amino acid chains that may be altered for various purposes, including improved skin penetration, particular receptor binding, stability, and solubility. Finkley and co-authors (206) reported that the facial creams containing GHK-Cu (copper tripeptide 1) applied for 12 weeks on 71 volunteers aged 50–59 resulted in a visible reduction of the signs of aging. In a separate investigation, the same authors tested the formulation on the eyes of 41 pairs of volunteers under comparable experimental conditions, where a cream with vitamin K was used as a control. The cream with GHK-Cu was found to enhance the suppleness and tightness of the skin in both experiments and lessened the appearance of both fine lines and deep wrinkles. Lintner and Peschard (207) found a significant variation in skin permeability amongst palmitoylated and non-palmitoylated peptides. The anti-wrinkle and wound-healing effects of the peptides pal-GHK and pal-AH were examined. The transcutaneous flow was disclosed using standard Franz diffusion cells, which showed increased interpenetration in the case of the palmitoylated analog. The collagen-derived pentapeptide KTTKS is another key peptide active component in cosmeceutical formulations (208). In a fascinating clinical investigation, its palmitoylated analog (pal-KTTKS) was tested and compared to the KTTKS peptide regarding stability and permeability. It was discovered that pal-KTTKS could penetrate all three layers of the skin

(stratum corneum, epidermis, and dermis), while unmodified KTTKS was not found in any of them (209). According to previous research, collagen may liberate bioactive peptides with various physiological activities after enzymatic digestion. Collagen peptides/hydrolysates have been found to help improve skin problems (210, 211). Kang et al. (212) employed hairless mice that had been exposed to UV radiation, which were administered 1,000 mg/kg collagen peptide for 9 weeks. Collagen peptides were found to upregulate the expression of hyaluronic acid synthase mRNA and the skin moisturizing factor filaggrin, boost hyaluronic acid concentration in skin tissue, and down-regulate the expression of hyaluronidase (HYAL-1 and HYAL-2) mRNA. Likewise, collagen peptide consumption may prevent skin moisture loss caused by ultraviolet (UVB) light (213). Overall, collagen and synthetic peptides have been widely used to develop anti-aging products and nutraceuticals.

Wound Healing Applications

Human skin wounds continue to be a substantial and growing public health and economic issue (214). The skin is the largest organ of the human body and serves as a physical barrier between the internal and external environments. Undoubtedly, skin wounds occur frequently in unfortunate accidents. When the skin defenses against hazardous stimuli are compromised, adverse outcomes such as infection, shock, and even death can occur (215, 216). The wound healing process can be slowed down in specific diseases (e.g., diabetes and infection), usually causing chronic wounds (217). Traditional wound healing medications, such as growth factors, cytokines, chemical compounds extracted or produced from plants, and other immunomodulatory agents, have proven to be especially challenging to translate into clinic treatments for chronic wound healing (218).

Bioactive peptides with high activity, specificity, and stability have sparked substantial interest in the associated field of study (219) compared with expensive pharmaceuticals and low activity, safety, and delivery issues. In this regard, in diabetic-ob/ob rats (mutant obese rats employed as animal models of type II diabetes), Carretero et al. (220) found that *in vivo* adenoviral delivery of LL-37 antimicrobial peptides to excisional wounds increased re-epithelialization and granulation tissue formation. Ramos et al. (221) also verified this, finding that LL-37 and PLL-37 (LL-37 derivative containing an N-terminal proline) improve re-epithelialization and angiogenesis in skin lesions with poor wound healing *in vitro* and *in vivo*. Song et al. (222) used electrospun silk fibroin nanofiber membranes to immobilize an LL-37 derivative, Cys-KR12. Cys-KR12 was chosen for its antibacterial and anti-biofilm properties vs. four different bacterial strains (*S. aureus, S. epidermidis, E. coli*, and *P. aeruginosa*) and contained residues 18–29 of the LL-37 sequence. The peptide-modified membranes were discovered to stimulate the proliferation of keratinocytes, fibroblasts, and monocytes, all of which are key to wound healing.

Moreover, collagen peptides serve as fake collagen breakdown peptides in the skin, causing fibroblast cells to create novel collagen fibers in response to a false signal. Collagen peptides also have chemotactic qualities, encouraging cell migration and proliferation, essential to wound healing (223). Recently,

marine organisms like fish, fish waste, starfish, sponges, and jellyfish have been investigated as reliable sources of collagen (224). Cheng et al. (225) lately discovered that collagen sponges generated from *Rhopilema esculentum* show potential hemostatic properties, implying that they could be a viable choice for wound treatment. Other biomaterials acquired from marine collagen, such as collagen gels, films, and membranes, have also shown practical applications in wound treatment (226).

Feed Applications

Enhancing feed utilization efficiency for milk, meat, and egg production is an important goal for animal agriculture. A proper nutrition strategy is required to digest and absorb dietary nutrients in the small intestine. Recently, peptides in animal feeding have received considerable attention (227, 228). Before feeding, chemical, enzymatic, or microbiological procedures are utilized to routinely generate peptides from animal and plant proteins to increase the nutritional quality and decrease any associated anti-nutritional effects (229). After consumption, the proteins in the feed are digested in the small intestine by enzymes and oligopeptidases into small peptides (di- and tri-peptides) and free amino acids (230). Nonetheless, depending on the physiological state of the animals and the composition of their meals, the types of peptides produced might vary substantially. To produce peptides for animal nutrition, only animal by-products, brewer by-products, and plant materials with anti-nutritional elements are hydrolyzed (231). Different peptide compounds have been added to the meals of calves (232), poultry (233), fish (234), and companion animals (235) to enhance their nutrition, gut function, and capacity to combat infectious diseases. According to Kim (236), fermented soybean meal (4.9%) might substitute 3.7% of spray-dried plasma protein in the diet of 3- to 7-week-old pigs given a corn and soybean meal-based diet with no effect on growth performance or feed efficiency. Comparable outcomes were gained for the Atlantic salmon fed a diet including 40% of protein from fermented soy white flakes (233). In the diet of juvenile red sea bream, 50% of the fish meal could be substituted with the equivalent quantity of soybean protein hydrolysate (234). As the fish meal is becoming limited worldwide, adding plant-based protein hydrolysate in diets is critical in aquaculture. Moreover, the hydrolysate of soy protein concentrate (19.7% in diet) can be employed to maintain a sturdy growth in calves as an alternative for expensive skim milk powder (230). In another study, El-Ayek et al. (237) found that black cumin cake can cost-effectively substitute 50% of the protein in forage formulations. El-Deek et al. (238) reported comparable results, confirming that up to 50% black seed cake protein may be used in broiler chick feed with no adverse effects on growth, meat quality, feed consumption, conversion rate, or safety.

Safety of Bioactive Peptides

Bioactive peptide safety is a significant perspective for clinical studies and food applications. The physiological impact of bioactive peptide consumption (from food and hydrolysate/concentrated forms) is thought to be harmless.

Nevertheless, because most toxicological investigations are conducted *in vitro* and in animals, the level of proof supporting the safety of bioactive intake must be increased. To date, just a few investigations on the potential toxicological impact on humans have been undertaken. In this context, according to an *in vitro* work conducted by Doorten et al. (239), daily ingestion of a hydrolysate derived from cow milk (2 g/kg body weight) was not likely to generate mutagenic or clastogenic effects. The scholars found a No Observed Adverse Effect Level (NOAEL) of 40 g/kg body weight/day, 140 times greater than the recommended daily intake. Moreover, Anadón et al. (240) found that acute (2,000 mg/kg) and daily (1,000 mg/kg for 4 weeks) ingestion of casein hydrolysate (rich in antihypertensive peptides) neither had any histological impact nor caused mortality in mice. Overall, peptides are more reactive than natural proteins due to their lower molecular weight and are made up of smaller chains of amino acids. As a result, it is critical to ensure their safety, which includes the absence of toxicity, cytotoxicity, and allergenicity (6). Strict and precise legislation is essential to safeguard consumers from potentially hazardous or deceptive products.

Peptide Therapeutics Market

Therapeutic peptides and proteins have risen as potential drug candidates for several decades. The peptide therapeutics market is moderately competitive and consists of several major parties. Some companies, which are currently overlooking the market, are Eli Lilly and Company, Pfizer, Inc., Amgen, Inc., Bristol-Myers Squibb Company, EVER NEURO PHARMA GMBH, Takeda Pharmaceutical Company Limited, Davisco Foods International, Tokiwa Yakuhin Co., Ltd., Reliv, Inc., Valio Ltd., and many others. The major partakers are involved in strategic alliances, such as acquisitions and collaborations, along with research activities for the global expansion of the product portfolio. For example, in June 2019, Eli Lilly and Company received the FDA approval for Emgality, a subcutaneously injected calcitonin gene-related peptide (CGRP) antibody, for migraine prevention and treating episodic cluster headache [1].

CONCLUSION AND FUTURE PERSPECTIVES

The advantages and activities of bioactive peptides derived from various sources were addressed in this review. Peptide extraction, purification, and identification were also covered. Bioactive proteins can be utilized to develop functional foods and are likely to be employed as a food additive in fatty products to extend their shelf life by increasing oxidative stability. New bioactive peptides derived from various food sources and their by-products for food, pharmaceutical, cosmetic, wound healing, feed, and safety were also discussed. Even though much is known about the structure and activity of peptides, more research into the link between these two aspects is required. Further

---

[1] https://www.researchandmarkets.com/reports/5265155/peptidetherapeutics-market-growth-trends. Last access: Dec 19, 2021.

investigation is needed on the stability of peptide activity and its regulatory factors, in addition to the extraction of bioactive peptides and qualification of prospective bioactivity. In addition, pre-clinical and clinical studies are needed to determine which levels are beneficial for health, their dose-response relation, bioavailability, pharmacokinetics, and whether they can be consumed with foods.

AUTHOR CONTRIBUTIONS

AZ and AA contributed significantly to analysis and manuscript preparation. AZ supported valuable discussion. JS-G, J-BE, and J-HS revised the whole manuscript. All authors collated papers, wrote the manuscript, read, and approved the final manuscript.

REFERENCES

1. Wang N, Manabe Y, Sugawara T, Paul NA, Zhao J. Identification and biological activities of carotenoids from the freshwater alga *Oedogonium intermedium*. *Food Chem.* (2018) 242:247–55. doi: 10.1016/j.foodchem.2017.09.075

2. Szymanowska U, Baraniak B. Antioxidant and potentially anti-inflammatory activity of anthocyanin fractions from pomace obtained from enzymatically treated raspberries. *Antioxidants.* (2019) 8:299. doi: 10.3390/antiox8080299

3. Dziki D, Gawlik-Dziki U, Biernacka B. *Cistus incanus* L. as an innovative functional. *Foods.* (2019) 8:1–12. doi: 10.3390/foods8080349

4. Zaky AA, Chen Z, Liu Y, Li S, Jia Y. Preparation and assessment of bioactive extracts having antioxidant activity from rice bran protein hydrolysates. *J Food Measur Character.* (2019) 13:2542–8. doi: 10.1007/s11694-019-00174-9

5. Zaky AA, Liu Y, Han P, Chen Z, Jia Y. Effect of pepsin–trypsin in vitro gastro-intestinal digestion on the antioxidant capacities of ultra-filtrated rice bran protein hydrolysates (molecular weight> 10 kDa; 3–10 kDa, and< 3 kDa). *Int J Pept Res Ther.* (2020) 26:1661–7. doi: 10.1007/s10989-019-09977-2

6. Korhonen H, Pihlanto A. Bioactive peptides: production and functionality. *Int Dairy J.* (2006) 16:945–60. doi: 10.1016/j.idairyj.2005.10.012

7. Ulug SK, Jahandideh F, Wu J. Novel technologies for the production of bioactive peptides. *Trends Food Sci Technol.* (2021) 108:27–39. doi: 10.1016/j.tifs.2020.12.002

8. Chakrabarti S, Jahandideh F, Wu J. Food-derived bioactive peptides on inflammation and oxidative stress. *BioMed Res Int.* (2014) 2014:1–11. doi: 10.1155/2014/608979

9. Unal G, Akalin AS. Antioxidant and angiotensin-converting enzyme inhibitory activity of yoghurt fortified with sodium calcium caseinate or whey protein concentrate. *Dairy Sci Technol.* (2012) 92:627–39. doi: 10.1007/s13594-012-0082-5

10. Mohanty D, Jena R, Choudhury PK, Pattnaik R, Mohapatra S, Saini MR. Milk derived antimicrobial bioactive peptides: a review. *Int J Food Prop.* (2016) 19:837–46. doi: 10.1080/10942912.2015.1048356

11. Wakabayashi H, Takase M, Tomita M. Lactoferricin derived from milk protein lactoferrin. *Curr Pharm Des.* (2003) 9:1277–87. doi: 10.2174/1381612033454829

12. Pritchard SR, Phillips M, Kailasapathy K. Identification of bioactive peptides in commercial Cheddar cheese. *Food Res Int.* (2010) 43:1545–8. doi: 10.1016/j.foodres.2010.03.007

13. Meisel H. Biochemical properties of peptides encrypted in bovine milk proteins. *Curr Med Chem.* (2005) 12:1905–19. doi: 10.2174/0929867054546618

14. Contreras MDM, Carrón R, Montero MJ, Ramos M, Recio I. Novel casein-derived peptides with antihypertensive activity. *Int Dairy J.* (2009) 19:566–73. doi: 10.1016/j.idairyj.2009.05.004

15. Choi J, Sabikhi L, Hassan A, Anand S. Bioactive peptides in dairy products. *Int J Dairy Technol.* (2012) 65:1–12. doi: 10.1111/j.1471-0307.2011.00725.x

16. FitzGerald RJ, Murray BA, Walsh DJ. Hypotensive peptides from milk proteins. *J Nutr.* (2004) 134:980S–8S. doi: 10.1093/jn/134.4.980S

17. Tuomilehto J, Lindström J, Hyyrynen J, Korpela R, Karhunen ML, Mikkola L, et al. Effect of ingesting sour milk fermented using Lactobacillus helveticus bacteria producing tripeptides on blood pressure in subjects with mild hypertension. *J Hum Hypertens.* (2004) 18:795–802. doi: 10.1038/sj.jhh.1001745

18. Haque E, Chand R, Kapila S. Biofunctional properties of bioactive peptides of milk origin. *Food Rev Int.* (2008) 25:28–43. doi: 10.1080/87559120802458198

19. López-Expósito I, Gómez-Ruiz JÁ, Amigo L, Recio I. Identification of antibacterial peptides from ovine αs2-casein. *Int Dairy J.* (2006) 16:1072–80. doi: 10.1016/j.idairyj.2005.10.006

20. Manso MA, López-Fandiño R. Angiotensin I converting enzyme–inhibitory activity of bovine, ovine, and caprine κ-casein macropeptides and their tryptic hydrolysates. *J Food Protect.* (2003) 66:1686–92. doi: 10.4315/0362-028X-66.9.1686

21. Fitzgerald RJ, Murray BA. Bioactive peptides and lactic fermentations. *Int J Dairy Technol.* (2006) 59:118–25. doi: 10.1111/j.1471-0307.2006.00250.x

22. Murakami M, Tonouchi H, Takahashi R, Kitazawa H, Kawai Y, Negishi H, et al. Structural analysis of a new anti-hypertensive peptide (β-lactosin B) isolated from a commercial whey product. *J Dairy Sci.* (2004) 87:1967–74. doi: 10.3168/jds.S0022-0302(04)70013-2

23. Hartmann R, Meisel H. Food-derived peptides with biological activity: from research to food applications. *Curr Opin Biotechnol.* (2007) 18:163–9. doi: 10.1016/j.copbio.2007.01.013

24. Bhandari D, Rafiq S, Gat Y, Gat P, Waghmare R, Kumar V. A review on bioactive peptides: physiological functions, bioavailability and safety. *Int J Pept Res Ther.* (2020) 26:139–50. doi: 10.1007/s10989-019-09823-5

25. Silva SV, Malcata FX. Caseins as source of bioactive peptides. *Int Dairy J.* (2005) 15:1–15. doi: 10.1016/j.idairyj.2004.04.009

26. Tidona F, Criscione A, Guastella AM, Zuccaro A, Bordonaro S, Marletta D. Bioactive peptides in dairy products. *Ital J Anim Sci.* (2009) 8:315–40. doi: 10.4081/ijas.2009.315

27. Wang LS, Huang JC, Chen YL, Huang M, Zhou GH. Identification and characterization of antioxidant peptides from enzymatic hydrolysates of duck meat. *J Agric Food Chem.* (2015) 63:3437–44. doi: 10.1021/jf506120w

28. Jang A, Jo C, Kang K-S, Lee M. Antimicrobial and human cancer cell cytotoxic effect of synthetic angiotensin-converting enzyme (ACE) inhibitory peptides. *Food Chem.* (2008) 107:327–36. doi: 10.1016/j.foodchem.2007.08.036

29. Lafarga T, Hayes M. Bioactive peptides from meat muscle and by-products: generation, functionality and application as functional ingredients. *Meat Sci.* (2014) 98:227–39. doi: 10.1016/j.meatsci.2014.05.036

30. Kim E-K, Lee S-J, Jeon B-T, Moon S-H, Kim B, Park T-K, et al. Purification and characterisation of antioxidative peptides from enzymatic hydrolysates of venison protein. *Food Chem.* (2009) 114:1365–70. doi: 10.1016/j.foodchem.2008.11.035

31. Ohata M, Uchida S, Zhou L, Arihara K. Antioxidant activity of fermented meat sauce and isolation of an associated antioxidant peptide. *Food Chem.* (2016) 194:1034–9. doi: 10.1016/j.foodchem.2015.08.089

32. Sun Y, Pan D, Guo Y, Li J. Purification of chicken breast protein hydrolysate and analysis of its antioxidant activity. *Food Chem Toxicol.* (2012) 50:3397–404. doi: 10.1016/j.fct.2012.07.047

33. Lee SJ, Kim YS, Hwang JW, Kim EK, Moon SH, Jeon BT, Park PJ. Purification and characterization of a novel antioxidative peptide from duck skin by-products that protects liver against oxidative damage. *Food Res Int.* (2012) 49:285–95. doi: 10.1016/j.foodres.2012.08.017

34. Di Bernardini R, Mullen AM, Bolton D, Kerry J, O'Neill E, Hayes M. Assessment of the angiotensin-I-converting enzyme (ACE-I) inhibitory and antioxidant activities of hydrolysates of bovine brisket sarcoplasmic proteins produced by papain and characterisation of associated bioactive peptidic fractions. *Meat Sci.* (2012) 90:226–35. doi: 10.1016/j.meatsci.2011.07.008

35. Adje EY, Balti R, Guillochon D, Nedjar-Arroume N. α 67-106 of bovine hemoglobin: a new family of antimicrobial and angiotensin I-converting enzyme inhibitory peptides. *Eur Food Res Technol.* (2011) 232:637–46. doi: 10.1007/s00217-011-1430-z

36. Banerjee P, Shanthi C. Isolation of novel bioactive regions frombovine *Achilles tendon* collagen having angiotensin I-converting enzyme-inhibitory properties. *Process Biochem.* (2012) 47:2335–46. doi: 10.1016/j.procbio.2012.09.012

37. Nedjar-Arroume N, Dubois-Delval V, Miloudi K, Daoud R, Krier F, Kouach M, et al. (2006). Isolation and characterization of four antibacterial peptides from bovine hemoglobin. *Peptides* 27, 2082–2089. doi: 10.1016/j.peptides.2006.03.033

38. Liu R, Wang M, Duan JA, Guo JM, Tang YP. Purification and identification of three novel antioxidant peptides from Cornu Bubali (water buffalo horn). *Peptides.* (2010) 31:786–93. doi: 10.1016/j.peptides.2010.02.016

39. Liu R, Xing L, Fu Q, Zhou GH, Zhang WG. A review of antioxidant peptides derived from meat muscle and by-products. *Antioxidants.* (2016) 5:32. doi: 10.3390/antiox5030032

40. Ohmori T, Nakagami T, Tanaka H, Maruyama S. Isolation of prolylendopeptidase-inhibiting peptides from bovine brain. *Biochem Biophys Res Commun.* (1994) 202:809–15. doi: 10.1006/bbrc.1994.2002

41. Lorenzo JM, Munekata PE, Gómez B, Barba FJ, Mora L, Pérez-Santaescolástica C, et al. Bioactive peptides as natural antioxidants in food products–a review. *Trends Food Sci Technol.* (2018) 79:136–47. doi: 10.1016/j.tifs.2018.07.003

42. Liu B, Aisa HA, Yili A. Isolation and identification of two potential antioxidant peptides from sheep abomasum protein hydrolysates. *Eur Food Res Technol.* (2018) 244:1615–25. doi: 10.1007/s00217-018-3074-8

43. Di Bernardini R, Rai DK, Bolton D, Kerry J, O'Neill E, Mullen AM, et al. Isolation, purification and characterization of antioxidant peptidic fractions from a bovine liver sarcoplasmic protein thermolysin hydrolyzate. *Peptides.* (2011) 32:388–400. doi: 10.1016/j.peptides.2010.11.024

44. Gallego M, Mora L, Hayes M, Reig M, Toldrá F. Effect of cooking and in vitro digestion on the antioxidant activity of dry-cured ham by-products. *Food Res Int.* (2017) 97:296–306. doi: 10.1016/j.foodres.2017.04.027

45. Chou C-H, Wang S-Y, Lin Y-T, Chen Y-C. Antioxidant activities of chicken liver hydrolysates by pepsin treatment. *Int J Food Sci Technol.* (2014) 49:1654–62. doi: 10.1111/ijfs.12471

46. Zhang Y, Kouguchi T, Shimizu K, Sato M, Takahata Y, Morimatsu F. Chicken collagen hydrolysate reduces proinflammatory cytokine production in C57BL/6.KOR-ApoEshl Mice. *J Nutr Sci Vitaminol.* (2010) 56:208–10. doi: 10.3177/jnsv.56.208

47. Singh BP, Vij S, Hati S. Functional significance of bioactive peptides derived from soybean. *Peptides.* (2014) 54:171–9. doi: 10.1016/j.peptides.2014.01.022

48. Malaguti M, Dinelli G, Leoncini E, Bregola V, Bosi S, Cicero AF, et al. Bioactive peptides in cereals and legumes: agronomical, biochemical and clinical aspects. *Int J Mol Sci.* (2014) 15:21120–35. doi: 10.3390/ijms151121120

49. Zhang M, Mu TH. Identification and characterization of antioxidant peptides from sweet potato protein hydrolysates by alcalase under high hydrostatic pressure. *Innov Food Sci Emerg Technol.* (2017) 43:92–101. doi: 10.1016/j.ifset.2017.08.001

50. Tang N, Zhuang H. Evaluation of antioxidant activities of zein protein fractions. *J Food Sci.* (2014) 79:2174–84. doi: 10.1111/1750-3841.12686

51. Montoya-Rodríguez A, de Mejía EG, Dia VP, Reyes-Moreno C, Milán-Carrillo J. Extrusion improved the anti-inflammatory effect of amaranth (*Amaranthus hypochondriacus*) hydrolysates in LPS-induced human THP-1 macrophage-like and mouse RAW 264.7 macrophages by preventing activation of NF-κ B signaling. *Mol Nutr Food Res.* (2014) 58:1028–41. doi: 10.1002/mnfr.201300764

52. Manfredini PG, Cavanhi VAF, Costa JAV, Colla LM. Bioactive peptides and proteases: characteristics, applications and the simultaneous production in solid-state fermentation. *Biocatal Biotransform.* (2021) 39:360–77. doi: 10.1080/10242422.2020.1849151

53. Magro AEA, Silva LC, Rasera GB, de Castro RJS. Solid-state fermentation as an efficient strategy for the biotransformation of lentils: enhancing their antioxidant and antidiabetic potentials. *Bioresour Bioproces.* (2019) 6:1–9. doi: 10.1186/s40643-019-0273-5

54. Zhu L, Chen J, Tang X, Xiong YL. Reducing, radical scavenging, and chelation properties of in vitro digests of alcalase-treated zein hydrolysate. *J Agric Food Chem.* (2008) 56:2714–21. doi: 10.1021/jf703697e

55. Rizzello CG, Lorusso A, Russo V, Pinto D, Marzani B, Gobbetti M. Improving the antioxidant properties of quinoa flour through fermentation with selected autochthonous lactic acid bacteria. *Int J Food Microbiol.* (2017) 241:252–61. doi: 10.1016/j.ijfoodmicro.2016.10.035

56. Garza NG, Koyoc JA, Castillo JA, Zambrano EA, Ancona D, Guerrero L, et al. Biofunctional properties of bioactive peptide fractions from protein isolates of moringa seed (*Moringa oleifera*). *J Food Sci Technol.* (2017) 54:4268–76. doi: 10.1007/s13197-017-2898-8

57. González-García E, Marina ML, García MC. Plum (*Prunus domestica* L.) by-product as a new and cheap source of bioactive peptides: extraction method and peptides characterization. *J Funct Foods.* (2014) 11:428–37. doi: 10.1016/j.jff.2014.10.020

58. Zaky AA, Liu Y, Han P, Ma A, Jia Y. Effect of flavorzyme digestion on the antioxidant capacities of ultra-filtrated rice bran protein hydrolyzates. *J Food Proces Preserv.* (2020) 44:e14551. doi: 10.1111/jfpp.14551

59. Yu M, He S, Tang M, Zhang Z, Zhu Y, Sun H. Antioxidant activity and sensory characteristics of Maillard reaction products derived from different peptide fractions of soybean meal hydrolysate. *Food Chem.* (2018) 243:249–57. doi: 10.1016/j.foodchem.2017.09.139

60. Freitas CS, Vericimo MA, da Silva ML, da Costa GCV, Pereira PR, Paschoalin VMF, et al. Encrypted antimicrobial and antitumoral peptides recoveredfrom a protein-rich soybean (Glycine max) by-product. *J Funct Foods.* (2019) 54:187–98. doi: 10.1016/j.jff.2019.01.024

61. Zarei M, Forghani B, Ebrahimpour A, Abdul-hamid A. *In vitro* and *in vivo* antihypertensive activity of palm kernel cake protein hydrolysates: sequencing and characterization of potent bioactive peptides. *Indus Crops Prod.* (2015) 76:112–20. doi: 10.1016/j.indcrop.2015.06.040

62. Zou Z, Wang M, Wang Z, Aluko RE, He R. Antihypertensive and antioxidant activities of enzymatic wheat bran protein hydrolysates. *J Food Biochem.* (2020) 44:1–13. doi: 10.1111/jfbc.13090

63. Kadam D, Lele SS. Value addition of oilseed meal: a focus on bioactive peptides. *J Food Measur Character.* (2018) 12:449–58. doi: 10.1007/s11694-017-9658-3

64. Wen C, Zhang J, Zhang H, Duan Y, Ma H. Effects of divergent ultrasound pretreatment on the structure of watermelon seed protein and the antioxidant activity of its hydrolysates. *Food Chem.* (2019) 299:125165. doi: 10.1016/j.foodchem.2019.125165

65. Moayedi A, Mora L, Aristoy MC, Hashemi M, Safari M, Toldrá F. ACEinhibitory and antioxidant activities of peptide fragments obtained from tomato processing by-products fermented using Bacillus subtilis: effect of amino acid composition and peptides molecular mass distribution. *Appl Biochem Biotechnol.* (2017) 181:48–64. doi: 10.1007/s12010-016-2198-1

66. Sun H, Yao X, Wang X, Wu Y, Liu Y, Tang J, et al. Chemical composition and in vitro antioxidant property of peptides produced from cottonseed meal by solid-state fermentation. *CYTA J Food.* (2015) 13:264–72. doi: 10.1080/19476337.2014.948042

67. Li XX, Han LJ, Chen LJ. In vitro antioxidant activity of protein hydrolysates prepared from corn gluten meal. *J Sci Food Agric.* (2008) 88:1660–6. doi: 10.1002/jsfa.3264

68. Fazhi X, Huihui P, Yang L, Lumu L, Kun Q, Xioling D. Separation and purification of small peptides from fermented sesame meal and their antioxidant activities. *Protein Pept Lett.* (2014) 21:966–74. doi: 10.2174/0929866521666140411113021

69. Hai-Lun HE, Xiu-Lan C, Cai-Yun S, Yu-Zhong Z, Bai-Cheng Z. Analysis of novel angiotensin-I-converting enzyme inhibitory peptides from protease-hydrolyzed marine shrimp *Acetes chinensis*. *J Peptide Sci.* (2006) 12:726–33. doi: 10.1002/psc.789

70. Kim SK, Ngo DH, Vo TS. Marine fish-derived bioactive peptides as potential antihypertensive agents. *Adv Food Nutr Res.* (2012) 65:249–60. doi: 10.1016/B978-0-12-416003-3.00016-0

71. Zhao Y, Li B, Dong S, Liu Z, Zhao X, Wang J, et al. A novel ACE inhibitory peptide isolated from *Acaudina molpadioidea* hydrolysate. *Peptides.* (2009) 30:1028–33. doi: 10.1016/j.peptides.2009.03.002

72. Ranathunga S, Rajapakse N, Kim SK. Purification and characterization of antioxidantive peptide derived from muscle of conger eel (*Conger myriaster*). *Eur Food Res Technol.* (2006) 222:310–5. doi: 10.1007/s00217-005-0079-x

73. Suetsuna K, Ukeda H. Isolation of an octapeptide which possesses active oxygen scavenging activity from peptic digest of sardine muscle. *Nipp Suis Gakk.* (1999) 65:1096–9. doi: 10.2331/suisan.65.1096

74. Wu HC, Chen HM, Shiau CY. Free amino acids and peptides as related to antioxidant properties in protein hydrolysates of mackerel (*Scomber austriasicus*). *Food Res Int.* (2003) 36:949–57. doi: 10.1016/S0963-9969(03)00104-2

75. Guo H, Kouzuma Y, Yonekura M. Structures and properties of antioxidative peptides derived from royal jelly protein. *Food Chem.* (2009) 113:238–45. doi: 10.1016/j.foodchem.2008.06.081

76. Hori K, Sato Y, Ito K, Fujiwara Y, Iwamoto Y, Makino H, et al. Strict specificity for high-mannose type N-glycans and primary structure of a red alga *Eucheuma serra* lectin. *Glycobiology.* (2007) 17:479–91. doi: 10.1093/glycob/cwm007

77. Odaka C, Sanders ML, Crews P. Jasplakinolide induces apoptosis in various transformed cell lines by a caspase-3-like protease-dependent pathway. *Clin Diagn Lab Immunol.* (2000) 7:947–52. doi: 10.1128/CDLI.7.6.947-952.2000

78. Freitas VM, Rangel M, Bisson LF, Jaeger RG, Machado-Santelli GM. The geodiamolide H, derived from brazilian sponge *Geodia corticostylifera*, regulates actin cytoskeleton, migration and invasion of breast cancer cells cultured in three-dimensional environment. *J Cell Physiol.* (2008) 216:583–94. doi: 10.1002/jcp.21432

79. Chen J, Ryu B, Zhang Y, Liang P, Li C, Zhou C, et al. Comparison of an angiotensin-I-converting enzyme inhibitory peptide from tilapia (*Oreochromis niloticus*) with captopril: inhibition kinetics, in vivo effect, simulated gastrointestinal digestion and a molecular docking study. *J Sci Food Agri.* (2020) 100:315–24. doi: 10.1002/jsfa.10041

80. Ngo DH, Vo TS, Ryu B, Kim SK. Angiotensin-I-converting enzyme (ACE) inhibitory peptides from Pacific cod skin gelatin using ultrafiltration membranes. *Process Biochem.* (2016) 51:1622–8. doi: 10.1016/j.procbio.2016.07.006

81. Je JY, Qian ZJ, Byun HG, Kim SK. Purification and characterization of an antioxidant peptide obtained from tuna backbone protein by enzymatic hydrolysis. *Process Biochem.* (2007) 42:840–6. doi: 10.1016/j.procbio.2007.02.006

82. Mendis E, Rajapakse N, Kim SK. Antioxidant properties of a radical-scavenging peptide purified from enzymatically prepared fish skin gelatin hydrolysate. *J Agric Food Chem.* (2005) 53:581–7. doi: 10.1021/jf048877v

83. Wang Y, Zhu F, Han F, Wang H. Purification and characterization of antioxidative peptides from salmon protamine hydrolysate. *J Food Biochem.* (2008) 32:654–71. doi: 10.1111/j.1745-4514.2008.00190.x

84. Sila A, Bougatef A. Antioxidant peptides from marine by-products: isolation, identification and application in food systems. A review. *J Funct Foods.* (2016) 21:10–26. doi: 10.1016/j.jff.2015.11.007

85. Oh JY, Kim EA, Lee H, Kim HS, Lee JS, Jeon YJ. Antihypertensive effect of surimi prepared from olive flounder (*Paralichthys olivaceus*) by angiotensin-I converting enzyme (ACE) inhibitory activity and characterization of ACE inhibitory peptides. *Process Biochem.* (2019) 80:164–70. doi: 10.1016/j.procbio.2019.01.016

86. Chi CF, Wang, B.,Wang YM, Zhang B, Deng SG. Isolation and characterization of three antioxidant peptides from protein hydrolysate of bluefin leatherjacket (*Navodon septentrionalis*) heads. *J Funct Foods.* (2015) 12:1–10. doi: 10.1016/j.jff.2014.10.027

87. Udenigwe CC, Aluko RE. Food protein-derived bioactive peptides: Production, processing, and potential health benefits. *J Food Sci.* (2012) 77:R11–24. doi: 10.1111/j.1750-3841.2011.02455.x

88. Bamdad F, Shin SH, Suh JW, Nimalaratne C, Sunwoo H. Anti-inflammatory and antioxidant properties of casein hydrolysate produced using high hydrostatic pressure combined with proteolytic enzymes. *Molecules.* (2017) 22:609. doi: 10.3390/molecules22040609

89. Hamada JS. Characterization of protein fractions of rice bran to devise effective methods of protein solubilization. *Cereal Chem.* (1997) 74:662–8. doi: 10.1094/CCHEM.1997.74.5.662

90. Phongthai S, Homthawornchoo W, Rawdkuen S. Preparation, properties and application of rice bran protein: a review. *Int Food Res J.* (2017) 24:25.

91. Anal AK, Noomhorm A, Vongsawasdi P. Protein hydrolysates and bioactive peptides from seafood and crustacean waste: their extraction, bioactive

properties and industrial perspectives. *Mar Proteins Peptid.* (2013) 36:709–35. doi: 10.1002/9781118375082.ch36

92. Yan QJ, Huang LH, Sun Q, Jiang ZQ, Wu X. Isolation, identification and synthesis of four novel antioxidant peptides from rice residue protein hydrolyzed by multiple proteases. *Food Chem.* (2015) 179:290–5. doi: 10.1016/j.foodchem.2015.01.137

93. Fabian C, Ju YH. A review on rice bran protein: Its properties and extraction methods. *Crit Rev Food Sci Nutr.* (2011) 51:816–27. doi: 10.1080/10408398.2010.482678

94. Wang M, Hettiarachchy NS, Qi M, Burks W, Siebenmorgen T. Preparation and functional properties of rice bran protein isolate. *J Agric Food Chem.* (1999) 47:411–6. doi: 10.1021/jf9806964

95. Amagliani L, O'Regan J, Kelly AL, O'Mahony JA. The composition, extraction, functionality and applications of rice proteins: a review. *Trends Food Sci Technol.* (2017) 64:1–12. doi: 10.1016/j.tifs.2017.01.008

96. Han Z, Cai MJ, Cheng JH, Sun DW. Effects of electric fields and electromagnetic wave on food protein structure and functionality: a review. *Trends Food Sci Technol.* (2018) 75:1–9. doi: 10.1016/j.tifs.2018.02.017

97. Sedaghat Doost A, Nikbakht Nasrabadi M, Wu J, A'Yun Q, Van der Meeren P. Maillard conjugation as an approach to improve whey proteins functionality: a review of conventional and novel preparation techniques. *Trends Food Sci Technol.* (2019) 91:1–11. doi: 10.1016/j.tifs.2019.06.011

98. Urbizo-Reyes U, San Martin-Gonz'alez MF, Garcia-Bravo J, L'opez Malo Vigil A, Liceaga AM. Physicochemical characteristics of chia seed (*Salvia hispanica*) protein hydrolysates produced using ultrasonication followed by microwave-assisted hydrolysis. *Food Hydrocol.* (2019) 97:105187. doi: 10.1016/j.foodhyd.2019.105187

99. Gharibzahedi SMT, Smith B. The functional modification of legume proteins by ultrasonication: a review. *Trends Food Sci Technol.* (2020) 98:107–16. doi: 10.1016/j.tifs.2020.02.002

100. Zhao Z-K, Mu T-H, Zhang M, Richel A. Effect of salts combined with high hydrostatic pressure on structure and gelation properties of sweet potato protein. *Lebensmittel-Wissenschaft und -Technologie.* (2018) 93:36–44. doi: 10.1016/j.lwt.2018.03.007

101. Vanga SK, Wang J, Raghavan V. Effect of ultrasound and microwave processing on the structure, in-vitro digestibility and trypsin inhibitor activity of soymilk proteins. *Lebensmittel-Wissenschaft und -Technologie.* (2020) 131:109708. doi: 10.1016/j.lwt.2020.109708

102. Mesías M, Wagner M, George S, Morales FJ. Impact of conventional sterilization and ohmic heating on the amino acid profile in vegetable baby foods. *Innov Food Sci Emerg Technol.* (2016) 34:24–8. doi: 10.1016/j.ifset.2015.12.031

103. Pereira RN, Teixeira JA, Vicente AA, Cappato LP, da Silva Ferreira MV, da Silva Rocha R, et al. Ohmic heating for the dairy industry: a potential technology to develop probiotic dairy foods in association with modifications of whey protein structure. *Curr Opin Food Sci.* (2018) 22:95–101. doi: 10.1016/j.cofs.2018.01.014

104. Li X, Ye C, Tian Y, Pan S, Wang L. Effect of ohmic heating on fundamental properties of protein in soybean milk. *J Food Process Eng.* (2018) 41:12660. doi: 10.1111/jfpe.12660

105. Sedaghat Doost A, Devlieghere F, Stevens CV, Claeys M, Van der Meeren P. Self-assembly of Tween 80 micelles as nanocargos for oregano and trans-cinnamaldehyde plant-derived compounds. *Food Chem.* (2020) 327:126970. doi: 10.1016/j.foodchem.2020.126970

106. Nasrabadi MN, Doost AS, Mezzenga R. Modification approaches of plant-based proteins to improve their techno-functionality and use in food products. *Food Hydrocoll.* (2021) 106789. doi: 10.1016/j.foodhyd.2021.106789

107. Zhang L, Wang L-J, Jiang W, Qian J-Y. Effect of pulsed electric field on functional and structural properties of canola protein by pretreating seeds to elevate oil yield. *Lebensmittel-Wissenschaft und -Technologie.* (2017) 84:73–81. doi: 10.1016/j.lwt.2017.05.048

108. Liang R, Cheng S, Wang X. Secondary structure changes induced by pulsed electric field affect antioxidant activity of pentapeptides from pine nut (*Pinus koraiensis*) protein. *Food Chem.* (2018) 254:170–84. doi: 10.1016/j.foodchem.2018.01.090

109. Zaky AA, Shim J-H, Abd El-Aty AM. A Review on extraction, characterization, and applications of bioactive peptides from pressed black cumin seed cake. *Front Nutr.* (2021) 8:743909. doi: 10.3389/fnut.2021.743909

110. Agyei D, Ongkudon CM, Wei CY, Chan AS, Danquah MK. Bioprocess challenges to the isolation and purification of bioactive peptides. *Food Bioprod Proces.* (2016) 98:244–56. doi: 10.1016/j.fbp.2016.02.003

111. Ibrahim HR, Isono H, Miyata T. Potential antioxidant bioactive peptides from camel milk proteins. *Anim Nutr.* (2018) 4:273–80. doi: 10.1016/j.aninu.2018.05.004

112. Gorska-Warsewicz H, Laskowski W, Kulykovets O, Kudlińska-Chylak A, Czeczotko M, Rejman K. Food products as sources of protein and amino acids—the case of Poland. *Nutrients.* (2018) 10:21977. doi: 10.3390/nu10121977

113. Toldra F, Reig M, Aristoy MC, Mora L. Generation of bioactive peptides during food processing. *Food Chem.* (2018) 267:395–404. doi: 10.1016/j.foodchem.2017.06.119

114. Esfandi R, Walters ME, Tsopmo A. Antioxidant properties and potential mechanisms of hydrolyzed proteins and peptides from cereals. *Heliyon.* (2019) 5:e01538. doi: 10.1016/j.heliyon.2019.e01538

115. Ajibola CF, Fashakin JB, Fagbemi TN, Aluko RE. Effect of peptide size on antioxidant properties of African yam bean seed (*Sphenostylis stenocarpa*) protein hydrolysate fractions. *Int J Mol Sci.* (2011) 12:6685–702. doi: 10.3390/ijms12106685

116. Sarmadi BH, Ismail A. Antioxidative peptides from food proteins: a review. *Peptides.* (2010) 31:1949–56. doi: 10.1016/j.peptides.2010.06.020

117. Görgüç A, Gençdag E, Yilmaz FM. Bioactive peptides derived from plant origin by-products: biological activities and techno-functional utilizations in food developments–a review. *Food Res Int.* (2020) 136:109504. doi: 10.1016/j.foodres.2020.109504

118. Haney EF, Hancock REW. Peptide design for antimicrobial and immunomodulatory applications. *Biopolymers.* (2013) 100:572–83. doi: 10.1002/bip.22250

119. Yadavalli SS, Carey JN, Leibman RS, Chen AI, Stern AM, Roggiani M, et al. Antimicrobial peptides trigger a division block in *Escherichia coli* through stimulation of a signalling system. *Nat Commun.* (2016) 7:1240. doi: 10.1038/ncomms12340

120. Kamali Alamdari E, Ehsani MR. Antimicrobial peptides derived from milk: a review. *J Food Biosci Technol.* (2017) 7:49–56.

121. Tang W, Zhang H, Wang L, Qian H, Qi X. Targeted separation of antibacterial peptide from protein hydrolysate of anchovy cooking wastewater by equilibrium dialysis. *Food Chem.* (2015) 168:115–23. doi: 10.1016/j.foodchem.2014.07.027

122. Aguilar-Toalá JE, Deering AJ, Liceaga AM. New insights into the antimicrobial properties of hydrolysates and peptide fractions derived from chia seed (*Salvia hispanica* L.). *Probiot Antimicrob Prot.* (2020) 12:1571–81. doi: 10.1007/s12602-020-09653-8

123. Omoni AO, Aluko RE. Effect of cationic flaxseed protein hydrolysate fractions on the *in vitro* structure and activity of calmodulin-dependent endothelial nitric oxide synthase. *Mol Nutr Food Res.* (2006) 50:958–66. doi: 10.1002/mnfr.200600041

124. Remesic M, Sun Lee Y, Hruby VJ. Cyclic opioid peptides. *Curr Med Chem.* (2016) 23:1288–303. doi: 10.2174/092986732366616042712
3005

125. Lesniak A, Leszczynski P, Bujalska-Zadrozny M, Pick CG, Sacharczuk M. Naloxone exacerbates memory impairments and depressive-like behavior after mild traumatic brain injury (mTBI) in mice with upregulated opioid system activity. *Behav Brain Res.* (2017) 326:209–16. doi: 10.1016/j.bbr.2017.03.015

126. Liu Z, Udenigwe CC. Role of food-derived opioid peptides in the central nervous and gastrointestinal systems. *J Food Biochem.* (2019) 43:1–7. doi: 10.1111/jfbc.12629

127. Ghelardini C, Di Cesare Mannelli L, Bianchi E. The pharmacological basis of opioids. *Clin Cases Mineral Bone Metabol.* (2015) 12:219–21. doi: 10.11138/ccmbm/2015.12.3.219

128. Kaur J, Kumar V, Sharma K, Kaur S, Gat Y, Goyal A, et al. Opioid peptides: an overview of functional significance. *Int J Pept Res Therapeut.* (2020) 26:33–41. doi: 10.1007/s10989-019-09813-7

129. Pihlanto-Leppala A. Bioactive peptides derived from bovine whey proteins. *Trends Food Sci Technol.* (2002) 11:347–56. doi: 10.1016/S0924-2244(01)00003-6

130. Noguchi T, Kato T, Wang L, Maeda Y, Ikeda H, Sato E, et al. Intracellular tumor-associated antigens represent effective targets for passive immunotherapy. *Cancer Res.* (2012) 72:1672–82. doi: 10.1158/0008-5472.CAN-11-3072

131. Kannan A, Hettiarachchy NS, Lay JO, Liyanage R. Human cancer cell proliferation inhibition by a pentapeptide isolated and characterized from rice bran. *Peptides.* (2010) 31:1629–34. doi: 10.1016/j.peptides.2010.05.018

132. Kim EK, Joung HJ, Kim YS, Hwang JW, Ahn CB, Jeon YJ, et al. Purification of a novel anticancer peptide from enzymatic hydrolysate of Mytilus coruscus. *J Microbiol Biotechnol.* (2012) 22:1381–7. doi: 10.4014/jmb.1207.07015

133. Dia VP, de Mejia EG. Lunasin induces apoptosis and modifies the expression of genes associated with extracellular matrix and cell adhesion in human metastatic colon cancer cells. *Mol Nutr Food Res.* (2011) 55:623–34. doi: 10.1002/mnfr.201000419

134. Hwang JS, Yoo HJ, Song HJ, Kim KK, Chun YJ, Matsui T, et al. Inflammation-related signaling pathways implicating TGFβ are revealed in the expression profiling of MCF7 cell treated with fermented soybean. *Chungkookjang Nutr Cancer.* (2011) 63:645–52. doi: 10.1080/01635581.2011.551987

135. Badger TM, Ronis MJJ, Simmen RCM, Simmen FA. Soy protein isolate and protection against cancer. *J Am Coll Nutr.* (2005) 24:146S–9S. doi: 10.1080/07315724.2005.10719456

136. Chen Z, Wang J, Liu W, Chen H. Physicochemical characterization, antioxidant and anticancer activities of proteins from four legume species. *J Food Sci Technol.* (2017) 54:964–72. doi: 10.1007/s13197-016-2390-x

137. Lee SY, Hur SJ. Antihypertensive peptides from animal products, marine organisms, and plants. *Food Chem.* (2017) 228:506–17. doi: 10.1016/j.foodchem.2017.02.039

138. Joffres MR, Hamet P, MacLean DR, L'italien GJ, Fodor G. Distribution of blood pressure and hypertension in Canada and the United States. *Am J Hypertens.* (2001) 14:1099–105. doi: 10.1016/S0895-7061(01)02211-7

139. Acquah C, Stefano ED, Udenigwe CC. Role of hydrophobicity in food peptide functionality and bioactivity. *J Food Bioactiv.* (2018) 4:88–98. doi: 10.31665/JFB.2018.4164

140. Marambe PW, Shand PJ, Wanasundara JPD. An *in-vitro* investigation of selected biological activities of hydrolysed flaxseed (*Linum usitatissimum* L.) proteins. *J Am Oil Chem Soc.* (2008) 85:1155–64. doi: 10.1007/s11746-008-1293-z

141. Wang X, Chen H, Fu X, Li S, Wei J. A novel antioxidant and ACE inhibitory peptide from rice bran protein: biochemical characterization and molecular docking study. *LWT Food Sci Technol.* (2017) 75:93–9. doi: 10.1016/j.lwt.2016.08.047

142. Kong X, Guo M, Hua Y, Cao D, Zhang C. Enzymatic preparation of immunomodulating hydrolysates from soy proteins. *Bioresour Technol.* (2008) 99:8873–9. doi: 10.1016/j.biortech.2008.04.056

143. Vo T, Ryu B, Kim S. Purification of novel anti-inflammatory peptides from enzymatic hydrolysate of the edible microalgal *Spirulina maxima*. *J Funct Foods.* (2013) 5:1336–46. doi: 10.1016/j.jff.2013.05.001

144. Ngo DH, Vo TS, Ngo DN, Wijesekara I, Kim SK. Biological activities and potential health benefits of bioactive peptides derived from marine organisms. *Int J Biol Macromol.* (2012) 51:378–83. doi: 10.1016/j.ijbiomac.2012.06.001

145. Wu J, Majumder K, Gibbons K. Bioactive proteins and peptides from egg proteins. In: Mine Y, Li-Chan E, Jiang B, editors, *Bioactive Proteins and Peptides as Functional Foods and Nutraceuticals.* Oxford: Wiley-Blackwell (2010). p. 247–63. doi: 10.1002/9780813811048.ch17

146. Kim SK, Wijesekara I. Development and biological activities of marine-derived bioactive peptides: a review. *J Funct Foods.* (2010) 2:1–9. doi: 10.1016/j.jff.2010.01.003

147. Zhao L, Wang X, Zhang X-L, Xie Q-F. Purification and identification of anti-inflammatory peptides derived from simulated gastrointestinal digest of velvet antler protein (*Cervus elaphus* Linnaeus). *J Food Drug Anal.* (2016) 24:376–84. doi: 10.1016/j.jfda.2015.10.003

148. Dumeus S, Shibu MA, Lin WT, Wang MF, Lai CH, Shen CY, et al. Bioactive peptide improves diet-induced hepatic fat deposition and hepatocyte

149. Dia VP, Bringe NA, De Mejia EG. Peptides in pepsin–pancreatin hydrolysates from commercially available soy products that inhibit lipopolysaccharide-induced inflammation in macrophages. *Food Chem.* (2014) 152:423–31. doi: 10.1016/j.foodchem.2013.11.155

150. Shahi MM, Rashidi MR, Mahboob S, Haidari F, Rashidi B, Hanaee J. Protective effect of soy protein on collagen-induced arthritis in rat. *Rheumatol Int.* (2012) 32:2407–14. doi: 10.1007/s00296-011-1979-7

151. Faustino M, Veiga M, Sousa P, Costa EM, Silva S, Pintado M. Agro-food byproducts as a new source of natural food additives. *Molecules.* (2019) 2019:1–23. doi: 10.3390/molecules24061056

152. Lam RSH, Nickerson MT. Food proteins: a review on their emulsifying properties using a structure-function approach. *Food Chem.* (2013) 141:975–84. doi: 10.1016/j.foodchem.2013.04.038

153. Garcia-Moreno PJ, Gregersen S, Nedamani ER, Olsen TH, Marcatili P, Overgaard MT, et al. Identification of emulsifier potato peptides by bioinformatics: application to omega-3 delivery emulsions and release from potato industry side streams. *Sci Rep.* (2020) 10:1–22. doi: 10.1038/s41598-019-57229-6

154. Liu F, Wang D, Sun C, McClements DJ, Gao Y. Utilization of interfacial engineering to improve physicochemical stability of β-carotene emulsions: multilayer coatings formed using protein and protein-polyphenol conjugates. *Food Chem.* (2016) 205:129–39. doi: 10.1016/j.foodchem.2016.02.155

155. Tsumura K, Kugimiya W, Inouye K. Emulsifying properties of a peptide from peptic hydrolysates of soy glycinin. *Food Sci Technol Res.* (2005) 11:46–51. doi: 10.3136/fstr.11.46

156. Alvarez D, Delles RM, Xiong YL, Castillo M, Payne FA, Laencina J. Influence of canola-olive oils, rice bran and walnut on functionality and emulsion stability of frankfurters. *LWT Food Sci Technol.* (2011) 44:1435–42. doi: 10.1016/j.lwt.2011.01.006

157. Talukder S, Sharma DP. Development of dietary fiber rich chicken meat patties using wheat and oat bran. *J Food Sci Technol.* (2010) 47:224–9. doi: 10.1007/s13197-010-0027-z

158. Kamani MH, Meera MS, Bhaskar N, Modi VK. Partial and total replacement of meat by plant-based proteins in chicken sausage: evaluation of mechanical, physico-chemical and sensory characteristics. *J Food Sci Technol.* (2019) 56:2660–9. doi: 10.1007/s13197-019-03754-1

159. Xiong T, Xiong W, Ge M, Xia J, Li B, Chen Y. Effect of high intensity ultrasound on structure and foaming properties of pea protein isolate. *Food Res Int.* (2018) 109:260–7. doi: 10.1016/j.foodres.2018.04.044

160. Elsohaimy SA, Refaay TM, Zaytoun MAM. Physicochemical and functional properties of quinoa protein isolate. *Ann Agri Sci.* (2015) 60:297–305. doi: 10.1016/j.aoas.2015.10.007

161. Tibin IM, Mustafa MA. Quality attributes of beef burger patties extended with soybean flour and water melon seed cakes. *J Vet Med Anim Prod.* (2018) 8:1893.

162. Hidayat BT, Wea A, Andriati N. Physicochemical, sensory attributes and protein profile by SDS-PAGE of beef sausage substituted with texturized vegetable proteins. *Food Res.* (2018) 2:20–31. doi: 10.26656/fr.2017.2(1).106

163. Carvalho GRd, Milani TMG, Trinca NRR, Nagai LY, Barretto ACdaS. Textured soy protein, collagen and maltodextrin as extenders to improve the physicochemical and sensory properties of beef burger. *Food Sci Technol.* (2017) 37:10–6. doi: 10.1590/1678-457x.31916

164. Karami Z, Akbari-adergani B. Bioactive food derived peptides: a review on correlation between structure of bioactive peptides and their functional properties. *J Food Sci Technol.* (2019) 56:535–47. doi: 10.1007/s13197-018-3549-4

165. Rowayshed G, Sharaf AM, El-Faham SY, Ashour M, Zaky AA. Utilization of potato peels extract as source of phytochemicals in biscuits. *J Basic Appl Res Int.* (2015) 8:190–201.

166. Zaky AA, Abd El-Aty AM, Ma A, Jia Y. An overview on antioxidant peptides from rice bran proteins: extraction, identification, and applications. *Crit Rev Food Sci Nutr.* (2020) 2020:1–13. doi: 10.1080/10408398.2020.1842324

167. Zaky AA, Chen Z, Qin M, Wang M, Jia Y. Assessment of antioxidant activity, amino acids, phenolic acids and functional attributes in defatted rice bran and rice bran protein concentrate. *Progr Nutr.* (2020) 22:e2020069. doi: 10.23751/pn.v22i4.8971

168. El-Faham SY, Mohsen M, Sharaf A, Zaky A. Utilization of mango peels as a source of polyphenolic antioxidants. *Curr Sci Int.* (2016) 5:529–42.

169. Zaky AA, Asiamah E, El-Faham SY, Ashour MM, Sharaf A. Utilization of grape pomace extract as a source of natural antioxidant in biscuits. *Eur Acad Res.* (2020) 8:108–26.

170. Sohaib M, Anjum FM, Sahar A, Arshad MS, Rahman UU, Imran A, et al. Antioxidant proteins and peptides to enhance the oxidative stability of meat and meat products: a comprehensive review. *Int J Food Prop.* (2017) 20:2581–93. doi: 10.1080/10942912.2016.1246456

171. Samaranayaka AG, Li-Chan EC. Food-derived peptidic antioxidants: a review of their production, assessment, and potential applications. *J Funct Foods.* (2011) 3:229–54. doi: 10.1016/j.jff.2011.05.006

172. Nikoo M, Benjakul S, Ehsani A, Li J, Wu F, Yang N, et al. Antioxidant and cryoprotective effects of a tetrapeptide isolated from *Amur sturgeon* skin gelatin. *J Funct Foods.* (2014) 7:609–20. doi: 10.1016/j.jff.2013.12.024

173. Shahidi F, Han XQ, Synowiecki J. Production and characteristics of protein hydrolysates from capelin (*Mallotus villosus*). *Food Chem.* (1995) 53:285–93. doi: 10.1016/0308-8146(95)93934-J

174. Kittiphattanabawon P, Benjakul S, Visessanguan W, Shahidi F. Gelatin hydrolysate from blacktip shark skin prepared using papaya latex enzyme: antioxidant activity and its potential in model systems. *Food Chem.* (2012) 135:1118–26. doi: 10.1016/j.foodchem.2012.05.080

175. Bougatef A, Nedjar-Arroume N, Manni L, Ravallec R, Barkia A, Guillochon D, et al. Purification and identification of novel antioxidant peptides from enzymatic hydrolysates of sardinelle (*Sardinella aurita*) by-products proteins. *Food Chem.* (2010) 118:559–65. doi: 10.1016/j.foodchem.2009.05.021

176. Sun J, He H, Xie BJ. Novel antioxidant peptides from fermented mushroom *Ganoderma lucidum*. *J Agric Food Chem.* (2004) 52:6646–52. doi: 10.1021/jf0495136

177. Yang JI, Ho HY, Chu YJ, Chow CJ. Characteristic and antioxidant activity of retorted gelatin hydrolysates from cobia (*Rachycentron canadum*) skin. *Food Chem.* (2008) 110:128–36. doi: 10.1016/j.foodchem.2008.01.072

178. Cai, L.,Wu X, Zhang Y, Li X, Ma S, Li J. Purification and characterization ofthree antioxidant peptides from protein hydrolysate of grass carp (*Ctenopharyngodon idella*) skin. *J Funct Foods.* (2015) 16:234–42. doi: 10.1016/j.jff.2015.04.042

179. Sivaraman B, Shakila RJ, Jeyasekaran G, Sukumar D, Manimaran U, Sumathi G. Antioxidant activities of squid protein hydrolysates prepared with papain using response surface methodology. *Food Sci Biotechnol.* (2016) 25:665–72. doi: 10.1007/s10068-016-0117-4

180. Shen Y, Hu R, Li Y. Antioxidant and emulsifying activities of corn gluten meal hydrolysates in oil-in-water emulsions. *J Am Oil Chem Soc.* (2020) 97:175–85. doi: 10.1002/aocs.12286

181. Li Y, Kong B, Liu Q, Xia X, Chen H. Improvement of the emulsifying and oxidative stability of myofibrillar protein prepared oil-in-water emulsions by addition of zein hydrolysates. *Process Biochem.* (2017) 53:116–24. doi: 10.1016/j.procbio.2016.11.010

182. Jridi M, Lassoued I, Nasri R, Ayadi MA, Nasri M, Souissi N. Characterization and potential use of cuttlefish skin gelatin hydrolysates prepared by different microbial proteases. *Biomed Res Int.* (2014) 2014:1–14. doi: 10.1155/2014/461728

183. Sakanaka S, Tachibana Y, Ishihara N, Juneja LR. Antioxidant properties of casein calcium peptides and their effects on lipid oxidation in beef homogenates. *J Agric Food Chem.* (2005) 53:464–8. doi: 10.1021/jf0487699

184. Peña-Ramos EA, Xiong YL. Whey and soy protein hydrolysates inhibit lipid oxidation in cooked pork patties. *Meat Sci.* (2003) 64:259–63. doi: 10.1016/S0309-1740(02)00187-0

185. Bechaux J, Gatellier P, Le Page JF, Drillet Y, Sante-Lhoutellier V. A comprehensive review of bioactive peptides obtained from animal byproducts and their applications. *Food Funct.* (2019) 10:6244–66. doi: 10.1039/C9FO01546A

186. Català-Clariana S, Benavente F, Giménez E, Barbosa J, Sanz-Nebot V. Identification of bioactive peptides in hypoallergenic infant milk formulas by CE-TOF-MS assisted by semiempirical model of electromigration behavior. *Electrophoresis.* (2013) 34:1886–94. doi: 10.1002/elps.201200547

187. You L, Zhao M, Regenstein JM, Ren J. *In vitro* antioxidant activity and *in vivo* anti-fatigue effect of loach (*Misgurnus anguillicaudatus*) peptides prepared by papain digestion. *Food Chem.* (2011) 124:188–94. doi: 10.1016/j.foodchem.2010.06.007

188. Han B-K, Park Y, Choi H-S, Suh HJ. Hepatoprotective effects of soluble rice protein in primary hepatocytes and in mice. *J Sci Food Agric.* (2016) 96:685–94. doi: 10.1002/jsfa.7153

189. Zhang R, Chen J, Jiang X, Yin L, Zhang X. Antioxidant and hypoglycaemic effects of tilapia skin collagen peptide in mice. *Int J Food Sci Technol.* (2016) 51:2157–63. doi: 10.1111/ijfs.13193

190. De Simone C, Picariello G, Mamone G, Stiuso P, Dicitore A, Vanacore D, et al. Characterisation and cytomodulatory properties of peptides from Mozzarella di Bufala Campana cheese whey. *J Pept Sci.* (2009) 15:251–8. doi: 10.1002/psc.1093

191. Meisel H, FitzGerald RJ. Biofunctional peptides from milk proteins: mineral binding and cytomodulatory effects. *Curr Pharm Des.* (2003) 9:1289–96. doi: 10.2174/1381612033454847

192. Mahmoud SS, Torchilin VP. Hormetic/cytotoxic effects of *Nigella sativa* seed alcoholic and aqueous extracts on MCF-7 breast cancer cells alone or in combination with doxorubicin. *Cell Biochem Biophys.* (2013) 66:451–60. doi: 10.1007/s12013-012-9493-4

193. Saisavoey T, Sangtanoo P, Reamtong O, Karnchanatat A. Antioxidant and anti-inflammatory effects of defatted rice bran (*Oryza sativa* L.) protein hydrolysates on raw 264.7 macrophage cells. *J Food Biochem.* (2016) 40:731–40. doi: 10.1111/jfbc.12266

194. Chauhan V, Kanwar SS. Bioactive peptides: synthesis, functions and Biotechnological applications. In: *Biotechnological Production of Bioactive Compounds*, eds M. L. Verma and A. K. Chandel (Amsterdam: Elsevier). (2020). p. 107–37. doi: 10.1016/B978-0-444-64323-0.00004-7

195. Marczak ED, Usui H, Fujita H, Yang Y, Yokoo M, Lipkowski AW, et al. New antihypertensive peptides isolated from rapeseed. *Peptides.* (2003) 24:791–8. doi: 10.1016/S0196-9781(03)00174-8

196. El-Salam MA, El-Shibiny S. Bioactive peptides of buffalo, camel, goat, sheep, mare, and yak milks and milk products. *Food Rev Int.* (2013) 29:1–23. doi: 10.1080/87559129.2012.692137

197. Reddi S, Kapila R, Ajay Kumar Dang AK, Kapila S. Evaluation of allergenic response of milk bioactive peptides using mouse mast cell. *Milchwissenschaft-Milk Sci Int.* (2012) 67:189.

198. Ledwoń P, Errante F, Papini AM, Rovero P, Latajka R. Peptides as active ingredients: a challenge for cosmeceutical industry. *Chem Biodiv.* (2021) 18:e2000833. doi: 10.1002/cbdv.202000833

199. Choi HI, Park JI, Kim HJ, Kim DW, Kim SS. A novel L-ascorbic acid and peptide conjugate with increased stability and collagen biosynthesis. *BMB Rep.* (2009) 42:743–6. doi: 10.5483/BMBRep.2009.42.11.743

200. Pickart L. The human tri-peptide GHK and tissue remodeling. *J Biomater Sci Polym Ed.* (2008) 19:969–88. doi: 10.1163/156856208784909435

201. Cheung RCF, Ng TB, Wong JH. Marine peptides: bioactivities and applications. *Mar Drugs.* (2015) 13:4006–43. doi: 10.3390/md13074006

202. Sable R, Parajuli P, Jois S. Peptides, peptidomimetics, and polypeptides from marine sources: a wealth of natural sources for pharmaceutical applications. *Mar Drugs.* (2017) 15:124. doi: 10.3390/md15040124

203. Tkaczewska J, Bukowski M, Mak P. Identification of antioxidant peptides in enzymatic hydrolysates of carp (*Cyprinus carpio*) skin gelatin. *Molecules.* (2019) 24:97. doi: 10.3390/molecules24010097

204. Aldag C, Teixeira DN, Leventhal PS. Skin rejuvenation using cosmetic products containing growth factors, cytokines, and matrikines: a review of the literature. *Clin Cosmet Investig Dermatol.* (2016) 9:411. doi: 10.2147/CCID.S116158

205. Schagen SK. Topical peptide treatments with effective anti-aging results. *Cosmetics.* (2017) 4:16. doi: 10.3390/cosmetics4020016

206. Finkley M, Appa Y, Bhandarkar S. Copper peptide and skin. In: Elsner P, Maibach H, editor, *Cosmeceuticals and Active Cosmetics: Drugs vs. Cosmetics.* New York NY: Marcel Dekker Press (2005). p. 549–63.

207. Lintner K, Peschard O. Biologically active peptides: from a laboratory bench curiosity to a functional skin care product. *Int J Cosmet Sci.* (2000) 22:207–18. doi: 10.1046/j.1467-2494.2000.00010.x

208. Katayama K, Seyer JM, Raghow R, Kang AH. Regulation of extracellular matrix production by chemically synthesized subfragments of type I collagen carboxy propeptide. *Biochemistry.* (1991) 30:7097–104. doi: 10.1021/bi00243a009

209. Choi YL, Park EJ, Kim E, Na DH, Shin YH. Dermal stability and *in vitro* skin permeation of collagen pentapeptides (KTTKS and palmitoyl-KTTKS). *Biomol Ther.* (2014) 22:321. doi: 10.4062/biomolther.2014.053

210. Kim D-U, Chung H-C, Choi J, Sakai Y, Lee B-Y. Oral intake of low-molecular-weight collagen peptide improves hydration, elasticity, and wrinkling in human skin: a randomized, double-blind, placebo-controlled study. *Nutrients.* (2018) 10:826. doi: 10.3390/nu10070826

211. Song H, Li B. Beneficial effects of collagen hydrolysate: a review on recent developments. *J Sci Tech Res.* (2017) 1:1–4. doi: 10.26717/BJSTR.2017.01.000217

212. Kang MC, Yumnam S, Kim SY. Oral intake of collagen peptide attenuates ultraviolet B irradiation-induced skin dehydration *in vivo* by regulating hyaluronic acid synthesis. *Int J Mol Sci.* (2018) 19:3551. doi: 10.3390/ijms19113551

213. Asserin J, Lati E, Shioya T, Prawitt J. The effect of oral collagen peptide supplementation on skin moisture and the dermal collagen network: evidence from an *ex vivo* model and randomized, placebo-controlled clinical trials. *J Cosmet Dermatol.* (2015) 14:291–301. doi: 10.1111/jocd.12174

214. Sen CK, Gordillo GM, Roy S, Kirsner R, Lambert L, Hunt TK, et al. Human skin wounds: a major and snowballing threat to public health and the economy. *Wound Rep Regener.* (2009) 17:763–71. doi: 10.1111/j.1524-475X.2009.00543.x

215. Heng MC. Wound healing in adult skin: aiming for perfect regeneration. *Int J Dermatol.* (2011) 50:1058–66. doi: 10.1111/j.1365-4632.2011.04940.x

216. Song Y, Wu C, Zhang X, Bian W, Liu N, Yin S, et al. A short peptide potentially promotes the healing of skin wound. *Biosci Rep.* (2019) 39:BSR20181734. doi: 10.1042/BSR20181734

217. Mustoe T. Understanding chronic wounds: a unifying hypothesis on their pathogenesis and implications for therapy. *Am J Surg.* (2004) 187:S65–70. doi: 10.1016/S0002-9610(03)00306-4

218. Larouche J, Sheoran S, Maruyama K, Martino MM. Immune regulation of skin wound healing: mechanisms and novel therapeutic targets. *Adv Wound Care.* (2018) 7:209–31. doi: 10.1089/wound.2017.0761

219. Li X, Wang Y, Zou Z, Yang M, Wu C, Su Y, et al. OM-LV20, a novel peptide from odorous frog skin, accelerates wound healing *in vitro* and *in vivo*. *Chem Biol Drug Design.* (2018) 91:126–36. doi: 10.1111/cbdd.13063

220. Carretero M, Escámez MJ, García M, Duarte B, Holguín A, Retamosa L, et al. *In vitro* and *in vivo* wound healing-promoting activities of human cathelicidin LL-37. *J Investig Dermatol.* (2008) 128:223–36. doi: 10.1038/sj.jid.5701043

221. Ramos R, Silva JP, Rodrigues AC, Costa R, Guardão L, Schmitt F, et al. Wound healing activity of the human antimicrobial peptide LL37. *Peptides.* (2011) 32:1469–76. doi: 10.1016/j.peptides.2011.06.005

222. Song DW, Kim SH, Kim HH, Lee KH, Ki CS, Park YH. Multi-biofunction of antimicrobial peptide-immobilized silk fibroin nanofiber membrane: implications for wound healing. *Acta Biomater.* (2016) 39:146–55. doi: 10.1016/j.actbio.2016.05.008

223. Banerjee P, Suguna L, Shanthi C. Wound healing activity of a collagen-derived cryptic peptide. *Amino Acids.* (2015) 47:317–28. doi: 10.1007/s00726-014-1860-6

224. Felician FF, Yu RH, Li MZ, Li CJ, Chen HQ, Jiang Y, et al. The wound healing potential of collagen peptides derived from the jellyfish *Rhopilema esculentum*. *Chin J Traumatol.* (2019) 22:12–20. doi: 10.1016/j.cjtee.2018.10.004

225. Cheng X, Shao Z, Li C, Yu L, Raja MA, Liu C. Isolation, characterization and evaluation of collagen from jellyfish *Rhopilema esculentum* Kishinouye for use in hemostatic applications. *PLoS ONE.* (2017) 12:e0169731. doi: 10.1371/journal.pone.0169731

226. Addad S, Exposito JY, Faye C, Ricard-Blum S, Lethias C. Isolation, characterization and biological evaluation of jellyfish

collagen for use in biomedical applications. *Mar Drugs.* (2011) 9:967–83. doi: 10.3390/md9060967

227. Wu G, Bazer FW, Cross HR. Land-based production of animal protein: impacts, efficiency, and sustainability. *Ann N Y Acad Sci.* (2014) 1328:18–28. doi: 10.1111/nyas.12566

228. Wu G, Fanzo J, Miller DD, Pingali P, Post M, Steiner JL, et al. Production and supply of high-quality food protein for human consumption: sustainability, challenges, and innovations. *Ann N Y Acad Sci.* (2014) 1321:1–19. doi: 10.1111/nyas.12500

229. Dieterich F, Boscolo WR, Pacheco MTB, Silva VSN, Gonçalves GS, Vidotti RM. Development and characterization of protein hydrolysates originated from animal agro industrial byproducts. *J Dairy Vet Anim Res.* (2014) 1:1–7. doi: 10.15406/jdvar.2014.01.00012

230. Hou Y, Wu Z, Dai Z, Wang G, Wu G. Protein hydrolysates in animal nutrition: Industrial production, bioactive peptides, and functional significance. *J Anim Sci Biotechnol.* (2017) 8:1–13. doi: 10.1186/s40104-017-0153-9

231. Pasupuleti VK, Holmes C, Demain AL. Applications of protein hydrolysates in biotechnology. In: *Protein Hydrolysates in Biotechnology*, eds V. K. PasupuletiArnold and L. Demain (New York, NY: Springer Science). (2010). p. 1–9. doi: 10.1007/978-1-4020-6674-0

232. Lalles JP, Toullec R, Pardal PB, Sissons JW. Hydrolyzed soy protein isolate sustains high nutritional performance in veal calves. *J Dairy Sci.* (1995) 78:194–204. doi: 10.3168/jds.S0022-0302(95)76629-2

233. Opheim M, Sterten H, Øverland M, Kjos NP. Atlantic salmon (*Salmo salar*) protein hydrolysate–effect on growth performance and intestinal morphometry in broiler chickens. *Livest Sci.* (2016) 187:138–45. doi: 10.1016/j.livsci.2016.03.005

234. Khosravi S, Rahimnejad S, Herault M, Fournier V, Lee CR, Bui HTD, et al. Effects of protein hydrolysates supplementation in low fish meal diets on growth performance, innate immunity and disease resistance of red sea bream Pagrus major. *Fish Shellfish Immunol.* (2015) 45:858–68. doi: 10.1016/j.fsi.2015.05.039

235. Nagodawithana TW, Nelles L, Trivedi NB. Protein hydrolysates as hypoallergenic, flavors and palatants for companion animals. In: *Protein Hydrolysates in Biotechnology*, eds V. K. PasupuletiArnold and L. Demain (New York, NY: Springer Science). (2010). p. 191–207. doi: 10.1007/978-1-4020-6674-0_11

236. Kim SW, Van Heugten E, Ji F, Lee CH, Mateo RD. Fermented soybean meal as a vegetable protein source for nursery pigs: I. Effects on growth performance of nursery pigs. *J Anim Sci.* (2010) 88:214–24. doi: 10.2527/jas.2009-1993

237. El-Ayek MY, Gabr AA, Mehrez AZ. Influence of substituting concentrate feed mixture by *Nigella sativa* meal on animal performance and carcass traits of growing lambs. *Egypt J Nutr Feeds.* (1999) 2:265–77.

238. El-Deek AA, Hamdy SM, Attia YA, Khalifah MM. *Nigella sativa* seed oil meal as a source of plant protein in broiler diets. *Egypt Poult Sci J.* (2009) 29:39–52.

239. Doorten APS, Vd Wiel JAG, Jonker D. Safety evaluation of an IPP tripeptide-containing milk protein hydrolysate. *Food Chem Toxicol.* (2009) 47:55–61. doi: 10.1016/j.fct.2008.10.001

240. Anadón A, Martínez MA, Ares I, Ramos E, Martínez-Larrañaga MR, Contreras MM, et al. Acute and repeated dose (4 weeks) oral toxicity studies of two antihypertensive peptides, RYLGY and AYFYPEL, that correspond to fragments (90–94) and (143–149) from αs1-casein. *Food Chem Toxicol.* (2010) 48:1836–45. doi: 10.1016/j.fct.2010.04.016

Translocation of Phthalates From Food Packaging Materials Into Minced Beef

Denis Baranenko[1]*, Mohamed Said Boulkrane[1], Irina Borisova[1], Bazhena Astafyeva[1], Weihong Lu[2] and A. M. Abd El-Aty[3,4]

[1] *International Research Centre "Biotechnologies of the Third Millennium", Faculty of Biotechnologies (BioTech), ITMO University, Saint-Petersburg, Russia,* [2] *Institute of Extreme Environment Nutrition and Protection, Harbin Institute of Technology, Harbin, China,* [3] *Department of Pharmacology, Faculty of Veterinary Medicine, Cairo University, Giza, Egypt,* [4] *Department of Medical Pharmacology, Medical Faculty, Ataturk University, Erzurum, Turkey*

There has been increased concern regarding the potential human health risks associated with exposure to phthalates. Research indicates that food intake is the most critical exposure pathway for phthalates. This study aimed to investigate packaged beef samples for the presence of dimethyl terephthalate (DMTP), di-n-butyl phthalate (DnBP), and diisooctyl phthalate (DiOP) and to assess their translocation from the common form of food packaging procured from various Saint-Petersburg and Leningrad region shops. The packaging samples include paper and different types of plastic. Phthalates were extracted by dichloromethane and analyzed by gas chromatography coupled with mass spectrometry (GC-MS). While DnBP had the highest mean values in beef from 34.5 to 378.5 μg·kg^{-1}, DiOP displayed the lowest mean values from LOD to 37 μg·kg^{-1}. The larger contact area and the presence of distributed fat on the surface of the minced meat resulted in significantly higher phthalate translocation than beef slices. Further, DMTP was not detected in any samples. However, the examined food packages do not meet the requirements of Russian, EU and USA legislation, as DnBP migrates to meat. Calculated maximum DnBP daily intake of 0.167 μg·kg^{-1}·day^{-1} for chilled minced beef in vacuum packaging did not exceed tolerable daily intake (TDI) level. The most alarming results are concerning the phthalates presence in beef farmed in the Leningrad region and not subjected to any plastic packaging. A full-scale study is warranted to determine the pathways and sources of phthalates migration in the food chain.

Keywords: xenobiotics, toxicity, GC-MS, meat, animal raw materials

INTRODUCTION

Over the past decades, a vast number of studies related to the existence of phthalate compounds in packaging materials and food have been published (1–4). Phthalates (diesters of ortho phthalic acid) are organic chemicals that are commonly used as plasticizers to make plastic polymers softer and more flexible. Additionally, they are used to produce lacquers and printing inks as additives to improve the flexibility, surface adhesion, color, elasticity, and wrinkle resistance to manufacturing adhesives, solvents, waxes, pharmaceuticals, and cosmetics insecticides, and packaging from regenerated cellulose (5).

The presence of phthalates in food poses a significant concern regarding their impact on human health (6). Following exposure and uptake, phthalates are rapidly metabolized by hydrolysis followed by conjugation (7). The first phase, which occurred in the intestine and parenchyma and catalyzed by esterases and lipases, the diester phthalate is hydrolyzed into the monoester phthalate (8). Monoester phthalates are more bioactive than non-hydrolyzed diester phthalates, as shown in *in vitro* and *in vivo* studies. Short-branched phthalates are mainly excreted as monoester phthalates *via* urine. In contrast, long-branched compounds are further biotransformed through hydroxylation and oxidation and then excreted in feces and urine as phase II conjugated compounds (9). Phthalates were also found in breast milk and amniotic fluid (10).

It was reported that exposure to phthalates and their metabolites might inadvertently be disrupting the endocrine system, act as carcinogens, and negatively impact the reproductive system (11). Some phthalates may have anti-androgenic and cause reproductive and developmental toxicity in animals (12). Researches demonstrated that phthalates could adversely affect the male reproductive system, causing asthma, rhinitis, and eczema in children, in addition to their impacts on metabolism and neurological development (13). Neurotoxicity, infertility, respiratory symptoms, epigenetic, immune and metabolic abnormalities are other endpoints of target organ toxicity caused by phthalates (14).

People are mainly exposed to phthalates from food, water, air, and consumer products, including building materials, household furnishings, clothing, cosmetics, pharmaceuticals, nutritional supplements, medical devices, dentures, children's toys, glow sticks, modeling clay, food packaging, automobiles, lubricants, waxes, cleaning materials, and insecticides (15). The routes of phthalate exposure ranked by their importance include food intake, dust ingestion, and indoor air inhalation (16). Mechanical stress or high temperature can cause chemical migration from packaging materials to food or drink (17). Phthalates are readily leached from products and released to the environment because of their weak bonds with bridging substrate (11).

In addition to the direct effect of phthalates through food items, their migration to the soil, groundwater, and dust can pose a significant risk to human health and/or sensitive environmental receptors. Plastics account for 25% of municipal solid waste (18). The most rational way for treating plastic is separate collection and recycling as it gives the possibilities for environmentally friendly management of every municipal solid waste stream (19). Even in this case, plastic materials should be handled, treated, and disposed of safely (20). In the case of landfilling of plastic materials, the impact of phthalates on environmental quality is associated with certain long-term related soil and groundwater contamination problems (21).

European Union has set limits and regulations for the content of chemical compounds in packaging. European Food Safety Authority has specified tolerable daily intakes (TDIs) of $0.01 \text{ mg} \times \text{kg}^{-1}$ bw for di-n-butyl phthalate (DnBP), $0.05 \text{ mg} \times \text{kg}^{-1}$ bw for di(2-ethylhexyl) phthalate (DEHP), $0.50 \text{ mg} \times \text{kg}^{-1}$ bw for benzylbutyl phthalate (BBP), and a group TDI of $0.15 \text{ mg} \times \text{kg}^{-1}$ bw for diisodecyl phthalate (DiDP) and

diisononyl phthalate (DiNP) (22–26). Russia has also established the rules governing the packaging components migration tests using simulators of food (Technical Regulations CU TR 005/2011 on the safety of the packaging). However, it is still inadequately controlled. Although there were many studies on phthalates in packaging materials and food in Europe and America (27–31), Russia lacks information. Hence, this study aimed to evaluate the migration of phthalates from various common packaging materials to beef sold in the Russian meat market.

MATERIALS AND METHODS

Standards, Solvents, and Chemicals

Phthalate standards, including dimethyl terephthalate (DMTP), di-n-butyl phthalate (DnBP), and diisooctyl phthalate (DiOP), were procured from ChromLab Ltd. (Lyubertsy, Russia). LC grade or glass-distilled solvents were used. Dichloromethane and hexane were from Merck (Darmstadt, Germany). HPLC gradient grade methanol was from J.T.Baker (Deventer, Netherlands). Water is produced using Milli-Q Type 1 Ultrapure Water Systems (Millipore, Burlington, Massachusetts, United States).

Standard stock solution for each analyte (DMTP, DnBP, and DiOP) was prepared in methanol at a 1 mg·ml^{-1} concentration. These solutions were further diluted in methanol, yielding various concentrations (0.005, 0.01, 0.1, and 0.5 mg·ml^{-1}) for constructing the calibration curves. All working solutions are prepared freshly before use.

During all manipulations, contact with any plastic material was not allowed. All glassware and accessories were rinsed with methanol, acetone, and n-hexane, immediately before and after use.

Sample Collection

Beef striploin (50 samples) and packaging materials (35 samples) were secured from various shopping areas in Saint-Petersburg and Leningrad region, Northwestern Federal District, Russia, between November 2020 and May 2021. Samples of beef striploin were selected with an average fat content of about 20%. It should be noted that the distribution networks of the Northwestern Federal District and the range of goods are common or very similar for beef and packaging materials compared to most regions of Russia.

Farm beef samples (40 samples) were obtained from striploin cuts weighing 4.5–5 kg each from three carcasses. These three striploin cuts were delivered to the laboratory in glass containers. In the laboratory, the cuts were carved into appropriate pieces and analyzed, minced and/or packed in five samples for each type of processing. Each sample was packaged and sealed in selected packaging material, as shown in **Table 1**. Each packaging sample was taken from a single roll or unit of packaging material. Samples of commercially packaged beef were purchased in quantities of five for each of the two types. The pH of the farm fresh beef was 5.7 ± 0.1 (24 h), increased to 6.1 ± 0.1 (120 h) after slaughter. The pH of the chilled commercially packaged beef samples was 6.0 ± 0.2. The water content of farm fresh beef, commercially packaged beef sample 1, and commercially packaged beef sample two were 64.5 ± 0.8, 65.7

N	Food	Packaging and conditions	Type of plastic
1	Farm fresh beef	Obtained at a farm right after slaughter and placed in a glass container	–
2	Chilled/minced farm beef	Cut or minced from the farm-fresh beef, vacuum sealed and stored at 2°C for 7 days	PET/PE[a]
3	Farm frozen beef	Cuts from farm-fresh beef, vacuum sealed and stored at −18°C for 14 days	PET/PE
4	Farm chilled beef	Cuts from farm-fresh beef, wrapped in packaging paper or a string bag, and stored at 2°C for 7 days	PAP[b] or PP[c]
5	Farm baked beef	Cuts from farm-fresh beef, wrapped in a baking sleeve or a polyethylene film, subjected to microwave heat treatment and stored at 2°C for 7 days	PET[d] or LDPE[e]
6	Chilled beef sample 1	Obtained from a shop–commercially packaged in a polyethylene bag	LDPE
7	Chilled beef sample 2	Obtained from a shop–commercially packaged using vacuum packaging	PET/PE

[a] *Polyethylene terephthalate/Polyethylene.*
[b] *Paper.*
[c] *Polypropylene.*
[d] *Polyethylene terephthalate.*
[e] *Low-density polyethylene.*

± 0.5, and 65.2 ± 0.7, whereas the fat contents were 16 ± 1, 17.3 ± 0.8, and 18.6 ± 0.7, respectively. Except for commercially packaged and minced beef, all samples were sliced at 10 ± 2 mm thickness. Some samples were subjected to microwave heat treatment for 10 min at a power of 900 W. Each sample was homogenized in a stainless-steel laboratory blender Grindomix GM200 (Retsch GmbH, Haan, Germany) before analysis. The blender was thoroughly cleaned after processing each sample to avoid cross-contamination.

Extraction

To ensure low backgrounds from phthalate contamination, all glassware was rinsed with glass-distilled acetone immediately before use and only glass-distilled or HPLC grade solvents were utilized. At all stages of analysis, contact between food samples and materials other than glass, PTFE, or stainless steel was avoided. Extraction using organic solvents is widely used for phthalates analysis in solid matrix samples, such as food-packaging materials and foods (32). An average sample with a mass of about 10 g was taken from each packaged striploin or minced beef. Average meat samples were blended with the same mass of sodium sulfate and 50 ml of dichloromethane. The supernatant was filtered and removed by rotary evaporation. The weight of extracted fat was determined. Plasticizers were then isolated from aliquots of the lipid material with hexane, then analyzed by gas chromatography coupled with mass spectrometry (GC-MS).

Gas Chromatography

Analysis was carried out by GC-2010 Plus gas chromatograph (Shimadzu, Kyoto, Japan) linked with gas chromatograph-mass spectrometer GCMS-TQ8040. The separation was performed on a cross bonded a 30 m × 0.25 mm I.D. Rxi-5Sil MS column (Restek, Bellefonte, Pennsylvania, USA) coated with 5% diphenyl 95% dimethylpolysiloxane (film thickness 0.25 μm). The oven temperature was programmed from 50°C (holding time 5 min) to 300°C at 5°C min^{-1}. One μl was injected in the injection mode (split ratio 1:10). Helium was used as the carrier gas (1.1 ml min−1), and the injection temperature was set at 250°C. The electron-impact ionization mass spectrometer was

operated as follows: ionization voltage, 70 eV; interface and ion source temperatures were 275°C and 200°C, respectively; scan mode, mass range 40.0–500.0; solvent cut time 2 min. Plasticizer identification was performed by comparing mass spectra with those in the mass spectral library (NIST, Gaithersburg, USA). The phthalates were detected using a SCAN mode (**Figure 1**).

A base peak and a qualifier ion were chosen by the intensity of signals for each phthalate (**Table 2**). The dominant product ion 149 *m/z* was used to quantify all phthalates, except for DMTP. The ion 163 *m/z* was used for DMTP quantification. The qualifier to target the ion ratio of each phthalate had to be <20% of the same in a standard solution for positive identification. The retention times on the Rxi-5Sil MS column, similarity range and the characteristic *m/z* values for these compounds are summarized in **Table 2**.

Quantification was based on comparing the areas of identified peaks with calibration curves in GC-MS Solution software (Shimadzu, Kyoto, Japan). In the studied concentration range, the calibration curves fitted a linear mode ($R^2 > 0.99$). The State Pharmacopeia of the Russian Federation (XIV edition, 2018) indicates that in most cases, linear models are used if they meet the condition $R \geq 0.99$. In our case, for the least-squares model, this corresponds to $R^2 \geq 0.9801$. Also, $R^2 > 0.99$ corresponds to the previously developed methods for determining phthalates in meat (33). Method performance is shown in **Table 3**.

To minimize the risk of contamination, each analytical batch was composed of several samples of blank solvent, standard calibration solutions, a reference, and several experimental samples (five replicates at the most). The whole procedure was carried out using minimum solvents and glassware and as fast and straightforward as possible. Mathematical statistics methods were used for data processing at a theoretical frequency of 0.95. To determine the significant differences between the values, a two-sample *t*-test was used for each pair of means.

RESULTS AND DISCUSSION

Fasano et al. (11) investigated the migration of phthalates from a common form of food packaging. They concluded that simulants may be helpful for identification and comparing

FIGURE 1 | GC–MS chromatograms of standard methanol solutions of DMTP, DnBP, and DiOP in SCAN mode.
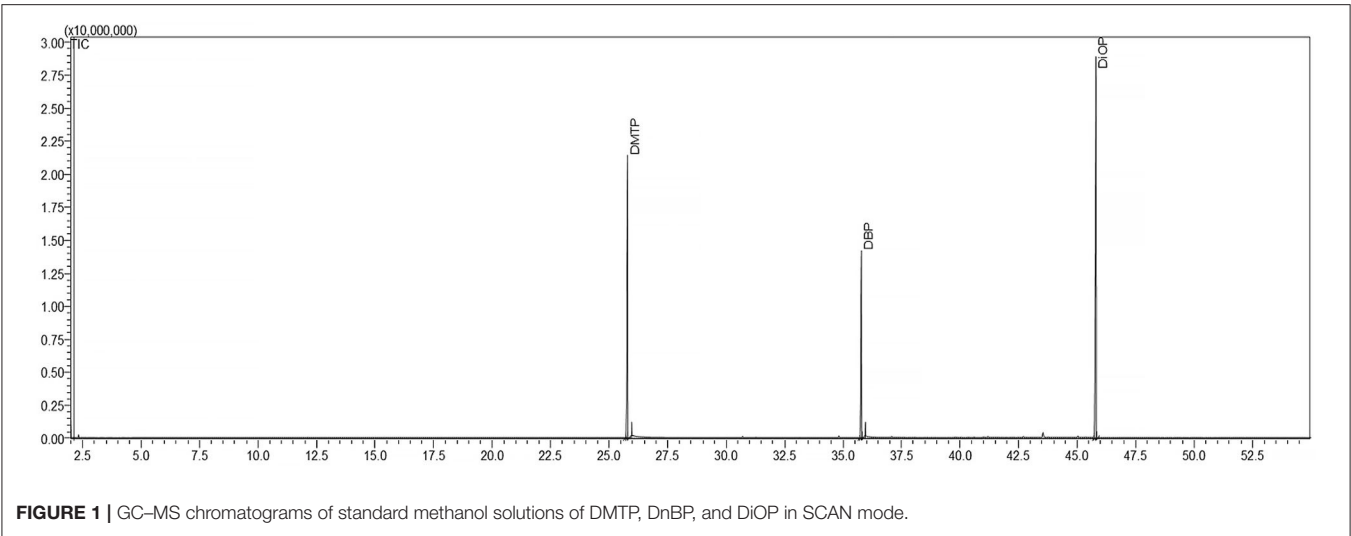
TABLE 2 | Conditions for GC-MS analysis of phthalates.

N	Phthalate compound	Retention time (min)	Base peak (m/z)	Qualifier ion (m/z)	Similarity (%)
1	DMTP	25.7 ± 0.2	163	194	96–98
2	DnBP	35.7 ± 0.2	149	278	93–96
3	DiOP	45.8 ± 0.3	149	390	90–95

TABLE 3 | Method performance for GC-MS analysis of phthalates.

N	Phthalate compound	Recovery (%)	RSD (%)	LOD ($\mu g \cdot kg^{-1}$)	LOQ ($\mu g \cdot kg^{-1}$)
1	DMTP	94	9	1	7
2	DnBP	93	7	2	7
3	DiOP	93	10	3	10

legislated maximum concentrations of compounds migrating from containers. However, this is not always adequate to real conditions, and lately, migration experiments should be performed directly in food. The use of mass spectrometry makes it possible to evaluate the migration of phthalates not only in simple phantom mixtures but also in real objects with a complex matrix (34). So, we used the meat samples as research objects in our study.

Figure 2 shows the typical chromatogram of chilled minced farm beef extract previously stored in a vacuum package. Selected conditions gave an excellent resolution of phthalates peaks, and the matrix did not interfere with the identification. This proves that phthalates could be adequately identified and quantified in all investigated samples.

The food's specific surface area, moisture, fat content, and thermal (microwave) treating impact the degree and rate of migration of harmful substances (11). That is why cut and minced samples were prepared for the research. The effect of temperature on migration was investigated for storage at 2 and −18°C, as well

as after heat treatment using microwave radiation. The results of various beef samples are presented in **Table 4**.

In general, the obtained values of phthalate concentrations vary wildly, even for the same type of plastic. This might be attributed to the fact that each plastic material uses different plasticizers and additives.

We have found phthalates in the farm-fresh beef that has been collected directly after the slaughter at the farm with no contact with any packaging materials. This finding suggests phthalates contamination of farm fodder or water, which necessitated further research.

The use of all packaging and processing options for farm fresh beef increased phthalate content compared to untreated and unpackaged samples. This indicates the migration of these xenobiotics from all types of the investigated packaging for almost any condition. The large contact area and the presence of more fat on the surface of the minced meat resulted in significantly higher phthalate migration (DnBP: 378.5 $\mu g \cdot kg^{-1}$, DiOP: 37 $\mu g \cdot kg^{-1}$) than beef slices (DnBP: 88.2 $\mu g \cdot kg^{-1}$, DiOP: 12.2 $\mu g \cdot kg^{-1}$). Deserves attention, frozen storage resulted in nearly the same phthalate levels (DnBP: 89 $\mu g \cdot kg^{-1}$, DiOP: 10 $\mu g \cdot kg^{-1}$) as refrigerated storage (DnBP: 88.2 $\mu g \cdot kg^{-1}$, DiOP: 12.2 $\mu g \cdot kg^{-1}$). This is probably due to phthalates migration during freezing and thawing since it is evident that the migration of components at −18°C should be very slow. This requires further research. However, as a primary recommendation, more intensive freezing of packaged meat products and defrosting outside plastic packaging can be proposed.

FIGURE 2 | GC–MS chromatogram of an extract of chilled minced farm beef in a vacuum package.
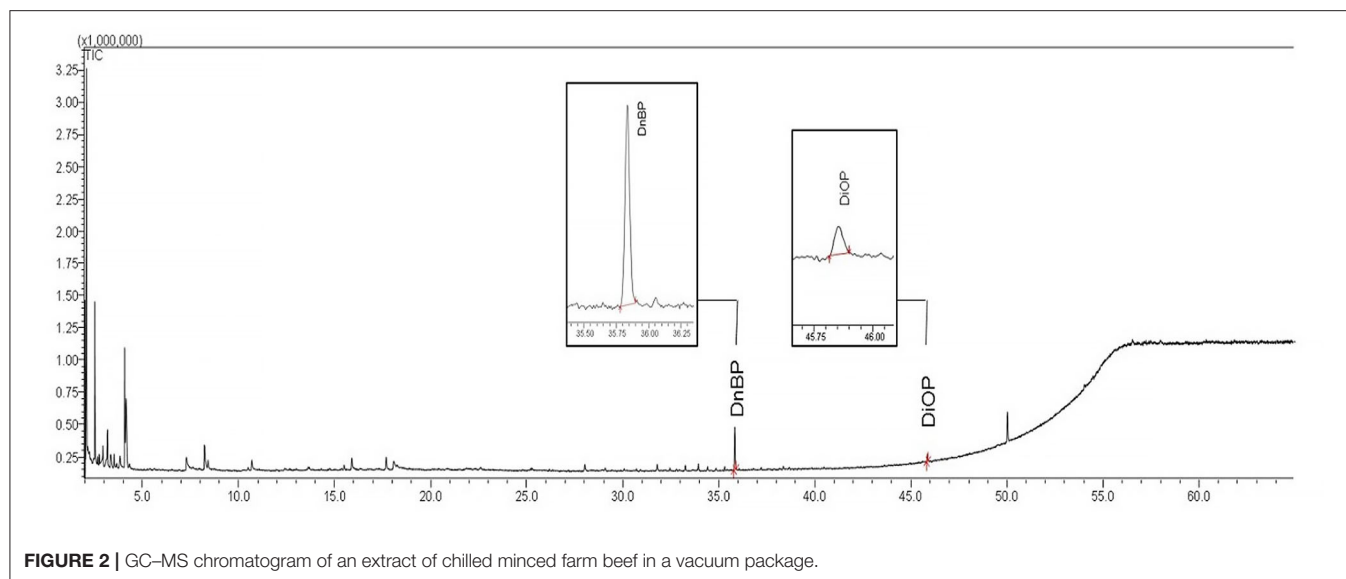
TABLE 4 | Levels of phthalates in beef samples $\mu g \cdot kg^{-1}$ (mean ± sd).

N	Food	Packaging	DMTP	DnBP	DiOP
1	Farm fresh beef	–	ND*	35.1 ± 0.2a	ND
2	Chilled minced farm beef	Vacuum package	ND	378.5 ± 0.1b	37 ± 1s
3	Chilled farm beef	Vacuum package	ND	88.2 ± 0.5c	12.2 ± 0.1t
4	Frozen farm beef	Vacuum package	ND	89 ± 1d	10 ± 1u
5	Chilled farm beef	Paper	ND	41 ± 2e	11 ± 2t,u
6	Chilled farm beef	String bag	ND	73.2 ± 0.4f	23.2 ± 0.3v
7	Baked farm beef	Baking sleeve	ND	34.5 ± 0.7a	15.2 ± 0.4w
8	Baked farm beef	Polyethylene package	ND	75 ± 3f	24 ± 2v
9	Chilled beef sample 1	Polyethylene package	ND	38 ± 2g	10 ± 1u
10	Chilled beef sample 2	Vacuum package	ND	43.8 ± 0.8h	<10**

*ND, not detected. ** <10 indicates that the value was lower than LOQ, but higher than LOD. Different lower-case letters indicate significant differences among samples for each phthalate (p < 0.05).

DnBP showed the highest mean values for most samples ranging from 34.5 to 378.5 $\mu g \cdot kg^{-1}$. DiOP displayed the lower mean values, ranging from LOD to 37 $\mu g \cdot kg^{-1}$. Particular attention should be paid to the fact that according to regulatory documents in Russia, DnBP presence in food is not allowed. The European Union regulation EC No. 11/2011 also states that DnBP is not allowed in fat-containing food. DiOP contents correspond to Russian normative documents (CU TR 005/2011). Also, they correspond to the European Union regulation EC No. 10/2011, which established a limit of 60 $mg \cdot kg^{-1}$ for DiOP in food products. Regarding phthalates regulation, the USA and the European Union have harmonized their directives and implemented a "threshold policy" (35). Thus, the conclusions drawn regarding the obtained DnBP and DiOP concentrations for the European Union are also relevant for the United States. Polyethylene terephthalate (PET) used in the study is usually made with the addition of DMTP, and it was expected to be found. However, DMTP could not be recovered and was not detected in any samples. Thus, the DMTP concentration was

below the LOD in the studied samples. One of the possible reasons for this may be its less use in the production of plastic packaging since it is more used as solvent and fixative in fragrances, additive in cosmetics, medical devices, and household and personal care products (36).

Analysis of phthalates in foods sold on the Belgian market revealed DnBP in 14 out of 22 meat and meat products with concentrations of up to 15.0 $\mu g \cdot kg^{-1}$ (37). These concentrations in beef correlated with predicted by environmental food transfer model for organic contaminants in Europe (5). DnBP was determined in all the analyzed samples of spices used to cook the chicken meat in concentrations ranging from 3.47 to 29.3 $\mu g \cdot kg^{-1}$ (38). The chicken meat samples roasted with spices in a plastic bag presented concentrations from 0.1 to 1.17 $\mu g \cdot kg^{-1}$ for DnBP. DnBP was the most frequently detected ortho-phthalate in USA fast food samples (39). It was detected in 81% of all food items in median concentrations of 2.4–4.8 $\mu g \cdot kg^{-1}$. A study of convenience meat products on the Chinese market (40) found a median DnBP content of 336 $\mu g \cdot kg^{-1}$ for 48 samples. Also,

TABLE 5 | Estimated DI levels of DnBP residues in beef and their percentage of TDI level in adults.

N	Food	Packaging	DI (µg·kg^{-1}·day^{-1})	% of TDI
1	Farm fresh beef	–	0.016	0.16
2	Chilled minced farm beef	Vacuum package	0.167	1.67
3	Chilled farm beef	Vacuum package	0.039	0.39
4	Frozen farm beef	Vacuum package	0.039	0.39
5	Chilled farm beef	Paper	0.018	0.18
6	Chilled farm beef	String bag	0.032	0.32
7	Baked farm beef	Baking sleeve	0.015	0.15
8	Baked farm beef	PE package	0.033	0.33
9	Chilled beef sample 1	PE package	0.017	0.17
10	Chilled beef sample 2	Vacuum package	0.019	0.19

it was found that the migration of the phthalates into foods increased with time and the temperature and their content in the convenience foods near the shelf-life was much higher than those which were just manufactured. This study confirms these trends concerning plastic packaging available on the Russian market. Research on phthalates in food packaged in various types of plastics worldwide suggests a need to carefully analyze their overall consumption and assess the associated health risks (33, 35).

Besides polymer packages, we found phthalates in foods stored in wrapping paper. The chilled farm beef samples wrapped in paper contained DnBP and DiOP 41 and 11 µg·kg^{-1}, respectively. The possible reason is the use of recycled cartons to produce paper. Using recycled fibers comes with new challenges, such as controlling potential packaging contamination by harmful chemicals introduced by using pre-and post-consumer waste. Numerous studies have revealed the migration of various contaminants, such as phthalates (41), diisopropyl naphthalenes, benzophenones and others (42). In a study conducted by USA Food and Drug Administration scientists reported detectable concentrations of DnBP in paper-based fast food packaging collected from restaurants (31). Also, this is understandable, as phthalate compounds are widely used additives for printing inks and lacquers in food contact materials.

Daily intake (DI) was determined and compared with its tolerable daily intake (TDI) value established by the European Food Safety Authority to assess the health risks of human exposure to phthalate residues in beef. The DnBP TDI value is 10 µg·kg^{-1} body weight a day (23). Since no TDI values have been established for DiOP, the risk assessment was carried out only in relation to the detected DnBP. The DI (µg·kg^{-1}·day^{-1}) was determined by multiplying the daily beef consumption (kg·day^{-1}) by obtaining mean DnBP concentration (µg·kg^{-1}) and dividing by human body weight (kg). The daily beef consumption value of 27.4 g (0.0274 kg·day^{-1}) was obtained by dividing the stated annual beef consumption in Russia by 10 kg·year^{-1} by 365 (43). An average body weight of 62 kg for adults was used as a reference value (44). The results are indicated in **Table 5**.

Thus, the daily intake did not exceed TDI for all types of packaging and beef processing. At the same time, the largest percentage of TDI was determined for chilled minced beef in vacuum packaging. In the annual and, accordingly, the average daily beef consumption is 1.36% (10 kg per year of beef from 735.6 kg per year of all food products) (45). Thus, if we assume a similar level of phthalates translocation from plastic packaging to other food products, as well as previously unaccounted drinking water, the daily intake of DnBP and other phthalates may exceed TDI. Thus, it is necessary to reduce the amount of plastic packaging and reduce the content and migration of phthalates into food from it. Also, an obvious conclusion is a need for the global introduction of new types of packaging materials without phthalates. Bio-based resources can be a base for producing biopolymers in food packaging applications instead of conventional plastics traditionally produced from fossil fuels. Microorganisms can produce biopolymers through fermentative processes of different bioresources (e.g., polyhydroxyalkanoates), and biomass may be produced directly from different types of plants (starch, cellulose, pectin, zein, gluten) and animal materials (chitosan, gelatin, caseins) (46). Biopolymer production does not include phthalates as glyceryl monoesters, glycerol, fatty acids, and polyethylene glycol are used as common plasticizers (47).

CONCLUSIONS

The Technical Regulations TR 005/2011 on the safety of the packaging were adopted in 2011 in the Russian Federation. This document defined allowable migration amounts for DiOP of 2.00 mg·L^{-1}, and migration of DnBP into food products was not allowed. The examined food packages from the Russian market do not meet the requirements of this standard, as DnBP migrates to food products. Perhaps the manufacturers are still using the previous instruction from 1972, according to which the allowable migration amounts for DnBP was 0.25 mg·L^{-1}. The obtained results require discussion by all participants of the production processes and the use and control of food packaging materials.

The most alarming results obtained in this study are the presence of phthalates in beef produced on a farm in the Leningrad region and not subjected to packaging. Presumably, phthalates could enter animals' diet along with fodder, compound feed, or water. A full-scale study is needed to determine the pathways and sources of phthalates migration in the food chain. The implementation of separate collection and recycling of plastic materials in Russia may be a way to reduce the contamination of farm animals food chains with phthalates. Moreover, this should be carried out in such a way as to avoid cross-contamination of materials, for example, recycled paper. In addition, it is necessary to strive to reduce the use of plastic packaging. At present, both the encapsulated forms of food ingredients (48) and the edible food coatings that increase food shelf-life are being developed to improve product stability during storage (49).

DATA AVAILABILITY STATEMENT

The raw data supporting the conclusions of this article will be made available by the authors, without undue reservation.

AUTHOR CONTRIBUTIONS

DB contributed to the study concept. DB and AE-A critically reviewed the article. DB, MB, IB, BA, and WL contributed to the design of the manuscript and figure preparation and edition. DB, MB, IB, BA, WL, and AE-A contributed to the acquisition and analysis of data and drafted the manuscript. All authors gave final approval for all aspects of the work, agreed to be fully accountable for ensuring the integrity and accuracy of the work, read, and approved the final manuscript.

FUNDING

REFERENCES

1. Fromme H, Gruber L, Schlummer M, Wolz G, Boehmer S, Angerer J, et al. Intake of phthalates and di(2-ethylhexyl)adipate: results of the integrated exposure assessment survey based on duplicate diet samples and biomonitoring data. *Environ Int.* (2007) 33:1012–20. doi: 10.1016/j.envint.2007.05.006

2. Bopp K, Altkofer W. Survey on intake of certain phthalic acid esters in South Germany: comparative study of two boarding schools with conventional and organic nutrition. *Dtsch Lebensm Rundsch.* (2009) 105:35–8.

3. *COT Statement on Dietary Exposure to Phthalates–Data from the Total Diet Study (TDS)*. London, United Kingdom: Committee on Toxicity of Chemicals in Food, Consumer Products and the Environment.

4. Schecter A, Lorber M, Guo Y, Wu Q, Yun SH, Kannan K, et al. Phthalate concentrations and dietary exposure from food purchased in New York State. *Environ Health Perspect.* (2013) 121:473–9. doi: 10.1289/ehp.1206367

5. Fierens T, Servaes K, Van Holderbeke M, Geerts L, De Henauw S, Sioen I, et al. Analysis of phthalates in food products and packaging materials sold on the Belgian market. *Food and Chem Toxicol.* (2012) 50:2575–83. doi: 10.1016/j.fct.2012.04.029

6. Dodson RE, Nishioka M, Standley LJ, Perovich LJ, Brody JG, Rudel RA. Endocrine disruptors and asthma-associated chemicals in consumer products. *Environ Health Perspect.* (2012) 120:935–43. doi: 10.1289/ehp.1104052

7. Rusyn I, Peters JM, Cunningham ML. Modes of action and species-specific effects of di-(2-ethylhexyl)phthalate in the liver. *Crit Rev Toxicol.* (2006) 36:459–79. doi: 10.1080/10408440600779065

8. Calafat AM, Ye X, Silva MJ, Kuklenyik Z, Kuklenyik Z, Needham LL. Human exposure assessment to environmental chemicals using biomonitoring. *Int J Androl.* (2006) 29:166–71. doi: 10.1111/j.1365-2605.2005.00570.x

9. Frederiksen H, Skakkebæk NE, Andersson AM. Metabolism of phthalates in humans. *Mol Nutr Food Res.* (2007) 51:899–11. doi: 10.1002/mnfr.200600243

10. Ghisari M, Bonefeld-Jorgensen EC. Effects of plasticizers and their mixtures on estrogen receptor and thyroid hormone functions. *Toxicol Let.* (2009) 189:67–7. doi: 10.1016/j.toxlet.2009.05.004

11. Fasano E, Bono-Blay F, Cirillo T, Montuori P, Lacorte S. Migration of phthalates, alkylphenols, bisphenol A and di(2-ethylhexyl)adipate from food packaging. *Food Control.* (2012) 27:132–8. doi: 10.1016/j.foodcont.2012.03.005

12. Silva MJ, Samandar E, Preau JJL, Reidy JA, Needham LL, Calafat AM. Quantification of 22 phthalate metabolites in human urine. *J Chromatogr B.* (2007) 860:106–12. doi: 10.1016/j.jchromb.2007.10.023

13. Meeker JD, Ferguson KK. Phthalates: human exposure and related health effects In: Schecter A, editor. *Dioxins and Health: Including Other Persistent Organic Pollutants and Endocrine Disruptors*. Hoboken: Wiley (2012). p. 415–43.

14. Snedeker SM, Rudel RA, Just AC. Phthalates in Food Packaging, Consumer Products, and Indoor Environments. In: Snedeker SM, editor. *Toxicants in Food Packaging and Household Plastics*. London: Springer (2014). p. 31–59.

15. Schettler T. Human exposure to phthalates *via* consumer products. *Int J Androl.* (2006) 29:134–9. doi: 10.1111/j.1365-2605.2005.00567.x

16. Wormuth M, Scheringer M, Vollenweider M, Hungerbuhler K. What are the sources of exposure to eight frequently used phthalic acid esters in Europeans? *Risk Analysis.* (2006) 26:803–24. doi: 10.1111/j.1539-6924.2006.00770.x

17. Rudel RA, Gray JM, Engel CL, Rawsthorne TW, Dodson RE, Ackerman JM, et al. Food packaging and bisphenol A and bis(2-ethyhexyl) phthalate exposure: findings from a dietary intervention. *Environ Health Perspect.* (2011) 119:914–20. doi: 10.1289/ehp.1003170

18. Kaspars K, Dzene KP, Blumberga D. Optimal strategies for municipal solid waste treatment–environmental and socio-economic criteria assessment. *Energy Procedia.* (2017) 128:512–19. doi: 10.1016/j.egypro.2017.09.071

19. Barisa A, Dzene I, Rosa M, Dobraja K. Waste-to-biomethane concept application: a case study of Valmiera city in Latvia. *Env Clim Tech.* (2015) 15:48–58. doi: 10.1515/rtuect-2015-0005

20. Aydin N. Review of Municipal Solid Waste Management in Turkey with a Particular Focus on Recycling of Plastics. *Energy Procedia.* (2017) 113:111–5. doi: 10.1016/j.egypro.2017.04.031

21. Yogalakshmi KN, Singh S. Plastic waste: environmental hazards, its biodegradation, and challenges. In: Saxena G, Bharagava RN, editors. *Bioremediation of Industrial Waste For Environmental Safety*. Singapore: Springer (2020). p. 99–133.

22. European Food Safety Authority (EFSA). Opinion of the Scientific Panel on food additives, flavourings, processing aids and materials in contact with food (AFC) related to di-Butylphthalate (DBP) for use in food contact materials. *EFSA J.* (2005) 3:242. doi: 10.2903/j.efsa.2005.242

23. European Food Safety Authority (EFSA). Opinion of the scientific panel on food additives, flavourings, processing aids and materials in contact with food (AFC) on a request from the commission related to butylbenzylphthalate (BBP) for use in food contact materials. *EFSA J.* (2005) 241:1–14. doi: 10.2903/j.efsa.2005.241

24. European Food Safety Authority (EFSA). Opinion of the scientific panel on food additives, flavourings, processing aids and materials in contact with food (AFC) on a request from the commission related to di-isononylphthalate (DINP) for use in food contact materials. *EFSA J.* (2005) 244:1–18. doi: 10.2903/j.efsa.2005.244

25. European Food Safety Authority (EFSA). Opinion of the scientific panel on food additives, flavourings, processing aids and materials in contact with food (AFC) on a request from the commission related to di-isodecylphthalate (DIDP) for use in food contact materials. *EFSA J.* (2005) 245:1–14. doi: 10.2903/j.efsa.2005.245

26. European Food Safety Authority (EFSA). Opinion of the scientific panel on food additives, flavourings, processing aids and materials in contact with food (AFC) on a request from the commission related to bis(2-ethylhexyl)phthalate (DEHP) for use in food contact materials. *EFSA J.* (2005) 243:1–20. doi: 10.2903/j.efsa.2005.243

27. Ibarra VG, de Quirós ARB, Losada PP, Sendón R. Identification of intentionally and non-intentionally added substances in plastic packaging materials and their migration into food products. *Anal Bioanal Chem.* (2018) 410:3789–803. doi: 10.1007/s00216-018-1058-y

28. Varshavsky JR, Morello-Frosch R, Woodruff TJ, Zota AR. Dietary sources of cumulative phthalates exposure among the US general population in NHANES 2005–2014. *Environ Int.* (2018) 115:417–29. doi: 10.1016/j.envint.2018.02.029

29. Alp AC, Yerlikaya P. Phthalate ester migration into food: effect of packaging material and time. *Eur Food Res Technol.* (2020) 246:425–35. doi: 10.1007/s00217-019-03412-y

30. Perestrelo R, Silva CL, Algarra M, Câmara JS. Evaluation of the occurrence of phthalates in plastic materials used in food packaging. *Appl Sci.* (2021) 11:2130. doi: 10.3390/app11052130

31. Carlos KS, de Jager LS, Begley TH. Determination of phthalate concentrations in paper-based fast food packaging available on the US market. *Food Addit Contam A.* (2021) 38:501–12. doi: 10.1080/19440049.2020.1859623

32. Gomez-Hens A, Aguilar-Caballos MP. Social and economic interest in the control of phthalic acid esters. *Trend Anal Chem.* (2003) 22:847–57. doi: 10.1016/S0165-9936(03)01201-9

33. Tsai MY, Ho CH, Chang HY, Yang WC, Lin CF, Lin CT, et al. Analysis of Pollution of Phthalates in Pork and Chicken in Taiwan Using Liquid Chromatography–Tandem Mass Spectrometry and Assessment of Health Risk. *Molecules.* (2019) 24:3817. doi: 10.3390/molecules24213817

34. Guerreiro TM, de Oliveira DN, Melo CFOR, de Oliveira Lima E, Catharino RR. Migration from plastic packaging into meat. *Food Res Int.* (2018) 109:320–4. doi: 10.1016/j.foodres.2018.04.026

35. Giuliani A, Zuccarini M, Cichelli A, Khan H, Reale M. Critical review on the presence of phthalates in food and evidence of their biological impact. *Inter J Env Res Pub Health.* (2020) 17:5655. doi: 10.3390/ijerph17165655

36. Wypych A. *Databook of Plasticizers.* ChemTec Publishing:Toronto (2017). p. 710.

37. Fierens T, Cornelis C, Standaert A, Sioen I, De Henauw S, Van Holderbeke M. Modelling the environmental transfer of phthalates and polychlorinated dibenzo-p-dioxins and dibenzofurans into agricultural products: the EN-forc model. *Env Res.* (2014) 133:282–93. doi: 10.1016/j.envres.2014.06.005

38. Moreira MA, André LC, de Lourdes Cardeal Z. Analysis of plasticiser migration to meat roasted in plastic bags by SPME–GC/MS. *Food Chem.* (2015) 178:195–200. doi: 10.1016/j.foodchem.2015.01.078

39. Edwards L, McCray NL, VanNoy BN, Yau A, Geller RJ, Adamkiewicz G, Zota AR. Phthalate and novel plasticizer concentrations in food items from U.S. fast food chains: a preliminary analysis. *J Expo Sci Environ Epidemiol.* (2021). doi: 10.1038/s41370-021-00392-8

40. Yang J, Song W, Wang X, Li Y, Sun J, Gong W, et al. Migration of phthalates from plastic packages to convenience foods and its cumulative health risk assessments. *Food Addit Contam Part B Surveill.* (2019) 12:151–8. doi: 10.1080/19393210.2019.1574909

41. Aurela B, Kulmala H, Soderhjelm L. Phthalates in paper and board packaging and their migration into Tenax and sugar. *Food Addit Contam.* (1999) 16:571–7. doi: 10.1080/026520399283713

42. Tiggelman I. *Migration of Organic Contaminants Through Paper and Plastic Packaging* [master's thesis]. [Stellenbosch], South Africa: University of Stellenbosch (2012).

43. Gorlov IF, Fedotova GV, Slozhenkina MI, Mosolova NI. The meat products supply of population in Russia. In: Popkova EG, editor. *Growth Poles of the Global Economy: Emergence, Changes and Future Perspectives.* Cham: Springer (2020). p. 311–8.

44. Walpole SC, Prieto-Merino D, Edwards P, Cleland J, Stevens G, Roberts I. The weight of nations: an estimation of adult human biomass. *BMC Public Health.* (2012) 12:439. doi: 10.1186/1471-2458-12-439

45. Antamoshkina EN, Rogachev AF. The model of statistical assessment of food security. In: Bogoviz AV, editor. *Complex Systems: Innovation and Sustainability in the Digital Age.* Cham: Springer (2020) p. 471–9.

46. Grujić R, Vujadinović D, Savanović D. Biopolymers as food packaging materials. In: Pellicer E, Nikolic D, Sort J, Baró M, Zivic F, Grujovic N, Pelemis S, editors. *Advances in Applications of Industrial Biomaterials.* Cham: Springer (2017) p. 139–60.

47. Vasiljevic L, Pavlovi S. Biodegradable Polymers Based on Proteins and Carbohydrates. In: Pellicer E, Nikolic D, Sort J, Baró M, Zivic F, Grujovic N, Pelemis S, editors. *Advances in Applications of Industrial Biomaterials.* Cham: Springer (2017) p. 87–101.

48. Zabodalova L, Ishchenko T, Skvortcova N, Baranenko D, Chernjavskij V. Liposomal beta-carotene as a functional additive in dairy products. *Agronomy Res.* (2014) 12:825–34.

49. Baranenko DA, Kolodyaznaya VS, Zabelina NA. Effect of composition and properties of chitosan-based edible coatings on microflora of meat and meat products. *Acta Sci Pol Technol Alimen.* (2013) 12:149–57.

Conflict of Interest: The reviewer (FO) declared a shared affiliation with one of the authors, (AE-A), to the handling editor at the time of review.

The authors declare that the research was conducted in the absence of any commercial or financial relationships that could be construed as a potential conflict of interest.

Publisher's Note: All claims expressed in this article are solely those of the authors and do not necessarily represent those of their affiliated organizations, or those of the publisher, the editors and the reviewers. Any product that may be evaluated in this article, or claim that may be made by its manufacturer, is not guaranteed or endorsed by the publisher.

Check for
updates

Tea Tree Oil Terpinen-4-ol Protects Gut Barrier Integrity by Upregulation of Tight Junction Proteins *via* the ERK1/2-Signaling Pathway

Yanhong Yong[1,2], Biao Fang[2], Yingxin Huang[2], Junyu Li[3], Tianyue Yu[3], Lianyun Wu[3], Canying Hu[3], Xiaoxi Liu[1], Zhichao Yu[2], Xingbin Ma[2], Ravi Gooneratne[4], Sidong Li[5], A. M. Abd El-Aty[6,7] and Xianghong Ju[1,2]*

[1] Shenzhen Institute of Guangdong Ocean University, Shenzhen, China, [2] Department of Veterinary Medicine, College of Agricultural Sciences, Guangdong Ocean University, Zhanjiang, China, [3] Department of Animal Science, College of Agricultural Sciences, Guangdong Ocean University, Zhanjiang, China, [4] Department of Wine, Food and Molecular Biosciences, Faculty of Agriculture and Life Sciences, Lincoln University, Lincoln, New Zealand, [5] College of Chemistry and Environment, Guangdong Ocean University, Zhanjiang, China, [6] Department of Pharmacology, Faculty of Veterinary Medicine, Cairo University, Giza, Egypt, [7] Department of Medical Pharmacology, Medical Faculty, Ataturk University, Erzurum, Turkey

Tea tree oil (TTO) exhibits a potent antioxidant, antibacterial, and anti-inflammatory activity and is commonly used in skincare products. However, it is not clear whether TTO can protect gut barrier damage in inflammatory bowel disease (IBD) patients. Herein, we report the impact of terpinen-4-ol (TER, the primary constituent of TTO), on lipopolysaccharide (LPS)-induced intestinal epithelial cell barrier function impairment in intestinal porcine epithelial cell lines (IPEC-J2) and dextran sulfate sodium (DSS)-induced IBD in mice. TER protected against LPS-induced damage in IPEC-J2 cells *in vitro* and attenuated DSS-induced colitis *in vivo*. Added TER promoted the tight junction (TJ) proteins expressing *in vitro* and *in vivo* and attenuated the LPS-induced upregulation of ERK phosphorylation in IPEC-J2 cells. However, when an inhibitor of ERK phosphorylation was added, TER did not promote the expression of TJ protein, denoting that the ERK signaling pathway mediates the upregulation of TJ proteins. Our data may propose the potential application of TER in treating IBD.

Keywords: inflammatory bowel disease, terpinen 4-ol, ERK1/2-signaling pathway, tight junction (TJ) proteins, mouse model

INTRODUCTION

Inflammatory bowel disease (IBDs) is a chronic inflammatory disease of the gastrointestinal tract, which comprises Crohn's disease (CD), ulcerative colitis (UC), and indeterminate colitis (1). This disease affects all ages, and the clinical features primarily include fever, weight loss, diarrhea, and blood in stool (2). Although the exact causes of CD and UC are not well documented, previous studies have shown that genetic factors, immune system dysfunction, and environmental factors might play a crucial role in its occurrence (3). The lesions of IBD patients are mainly confined to the colorectal mucosa and submucosa. They are characterized by mucosal barrier damage and impaired tight junction (TJ) functions, resulting in a loss in gut barrier integrity (4).

Tight junctions between epithelial cells play a role in maintaining the permeability and integrity of the intestinal mucosal barrier. Occludin, claudins, and zonula occludens-1 (ZO-1) are the

essential adhesion proteins responsible for the efficient functioning of TJs in the intestinal lining (5). The intestinal mucosal barrier is damaged in IBD patients, and the expression of the TJ proteins ZO-1, claudin, and occludin was decreased in the intestine (6). Otherwise, the upregulation of both ZO-1 and occludin expression significantly improves the integrity, reduces the intestinal mucosal barrier permeability, and prevents the infiltration of harmful substances in IBD patients (7, 8).

There are no drugs to cure IBD, and, at best, they serve to minimize the disease process (9). Drugs commonly used for IBD treatment, include corticosteroids, immunosuppressants, and immunomodulators, which may induce adverse effects on long-term usage (10). Therefore, it has been proposed that IBD patients be treated to restore the mucosal barrier function and thereby relieve the clinical symptoms and cure IBD (11). Given that TJ protein expression levels are closely related to the mucosal barrier function, we speculated that developing a "natural" drug that can normalize TJ function may be an approach for treating IBD.

Tea tree oil (TTO) is extracted from *Melaleuca alternifolia*. Because of its broad-spectrum antimicrobial (bacteria, fungi, and viruses), anti-cancer, anti-tussive, and antioxidant properties (12). TTO is widely used to treat acne, athlete's foot, and contact dermatitis. TTO contains over 100 components, including terpineol, zinc, and diheptoxy-sulfanylidene-sulfido-λ5–phosphane (13), the most crucial being terpinen-4-ol (TER), which accounts for >30% of all TTO components. Currently, TER is widely used in the food industry. For instance, as an antistaling agent, TER can alter the microbial biofilm formation in foods, thereby preventing food deterioration and reducing the incidence of certain foodborne illnesses (14). TER has inhibitory activity against certain aerobic heterotrophic bacteria in food (15). It has also been used as a spice to reduce breast cancer incidence (16). Mechanistically, TER can downregulate the secretion of the inflammatory signaling molecule, NO, which is induced by lipopolysaccharide (LPS) and dioctyl sodium sulfosuccinate (DSS) (17, 18). In addition, TER plays a role in regulating the mitogen-activated protein kinase (MAPK)-signaling pathway (19), which is intimately involved in the expression of TJ proteins (20). Hence, we hypothesized that TER would be a promising candidate for IBD therapy. In this study, we examined the effects and mechanisms of TER in protection against LPS/DSS-induced inflammation, both *in vitro* and *in vivo*.

MATERIALS AND METHODS

Fourier-Transform Infrared Spectroscopy (FTIR) Analysis

TER was a gift from Professor Sidong Li's laboratory. His group isolated TER from TTO, the essential oil extracted from *Melaleuca alternifolia*. The protocol of FTIR analysis was conducted as described by Linshi and modifications (21). Briefly, samples were dissolved in heavy water (D_2O) and detected with a Bruker Tensor 27 infrared spectrometer (Shanghai, China) with a resolution of 4.0 cm^{-1} and a scan range of 400–4,000 cm^{-1}.

An average of 64 scans was required to obtain information about the structure.

Cell Culture

IPEC-J2 cells were generously donated by Dr. Bruce Schultz of Kansas State University. The cells were seeded in a T25 flask (Corning Inc., Corning, NY, USA) and cultured in an incubator at 37 °C and 5% CO_2. The cells were grown in DMEM/F12 (Sigma-Aldrich, St. Louis, MO, USA) added with 100 U/mL penicillin, 100 μg/mL streptomycin, and 10% fetal bovine serum. After the cells were grown to sub-confluence in 24-well plates, the culture medium was removed, and the cells were washed twice with phosphate-buffered saline (PBS). Subsequently, the cells were exposed to LPS with or without TER.

Cell Viability Assay

A Cell Counting Kit-8 (CCK8, MedChemExpress, Shanghai, China) was used to detect the viability of cells as described by Linshi and modifications (21). Briefly, the IPEC-J2 cells were scattered into 96-well plates and cultured for 24 h, then treated with TER (0, 0.001, 0.002, 0.004, 0.006, 0.008, 0.01, 0.016, and 0.02%) for another 24 h, then incubated with 10 μL of CCK8 solution. Next, the absorbance at 450 nm was detected by the plate reader.

Determination of Epithelial Cell Integrity

The protocol of epithelial cell integrity detection was according to the methods reported by Linshi et al. (21). Briefly, cells were scattered at a 1×10^5 cells/mL density into Trans-well-COL (Corning). The cells were cultured in a 37 °C, 5% CO_2 incubator for 13–15 days until they reached a complete polarization, and the culture media was refreshed per 2 days. After the fused monolayer epithelial cells were formed, serial concentrations (as described above) of TER were added and treated for 24 h. Next, 10 μg/mL LPS was added to Trans-well plates' upper compartment (22). The Millicell ERS-2 Voltohmmeter (Millipore, Billerica, MA, USA) were used to measure Trans-epithelial electrical resistance (TEER) of monolayer epithelia at 0, 12, and 24 h. 4-kDa fluorescein isothiocyanate-labeled dextran (FITC-dextran, Sigma-Aldrich). FITC-dextran was dissolved in DMEM/F12 and added to the upper compartment with a 2.2 mg/mL concentration. Two hours later, the lower compartment fluorescence intensity was detected by fluorometry (Tecan Group, Switzerland; excitation, 490 nm; emission, 520 nm).

qRT-PCR

The total RNA of cells and tissue were extracted by the standard method using TRIzol® Reagent (Takara, Dalian, China). The quality of extracted RNA was analyzed by the ratio of A260/A280 using spectrometry. Then, the RNA was reverse transcribed to cDNA using the PrimeScript RT reagent kit (Takara, Dalian, China). Next, the SYBR® Premix Ex Taq™ II (Takara, Dalian, China) were used to perform qRT-PCR. The gene expression level was analyzed by the ΔΔCT method (23). The primers used in the reaction are shown in **Table 1**.

Western Blotting

The western blotting was performed as Linshi reported methods and modification. RIPA Lysis Buffer (Beyotime Biotechnology, Shanghai, China) and extraction kits (ThermoFisher Scientific, Shanghai, China) were used to isolate the total proteins, a nuclear protein, and cytoplasmic proteins, respectively. The protein concentration was analyzed using a BCA reagent (CWBIO, Beijing, China) followed by SDS-PAGE and electrotransfer of separated protein lysates to nitrocellulose membranes (Millipore). After 1 h of blocking, the membranes were incubated with a primary antibody at 4°C for overnight, then incubated with the secondary antibody for 2 h at room temperature. Positive bands were measured by enhanced chemo-luminescence (Tanon, Shanghai, China). Gel-Pro Analyzer software version 4.0 (Media Cybernetics, Silver Spring, MD, USA) was used to analyse the densitometry. Antibodies against ZO-1 (ab96587), occludin (ab167161), claudin-1 (ab129119), and claudin-4 (ab15104) were obtained from Abcam (Cambridge, MA, USA). The antibody against ERK (4695S), P-ERK (4370S), and β-actin (4970S) were secured from CST (CST, MA, USA).

TABLE 1 | Primer sequence.

Primer	Sequence (5′–3′)
claudin-1 forward	GTGGATGTCCTGCGTGTC
claudin-1 reverse	GTGTTGGGTAAGATGT TGTTTT
claudin-4 forward	TTCATCGGCAGCAACAT
claudin-4 reverse	AGGACACGGGCACCAT
Occludin forward	ATCAACAAAGGCAA
Occludin reverse	CTCCGTAATGACCAGA
ZO-1 forward	GCCTCCTGAGTTTGATAGTG
ZO-1 reverse	TCGGCAGACCTTGAAATAGA
β-actin forward	TGCGGGACATCAAGGAGAAG
β-actin reverse	AGTTGAAGGTAGT TTCGTGG

Enzyme-Linked Immunosorbent Assay

The cell culture supernatant was stored at −20 °C before analysis. According to the manufacturer's instructions, the IL-6 concentration and TNF-α concentration were detected by ELISA Kit (IL-6, P6000B; TNF-α, PTA00; R & D Systems, Inc. Minneapolis, MN, USA). The plates were read by a microplate reader (BioTek Instruments, INC, USA) at 405 nm wavelength.

Animal Experiments

The six-week-old male mice (C57BL6/J) were reared in the Animal Housing Unit and controlled environmental temperature around 24 ± 1°C with a 12-h light/12-h dark cycle. The experimental protocols used were as follows (a brief protocol is shown in **Figure 1**). The mice were randomly allocated into one of six groups (five animals per group), namely the control, PBS (PBS, i.p.), DSS, DSS + TER-L (5 mg·kg^{-1}·day^{-1}, i.p.), DSS + TER-M (10 mg·kg^{-1}·day^{-1}, i.p.), and DSS + TER-H (20 mg·kg^{-1}·day^{-1}, i.p.). After TER pre-treatment, DSS (2%, v/w, MW 36,000–50,000, MP Biomedicals, Aurora, OH) was added to drinking water from days 15 to 21. All experimental protocols were approved by the Animal Ethics Committee of Guangdong Ocean University, China (Clearance No. 2018-0008) and performed according to the European Community Ethical Guidelines (Directive 2010/63/EU).

Assessment of Colitis

The method for colitis assessment was followed by Linshi's reported and minimal modification (21). The animal's body weights (BWs) were recorded daily. All animals were euthanized on day 21 with CO_2, and the blood, colon, and colon contents were collected. Two 5-mm sections of each colon were obtained and fixed in 4% paraformaldehyde and Carnoy's fixative (dry methanol: chloroform: glacial acetic acid at a volume ratio of 60:30:10). The rest of the colon was rinsed with saline and stored at −80°C pending analysis. After fixation, colon samples were dehydrated and embedded in paraffin wax. 5 μm slices were prepared using a microtome (Thermo Fisher) and stained with haematoxylin/eosin (H&E) and periodic acid–Schiff (PAS). The stained slices were covered with coverslips using neutral balsam
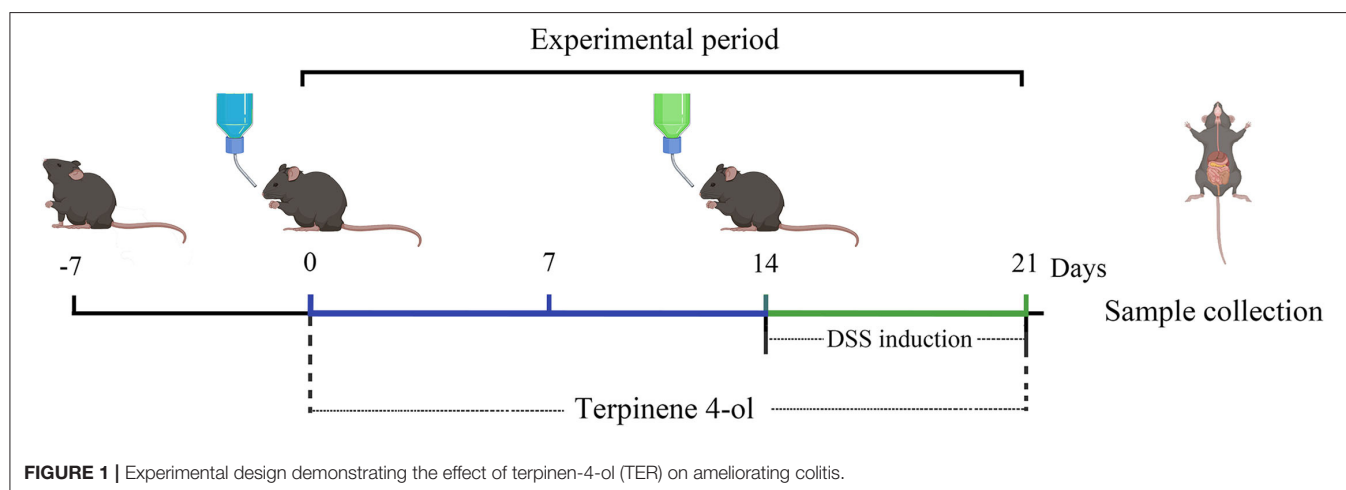
FIGURE 1 | Experimental design demonstrating the effect of terpinen-4-ol (TER) on ameliorating colitis.

FIGURE 2 | The characterization of TER. **(A)** The infrared spectrum of TER. **(B)** The chemical structure of TER intestinal epithelial cells pretreated with different TER concentrations for 24 h followed by treatment with LPS (10 μg/mL) for 24 h. The effects of TER on **(B,C)** cytotoxicity and **(D)** cell viability were observed in IPEC-J2 cells exposed to LPS. The data are expressed as the mean ± standard error of three independent experiments. * $P < 0.05$, ** $P < 0.01$, compared with the blank control group. # $P < 0.05$, ## $P < 0.01$, compared with the blank LPS group.

as an adhesive. The thickness of the muscle layer, the height of the villus, and the number of goblet cells was calculated by Image-Pro Plus software, version 6.0 (Media Cybernetics, Silver Spring, MD, USA).

Statistical Analyses

GraphPad Prism® 5.0 (GraphPad Software, La Jolla, CA, USA) was used for all statistical analyses and graphs. Error bars refer to the standard error of the mean (SEM). The means ± SEM presented are from at least three experiments. The two means were compared using Student's t-test.

RESULTS

Chemical Profile of TER

As assessed by FTIR spectroscopy, the structure characteristics and molecular mass of TER are shown in **Figures 2A,B**. The IR spectra revealed detection at 3,454 cm^{-1} (-OH stretching); 2,962 cm^{-1}, 2,838 cm^{-1} (-CH$_2$ stretching); 2,914 cm^{-1} (C=C stretching); 1,448 cm^{-1} (-C-OH); 3,400
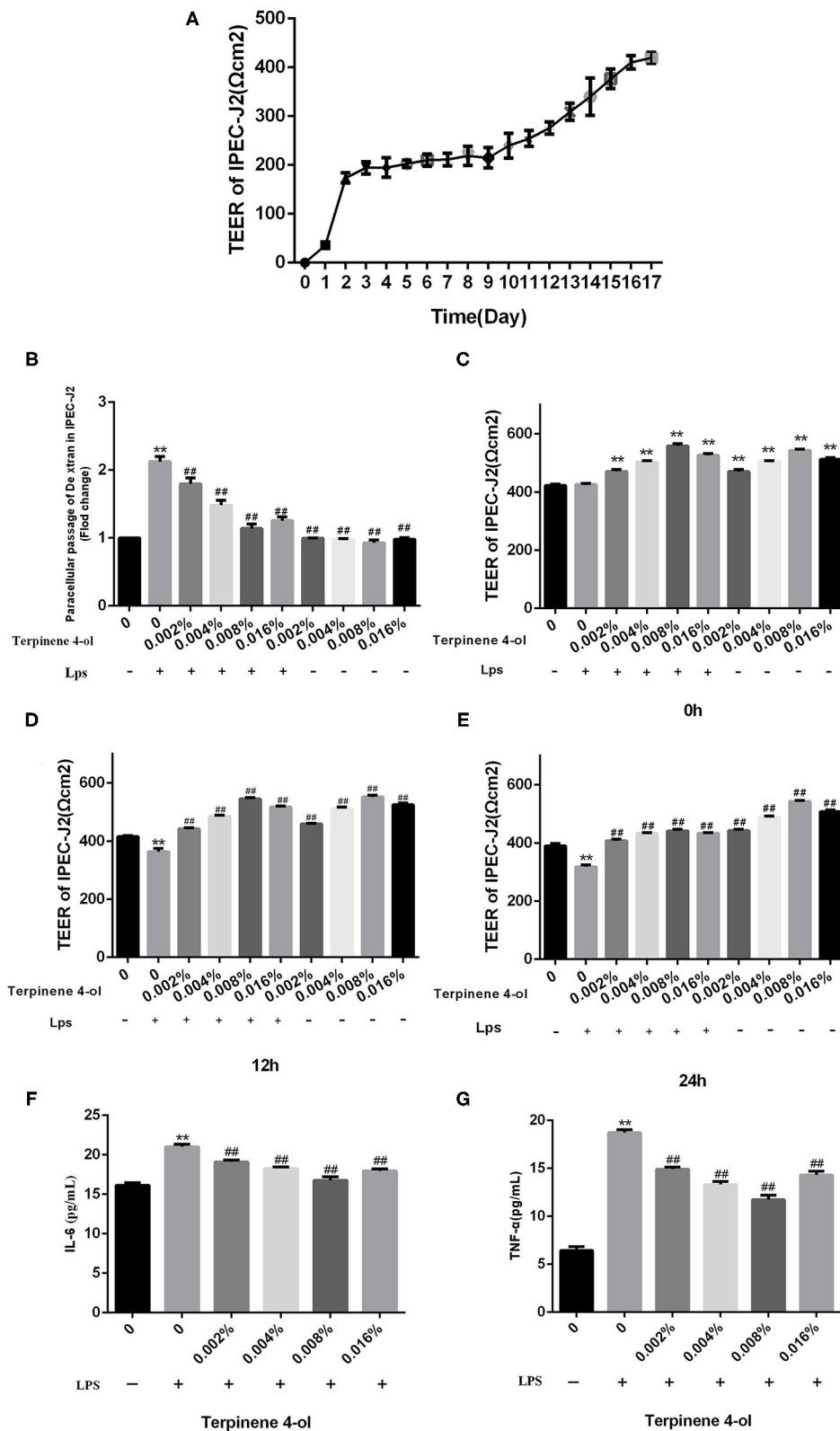
FIGURE 3 | Effects of TER on LPS-induced intestinal epithelial cell permeability and inflammatory cytokines. The protective effects of TER on fused monolayers of intestinal epithelial cells were examined by measuring the TEER values of fused intestinal epithelial monolayers at different time points and FITC-dextran permeability.

(Continued)

FIGURE 3 | (A) TEER values. Cells were treated with LPS on day 17 after differentiation, and TEER values were detected at different times **(B–D)**. Cell permeability was measured by determining FITC-dextran permeability after 24 h of LPS exposure in TER-treated cells **(E)**. The IL-6 **(F)** and TNF-α **(G)** levels in the culture supernatants of cells pretreated with TER for 24 h and then exposed to LPS for 3 h were measured by ELISA. ** and ## display similar means with above mentioned.

FIGURE 4 | Effect of TER on tight junction proteins in IPEC-J2 cells. The expression of ZO-1 **(A)**, occluding **(B)**, claudin-1 **(C)**, and claudin-4 **(D)** genes were analyzed by qRT-PCR. ** and ## display similar means with above mentioned.
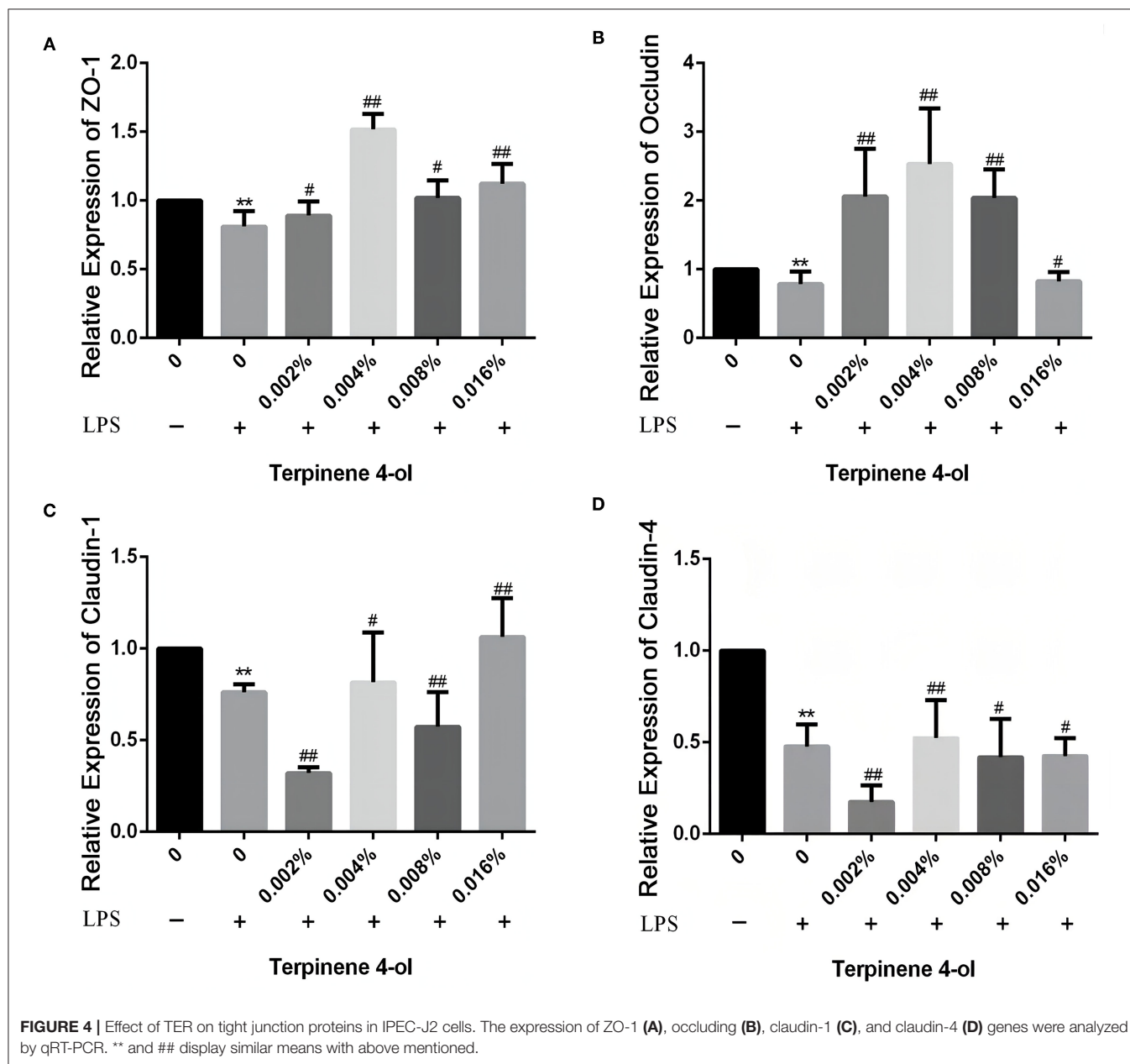
cm^{-1} (-OH stretching vibration); 1,680 cm^{-1} (-OH bending); and 1,050 cm^{-1} (C-O-C stretching). The spectral results were similar to the TER structure reported in previous studies (24, 25).

Cell Viability After Exposed to TER

Cells were treated with different TER concentrations for 24 h to determine the highest non-toxic TER concentration. **Figure 2C** shows that TER did not significantly inhibit IPEC-J2 cell proliferation. At concentrations between 0.002% and 0.016%, the viability rate of IPEC-J2 significantly increased ($P < 0.05$). The viability rate of IPEC-J2 cells significantly decreased following LPS exposure (**Figure 2D**). However, upon TER pretreatment, the cell viability rate increased significantly ($P < 0.05$). The most effective TER concentrations ranged between 0.001% and 0.016%.
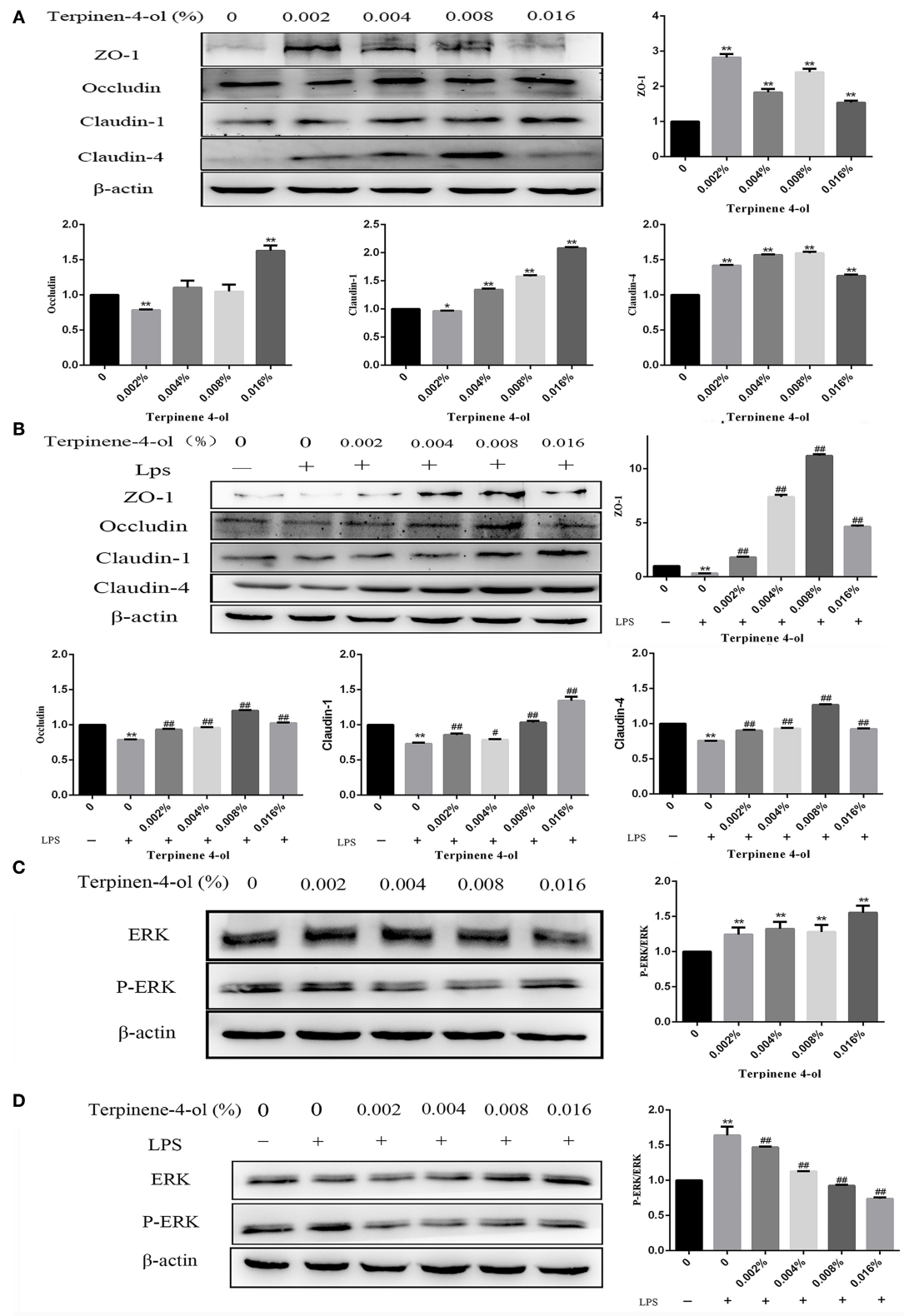
FIGURE 5 | Effect of TER on tight junction (TJ) proteins and phosphorylated ERK expression in IPEC-J2 cells. **(A)** The TJ proteins expression were detected in cells exposed to a serial concentration of TER. **(B)** The TJ proteins' expression in cells incubated with TER for 24 h and then exposed to LPS. **(C)** ERK and phosphorylated ERK expression in cells incubated with TER for 24 h. **(D)** ERK and phosphorylated ERK expression in cells incubated with TER for 24 h and then exposed to LPS. **
and ## display similar means with above mentioned.

FIGURE 6 | Effect of ERK phosphorylation inhibition on tight junction (TJ) protein expression. **(A)** The expression of phosphorylated ERK and **(B)** TJ proteins were detected in cells pretreated with the ERK inhibitor PD98059 (50 μM) for 1 h before treatment with TER or LPS. ** and ## display similar means with above mentioned.
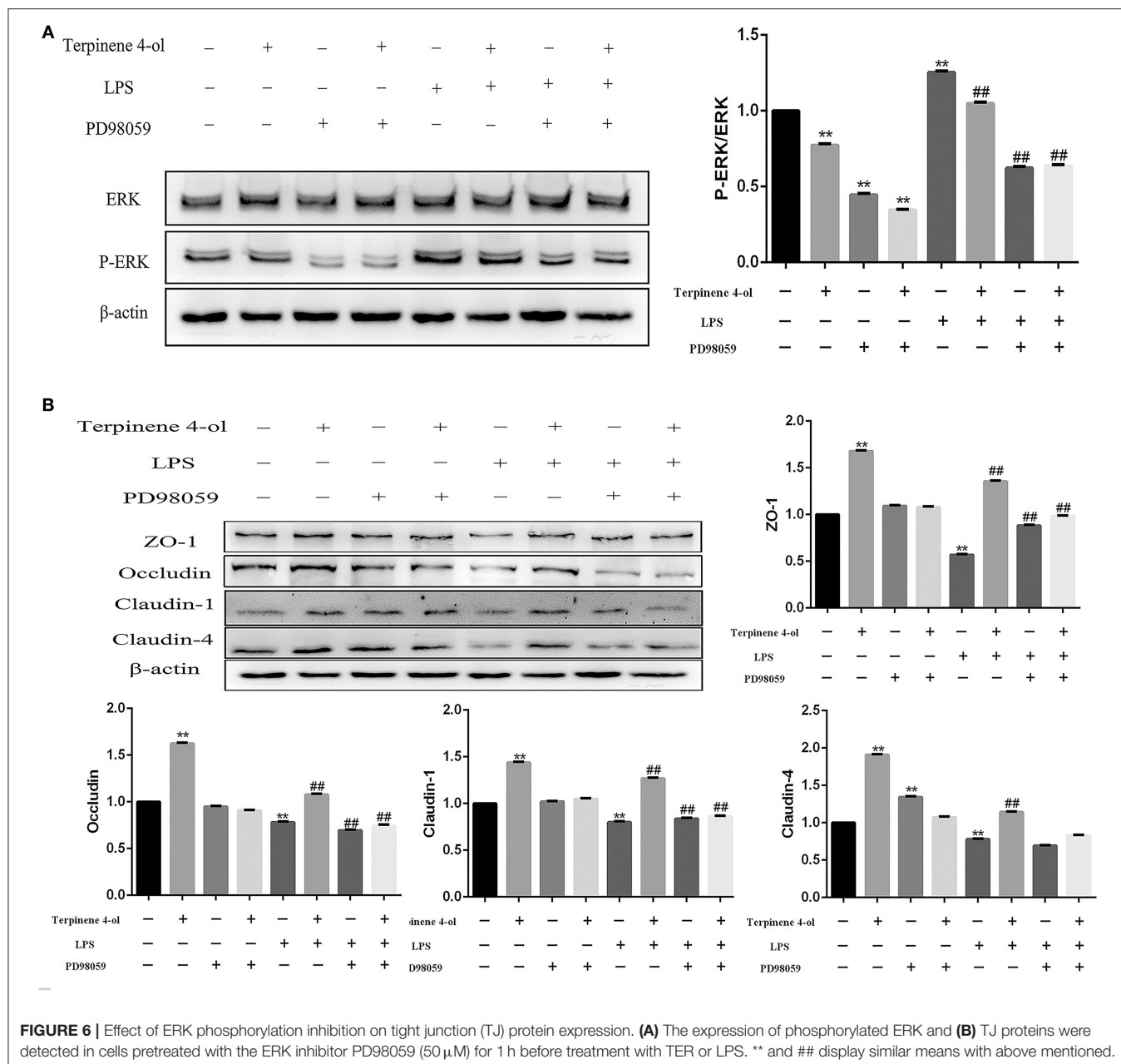
Effect of TER on the Intestinal Epithelial Cell Monolayer Integrity Exposed to LPS

The effects of TER on intestinal epithelial cell permeability were determined by gauging TEER values and concentration of FITC-dextran after being exposed to LPS. The TEER values of IPEC-J2 epithelial cells fused monolayers were stable at 16 d after seeding, indicating that the single-layered epithelium fusion was successfully constructed (**Figure 3A**). The TEER values of the epithelial monolayer significantly increased after pre-treating with different TER concentrations for 24 h. When fused IPEC-J2 epithelial cell monolayers were exposed to LPS (10 μg/mL), the TEER values significantly decreased ($P < 0.05$) and the

permeability to FITC-dextran was remarkably increased ($P < 0.01$). Adding different concentrations of TER significantly ($P < 0.01$) reversed the LPS-dependent decrease in TEER values and increased FITC-dextran permeability in IPEC-J2 monolayers (**Figures 3B–E**).

Effect of TER on IL-6 and TNF-α Expression in IPEC-J2 Cells Exposed to LPS

The cells were centrifuged, and the supernatant was collected to detect the expression of IL-6 and TNF-α. As shown in **Figures 3F,G**, the IL-6 and TNF-α levels, all of which were
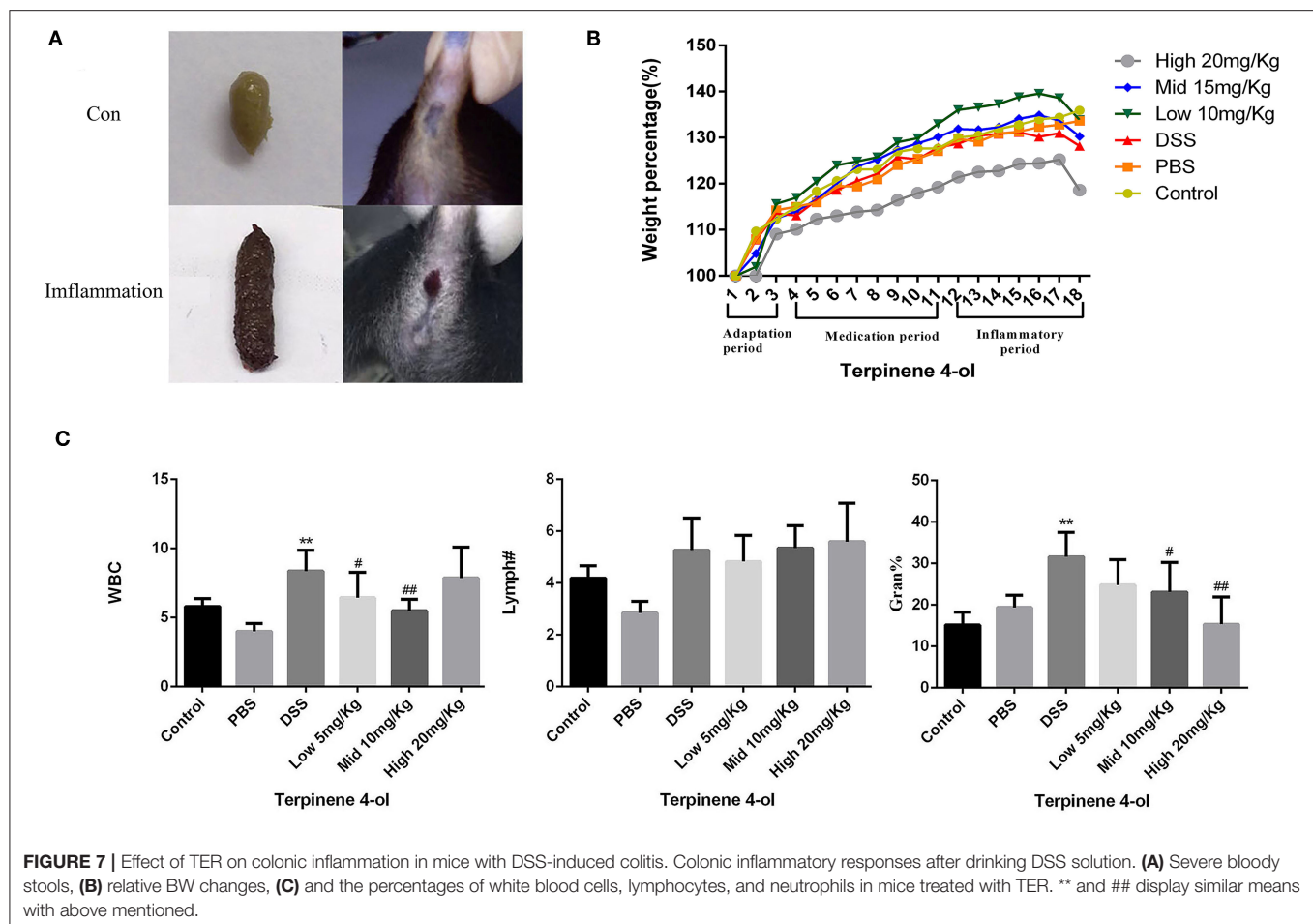
FIGURE 7 | Effect of TER on colonic inflammation in mice with DSS-induced colitis. Colonic inflammatory responses after drinking DSS solution. **(A)** Severe bloody stools, **(B)** relative BW changes, **(C)** and the percentages of white blood cells, lymphocytes, and neutrophils in mice treated with TER. ** and ## display similar means with above mentioned.

significantly increased ($P < 0.01$) in the supernatants of IPEC-J2 cells challenged by LPS, but were significantly decreased ($P < 0.01$) when pre-treated with TER.

Effect of TER on TJ Proteins Expressing in IPEC-J2 Cells Exposed to LPS

Following 24 h pretreatment with TER, the TJ protein expression in IPEC-J2 cells were measured by qPCR and western blotting. TER significantly upregulated the expression of tight junction proteins, such as ZO-1, occludin, claudin-1, and claudin-4. Interestingly, when cells were exposed to LPS for 3 h, the above-mentioned proteins level was significantly decreased ($P < 0.05$). However, TER pretreatment significantly inhibited LPS-induced decreased TJ proteins at both mRNA (**Figures 4A–D**) and protein (**Figures 5A,B**) levels.

Effects of TER on ERK Protein and Its Phosphorylation in IPEC-J2 Cells

Following 24-h pretreatment with TER, ERK and phosphorylated ERK in cells were measured by immunoblotting. TER treatment was significantly downregulated ($P < 0.05$) the expression of phosphorylated ERK in IPEC-J2 cells (**Figure 5C**). Following exposure to LPS for 3 h, the phosphorylated ERK levels were

significantly increased ($P < 0.05$). However, pre-treatment of the cells with TER for 24 h and subsequent exposure to LPS resulted in a phosphorylated ERK decrease (**Figure 5D**, $P < 0.05$).

Effects of Blocking ERK Phosphorylation on TJ Protein Expression

To examine the role of ERK in regulating TJ proteins expression, cells were incubated with an ERK inhibitor (PD98059, 50 nM) for 1 h before treatment with TER (0.008%) or LPS (10 μg/mL). The level of phosphorylated ERK was significantly decreased ($P < 0.01$) after adding the inhibitor (**Figure 6A**), suggesting that the ERK pathway was successfully blocked. Although the expression of TJ proteins was upregulated significantly ($P < 0.01$) in cells pre-treated with TER alone, but the ERK inhibitor significantly attenuated ($P < 0.01$) the upregulation of TJ proteins induced by TER. In TER-pretreated cells that were later exposed to LPS, the inhibitor significantly decreased ($P < 0.01$) the expression of TJ proteins (**Figure 6B**).

Effects of TER on DSS-Induced Colonic Inflammation in Mice

The mice given DSS-containing water showed reduced food intake, lethargy, dry hair, slow responses to stimulation and
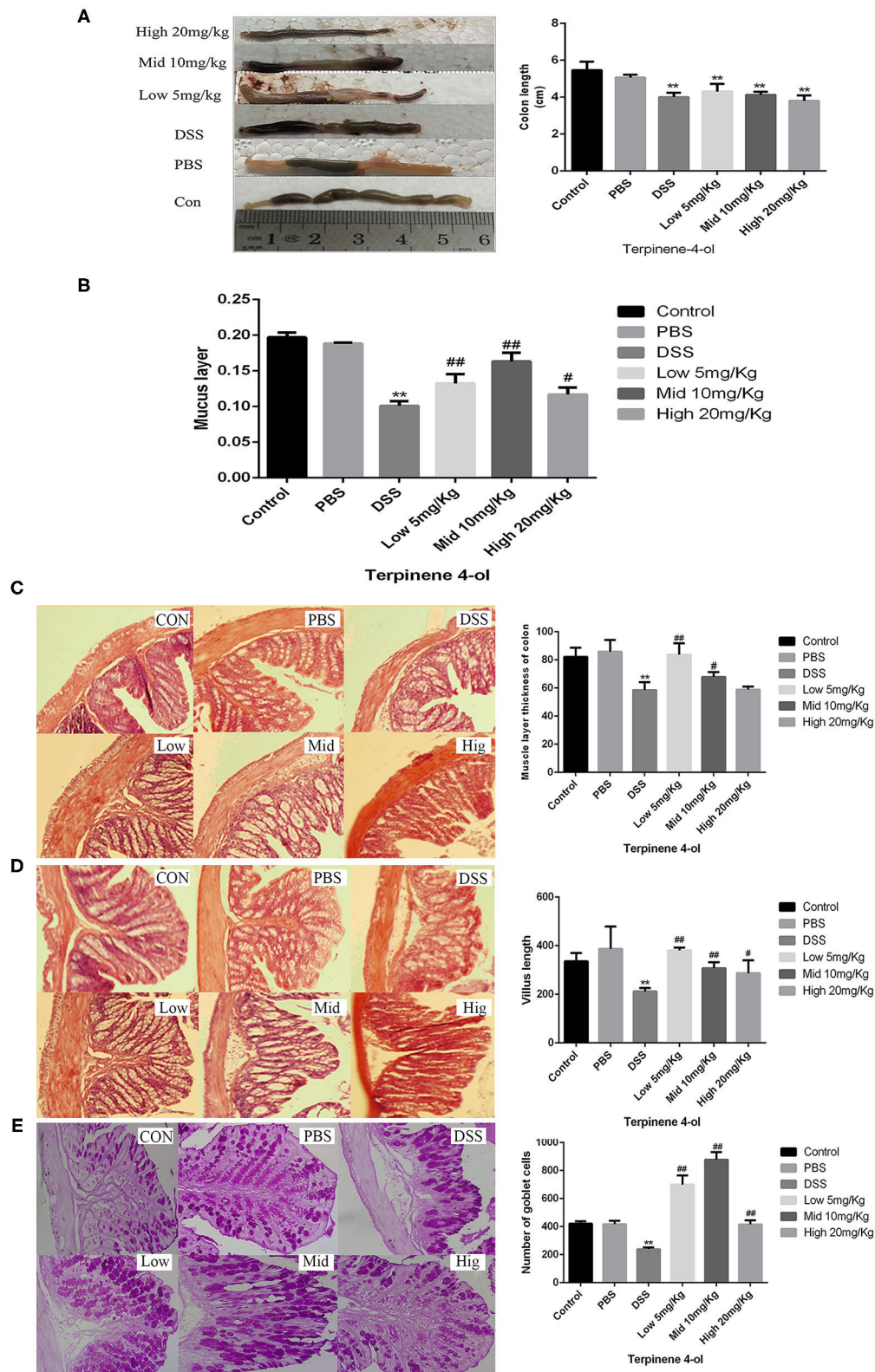
FIGURE 8 | Effect of terpinen-4-ol (TER) treatment on colonic histopathology and the intestinal mucosal layer thickness in dextran sulfate sodium (DSS)-induced colitis. Effect of TER treatment on the colon length **(A)**, mucus layer thickness **(B)**, muscle layer thickness **(C)**, villus length **(D)**, and the number of goblet cells **(E)** in mice with DSS-induced colitis. ** and ## display similar means with above mentioned.

FIGURE 9 | Effect of terpinen-4-ol (TER) on the tight junction (TJ) and ERK-pathway protein expression in mice. **(A)** Expression of colon TJ proteins and **(B)** ERK-signaling proteins in mice after drinking DSS solution. ** and ## display similar means with above mentioned.
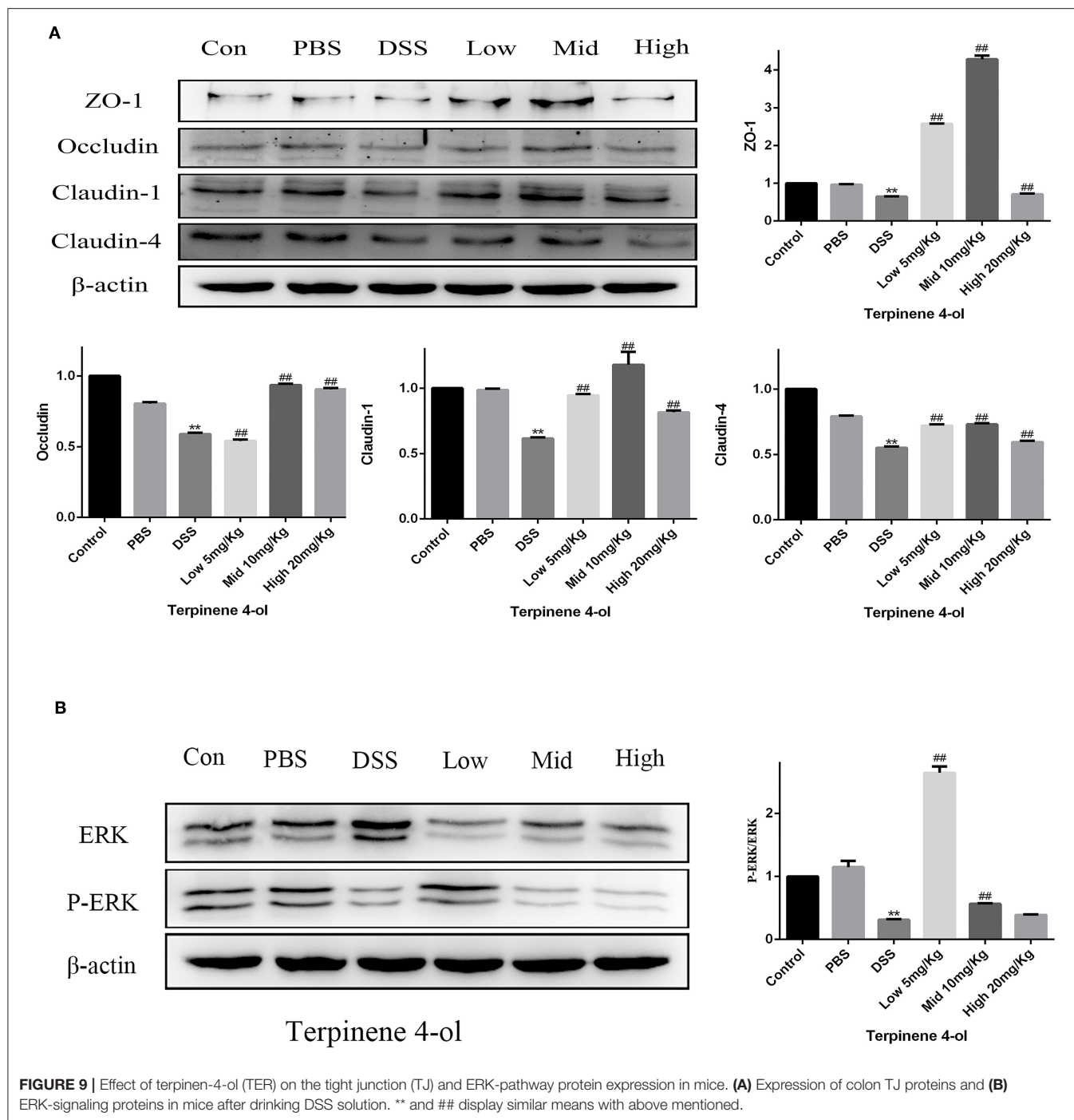
impotence. Severe bloody stools and/or anal bleeding was also noticed (**Figure 7A**). The BWs of mice in the control and the PBS-treated groups increased steadily, whereas it decreased in those administered DSS alone on day 3 post-treatment. Lower BW losses were observed in mice exposed to both low- and moderate- levels of TER than in the DSS group

in contrast to higher BW losses in mice exposed to a high TER level (**Figure 7B**). Routine blood test results showed that the proportions of leukocytes, lymphocytes, and neutrophils increased in the DSS-treated mouse. However, TER (low and moderate doses) administration attenuated the increase of inflammatory response induced by DSS in mice (**Figure 7C**).

FIGURE 10 | The putative signal pathway of terpinen-4-ol (TER) protects gut integrity in IPEC-J2 cells. TER attenuated LPS induces downregulation of tight junction proteins via the ERK1/2 signal pathway.
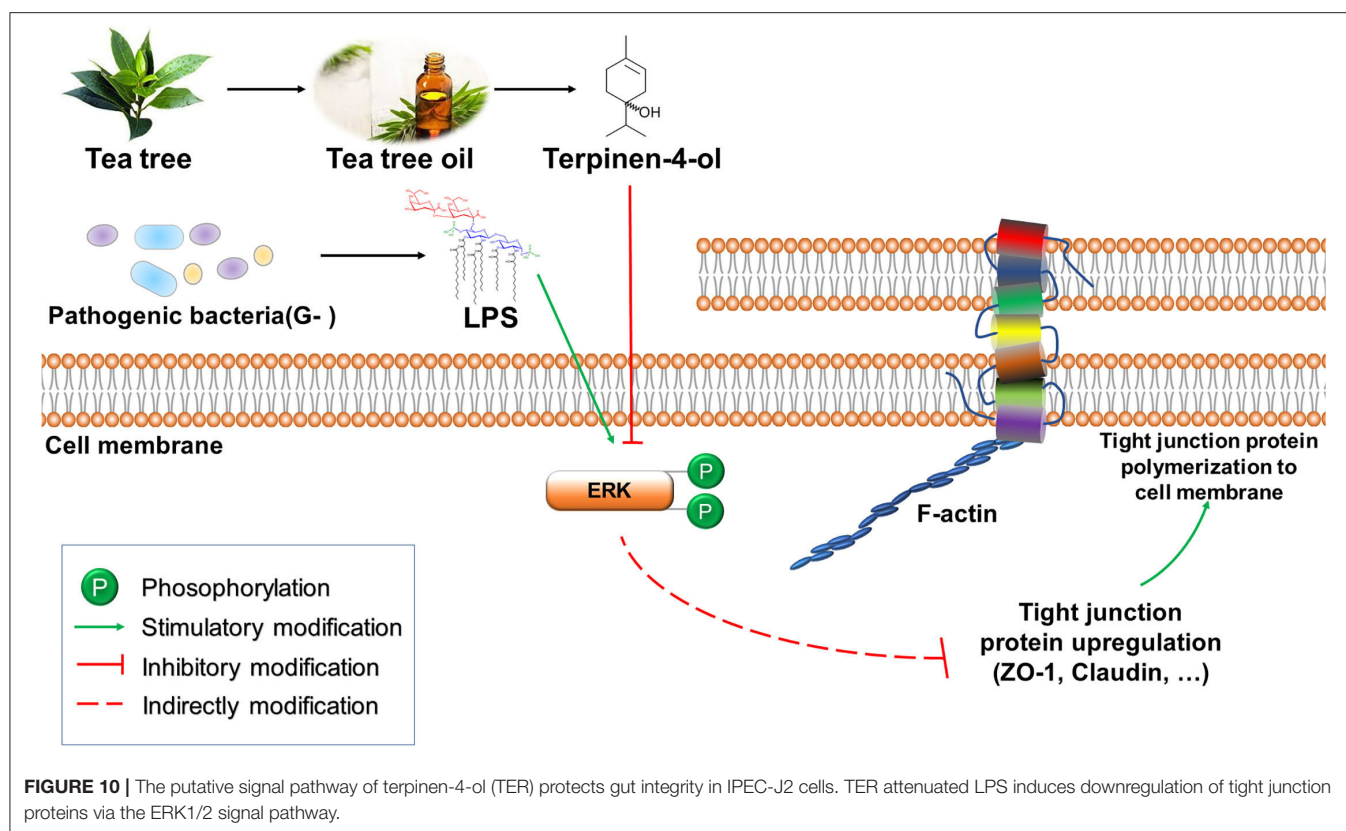
TER Attenuated Mice Colitis Induced by DSS

The colon structure in control mice was normal under the microscope. However, in DSS-treated mice, significant inflammatory responses, such as the short of colon length (**Figure 8A**), the disappear of intestinal mucous layer (**Figure 8B**), the thickness of the muscle layer of the colon (**Figure 8C**), the short of intestinal villus (**Figure 8D**), and marked decrease of the number of goblet cell (**Figure 8E**) have appeared. Interestedly, both lower concentration and middle concentration of TER added protected the goblet cells and the mucosal integrity in DSS-induced colitis mice.

Effect of TER on TJ Proteins and ERK-Pathway Protein Expression *in vivo*

Compared with the control and PBS groups, TJ protein expression levels were markedly reduced ($P < 0.05$) in the DSS treated group but increased in TER pre-treated groups (**Figure 9A**, $P < 0.05$). Meanwhile, the expression of phosphorylated ERK was remarkably decreased in the DSS treated group compared with control but increased in mice with a lower dose of TER administration (**Figure 9B**, $P<0.05$), suggesting that TER upregulated the expression of tight junction proteins was related to phosphorylated ERK.

DISCUSSION

TER has attracted considerable interest as a bactericidal product in potential applications due to its unique biological activity, including antibacterial and antioxidant activities. Our study showed that TER protected IPEC-J2 cells against LPS-induced inflammation and DSS-induced colitis. Furthermore, we also showed the role of TJ proteins in LPS-or DSS-induced gut barrier damage via the ERK1/2-signaling pathway (**Figure 10**).

During growth and metabolic processes, cells secrete highly active biological oxidants, such as NO and hydroxyl radicals. Physiological doses of biological oxidants are essential for normal cellular metabolic processes and regulating various physiological functions. However, excessive oxidants will induce oxidative stress and subsequent cellular damage in the animal. A variety of pathogens and their secreted molecules, such as LPS, induce cells to produce high levels of oxidants (26). Essential oils containing TER can downregulate LPS-induced NO secretion (17), allowing normal cell growth and metabolism (27). In this study, we found a significant decrease in the viability of IPEC-J2 cells when exposed to LPS. On the contrary, the viability rate was significantly increased when pretreated with TER before LPS exposure. This phenomenon could be due to (i) pretreatment of TER significantly increased the IPEC-J2 cell proliferation rate, and (ii) TER protecting the intestinal barrier integrity, which attenuated the toxicity of LPS.

Inflammatory responses represent the initial pathological process during tissue damage in multiple diseases (28). Nuclear

factor-kappa B (NF-κB) is activated when cells are activated by LPS, leading to an increase of intracellular inflammatory factors (29, 30). TER can significantly inhibit the activation of NF-κB, thereby reducing the inflammatory response (31). IL-6 and TNF-α were upregulated in IPEC-J2 cells after LPS stimulation, but pretreatment of the cells with TER, the above-mentioned phenomenon, disappeared. This indicates that TER exhibited significant anti-inflammatory activity.

When a pathogen invades the intestinal mucosal barrier, it can cause epithelial cell damage, activate inflammatory factors and mucosal immune activity, impair intestinal TJs (32), all of which can result in intestinal inflammation (33). This study demonstrated that TER improved intestinal barrier integrity. The mechanism may be related to the expression of TJ proteins, as TER pretreatment significantly ameliorated LPS- or DSS-induced damage to the epithelial integrity and decrease of tight junction proteins. The activating of p38 MAPK- and ERK1/2-pathways is related to inflammatory cytokine secretion in intestinal cells (34). The amelioration of *Lactobacillus pentosus*-induced colitis was based on inhibiting MAPKs and TJ protein expression (20, 35). In human corneal epithelial cells, TJ disruption occurred when the ERK1/2 pathway activated. In this study, TER attenuated LPS induced tight junction proteins decrease and ERK1/2 activation.

Similarly, pretreatment of IPEC-J2 cells with ERK1/2 inhibitor effectively inhibited the LPS-induced ERK1/2 activation and the TJ protein decrease. Moreover, TER attenuated colitis in DSS-treated mice was accompanied by TJ protein upregulation and inhibition of ERK1/2 phosphorylation in mice exposed to moderate and high TER doses, suggesting that ERK1/2 signaling is involved in TJ protein regulation by TER. In the LPS-induced inflammatory response of RAW264.7 macrophages, pedunculoside remarkably inhibited the phosphorylation of ERK1/2 to reduce the inflammatory cytokine production (32). However, as the phosphorylated ERK1/2 was significantly decreased in DSS alone and low dose TER treated mice, we speculate that cyclic changes in ERK1/2 expression may occur during the treatment process in the mice. For example, heat stress (HS) increased intestinal permeability and associated cyclic changes in TJ gene expression within 7 days (36), and ERK1/2 expression is quickly upregulated in acute HS but decreased sharply in pigs subjected to chronic HS (37).

In our study, TER remarkably improved DSS-induced colitis in mice and enhanced immune function. In addition, TER inhibited potential oxidative stress factors caused by DSS, thereby potentially protecting the intestinal barrier integrity by inhibiting intestinal cell apoptosis. Goblet cells are important mucus-secreting cells in the body (38). When goblet cells are reduced, mucus is secreted in insufficient quantities. The mucosal barrier function is impaired, resulting in inflammation (39). Our research also showed that TER ameliorated the DSS-induced decrease in the number of colonic goblet cells and the mucus layer thickness in mice. However, further study is required to elucidate the mechanism(s) by which goblet cells respond to TER.

In conclusion, the data demonstrate that TER attenuates LPS- or DSS-induced downregulation of TJ proteins via the ERK1/2-signaling pathway, which could be used as a novel therapeutic approach for treating IBD.

DATA AVAILABILITY STATEMENT

The original contributions presented in the study are included in the article/**Supplementary Material**, further inquiries can be directed to the corresponding author.

ETHICS STATEMENT

The animal study was reviewed and approved by Animal Ethics Committee of Guangdong Ocean University.

AUTHOR CONTRIBUTIONS

XJ, YY, and BF designed the study. YY, BF, YH, JL, TY, LW, CH, XL, ZY, and XM participated in the experiments. YY, BF, XJ, SL, RG, and AA wrote and revised the manuscript. All authors approved the final manuscript.

FUNDING

SUPPLEMENTARY MATERIAL

The Supplementary Material for this article can be found online at: https://www.frontiersin.org/articles/10.3389/fnut.2021.805612/full#supplementary-material

REFERENCES

1. Yashiro M. Ulcerative colitis-associated colorectal cancer. *World J Gastroenterol.* (2014) 20:16389. doi: 10.3748/wjg.v20.i44.16389

2. Laugesen K.B, Tøttrup A. Colorectal cancer in ulcerative colitis. Ugeskr Laeger. (2014). 176.

3. Lee SH, Kwon JE, Cho ML. Immunological pathogenesis of inflammatory bowel disease. *Intestinal Research.* (2018) 16:26–42. doi: 10.5217/ir.2018.16.1.26

4. Marchesi JR, Adams DH, Fava F, Hermes GDA, Hirschfield GM, Hold G. et al. N. The gut microbiota and host health: A new clinical frontier. *Gut.* (2016) 65:330. doi: 10.1136/gutjnl-2015-309990

5. Zihni C, Mills C, Matter K, Balda MS. Tight junctions: From simple barriers to multifunctional molecular gates. *Nat Rev Mol Cell Biol.* (2016) 17:564. doi: 10.1038/nrm.2016.80

6. Hu CAA, Hou Y, Yi D, Qiu Y, Wu G, Kong X, et al. Autophagy and tight junction proteins in the intestine and intestinal diseases. *Anim Nutr.* (2015) 1:43–7. doi: 10.1016/j.aninu.2015.08.014

7. Wu Y JZ, Zheng C, et al. Effects of protein sources and levels in antibiotic-free diets on diarrhea, intestinal morphology, and expression of tight junctions in weaned piglets. *Anim Nutr.* (2015) 1:90–6. doi: 10.1016/j.aninu.2015.08.013

8. Mccarthy KM, Skare IB, Stankewich MC, Furuse M, Tsukita S, Roger RA, et al. Occludin is a functional component of the tight junction. *J Cell Sci.* (1996) 109:2287. doi: 10.1242/jcs.109.9.2287

9. Baig MM, A. Fatima, S, Fatima, M, Siddiqui, S, Ali S.A, Ilyas, Prescription pattern MN, and cost of illness (coi) of inflammatory bowel disease (ibd) in a tertiary care hospital. *Int J Pharm Pharm Sci.* (2016) 9:44. doi: 10.22159/ijpps.2017v9i1.14248

10. Murthy SK, Nguyen GC. Increased risk of venous thromboembolic events with corticosteroid versus biologic therapy for inflammatory bowel disease. *Clin Gastroenterol Hepatol.* (2016) 14:166. doi: 10.1016/j.cgh.2015.04.022

11. Groschwitz KR, Hogan SP. Intestinal barrier function: Molecular regulation and disease pathogenesis. *J Allergy Clin Immunol.* (2009) 124:3–20. doi: 10.1016/j.jaci.2009.05.038

12. Hammer; Carson; Riley. Antifungal effects of Melaleuca alternifolia (tea tree) oil and its components on Candida albicans, Candida glabrata and Saccharomyces cerevisiae. *J Antimicrob Chemother.* (2004) 53:1081–5. doi: 10.1093/jac/dkh243

13. Carson CF, Hammer KA, Riley TV. Melaleuca alternifolia (tea tree) oil: A review of antimicrobial and other medicinal properties. *Clin Microbiol Rev.* (2006) 19:50. doi: 10.1128/CMR.19.1.50-62.2006

14. Kerekes E-B, Deak E, Takó M, Tserennadmid R, Petkovits T, VágvLgyi C, et al. Anti-biofilm forming and anti-quorum sensing activity of selected essential oils and their main components on food-related micro-organisms. *J Appl Microbiol.* (2013) 115:933–42. doi: 10.1111/jam.12289

15. Busatta C, Vidal RS, Popiolski AS, Mossi AJ, Dariva C, Rodrigues MRA, et al. Application of Origanum majorana l. Essential oil as an antimicrobial agent in sausage. *Food Microbiology.* (2008) 25:207–11. doi: 10.1016/j.fm.2007.07.003

16. Al-Kalaldeh JZ, Abu-Dahab R, Afifi FU. Volatile oil composition and antiproliferative activity of Laurus nobilis, Origanum syriacum, Origanum vulgare, and Salvia triloba against human breast adenocarcinoma cells. *Nutr Res.* (2010) 30:271–8. doi: 10.1016/j.nutres.2010.04.001

17. Gostner J,M. Becker, K, Ueberall, F, Fuchs, The good D, and bad of antioxidant foods: An immunological perspective. *Food Chem Toxicol.* (2015) 80:72–9. doi: 10.1016/j.fct.2015.02.012

18. Souza CF, Baldissera MD, Silva LdL, Geihs MA, Baldisserotto B, et al. Is monoterpene terpinen-4-ol the compound responsible for the anesthetic and antioxidant activity of, Melaleuca alternifolia, essential oil (tea tree oil) in silver catfish?[j]. *Aquaculture.* (2018) 486:217–23. doi: 10.1016/j.aquaculture.2017.12.025

19. Nogueira MNM, Aquino SG, Junior CR, Spolidorio DMP. Terpinen-4-ol and alpha-terpineol (tea tree oil components) inhibit the production of il-1β, il-6 and il-10 on human macrophages. *Inflamm Res.* (2014) 63:769–78. doi: 10.1007/s00011-014-0749-x

20. Jin-Ju J, Kyung-Ah K, Se-Eun J, Jae-Yeon W, Myung Joo H, Dong-Hyun K. Orally administrated Lactobacillus pentosus var. Plantarum c29 ameliorates age-dependent colitis by inhibiting the nuclear factor-kappa b signaling pathway via the regulation of lipopolysaccharide production by gut microbiota. *PLoS ONE.* (2015) 10:e0116533. doi: 10.1371/journal.pone.0116533

21. Shi L, Fang B, Yong Y, Li X, Gong D, Li J, et al. Chitosan oligosaccharide-mediated attenuation of lps-induced inflammation in ipec-j2 cells is related to the tlr4/nf-kappab signaling pathway. *Carbohydr Polym.* (2019) 219:269–79. doi: 10.1016/j.carbpol.2019.05.036

22. Lu YC, Yeh WC, Ohashi PS. Lps/tlr4 signal transduction pathway. *Cytokine.* (2008) 42:145–51. doi: 10.1016/j.cyto.2008.01.006

23. Yoshida LS, Kakegawa T, Yuda Y, Takanoohmuro H. Shikonin changes the lipopolysaccharide-induced expression of inflammation-related genes in macrophages. *J Nat Med.* (2017) 71:1–12. doi: 10.1007/s11418-017-1106-5

24. Xia JQ, De Yu Z, Rui L, Qing ZW, Jing D, Guang CX. *In vitro* evaluation of the biomedical properties of chitosan and quaternized chitosan for dental applications. *Carbohydr Res.* (2009) 344:1297–302. doi: 10.1016/j.carres.2009.07.001

25. Yang Z, Xiao Z, Ji H. Solid inclusion complex of terpinen-4-ol/β-cyclodextrin: Kinetic release, mechanism and its antibacterial

activity. *Flavour Fragr J.* (2015) 30:179–87. doi: 10.1002/ffj.3229

26. Ray PD, Huang B-W, Tsuji Y. Reactive oxygen species (ros) homeostasis and redox regulation in cellular signaling. *Cell Signal.* (2012) 24:981–90. doi: 10.1016/j.cellsig.2012.01.008

27. Hajimehdipoor H, Samadi N, Mozaffarian V, Rahimifard N, Shoeibi S, Hamedani MP. Chemical composition and antimicrobial activity of Oliveria decumbens volatile oil from west of Iran. *J Medicinal Plants.* (2010) 4:1411–8.

28. Kim N, Dixit VM. Signaling in innate immunity and inflammation. *Cold Spring Harb Perspect Biol.* (2012) 4:829–41. doi: 10.1101/cshperspect.a006049

29. Hart P.H. Brand, C, Carson C.F, Riley T.V, Prager R.H, Finlay-Jones, Terpinen-4-ol JJ, the main component of the essential oil of Melaleuca alternifolia (tea tree oil), suppresses inflammatory mediator production by activated human monocytes. *Inflammat Res.* (2000) 49:619–26. doi: 10.1007/s000110050639

30. Homeyer DC, Sanchez CJ, Katrin M, Beckius ML, Murray CK, Wenke JC, et al. *In vitro* activity of Melaleuca alternifolia (tea tree) oil on filamentous fungi and toxicity to human cells. *Medical Mycology.* (2015) 53:285–94. doi: 10.1093/mmy/myu072

31. Hua KF, Yang TJ, Chiu HW, Ho CL. Essential oil from leaves of Liquidambar formosana ameliorates inflammatory response in lipopolysaccharide-activated mouse macrophages. *Nat Prod Commun.* (2014) 9:869. doi: 10.1177/1934578X1400900638

32. Liu K, Li G, Guo W, Zhang J. The protective effect and mechanism of pedunculoside on dss (dextran sulfate sodium) induced ulcerative colitis in mice. *Int Immunopharmacol.* 88:107017. doi: 10.1016/j.intimp.2020.107017

33. Fermín SDM, Isabel R,C. Cristina, M, Olga, Intestinal inflammation MA, and mucosal barrier function. *Inflamm Bowel Dis.* (2014) 20:2394–404. doi: 10.1097/MIB.0000000000000204

34. O'Brien D OCT, Shanahan F, et al. O'brien d, o'connor t, shanahan f, et al. Activation of the p38 mapk and erk1/2 pathways is required for fas-induced il-8 production in colonic epithelial cells. *Ann N. Y. Acad Sci.* (2002) 973:161–5. doi: 10.1111/j.1749-6632.2002.tb04627.x

35. Wu HL, Gao X, Jiang ZD, Duan ZT, Wang SK, He B, et al. et al. Attenuated expression of the tight junction proteins is involved in clopidogrel-induced gastric injury through p38 mapk activation. *Toxicology.* (2013) 304:41–8. doi: 10.1016/j.tox.2012.11.020

36. Pearce SC, Mani V, Boddicker RL, Johnson JS, Weber TE, Ross J, et al. Heat stress reduces intestinal barrier integrity and favors intestinal glucose transport in growing pigs. *PloS ONE.* (2013) 8:e70215. doi: 10.1371/journal.pone.0070215

37. Pearce SC, Mani V, Boddicker RL, Johnson JS, Weber TE, Ross J, et al. et al. Heat stress reduces barrier function and alters intestinal metabolism in growing pigs. *J Animal Sci.* (2012) 90:257–9. doi: 10.2527/jas.52339

38. Moors E, Singh T, Siderius C, Balakrishnan S, Mishra A. Climate change and waterborne diarrhoea in northern India: Impact and adaptation strategies. *Sci Total Environ.* (2013) 468–9. doi: 10.1016/j.scitotenv.2013.07.021

39. Deckers J, Madeira FB, Hammad H. Innate immune cells in asthma. *Trends Immunol.* (2013) 34:540–7. doi: 10.1016/j.it.2013.08.004

Publisher's Note: All claims expressed in this article are solely those of the authors and do not necessarily represent those of their affiliated organizations, or those of the publisher, the editors and the reviewers. Any product that may be evaluated in this article, or claim that may be made by its manufacturer, is not guaranteed or endorsed by the publisher.

A Competitive Assay Based on Dual-Mode Au@Pt-DNA Biosensors for On-Site Sensitive Determination of Carbendazim Fungicide in Agricultural Products

Ge Chen[1]*, Rongqi Zhai[1], Guangyang Liu[1], Xiaodong Huang[1], Kaige Zhang[1], Xiaomin Xu[1], Lingyun Li[1], Yanguo Zhang[1], Jing Wang[2], Maojun Jin[2], Donghui Xu[1]* and A. M. Abd El-Aty[3,4,5]

[1] Key Laboratory of Vegetables Quality and Safety Control, Laboratory of Quality and Safety Risk Assessment for Vegetable Products, Ministry of Agriculture and Rural Affairs, Institute of Vegetables and Flowers, Chinese Academy of Agricultural Sciences, Beijing, China, [2] Key Laboratory of Agro-Product Quality and Safety, Ministry of Agriculture and Rural Affairs, Institute of Quality Standard and Testing Technology for Agro-Products, Chinese Academy of Agricultural Sciences, Beijing, China, [3] State Key Laboratory of Biobased Material and Green Papermaking, College of Food Science and Engineering, Qilu University of Technology, Shandong Academy of Science, Jinan, China, [4] Department of Pharmacology, Faculty of Veterinary Medicine, Cairo University, Giza, Egypt, [5] Department of Medical Pharmacology, Faculty of Medicine, Atatürk University, Erzurum, Turkey

Carbendazim (CBZ), a systemic, broad-spectrum benzimidazole fungicide, is widely used to control fungal diseases in agricultural products. Its residues might pose risks to human health and the environment. Therefore, it is warranted to establish a rapid and reliable method for its residual quantification. Herein, we proposed a competitive assay that combined aptamer (DNA) specific recognition and bimetallic nanozyme gold@platinum (Au@Pt) catalysis to trace the CBZ residue. The DNA was labeled onto bimetallic nanozyme Au@Pt surface to produce Au@Pt probes (Au@Pt-DNA). The magnetic Fe_3O_4 was functionalized with a complementary strand of DNA (C-DNA) to form Fe_3O_4 probes (Fe_3O_4-C-DNA). Subsequently, the CBZ and the Fe_3O_4 probes competitively react with Au@Pt probes to form two Au@Pt-DNA biosensors (Au@Pt-ssDNA-CBZ and Au@Pt-dsDNA-Fe_3O_4). The Au@Pt-ssDNA-CBZ biosensor was designed for qualitative analysis through a naked-eye visualization strategy in the presence of CBZ. Meanwhile, Au@Pt-dsDNA-Fe_3O_4 biosensor was developed to quantitatively analyze CBZ using a multifunctional microplate reader. A competitive assay based on the dual-mode Au@Pt-DNA biosensors was established for onsite sensitive determination of CBZ. The limit of detection (LOD) and recoveries of the developed assay were 0.038 ng/mg and 71.88-110.11%, with relative standard deviations (RSDs) ranging between 3.15 and 10.91%. The assay demonstrated a good correlation with data acquired from liquid chromatography coupled with mass spectrometry/mass spectrometry analysis. In summary, the proposed competitive assay based on dual-mode Au@Pt-DNA biosensors might have a great potential for onsite sensitive detection of pesticides in agro-products.

Keywords: carbendazim, Au@Pt-DNA, pesticide residue, biosensor, aptamer

INTRODUCTION

Carbendazim (CBZ) is a broad-spectrum benzimidazole fungicide used to protect a wide variety of crops against fungal disease, thus producing high-quality crops with optimal yields (1, 2). CBZ, which interferes with DNA biosynthesis during fungal cell division, was defined as a major agrochemical pollutant, hazardous to humans and the environment. Because of its long half-life and severe toxicity, residues might threaten safe consumption and negatively influence food quality (3). There is an urgent need to develop analytical methods to determine residual trace levels of CBZ in agro-products to protect public health. To date, a variety of classical quantitive analyses, including liquid chromatography coupled with mass spectrometry (LC-MS) (4) and gas chromatography coupled with tandem mass spectrometry (GC-MS/MS) (5), have been routinely used to monitor CBZ residues in the agricultural products. Although these analytical methods provide high stability and accuracy, preparation steps are laborious, time-consuming, requiring professional operators and expensive instruments (2), restricting their applications. Therefore, a sensitive, rapid, and simple analytical method is needed to detect CBZ. Currently, the rapid immunoassay for detecting CBZ with high sensitivity and specificity (6) overcomes the pitfalls of the traditional analytical methods (7). However, the antibodies are prone to degradation and denaturation during field applications (8), resulting in difficultly in specifically recognizing the target (9). Moreover, antibodies are more complicated, and the manufacturing process is costly and time consuming (10). Furthermore, haptens synthesized from the CBZ analogs can attach to the appropriate functional groups, enabling the conjugation with the protein (11). Hence, a stable, specific, and cost-effective recognition receptor for CBZ is strongly required to replace the traditional immunoassays.

As molecular recognition elements, aptamers are artificially synthesized single-stranded nucleotide sequences, screened through systematic evolution of ligands by exponential enrichment (SELEX) techniques, and could specifically bind the target analyte (12). Aptamers have attracted significant attention because of their advantages of easy synthesis, low cost, and high affinity (13). Unlike antibodies, aptamers are relatively stable under extreme temperature conditions for a short time (14). Therefore, several platforms of aptamer sensors, such as fluorescence (15), colorimetry (16), and electrochemistry (17), have been developed for the detection of pesticides. To improve the stability and sensitivity of aptamer-based assays, nanomaterials (one of the most interesting sensing materials) are bioconjugated with aptamers for selective and sensitive detection of analytes. The nanomaterials with some enzyme-mimicking characteristics are defined as nanozymes (18). Nanozyme, an emerging alternative to the natural enzyme (19), displayed the following advantages: simple preparation methods, high stability, easy surface modification, and low cost (20). Some enzyme-like bimetallic nanomaterials Au@Pt are of great interest because of their multifunctional and synergistic properties (21). Au@Pt combines good chemical stability of Au with specific catalytic activities of Pt (22). Moreover, the DNA could be firmly bound to the surface of Au@Pt (23). Meanwhile, the recent reports have demonstrated that Au@Pt exhibited high-catalytic properties (24, 25).

Herein, a competitive assay based on dual-mode Au@Pt-DNA biosensors for onsite sensitive determination of CBZ fungicide is shown in **Figure 1**. One promising strategy is to reversibly bind target-specific aptamers (DNA) to the Au@Pt surface. The magnetic Fe_3O_4 was functionalized with a complementary strand of DNA (cDNA) to form Fe_3O_4 probes (Fe_3O_4-C-DNA). The CBZ and the Fe_3O_4 probes competitively react with DNA-modified nanozyme Au@Pt to form two Au@Pt-DNA biosensors (Au@Pt-ssDNA-CBZ and Au@Pt-dsDNA-Fe_3O_4 biosensors, respectively). The aptamers only extend from the Au@Pt surface, specifically in the presence of the CBZ (26), which forms Au@Pt-ssDNA-CBZ biosensor for the qualitative analysis through visualization by naked-eye from light blue to dark blue (19). In addition, Au@Pt-dsDNA-Fe_3O_4 biosensor was established for quantitative analysis of CBZ by constructing a calibration curve for trace residual determination of CBZ in agricultural products.

MATERIALS AND METHODS

Materials and Reagents

Gold (Au) chloride hydrate ($HAuCl_4 \cdot xH_2O$), chloroplatinic acid ($H_2PtCl_6 \cdot 6H_2O$), sodium citrate ($C_6H_5Na_3O_7 \cdot 2H_2O$, purity > 99%), Fe_3O_4 (10 mg/ml), 1-ethyl-3-[3-(dimethylamino) propyl] carbodiimide (EDC), and N-hydroxysuccinimide (NHS) were acquired from Sigma-Aldrich (St. Louis, MO, USA). L-ascorbic acid ($C_6H_8O_6$, LAA) was procured from Macklin Biochemical Co., Ltd (Shanghai, China). Carboxyl-functionalized magnetic particles (Fe_3O_4, 10 mg/ml) were secured from Invitrogen (Grand Island, NY). CBZ standard ($C_9H_9N_3O_2$, purity > 99%) was obtained from Dr. Ehrenstorfer GmbH (Augsburg, Germany). Polyethylene glycol 20,000 (PEG 20,000), Tween-20, Tris-EDTA buffer (TE, pH 8.0), and 3,3',5,5'-tetramethylbenzidine (TMB) substrate were purchased from Solarbio (Beijing, China). Primary secondary amine (PSA) and octadecyl (C18) were picked up from Shimadzu (Kyoto, Japan). Anhydrous magnesium sulfate ($MgSO_4$), sodium chloride (NaCl), potassium chloride (KCl), disodium phosphate (Na_2HPO_4), potassium dihydrogen phosphate (KH_2PO_4), and other analytical grade reagents were supplied by Sinopharm Chemical Reagent Co., Ltd. (Beijing, China). Hydrochloric acid (HCl) and nitric acid (HNO_3) were provided by Beijing Chemical Industry Group Co., Ltd. (Beijing, China). The CBZ aptamer (DNA) and C-DNA (the sequence of DNA and C-DNA designed in **Supplementary Table 1**) were synthesized by Sangon Co., Ltd. (Shanghai, China). A 96-well micro-plate (Transplant, flat bottom) was supplied by Costar, Inc. (Kennebunk, ME, USA). The HPLC-grade acetonitrile (ACN) and methanol (MeOH) were obtained from Thermo Fisher Scientific (Pittsburgh, PA, USA). Ultrapure water was purified by a Milli-QRC purification system (Millipore, Bedford, MA, USA). Aqua regia is a mixture of HCl and HNO_3 (HCl/HNO_3 = 3/1). The 0.01 M phosphate-buffered saline (PBS buffer, pH 7.4) consists of 0.2 g KCl, 0.27 g KH_2PO_4, 8 g NaCl, and 1.14 g Na_2HPO_4. Washing buffer (PBST:

FIGURE 1 | Schematic illustration of a competitive assay based on dual-mode Au@Pt-DNA biosensors for the sensitive determination of CBZ fungicide.
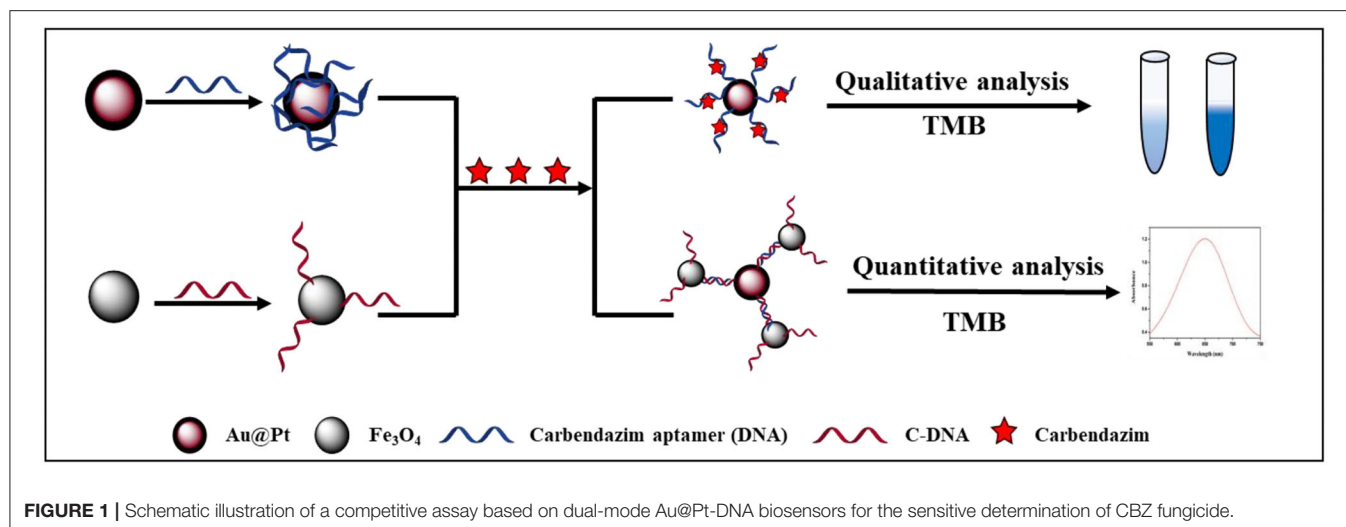
PBS buffer containing 0.05% Tween-20) was prepared for washing micro-plates.

Preparation of Au@Pt Nanomaterials

The Au@Pt nanomaterials were prepared by the seed-mediated growth method (27). All the glassware was thoroughly soaked in aqua regia and rinsed with ultrapure water. At first, the seeds of gold nanoparticles (AuNPs) were prepared with mirror modifications (28). AuNPs were synthesized by a chemical reduction method where $HAuCl_4$ was used as a precursor, and trisodium citrate was used as a reducing agent and stabilizing agent (29, 30). One milliliter $HAuCl_4$ (10%, *w/v*) aqueous solution and 99 ml distilled water were added to a round-bottomed flask. After that, 10 ml of trisodium citrate (38.8 mM) solution was quickly added when the aforementioned mixture heated to boiling under vigorous stirring and refluxing using a magnetic stirring heater (Zhengzhou, China). The color of the solution was changed from yellow to wine red, and the mixture was left to stir for another 20 min.

Second, Au@Pt was synthesized using AuNPs (30 ml) as seeds as follows: H_2PtCl_6 (1.0 mM, 10 ml) solution and LAA (5 mM, 10 ml) were added to the AuNPs solution and heated to boiling until the color changes from wind red to brown-red. Then, the aforementioned aqueous solution was left to stir for another 30 min to ensure a comprehensive reduction of H_2PtCl_6. The synthetic Au@Pt was cooled to room temperature, stored in the dark at 4°C, and then filtered through a cellulose nitrate filter.

Construction of Au@Pt Probe

Sangon Biotech Co., Ltd. synthesized the aptamer (DNA) of CBZ. The aptamer (DNA) sequence of CBZ was acquired from literature (31). Before using the aptamer (DNA) of CBZ (35.08 μg), it should be activated. At first, 18 μl TE buffer was added into the microcentrifuge tube with the aptamer (DNA) of CBZ to dissolve, and 18 μl TCEP solution was then added to reduce the disulphide bonds to single sulfhydryl groups. Subsequently, the DNA solution was shaken for 3 h under 200 rpm. After that, the activated DNA reacts with Au@Pt solution to form an

Au@Pt probe (Au@Pt-DNA). The 30% PEG and 0.1 M PBS were selected to stabilize the Au@Pt probe to achieve 0.5% PEG and 0.01 M PBS in the final solution and avoid the aggregation of the Au@Pt probe (Au@Pt-DNA). Afterward, unbound aptamer of CBZ (DNA) was removed by centrifugation at 10,000 rpm for 30 min. The Au@Pt probe was kept refrigerated at 4°C for further analysis.

Construction of Fe₃O₄ Probe

At first, the C-DNA (33.26 μg) should be activated before conjugation with Fe_3O_4. The TE buffer (pH 8.5, 18 μl) was added to the C-DNA. Next, the NHS (10 mg/ml, 100 μl) and EDC (10 mg/ml, 100 μl) were selected to activate the carboxyl group of Fe_3O_4 (10 μl, 10 mg/ml) with gentle shaking for 30 min. The Fe_3O_4 was magnetically separated and washed three times with MES buffer (15 mM) for 1 min. The washed Fe_3O_4 was resuspended in PBS buffer (pH 7.4, 0.1 mol/L). After that, the activated C-DNA was added to Fe_3O_4 solution to construct Fe_3O_4 probe (Fe_3O_4-C-DNA) for 18 h at 4°C. The Fe_3O_4 probe was washed three times with PBS buffer to remove the unconjugated C-DNA. Finally, the Fe_3O_4 probe was resuspended in 500 μl PBS (pH 7.4, 0.1 mol/L) and stored at 4°C for further use.

A Competitive Assay Based on Au@Pt-DsDNA-Fe₃O₄ Biosensor

In general, the quantitative analysis of CBZ was carried out as follows: at first, 150 μl Au@Pt-DNA (0.3 nmol/L) was added to a 0.5-ml microcentrifuge tube. Then, different concentrations of CBZ standard were prepared by PBS solution containing 10% methanol or supernatant of actual samples extract in advance. Afterward, 60 μl CBZ was added to Au@Pt-DNA solution, followed by adding a 60 μl Fe_3O_4 probe (diluted by probe buffer, 0.1 mg/L) to construct a competitive assay at room temperature. The aforementioned mixture was washed three times, followed by separation under a magnetic field for 1 min. After that, the Au@Pt-dsDNA-Fe_3O_4 mixture was resuspended

FIGURE 2 | Characterization of Au@Pt and Au@Pt probes. **(A)** TEM of Au@Pt; **(B)** EDS of Au@Pt probe; **(C)** UV-Vis spectra of Au@Pt and Au@Pt probes; and **(D)** FTIR spectra of Au@Pt and Au@Pt probes.
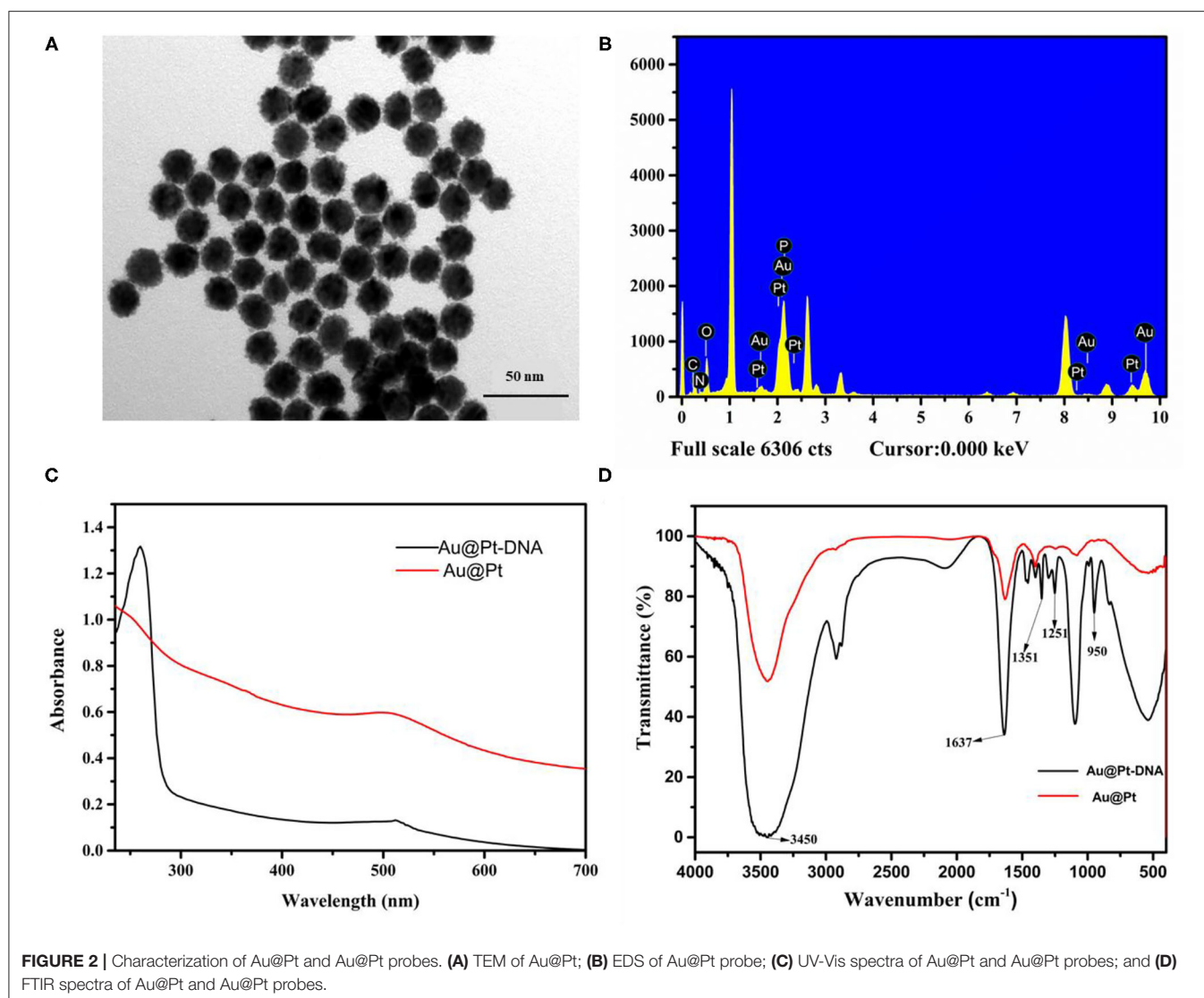
in PBS buffer to catalyze TMB for the trace detection of CBZ using a multifunctional microplate reader (Salzburg, Austria).

Sample Preparation

The leeks and rice samples were obtained from the Shangdong vegetable production field to evaluate the feasibility of the developed assay. Blank samples (free from CBZ) were used for creating a calibration curve and recovery experiments. The leeks and rice samples were pretreated with QuEChERS (quick, easy, cheap, effective, rugged, and safe) method designed by the Anastassiades team (32) with slight modifications. Standard concentrations (10, 50, and 100 $\mu g \cdot kg^{-1}$) were used as spiking levels to homogenized samples (10 g for leeks, 5 g for rice) in 50-ml centrifuge tubes. Afterward, the spiked samples were allowed to equilibrate at room temperature for 4 h. Subsequently, 10 ml acetonitrile was added, followed by a 2 min vortex mix. Next, 2 g anhydrous $MgSO_4$ and 1 g NaCl were added for dehydration and stratification (vigorous shaking for 1 min). The supernatant was

transferred into a 10-ml plastic tube, vortexed for another 1 min, and centrifuged at 5,000 rpm (at 4°C) for 5 min. Subsequently, 5 ml supernatant was purified using a purification cartridge (52 mg PSA, 52 mg C18, and 26 mg GCB), vortexed again for 1 min, and then centrifuged at 10,000 rpm (at 4°C) for 5 min. Finally, the supernatant was filtered through a 0.22-μm filter (Jinteng, China) for competitive assay based on Au@Pt-dsDNA-Fe_3O_4 biosensor and LC-MS/MS analysis.

RESULTS

Characterization of Au@Pt and Au@Pt Probe

Using Au as seeds, a thin Pt layer was deposited on the surface of the Au core to achieve Au@Pt. The morphology of Au@Pt nanoparticles was characterized by transmission electron microscopy (TEM). As shown in **Figure 2A**, the Au@Pt showed uniform spherical shapes with an average

FIGURE 3 | Optimization of the experimental conditions. **(A)** pH; **(B)** DNA concentration; and **(C)** reaction time.
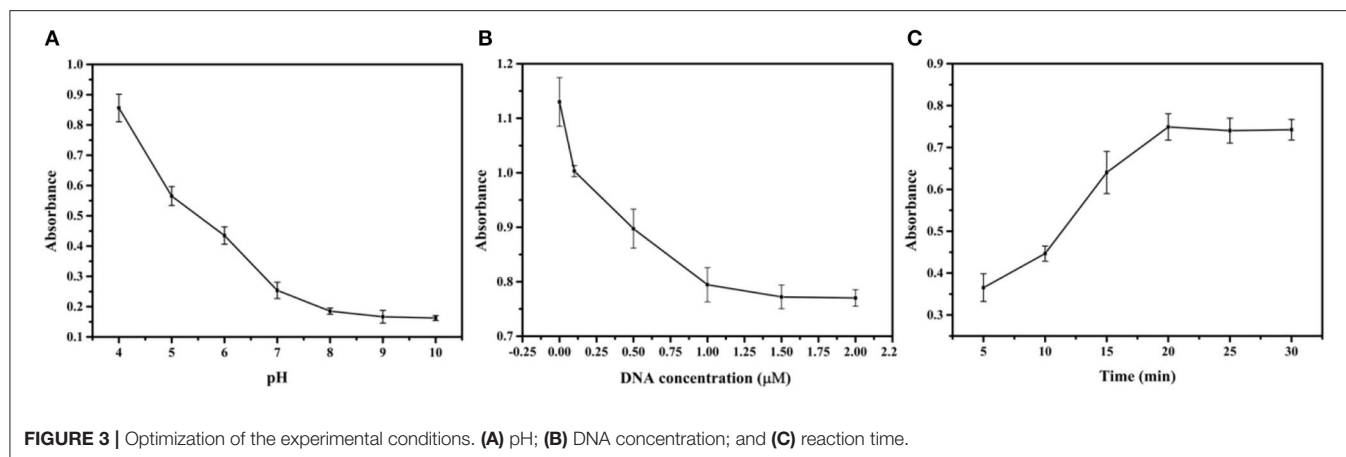
particle size of 20 nm. Compared with smooth Au (as shown in **Supplementary Figure 1A**). The particle size of Au@Pt was increased by ∼5 nm indicating the existence of smooth AuNPs surface of a 5 nm layer Pt. The TEM images of Au@Pt demonstrated that the Au@Pt core-shell structure was successfully prepared. Then, the Au@Pt and Au@Pt probes were carefully characterized by energy dispersive spectrometer (EDS). As presented in **Figure 2B**, the EDS of Au@Pt probe has shown that P element signal except for Au and Pt, which are from Au@Pt nanoparticles (as depicted in **Supplementary Figure 1B**). Therefore, the P characteristic element can be inferred from the DNA. The EDS (Hitachi Co., Ltd., Tokyo, Japan) of Au@Pt and Au@Pt probes indicate that the DNA was successfully modified on the Au@Pt surface. To further confirm the successful preparation of the Au@Pt probe, the UV–vis spectra (Shimadzu, Japan) were used to verify the synthesized Au@Pt probe. The UV–vis spectra of Au@Pt (red line) have a maximum absorbance at 508 nm. Compared with Au@Pt, a prominent characteristic absorbance peak near 260 nm was noticed in UV–vis spectroscopy of Au@Pt probe (black line), as presented in **Figure 2C**. As reported, the maximum absorption peak of DNA occurs at 260 nm (23), denoting that the Au@Pt surface was conjugated with DNA. In addition, the Au@Pt probe was characterized by FT-IR (Pittsburgh, USA), as depicted in **Figure 2D**. Peaks around 3,450 and 1,637 cm^{-1} are derived from the O–H stretching, representing the H-O-H bending vibration of water. The characteristic peaks of 1,351, 1,251, and 950 cm^{-1} were observed except for 3,450 and 1,637 cm^{-1} in the Fourier-transform infrared spectroscopy (FTIR) spectra of the Au@Pt probe. These characteristic peaks, corresponding to C=C, C-N, and C-H, respectively, can be inferred from bases of DNA. These results denote that the DNA was successfully modified on the surface of Au@Pt.

Optimization of the Experimental Conditions

This section investigated the influence of important factors, such as pH value, DNA concentration, and reaction time, to achieve the optimal experimental conditions for CBZ detection. The pH plays a crucial role in the preparation of the Au@Pt probe. A series of pH ranges (4.0, 5.0, 6.0, 7.0, 8.0, 9.0, and 10.0) was set to estimate the optimal value for forming the Au@Pt probe. The catalytic efficiency of the Au@Pt probe was decreased with increasing the pH value to 8.0 (as depicted in **Figure 3A**). The DNA is easily degraded under acidic conditions (low pH value). The Au@Pt probe catalytic efficiency was increased because more catalytic active sites were exposed with a low concentration of DNA modified on the surface of Au@Pt nanomaterials. Thus, the optimal pH value was set at 8.0 for this assay. The sensitivity of the competitive assay based on Au@Pt-dsDNA-Fe$_3$O$_4$ biosensor depends on the DNA concentrations modified on the surface of Au@Pt. Then, the DNA concentration was carefully optimized as well. Different DNA concentrations (0, 0.1, 0.5, 1.0, 1.5, and 2.0 μM) were designed to prepare the Au@Pt probe. Like the influence of pH, the catalytic efficiency of the Au@Pt probe was reduced with a high concentration of DNA, as can be displayed from **Figure 3B**, reaching maximum absorbance at 1.0 μM. Notably, this evidence demonstrated that the optimal concentration of DNA was 1.0 μM in this assay. It is essential to optimize the reaction time between CBZ and Au@Pt probe to detect CBZ rapidly. In turn, a set of reaction times (5, 10, 15, 20, 25, and 30 min) were designed to achieve the optimal reaction time. As time increased, the catalytic efficiency of the Au@Pt probe was improved, reaching the maximum absorbance at 20 min (as shown in **Figure 3C**). Thus, 20 min was identified as the optimized reaction time for the following experiments.

Qualitative Analysis

The CBZ and the Fe$_3$O$_4$ probe competitively react with DNA-modified nanomaterials Au@Pt to form Au@Pt-ssDNA-CBZ biosensor and Au@Pt-dsDNA-Fe$_3$O$_4$ biosensor, respectively. The Au@Pt-ssDNA-CBZ biosensor solution color dramatically changed from light blue to dark blue with Au@Pt-ssDNA-CBZ biosensor to catalyze TMB when the concentration of CBZ increased from 0 to 100 ng/ml (as shown in **Figure 4A**). The catalytic efficiency of the Au@Pt-ssDNA-CBZ biosensor was improved by increasing the CBZ concentration. The Au@Pt-ssDNA-CBZ biosensor catalytic efficiency was increased because more catalytic active sites were exposed in the presence of CBZ, which was bonded to the DNA on the surface of

FIGURE 4 | Construction of the calibration curve. **(A)** UV–vis spectra absorbance for various concentrations of carbendazim (CBZ); **(B)** the absorbance scan with CBZ concentration (0.00–100 ng/ml); and **(C)** calibration curve of a competitive assay based on Au@Pt-dsDNA-Fe$_3$O$_4$ biosensor ($n = 3$).
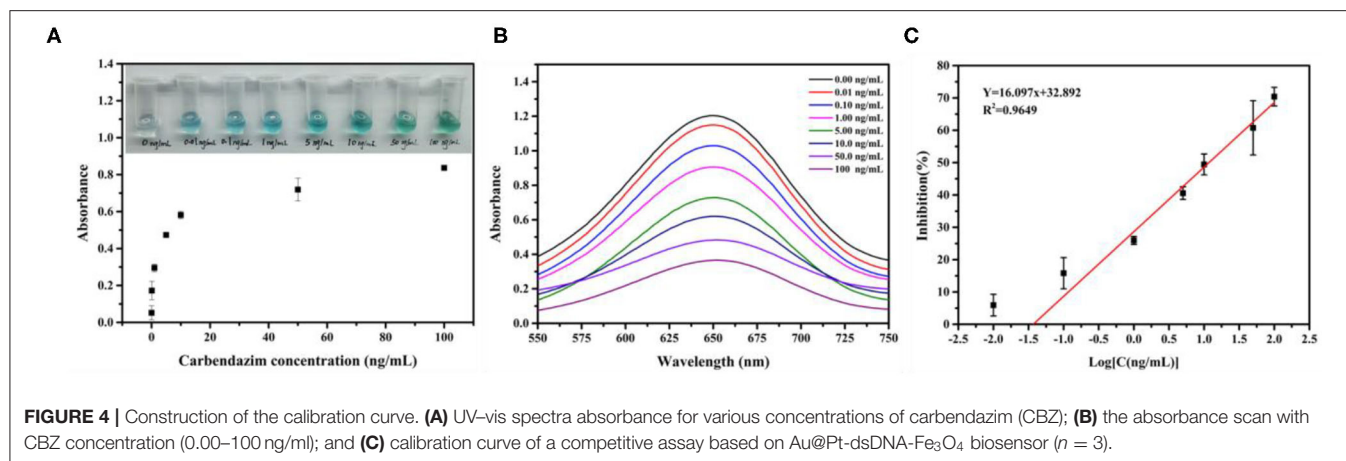
TABLE 1 | Calibration curve of carbendazim (CBZ) in field incurred samples ($n = 3$).

Samples	Spiked concentration (ng/mg)	Recovery (%)	RSD (%)	IC$_{50}$ (ng/mg)	LOD (ng/mg)	R^2
Leek	10	71.88 ± 0.04	10.91	7.56	0.044	0.9613
	50	96.40 ± 0.01	3.93			
	100	110.11 ± 0.02	6.76			
Rice	10	91.62 ± 0.03	6.52	6.08	0.041	0.9453
	50	89.86 ± 0.01	4.21			
	100	107.45 ± 0.01	3.16			

C_{50}: Represents the concentration at which a substance exerts half of its maximal inhibitory effect.

Au@Pt nanomaterials. Hence, the designed Au@Pt-ssDNA-CBZ biosensor could use as a qualitative analysis biosensor for on-site pesticide monitoring in the agro-products.

Quantitative Analysis (Calibration Curves)

The calibration curve was established based on Au@Pt-dsDNA-Fe$_3$O$_4$ biosensor catalysis in the competitive assay. The absorbance intensity decreased as the CBZ concentration increased in this study, as depicted in **Figure 4B**. It displayed a maximum absorbance at 650 nm. The calibration curve of the competitive assay based on Au@Pt-dsDNA-Fe$_3$O$_4$ biosensor for detection of CBZ pesticide was established under the optimal condition (**Figure 4C**). The calibration regression equation of curve ($Y = 16.097\text{x} + 32.892$) was achieved with a wide linear range. Y represented the inhibition rate (%) and the logarithmic (Log) concentration of CBZ as the X abscissa axis. A low-detection limit (0.038 ng/mg) was acquired with a good linear relationship ($R^2 = 0.9649$). The RSDs ranged from 1.56 to 10.22%. The LOD of this assay was lower than the maximum residue limit (MRL) of CBZ enacted by China (GB 2763–2021) in various agro-products.

Assay Evaluation

The method was validated in terms of accuracy, precision, and LODs. The accuracy (recoveries of the proposed assay),

precision (RSDs of the proposed assay), LODs, and correlation coefficients (R^2 of regression equation) were used to evaluate the reliability, applicability, and sensitivity of the assay. To determine the validation parameters, three concentrations (10, 50, and 100 ng/mg) of CBZ standard solutions were chosen. For leek samples, the average recoveries ranged from 71.88 to 110.11% with RSDs (3.93–10.91%), and a low LOD (0.044 ng/mg) and IC$_{50}$ (7.56 ng/mg) were acquired in the competitive assay. Like leeks', average recoveries of rice, RSDs, LOD, and IC$_{50}$ were 89.86–107.45%, 4.21–6.52%, 0.041 ng/mg and 6.08 ng/mg, respectively (**Table 1**). The regression equations were $Y = 17.905\text{x} + 34.267$ and $Y = 18.718\text{x} + 36.535$ for leeks and rice, respectively. Hence, good correlations (R^2 0.9613 for leeks and 0.9453 for rice) were gained using the competitive assay (**Table 1**, **Supplementary Figure 3**). Therefore, the Au@Pt-dsDNA-Fe$_3$O$_4$ biosensor of this competitive assay holds the potential as a sensitive and reliable assay for residual trace detection of pesticides.

Specificity

Specificity, recognizing the target molecule, is essential in the performance evaluation [33]. The accuracy of the assay method is mainly based on the specificity of the CBZ aptamer [2]. Several commonly used fungicides and insecticides (100 ng/ml solution of imidacloprid, procymidone, chlorpyrifos, and acetamiprid)
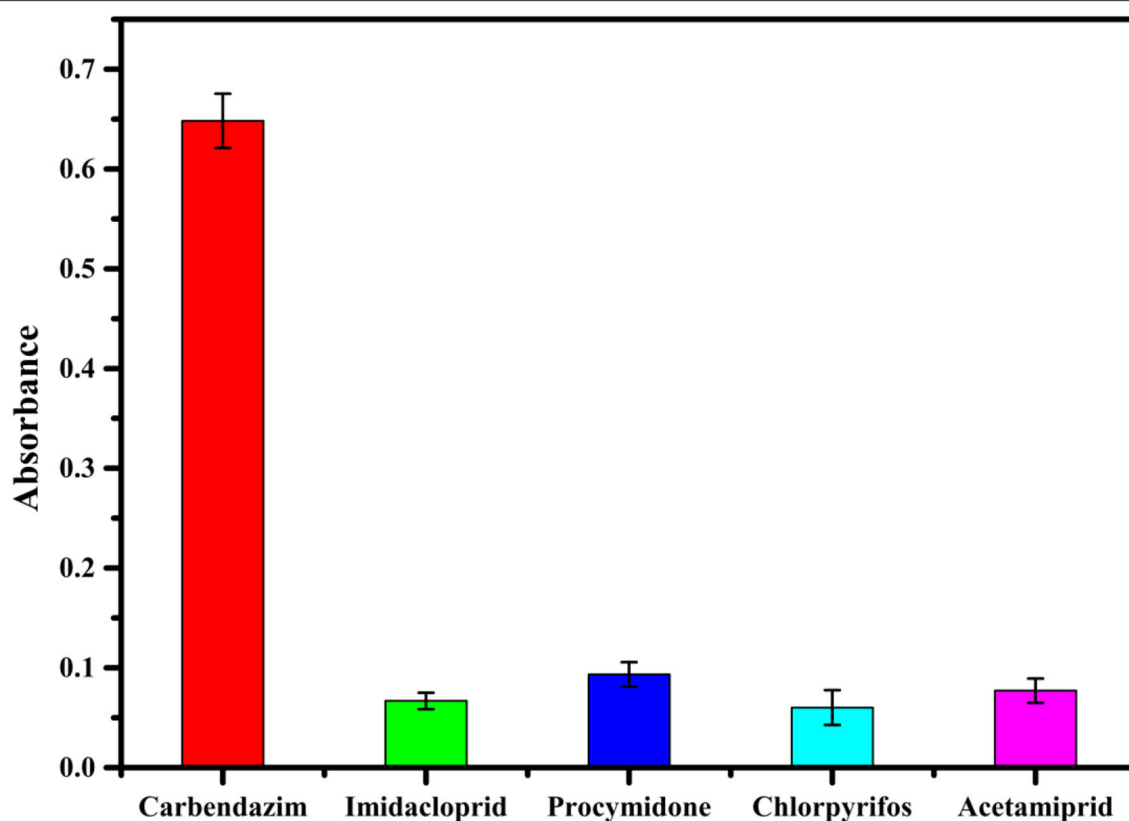
FIGURE 5 | Specificity between CBZ and other unrelated pesticides.

were investigated to evaluate the specificity of the proposed competitive assay for detection of CBZ. As can be inferred from **Figure 5**, the absorbance of the Au@Pt-ssDNA-CBZ biosensor increased only in the presence of CBZ. In contrast, other pesticides caused minor changes in absorbance. Hence, imidacloprid, procymidone, chlorpyrifos, and acetamiprid have a negligible effect on the proposed competitive assay in the presence of CBZ.

Confirmation Analysis

To further confirm the proposed accuracy of the assay, the blank leeks and rice samples were randomly selected to establish the correlation between the competitive assay and LC-MS/MS method (the parameters of LC-MS/MS shown in **Supplementary Table 2**). Five concentrations (5, 10, 20, 50, and 100 ng/mg) of CBZ were spiked to blank leek ($n = 24$) and rice ($n = 24$) samples with vigorous shaking. Half of the samples were analyzed by the proposed competitive assay based on Au@Pt-dsDNA-Fe$_3$O$_4$ biosensor, and the rest were quantified with LC-MS/MS. The correlation coefficients were achieved to assess the association between both methods. The correlation coefficients were 0.9339 and 0.9321 for leek and rice, respectively (**Figure 6**, **Supplementary Table 3**). These findings denote that competitive assay has good reliability to satisfy the requirements for pesticide detection in agro-products.

DISCUSSION

This study proposed dual-mode Au@Pt-DNA biosensors (Au@Pt-ssDNA-CBZ biosensor and Au@Pt-dsDNA-Fe^{3}O^4 biosensor) to analyze CBZ residues agricultural products.

The construction of the Au@Pt probe is the main key factor for Au@Pt-DNA biosensors. The EDS, UV–vis and FT-IR techniques were used to characterize the Au@Pt probe. Compared with Au@Pt nanoparticles (as depicted in **Supplementary Figure 1B**), the EDS of the Au@Pt probe has shown a *P* element signal (**Figure 2B**). It has been deduced that the *P* element is derived from DNA. A prominent characteristic absorbance peak (near 260 nm) was noticed in UV–vis spectroscopy of the Au@Pt probe (**Figure 2C**). As reported, the maximum absorption peak of DNA occurs at 260 nm [23]. The characteristic peaks of 1,351, 1,251, and 950 cm^{-1}, corresponding to C=C, C-N, and C-H, were observed in the FTIR spectra of the Au@Pt probe, as shown in **Figure 2D**. These results denote that the Au@Pt probe was successfully prepared.

The pH value, DNA concentration, and reaction time were investigated for establishing the assay based on Au@Pt-DNA biosensors to detect CBZ. The DNA is easily degraded under acidic conditions. The catalytic efficiency of the Au@Pt probe achieved the best results when the pH value reached 8.0 (**Figure 3A**). Similarly, the concentration of DNA at 1.0 μM, the catalytic efficiency of the Au@Pt probe reached maximum

FIGURE 6 | Correlation between the concentrations of CBZ measured by the proposed competitive assay based on Au@Pt-dsDNA-Fe$_3$O$_4$ mediated biosensor and LC–MS/MS in **(A)** leeks and **(B)** rice.
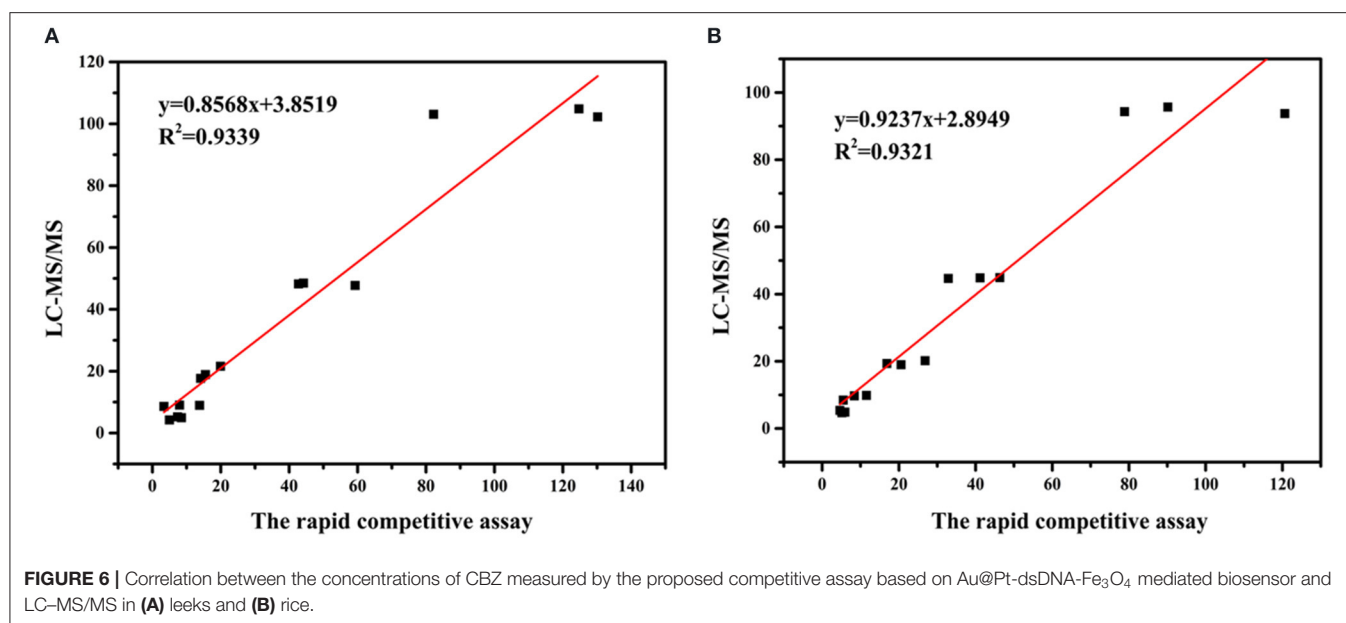
absorbance (**Figure 3B**). The Au@Pt probe with low DNA concentration achieves poor sensitivity. However, the higher DNA concentration inhibits the Au@Pt probe catalysis efficiency because too much DNA concentration might be covering the catalytic site on the Au@Pt nanozyme.

The Au@Pt-ssDNA-CBZ biosensor solution color dramatically changed from light blue to dark blue with Au@Pt-ssDNA-CBZ biosensor to catalyze TMB when the concentration of CBZ increased from 0 to 100 ng/ml (as shown in **Figure 4A**). The catalytic efficiency of the Au@Pt-ssDNA-CBZ biosensor improved by increasing the CBZ concentration because more catalytic active sites of Au@Pt were exposed in the presence of CBZ that was bonded to the DNA on the surface of Au@Pt nanomaterials. Hence, the designed Au@Pt-ssDNA-CBZ biosensor could use as a qualitative analysis biosensor for on-site pesticide monitoring in agro-products through naked-eye visualization.

In addition, the Au@Pt-dsDNA-Fe$_3$O$_4$ biosensor was regarded as quantitate analysis biosensor to establish a sensitive and reliable assay for residual trace detection of pesticides. The regression equation of calibration curve' ($Y = 16.097x + 32.892$, $R^2 = 0.9649$) was achieved. This assay acquired a low LOD (0.038 ng/mg) with RSDs ranged from 1.56 to 10.22% (**Figure 4C**). The leeks and rice samples were selected to monitor the residual levels of CBZ using the proposed assay. As shown in **Table 1**, the mean recoveries (leeks: 71.88–110.11%, rice: 89.86–107.45%) meet the EU guidance document for pesticide residue testing (SANTE/11813/2017). This assay acquired a low LOD (0.038 ng/mg) with RSDs ranging from 1.56 to 10.22%. Therefore, the Au@Pt-dsDNA-Fe$_3$O$_4$ biosensor of this competitive assay holds the potential as a sensitive and reliable assay for residual trace detection of pesticides. Compared with other assays based on nanomaterials, such as Au/Fe$_3$O$_4$ (6), UCNPs-MnO$_2$ (34), AuNPs (35, 36), Nd$_2$O$_3$ (37), and MoS$_2$/MWCNTs (38) for CBZ detection is compiled in **Table 2**. As shown, this proposed

TABLE 2 | Various assays for detection of CBZ based on nanomaterials.

Nanomaterials	Recovery (%)	LOD	Reference
Au@Pt	71.88–110.11%	0.037 ng/mg	This work
Au/Fe$_3$O$_4$	102.4–115.0%	0.44 ng/ml	(6)
UCNPs-MnO$_2$	85.58–109.40%	0.05 ng/ml	(34)
AuNPs	94.9–104.8%	2.2 nM	(35)
AuNPs	96.3–111.2%	2.33 nM	(36)
Nd$_2$O$_3$	-	0.027 mM	(37)
MoS$_2$/MWCNTs	89.18–105.56%	7.4 nM	(38)

competitive assay based on dual-mode Au@Pt-DNA biosensors acquires much lower LOD than other nanomaterials. Besides, the LOD of this assay is much lower than the MRL of CBZ set by China in various agro-products.

CONCLUSIONS AND FUTURE PERSPECTIVES

A competitive assay based on dual-mode Au@Pt-DNA biosensors combined aptamer (DNA) specific recognition property, bimetallic nanomaterials Au@Pt catalysis, and Fe$_3$O$_4$ magnetic separation was proposed to trace the CBZ residue. The qualitative Au@Pt-ssDNA-CBZ biosensor with aptamer (DNA) specific recognition property monitors pesticides through light blue to dark blue visualization and quantitative Au@Pt-dsDNA-Fe$_3$O$_4$ biosensor with bimetallic nanomaterials Au@Pt catalysis and Fe$_3$O$_4$ magnetic separation detect CBZ residue, respectively. Overall, this proposed competitive assay holds the potential as a sensitive and reliable assay for residual trace detection of pesticides and can be used for rapid on-site pesticide

monitoring, reducing false-negative results, and improving screening efficiency and sensitivity.

DATA AVAILABILITY STATEMENT

The original contributions presented in the study are included in the article/**Supplementary Material**, further inquiries can be directed to the corresponding authors.

AUTHOR CONTRIBUTIONS

GC and DX investigated, designed, and wrote the original draft. RZ, GL, and XH investigated and supervised the article. KZ, XX, LL, and YZ visualized and investigated. MJ, JW, and AA were involved in investigation and writing (review and editing) the manuscript. All the authors contributed to the article and approved the submitted version.

SUPPLEMENTARY MATERIAL

The Supplementary Material for this article can be found online at: https://www.frontiersin.org/articles/10.3389/fnut.2022.820150/full#supplementary-material

REFERENCES

1. Chuang S, Yang H, Wang X, Xue C, Jiang J, Hong Q. Potential effects of Rhodococcus qingshengii strain djl-6 on the bioremediation of carbendazim-contaminated soil and the assembly of its microbiome. *J Hazard Mater.* (2021) 414:125496. doi: 10.1016/j.jhazmat.2021.125496

2. Fu R, Zhou J, Liu Y, Wang Y, Liu H, Pang J, et al. Portable and quantitative detection of carbendazim based on the readout of a thermometer. *Food Chem.* (2021) 351:129292. doi: 10.1016/j.foodchem.2021.129292

3. Liu Z, Chen Y, Han J, Chen D, Yang G, Lan T, et al. Determination, dissipation dynamics, terminal residues and dietary risk assessment of thiophanate-methyl and its metabolite carbendazim in cowpeas collected from different locations in China under field conditions. *J Sci Food Agric.* (2021) 101:5498–507. doi: 10.1002/jsfa.11198

4. Li P, Sun P, Dong X, Li B. Residue analysis and kinetics modeling of thiophanate-methyl, carbendazim, tebuconazole, and pyraclostrobin in apple tree bark using QuEChERS/HPLC-VWD. *Biomed Chromatogr.* (2020) 34:e4851. doi: 10.1002/bmc.4851

5. Chu Y, Tong Z, Dong X, Sun M, Gao T, Duan J, et al. Simultaneous determination of 98 pesticide residues in strawberries using UPLC-MS/MS and GC-MS/MS. *Microchem J.* (2020) 156:104975. doi: 10.1016/j.microc.2020.104975

6. Li Q, Dou X, Zhao X, Zhang L, Luo J. Xing, X, et al. A gold/Fe$_3$O$_4$ nanocomposite for use in a surface plasmon resonance immunosensor for carbendazim. *Microchim Acta.* (2019) 186:313. doi: 10.1007/s00604-019-3402-0

7. Koukouvinos G, Karachaliou CE, Raptis I, Petrou P, Livaniou E, Kakabakos S. Fast and sensitive determination of the fungicide carbendazim in fruit juices with an immunosensor based on white light reflectance spectroscopy. *Biosensors.* (2021) 11:153. doi: 10.3390/bios11050153

8. Qiao Q, Guo X, Wen F, Chen L, Xu Q, Zheng N, et al. Aptamer-based fluorescence quenching approach for detection of aflatoxin M1 in milk. *Front Chem.* (2021) 9:653869. doi: 10.3389/fchem.2021.653869

9. Zhao X, Zhang X, Qin M, Song Y, Zhang J, Xia X, et al. Determination of carbendazim by aptamer-based fluorescence resonance energy transfer (FRET). *Anal Lett.* (2020) 54:2198–210. doi: 10.1080/00032719.2020.1849250

10. Zikos C, Evangelou A, Karachaliou CE, Gourma G, Blouchos P, Moschopoulou G, et al. Commercially available chemicals as immunizing haptens for the development of a polyclonal antibody recognizing carbendazim and other benzimidazole-type fungicides. *Chemosphere.* (2015) 119:16–20. doi: 10.1016/j.chemosphere.2014.03.049

11. Yan H, Liu L, Xu N, Kuang H, Xu C. Development of an immunoassay for carbendazim based on a class-selective monoclonal antibody. *Food Agric Immunol.* (2015) 26:659–70. doi: 10.1080/09540105.2015.1007446

12. Zhou W, Huang PJ, Ding J, Liu J. Aptamer-based biosensors for biomedical diagnostics. *Analyst.* (2014) 139:2627–40. doi: 10.1039/c4an00132j

13. Fan K, Yang R, Zhao Y, Zang C, Miao X, Qu B, et al. A fluorescent aptasensor for sensitive detection of isocarbophos based on AT-rich three-way junctions DNA templated copper nanoparticles and Fe$_3$O$_4$@GO. *Sens Actuators B.* (2020) 321:128515. doi: 10.1016/j.snb.2020.128515

14. McConnell EM, Nguyen J, Li Y. Aptamer-based biosensors for environmental monitoring. *Front Chem.* (2020) 8:434. doi: 10.3389/fchem.2020.00434

15. Shi YQ Li WT, Feng XP, Lin L, Nie PC, Shi JY, et al. Sensing of mercury ions in Porphyra by Copper@Gold nanoclusters based ratiometric fluorescent aptasensor. *Food Chem.* (2021) 344:10. doi: 10.1016/j.foodchem.2020.128694

16. Zhang WW, Wang YL, Nan MN Li YC, Yun JM, Wang Y, et al. Novel colorimetric aptasensor based on unmodified gold nanoparticle and ssDNA for rapid and sensitive detection of T-2 toxin. *Food Chem.* (2021) 348:8. doi: 10.1016/j.foodchem.2021.129128

17. Nan MN Bi Y, Xue HL, Long HT, Xue SL, Pu LM, et al. Modification performance and electrochemical characteristics of different groups of modified aptamers applied for label-free electrochemical impedimetric sensors. *Food Chem.* (2021) 337:6. doi: 10.1016/j.foodchem.2020.127761

18. Wei H, Wang EK. Nanomaterials with enzyme-like characteristics (nanozymes): next-generation artificial enzymes. *Chem Soc Rev.* (2013) 42:6060–93. doi: 10.1039/c3cs35486e

19. Weerathunge P, Behera BK, Zihara S, Singh M, Prasad SN, Hashmi S, et al. Dynamic interactions between peroxidase-mimic silver nanozymes and chlorpyrifos-specific aptamers enable highly-specific pesticide sensing in river water. *Anal Chim Acta.* (2019) 1083:157–65. doi: 10.1016/j.aca.2019.07.066

20. Wang Q, Wei H, Zhang Z, Wang E, Dong S. Nanozyme: An emerging alternative to natural enzyme for biosensing and immunoassay. *TrAC, Trends Anal Chem.* (2018) 105:218–24. doi: 10.1016/j.trac.2018.05.012

21. Sim S, Beierle A, Mantos P, McCrory S, Prasankumar RP, Chowdhury S. Ultrafast relaxation dynamics in bimetallic plasmonic catalysts. *Nanoscale.* (2020) 12:10284–91. doi: 10.1039/D0NR00831A

22. Lu C, Tang L, Gao F, Li Y, Liu J, Zheng J. DNA-encoded bimetallic Au-Pt dumbbell nanozyme for high-performance detection and eradication of *Escherichia coli* O157:H7. *Biosens Bioelectron.* (2021) 187:113327. doi: 10.1016/j.bios.2021.113327

23. Chen G, Liu G, Jia H, Cui X, Wang Y, Li D, et al. A sensitive bio-barcode immunoassay based on bimetallic Au@Pt nanozyme for detection of organophosphate pesticides in various agro-products. *Food Chem.* (2021) 362:130118. doi: 10.1016/j.foodchem.2021.130118

24. Tian J, Liang Z, Hu O, He Q, Sun D, Chen Z. An electrochemical dual-aptamer biosensor based on metal-organic frameworks MIL-53 decorated with Au@Pt nanoparticles and enzymes for detection of COVID-19 nucleocapsid protein. *Electrochim Acta.* (2021) 387:138553. doi: 10.1016/j.electacta.2021.138553

25. Wei SS, Xiao HL, Gu M, Chen ZC, Cao LL. Ultrasensitive label-free electrochemical immunosensor based on core-shell Au@PtNPs functionalized rGO-TEPA/PB nanocomposite for HBsAg detection. *J Electroanal Chem.* (2021) 890:9. doi: 10.1016/j.jelechem.2021.115216

26. Ma JL, Yin BC, Wu X, Ye BC. Copper-mediated dna-scaffolded silver nanocluster switch for detection of pyrophosphate and alkaline phosphatase. *Anal Chem.* (2016) 88:9219–25. doi: 10.1021/acs.analchem.6b02465

27. Jin X, Chen L, Zhang YT, Wang XL, Zhou ND, A. lateral flow strip for on-site detection of tobramycin based on dual-functional platinum-decorated gold nanoparticles. *Analyst.* (2021) 146:3608–16. doi: 10.1039/D1AN00403D

28. Chen G, Jin M, Ma J, Yan M, Cui X, Wang Y, et al. Competitive bio-barcode immunoassay for highly sensitive detection of parathion based on bimetallic nanozyme catalysis. *J Agric Food Chem.* (2021) 68:660–8. doi: 10.1021/acs.jafc.9b06125

29. Sajwan RK, Lakshmi G, Solanki PR. Fluorescence tuning behavior of carbon quantum dots with gold nanoparticles *via* novel intercalation effect of aldicarb. *Food Chem.* (2021) 340:9. doi: 10.1016/j.foodchem.2020.127835

30. Wu X, Song Y, Yan X, Zhu C, Ma Y, Du D, et al. Carbon quantum dots as fluorescence resonance energy transfer sensors for organophosphate pesticides determination. *Biosens Bioelectron.* (2017) 94:292–7. doi: 10.1016/j.bios.2017.03.010

31. Eissa S, Zourob M. Selection and characterization of DNA aptamers for electrochemical biosensing of carbendazim. *Anal Chem.* (2017) 89:3138–45. doi: 10.1021/acs.analchem.6b04914

32. Anastassiades M, Lehotay SJ, Stajnbaher D, Schenck FJ. Fast and easy multiresidue method employing acetonitrile extraction/partitioning and "dispersive solid-phase extraction" for the determination of pesticide residues in produce. *J AOAC Int.* (2003) 86:412–31. doi: 10.1093/jaoac/86.2.412

33. Ouyang Q, Wang L, Ahmad W, Rong Y, Li H, Hu Y, et al. A highly sensitive detection of carbendazim pesticide in food based on the upconversion-MnO₂ luminescent resonance energy transfer biosensor. *Food Chem.* (2021) 349:129157. doi: 10.1016/j.foodchem.2021.129157

34. Zhang XL, Wu D, Zhou XX Yu YX, Liu JC, Hu N, et al. Recent progress in the construction of nanozyme-based biosensors and their applications to food safety assay. *TrAC, Trends Anal Chem.* (2019) 121:22. doi: 10.1016/j.trac.2019.115668

35. Wang S, Su L, Wang L, Zhang D, Shen G, Ma Y. Colorimetric determination of carbendazim based on the specific recognition of aptamer and the poly-diallyldimethylammonium chloride aggregation of gold nanoparticles. *Spectrochim Acta, Part A.* (2020) 228:117809. doi: 10.1016/j.saa.2019.117809

36. Zhou Y, Li Y, Han P, Dang Y, Zhu M, Li Q, et al. A novel low-dimensional heteroatom doped Nd₂O₃ nanostructure for enhanced electrochemical sensing of carbendazim. *New J Chem.* (2019) 43:14009–19. doi: 10.1039/C9NJ02778E

37. Zhu X, Liu P, Ge Y, Wu R, Xue T, Sheng Y, et al. MoS₂/MWCNTs porous nanohybrid network with oxidase-like characteristic as electrochemical nanozyme sensor coupled with machine learning for intelligent analysis of carbendazim. *J Electroanal Chem.* (2020) 862:113940. doi: 10.1016/j.jelechem.2020.113940

38. Su L, Wang S, Wang L, Yan Z, Yi H, Zhang D, et al. Fluorescent aptasensor for carbendazim detection in aqueous samples based on gold nanoparticles quenching Rhodamine B. *Spectrochim Acta, Part A.* (2020) 225:117511. doi: 10.1016/j.saa.2019.117511

Residue, Dissipation Pattern, and Dietary Risk Assessment of Imidacloprid in Chinese Chives

Rongqi Zhai[1], Kaige Zhang[1], Ge Chen[1]*, Guangyang Liu[1], Xiaodong Huang[1], Mingkun Gao[1], Jie Zhou[1], Xiaomin Xu[1], Lingyun Li[1], Yanguo Zhang[1], Jing Wang[2], Maojun Jin[2], Donghui Xu[1]* and A. M. Abd El-Aty[3,4]

[1] Key Laboratory of Vegetables Quality and Safety Control, Laboratory of Quality & Safety Risk Assessment for Vegetable Products, Institute of Vegetables and Flowers, Ministry of Agriculture and Rural Affairs, Chinese Academy of Agricultural Sciences, Beijing, China, [2] Key Laboratory of Agro-Product Quality and Safety, Institute of Quality Standard and Testing Technology for Agro-Products, Ministry of Agriculture and Rural Affairs, Chinese Academy of Agricultural Sciences, Beijing, China, [3] Department of Pharmacology, Faculty of Veterinary Medicine, Cairo University, Giza, Egypt, [4] Department of Medical Pharmacology, Faculty of Medicine, Atatürk University, Erzurum, Turkey

The demand for Chinese chives is growing as they are also rich in vitamins, fiber, and sulfur nutrients. Chinese chives should be sprayed with imidacloprid to control pests and diseases to safeguard their yield and to meet the demands of East Asian consumers for Chinese chives. Overspraying of imidacloprid can lead to residues in Chinese chives, posing a severe risk to human health. To reduce the harmful effects of imidacloprid residues on humans, we investigated the imidacloprid dissipation pattern and the final residue on Chinese chives using the quick, easy, cheap, effective, rugged, and safe (QuEChERS) method combined with liquid chromatography-tandem mass spectrometry (LC-MS/MS). Good linearity ($R^2 = 0.9988$), accuracy (expressed as recovery % of 78.34–91.17%), precision [expressed as relative SDs (RSDs) of 0.48–6.43%], and sensitivity [a limit of quantification (LOQ) $\leq 8.07 \times 10^4$ mg/kg] were achieved. The dissipation dynamics were consistent with the first-order kinetics, with a half-life of 2.92 days. The final residual levels on Chinese chives were 0.00923–0.166 mg/kg, which is lower than the maximum residue limits (MRLs) of 1 mg/kg for imidacloprid on Chinese chives. A risk assessment index of <1 indicates that Chinese chives are safe for consumption.

Keywords: imidacloprid pesticides, dissipation dynamics, Chinese chives, sample preparation, risk assessment

INTRODUCTION

Chinese chives (*Allium tuberosum*) are among the most important vegetables to East Asians (1). It is rich in vitamins, fiber, and sulfur compounds with antiseptic properties (2, 3). According to traditional Chinese medicine, it has aphrodisiac, anti-cancer, antioxidant, and other healing properties and treats abdominal pain and asthma (4–6). Modern medicine shows that the dietary fiber in Chinese chives could promote intestinal peristalsis and accelerate the body's metabolism, thereby preventing colorectal cancer. It also decreases cholesterol absorption and prevents atherosclerosis and coronary heart disease (7, 8). Therefore, the economic value of chives is increasing, which leads to the expansion of the planting area.

As Chinese chives are planted on a large scale, plant pests and diseases increased accordingly. The Chinese chives maggot (*Bradysiaodoriphaga*), with a short reproductive cycle, high fertility,

TABLE 1 | Imidacloprid elution conditions.

Time (min)	Flow rate (mL/min)	Methanol (%)	Ammonium acetate solution (1 mmol,%)
0	0.3	20	80
8	0.3	95	5
12	0.3	95	5
12.1	0.3	20	80

and overwintering under protected conditions, becomes an annual pest occurrence (9). The rate of affected plants can reach 20–50%. The damage of Chinese chives maggot is the most severe problem (10). Farmers spray imidacloprid to control pests, which acts as an inhibitor of nicotinic acetylcholine receptors (nAChRs) in the central nervous system of insects, causing disruption of the insect's nervous system and, eventually, leading to death (11, 12). It fails to decompose thoroughly, resulting in long residual levels (13) that would result in harmful health effects.

The residue dissipation of imidacloprid has been reported in Chinese chives. However, few studies detected the imidacloprid residues using a liquid chromatography-tandem mass spectrometry (LC-MS/MS), and assessed its dietary risk in Chinese chives (14, 15). Studying pesticide residues and dissipation of imidacloprid is vital in Chinese chives because of its high residual pesticide and less-relevant dissipation dynamics (16). This study developed a method to analyze the imidacloprid residues in Chinese chives using QuEChERS combined with LC-MS/MS. Furthermore, we determined the dissipation pattern and the dietary risk assessment to help planters to further master the spraying and the harvesting period of imidacloprid in Chinese chives, thus, reducing the risk to the environment and the human health. Secondly, the study further explored the quick sample preparation of imidacloprid in Chinese chives. Finally, the study compared the recoveries, relative SDs (RSDs) of QuEChERS, and quick extraction to select a more suitable sample preparation for imidacloprid in Chinese chives.

MATERIALS AND METHODS

Chemicals and Equipment

Imidacloprid, water-dispersible granules (10% WG), was obtained from Hebei Noda Agrochemical Co., Ltd. Imidacloprid standard (100 mg/kg), was procured from Beijing Manhage Bio-Technology Co. Ltd. Acetonitrile (chromatographic grade), and was purchased from Merck AG, Germany. Anhydrous magnesium sulfate (analytical grade) was secured from Xilong Chemical Co., Ltd. Sodium chloride (analytical grade) and was supplied by Tianjin Huihang Chemical Technology Co., Ltd. Dispersed solid-phase extraction purifier (52-mg PSA; 52-mg C18; 26-mg GCB) was obtained from Shimadzu Corp. (Kyoto, Japan).

Field Experiment and Sampling

Final residue and dissipation field trials were carried out following the "Guideline for Testing of Pesticide Residues in

Crops" (NY/T 788–2018) (Ministry of Agriculture and Rural Affairs of the People's Republic of China, 2018). The final residual experiments were conducted in May 2020 at Tongzhou Beijing. The experiment set up a protective belt around each 50-m^2 plot, including a control plot without application of imidacloprid, an experiment plot of imidacloprid dissipation, and an experiment plot of final imidacloprid residue was reserved during the whole growth period.

Imidacloprid, at 10% WG, was applied at a dosage of 0.429 g/L when Chinese chives grew to 10–30 cm to investigate its dissipation. Fresh samples of at least 2 kg Chinese chives that have been drugged and are growing normally were randomly collected from 24 points of each plot. The fresh samples were collected and packed into sample containers that were wrapped and labeled after 2 h, 8 days, 18 days, and 25 days following the last application.

Soil and wilted leaves attached to the Chinese chives were removed. The samples were cut and mixed, homogenized with a beater, and packed into sample boxes. The sample boxes were labeled and stored at −20°C in the refrigerator.

Sample Preparation

As the composition of Chinese chives substrate is more complex than other vegetables, the sample preparation was carried out with two different methods.

Method 1 (QuEChERS): Chinese chives homogenate (10 g) was weighed and placed in a 50-mL centrifuge tube. Then, 10-mL acetonitrile was added to the centrifuge tube and vortexed for 1 min. After that, 4-g anhydrous magnesium sulfate and 1-g sodium chloride were added, vortexed again for 1 min, and centrifuged at 6,000 r/min for 5 min. The supernatant (9 mL) was transferred to a 50 mL centrifuge tube containing 90-mg dispersed solid-phase extraction purifier, vortexed for 30 s, and centrifuged at 6,000 r/min for 2 min. The sample was filtered through a 0.22-μm membrane and transferred into a glass vial for LC-MS/MS.

Method 2 (quick extraction): Chinese chives homogenate (1 g) was weighed and was placed in a 10-mL centrifuge tube. Next, 4 mL of an aqueous solution of 2, 5, and 10% of methanol were added respectively to the different centrifuge tubes, shaken manually for 30 s, and left undisturbed for 1 min. The sample was filtered through a 0.22-μm membrane and transferred into a glass vial for LC-MS/MS.

Liquid Chromatography-Tandem Mass Spectrometry (LC-MS/MS)

A Shimadzu LC-30A, MS8050 HPLC–MS/MS (Shimadzu Corp., Kyoto, Japan) instrument, equipped with an electrospray ionization (ESI), was adopted here. A Phenomenex-C18 column (50 mm × 3 mm, 2.6 μm) with an injection volume of 1 μL; column temperature of 40°C; flow rate of 0.3 ml/min; and elution conditions are shown in **Table 1**. The mass spectrometer was operated with electrospray in the positive ion mode (ESI$^+$), and the ions were monitored in the multiple reaction monitoring (MRM) mode. Mass spectrometric conditions: ion source temperature 400°C; ion pairs and collision energy and other parameters are shown in **Table 2**.

TABLE 2 | Characteristic monitoring ion of imidacloprid.

Name	Qualitative ion (*m/z*)	Quantification ion(*m/z*)	Retention time /min	Q1 Pre bias/V	Q3 Pre bias /V	Collision energy /eV
Imidacloprid	256.10/175.10	256.10/209.10	2.701	−27−27	−27 −22	−16−14

Dissipation Kinetics

The residue levels of imidacloprid on Chinese chives decreased with application time in Chinese chives, expressed by the first-order kinetic equation:

$$C_t = C_0 e^{-kt} \qquad (1)$$

$$T_{1/2} = \ln 2/k \qquad (2)$$

where C_t and C_0 represent the pesticide residual levels (mg/kg) at times t and 0 (days), respectively.

Dietary Exposure Assessment

We assessed the risk of imidacloprid in Chinese chives using a chronic dietary risk quotient (RQc) based on a risk factor approach (17).

$$RQc = \frac{NEDI}{ADI} \qquad (3)$$

$$NEDI = \frac{\sum(Fi \times STMR)}{bw} \qquad (4)$$

NEDI (mg/kg· bw/day): the national estimated daily intake; Fi (kg/day): the average daily *per capita* consumption of a particular food in China; STMR (mg/kg): supervised trials median residue; bw: the average body weight of Chinese adults (63 kg); ADI (mg/kg bw/day): the acceptable daily intake.

$$RQa = \frac{NESTI}{ARfD} \qquad (5)$$

$$NESTI = \frac{LP \times HR}{bw} \qquad (6)$$

NESTI (mg/kg·bw/day): the national estimated short-term intake; LP (kg/day): the large portion of specific food item consumed per day; HR (mg/kg): the highest residue; ARfD (mg/kg·bw/day): the acute reference dose. ARfD of imidacloprid was established to be 0.4 mg/kg·bw/day.

According to Mao et al. (18), the *per capita* annual consumption of Chinese chives was 33.40 kg, and the *Fi* of Chinese chives was 0.0915 kg/day. As the LP of Chinese chives was not reported, it has to be replaced by dark green vegetables (LP = 0.5 kg) (19). The RQ < 1 and RQ > 1 indicate whether the risk of the evaluated pesticide is acceptable and unacceptable to consumers, respectively.
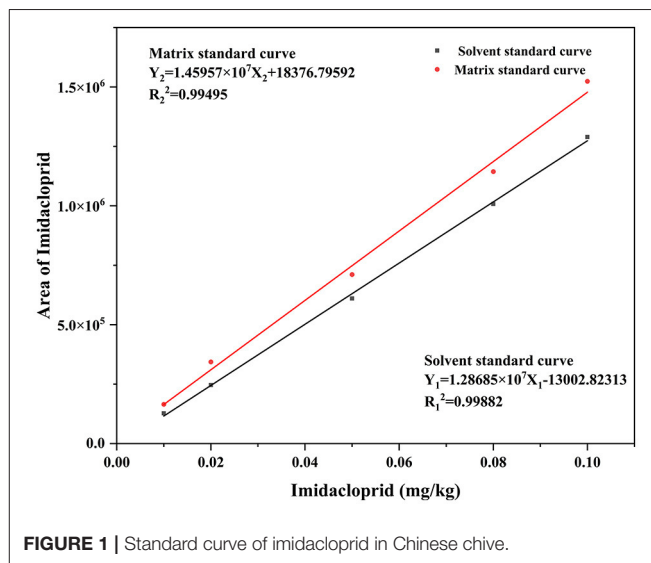
FIGURE 1 | Standard curve of imidacloprid in Chinese chive.

RESULTS AND DISCUSSION

Method Validation

According to NY/T 788-2018, the analytical method was validated using accuracy, precision, quantification limit, detection limit, matrix effect (ME), and linearity. The method's linearity was evaluated by plotting matrix-matched calibration curves at five concentrations within 0.01–0.10 mg/kg. The ME represents the ratio of the slope of the matrix matching curve to the slope of the solvent curve. The values >1 and <1 represent a signal enhancement and suppression effects, respectively (20). The imidacloprid standard was prepared in acetonitrile and blank solution at a concentration rate of 0.01, 0.02, 0.05, 0.08, and 0.1 mg/kg. The solvent and matrix-matched calibrations for imidacloprid are $Y_1 = 1.28685 \times 10^7 X_1 - 13002.82313$, $R_1^2 = 0.99882$ and $Y_2 = 1.45957 \times 10^7 X_2 + 18376.79592$, $R_2^2 = 0.99495$ (**Figure 1**). The calculated ME was >1, denoting that the Chinese chives mechanism has an enhancement effect.

Accuracy and precision are expressed as recovery (recovery of 70–120%), and relative standard deviation (RSD ≤ 20%) is according to NY/T 788-2018 (21). The average recoveries of imidacloprid were 78.34–91.17%, with RSD between 0.48 and 6.43% using QuEChERS; the finding that met the NY/T788-2018 requirements. These results showed a satisfactory accuracy and precision of imidacloprid in Chinese chives matrices.

Comparison of QuEChERS and Quick Extraction

The extraction efficiency (expressed as recovery ± RSD) of the 2 tested methods was assessed by spiking three different

FIGURE 2 | Average recovery of spiked levels using QuEChERS and Quick extraction in Chinese chive.
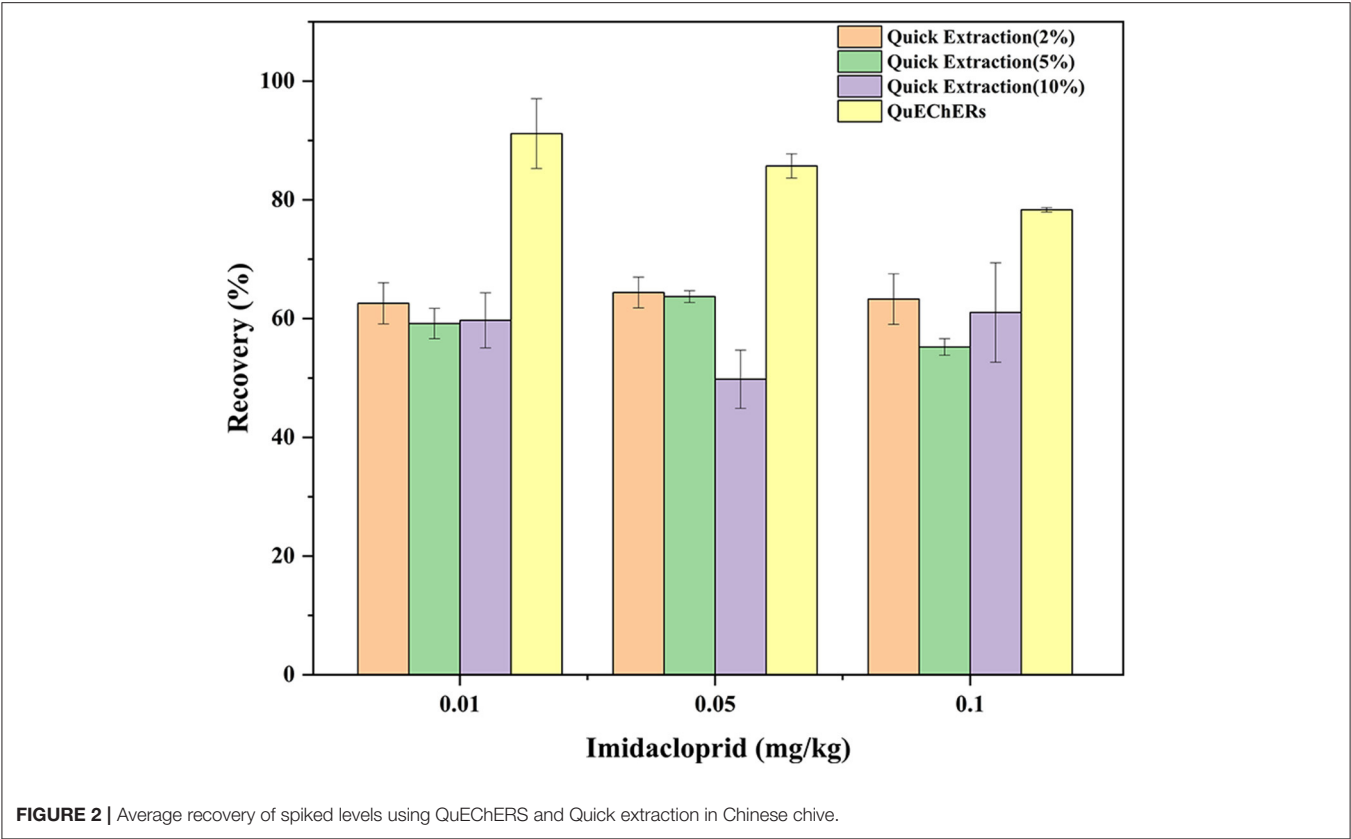
TABLE 3 | Recoveries and relative standard deviations (RSD) of imidacloprid in Chinese chives.

Spiked	QuEChERS		Quick extraction					
(mg/kg)			Methanol (2%)		Methanol (5%)		Methanol (10%)	
	Recovery (%)	RSD (%)	Recovery (%)	RSD (%)	Recovery (%)	RSD (%)	Recovery (%)	RSD (%)
0.01	91.17	6.43	62.57	5.54	59.18	4.31	59.71	7.78
0.05	85.72	2.37	64.40	4.02	63.71	1.55	49.80	9.85
0.1	78.34	0.48	63.29	6.73	55.22	2.53	61.03	13.71

TABLE 4 | Dissipation kinetic equations, half-lives, and other related parameters of imidacloprid in Chinese chives.

Initial deposit (mg/kg)	Dissipation kinetic equations	Correlation coefficient (R^2)	Half-life (d)
0.1666	$C_t = 165.290e^{-0.108t}$	$R^2 = 0.9831$	2.92

concentration levels (0.01, 0.05, and 0.1 mg/kg) of imidacloprid to a blank matrix in six replicates ($n = 6$)(**Figure 2**). The results are summarized in **Table 3**. We tested acetonitrile, ethyl acetate, acetone, and methanol as an extraction solvent to determine the imidacloprid residues in agricultural products (22). It has to be noted that acetonitrile is more expensive and toxic, ethyl acetate is not miscible with an aqueous solution, and

acetone requires availability to purchase the organic solvents. Hence, all the above organic solvents were excluded (23–25). We have chosen methanol as a quick extraction solvent. Methanol has low environmental toxicity, cheap, and easy to obtain. To obtain a satisfactory recovery, different ratios of aqueous methanol solutions were optimized. The average recoveries of imidacloprid were 62.57–64.40%, 55.22–63.71%, and 49.80–61.03% with RSD between 4.02 and 6.73%, 1.55 and 4.31%, and 7.78 and 13.71% using an aqueous solution of 2, 5, and 10% methanol, respectively. The recovery is inconsistent with the standard NY/T 788-2018 using methanol aqueous solution as an extractant. Thus, the ratio and composition of the extractant need to be further improved. On the other hand, the average recoveries of imidacloprid were 78.34–91.17%, with RSD between 0.48 and 6.43% using
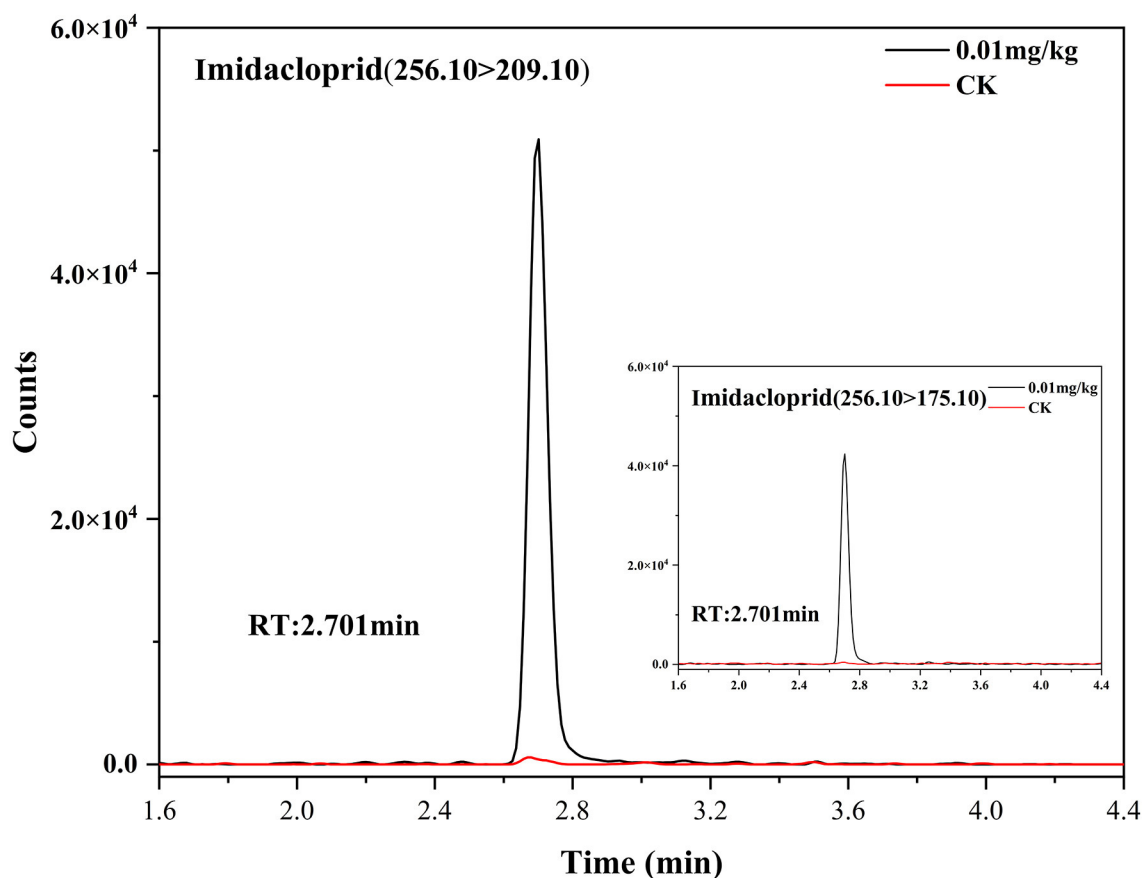
FIGURE 3 | Extracted ion chromatograms of imidacloprid in control and spiked sample (0.01 mg/kg) for Chinese chive.
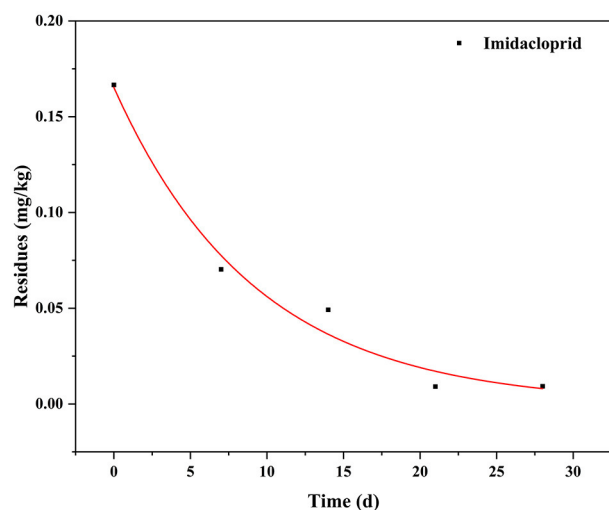
FIGURE 4 | Dissipation curves of imidacloprid in Chinese chive.

QuEChERS in Chinese chives, which met the experimental criteria. The extracted ion chromatograms of imidacloprid in blank and spiked samples are shown in **Figure 3**. The following

method validation and dissipation dynamics were performed using QuEChERS.

In QuEChERS, the adsorbents PSA, C-18, and GCB were used to adsorb organic acids, vitamins, and pigments. Moreover, anhydrous magnesium sulfate and sodium chloride were used to remove the water from the samples (22, 26). Most importantly, extraction with 100% acetonitrile results in higher recoveries. The quick extraction method used different ratios of methanolic aqueous solutions without purification. The steps of salting out and purification had less effect on the extraction rate of imidacloprid in the QuEChERS method. The main reason for the high extraction rate of QuEChERS was that the acetonitrile is more polar than methanol, and its proportion was 100%. The proportion of organic solvent was higher, contributing to the high extraction efficiency of the QuEChERS method.

Dissipation of Imidacloprid in Chinese Chives

The dissipation data and curves of imidacloprid in Chinese chives are shown in **Table 4** and **Figure 4**. The dissipation dynamic under field conditions followed a first-order kinetics model, with correlation coefficients (R^2) of 0.9831. The dissipation dynamics show a fast pre-late stage and a flat mid-stage. The

TABLE 5 | Effect of different factors on imidacloprid dissipation.

Crop type	Volume	Application times	Application interval (d)	Mix with other pesticides	R^2	Half-time (d)	References
Tomato	2.5 L ha^{-1}	1	-	No	0.90	14.43	(29)
Rice	20 g ai ha^{-1}	2	10	No	0.992	7.16	(30)
Brinjal	42 g ai ha^{-1}	3	7	No	-	2.31	(31)
Cardamom	20 g ai ha^{-1}	1	-	No	0.98	3.63	(32)
Green chilies	20 g ai ha^{-1}	2	7	No	0.996	2.08	(33)
Tea	30 g ai ha^{-1}	1	-	No	0.972	2.45	(34)
Cabbage	32.38 g ha^{-1}	1	-	No	0.934	33.0	(35)
Celery	56.2 g ai ha^{-1}	1	-	Yes	0.99	46.5	(36)

TABLE 6 | Dietary exposure risk assessment.

Matrix	PHI (d)	Residue (mg/ kg)	STMR (mg/ kg)	NEDI (mg/kg· bw/d)	RQc (%)	HR (mg/kg)	NESTI (mg/kg bw/d)	RQa (%)
Chinese chives	7	0.0703	0.0703	0.000102	0.170	0.167	0.00132	0.331
	14	0.0492	0.0492	0.0000715	0.119	0.0703	0.000558	0.139

initial residues were 0.1666 mg/kg with half-lives ($T_{1/2}$) of 2.92 days. Approximately 90% of imidacloprid residues were dissipated 28 days after application. The dissipation dynamics suggested that imidacloprid is readily degraded in Chinese chives during its growth. Other experimental field studies have shown that the dissipation dynamics of imidacloprid are affected by various factors, including crop type, climate and environmental conditions, application dose and timing, and co-application with other pesticides (27, 28). In this context, Li et al. (29) investigated the final residues and the dissipation dynamics of imidacloprid in tomatoes by LC-MS/MS, with a half-life of 14.43 days and $R^2 = 0.90$. Imidacloprid in tomatoes decreased rapidly during the first 7 days. It tended to decrease slowly after 14 days, consistent with a rapid degradation trend in the first period and a slight decrease in the second period. The same trend of imidacloprid dissipation was observed in other crops, as detailed in **Table 5**. The present study is consistent with previous studies, presenting trends in line with each other. Different crop types and environmental factors can influence the dissipation of imidacloprid. However, volatilization is the main factor of imidacloprid dissipation under outdoor conditions, leading to imidacloprid dissipation (37).

Dietary Exposure Assessment

The acute and chronic dietary risk of total residues of imidacloprid in Chinese chives was assessed (**Table 6**). For a Chinese adult weighing 63 kg, the average consumption of Chinese chives was 0.0915 kg/d, and the ADI of imidacloprid was 0.06 mg/kg bw/day. According to Eqs. (3)–(4), the RQc of imidacloprid was 0.119–0.170% in Chinese chives, which is <100%. The large portion that is reported for Chinese chives was 0.5 kg/d. The highest residue of Chinese chives was 0.167 mg/kg. The ARfD of imidacloprid was

established to be 0.4 mg/kg bw/day. According to Eqs. (5)-(6), the RQa of imidacloprid was 0.139–0.331% in Chinese chives, which is <100%. These results suggest that the acute and chronic dietary risk of imidacloprid is not threatening the health of the average Chinese consumers for Chinese chives.

Moreover, the *Fi* ratio of different age groups to the body weight was significantly different. Therefore, 6 distinct groups were selected, representing young children (2–4 years old), young adults (18–30 years old), and elderly (60–70 years old) for risk assessment. The NEDI and RQc were calculated by combining data on diet, bodyweight of Chinese, and the final residues of imidacloprid in Chinese chives determined in this study (38). In addition, the highest STMR (0.0703 mg/kg) at the recommended PHI (7 days) in the final residues was selected for evaluation. Following the principle of risk maximization, the Fi of Chinese chives was calculated using the vegetable. **Table 7** shows that the RQc was <100% and decreased gradually with age. The RQc of children (2–4 years old) was the highest. The dietary exposure of females was slightly higher than that of males in the same age group due to differences in body weight and dietary habits between the sexes.

CONCLUSION

Herein, imidacloprid residual levels and dissipation dynamics on Chinese chives under outdoor conditions were determined using QuERChERS preparation and LC-MS/MS based on the application dose, frequency, and harvest interval criteria implemented in NY/788-2018. Furthermore, risk assessment was performed according to the risk quotient method. The pattern of imidacloprid dissipation in Chinese chives was best fitted to

TABLE 7 | The exposure risk of imidacloprid among different age groups in China.

Age	Gender [a]	Fi(kg/d)	Bw(kg)	NEDI(mg/kg·bw/d)	RQc (%)
2–4	M	0.2234	14.1	0.00111	1.86
	F	0.2234	13.4	0.00117	1.95
18–30	M	0.3550	60.5	0.000412	0.687
	F	0.3550	52.6	0.000474	0.791
60–70	M	0.3664	61.3	0.000420	0.700
	F	0.3664	54.3	0.000474	0.791

[a] M, male; F, female.

first-order kinetics with a half-life of 2.92 days. A recommended dosage of 10% WG under outdoor conditions and a spray interval of 7 days will not cause any harm to humans.

DATA AVAILABILITY STATEMENT

The original contributions presented in the study are included in the article/supplementary material, further inquiries can be directed to the corresponding authors.

AUTHOR CONTRIBUTIONS

RZ, KZ, and GC: investigation and writing – original draft. GL, XH, MG, and JZ: investigation and visualization. XX, LL, and YZ: visualization and supervision. JW, MJ, DX, and AA: validation and writing – review and editing. All authors contributed to the article and approved the submitted version.

REFERENCES

1. Zhang WN, Zhang HL, Lu CQ, Luo JP, Zha XQ. A new kinetic model of ultrasound-assisted extraction of polysaccharides from Chinese chive. *Food Chem.* (2016) 212:274–81. doi: 10.1016/j.foodchem.2016.05.144

2. Gao Q, Li XB, Sun J, Xia ED, Tang F, Cao HQ, et al. Isolation and identification of new chemical constituents from Chinese chive (Allium tuberosum) and toxicological evaluation of raw and cooked Chinese chive. *Food Chem Toxicol.* (2018) 112:400–11. doi: 10.1016/j.fct.2017.02.011

3. Nishiwaki Y, Takahashi T, Wada E, Nishimura Y. Nondestructive Mineral Imaging of Chinese Chive Leaves Withered by Physiological Damage Using Microbeam Synchrotron Radiation X-Ray Fluorescence Analysis. *Anal Sci.* (2021) 37:1459–63. doi: 10.2116/analsci.21N002

4. Tang X, Olatunji OJ, Zhou Y, Hou X. Allium tuberosum: Antidiabetic and hepatoprotective activities. *Food Res Int.* (2017) 102:681–9. doi: 10.1016/j.foodres.2017.08.034

5. Mosavat SH, Ghahramani L, Sobhani Z, Haghighi ER, Chaijan MR, Heydari M. The effect of leek (Allium iranicum (Wendelbo)) leaves extract cream on hemorrhoid patients: A double blind randomized controlled clinical trial. *Eur J Integr Med.* (2015) 7:669–73. doi: 10.1016/j.eujim.2015.08.008

6. Thompson CM, Gaylor DW, Tachovsky JA, Perry C, Carakostas MC, Haws LC. Development of a chronic noncancer oral reference dose and drinking water screening level for sulfolane using benchmark dose modeling. *J Appl Toxicol.* (2013) 33:1395–406. doi: 10.1002/jat.2799

7. Strati IF, Kostomitsopoulos G, Lytras F, Zoumpoulakis P, Proestos C, Sinanoglou VJ. Optimization of Polyphenol Extraction from Allium ampeloprasum var. porrum through Response Surface Methodology. *Foods.* (2018) 7:162. doi: 10.3390/foods7100162

8. Oh M, Kim SY, Park S, Kim KN, Kim SH. Phytochemicals in Chinese Chive (Allium tuberosum) Induce the Skeletal Muscle Cell Proliferation via PI3K/Akt/mTOR and Smad Pathways in C2C12 Cells. *Int J Mol Sci.* (2021) 22:2296. doi: 10.3390/ijms22052296

9. Yan H, Zhang B, Wang E, Xu X, Wei GS. Combining predatory mites and film mulching to control Bradysiacellarum (Diptera: Sciaridae) on Chinese chives, Allium tuberosum. *Exp Appl Acarol.* (2022) 86:117–27. doi: 10.1007/s10493-021-00681-9

10. Gul H, Ullah F, Hafeez M, Tariq K, Desneux N, Gao X, et al. Sublethal concentrations of clothianidin affect fecundity and key demographic parameters of the chive maggot, Bradysiaodoriphaga. *Ecotoxicology.* (2021) 30:1150–60. doi: 10.1007/s10646-021-02446-x

11. Ding Q, Xu X, Sang Z, Wang R, Ullah F, Gao X, et al. Characterization of the insecticide detoxification carboxylesterase Boest1 from Bradysiaodoriphaga Yang et Zhang (Diptera: Sciaridae). *Pest Manag Sci.* (2021) 78:591–602. doi: 10.1002/ps.6667

12. Loser D, Grillberger K, Hinojosa MG, Blum J, Haufe Y, Danker T, et al. Acute effects of the imidacloprid metabolite desnitro-imidacloprid on human nACh receptors relevant for neuronal signaling. *Arch Toxicol.* (2021) 95:3695–716. doi: 10.1007/s00204-021-03168-z

13. Chen C, Shi X, Desneux N, Han P, Gao X. Detection of insecticide resistance in Bradysiaodoriphaga Yang et Zhang (Diptera: Sciaridae) in China. *Ecotoxicology.* (2017) 26:868–75. doi: 10.1007/s10646-017-1817-0

14. Zhou Y, Piao X, Liao X, Liu J, Zhu H, Ma H, et al. Determination and chronic dietary exposure assessment ofprocrymidone residue in Chinese chives. *Chin J of Pesticide Sci.* (2021) 23:373–9. doi: 10.16801/j.issn.1008-7303.2021.0007

15. Liu J, Hu Y, Yang Y, Zhang J, Zhong H, Liu L. Residue Level and Digestion Rate of Procymidone in Chinese Chives. *Agrochemicals.* (2021) 60:756–8. doi: 10.16820/j.cnki.1006-0413.2021.10.012

16. Lv B, Liu M, Xing S. Analysis of the national food safety supervision and sampling inspectionresult on vegetables in 2018. *J Food Saf Qual.* (2019) 10:5715–21. doi: 10.19812/j.cnki.jfsq11-5956/ts.2019.17.027

17. Yang L, Zhou X, Deng Y, Gong D, Luo H, Zhu P. Dissipation behavior, residue distribution, and dietary risk assessment of fluopimomide and dimethomorph in taro using HPLC-MS/MS. *Environ Sci Pollut Res Int.* (2021) 28:43956–69. doi: 10.1007/s11356-021-13713-z

18. Mao J, Li H, Chen Z, Zhang W, Guo C, Fang L, et al. Dissipation Dynamics and Preliminary Dietary Risk Assessment of Clothianidin and Cyromazine in Chinese Chives. *Shandong Agric Sci.* (2019) 51:118–23. doi: 10.14083/j.issn.1001-4942.2019.03.025

19. Zhang Q, Qin Z, Bai X, Jiang J. The acute dietary risk assessment of pesticide residues from fresh edible vegetables for human health. *Chin Agri Sci Bulletin.* (2013) 29:200–5. doi: 10.16498/j.cnki.hnnykx.20013.29.032

20. Zhou J, Dong C, An W, Zhao Q, Zhang Y, Li Z, et al. Dissipation of imidacloprid and its metabolites in Chinese prickly ash (Zanthoxylum) and their dietary risk assessment. *Ecotoxicol Environ Saf.* (2021) 225:112719. doi: 10.1016/j.ecoenv.2021.112719

21. Fu Y, Wang Q, Zhang L, Ling S, Jia H, Wu Y. Dissipation, occurrence, and risk assessment of 12 pesticides in Dendrobium officinale Kimura et Migo. *Ecotoxicol Environ Saf.* (2021) 222:112487. doi: 10.1016/j.ecoenv.2021.112487

22. Zhang C, Deng Y, Zheng J, Zhang Y, Yang L, Liao C, et al. The application of the QuEChERS methodology in the determination of antibiotics in food: a review. *TrAC Trends Anal Chem.* (2019) 118:517–37. doi: 10.1016/j.trac.2019.06.012

23. Aguilera-Luiz MM, Martínez Vidal JL, Romero-González R, Garrido Frenich A. Multiclass method for fast determination of veterinary drug residues in baby food by ultra-high-performance liquid chromatography–tandem mass spectrometry. *Food Chem.* (2012) 132:2171–80. doi: 10.1016/j.foodchem.2011.12.042

24. Herrera-Herrera AV, Hernandez-Borges J, Rodriguez-Delgado MA. Fluoroquinolone antibiotic determination in bovine, ovine and caprine milk using solid-phase extraction and high-performance liquid chromatography-fluorescence detection with ionic liquids as mobile phase additives. *J Chromatogr A.* (2009) 1216:7281–7. doi: 10.1016/j.chroma.2009.02.025

25. Lombardo-Agüí M, García-Campaña AM, Cruces-Blanco C, Gámiz-Gracia L. Determination of quinolones in fish by ultra-high performance liquid chromatography with fluorescence detection using QuEChERS as sample treatment. *Food Control.* (2015) 50:864–8. doi: 10.1016/j.foodcont.2014.10.027

26. Qi P, Wang J, Liu Z, Wang Z, Xu H, Di S, et al. Integrated QuEChERS strategy for high-throughput multi-pesticide residues analysis of vegetables. *J Chromatogr A.* (2021) 1659:462589. doi: 10.1016/j.chroma.2021.462589

27. Zhang Q, Wang X, Rao Q, Chen S, Song W. Imidacloprid dissipation, metabolism and accumulation in Agaricusbisporus fruits, casing soil and compost and dietary risk assessment. *Chemosphere.* (2020) 254:126837. doi: 10.1016/j.chemosphere.2020.126837

28. Yen JH, Liao CS, Kuo YW, Chen WC, Huang WT. Effect of growing groundcover plants in a vineyard on dissipation of two neonicotinoid insecticides. *Sustainability.* (2019) 11:798. doi: 10.3390/su11030798

29. Li J, Jiang Y, Li D. Determination of imidacloprid and its relevant metabolites in tomato using modified QuEChERS combined with ultrahigh-pressure liquid chromatography/Orbitrap tandem mass spectrometry. *J Sci Food Agric.* (2019) 99:5211–8. doi: 10.1002/jsfa.9769

30. Akoijam R, Singh B. Persistence and metabolism of imidacloprid in rice. *Bull Environ ContamToxicol.* (2014) 92:609–15. doi: 10.1007/s00128-013-1190-5

31. Mandal K, Chahil GS, Sahoo SK, Battu RS, Singh B. Dissipation kinetics of beta-cyfluthrin and imidacloprid in brinjal and soil under subtropical conditions of Punjab, India. *Bull Environ Contam Toxicol.* (2010) 84:225–9. doi: 10.1007/s00128-009-9903-5

32. Pratheeshkumar N, Chandran M, Beevi SN, Mathew TB, George T, Paul A, et al. Dissipation kinetics and effect of processing on imidacloprid and its metabolites in cardamom (Elettaria cardamomum Maton). *Environ Monit Assess.* (2016) 188:53. doi: 10.1007/s10661-015-5058-5

33. Varghese TS, Mathew TB, George T, Beevi SN, Xavier G. Persistence and dissipation of neonicotinoid insecticides on chilli fruits. *Qual Assur Saf Crops Foods.* (2015) 7:487–91. doi: 10.3920/QAS2013.0265

34. Hou RY, Hu JF, Qian XS, Su T, Wang XH, Zhao XX, et al. Comparison of the dissipation behaviour of three neonicotinoid insecticides in tea. *Food Addit Contam Part A Chem Anal Control Expo Risk Assess.* (2013) 30:1761–9. doi: 10.1080/19440049.2013.820356

35. Chen Y, Nie E, Huang L, Lu Y, Gao X, Akhtar K, et al. Translocation and metabolism of imidacloprid in cabbage: Application of (14)C-labelling and LC-QTOF-MS. *Chemosphere.* (2021) 263:127928. doi: 10.1016/j.chemosphere.2020.127928

36. Kang L, Liu H, Zhao D, Pan C, Wang C. Pesticide Residue Behavior and Risk Assessment in Celery after Se Nanoparticles Application. Foods. (2021) 10:1987. doi: 10.3390/foods10091987

37. Celik S, Kunc S, Asan T. Degradation of some pesticides in the field and effect of processing. *Analyst.* (1995) 120:1739–43. doi: 10.1039/AN9952001739

38. Yang Q, Ji M, Zu G. Residues behavior and dietary exposure risk assessment of cyazofamid and its main metabolite CCIM in tomato and grape. *Chin J Pesticide Sci.* (2020) 22:815–22. doi: 10.16801/j.issn.1008-7303.2020.0094

Feasibility of Ultrasound-Assisted Extraction for Accelerated Cold Brew Coffee Processing: Characterization and Comparison With Conventional Brewing Methods

Xingchen Zhai[1†], Mengnan Yang[1†], Jing Zhang[1], Lulu Zhang[1], Yarong Tian[1], Chaonan Li[1], Lina Bao[1], Chao Ma[1*] and A. M. Abd El-Aty[2,3*]

[1] Beijing Key Laboratory of Forest Food Processing and Safety, College of Biological Science and Technology, Beijing Forestry University, Beijing, China, [2] Department of Pharmacology, Faculty of Veterinary Medicine, Cairo University, Giza, Egypt, [3] Department of Medical Pharmacology, Faculty of Medicine, Atatürk University, Erzurum, Turkey

A long extraction time for traditional cold coffee brewing considerably reduces the production efficiency of this type of beverage. Herein, a new ultrasound-assisted cold brewing (UAC) method was established. The feasibility of UAC was assessed by comparison with main physicochemical characteristics, non-volatile and volatile compounds in coffee extracts produced by hot brewing and conventional static cold brewing methods. Compared to the static cold brews, the levels of total dissolved solids, total lipids, proteins, and titrated acids of UAC coffee extracts increased by 6–26%, 10–21%, 26–31%, and 12–15%, respectively. Caffeine, chlorogenic acid, and trigonelline concentrations were also determined by HPLC. Based on the volatile profiles obtained by HS-SPME-GC/MS, the aroma compounds in UAC was significantly different ($p <$ 0.05) from hot brews but similar to static cold ones, suggesting that ultrasonication compensated for the time of the static cold brewing, thereby considerably shortening the extraction time (1 h vs. 12 h). This work demonstrated that the combination of ultrasound-assisted with cold brew could produce coffee with good flavor and increase the extraction efficiency, which may provide an option for the acceleration of the cold brew coffee process.

Keywords: coffee, cold brew, hot brew, ultrasound-assisted extraction, volatile compounds

INTRODUCTION

Coffee is the most widely consumed beverage worldwide and one of the most commercial food products. From an engineering point of view, coffee brewing is a solid–liquid extraction, where the roasted and ground coffee is in intimate contact with water. Depending on the extraction technique, water acts as a solvent to extract soluble and non-soluble compounds. These compounds eventually appear in the form of dissolved or suspended solids in the extract, which substantially impact the sensory properties of coffee (1). Traditionally, coffee has been prepared with hot water (near the boiling point) within just a few minutes (2). The high temperature is the driving force for extraction. With the increasing demands for coffee with unique sensory characteristics, cold brew coffee has

emerged and spread rapidly, which is prepared with water at 20–25°C or lower temperatures and requires a more extended period than the conventional hot brew methods, varying from 8 to 24 h (2, 3). The unique extraction conditions make cold brewing coffee have an utterly different flavor than hot brewing coffee, manifested as intense sweetness, chocolate, floral and fruity aroma, with moderate bitterness and acidity (4). According to market analysis, the global market size for cold brew coffee was valued at USD 339.7 million in 2018 and is expected to reach USD 1.63 billion by 2025 (5).

Significant differences were found in the chemical, physical parameters, and sensory profiles (such as bitter, sweet, astringency) between cold brew and cold drip coffee extractions (6). Rao et al. (7) indicated that cold brew coffees showed decreased acidity, fewer total dissolved solids (TDS), and a lower concentration of browned compounds than hot brewing extractions. According to Fuller and Rao (8), caffeine and chlorogenic acid (CGA) concentrations reached an equilibrium between 6 and 7 h in cold brew samples based on first-order kinetics. Compared to hot brew coffee, substantially higher caffeine concentrations were found in cold counterparts, while there were no significant differences in CGA concentrations. Despite the physicochemical properties of classic cold brew coffee research, there are a few studies on alternative methods to reduce the long cold extraction time. Recently, Morgan Caudill (9) accelerated cold brew extraction through microwave heat treatment, but the temperature still needs to reach up to 80°C. Ultrasound-assisted extraction is a green and economical technology with high efficiency for food and natural products, and it acts with combined mechanisms between fragmentation, erosion, capillarity, detexturation, and sonoporation (10). Ultrasound has been reported to increase the yield of flavonoids extraction from sea buckthorn (11), saponin from ginseng (12), and triglycerides from coffee (13). Probably, ultrasound-assisted is an alternative method to improve the cold brewing efficiency and to create faster commercialization of cold brewing.

Therefore, the present study aimed to explore the feasibility of ultrasound-assisted cold brew (UAC) as an alternative extraction method to shorten the long extraction time required by the traditional cold brewing methods.

MATERIALS AND METHODS

Materials and Reagents

Arabica coffee (originating from Brazil) from Basic ElementsCatering Services Co., LTD (Gu'an, China) were was used in all the trials. Caffeine, CGA, and trigonelline were obtained from Chengdu Effa Biological Technology Co., Ltd (Chengdu, China). Folin–Ciocalteu was purchased from Coolaber Technology Co., Ltd (Beijing, China). Other chemicals, such as gallic acid, sodium carbonate, n-hexane, and sodium

chloride, were of analytical grade and secured from Sinopharm Chemical Reagent Co., Ltd (Shanghai, China).

Coffee Extracts Preparation

Roasted coffee beans were ground until they passed through a 20-mesh sieve. All samples were prepared using the same commercial brand of mineral water and the same coffee to water ratio (1:18).

For hot brewing, hot boiled (HB) coffee was prepared with coffee (16.5 g) and hot water (313.5 g, 95°C) was mixed for 5 min. Three-stage water (92°C) injection was performed for pour-over (PO) coffee. Firstly, 30 g water was added to coffee to stew and steam for 40 s. Then water was slowly added to 150 g. Finally, the remained hot water was injected to complete the extraction for a total time of about 3 min. All filtered samples from different methods were used for further analysis.

Cold brew coffee was prepared by immersion methods performed under static (4 or 10°C) or ultrasonic conditions. Conventional cold brews were produced by coffee immersed in water at 4 or 10°C for 12 h (short for 4 and 10B). UAC coffee was prepared by probe-ultrasound equipment with 200 W for 60 min (Biosafer 3D, Saifei China Technology Co., LTD) at room temperature. When extraction ended, the beverage was filtered through a paper coffee filter for further analysis.

Physicochemical Analysis

Extraction Yield, Color Values, pH, and TDS

The following equation measured the extraction yield (EY): $EY(\%) = (W_2 - W_1)/W_0 \times 100\%$, where W_2 defines the total mass of extract obtained in the evaporating dish, W_1 as the empty evaporating dish mass, and W_0 as the initial coffee mass used in the extraction.

A Chroma meter (SR60, Sanenshi, Shenzhen, China), pH meter (LE438, METTLER TOLEDO, Zurich, Switzerland), and refractometer (LH-Q20, Luheng, Hangzhou, China) were used to measure color (L, a, b values), pH, and total dissolved solids (TDS) of different coffee extracts, respectively.

Extraction Rate of Total Phenols (TPC), Lipids (TL), Proteins (Tpro), and Titratable Acidity (TA)

Total phenols was measured using the Folin-Ciocalteu method described by Cordoba et al. (2) with minor modifications. A 0.1 mL coffee extraction sample, 6 mL distilled water, 0.5 mL Folin-Ciocalteu reagent, and 1.5 mL 20% Na_2CO_3 solution were added, followed by distilled water to make 10 mL. All mixed samples were incubated at room temperature for 2 h before measuring the absorbance at 765 nm. The results were expressed as total phenolic content in micrograms of gallic acid equivalents per millilietr of solution. After that, TPC was calculated by $TPC(\%) = c \times V \times N/W \times 100\%$, where c defined as total phenolic content ($\mu g/mL$); V is the volume of coffee extracts (mL); N as diluted multiples; and W is the coffee mass corresponding to the coffee extraction (μg).

Soxhlet extraction (SE) was used to evaluate TL as recommended by the Association of Official Analytical Chemists (AOAC). SE was conducted for 6–8 h with 10 mL of coffee extraction sample and petroleum ether in a water bath, and then

---

Abbreviations: HB, Hot boiled method; PO, Pour-over method; 4CB, 4°C cold brewing method; 10CB, 10°C cold brewing method; UAC, Ultrasound-assisted cold brewing method; EY, Extraction yield; TDS, Total dissolved solids; TL, Total lipid extraction rate; TPC, Total phenolic extraction rate; Tpro, Total protein extraction rate; TA, Total acid extraction rate; CGA, Chlorogenic acid.

the suspension was filtered with filter paper. Petroleum ether was evaporated in the fume hood. The lipids extracted were placed into a vacuum drying oven until they reached a constant mass. Afterward, TL (%) in coffee was obtained by gravimetric analysis, which was expressed as lipids amount extracted from coffee per unit mass.

Total protein extraction rate was determined by the Kjeldahl method. A 10 mL coffee sample was put in the digestive tube, then 4 g potassium sulfate, 0.25 g copper sulfate pentahydrate, and 10 mL concentrated sulfuric acid were added consecutively. Following total digestion in a furnace in a fume hood for 1–2 h, a fully automated Kjeldahl apparatus (KDY-9830, Tongrunyuan Co., Beijing, China) was used to measure the protein content, and Tpro (%) was expressed as protein amount extracted from coffee per unit mass.

For TA, 20 mL of coffee extraction was titrated with 0.1 mol/L NaOH solution at a pH of 6.5, and the TA (%) was expressed as CGA amount extracted from coffee per unit mass.

Caffeine, CGA, and Trigonelline Measurement

Caffeine, CGA, and trigonelline were measured by HPLC (LC-20A, Shimadzu Co., Kyoto, Japan) fitted with a Diamosil C18 column (Dikma, Beijing, China, 250 mm × 4.6 mm) run at 30°C with a mobile phase flow rate of 1.0 mL/min and an injection volume of 10 μL. For caffeine, separation was carried out with an isocratic gradient of a mixture of 90% mobile phase A and 10% mobile phase B (A: 0.1% aqueous phosphoric acid; B: acetonitrile). CGA was determined using the same mobile phase as caffeine, while the isocratic gradient was set to a mixture of 75% mobile phase A and 25% mobile phase B. As for trigonelline, elution was performed using an isocratic gradient of a mixture of 80% mobile phase A and 20% mobile phase B (A: 0.05%SDS-0.1% aqueous acetic acid; B: 0.1% acetic acid in methanol). Caffeine, CGA, and trigonelline were detected using a diode array detector at 272, 327, and 265 nm, respectively. Five concentrations for each compound were used to prepare the calibration curve, and regression equations were fitted by plotting of area of the standard solutions against concentrations.

Volatile Compound Analysis

The volatile compounds from hot and cold brew coffee extracts were obtained by headspace–solid-phase microextraction (HS-SPME) and analyzed by gas chromatography coupled with mass spectrometry (GC/MS), according to the method reported by Moreno et al. (14) with minor modifications. Each extraction sample (2 mL) was equilibrated with 2 g sodium chloride for 30 min in a 25-mL sealed vial at 60°C using a magnetic stirrer with a speed of 260 rpm. The volatile compounds released from the headspace of each sample were collected using 50 μm/DVB/CAR/PDMS long fiber (SAAB-57348U, Anpu Experimental Technology Co., Shanghai, China) and directly injected into a gas chromatography–mass spectrometry (QP2010 Ultra, Shimazu, Tokyo, Japan). A RTX-5MS capillary column (Restek, Bellefonte, PA, USA, 30 m × 0.25 mm i.d., 0.25 μm) was used. The column oven was programmed from 40°C (after 5 min) to 120°C at 5°C/min, then to 280°C at 10°C /min, and maintained at the final temperature for 5 min. The injector and

TABLE 1 | Factors and levels of OED L_9 (3^3) design.

Independent variable	Range and levels		
	1	**2**	**3**
Coffee to water ratio	1:12	1:15	1:18
Extraction time (min)	20	30	60
Ultrasonic power (W)	100	150	200

ion source temperatures were maintained at 280 and 230°C, respectively. The carrier gas was 1 mL/min of He, with a split injection of 40:1. Qualitative elucidation of the volatile compounds was performed by comparing their mass spectra with those of NIST14 or NIST14s mass spectra library. Quantification was conducted by the internal standard method using 4-methyl-2-amyl alcohol as the internal standard.

To assess the influence of the volatile compounds of coffee extraction, the odor activity values (OAVs) were calculated by the following equation: $OAV_i = C_i/OT_i$, where C_i referred to the concentration of a particular aroma in coffee extraction (μg/L), and OT_i referred to the aroma threshold in water from literature (μg/L) (15). Only compounds with an OAV > 1 contributed to the coffee aroma.

Orthogonal Experimental Design

An L_9 (3^3) OED was used to obtain the optimal conditions for the production of UAC coffee with three operational parameters, including coffee to water ratio (1:12, 1:15, and 1:18), extraction time (20 min, 30 min, and 60 min), and ultrasonic power (100 W, 150 W, and 200 W) in three levels, respectively. The EY (%) of coffee was chosen as the observed index. The parameters, their ranges, and levels are listed in **Table 1**. Also, the quality parameters of the coffee obtained under optimized conditions were evaluated according to the methods displayed in Section Physicochemical Analysis.

Statistical Analyses

All measurements were carried out three times. One-way analysis of variance (ANOVA), followed by Ducan's test at a 5% significance level, was applied using SPSS Statistics 22.0. The result figures were drawn based on Microsoft Excel 2010, Origin Pro 2019, and SIMCA 14.1.

RESULTS AND DISCUSSION

Comparison of Extraction Effects of Hot- and Cold-Brewing

Coffee comprises carbohydrates, lipids, proteins, melanoidins, organic acids, CGA, and nitrogen-containing compounds, such as caffeine and trigonelline (16). The chemicals in roasted coffee are extracted at different rates due to water solubility variations. EY is the ratio of the mass of extracted coffee solubles to the mass of the coffee grains used, which determines the coffee's flavor. The EYs of hot- and cold-brewing were evaluated using the same

ratio of coffee/water. As shown in **Supplementary Table 1**, hot-brewing exhibited higher EYs than cold-brewing. The extraction temperature for hot-brewing was near 100°C, which is a high-energy system leading to a faster rate of diffusion of coffee grain in water and the release of components in the process of solid–liquid mass transfer (17). Regarding cold-brewings, the EY of UAC was higher than 4 and 10 CB, with significantly shorter extraction time, which may be because the acoustic cavitation that occurred throughout ultrasonication can accelerate the release, diffusion, and dissolution of the active components in coffee. Ahmed et al. (18) also proposed that the combination of ultrasonication and agitation enhanced various phytochemicals in cold-brew coffee, such as color values, TDS, antioxidant activities, and most organic acids. According to Brewing Control Charts of the Specialty Coffee Association (SCA), the EY should be 18–22%, with 0.79–1.38% TDS. With the emergence of more and more new brewing methods, the applicability of this classic chart developed in the 1950s is rapidly decreasing (19). Therefore, the ranges of EY and TDS for the present study were acceptable.

Soluble sugars are the main components of dissolved solids in coffee, mainly influencing the sweetness and viscosity (20). Compared with other methods, UAC exhibited the highest TDS (**Supplementary Table 1**). More water can move into the cells because the tissue and cell wall disruption by sonoporation during ultrasonication leads to increased permeability of cell membranes and more soluble solids passing through the cell membrane (18), which compensates for the time effect cold-brew at 4 and 10°C. The higher TDS may make UAC coffee sweeter, also with a relatively high pH. In this study, cold brew coffees displayed higher pH values (less acidic) than hot counterparts. Several pieces of research have reported that the pH, together with TA, in hot coffee extracts was higher than that measured in cold coffee extracts, indicating hot-brewing was able to extract more acids and additional acidic compounds (2), as the solubility of organic acids increased with temperature (21). The pH measurement mainly quantifies the concentration of hydrogen ions in an aqueous solution. At the same time, TA evaluates all acidic protons, including undissociated protons that a strong base can neutralize. Although many researchers want to establish correlations between pH, TA, and perceived acidity, no agreement has been reached as yet (19). In this work, UAC extractions presented the highest pH value and a relatively high TA, which might make the UAC coffee less acidic than the others. However, this needs further sensory evaluation to be verified.

Generally, raw coffee beans are green in color. As the temperature rises during roasting, the Maillard reaction and Strecker degradation give the beans a new color and aroma. Herein, the values of a^* and b^* for all samples were close to zero, so the red–green, and yellow–blue differences could be ignored. While hot-brewing coffee had lower L^* and a^* values, indicating darker color in hot-brewing extracts, consistent with actual images (**Figure 1B**), cold-brewing coffees exhibited hazelnut color with a hint of brown, and the color of UAC counterpart was the brightest, owing to the highest L^* value observed. Also, cold coffee brews showed significant differences compared with hot ones with regard to TPC, TL, Tpro, and

TA (**Figure 1A**). The TPC values were comparable in the cold brews, significantly lower than HB and PO coffees. Several phenolic substances in coffee, such as CGA, will be accelerated to release by high temperatures. This is also the reason for the highest TPC and TA of HB coffee. Since coffee's sour and astringency flavor is mainly provided by phenols and their degradation products (22), low TPC makes UAC coffee slightly sweet and tasty. Some shear forces are generated within the liquid (water) for total lipids and proteins extraction by UAC. The vicinity of solid materials (coffee) and the collapse of a cavitation bubble close to the cell could cause its rupture (23), making UAC coffee exhibit a relatively high TL and Tpro. Lipids in coffee brews can form emulsions that retain aromatic compounds to strengthen the aroma and provide coffee with a mellow and long aftertaste (24). Protein contents generally impact Maillard reaction and caramelization, thus affecting the formation of coffee flavor substances and the sensory quality of coffee, such as color, taste, and aroma. Franca et al. (25) showed that high-quality coffee beans have a higher protein content, while Macrae (26) suggested no necessary relationship between protein content and coffee flavor quality. To better display multidimensional data, a spider plot was also used to visually show the main physicochemical characteristics and the EY obtained by different brewing methods (**Figure 1C**). Among the three cold-brewing methods, the EY of UAC was slightly higher than that of the other two counterparts, which demonstrated that ultrasound directly acts on mass transfer improvement and impacts positively on the basic mechanisms of extractions: desorption and diffusion of a solute out of the raw material structure (27). The ultrasonic capillary effect could also explain the enhanced extraction effect, but its detailed mechanism is not fully understood (10). Overall, regarding extraction ability and general physicochemical characteristics in coffee, UAC was an effective cold brewing method, even better than static cold extraction at 4 and 10°C.

Effects of Hot- and Cold-Brewing on Caffeine, CGA, and Trigonelline Contents

The most abundant alkaloids in coffee are caffeine and trigonelline, vital to the coffee flavor. CGA is also present in coffee, with relatively high amounts contributing to the health benefits. Therefore, HPLC was adopted in their analysis to clarify the differences between hot and cold brews. The hot brewing methods produced higher caffeine, CGA, and trigonelline contents (**Table 2**), according to linear regression equations (**Supplementary Table 2**). Caffeine has a limited solubility at an ambient temperature of 16 mg/mL (8) and is less sensitive to roasting temperature than CGA. This may explain why 4 and 10 CB exhibited similar caffeine concentrations. CGA, unlike caffeine, is freely soluble in water (8), and this facilitates its extraction by both hot and cold brewing methods. Concentrations were the highest in PO coffees (1.53 mg/mL for CGA and 0.54 mg/mL for trigonelline) because the dynamic PO method (add water in three stages) involved the continuous renewal of the extraction. Compared to a static system, this is definitely a more efficient way of extracting relevant molecules
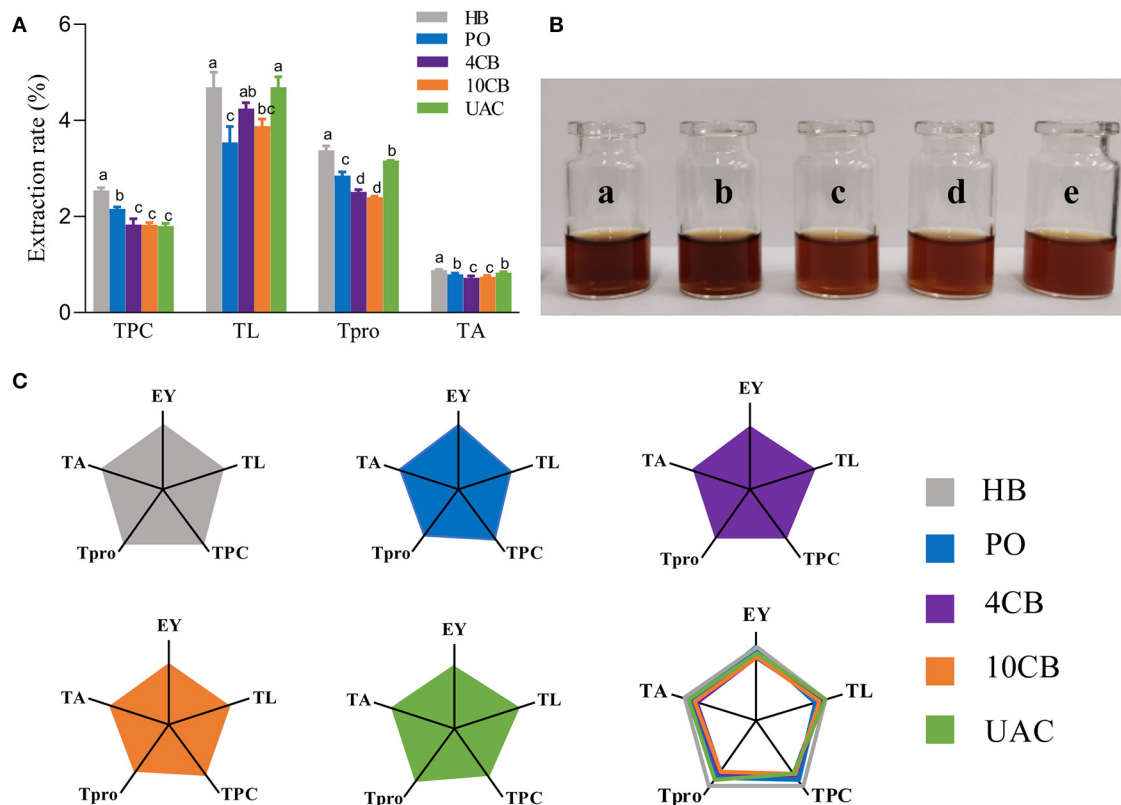
FIGURE 1 | (A) The effects of different brewing methods on TPC, TO, Tpro, and TA. Different letters indicate statistically significant differences ($p < 0.05$) among treatments. **(B)** Actual images of a) hot boiled, b) pour-over, c) 4°C cold brew, d) 10°C cold brew, and e) ultrasound-assisted cold brewed coffee samples. **(C)** Spider plots of main physicochemical characteristics yielded by hot and cold brewing coffee methods. EY, Extraction yield; TL, total lipid extraction rate; TPC, total phenolic extraction rate; Tpro, total protein extraction rate; TA, total acid extraction rate. HB, Hot boiled, PO, Pour-over, 4 CB, 4°C cold-brew, 10 CB, 10°C cold brew, UAC, Ultrasound-assisted cold brew.

(6). Fuller et al. (8) have investigated the extraction kinetics and equilibrium concentrations of caffeine and CGA in cold brew coffee and proved that caffeine and CGA reached nearly steady-state concentrations after 400 min. Since extraction time in UAC was only 60 min, the contents of caffeine and CGA obtained were significantly lower than that of static cold brews (12 h). Although CGA and its derivatives are important flavor-regulating substances of coffee, they also contribute to the acidity, astringency, and bitterness of the final coffee beverages (6). Also, caffeine and trigonelline represent a maximum of 10–30% and 1% of the total bitter taste intensity, respectively (28). Many researchers considered that CGA, trigonelline, and caffeine's degradation products were related to the bitterness of coffee beverages (29). Therefore, UAC coffee with relatively lower CGA (1.25 mg/mL) and trigonelline (0.42 mg/mL) contents may make it less bitter than other coffees. Similarly, the previous study has described that over-brewing cold brew coffee may result in unpalatable flavor due to degradation of CGA and other relatively slow-extracting compounds such as 4-vinylcatechol oligomers (30). Angeloni et al. (6) also ascribed the higher concentrations of caffeine and CGA to the prolonged contact time during conventional cold brewing compared to hot brewed coffees.

Volatile Compound Profiles of Hot and Cold Brew Coffees

Flavor is a key attribute in determining coffee products' quality and consumer acceptance. The volatiles present in the coffee brew depends on the extraction technique. Therefore, in the present study, HS-SPME-GC/MS was used for qualitative and quantitative analysis of volatile components in hot and cold brew coffees (**Table 3**). Total ion chromatograms of volatiles with different methods are shown in **Supplementary Figure 1**.

Qualitative Analysis

A total of 97 volatile compounds were identified in hot and cold coffee brews, including furans (16), pyrazines (16), alcohols (10), pyrroles (7), aldehydes (4), ketones (11), phenols (7), pyridines (3), acids (3), esters (11), and others (9). Lopez-Galilea et al. (31) have reported that pyrazines, furans, aldehydes, and ketones have a high impact on the aroma of coffee. The current results showed that most of the volatile compounds identified in hot and cold coffee extractions belonged to these chemical classes. For the cold brews, 53 volatile compounds were found in UAC coffee, between 4 CB (52) and 10 CB (56). Three special volatiles were found in the UAC coffee, including phenylacetaldehyde, 4'-propyl-1,1'-biphenyl (cyclohexyl)-4-butyrate, and furfuryl acetate, which

Brewing methods		Extraction conditions	Caffeine (mg/mL)	CGA (mg/mL)	Trigonelline (mg/mL)
Hot brewing	HB	95°C, 5 min	0.64 ± 0.00[b]	1.29 ± 0.00[c]	0.49 ± 0.00[c]
	PO	92°C, 3 min (three-stage)	0.68 ± 0.00[a]	1.53 ± 0.05[a]	0.54 ± 0.00[a]
Cold brewing	4 CB	4°C, 12 h	0.60 ± 0.00[c]	1.37 ± 0.00[b]	0.50 ± 0.00[b]
	10 CB	10°C, 12 h	0.60 ± 0.00[c]	1.35 ± 0.04[b]	0.31 ± 0.00[e]
	UAC	200 W, RT, 60 min	0.56 ± 0.00[d]	1.25 ± 0.00[c]	0.42 ± 0.00[d]

HB, Hot boiled; PO, Pour-over; 4CB, 4°C cold brew; 10CB, 10°C cold brew; UAC, Ultrasound-assisted cold brew; CGA, Chlorogenic acid. Different letters indicate statistically significant differences (P < 0.05) among treatments.

belonged to aldehydes and esters. Aldehydes have been described as having chocolate and malty odors (1), and esters are related to fruity flavor in coffee (32). Both roasting process and extraction technology influence the presence of volatile compounds in the final coffee. Venn diagrams (**Figure 2B**) clearly showed the volatiles in different groups. Although cold-brew coffee's overall volatiles were less than their hot counterparts, the cold coffee beverages had a unique and acceptable flavor.

The abundance of 97 volatile compounds in hot and cold coffee extractions was analyzed by hierarchical clustering (**Figure 2A**). The coffee samples were divided into two groups, where HB and PO coffee were classified as one group. Both were performed at relatively high temperatures, contributing to more volatiles, especially furans and pyrazines. Cold-brew extractions were divided into a second group, and the volatiles between 10 CB and UAC were more similar. To further clarify the effects of different extraction methods on volatile components, the main volatiles (content greater than 0.1 μg/mL) were selected for principal component analysis (PCA). As shown in **Figure 2C**, two principal components represented more than 83.5% of the total variance in the volatiles, and PC1 and PC2 of the PCA analysis model explained 61.4 and 22.1% of the variance, respectively. The hot and cold brewing methods were clearly separated by PC1, indicating the main volatile compounds differed between hot and cold counterparts. Phenols, ketones, and furans, such as guaiacol, 2,3-pentanedione, and 5-methyl-2-acetylfuran, were grouped in the first quadrant with PO coffees. While pyrazines and acids, including 2-ethyl-3-methylpyrazine, 2-ethylpyrazine, and cyclohexanacetic acid, were grouped in the fourth quadrant with HB extractions, most of the volatiles correlated with 4 CB, 10 CB, and UAC coffee beverages were concentrated in the negative axis of PC1, such as furfuryl acetate and some ketones derivatives, further indicating that there was no significant difference in the aroma and flavor among cold brew coffees, which was consistent with cluster analysis results (**Figure 2A**).

Quantitative Analysis

The species and contents of the volatile compounds were identified in hot and cold brew coffees by HS-SPME-GC/MS, and are presented in **Figure 3A** and **Table 3**. It was observed that the volatile profiles of different extractions were generally similar. Furans were the most abundant class of volatiles detected

in coffees, which could be formed through thermal degradation of carbohydrates, ascorbic acid, or unsaturated fatty acids during coffee roasting (33). UAC extractions contained 19.73 μg/mL furans, accounting for 40.31% of the total volatiles, and were slightly lower than that of 4 CB (31.38 μg/mL) and 10 CB (25.94 μg/mL). Compared to other volatiles in coffee, furans had relatively high thresholds and mainly exhibited malty and sweet roasted aromas. 3-Furan methanol, 5-methylfuran aldehyde, and furan formaldehyde were found in large amounts in UAC coffees, associated with almond notes, caramel, and burnt sugar.

Pyrazines had the second-highest number of volatile compounds in all samples, including UAC coffee. They are mainly generated by Strecker degradation of aldehydes interacting with amino ketones provided by amino acids (34). The contents of pyrazine compounds in PO and HB coffee were approximately 2 times the cold brews, indicating more potent nutty and roasty aromas in hot brew coffees. The contents of pyrazines in UAC extractions were 9.64 μg/mL (19.69%), and 2,6-dimethylpyrazine and 2-ethyl-6-methylpyrazine were more abundant.

Heterocyclic compounds, such as pyridines and pyrroles, were also detected in hot and cold brew coffees. In general, pyridines in coffee mainly include alkylpyridine and acylpyridene, which endow coffee roasting/burnt flavor and biscuit aroma, respectively. Acylpyridine was only identified in hot brew coffee samples, indicating a unique biscuit aroma. Pyrroles have been reported as furan degradation products and amino acid derivatives (2), responsible for a peculiarly sweet and slightly flared smell in coffee (35). Pyridines and pyrroles showed low concentrations in UAC coffees (4.11 μg/mL and 4.04 μg/mL, respectively), indicating a relatively weak burnt and smoky aroma.

There were also some ketones and phenols present in coffees. Ketones are known to be responsible for buttery, caramel-like, or fruity odor notes (31), and phenols have been described as having smoky, spicy, and burnt aromas (36). The content of ketones in UAC extractions was the lowest (3.39 μg/mL), which was about one-third of that in PO coffee. In contrast, phenols were 3.05 μg/mL in content, slightly higher than 4 CB. The UAC method demonstrated the low extraction ability of ketones and phenols in coffee.

Table 4 shows the compounds with OAV values greater than 1, and the sensory descriptors and the odor perception

TABLE 3 | Volatile components in coffee extracts with different brewing methods.

NO.	Category	CAS	Compounds	Contents (μg/mL)				
				HB	PO	4 CB	10 CB	UAC
1	Furans	3188-00-9	2-Methyl tetrahydro-3-furanone	0.44	0.51	0.30	0.21	0.13
2		4412-91-3	3-Furyl alcohol	14.95	16.21	10.86	9.13	7.26
3		1192-62-7	2-Acetylfuran	2.56	2.25	1.47	1.16	0.83
4		4466-24-4	2-N-butyl furan	1.06	0.66	0.50	—	0.25
5		620-02-0	5-Methylfuran aldehyde	21.31	20.89	10.52	9.09	6.35
6		3194-15-8	2-Propionylfuran	1.01	0.52	—	0.23	0.22
7		5989-33-3	Cis-α,α-5-trimethyl-5-vinyl tetrahydrofuran-2-methanol	2.96	2.03	1.54	0.37	0.78
8		10599-69-6	2-Methyl-5-propionylfuran	—	—	—	0.16	0.12
9		31681-26-2	α -Propyl-2-furan acetaldehyde	0.73	0.71	—	—	—
10		1193-79-9	5-Methyl-2-acetyl-furan	1.12	1.69	—	0.89	0.61
11		19377-82-3	2-N-(furanyl) furosemide	—	1.44	—	—	—
12		98-01-1	Furfural	8.35	10.68	5.02	3.86	2.60
13		488-05-1	3-Methyl-1- (3-methyl-2-furanyl)—1-butanone	—	0.55	—	—	—
14		3777-71-7	2-Heptyl furan	—	—	0.37	0.21	0.15
15		3208-16-0	2-Ethylfuran	—	—	0.80	0.49	0.30
16		10410-20-5	2-(1-Hydroxy-1-methyl-2-oxo-propyl)-2, 5-dimethylfuran-3 (2H) -ketone	—	—	—	0.17	0.13
17	Pyrazines	71257-37-9	3, 4-Dihydropyrrole and [1,2-a] pyrazine	—	—	—	0.28	—
18		5910-89-4	2,3-Dimethylpyrazine	0.38	0.35	0.21	0.11	0.13
19		23747-48-0	5-Methyl-6,7-dihydro-5H-cyclopentaminopyrazine	0.49	0.52	0.37	0.27	0.19
20		22047-26-3	2-Acetyl-6-methylpyrazine	0.32	0.30	—	0.20	0.16
21		18217-82-8	2-Methyl-5-[(E)-1-allyl] pyrazine	0.32	0.46	0.34	0.21	—
22		14667-55-1	2,3,5-Trimethylpyrazine	—	7.50	3.97	2.65	2.05
23		13925-09-2	2-Vinyl-6-methylpyrazine	—	—	—	0.28	—
24		13925-08-1	2-Vinyl-5-methylpyrazine	—	0.22	—	—	—
25		13925-07-0	2-Ethylalkyl-3,5-dimethylpyrazine	—	1.67	—	—	—
26		13925-03-6	2-Ethyl-6-methylpyrazine	5.52	4.43	2.84	1.99	1.48
27		13925-00-3	2-Ethylpyrazine	2.05	1.13	0.74	0.64	0.48
28		13360-65-1	3-Ethyl-2,5-methylpyrazine	5.54	4.20	3.22	1.80	1.39
29		109-08-0	2-Methylpyrazine	3.04	3.96	1.99	1.47	1.05
30		108-50-9	2, 6-Dimethylpyrazine	9.29	9.53	4.84	3.71	2.61
31		15707-23-0	2-Ethyl-3-methylpyrazine	13.64	—	—	—	—
32		98-96-4	Pyrazinamide	—	—	—	0.14	0.10
33	Alcohols	98-55-5	Alpha terpineol	—	0.25	0.30	0.14	—
34		78-70-6	Linalool	0.84	0.30	0.57	0.20	0.19
35		768-95-6	1-Adamantanol	0.94	0.92	0.63	0.40	0.29
36		60-12-8	Phenethyl alcohol	—	—	—	0.64	0.48
37	Alcohols	59-42-7	3-Hydroxyl-α-(methyl amino) methyl benzyl alcohol	—	0.20	—	—	—
38		64-17-5	Ethyl alcohol	0.33	—	—	—	—
39		111-55-7	Glycol diacetate	0.71	—	—	—	—
40		543-49-7	2-Heptanol	—	—	0.24	—	—
41		14003-34-0	3-Methyl-3-quinolol	—	—	—	0.14	—
42		1075-04-3	1-Phenylpropane-1,2-diol	—	—	—	0.93	0.68
43	Pyrroles	86688-96-2	(Pyrrole-3-yl)-acetic acid	—	—	1.22	0.41	0.27
44		2167-14-8	Tea pyrrole	0.16	—	—	—	—
45		19713-89-4	3, 4-Dimethyl-1-H-pyrrol-2-carboxyaldehyde	1.43	—	0.40	0.26	0.31
46		1192-58-1	N-methyl-2-pyrrole formaldehyde	—	4.32	2.99	2.35	1.60
47		1072-83-9	2-Acetyl-pyrrole	2.74	0.85	1.10	1.85	1.32
48		1438-94-4	1-Furfuryl pyrrole	—	—	0.47	—	0.26
49		1003-29-8	2-Pyrrolidoformaldehyde	—	—	0.24	—	0.28

(Continued)

TABLE 3 | Continued

NO.	Category	CAS	Compounds	Contents (μg/mL)				
				HB	PO	4 CB	10 CB	UAC
50	Aldehydes	96-17-3	2-Methylbutylaldehyde	0.56	0.52	0.50	0.16	0.14
51		78-84-2	Isobutyraldehyde	—	0.28	—	—	—
52		590-86-3	Isovaleraldehyde	0.40	0.32	0.38	0.09	0.08
53		122-78-1	Phenylacetaldehyde	0.44	0.22	—	—	0.10
54	Ketones	875-59-2	4-Hydroxy-2-methyl acetophenone	6.84	6.82	3.49	2.31	1.46
55		75-97-8	Tert-butyl methyl ketone	—	—	—	0.54	—
56		600-14-6	2,3-Glutaric ketone	0.78	1.10	0.49	0.22	0.16
57	Ketones	592-20-1	Acetoxy-2-acetone	—	1.00	0.52	0.30	0.39
58		1575-57-1	1-Acetoxy-2-butanone	—	0.38	0.19	0.15	0.16
59		67-64-1	Acetone	—	0.44	—	—	—
60		21835-01-8	3-Ethyl-2-hydroxy-2-cyclopentene-1-ketone	—	0.68	—	—	—
61		765-70-8	3-Methylcyclopentane-1,2-dione	0.69	—	—	—	—
62		699-83-2	2,6-Dihydroxyacetophenone	—	—	2.71	—	1.22
63		34598-80-6	2, 4-Dimethylcyclopentane-1,3-dione	—	—	1.21	—	—
64		5751-48-4	2-Methylchromone	—	—	—	0.14	—
65	Phenols	95-48-7	2-Cresol	—	—	0.51	—	0.39
66		90-05-1	Guaiacol	2.54	4.92	1.94	1.89	1.77
67		2785-89-9	4-Ethyl-2-methoxyphenol	3.71	3.00	—	2.66	—
68		108-95-2	Phenol	—	—	—	1.19	0.89
69		2836-00-2	3-Amino-4-methylphenol	—	1.20	—	—	—
70		1138-52-9	3, 5-Di-tert-butylphenol	—	0.67	—	0.37	—
71		106-44-5	Paracresol	—	1.13	—	0.37	—
72	Pyridines	110-86-1	Pyridine	16.63	12.10	11.16	4.06	4.11
73		67402-83-9	1-Acetyl-1,4-dihydropyridine	0.33	0.30	—	—	—
74		17747-43-2	3-Acetoxyridine	—	0.16	—	—	—
75	Acids	503-74-2	Isopropylaceticacid	0.90	—	1.40	—	—
76		53387-38-5	Cyclohexylacetic Acid	1.29	—	—	0.29	—
77		631-61-8	Ammonium acetate	0.27	—	—	—	—
78	Esters	623-17-6	Furfuryl acetate	—	—	—	—	0.31
79		547-65-9	2-Methylenyl butyrolactone	—	0.22	—	0.17	—
80		62873-16-9	α-methylene-γ-valerolactone	—	0.32	—	—	—
81		36760-43-7	S-phenyl-tert-butyl thiocarbonate	1.47	1.17	0.57	—	0.43
82		68555-59-9	α,2, 2, 6-Tetramethylcyclohexyl acetate, propyl	0.23	—	—	—	—
83		1129-41-5	1-Acetoxy-2-butanone	1.34	—	—	—	—
84		79-20-9	Acetone	—	—	0.35	—	—
85		6203-89-0	3-Ethyl-2-hydroxy-2-cyclopentene-1-ketone	—	—	0.42	—	—
86		13290-00-1	3-Methylcyclopentane-1, 2-dione	—	—	0.36	—	—
87		7779-73-9	2, 6-Dihydroxyacetophenone	—	—	—	0.25	—
88		103130-72-9	2, 4-Dimethylcyclopentane-1, 3-dione	—	—	—	—	0.08
89	Others	96-37-7	2-Methylchromone	1.82	1.12	0.89	0.33	0.99
90		6596-35-6	Four hydrogen naphthalene anthracene	0.72	0.38	0.32	—	0.28
91		6380-23-0	3, 4-Dimethoxy styrene	0.84	0.55	0.48	0.20	—
92		491-36-1	4-Hydroxyquinazoline	—	0.56	0.50	0.23	0.19
93		4634-87-1	2, 6-Dimethyl-2, 4-heptadiene	—	—	—	0.26	0.24
94		4437-22-3	2, 2-Difuryl ether	1.19	0.73	0.82	0.53	0.24
95		3891-99-4	2,6, 10-Trimethyltridecane	0.40	0.22	0.28	0.07	0.12
96		1921-70-6	2,6,10, 14-Tetramethylpentadecane	—	0.62	0.36	—	0.16
97		55401-75-7	9-Dodecyl tetoxanthracene	0.97	—	0.51	—	—

HB, Hot boiled; PO, Pour-over; 4CB, 4°C cold brew; 10 CB, 10°C cold brew; UAC, Ultrasound-assisted cold brew.

FIGURE 2 | Cluster heatmap **(A)** and Venn diagrams **(B)** of volatile compounds produced by different coffee brewing methods. **(C)** Principal component analysis (PCA) biplot of volatile compounds in hot and cold brew coffees. (1: 2-Propionylfuran, 2: 2, 2-Difuryl ether, 3: Isopropylacetic acid, 4: 3, 4-Dimethyl-1H-pyrrol-2-carboxaldehyde, 5: (Pyrrole-3-yl) -acetic acid, 6: 2-N-(furanyl) furosemide, 7: 5-Methyl-2-acetyl-furan, 8: 4-Ethyl-2-methoxyphenol, 9: 2-n-butyl furan, 10: Phenol, 11: Cyclohexylacetic Acid, 12: Methylcyclopentane, 13: 2-Acetyl-pyrrole,14: 4-Hydroxy-2-methyl acetophenone, 15: 2-Ethylalkyl-3, 5-dimethylpyrazine, 16: 2-Ethylpyrazine, 17: 2, 3-Pentanedione, 18: Cis -α,α−5-trimethyl-5-vinyl tetrahydrofuran-2-methanol, 19: 2-Acetylfuran, 20: 3-Ethyl-2, 5-methylpyrazine, 21: Guaiacol, 22: 2-Ethyl-6-methylpyrazine, 23: 2,3,5-Trimethylpyrazine, 24: 2-Methylpyrazine, 25: Pyridine, 26: N-methyl-2-pyrrole formaldehyde, 27: Furfuryl acetate, 28: 2, 6-Dimethylpyrazine, 29: Furfural, 30: 3-Furyl alcohol, 31: 5-Methylfuran aldehyde, 32: 3-Methyl phenyl methyl carbamate, 33: S-phenyl-tert-butyl thiocarbonate, 34: 2-Ethyl-3-methylpyrazine, 35: Paracresol, 36: 3-Amino-4-methylphenol, 37: 2, 4-Dimethylcyclopentane-1, 3-dione, 38: 2,6-Dihydroxyacetophenone). HB, Hot boiled, PO, Pour-over, 4 CB, 4°C cold brew, 10 CB,10°C cold brew, UAC, Ultrasound-assisted cold brew.

threshold values were taken from the literature results (31, 37). Twenty-nine compounds were determined in five kinds of coffees at concentrations higher than their corresponding odor threshold value, including pyrazines (6), furans (5), phenols (5), aldehydes (4), ketones (2), alcohols (2), pyrroles (2), pyridines (2), and ester (1), which possibly contributed to the overall coffee aroma. According to **Table 4**, the aromas can be summarized into eight categories: caramel-like, sweet, frumentaceous, fruity, nutty, floral, roasty, medicinal, and spicy aroma (**Figure 3B**), which revealed apparent differences in the aroma profiles of the respective extraction methods. Caramel-like is the strongest

aroma, which was mainly contributed by guaiacol (OAV > 3000) and 3-ethyl-2,5-dimethylpyrazine (OAV > 200). According to Semmelroch & Grosch (36), these two compounds played an essential role in the aroma of coffees. Sweet, frumentaceous, fruity, and nutty aromas were also abundant in coffees, mainly owing to isovaleraldehyde (OAV > 400) and some pyrazine derivatives. While floral, roasty, medicinal, and spicy aroma had relatively little effect on flavor, On the whole, the aroma of coffee extracted by UAC might be less intense than that of hot extractions, but was similar to that of 10 CB extractions.
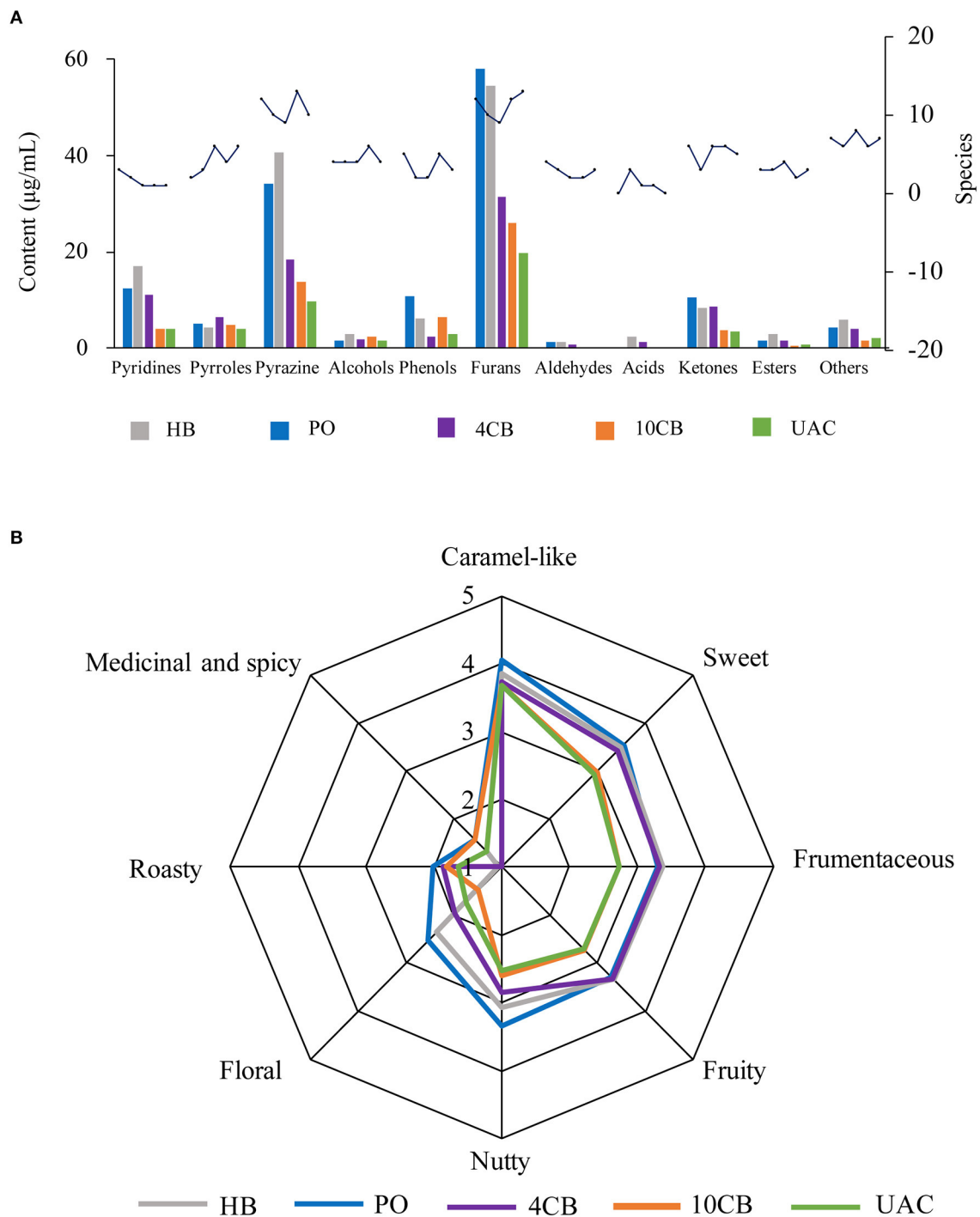
FIGURE 3 | Contents and species of volatile compounds **(A)** and spider plots of aroma attributes **(B)** for different coffee brewing methods. HB, Hot boiled, PO, Pour-over, 4 CB, 4°C cold brew, 10 CB, 10°C cold brew, UAC, Ultrasound-assisted cold brew.

Optimization of UAC Coffee

Compared to hot-brewing, the coffee produced by cold-brewing has a unique sensory flavor and good market prospect. However, the problems of long extraction time and high energy consumption limit the large-scale production of cold-brewing. The above results showed that UAC considerably shortened cold extraction time (1 h vs. 12 h) and made main physicochemical characteristics achieve the levels of coffee produced through

TABLE 4 | Odor thresholds and odor activity values (OAVs) of potent volatile compounds in coffee extracts with different brewing methods.

NO.	Compounds	Odor descriptors	Odor threshold (µg/L)	Odor activity value (OAV)				
				HB	PO	4 CB	10 CB	UAC
1	3-Furyl alcohol	Peculiar bitter, spicy	2,000	7.47	8.10	5.43	4.56	3.63
2	2-N-butyl furan	Wine, bread, meat	5	211.60	132.83	100.10	—	49.53
3	5-Methylfuran aldehyde	Caramel	1,110	19.20	18.82	9.48	8.19	5.72
4	2-Ethylfuran	Sweet	2.3	—	—	345.65	211.07	131.72
5	2-Acetyl-6-methylpyrazine	Roasty, nutty	62	5.18	4.91	—	3.17	2.56
6	2,3, 5-Trimethylpyrazine	Nutty, sweet, floral	1,800	—	4.17	2.21	1.47	1.14
7	2-Ethylalkyl-3,5-dimethylpyrazine	Nutty, sweet	1	—	1,671.63	—	—	—
8	2-Ethyl-6-methylpyrazine	Caramel, nutty	100	55.15	44.27	28.44	19.92	14.85
9	3-Ethyl-2,5-methylpyrazine	Almond, chocolate, caramel	5	1,107.73	839.21	644.38	360.86	277.22
10	2, 6-Dimethylpyrazine	Roasty, chocolate	9,000	1.03	1.06	0.54	0.41	0.29
11	2-Ethyl-3-methylpyrazine	Nutty, chocolate, peanut	130	104.92	—	—	—	—
12	Linalool	Floral, spices, wood	6	140.41	50.80	95.81	32.80	31.12
13	2-Heptanol	Lemon, grassy	65.2	—	—	3.61	—	—
14	N-methyl - 2-pyrrole formaldehyde	Roasty, almond	37	—	116.86	80.73	63.59	43.25
15	1-Furfuryl pyrrole	Hazelnut, cocoa	100	—	—	4.70	—	2.62
16	2-Methylbutylaldehyde	Apple, malt, and fermented	1.3	432.44	403.40	386.37	123.11	105.77
17	Isobutyraldehyde	Fruity, malt, and grassy	0.9	—	306.57	—	—	—
18	Isovaleraldehyde	Apple, chocolate, cheesy, sweet	0.2	1,998.30	1,619.64	1,894.72	465.63	402.77
19	Phenylacetaldehyde	Sweet, grassy, floral, chocolate	4	109.40	55.30	—	—	24.93
20	2, 3-Glutaric ketone	Creamy	30	26.03	36.59	16.33	7.22	5.48
21	3-Furyl alcohol	Caramel, nutty, bread	300	2.31	—	—	—	—
22	2-N-butyl furan	Caramel	0.381	6,666.67	12,919.95	5,104.40	4,973.02	4,652.80
23	5-Methylfuran aldehyde	Spicy, smoky	540	6.88	5.55	—	4.93	—
24	2-Ethylfuran	Phenolic, medicinal	58.6	—	—	—	20.24	15.19
25	2-Acetyl-6-methylpyrazine	Alkylphenolic	200	—	3.35	—	1.83	—
26	2,3, 5-Trimethylpyrazine	Medicinal, phenolic	55	—	20.46	—	6.81	—
27	2-Ethylalkyl-3, 5-dimethylpyrazine	Special smell, pungent	2,000	8.32	6.05	5.58	2.03	2.05
28	2-Ethyl-6-methylpyrazine	Nutty	32.19	—	4.97	—	—	—
29	3-Ethyl-2, 5-methylpyrazine	Fruity	1,030	—	—	—	—	0.30

HB, Hot boiled; PO, Pour-over; 4 CB, 4°C cold brew; 10 CB,10°C cold brew; UAC, Ultrasound-assisted cold brew.

conventional cold-brewing methods. The aroma was similar to that of 10 CB coffee. Therefore, UAC can replace conventional cold extractions, significantly improving the extraction efficiency and ensuring the quality of coffee.

The coffee-to-water ratio is significantly associated with mass transfer during the extraction process. Studies show that using a lower coffee/water ratio decreases the titratable acidity/total polyphenol concentration ratio and changes the coffee flavor (38). While a high amount of coffee decreases bed permeability, resulting in excessive pressure and possible over extraction (17), EY can be defined as a specified component released from the coffee matrix at a given time (19). So extraction time is another crucial factor for coffee flavor and quality. Likewise, ultrasound has been proposed as an effective technology to reach higher EY than conventional extraction methods due to faster extraction kinetics, with ultrasonic power as the most critical parameter. Therefore, the UAC conditions, including coffee/water ratio, extraction time, together with ultrasonic power, were optimized by OED.

Based on the optimal conditions obtained from single-factor experiments [coffee-to-water ratio, 1:15; extraction time, 60 min; ultrasonic power, 150 W (**Supplementary Figure 2**)], the OED L$_9$ (3^3) was employed to investigate the effects of coffee/water, extraction time, and ultrasonic power. The details of the OED are shown in **Supplementary Table 3**. The K values (K1, K2, and K3) were the average sum of indicators at each factor level, and the R-value was the influence of the experimental parameters. Higher R indicates the factor has a more decisive influence. Therefore, the optimal conditions were coffee/water = 1:15, extraction time, 60 min, with ultrasonic power 200 W, leading to the increased EY, high to 17.72%. Using the OED substantially reduced the number of experiments required, saving the time and cost spent on conducting experiments.

After that, the physicochemical characteristics, including TDS, TPC, TO, Tpro, TA, pH, color, and main no-volatiles including caffeine, CGA, and trigonelline contents, were evaluated under optimal condition (**Supplementary Table 4**). Compared to unoptimized UAC coffee, almost all component extraction rates

increased, while L^* value and CGA content slightly decreased, indicating darker color with a lesser bitter taste in UAC coffee after optimization.

CONCLUSIONS AND PERSPECTIVES

Cold brew coffee is rapidly growing, despite the lack of a standardized procedure for its production. In this work, cold brewing (immersion at $4°C/10°C$ and UAC) and hot brewing (HB and PO) extractions with the same coffee-to-water ratio were performed to identify any differences concerning the contents of physicochemical characteristics, mainly non-volatile components and volatiles. Results showed that the traditional cold-brewing method could be optimized by sonication, leading to shorter extraction time and improved extraction efficiency. Based on our data, the UAC-generated beverages displayed higher TDS, TL, Tpro, TA, and pH than static cold immersion coffee, with comparable contents of caffeine, CGA, and trigonelline. The superior quality aroma of coffee appeared to be related to well-defined temperature and pressure parameters because compounds with high polarity, such as alcohols, ketones, pyrazines and aldehydes, tend to percolate more quickly in the greatest abundance contributing to the potency and intensity of the coffee aroma in hot extractions. UAC coffee was mainly associated with flavor attributes such as caramel, nutty, roasty and sweet aromas, which had no significant difference from traditional cold brews. Further research is needed to characterize the UAC coffee by its sensory evaluation and consumer acceptability. Another vital issue that must be considered is the safety of cold brew coffee. Due to the long-brewing time for conventional cold brewing methods, it tends to facilitate the activity of microorganisms to cause microbiological food safety hazards. However, few published studies focused on the safety of cold coffee brews. Recently, Kyroglou (4) mentioned that various species of pathogenic bacteria might be viable in the cold brew for 7–28 days. Sonication is considered a non-thermal food preservation method that can inactivate microorganisms, so UAC may have an additional and surprising effect on cold brew coffee's bacteriostasis, which needs further research.

On the whole, with the optimum conditions for UAC, a new cold brew method was established, which can reduce the extraction time and improve extraction efficiency, with a similar aroma and flavor to original cold brew coffee. This study attempts to contribute to the processing of cold brew coffee, bringing in a promising fast extraction procedure that will shed light on the commercialization of the process. Future work should be conducted to evaluate other parameters for UAC; such as species of coffee beans, degree of grinding, roasting, and temperature; and the safety issues concerning cold coffee brew consumption, which will promote completing the work for industrial application of UAC brewing coffee.

DATA AVAILABILITY STATEMENT

The original contributions presented in the study are included in the article/**Supplementary Material**, further inquiries can be directed to the corresponding author/s.

AUTHOR CONTRIBUTIONS

XZ conducted most of the statistical analyses, wrote, and edited the manuscript. MY and JZ conducted the research. LZ provided expertise regarding the volatiles aspects of the work. YT and CL completed the optimization of UAC coffee. LB helped analyze the volatiles data. CM designed the experiments and provided consultation in terms of chemical and physical analyses. AA formal analysis, writing–review & editing. All authors contributed to this work. All authors contributed to the article and approved the submitted version.

SUPPLEMENTARY MATERIAL

The Supplementary Material for this article can be found online at: https://www.frontiersin.org/articles/10.3389/fnut.2022.849811/full#supplementary-material

REFERENCES

1. Sánchez López JA, Wellinger M, Gloess AN, Zimmermann R, Yeretzian C. Extraction kinetics of coffee aroma compounds using a semi-automatic machine: on-line analysis by PTR-ToF-MS. *Int J Mass Spectrom.* (2016) 401:22–30. doi: 10.1016/j.ijms.2016.02.015

2. Cordoba N, Pataquiva L, Osorio C, Moreno FLM, Ruiz RY. Effect of grinding, extraction time and type of coffee on the physicochemical and flavour characteristics of cold brew coffee. *Sci Rep.* (2019) 9:8440. doi: 10.1038/s41598-019-44886-w

3. Cordoba Castro N. Chemical and sensory evaluation of cold brew coffees using different roasting profiles and brewing methods. *Food Res Int.* (2021) 141:110141. doi: 10.1016/j.foodres.2021.110141

4. Kyroglou S, Thanasouli K, Vareltzis P. Process characterization and optimization of cold brew coffee: effect of pressure, temperature, time and

solvent volume on yield, caffeine and phenol content. *J Sci Food Agric.* (2021) 101:4789–98. doi: 10.1002/jsfa.11125

5. Yu JM, Chu M, Park H, Park J, Lee KG. Analysis of volatile compounds in coffee prepared by various brewing and roasting methods. *Foods.* (2021) 10:1347. doi: 10.3390/foods10061347

6. Angeloni G, Guerrini L, Masella P, Innocenti M, Bellumori M, Parenti A. Characterization and comparison of cold brew and cold drip coffee extraction methods. *J Sci Food Agric.* (2019) 99:391–9. doi: 10.1002/jsfa.9200

7. Rao NZ, Fuller M, Grim MD. Physiochemical characteristics of hot and cold brew coffee chemistry: The effects of roast level and brewing temperature on compound extraction. *Foods.* (2020) 9:902. doi: 10.3390/foods9070902

8. Fuller M, Rao NZ. The effect of time, roasting temperature, and grind size on caffeine and chlorogenic acid concentrations in cold brew coffee. *Sci Rep.* (2017) 7:17979. doi: 10.1038/s41598-017-18247-4

9. Caudill M, Osborne J, Sandeep KP, Simunovic J, Harris GK. Viability of microwave technology for accelerated cold brew coffee processing vs conventional brewing methods. *J Food Eng.* (2022) 317:110866. doi: 10.1016/j.jfoodeng.2021.110866

10. Chemat F, Rombaut N, Sicaire AG, Meullemiestre A, Fabiano-Tixier AS, Vian M. Ultrasound assisted extraction of food and natural products. Mechanisms, techniques, combinations, protocols and applications: a review. *Ultrason Sonochem.* (2016) 34. doi: 10.1016/j.ultsonch.2016.06.035

11. Proestos C, Komaitis M. Ultrasonically assisted extraction of phenolic compounds from aromatic plants: comparison with conventional extraction technics. *J Food Qual.* (2006) 29:567–82. doi: 10.1111/j.1745-4557.2006.00096.x

12. Wang L, Weller CL. Recent advances in extraction of nutraceuticals from plants. *Trends Food Sci Technol.* (2006) 17:300–12. doi: 10.1016/j.tifs.2005.12.004

13. Zamanipoor MH, Yakufu B, Tse E, Rezaeimotlagh A, Hook JM, Bucknall MP, et al. Brewing coffee? – Ultra-sonication has clear beneficial effects on the extraction of key volatile aroma components and triglycerides. *Ultrason Sonochem.* (2020) 60:104796. doi: 10.1016/j.ultsonch.2019.104796

14. Moreno FL, Quintanilla-Carvajal MX, Sotelo LI, Osorio C, Raventós M, Hernández E, et al. Volatile compounds, sensory quality and ice morphology in falling-film and block freeze concentration of coffee extract. *J Food Eng.* (2015) 166:64–71. doi: 10.1016/j.jfoodeng.2015.05.018

15. Averbeck M, Schieberle PH. Characterisation of the key aroma compounds in a freshly reconstituted orange juice from concentrate. *Eur Food Res Technol.* (2009) 229:611–22. doi: 10.1007/s00217-009-1082-4

16. Ludwig I, Clifford M, Lean M, Ashihara H, Crozier A. Coffee: biochemistry and potential impact on health. *Food Funct.* (2014) 5:1695–717. doi: 10.1039/C4FO00042K

17. Roman Corrochano B, Melrose J, Bentley AC, Fryer P, Bakalis S. A new methodology to estimate the steady-state permeability of roast and ground coffee in packed beds. *J Food Eng.* (2014) 150. doi: 10.1016/j.jfoodeng.2014.11.006

18. Ahmed M, Jiang GH, Park JS, Lee KC, Seok YY, Eun JB. Effects of ultrasonication, agitation and stirring extraction techniques on the physicochemical properties, health-promoting phytochemicals and structure of cold-brewed coffee. *J Sci Food Agric.* (2019) 99:290–301. doi: 10.1002/jsfa.9186

19. Cordoba N, Fernandez-Alduenda M, Moreno FL, Ruiz Y. Coffee extraction: A review of parameters and their influence on the physicochemical characteristics and flavour of coffee brews. *Trends Food Sci Technol.* (2020) 96:45–60. doi: 10.1016/j.tifs.2019.12.004

20. Wagemaker TAL, Carvalho CRL, Maia NB, Baggio SR, Guerreiro Filho O. Sun protection factor, content and composition of lipid fraction of green coffee beans. *Ind Crops Prod.* (2011) 33:469–73. doi: 10.1016/j.indcrop.2010.10.026

21. Severini C, Ricci I, Marone M, Derossi A, De Pilli T. Changes in the aromatic profile of Espresso coffee as a function of the grinding grade and extraction time: a study by the electronic nose system. *J Agric Food Chem.* (2015) 63:2321–7. doi: 10.1021/jf505691u

22. Farah A, Monteiro M, Calado V, Franca A, Trugo LC. Correlation between cup quality and chemical attributes of Brazilian coffee. *Food Chem.* (2006) 98:373–80. doi: 10.1016/j.foodchem.2005.07.032

23. Veillet S, Tomao V, Chemat F. Ultrasound assisted maceration: An original procedure for direct aromatisation of olive oil with basil. *Food Chem.* (2010) 123:905–11. doi: 10.1016/j.foodchem.2010.05.005

24. Toci AT, Neto VJMF, Torres AG, Farah A. Changes in triacylglycerols and free fatty acids composition during storage of roasted coffee. *LWT - Food Sci Technol.* (2013) 50:581–90. doi: 10.1016/j.lwt.2012.08.007

25. Franca A, Oliveira L, Mendonça J, Silva X. Physical and chemical attributes of defective crude and roasted coffee beans. *Food Chem.* (2005) 90:89–94. doi: 10.1016/j.foodchem.2004.03.028

26. Macrae R. *Carbohydrates in Coffee*. New York: Wiley. (1985).

27. Vinatoru M. An overview of the ultrasonically assisted extraction of bioactive principles from herbs. *Ultrason Sonochem.* (2001) 8:303–13. doi: 10.1016/S1350-4177(01)00071-2

28. Ginz M, Engelhardt UH. Identification of new diketopiperazines in roasted coffee. *Eur Food Res Technol.* (2001) 213:8–11. doi: 10.1007/s002170100322

29. Masi C, Dinnella C, Monteleone E, Prescott J. The impact of individual variations in taste sensitivity on coffee perceptions and preferences. *Physiol Behav.* (2015) 138:219–26. doi: 10.1016/j.physbeh.2014.10.031

30. Blumberg S, Frank O, Hofmann T. Quantitative studies on the influence of the bean roasting parameters and hot water percolation on the concentrations of bitter compounds in coffee brew. *J Agric Food Chem.* (2010) 58:3720–8. doi: 10.1021/jf9044606

31. López-Galilea I, Fournier N, Cid C, Guichard E. Changes in headspace volatile concentrations of coffee brews caused by the roasting process and the brewing procedure. *J Agric Food Chem.* (2006) 54:8560–6. doi: 10.1021/jf061178t

32. Czerny M, Grosch W. Potent odorants of raw Arabica coffee. Their changes during roasting. *J Agric Food Chem.* (2000) 48:868–72. doi: 10.1021/jf990609n

33. Crews C, Castle L. A review of the occurrence, formation and analysis of furan in heat-processed foods. *Trends Food Sci Technol.* (2007) 18:365–72. doi: 10.1016/j.tifs.2007.03.006

34. Furong W, Jiaqi H, Hailiang S, Yali Y, Yurong G. Formation mechanism of pyrazine compounds in the sunflower oil. *Sci Technol Food Ind.* (2020) 41:330–5. doi: 10.13386/j.issn1002-0306.2020.02.053

35. Toci AT, Farah A. Volatile fingerprint of Brazilian defective coffee seeds: corroboration of potential marker compounds and identification of new low quality indicators. *Food Chem.* (2014) 153:298–314. doi: 10.1016/j.foodchem.2013.12.040

36. Semmelroch P, Grosch W. Studies on character impact odorants of coffee brews. *J Agric Food Chem.* (1996) 44:537–43. doi: 10.1021/jf9505988

37. Córdoba N, Moreno FL, Osorio C, Velásquez S, Fernandez-Alduenda M, Ruiz-Pardo Y. Specialty and regular coffee bean quality for cold and hot brewing: Evaluation of sensory profile and physicochemical characteristics. *LWT.* (2021) 145:111363. doi: 10.1016/j.lwt.2021.111363

38. Wang X, William J, Fu Y, Lim LT. Effects of capsule parameters on coffee extraction in single-serve brewer. *Food Res Int.* (2016) 89:797–805. doi: 10.1016/j.foodres.2016.09.031

Physicochemical and Functional Properties of Membrane-Fractionated Heat-Induced Pea Protein Aggregates

Nancy D. Asen[1] and Rotimi E. Aluko[1,2]*

[1] Department of Food and Human Nutritional Sciences, University of Manitoba, Winnipeg, MB, Canada, [2] The Richardson Center for Functional Foods and Nutraceuticals, University of Manitoba, Winnipeg, MB, Canada

This study was carried out to investigate the effect of heat pre-treatment of pea proteins at different pH values on the formation of functional protein aggregates. A 10% (w/v) aqueous mixture of pea protein concentrate (PPC) was adjusted to pH 3.0, 5.0, 7.0, or 9.0 followed by heating at 100°C for 30 min, cooled and centrifuged. The supernatant was sequentially passed through 30 and 50 kDa molecular weight cut-off membranes to collect the <30, 30–50, and >50 kDa fractions. The >50 kDa fractions from pH 3.0 (FT3), 5.0 (FT5), 7.0 (FT7), and 9.0 (FT9) treatments had >60% protein content in contrast to the ≤20% for the <30 and 30–50 kDa fractions. Therefore, the >50 kDa fractions were collected and then compared to the untreated PPC for some physicochemical and functional properties. Protein aggregation was confirmed as the denaturation temperature for FT3 (124.30°C), FT5 (190.66°C), FT7 (206.33°C) and FT9 (203.17°C) was significantly ($p < 0.05$) greater than that of PPC (74.45°C). Scanning electron microscopy showed that FT5 had a compact structure like PPC while FT3, FT7, and FT9 contained a more continuous network. In comparison to PPC, the >50 kDa fractions showed improved solubility (>60%), oil holding capacity (~100%), protein content (~7%), foam capacity (>10%), foam stability (>7%), water holding capacity (>16%) and surface hydrophobicity (~50%). Least gelation concentration of PPC (18%), FT3 (25%), FT5 (22%), FT7 (22%), and FT9 (25%) was improved to 16, 18, 20, 16, and 18%, respectively, after addition of NaCl.

Keywords: pea protein, heat treatment, protein aggregates, polypeptide composition, pH, surface hydrophobicity, functional properties

INTRODUCTION

Utilization of protein as a food ingredient and additive is an age long global tradition and this is seen in wide applications from small scale (e.g., private home kitchens) to industrial scale food processing. Protein is valued by food formulators and the industry for properties such as gelation (e.g., pasta and sausages), foam (e.g., meringues and cakes), emulsification (e.g., salad dressings and soups), fat holding (e.g., yogurts and fish meat products), and water binding (e.g., meat and bread) (1). In addition, proteins contribute nutritional benefit to foods through amino acids,

which are essential for human growth and preservation. Food proteins are derived from plant and animal sources with the most popular being meat, poultry, seafood, beans, peas, lentils, eggs, nuts, seeds, and soy. The recent trend in food applications is the exploration of plant proteins as alternatives to animal proteins, especially to meet the triad of health, socioeconomic and environmental demands in addition to the challenge to produce and distribute quality protein to feed >9 billion people by 2050 (2). The reason for this trend is that plant proteins have several advantages over animal equivalents, including higher levels of unsaturated fatty acids, low cost, ready availability, low greenhouse gas emission, reduced carbon footprint and an alternative protein source for vegetarians and vegans (3, 4). As a result, high consumer preference for plant proteins as alternative protein source has been discussed (5). One of the most commercially utilized plant proteins comes from the yellow field pea seed. In addition to the benefits of plant proteins, and unlike other grain proteins from wheat and soybean, pea proteins are less allergenic and possess nitrogen fixing ability, which makes it an important agricultural crop for rotation to maintain soil health (6, 7). Several works have shown the potential use of pea protein as a food ingredient to improve emulsification, gelation, and foaming properties with possible development of novel foods like beverages, baked goods, soups, snacks, dips, and salad dressings (8, 9). Peas have been a popular source of protein in developing countries for decades, however, until recently, consumption as part of manufactured food products have been very limited mainly due to availability of many affordable alternative protein sources like soybean and milk.

The main pea proteins are the globulins (55–65%) but albumins, prolamin, and glutenins are also present. The globulin fraction consists mainly of legumin (11S), vicilin (7S), and convicilin (7S). Legumins have three acidic subunits and three basic subunits with molecular weight (MW) of 36.8, 36.4, and 34.4 kDa for acidic and ∼20 kDa for basic subunits. The vicilin β + γ subunit has MW of 23.6–31.6 kDa while vicilin basic subunit (α + β + γ) has MW 54.6 kDa and subunit γ is 17.4 kDa in size (10). Two-dimensional gel electrophoresis of pea seed albumins showed three groups, high molecular weight (∼50–110 kDa), average molecular weight (∼20–35 kDa) and low MW (∼ 6–17 kDa) (10, 11). About 638 amino acids were found in the protein primary structure of different pea seed cultivars (12). Pea proteins contain a wide variety and well-balanced profile of amino acids belonging to different classes of positively charged, negatively charged, branched-chain, aromatic and hydrophobic (9). However, previous works have shown that like other legumes, sulfur-containing amino acids (methionine and cysteine) are limiting in pea proteins (13, 14). The main amino acid in pea legumin α-chain is Glu, while the β-chain is rich in Val, Ala, and Leu and presence of high levels of Glu in proteins enhance protein-solvent interactions, which improves functionality (15). However, the globular nature of pea proteins hinders their flexibility as the structure is densely packed due to the presence of disulfide linkages, low surface charge density, hydrophobic effects, hydrogen bonds, electrostatic and van der Waals forces, which ultimately impairs solubility and other protein functionalities (16–19). Furthermore, the secondary structure of pea proteins is higher in the rigid β-sheet (30–41%), which contributes to the low solubility when compared to animal proteins (egg white and whey) with lots of the flexible α-helical structure (17–19). Inherent properties like beany flavor and the presence of antinutritional materials in pea protein also reduce its quality and value as a food ingredient (20). As a result of this complex conformation, globular proteins require some degree of pre-treatment to isolate specific fractions with enhanced functionality.

Techniques engaged in the modulation of protein structure could be largely classified as physical (ultrasound, thermal, high pressure), chemical (glycosylation, complex formation), and enzymatic. Heat treatment is a relatively cheap and simple method employed for food processing and preservation in which all the hierarchical structures of the protein could be affected (21). Literature is replete with studies where soybean and milk protein are thermally treated using a variety of methods. The effect of ohmic heat (17, 23, 30, and 37 V/cm) on structural and functional properties of soybean protein was studied and the outcome was improved amino acid content and emulsification activity index by 14 and 38%, respectively, while foaming properties, emulsion stability index, sulfhydryl content, and surface hydrophobicity declined (22); however, the study reported no significant structural changes in the protein. Pre-heating at 90°C for 2.5 min improved solubility, surface hydrophobicity, and the gelling properties of soy protein isolate and soy-egg composite gels (23). The significant increase in solubility was attributed to the formation of soluble macro-complexes. A functional whey protein powder with high water binding capacity was produced by addition of lactose at pH 10 and dry heating at 120°C for >30 min (24). Ryan and Foegeding (25) reported the presence of soluble whey protein aggregates after pre-treatment at 90°C for 10 min at pH 7.5. A few works have also been reported in literature about thermal treatment of pea protein. The application of heat to pea proteins at slightly above the denaturation temperature (>82°C) has been suggested to improve flexibility of the molecules (26). Another study on the solubility and heat stability of pea protein isolate showed high solubility (>92%) after heat treatment at 121°C for 2.8 min because of the formation of soluble aggregates and increased heat stability (15). During denaturation, pea protein subunits dissociate, and the structure unfolds to form aggregates at elevated temperatures. Some of the aggregates formed at elevated temperatures are stabilized by disulfide linkages and hydrophobic interactions (27, 28). Previous works have focused on the effect of heat pretreatment on functional and physicochemical properties of the native protein concentrate or isolate with or without pH adjustments and without fractionation. However, there is the need to evaluate the effect of pH and protein size on the properties of heat-induced protein aggregates. Therefore, the aim of this work was to determine the structural and functional properties of >50 kDa pea protein aggregates prepared at different pH values and isolated by membrane ultrafiltration. The aggregates were compared with the native unaggregated pea protein concentrate to measure potential relevance as ingredients for the food industry.

MATERIALS AND METHODS

Materials and Chemicals

The yellow field pea protein concentrate (PPC) was purchased from Nutri-Pea Limited (Portage La Prairie, MB, Canada). Other chemical reagents used were purchased from Sigma-Aldrich (St. Louis, MO, USA) and Fisher Scientific Company (Oakville, ON, Canada). All the chemicals and reagents were of high purity analytical grade with double distilled water used for their preparation.

Preparation of Protein Aggregates

A 10% (w/v) mixture of the PPC (68.6% protein content) was prepared using distilled water and stirred for 10 min. The mixture was then adjusted to pH 3.0, 5.0, 7.0, or 9.0 using 0.1 M NaOH or 0.1 M HCl and the containers hermetically sealed to allow for maximum heat penetration in the mixture followed by immersion in a shaking water bath at $100°C$ for 30 min. After cooling rapidly in an ice bath to $\sim20°C$, the heated protein mixture was centrifuged at $7,000 \times g$ for 30 min and the supernatant saved while precipitate was discarded.

Fractionation of the Protein Aggregates

The supernatants obtained from the heated protein mixtures were each sequentially passed through Amicon®stirred ultrafiltration cell fitted with a 30 kDa molecular weight cut-off (MWCO) membrane and the permeate collected as the <30 kDa fraction. The retentate was mixed with an equal amount of distilled water and passed through a 50 kDa MWCO membrane (coupled with diafiltration) and the permeate collected as 30–50 kDa fraction while the retentate was labeled as >50 kDa fraction. The three fractions were freeze-dried and stored at $-20°C$. The PPC and freeze-dried ultrafiltration fractions were dissolved in 0.1 M NaOH, and total protein content determined using the Lowry method (29). Based on the low protein contents of the <30 and 30–50 kDa fractions, only the freeze dried >50 kDa fractions, which had a high protein content like the PPC were used to perform all the following experiments. All the analysis were carried out in triplicates and reported as mean and standard deviation.

Protein Solubility, Content, and Yield

Protein solubility of the >50 kDa aggregated proteins was determined as previously described (30). Briefly, 10 mg of the protein was suspended in 1 mL buffers (pH 3.0–9.0) followed by vortexing and centrifugation at $10,000 \times g$ for 20 min. The protein content of the supernatant was determined with bovine serum albumin as the standard (29) and expressed as percentage ratio of the total protein to obtain protein solubility values. The gross protein yield was analyzed as described by Famuwagun et al. (31).

Surface Hydrophobicity

The surface hydrophobicity of the samples was determined according to the method described by Haskrad and Li-Chan (32). The stock sample was prepared using 10 mg/mL in 10 mM phosphate buffer, pH 7.0. The mixture was vortexed, kept for 1 h and then centrifuged at $10,000 \times g$ for 10 min at $25°C$. Serial dilutions of the supernatant were prepared to obtain 0.5–2.5 mg/mL protein concentrations. Using a 96 well-microplate, 5 µL of 8 mM l-anilinonaphthalene-8-sulphonate (ANS) in 10 mM phosphate buffer (pH 7.0) was added to 200 µL of sample followed by fluorescence intensity (FI) measurement at excitation and emission wavelengths of 390 and 470 nm, respectively. The surface hydrophobicity was calculated as the slope of a plot of the FI vs. protein concentration.

Determination of Polypeptide Composition and Profile

The polypeptide composition was determined using the reducing (R) and non-reducing (NR) sodium dodecyl sulfate-polyacrylamide gel electrophoresis (SDS-PAGE) as previously described by Aderinola et al. (33). Briefly, a 2.5% (w/v) sample was prepared with the NR buffer (Tris-HCl buffer, pH 8.0 containing 10%, w/v SDS) or R buffer (Tris-HCl buffer, pH 8.0 containing 10%, w/v SDS and 10%, v/v β-mercaptoethanol). The mixtures were heated at $95°C$ for 10 min, cooled and then centrifuged at $10,000 \times g$ for 10 min. The supernatant (1 µL) was loaded onto 8–25% gradient gels and electrophoresis performed with the Phastsystem™ Separation and Development units according to the manufacturer's instructions (Cytiva, Montreal, PQ, Canada). The gels were stained with Coomassie brilliant blue.

Determination of Sulfhydryl Group (SH) and Disulfide Linkages (SS)

The SS and free SH contents were determined as described by Tang et al. (34). Protein dispersions (7.5 mg/mL each) were prepared using Tris-Gly buffer (0.086 M Tris, 0.09 M glycine, 0.004 M EDTA, pH 8.0) containing 8 M urea and stirred overnight at room temperature. To obtain the SH content, 1 mL of the stirred protein dispersion was added to 4 mL Tris-Gly buffer and 0.05 mL Ellman's reagent (5,5-dithio-bis-2-nitrobenzoic acid in Tris-Gly buffer), incubated for 20 min at $25°C$ and absorbance measured at 412 nm. To determine total SH content (free SH and reduced SS), 1 mL of the stirred protein dispersion was mixed with 4 mL Tris-Gly buffer and 0.05 mL 2-mercaptoethanol (ME) and incubated for 1 h at $25°C$. A 10 mL aliquot of 12% (w/v) trichloroacetic acid (TCA) was added to the solution and incubated for another 1 h. The mixture was centrifuged at $5,000 \times g$ for 10 min and precipitate resuspended in 5 mL of the TCA solution and centrifuged again (this was performed three times to remove the ME). The final precipitate was suspended in 10 mL of Tris-Gly buffer and 0.04 mL Ellman's reagent was added to 4 mL of the suspension, incubated for 20 min and absorbance taken at 412 nm.

Calculations were made as follows:

$$\mu molSH/g = [73.53 \times (A_{412} \times D)/C] \qquad (1)$$

Where A_{412} is the absorbance at 412 nm, C is the sample concentration (mg/mL), D is the dilution factor (5 and 10 for free SH and total SH content, respectively), and the constant 73.53 was calculated from $10^6/(1.36 \times 10^4)$, the 10^6 being conversion from molar to µM/mL and from mg solids to g solids

while 1.36×10^4 is the molar absorptivity. The SS content was calculated by subtracting the free SH content from the total SH content and dividing the result by 2.

Determination of the Surface Charge (Zeta Potential) for the Native Protein and Fractions

Electrophoretic mobility (μ_e) of homogenous solutions (0.05%, w/v) of the protein samples was measured at room temperature using PALS Zeta Potential Analyzer Ver 5.67 (Brookhaven Instruments Corp., Holtsville, NY) and the zeta potential (ζ, mV) was determined as a function of pH and protein type. The solutions were dispensed in a 1.5 mL cuvette and measurements taken at pH 3.0, 5.0, 7.0 and 9.0 after adjustments based on the prior determined particle size (50–200 nm).

$$\mu_e = \frac{v}{E} \tag{2}$$

$$\zeta = \frac{(4\pi\eta)}{\varepsilon} f(\mathcal{K}\dashv) \cdot \mu_e \tag{3}$$

Where μ_e is the migration of particles through an electric field, v is the velocity of the particles in the electrical field and E is the Electrical field. Zeta potential was calculated from Helmholtz–Smoluchowski equation where ζ is the Zeta Potential, η is the Viscosity of the medium, ε is the Dielectric constant, and $f(\mathcal{K}\dashv)$ is the Debye function. The Smoluchowki approximation f (kα) for this study was taken as 1.5.

Thermal Properties

The effect of heat treatment on the denaturation temperature and enthalpy was determined using a differential scanning calorimeter (DSC Q200, TA Instruments, New Castle, DE). Dry protein flours (95–99 mg) were weighed in pans (TA Instruments, New Castle, DE) and hermetically sealed. The thermal curve was obtained by heating the sample from 40 to 250°C at 10 C/min in a standard DSC cell. Enthalpy of denaturation (ΔH) and denaturation temperature (T_d) were obtained from the endothermic peaks in the thermograms using Universal Analysis 2000 software (Version 4.5A). The DSC had been calibrated against both sapphire and indium standards and an empty pan was used as reference.

Scanning Electron Microscope Images

The electron micrographs of dried protein powders were determined in a high-resolution Quanta™ FEG 650 Schottky field emission scanning electron microscope (Hillsboro, OR, USA). Samples were sprinkled over a double-sided carbon tape and fixed on SEM stubs.

Emulsifying Properties

The oil-in-water emulsions were prepared by mixing protein samples (10, 15, and 20 mg/mL, based on protein content) that were prepared in 0.1 M phosphate buffer at pH 3.0, 5.0, 7.0, or 9.0 with 1 mL of pure canola oil added. The mixture was homogenized at 20,000 rpm for 1 min using the 20 mm non-foaming shaft on a Polytron® PT 3100 homogenizer. Emulsifying activity (EAI) and stability (ESI) index were

determined as described by Pearce and Kinsella (35). A 50 µL aliquot of the emulsion was taken from the bottom of the tube at 0 and 10 min after homogenization and then added to 10 mL of 0.1% (w/v) SDS solution. Absorbance of the diluted emulsion was read at 500 nm and calculations done as follows:

$$EAI\ (m^2/g) = 2 \times (2.303 x A_0 x N)/(cx\phi x 10000) \tag{4}$$

$$ESI\ (min) = (A_0/\Delta A)/t \tag{5}$$

Where, A_0 is the absorbance of the fresh emulsion dilution at time zero, N is the dilution factor (200), c is the protein concentration per volume (g/ mL), ϕ is the oil volume fraction, ΔA is the change in absorbance 10 min (A_0) after homogenization (A_0-A_{10}) and t is time interval (10 min).

Foaming Properties

The foams were prepared by a method described by Aderinola et al. (33). The protein mixtures (10, 15, and 20 mg/mL) were prepared in 0.1 M phosphate buffers at pH 3.0, 5.0, 7., or 9.0 and homogenized at 20,000 rpm for 1 min using a 20 mm foaming shaft on the Polytron® PT 3100 homogenizer (Kinematica AG, Lucerne, Switzerland). The foam capacity and stability were determined as follows:

$$\text{Foam capacity (\%)} = (\text{foam volume after whipping/}$$
$$\text{initial volume before whipping}) \times 100 \tag{6}$$
$$\text{Foam stability (\%)} = (\text{foam volume after 30 min/}$$
$$\text{foam volume after whipping}) \times 100 \tag{7}$$

Water Holding and Oil Holding Capacity

WHC and OHC were determined as previously described by Ajibola et al. (30) with slight modifications. A 20 mg/mL sample was prepared by dispersing 0.2 g sample in 10 mL buffers at pH 3.0, 4.0, 5.0, 6.0, 7.0, 8.0, or 9.0 (or oil) contained in a 50 mL pre-weighed centrifuge tube. The dispersion was vortexed for 1 min, allowed to stand for 30 min and then centrifuged at $7,000 \times g$ for 25 min at 25°C. The supernatant was decanted, and excess water or oil was drained for 15 min; the gram of water or oil retained per gram of sample was calculated.

Least Gelation Concentration

LGC was determined as previously described (33). The protein samples were suspended in water or 0.5% (w/v) NaCl at different concentrations (5–25%, w/v) and the mixtures vortexed, placed in a water bath at 95°C for 1 h, cooled under running tap water and stored in the refrigerator (4°C) for 14 h. The LGC is the sample concentration at which the gel did not slip when the tube was inverted.

Statistical Analysis

Protein aggregates were produced from three separate experiments and then combined for analyses. Samples were then analyzed in triplicates and the mean values subjected to analysis of variance. Significant differences ($p < 0.05$) between mean values were determined by the Duncan's multiple range test using IBM SPSS Statistics for Windows, Version 26.0.

RESULTS AND DISCUSSION

Protein Content and Yield

Table 1 reveals that protein content was dependent on the fraction size as the lower MW fractions (<30 and 30–50 kDa) had ≤20% while the bigger >50 kDa fraction contained >60% protein. The results suggest that most of the protein aggregates were in the >50 kDa fraction, which indicates successful heat-induced polymerization of the pea proteins. The rationale for analyzing higher molecular weight (HMW) fractions for physicochemical and techno-functional properties is because higher protein content enhances most of the functional properties (36, 37). The lower protein content of the <50 kDa fractions is indicative of the abundance of low molecular weight (LMW) non-proteins substances. Membrane ultrafiltration produces protein ingredients through application of selective barrier or sieve-like materials to fractionate, purify, and concentrate (38). Since the fractionation protocol was consecutive first with 30 kDa and then 50 kDa, removal of non-protein materials (permeates) at these stages also contributed to the higher protein content of the final retentate (>50 kDa fraction). The LMW (<50 kDa) proteins probably contained albumin polypeptides, sugars, and secondary metabolites like phenolic compounds (39, 40). The HMW fractions were renamed as FT3, FT5, FT7, and FT9 (fractionated at pH 3.0, 5.0, 7.0, and 9.0, respectively), and used in the comparative study with unfractionated PPC which is a conventional ingredient in the food processing industry. FT5 contained 64.5% protein, which was slightly lower than that of PPC, FT3, FT7, and FT9. The lower protein content at pH 5.0 may be because this is the least point of solubility, hence protein unfolding necessary to enhance aggregation was less. The results are consistent with the higher amounts (gross yield) of <50 kDa fractions at pH 5 when compared to the other pH values where solubility is higher and hence the propensity to form bigger aggregates is greater. However, yield of the >50 kDa fraction was highest at pH 3.0 and 7.0, which suggest optimal conditions for protein-protein interactions. In contrast, formation of protein aggregates was less efficient at pH 9.0, which is the farthest from the isoelectric point and could be attributed to excessive levels of negative charges. The high density of negative charges at pH 9.0 would have reduced protein-protein interactions during heat treatment, and hence lower yield of the >50 kDa aggregates when compared to pH 3.0, 5.0, and 7.0.

Sulfhydryl Groups (SH) and Disulfide Linkages (SS)

During heat treatment, proteins undergo structural and conformational changes namely unfolding (denaturation), exposure of hidden reactive groups and SCAA, protein-protein interactions *via* hydrophobic interaction and the formation of new disulfide linkages through reaction between two SH side chains of two cysteine residues. Results as shown in **Table 2** reveal that the FT3 and FT9 had similar total SH contents as the PPC while FT5 was significantly lower and FT7 had the highest value. The results had direct relationship with the protein contents of the samples. Similarly, the exposed SH result showed

lowest value for FT5, which suggest that at pH 5.0 most of this group were situated away from the protein aggregate surface when compared to the aggregates formed at pH 3.0, 7.0, and 9.0. The FT5 also contained significantly ($p < 0.05$) lower number of SS, which is consistent with the smaller number of total SH groups when compared to the other protein aggregates. The presence of exposed SH has been shown to positively influence protein solubility (41, 42), which is an important functionality in promoting the use of proteins as food ingredients. Exposed SH in a protein could be an index for conformational changes such as structural unfolding or the cleaving of the SS bonds during processing. Therefore, the results suggest that the FT5 is a less unfolded protein aggregate than the FT3, FT7, and FT9. Previous works have also suggested that a shift toward alkalinity increases the total number of SS groups, due to formation of more intra and intermolecular bonds during SH/SS interchange reactions, which leads to reductions in number exposed SH (43, 44). This may explain the significant decrease in exposed SH observed in this work for FT9, which was formed at pH 9.0 when compared to pH 7.

Surface Charge and Hydrophobicity (Ho)

Surface charge and hydrophobicity of proteins influence the solubility and subsequently, other functional properties such as foaming, thickening, gelation, and emulsification properties. The surface charge on proteins is the intrinsic effect of ionizable groups (amino and carboxyl) present and the average charge is measured as the zeta potential (17). The result as shown in **Figure 1** reveals that the net surface charge of PPC and the fractions are relatively low under which conditions the electrostatic repulsive forces are low and incidence of protein to protein interactions is eminent (14). Notwithstanding, surface charge of PPC was highest at pH 3.0 and 5.0 (13 and 14 mV, respectively), and at pH 9.0, which suggests the presence of electropositive and negative charges on the surface of the native protein at acidic and alkaline pH, respectively. The surface charge of other pea protein isolates extracted by different methods was reported to be ~21 mV at pH 7.0, which is low when compared to other legumes (17). Similarly, Hayati Zeidanloo et al. (45) showed that variations exist in surface charge of pea protein prepared by different methods (between −21.73 and 24.96 mV at pH 7.0). On the contrary, another study reported that the surface charge of lab prepared field protein isolate was −44.2 mV and higher than that of kidney bean (40.0 mV) and amaranth protein isolates (37.3 mV) (46). Cui et al. (43) also reported high surface charge of four yellow pea protein cultivar at pH 3.0–8.0 ranging between −30 and 30 mV. The study suggested a direct relationship between the surface charge of the proteins and solubility, which was not the case with the present study. Apart from FT9, which had relatively high surface charge at pH 9.0 (−19.4 mV), the aggregates had low surface charge at both low and high pH (~-2 to −4 mV). Although not statistically significant ($p > 0.05$), FT3 and FT7 had a slightly higher charge than FT5 at high pH values. Bogahawaththa et al. (15) showed that heat treatment of pea protein at 121°C (pH 6.8–7.5) improved the surface charge by at least 5% but a decrease of at least 14% occurred after ultra-heat treatment (140°C). The referenced study also

TABLE 1 | Protein content and yield of >50 kDa pea protein aggregates isolated by membrane ultrafiltration after heat treatment (100°C) at different pH values.

Samples[*]	Treatment pH	Molecular weight (kDa)	[†] Protein content (%)	[†] Protein yield (%)
PPC (control)			68.6 ± 0.05^b	
PPT1	3.0	<30	2.24 ± 0.96^h	1.14 ± 0.05^e
PPT2		30–50	6.24 ± 0.36^g	1.30 ± 0.05^e
PPT3 (FT3)		>50	68.4 ± 0.02^b	35.2 ± 4.53^a
PPT4	5.0	<30	14.1 ± 0.41^e	1.85 ± 0.05^e
PPT5		30–50	16.3 ± 0.24^e	2.80 ± 0.04^e
PPT6 (FT5)		>50	64.5 ± 0.04^c	22.7 ± 1.06^c
PPT7	7.0	<30	11.4 ± 1.09^f	0.55 ± 0.04^f
PPT8		30–50	10.8 ± 1.10^f	0.25 ± 0.02^f
PPT9 (FT7)		>50	73.8 ± 1.10^a	27.9 ± 3.53^b
PPT10	9.0	<30	10.4 ± 0.81^f	0.66 ± 0.01^f
PPT11		30–50	20.4 ± 0.50^d	1.39 ± 0.33^e
PPT12 (FT9)		>50	71.2 ± 0.17^a	15.0 ± 0.44^d

[a−h] For each column, different letters indicate significant differences ($p \leq 05$).

[*] Untreated pea protein concentrate (PPC) and ultrafiltration fractions (FT1–FT12).

[†] Mean of triplicate determinations ± standard deviation.

TABLE 2 | Sulfhydryl groups and surface hydrophobicity (H_o) of pea protein aggregates isolated by membrane ultrafiltration after heat treatment (100°C) at different pH values.

Samples[*]	[†] Sulfhydryl groups (μmol/g)			[†] H_o
	Total sulfhydryl	Exposed sulfhydryl	Disulfide bonds	
PPC	68.81 ± 0.30^b	18.28 ± 0.00^b	25.26 ± 0.13^{ab}	11.22 ± 0.24^c
FT3	69.27 ± 0.30^b	20.16 ± 0.22^{ab}	24.55 ± 0.17^b	4.97 ± 0.32^e
FT5	44.50 ± 0.20^c	8.40 ± 0.15^c	18.05 ± 0.04^c	8.73 ± 0.15^{cd}
FT7	75.23 ± 0.06^a	22.61 ± 0.08^a	26.51 ± 0.04^a	58.9 ± 0.44^b
FT9	69.33 ± 0.25^b	19.36 ± 0.01^b	25.00 ± 0.12^{ab}	278.7 ± 0.10^a

[a−d] For each column, different letters indicate significant differences ($p \leq 05$).

[*] Untreated pea protein concentrate (PPC) and the >50 kDa protein aggregates formed at pH 3.0 (FT3), 5.0 (FT5), 7.0 (FT7), and 9.0 (FT9).

[†] Mean of triplicate determinations ± standard deviation.

showed that the surface charge of supernatants derived from most of the heated protein solutions was lower than the those measured from the bulk samples by at least 8%. In this study, supernatants from protein solutions were analyzed for surface charge and may explain the reason for the observed low values because the isolated proteins consisted mainly of aggregates. Factors that could impact the surface charge of proteins includes amino acid composition, protein conformation, environment (ionic strength, pH, and temperature of solvent) and protein concentration (17, 39). **Table 2** also shows that FT7 and FT9 had significantly ($p < 0.05$) higher H_o values than PPC, FT3, and FT5, which suggest a more open protein conformation at pH above the isoelectric point. The results indicate that at pH 7.0 and 9.0, the increased net charge on proteins may have reduced protein-protein interactions accompanied by dissociation of the aggregates to expose hydrophobic patches (47). The FT3 and FT5 had similar H_o as the PPC, which indicates that at pH 3.0 and 5.0, the protein aggregates had conformations with most of the hydrophobic groups shifted into the core and away from the hydrophilic environment (48). Hydrophobicity means "water

fearing," which implies that the higher the surface hydrophobicity of a protein, the lower the solubility and vice versa. However, contrary views suggesting a positive relationship between surface hydrophobicity and solubility have been reported (49).

Polypeptide Composition and Profile

Polypeptide composition of the aggregates and native pea protein was determined using reducing and non-reducing gel electrophoresis, which separation is based on molecular weight. **Figure 2** shows that polypeptide sizes ranged from ~8.0–200 kDa for both gels while bigger protein aggregates ($\geq$200 kDa) were immobilized at the point of sample application (PSA) and did not enter the gel, especially under non-reducing condition. The reduction in intensity of the >200 kDa band (PSA) under reducing condition is an indication that some of the protein aggregates that did not enter the gel under non-reducing electrophoresis were held together by disulfide bonds. The profile revealed a wide variety of polypeptides attributed to be constituents of vicilin (7S) and legumins (11S). Under reducing condition,

the PPC produced 11 bands, which indicates dissociation of 11S fraction in the presence of a reducing agent as previously reported (50–52). The polypeptide profiles of the isolated aggregates were like that of PPC, which confirms heat-induced interactions of the native proteins led to polymer formation.

Scanning Electron Microscope Images

SEM provides information about the surface topography, morphology and composition by the detecting electrons scattered on the surface of the protein (53). PPC contains large amounts of 11S and 7S proteins, which are represented in different sizes (54). The microstructure of the native pea protein and that of the isolated protein aggregates are shown in **Figures 3A–E**. The images revealed that heat treatment at different pH values produced proteins with varying morphologies. PPC showed a mixture of distinct spherical and wrinkled shapes, which is characteristic of high levels of folded native proteins. FT3, FT7, and FT9 were amorphous floating mass that showed greater aggregation and network formation completely different from the native protein form. FT3 (**Figure 3B**) and FT9 (**Figure 3E**) showed more signs of network formation than FT5 (**Figure 3C**) and FT7 (**Figure 3D**). FT5 showed distinct aggregate forms with reduced level of continuous network formation but was still morphologically different from PPC.

Thermal Properties

Thermal properties reflect protein transition from one state to another (i.e., native to denatured state) under heat application and is an index for temperature-induced protein unfolding and thermal stability (51). As shown in **Table 3**, the T_o and T_d

FIGURE 1 | Surface charge of the native protein (PPC) and isolated fractions at pH 3.0, 5.0, 7.0, and 9.0. measured as the zeta potential (mV). PPC was heated at 100°C and varying pH, centrifuged, and the supernatant passed consecutively through 30 and 50 kDa membranes. The final retentate from the 50 kDa membrane was collected as FT3, FT5, FT7, and FT9 for heat treatments at pH 3.0, 5.0, 7.0, and 9.0, respectively.

FIGURE 2 | SDS-PAGE under reducing **(A)** and non-reducing **(B)** conditions. PSA, point of sample application. Lanes: 1, standard proteins; 2, pea protein concentrate (PPC); 3, FT3; 4, FT5; 5, FT7; 6, FT9. PPC was heated at 100°C and varying pH, centrifuged and the supernatant passed consecutively through 30 and 50 kDa membranes. The final retentate from the 50 kDa membrane was collected as FT3, FT5, FT7, and FT9 for heat treatments at pH 3.0, 5.0, 7.0, and 9.0, respectively.

FIGURE 3 | Scanning electromicrographs of: **(A)** pea protein concentrate (PPC), **(B)** FT3, **(C)** FT5, **(D)** FT7, and **(E)** FT9 at 1,000× magnification. PPC was heated at 100°C and varying pH, centrifuged, and the supernatant passed consecutively through 30 and 50 kDa membranes. The final retentate from the 50 kDa membrane was collected as FT3, FT5, FT7, and FT9 for heat treatments at pH 3.0, 5.0, 7.0, and 9.0, respectively.

reported for PPC correspond with values reported by Oliete et al. (52) for native pea globulins at 65.11 and 76.66°C respectively. However, some previous works have reported T_o and T_d values of ∼70 and 80°C, respectively for laboratory prepared native pea proteins (55, 56). Reducing heating rate from 10 to 5°C/ min was reported to decrease T_o and T_d by 4°C but ΔH_d was not affected (51). The T_o explains structural unfolding of the polypeptides and protein, T_d indicates the heat stability of the proteins and ΔH_d represents the enthalpy changes that occur during the denaturation process and reflects the extent of ordered structure of a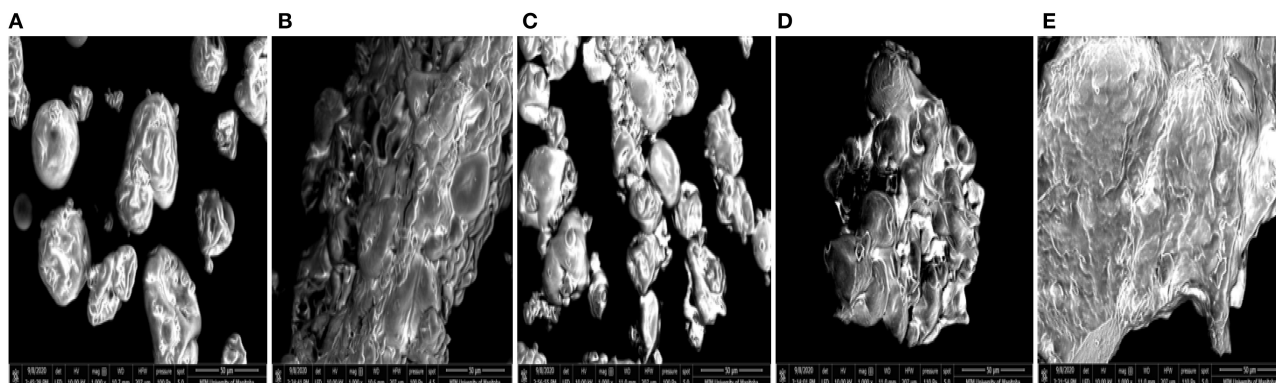 protein (51). This means PPC had less ordered protein structure prior to the thermal treatment, which could also suggest the presence of partially denatured protein in the untreated PPC. In contrast, the isolated protein aggregates all had significantly ($p < 0.05$) higher thermal properties that increased as the environment during thermal treatment was changed from pH 3.0 to pH 9.0. This means the heat and pH treatments produced polypeptides with more compact tertiary structure and stronger protein-protein interactions than the PPC (44). The exothermic reaction also means weakening and disruption of hydrophobic bonds (57). Therefore, the higher ΔH_d values obtained for the aggregated proteins also confirm the presence of a more extensive network of hydrophobic interactions when compared to the untreated PPC. The low ΔH_d values indicate that the protein aggregates were held together mainly by the non-covalent hydrophobic bonds (57). The increases in T_o and T_d values from pH 3.0 (FT3) to pH 9.0 (FT9) are consistent with changes in surface hydrophobicity (**Table 2**), which further supports the role of hydrophobic interactions as the main interactive forces responsible for formation of the protein aggregates.

Protein Solubility

Protein solubility is a measure of equilibrium between protein-protein and protein-solvent interactions and is a pivotal property with respect to protein utilization in food processing, which depends largely on hydration properties of the ingredients. These properties are influenced by the composition, sequence, conformation, and surface charge of the protein moiety. Protein

TABLE 3 | Thermal properties of pea protein aggregates isolated by membrane ultrafiltration after heat treatment (100°C) at different pH values.

Samples*	Onset temperature $(T_o)°C^\dagger$	Maximum temperature $(T_d)°C^\dagger$	ΔH (J/g of sample)†
PPC	66.50 ± 0.20[d]	74.45 ± 1.50[e]	0.06 ± 0.01[c]
FT3	89.15 ± 0.04[c]	124.30 ± 0.5[d]	1.43 ± 0.04[b]
FT5	160.12 ± 6.20[b]	190.66 ± 1.56[b]	2.47 ± 0.33[a]
FT7	176.56 ± 3.30[a]	206.33 ± 0.17[a]	1.87 ± 0.15[a]
FT9	171.36 ± 0.5[a]	203.17 ± 0.38[a]	1.58 ± 0.61[a]

$^{a-e}$For each column, different letters indicate significant differences ($p \leq 05$).

*Untreated pea protein concentrate (PPC) and the >50 kDa protein aggregates formed at pH 3.0 (FT3), 5.0 (FT5), 7.0 (FT7), and 9.0 (FT9).

† Mean of triplicate determinations ± standard deviation.

functionality especially emulsification, gelation and foaming largely depends on solubility (58). The results in **Figure 4** revealed that FT3 had a superior solubility of ∼60% in comparison with PPC (∼30%) at both acidic and alkaline environments. PPC and the other fractions exhibited improved solubility toward alkaline pH, which agrees with reports on native and heat-treated legumes (58). Apart from FT5 which had the lowest solubility, all the other fractions had better solubility than PPC. The reason for the low solubility of the FT5 could be attributed to isolation close to the isoelectric point of the protein, which would have produced compact and less flexible protein aggregates as evident in **Figure 3C**. In contrast, the FT3, FT7, and FT9 had superior solubility due to the presence of repulsive electrostatic interactions within the environment during heat-induced aggregation, hence more flexible and less compact protein structures (**Figures 3B,D,E**). Increased solubility occurs with the presence of net positive and negative charges, which introduces electrostatic repulsive forces between the protein molecules and attraction between the protein and water molecules. However, only FT3 displayed the

FIGURE 4 | pH solubility profile of pea protein concentrate (PPC) and >50 kDa pea protein aggregates. PPC was heated at 100°C and varying pH, centrifuged and the supernatant passed consecutively through 30 and 50 kDa membranes. The final retentate from the 50 kDa membrane was collected as FT3, FT5, FT7, and FT9 for heat treatments at pH 3.0, 5.0, 7.0, and 9.0, respectively.
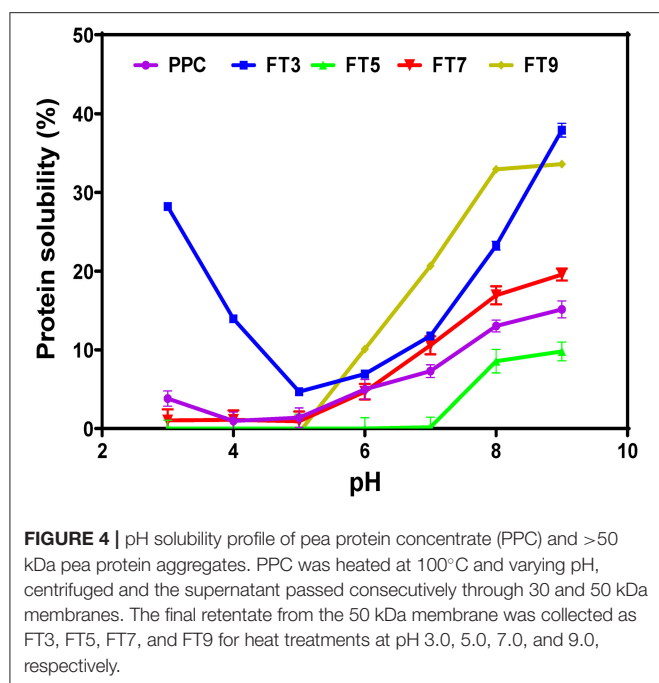
U-shape solubility profile that is typical of most plant proteins. Although heating and aggregation impair solubility and other protein functionalities, heat treatment for longer periods has been shown to produce aggregates with improved solubility (15).

Emulsifying Activity and Stability Index

Emulsifying activity index (EAI, m²/g) is the area of oil/water interface that can be emulsified per unit weight of protein and is dependent on the adsorption of proteins onto the interfacial layer (17). The EAI profile (**Figure 5**) looked very similar to the protein solubility profile showing pH dependency with the lowest activity observed at pH 5.0 (58). The higher EAI at pH 9.0 is consistent with a previous report by Chang et al. (48). The results confirm the important role of increased protein-water interactions (solubility) in enhancing emulsification of oil droplets (19). Similarly, EAI was dependent on the sample type and protein concentration ($p < 0.05$). FT3 had slightly better EAI than all the fractions and the control by ∼6%, which indicates greater unfolding and dissociation during emulsification that led to increased surface activity and enhanced adsorption at the oil-water interface. The low EAI of FT5 could be attributed to a combination of the compact structure as revealed by SEM (**Figure 3C**) and low solubility, which reduced ability to form interfacial membranes around the oil droplets.
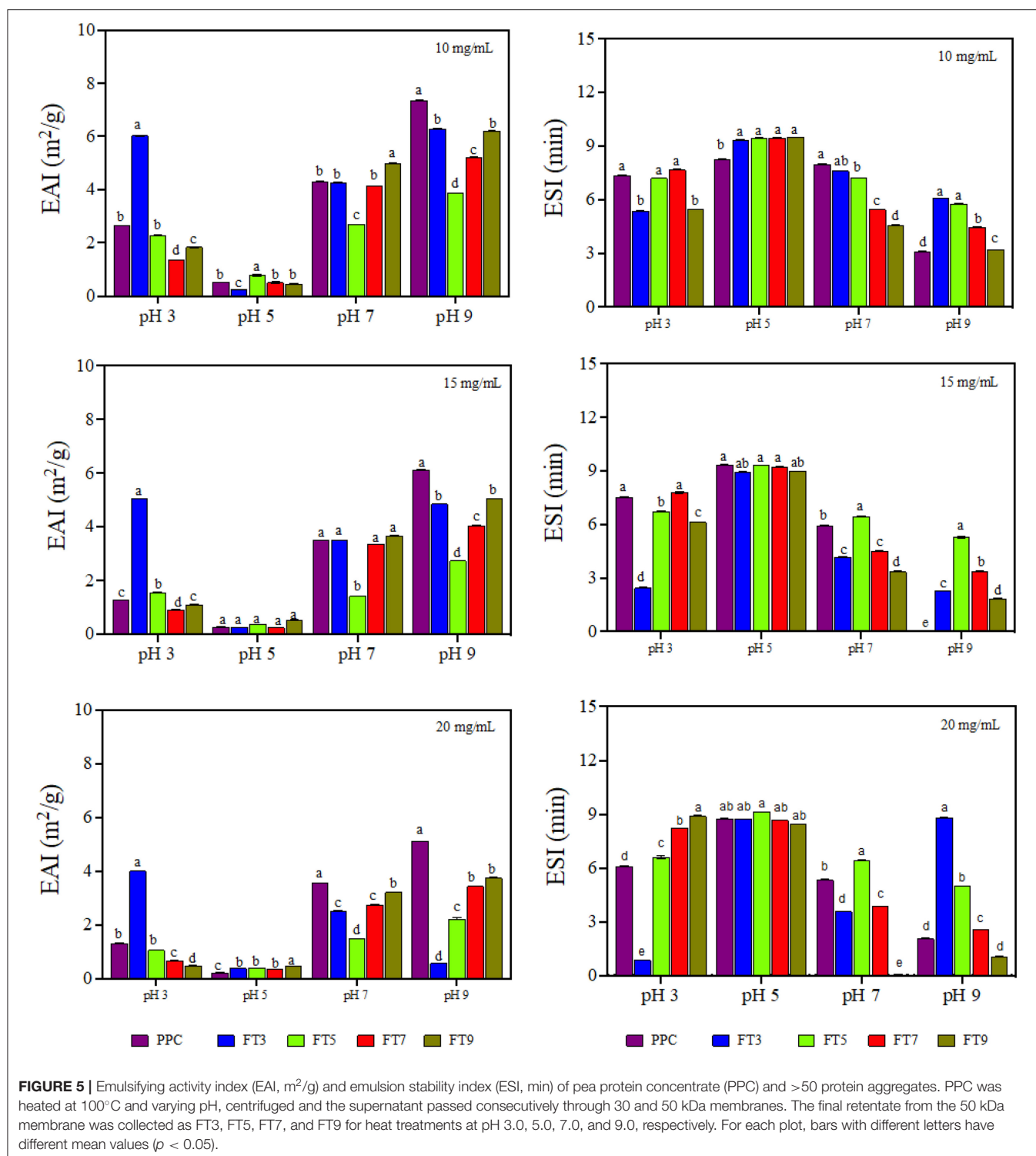
The current study revealed that the relationship between emulsifying activity of a protein and the physicochemical properties is complex and dependent on many other factors as previously suggested (48). EAI declined with increasing protein concentration (10 > 15 > 20 mg/mL), which indicates molecular crowding and increased viscosity of the continuous phase to prevent adequate formation of the interfacial membrane. Emulsifier concentration influences emulsification activity

because of the amount of protein that covers the interfacial layer and protein concentration could reach a saturation point at higher levels (59). Chen et al. (60) reported increase in the emulsification properties of thermally treated pea protein when the concentration in the emulsion increased to 10 mg/mL but above this concentration, the interfacial saturation point of the protein was reached. However, Aziz et al. (61) reported that increasing corn protein concentration (0.1–2%, w/v) improved the EAI, which suggests that the type of protein is also important.

Emulsion stability index (ESI) is the measure of the ability of the formed emulsion to resist changes to the structure over time (62). ESI is an indicator of the shelf life and stability of the food product against external stressors of the environment, freeze thaw and transportation but with dependence on the characteristics of the interfacial layer (17). The ESI result revealed pH dependency but was not influenced by protein concentration nor sample type (**Figure 5**). The emulsions prepared at pH 5.0 were more stable by ∼30% and the least stability was obtained at pH 9.0, which reflects the role of protein charge. This is because the proteins have least charge at pH 5.0, which would have reduced protein-protein repulsion and lead to formation of stronger interfacial membranes. In contrast, the high charge density at pH 9.0 led to strong protein-protein repulsions, hence weak interfacial membranes were formed.

Foam Properties

Foams are made of air bubbles dispersed in a continuous phase which could be a liquid (e.g., whipped cream) or a solid (e.g., marshmallows). Food proteins are very popular foaming agents in the food industry because of their ability to adsorb at the air-water interface of the foam followed by rapid reduction of the interfacial tension and formation of cohesive film around the dispersed air bubbles (63). Foam properties are measured using the foam capacity (foamability) and foam stability. Foamability is the foam volume after introduction of a gas and reflects the level of air in the dispersed phase while foam stability is the rate at which the foam volume decreases over time mostly due to effect from external stressors and gravity (64). As shown in **Figure 6**, FT3 had significantly ($p < 0.05$) higher foaming capacity by ∼10% in comparison to PPC while FT5 had a decline in activity by 31%. Foaming capacity of FT7 and FT9 was not significantly different from PPC but in general the values increased at a higher protein concentration (20 mg/mL) and at pH 3.0. Chao and Aluko (65) had earlier reported improved foam capacity at high concentrations of heat pretreated pea protein due to increased availability of polypeptide chains. However, the study also showed that foam capacity reduced when the pea protein was treated at 90–100 °C. Furthermore, findings from Chao and Aluko (65) also suggest pH-dependent foam capacity and treatments at pH 7.0 had better capacity than pH 3.0 and 5.0 resulting from increased flexibility and net charge. Statistically, there were significant differences ($p < 0.05$) in the foam capacity at 10, 15, and 20 mg/mL protein concentrations, with values influenced by sample type, pH, and protein concentrations. This finding is consistent with literature as the ability of protein to foam depends on the nature of the protein such as the surface properties (surface hydrophobicity and charges)

FIGURE 5 | Emulsifying activity index (EAI, m²/g) and emulsion stability index (ESI, min) of pea protein concentrate (PPC) and >50 protein aggregates. PPC was heated at 100°C and varying pH, centrifuged and the supernatant passed consecutively through 30 and 50 kDa membranes. The final retentate from the 50 kDa membrane was collected as FT3, FT5, FT7, and FT9 for heat treatments at pH 3.0, 5.0, 7.0, and 9.0, respectively. For each plot, bars with different letters have different mean values ($p < 0.05$).

and the processing conditions such as pH, temperature, ionic strength, and shear force (66). Foamability of the protein aggregates had a strong relationship with solubility, which corresponds to reports by Shevkani et al. (67) that cowpeas protein with higher solubility was associated with superior foaming capacity.

From **Figure 6**, foam stability was observed to be dependent on the protein concentration, sample type and pH ($p < 0.05$) with the best stability obtained at pH 3.0 and 20 mg/mL. FT3 and FT7 had ∼7% foam stability increases in comparison with PPC but there was no significant difference between FT5, FT9, and PPC. The reason could be that the greater presence of

FIGURE 6 | (A) Foaming capacity and **(B)** foam stability of pea protein concentrate (PPC) and >50 protein aggregates. PPC was heated at 100°C and varying pH, centrifuged and the supernatant passed consecutively through 30 and 50 kDa membranes. The final retentate from the 50 kDa membrane was collected as FT3, FT5, FT7, and FT9 for heat treatments at pH 3.0, 5.0, 7.0, and 9.0, respectively. For each plot, bars with different letters have different mean values ($p < 0.05$).

surface charge (electrostatic repulsive forces) at pH 3.0 and 7.0 facilitated increased repulsions between the encapsulated air bubbles, hence better foam stability when compared to pH 5.0 (17). A previous work has also shown that foam stability improved toward alkalinity in native and heat-treated legumes with better stability at pH 7.0 (58).

Water and Oil Holding Capacity (WHC and OHC)

WHC is the amount of water that 1 g of the protein can hold to prevent expulsion from within the matrix (14). OHC shows how much oil is entrapped within the protein matrix and influences flavor retainment and mouth feel of the food

product (14). Factors that influence WHC and OHC are the surface properties of the protein (hydrophobic interactions, surface charges, covalent, and non–covalent bonds), protein structure (molecular weight, pores, and capillary sizes) and the surrounding environment (pH, ionic strength, and temperature) (30). As shown in **Figure 7**, except for FT5, the isolated protein aggregates had ∼16% improvement in WHC than the PPC at acidic pH and ∼50% at neutral and alkaline pH. The protein aggregates had similar WHC values at pH 7.0, 8.0, and 9.0 but were distinct from the PPC. Similarly, FT3, FT7, and FT9 had significantly higher ($p < 0.05$) OHC (∼100%) in comparison with PPC and FT5 (**Table 4**). The OHC of the samples and control declined in the order FT9 > FT3 > FT7 > FT5 > PPC.
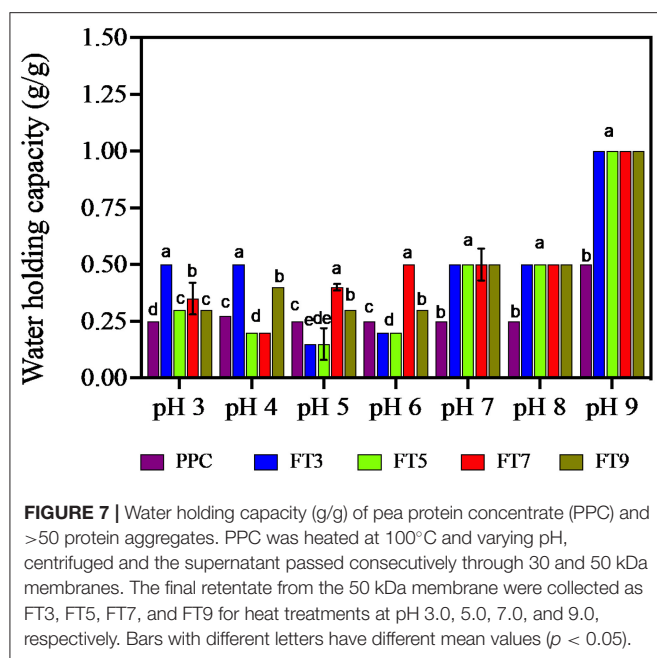
FIGURE 7 | Water holding capacity (g/g) of pea protein concentrate (PPC) and >50 protein aggregates. PPC was heated at 100°C and varying pH, centrifuged and the supernatant passed consecutively through 30 and 50 kDa membranes. The final retentate from the 50 kDa membrane were collected as FT3, FT5, FT7, and FT9 for heat treatments at pH 3.0, 5.0, 7.0, and 9.0, respectively. Bars with different letters have different mean values (*p* < 0.05).

WHC indicates that the protein aggregates may be useful in products where good interactions with water is required, such as in soups and gravies while their OHC values point to usefulness in baked goods.

Least Gelation Concentration (LGC)

Food gels are three-dimensional structures, which are held together by non-covalent interactions (van Der Waals forces, hydrophobic interactions, hydrogen bond, electrostatic forces) and the covalent sulfhydryl/disulfide linkages. The indices for a superior gel quality are hardness, paste viscosity and minimum gelation concentrations (68). Proteins with superior LGC require less concentration to form high quality gels. Gelation kinetics of soybean protein aggregates was shown to be faster and the gel structures more homogenous although the gel strength was not different when compared to the native protein (69). However, in this study, heat treatment impaired LGC as the PPC performed better with a lower LGC value than the aggregated proteins (**Table 4**). The results suggest that when compared to the untreated PPC, increased polymer size caused by heat treatment led to poor unfolding ability of the protein aggregates, which is required for protein network formation. However, addition of 0.5% (w/v) NaCl led to improved LGC, but this effect was more pronounced for the isolated protein aggregates than the untreated PPC. For example, while LGC improved by only 2% for the PPC, the presence of NaCl led to up to 7% reduction in amount of aggregated proteins needed to form a gel. As expected, the highly compact structure of the FT5 may have reduced the effect of NaCl addition as only a 2% reduction was achieved when compared to 6–7% for other protein aggregates. The positive effect of NaCl confirms that the protein aggregates are held together mostly by non-covalent interactions, which were readily interrupted to produce protein units with a more flexible structural conformation, thus favoring stronger network

TABLE 4 | Oil holding capacity (g/g) and least gelation concentration (LGC) of pea protein aggregates isolated by membrane ultrafiltration after heat treatment (100°C) at different pH values.

Samples*	*Oil holding capacity (g/g)	**LGC without NaCl (%)	**LGC with 0.5% NaCl (%)
PPC	0.23 ± 0.00^c	18	16
FT3	0.64 ± 0.04^b	25	18
FT5	0.34 ± 0.00^d	22	20
FT7	0.62 ± 0.01^b	22	16
FT9	0.87 ± 0.02^a	25	18

*Mean ± standard deviations of triplicate determinations. **Mean of triplicate determinations. Letters a-e represents statistical significance at $p \leq 05$. For each column, different letters indicate significant differences ($p \leq 05$). Untreated pea protein concentrate (PPC) and the >50 kDa protein aggregates formed at pH 3.0 (FT3), 5.0 (FT5), 7.0 (FT7), and 9.0 (FT9).

formation. The monovalent NaCl ions could have also influenced gelation through screening of repulsive forces on the protein surface, which enhanced protein-protein interactions (69).

CONCLUSION

Findings from this study gave valuable information about the structural and functional changes that occurred when pea protein was modified under heat treatment at varying pH conditions. As revealed by SEM, the effect of pH during heat treatment was pronounced because FT3, FT7, and FT9 showed a more flexible protein aggregate arrangement and network formation, and for FT9 at pH 9, higher surface charge, which translated to better functional properties when compared to FT5. The protein aggregates were held together by non-covalent interactions, therefore addition of NaCl was able to increase efficiency of gel formation. Overall, heat treatment at pH 3.0 produced >50 kDa aggregates with better solubility at acidic pH as well as superior emulsifying and foaming properties than similar protein aggregates produced at pH 5.0, 7.0, and 9.0. The outcome of this research may benefit the food industry in the production of novel pea protein ingredients for use in baked goods, beverages, soups, salad dressings and foam products like ice cream, meringue, and marshmallows. A noted drawback and limitation of the study is that the distinct morphology of individual aggregates could not be observed by the SEM. Heat induced aggregation of globular proteins leads to the formation of primary and secondary aggregates with different morphologies and each structure presents a unique functionality in food applications. Therefore, future studies are suggested to characterize the structure-function relationship of the different aggregates. Also, comparative studies with heat-induced aggregates formed from other standard proteins like dairy and soybean are required using the same processing conditions.

DATA AVAILABILITY STATEMENT

The original contributions presented in the study are included in the article/supplementary material, further inquiries can be directed to the corresponding author/s.

AUTHOR CONTRIBUTIONS

RA: conceptualization, funding, supervision, and review and editing. NA: analysis, investigation, and original draft. Both authors contributed to the article and approved the submitted version.

FUNDING

REFERENCES

1. Aryee ANA, Agyei D, Udenigwe CC. Impact of selected process parameters on solubility and heat stability of pea protein isolate. In: Yada R, editor. *Proteins in Food Processing*. Amsterdam: Elsevier Science & Technology (2018). p. 27–46. doi: 10.1016/B978-0-08-100722-8.00003-6

2. Sim SYJ, Srv A, Chiang JH, Henry CJ. Plant proteins for future foods: a roadmap. *Foods.* (2021) 10:1967. doi: 10.3390/foods10081967

3. Fasolin LH, Pereira RN, Pinheiro AC, Martins JT, Andrade CCP, Ramos OL, et al. Emergent food proteins – towards sustainability, health, and innovation. *Food Res Int.* (2019) 125:108586. doi: 10.1016/j.foodres.2019.108586

4. Taufik D, Verain MCD, Bouwman EP, Reinders MJ. Determinants of real-life behavioural interventions to stimulate more plant-based and less animal-based diets: a systematic review. *Trends Food Sci Technol.* (2019) 93:281–303. doi: 10.1016/j.tifs.2019.09.019

5. Onwezen MC, Bouwman EP, Reinders MJ, Dagevos H. A systematic review on consumer acceptance of alternative proteins: pulses, algae, insects, plant-based meat alternatives, and cultured meat. *Appetite.* (2021) 159:105058. doi: 10.1016/j.appet.2020.105058

6. Bessada SMF, Barreira JCM, Oliveira MBPP. Pulses and food security: dietary protein, digestibility, bioactive and functional properties. *Trends Food Sci Technol.* (2019) 93:53–68. doi: 10.1016/j.tifs.2019.08.022

7. Sharif HR, Williams PA, Sharif MK, Abbas S, Majeed H, Masamba KG, et al. Current progress in the utilization of native and modified legume proteins as emulsifiers and encapsulants – a review. *Food Hydrocoll.* (2018) 76:2–16. doi: 10.1016/j.foodhyd.2017.01.002

8. Jiang J, Zhu B, Liu Y, Xiong YL. Interfacial structural role of pH-shifting processed pea protein in the oxidative stability of oil/water emulsions. *J Agric Food Chem.* (2014) 62:1683–91. doi: 10.1021/jf405190h

9. Adebiyi AP, Aluko RE. Functional properties of protein fractions obtained from commercial yellow field pea *(Pisum sativum L.)* seed protein isolate. *Food Chem.* (2011) 128:902–8. doi: 10.1016/j.foodchem.2011.03.116

10. Dziuba J, Szerszunowicz I, Nałecz D, Dziuba M. Proteomic analysis of albumin and globulin fractions of pea *(Pisum sativum L.)* seeds. *Acta Sci Pol Technol Aliment.* (2014) 13:181–90. doi: 10.17306/J.AFS.2014.2.7

11. Djoullah A, Djemaoune Y, Husson F, Saurel R. Native-state pea albumin and globulin behavior upon transglutaminase treatment. *Proc Biochem.* (2015) 50:1284–92. doi: 10.1016/j.procbio.2015.04.021

12. Boeckmann B, Bairoch A, Apweiler R, Blatter M-C, Estreicher A, Gasteiger E, et al. The SWISS-PROT protein knowledgebase and its supplement TrEMBL in 2003. *Nucleic Acids Res.* (2003) 31:365–70. doi: 10.1093/nar/gkg095

13. Rubio LA, Alicia P, Ruiz R, Angeles M, Clemente A. Characterization of pea (*Pisum sativum*) seed. *J Sci Food Agric.* (2013) 94:280–7. doi: 10.1002/jsfa.6250

14. Stone AK, Karalash A, Tyler RT, Warkentin TD, Nickerson MT. Functional attributes of pea protein isolates prepared using different extraction methods and cultivars. *Food Res Int.* (2015) 76:31–8. doi: 10.1016/j.foodres.2014.11.017

15. Bogahawaththa D, Bao Chau NH, Trivedi J, Dissanayake M, Vasiljevic T. Impact of selected process parameters on solubility and heat stability of pea protein isolate. *LWT Food Sci Technol.* (2019) 102:246–53. doi: 10.1016/j.lwt.2018.12.034

16. Saldanha do Carmo C, Nunes AN, Silva I, Maia C, Poejo J, Ferreira-Dias S, et al. Formulation of pea protein for increased satiety and improved foaming properties. *RSC Adv.* (2016) 6:6048–57. doi: 10.1039/C5RA22452G

17. Shevkani K, Singh N, Kaur A, Chand J. Structural and functional characterization of kidney bean and field pea protein isolates: a comparative study. *Food Hydrocoll.* (2015) 43:679–89. doi: 10.1016/j.foodhyd.2014.07.024

18. Subirade M, Jacques G, Pezolet M. Conformational changes upon dissociation of a globular protein from pea: a Fourier

transform infrared spectroscopy study. *Biochim Biophys Acta.* (1994) 1205:239–47. doi: 10.1016/0167-4838(94)90239-9

19. Karaca AC, Low N, Nickerson M. Emulsifying properties of canola and flaxseed protein isolates produced by isoelectric precipitation and salt extraction. *Food Res Int.* (2011) 44:2991–8. doi: 10.1016/j.foodres.2011.07.009

20. Zha F, Dong S, Rao J, Chen B. The structural modification of pea protein concentrate with gum Arabic by controlled Maillard reaction enhances its functional properties and flavor attributes. *Food Hydrocoll.* (2019) 92:30–40. doi: 10.1016/j.foodhyd.2019.01.046

21. Peng W, Kong X, Chen Y, Zhang C, Yang Y, Hua Y. Effects of heat treatment on the emulsifying properties of pea proteins. *Food Hydrocoll.* (2016) 52:301–10. doi: 10.1016/j.foodhyd.2015.06.025

22. Li X, Ye C, Tian Y, Pan S, Wang L. Effect of ohmic heating on fundamental properties of protein in soybean milk. *J Food Process Eng.* (2018) 41:e12660. doi: 10.1111/jfpe.12660

23. Zhang M, Yang Y, Acevedo NC. Effects of pre-heating soybean protein isolate and transglutaminase treatments on the properties of egg-soybean protein isolate composite gels. *Food Chem.* (2020) 318:126421. doi: 10.1016/j.foodchem.2020.126421

24. Famelart M-H, Croguennec T, Sevrin T. Optimisation of microparticle formation by dry heating of whey proteins. *J Food Eng.* (2021) 291:110221. doi: 10.1016/j.jfoodeng.2020.110221

25. Ryan KN, Foegeding EA. Formation of soluble whey protein aggregates and their stability in beverages. *Food Hydrocoll.* (2015) 43:265–274. doi: 10.1016/j.foodhyd.2014.05.025

26. Wang N, Maximiuk L, Toews R. Pea starch noodles: effect of processing variables on characteristics and optimisation of twin-screw extrusion process. *Food Chem.* (2012) 133:742–53. doi: 10.1016/j.foodchem.2012.01.087

27. Lam ACY, Can Karaca A, Tyler RT, Nickerson MT. Pea protein isolates: structure, extraction, and functionality. *Food Rev Int.* (2018) 34:126–47. doi: 10.1080/87559129.2016.1242134

28. Mession J-L, Chihi ML, Sok N, Saurel R. Effect of globular pea proteins fractionation on their heat-induced aggregation and acid cold-set gelation. *Food Hydrocoll.* (2015) 46:233–43. doi: 10.1016/j.foodhyd.2014.11.025

29. Markwell MAK, Haas SM, Bieber LL, Tolbert NE. A modification of the lowry procedure to simplify protein determination in membrane and lipoprotein samples. *Anal Biochem.* (1978) 87:206–10. doi: 10.1016/0003-2697(78)90586-9

30. Ajibola CF, Malomo SA, Fagbemi TN, Aluko RE. Polypeptide composition and functional properties of African yam bean seed *(Sphenostylis stenocarpa)* albumin, globulin, and protein concentrate. *Food Hydrocoll.* (2016) 56:189–200. doi: 10.1016/j.foodhyd.2015.12.013

31. Famuwagun AA, Alashi AM, Gbadamosi SO, Taiwo KA, Oyedele DJ, Adebooye OC, et al. Comparative study of the structural and functional properties of protein isolates prepared from edible vegetable leaves. *Int J Food Propert.* (2020) 23:955–70. doi: 10.1080/10942912.2020.1772285

32. Haskard CA, Li-Chan ECY. Hydrophobicity of bovine serum albumin and ovalbumin determined using uncharged (PRODAN) and anionic (ANS-) fluorescent probes. *J Agric Food Chem.* (1998) 46:2671–7. doi: 10.1021/jf970876y

33. Aderinola TA, Alashi AM, Nwachukwu ID, Fagbemi TN, Enujiugha VN, Aluko RE. In vitro digestibility, structural and functional properties of *Moringa oleifera* seed proteins. *Food Hydrocoll.* (2020) 101:105574. doi: 10.1016/j.foodhyd.2019.105574

34. Tang C, Sun X, Yin S. Physicochemical, functional, and structural properties of vicilin-rich protein isolates from three phaseolus legumes: effect of heat treatment. *Food Hydrocoll.* (2009) 23:1771–8. doi: 10.1016/j.foodhyd.2009.03.008

35. Pearce KN, Kinsella JE. Emulsifying properties of proteins: evaluation of a turbidimetric technique. *J Agric Food Chem.* (1978) 26:716–23. doi: 10.1021/jf60217a041

36. Pedrosa MM, Varela A, Domínguez-Timón F, Tovar CA, Moreno HM, Borderías AJ, et al. Comparison of bioactive compounds content and techno-functional properties of pea and bean flours and their protein isolates. *Plant Foods Hum Nutr.* (2020) 75:642–50. doi: 10.1007/s11130-020-00866-4

37. Wang L, Liu H, Liu L, Wang Q, Li Q, Du Y, et al. Protein contents in different peanut varieties and their relationship to gel property. *Int J Food Propert.* (2014) 17:1560–76. doi: 10.1080/10942912.2012.723660

38. Ramirez J. *Ultrafiltration: Methods, Applications, and Insights.* New York, NY: Nova Science Publishers, Inc (2017).

39. Djoullah A, Husson F. Gelation behaviors of denatured pea albumin and globulin fractions during transglutaminase treatment. *Food Hydrocoll.* (2018) 77:636–45. doi: 10.1016/j.foodhyd.2017.11.005

40. Taherian AR, Mondor M, Labranche J, Drolet H, Ippersiel D, Lamarche F. Comparative study of functional properties of commercial and membrane processed yellow pea protein isolates. *Food Res Int.* (2011) 44:2505–14. doi: 10.1016/j.foodres.2011.01.030

41. Mundi S, Aluko RE. Physicochemical and functional properties of kidney bean albumin and globulin protein fractions. *Food Res Int.* (2012) 48:299–306. doi: 10.1016/j.foodres.2012.04.006

42. Yildiz G, Ding J, Andrade J, Engeseth NJ, Feng H. Effect of plant protein-polysaccharide complexes produced by mano-thermo-sonication and pH-shifting on the structure and stability of oil-in-water emulsions. *Innovat Food Sci Emerg Technol.* (2018) 47:317–25. doi: 10.1016/j.ifset.2018.03.005

43. Cui L, Bandillo N, Wang Y, Ohm J-B, Chen B, Rao J. Functionality, and structure of yellow pea protein isolate as affected by cultivars and extraction pH. *Food Hydrocoll.* (2020) 108:106008. doi: 10.1016/j.foodhyd.2020.106008

44. Ladjal-Ettoumi Y, Boudries H, Chibane M, Romero A. Pea, chickpea and lentil protein isolates: physicochemical characterization and emulsifying properties. *Food Biophys.* (2016) 11:43–51. doi: 10.1007/s11483-015-9411-6

45. Hayati Zeidanloo M, Ahmadzadeh Ghavidel R, Ghiafeh Davoodi M, Arianfar A. Functional properties of grass pea protein concentrates prepared using various precipitation methods. *J Food Sci Technol.* (2019) 56:4799–808. doi: 10.1007/s13197-019-03930-3

46. Shevkani K, Singh N. Relationship between protein characteristics and film-forming properties of kidney bean, field pea and amaranth protein isolates. *Int J Food Sci Technol.* (2015) 50:1033–43. doi: 10.1111/ijfs.12733

47. Tcholakova S, Vankova N, Denkov ND, Danner T. Emulsification in turbulent flow: 3. Daughter drop-size distribution. *J Colloid Interface Sci.* (2007) 310:570–89. doi: 10.1016/j.jcis.2007.01.097

48. Chang C, Tu S, Ghosh S, Nickerson MT. Effect of pH on the inter-relationships between the physicochemical, interfacial, and emulsifying properties for pea, soy, lentil, and canola protein isolates. *Food Res Int.* (2015) 77:360–7. doi: 10.1016/j.foodres.2015.08.012

49. Wagner JR, Sorgentini DA, Añón MC. Relation between solubility and surface hydrophobicity as an indicator of modifications during preparation processes of commercial and laboratory-prepared soy protein isolates. *J Agric Food Chem.* (2000) 48:3159–65. doi: 10.1021/jf990823b

50. Chihi ML, Mession JL, Sok N, Saurel R. Heat-induced soluble protein aggregates from mixed pea globulins and β-lactoglobulin. *J Agric Food Chem.* (2016) 64:2780–91. doi: 10.1021/acs.jafc.6b00087

51. Mession J-L, Sok N, Assifaoui A, Saurel R. Thermal denaturation of pea globulins (*Pisum sativum* L.) – molecular interactions leading to heat-induced protein aggregation. *J Agric Food Chem.* (2013) 61:1196–204. doi: 10.1021/jf303739n

52. Oliete B, Potin F, Cases E, Saurel R. Modulation of the emulsifying properties of pea globulin soluble aggregates by dynamic high-pressure fluidization. *Innovat Food Sci Emerg Technol.* (2018) 47:292–300. doi: 10.1016/j.ifset.2018.03.015

53. Akhtar K, Khan SA, Khan SB, Asiri AM. *Scanning Electron Microscopy: Principle and Applications in Nanomaterials Characterization.* Cham: Springer International Publishing (2018). p. 113–45. doi: 10.1007/978-3-319-92955-2_4

54. Liu S, Elmer C, Low NH, Nickerson MT. Effect of pH on the functional behaviour of pea protein isolate–gum Arabic complexes. *Food Res Int.* (2010) 43:489–95. doi: 10.1016/j.foodres.2009.07.022

55. Liang HN, Tang C he. Pea protein exhibits a novel Pickering stabilization for oil-in-water emulsions at pH 3.0. *LWT Food Sci Technol.* (2014) 58:463–9. doi: 10.1016/j.lwt.2014.03.023

56. Sun XD, Arntfield SD. Gelation properties of salt-extracted pea protein isolate induced by heat treatment: effect of heating and cooling rate. *Food Chem.* (2011) 124:1011–6. doi: 10.1016/j.foodchem.2010.07.063

57. Akharume F, Santra D, Adedeji A. Physicochemical and functional properties of proso millet storage protein fractions. *Food Hydrocoll.* (2020) 108:105497. doi: 10.1016/j.foodhyd.2019.105497

58. Barac MB, Pesic MB, Stanojevic SP, Kostic AZ, Bivolarevic V. Comparative study of the functional properties of three legume seed isolates: adzuki, pea and soybean. *J Food Sci Technol.* (2015) 52:2779–2787. doi: 10.1007/s13197-014-1298-6

59. Delahaije RJ, Gruppen H, Giuseppin ML, Wierenga PA. Quantitative description of the parameters affecting the adsorption behaviour of globular proteins. *Coll Surf B Biointerf.* (2014) 123:199–206. doi: 10.1016/j.colsurfb.2014.09.015

60. Chen M, Lu J, Liu F, Nsor-Atindana J, Xu F, Goff HD, et al. Study on the emulsifying stability and interfacial adsorption of pea proteins. *Food Hydrocoll.* (2019) 88:247–55. doi: 10.1016/j.foodhyd.2018.09.003

61. Aziz A, Khan NM, Ali F, Khan ZU, Ahmad S, Jan AK, et al. Effect of protein and oil volume concentrations on emulsifying properties of acorn protein isolate. *Food Chem.* (2020) 324:126894. doi: 10.1016/j.foodchem.2020.126894

62. Boye J, Zare F, Pletch A. Pulse proteins: processing, characterization, functional properties and applications in food and feed. *Food Res Int.* (2010) 43:414–31. doi: 10.1016/j.foodres.2009.09.003

63. Martin AH, Castellani O, Jong Govardus AH, Bovetto L, Schmitt C. Comparison of the functional properties of RuBisCO protein isolate extracted from sugar beet leaves with commercial whey protein and soy protein isolates. *J Sci Food Agric.* (2019) 99:1568–76. doi: 10.1002/jsfa.9335

64. Raikos V, Campbell L, Euston SR. Rheology, and texture of hen's egg protein heat-set gels as affected by pH and the addition of sugar and/or salt. *Food Hydrocoll.* (2007) 21:237–44. doi: 10.1016/j.foodhyd.2006.03.015

65. Chao D, Aluko RE. Modification of the structural, emulsifying, and foaming properties of an isolated pea protein by thermal pretreatment. *CyTA J Food.* (2018) 16:357–66. doi: 10.1080/19476337.2017.1406536

66. Foegeding EA, Luck PJ, Davis JP. Factors determining the physical properties of protein foams. *Food Hydrocoll.* (2006) 20:284–92. doi: 10.1016/j.foodhyd.2005.03.014

67. Shevkani K, Kaur A, Kumar S, Singh N. Cowpea protein isolates: functional properties and application in gluten-free rice muffins. *LWT Food Sci Technol.* (2015) 63:927–33. doi: 10.1016/j.lwt.2015.04.058

68. Wong D, Vasanthan T, Ozimek L. Synergistic enhancement in the co-gelation of salt-soluble pea proteins and whey proteins. *Food Chem.* (2013) 141:3913–9. doi: 10.1016/j.foodchem.2013.05.082

69. Chen N, Chassenieux C, Nicolai T. Kinetics of NaCl induced gelation of soy protein aggregates: effects of temperature, aggregate size, and protein concentration. *Food Hydrocoll.* (2018) 77:66–74. doi: 10.1016/j.foodhyd.2017.09.021

Conflict of Interest: The authors declare that the research was conducted in the absence of any commercial or financial relationships that could be construed as a potential conflict of interest.

Publisher's Note: All claims expressed in this article are solely those of the authors and do not necessarily represent those of their affiliated organizations, or those of the publisher, the editors and the reviewers. Any product that may be evaluated in this article, or claim that may be made by its manufacturer, is not guaranteed or endorsed by the publisher.

frontiers | Frontiers in Nutrition

Structural Elucidation and Activities of *Cordyceps militaris*-Derived Polysaccharides: A Review

Miao Miao, Wen-Qian Yu, Yuan Li, Yan-Long Sun* and Shou-Dong Guo*

Institute of Lipid Metabolism and Atherosclerosis, Innovative Drug Research Centre, School of Pharmacy, Weifang Medical University, Weifang, China

Cordyceps militaris is a parasitic edible fungus and has been used as tonics for centuries. Polysaccharides are a major water-soluble component of *C. militaris*. Recently, *C. militaris*-derived polysaccharides have been given much attention due to their various actions including antioxidant, anti-inflammatory, anti-tumor, anti-hyperlipidemic, anti-diabetic, anti-atherosclerotic, and immunomodulatory effects. These bioactivities are determined by the various structural characteristics of polysaccharides including monosaccharide composition, molecular weight, and glycosidic linkage. The widespread use of advanced analytical analysis tools has greatly improved the elucidation of the structural characteristics of *C. militaris*-derived polysaccharides. However, the methods for polysaccharide structural characterization and the latest findings related to *C. militaris*-derived polysaccharides, especially the potential structure-activity relationship, have not been well-summarized in recent reviews of the literature. This review will discuss the methods used in the elucidation of the structure of polysaccharides and structural characteristics as well as the signaling pathways modulated by *C. militaris*-derived polysaccharides. This article provides information useful for the development of *C. militaris*-derived polysaccharides as well as for investigating other medicinal polysaccharides.

Keywords: *Cordyceps militaris*, polysaccharide, structure-activity relationship, bioactivity, mechanisms of action

Abbreviations: ABC, ATP-binding cassette; apo, apolipoprotein; Ara, arabinose; CM1, heteropolysaccharide; COSY, correlated spectroscopy; CVD, cardiovascular disease; DEPT, polarization transfer spectroscopy; ERK, extracellular regulated kinase; ESI-MS, electrospray ionization mass spectrometry; FT-IR, Fourier transform infrared; Gal, galactose; GalA, galacturonic acid; GC, gas chromatography; GC-MS, gas chromatography-mass spectrometry; Glc, glucose; GlcA, glucuronic acid; HDL-C, high density lipoprotein cholesterol; HILIC-MS, Hydrophilic interaction chromatography coupled to mass spectrometric detection; HMBC, heteronuclear multiple bond correlation spectroscopy; HMQC, heteronuclear multiple quantum coherence spectroscopy; HPLC, high-performance liquid chromatography; HPLC-MS/MS, HPLC-tandem mass spectrometry; IFN, interferon; IL, interleukin; JNK, C-Jun Kinase; LDL, low-density lipoprotein; LDL-C, LDL cholesterol; LDLR, Low-density lipoprotein receptor; LPS, Lipopolysaccharide; MALDI, matrix-assisted laser desorption/ionization; MALDI-TOF, MALDI-time of flight; Man, mannose; MAPK, mitogen-activated protein kinase; MS, mass spectrometry; Mw, molecular weight; NF-κB, nuclear factor kappa-B; NMR, nuclear magnetic resonance; NO, nitric oxide; NOESY, nuclear overhauser effect spectroscopy; Nrf2, nuclear factor erythroid 2-related factor 2; PCSK9, proprotein convertase subtilisin/kexin-type 9; PKB/AKT, phosphoinositide-3-kinase/protein kinase B; PMP, 1-phenyl-3-methyl-5-pyrazolone; PRR, pattern recognition receptor; RCT, reverse cholesterol transport; SOD, superoxide dismutase; TC, total cholesterol; TFA, trifluoroacetic acid; TG, triglyceride; TGF-β1, transforming growth factor β1; TLR, Toll-like receptor; TNF, tumor necrosis factor; TOCSY, total correlation spectroscopy; VEGF, vascular endothelial growth factor.

INTRODUCTION

Cordyceps species have been used as medicine, tonics, and food for centuries in many countries (1, 2). Approximately 750 Cordyceps species are mainly distributed in Asia, Europe, and North America (1). *Cordyceps militaris* (Yong Chong Cao, 蛹虫草) is a well-developed Cordyceps species (3, 4). Pharmacological studies have suggested that artificially cultivated *C. militaris* is useful against many diseases, especially non-communicable diseases (5–7). Some medicinal and tonic products of *C. militaris* have been developed and commercialized around the world, especially in Asian countries (3, 8). The annual output value of *C. militaris*-derived products is estimated to be 10 billion RMB in China (9).

The primary metabolite, polysaccharide, is one of the major water-soluble bioactive components of *C. militaris* (3, 6). Compared to the secondary metabolites, *C. militaris*-derived polysaccharides have not been well characterized (1, 2, 4, 10–12). Four years' ago, Zhang et al. reviewed the extraction, isolation, purification, structural characteristics, and bioactivities of *C. militaris*-derived polysaccharides (3). The pharmaceutical mechanisms of *C. militaris* polysaccharides including antioxidant, immunomodulatory, and anti-tumor activities have also been reviewed recently (7). The activity of the polysaccharide is determined by its monosaccharide composition, molecular weight (Mw), glycosidic linkage, and degree of branching. With increasing use of advanced analytical tools, the structural characterization of polysaccharides has improved greatly during the past several years. However, the structural characteristics of these polysaccharides in relation to some bioactivities such as anti-diabetic, and anti-hyperlipidemic, and anti-atherosclerotic effects have not been well summarized. Furthermore, these is a lack of graphic representations that clearly show the reaction processes involved in structural elucidation and the signaling pathways mediated by *C. militaris*-derived polysaccharides. This is the motivation to review the advances in the methods used for structural elucidation and to further describe the structural characteristics and the signaling pathways that are modulated by *C. militaris*-derived polysaccharides. In this article, we review the related literature mainly from the year of 2019 to the present that were obtained as search results from PubMed using "*C. militaris* and polysaccharide" or "mass spectrometry and polysaccharide" as keywords.

METHODS FOR ELUCIDATION OF POLYSACCHARIDE STRUCTURE

Fourier Transform Infrared Spectrometry

Except for chemical methods, Fourier transform infrared (FT-IR) spectrometer is a common and easily available tool to quickly identify polysaccharides. In FT-IR spectrum, a strong U-type band observed at approximately 3,400 cm^{-1} represents the typical O-H stretching vibration, and the weak bands at around 2,930 cm^{-1} represent the typical C-H stretching vibration. Furthermore, the strong band presents at approximately 1,050 cm^{-1} is arisen from the C-O-C glycosidic bond vibration,

while the band at around 1,600 and 1,655 cm^{-1} can be assigned to C = O stretching vibration and the bending vibration of -NH- (-CONH-), respectively (6). The peak at approximately 1,250 cm^{-1} suggests the presence of sulfate in axial position. Of importance, the bands between 1,000 and 800 cm^{-1} are useful for determination of α- and β-configurations of glycosyls. For instance, the bands at around 880 cm^{-1} suggest the potential presence of mannosyl and galactosyl residues in a β-configuration; and the bands at approximately 810 and 850 cm^{-1} may arise from α-D mannosyl and α-D glucosyl residues, respectively (13–16).

Monosaccharide Composition Determination

To accurately determine monosaccharide composition, a complete acid hydrolysis of polysaccharide is needed. Theoretically, all strong acids can be used to release monosaccharides at a concentration of 2–4 mol/L. Considering the next neutralization step, trifluoroacetic acid (TFA) with a good volatility is the most popular acid because it can be easily removed by a rotary evaporator (17, 18). In brief, approximately 10 mg of polysaccharide dissolved in 1–2 mL of 2.0 mol/L of TFA is put into a 5 mL ampule container, which is sealed and maintained at 110°C for 6 h. Next, neutral monosaccharides can be detected by gas chromatography (GC) after the monosaccharides are converted into acetylated aldononitrile derivatives, however, acidic monosaccharides need to be converted into their corresponding alditols by an appropriate reductant, such as sodium borohydride, before chemical derivatization (14). Compared to GC, high-performance liquid chromatography (HPLC) is more popular because this method can detect all the reducing monosaccharides (neutral, acidic, and basic) after monosaccharide derivatization with 1-phenyl-3-methyl-5-pyrazolone (PMP) (**Figure 1A**). Moreover, HPLC combined with PMP derivatization can detect more than ten kinds of monosaccharides with a high sensitivity and resolution in a single run (16, 19). Ion chromatography is another method for determining monosaccharide composition without any kind of derivatization. However, some natural monosaccharides, such as galactose/N-acetyl glucosamine or mannose/xylose, have comparably bad resolution on ion chromatography (16). Recently, an HPLC-tandem mass spectrometry (HPLC-MS/MS) method was developed for simultaneous detection of 17 monosaccharides including aldoses, ketoses, amino sugars, and uronic acids, in the multiple reaction monitoring mode after aldononitrile acetate derivatization (20). Additionally, GC-mass spectrometry (GC-MS) can be used for determination of the absolute configuration (D or L) of monosaccharides (21).

Glycosyl Linkage Determination

Periodate oxidation-Smith degradation is a traditional method used to assess glycosidic linkages (8, 22). Glycosyls with distinct linkages may produce different reaction products (**Figure 1B**), which can be analyzed by thin layer chromatography and GC. However, it is impossible to assign glycosidic linkage of a polysaccharide that is composed of more than one
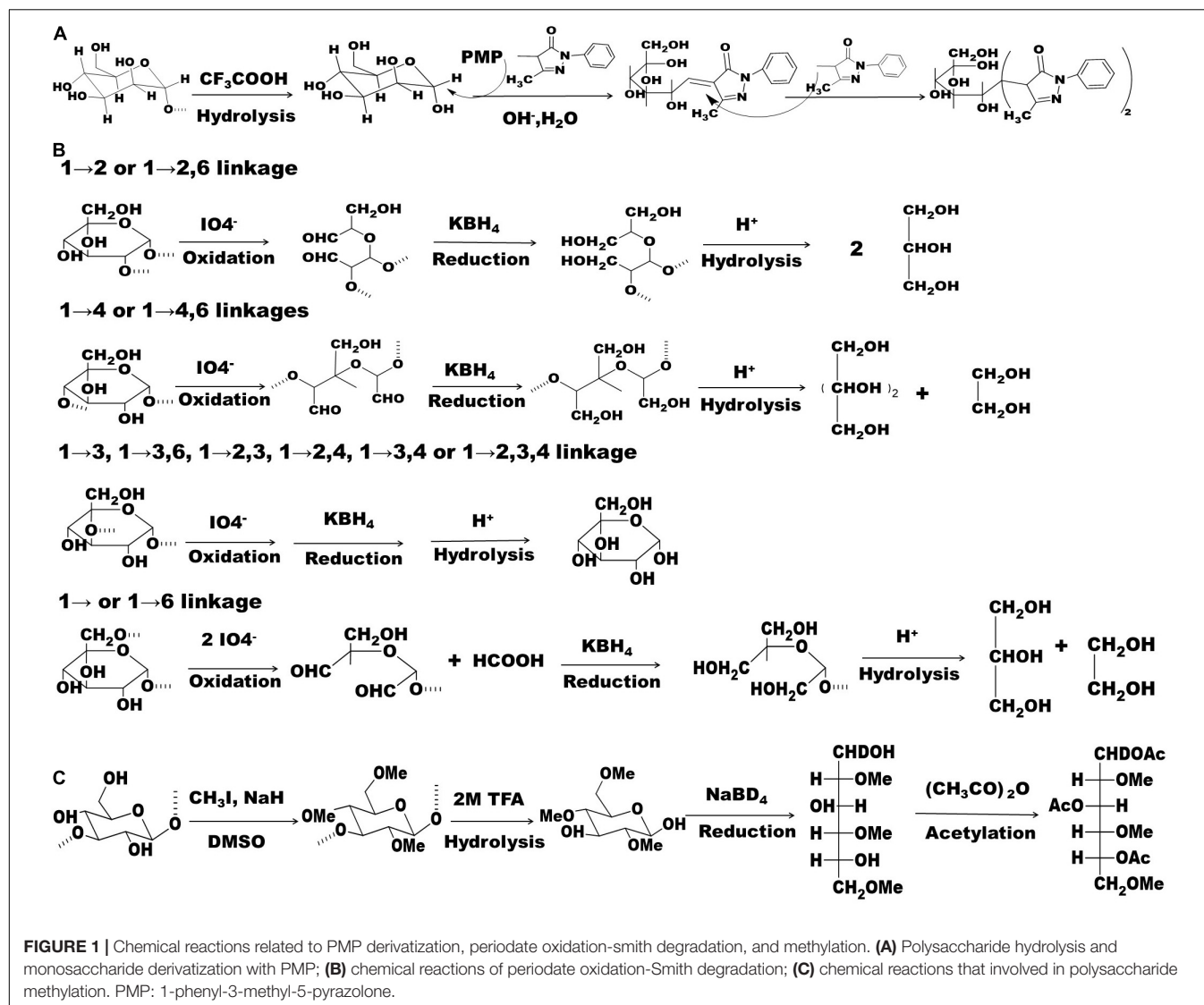
FIGURE 1 | Chemical reactions related to PMP derivatization, periodate oxidation-smith degradation, and methylation. **(A)** Polysaccharide hydrolysis and monosaccharide derivatization with PMP; **(B)** chemical reactions of periodate oxidation-Smith degradation; **(C)** chemical reactions that involved in polysaccharide methylation. PMP: 1-phenyl-3-methyl-5-pyrazolone.

type of monosaccharide (13). Therefore, this method has been gradually replaced by methylation and nuclear magnetic resonance (NMR) analysis.

Methylation Analysis

Methylation analysis is a classical and putative method used to determine glycosidic linkages (**Figure 1C**). In brief, approximately 2–3 mg of polysaccharide is needed to perform this assay. During the reaction process, anhydrous conditions and protection with nitrogen are strongly suggested. FT-IR is generally used to evaluate the completeness of methylation. In an FT-IR spectrum, the absence of the U-type peak at approximately 3,400 cm^{-1} and the significant increase of C-H stretching variation at around 2,930 cm^{-1} indicate a complete methylation reaction (15, 16). Next, permethylated polysaccharide is completely hydrolyzed as mentioned in the monosaccharide composition analysis above. The resulting hydrolysates are reduced with sodium borodeuteride (NaBD$_4$),

and then acetylated with acetic anhydride. To keep in alignment with the database, use of sodium borohydride (NaBH$_4$) as a reductant is not encouraged. The final methylated alditol acetates are generally analyzed using GC-MS (16). The open accessed Complex Carbohydrate Structure Database created by the Complex Carbohydrate Research Center of the University of Geogia[1] is generally used to explain the GC-MS data, thereby determining glycosidic linkages. A comparison of the total amount of branched glycosyls with the total amount of glycosyls that derived from the non-reducing end is useful in evaluating the correctness of the methylation analysis. However, polysaccharides with substitutions, such as *O*-methyl, are not considered in this type of comparison (16). Recently, an ultra-HPLC-MS/MS method was developed for the rapid determination of glycoside linkages of polysaccharide and oligosaccharide in a multiple reaction monitoring mode. The

---

[1]https://glygen.ccrc.uga.edu/ccrc/specdb/ms/pmaa/pframe.html

permethylated samples are hydrolyzed and derivatized with PMP before analysis and the resulting linkage profiles can be determined and quantified by the library containing 22 kinds of glycosidic linkages that are built using oligosaccharide standards (23).

Nuclear Magnetic Resonance Analysis

NMR spectroscopy is another powerful tool for determination of glycosidic linkages of carbohydrate. One-dimensional (1D-) (^{1}H-, and ^{13}C-NMR) and two-dimensional (2D-) NMR experiments, including distortionless enhancement by polarization transfer spectroscopy (DEPT), [1]H-^{1}H correlated spectroscopy (COSY), [1]H-^{13}C heteronuclear multiple quantum coherence spectroscopy (HMQC), [1]H-^{13}C heteronuclear multiple bond correlation spectroscopy (HMBC), total correlation spectroscopy (TOCSY), and nuclear overhauser effect spectroscopy (NOESY), are usually performed for accurately determining glycosidic linkages. In the 1D-NMR spectra, the anomeric signals always display in down-field regions, which could provide useful information for determining distinct glycosyls and even for quantitative analysis of the various glycosyls. However, the rest signals (H2-H6 or C2-C5) of heteropolysaccharides usually overlap with each other in the ^{1}H- and ^{13}C-NMR spectra, which makes it hard for a correct assignment. 2D-NMR experiments play key roles in structural elucidation of polysaccharides. ^{1}H-^{1}H COSY or TOCSY can give valuable information on the associated protons within a sugar ring. In general, the correlation between H1-H3 is easily identified even in the ^{1}H-^{1}H COSY spectrum of a heteropolysaccharide. However, it is difficult to accurately assign the correlation between H3-H6 due to the large degree of overlap of these proton signals in the ^{1}H-NMR spectrum. An HMQC experiment is valuable in determining the direct correlation between protons and carbons, such as H_1/C_1 or H_3/C_3. In comparison with ^{13}C-NMR spectrum, DEPT spectrum can provide useful information of *O*-6 substituted signals, which show inverted peaks at approximately 66 ppm. The long-range couplings (within 3 bonds) between carbon and proton signals in the HMBC spectrum are useful in making up the missing correlations within a sugar ring and even those between the connective glycosyls. Furthermore, NOESY and TOCSY provide complementary information based on bond connectivity. The solvent and relaxation rates of the protons can significantly influence the sensitivity of these correlation signals (24). Collectively, HMBC, NOESY, and TOCSY spectra are important in the construction of glycosyl connections.
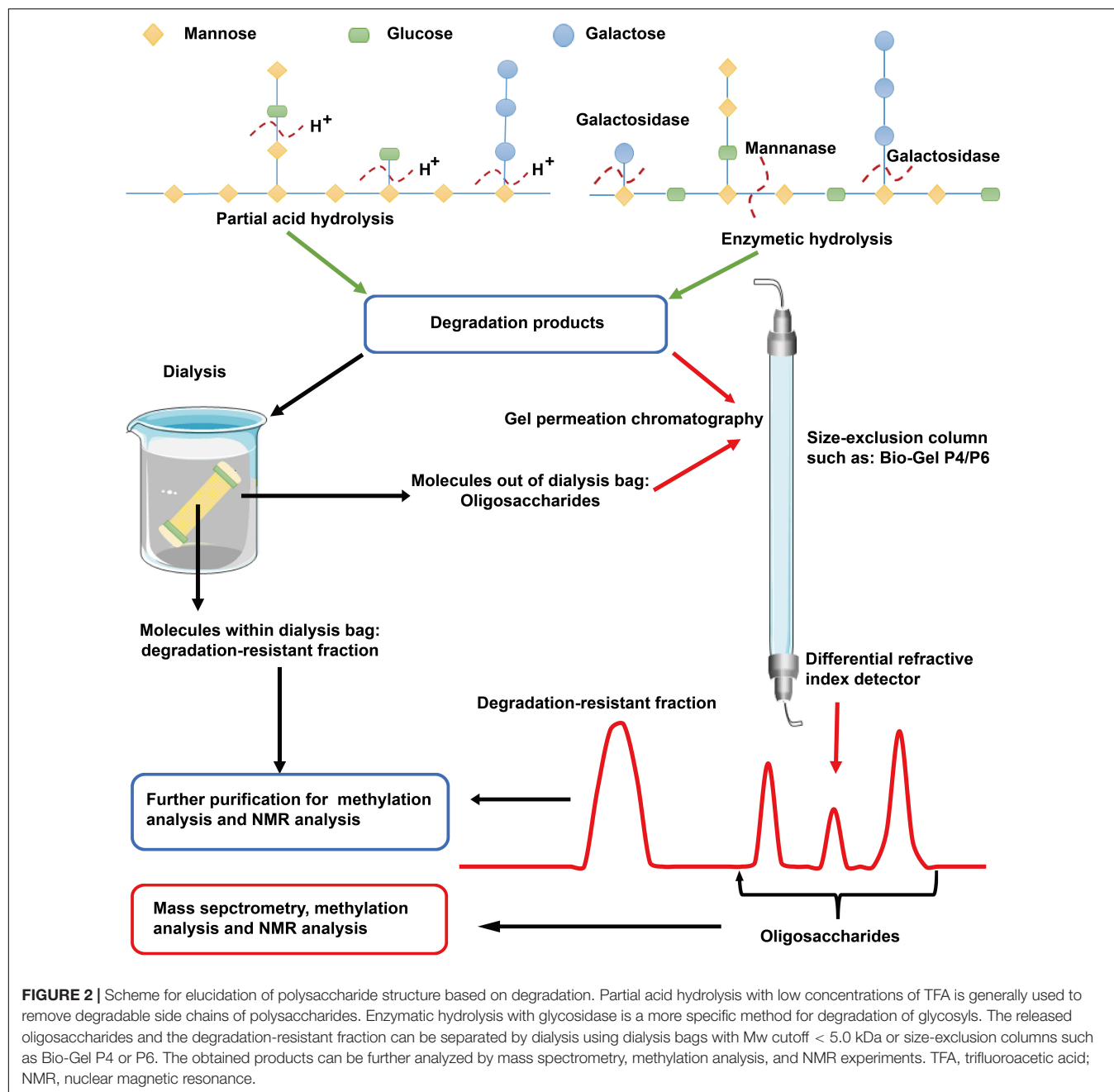
Given the complex linkages of glycosyls and heavy overlap of NMR signals, it is virtually impossible to assign all the NMR signals for most of the polysaccharides. However, some NMR signals can be assigned in combination with methylation analysis and using the available literature. Furthermore, NMR data are useful for determining the α- and β-configurations of glycosyls based on carbon-proton spin-coupling constants (25). As for the D-type pyranosyls in the $^4C_1$ conformation, a $^1J_{C1,H1}$ at ~170 *Hz* indicates an α-anomeric sugar configuration, and a $^1J_{C1,H1}$ at ~160 *Hz* suggests a β-anomeric sugar configuration (16). Alternatively, anomeric proton signals in the region of 5.60–4.90

and 4.90–4.30 ppm may be assigned as α- and β-anomers, respectively. It seems that anomeric protons of galactosyl in a β-D configuration does not match the latter rules. However, anomeric carbons in galactosyls in the β-D configuration always show a downfield chemical shift in ^{13}C-NMR spectrum (greater than 104 ppm in general), which is useful to determine the α- and β-configuration of these galactosyls (15, 16). Of importance, an accurate monosaccharide composition analysis is the basis for assignment of glycosyl linkage patterns.

The NMR signals of homopolysaccharides with simple glycosyl linkages are easily assigned. For instance, the structural characteristics of the *C. militaris*-derived β-D-(1→6)-glucan and the glucan mainly consisted of →4)-α-D-Glc*p* (1→ glycosyls are elucidated by our lab (14, 15). Furthermore, glycosyls in a specific configuration and linkage pattern usually show similar chemical shifts in NMR spectra. For example, the galactosyls in the β-D-configuration may present as the side chains in *C. militaris*-derived polysaccharides in the form of →2)-β-D-Gal*f* (1→ and/or β-D-Gal*f* (1→ glycosyls, whose anomeric carbon generally present at approximately 106 ppm in the ^{13}C-NMR spectrum (15). The anomeric signals of →2,6)-α-D-Man*p* (1→, α-D-Man*p* (1→, and →6)-α-D-Man*p* (1→ glycosyls are generally present at approximately 100.5, 102.0, and 98.0 ppm, respectively. Furthermore, O-methyl is also found in *C. militaris*-derived polysaccharides, and this kind of methyl shows a chemical shift at approximately 54.0 ppm in ^{13}C-NMR spectra (15, 26). The new magnets beyond 1 G*Hz* have greatly enhanced the sensitivity and resolution of the NMR signals, and the [13]C-, [15]N-, and ^{19}F-labeling strategies can further improve the sensitivity and resolution (27). Solid-state NMR spectroscopy in combination with magic angle spinning techniques can provide detailed signals in a non-destructive manner. This method has also been used to determine the structure of polysaccharides in different forms and even in plant and cell walls (28–31). The application of solid-state NMR has been reviewed recently by different teams (32–34).

Mass Spectrometry

Hydrolysis is helpful in elucidating the structure of polysaccharide (**Figure 2**). Partial hydrolysis with TFA at a concentration of < 0.1 M (such as 0.05 M) is generally used to remove degradable side chains of polysaccharides (35). The released oligosaccharides and the resistant backbone can be further analyzed by methylation and NMR experiments (26). Data obtained before and after partial hydrolysis are usually combined to elucidate the fine structure of a polysaccharide. Enzymatic hydrolysis is another valuable method for determining glycosidic linkages in polysaccharides. Based on enzymatic digestion (such as, α-amylase, β-glucanase, arabinanase, xylanase, galactanase, and pectinase), →4)-α-D-Glc*p* (1→, →4)-β-D-GlcA*p* (1→, and →4)-α-D-Gal*p* (1→ glycosyls are found to exist in wild and cultured *C. militaris* and other species of Cordyceps (17, 18, 36). The saccharide mapping profiles obtained in combination with high performance thin layer chromatography is valuable in distinguishing polysaccharides from different species of Cordyceps (17, 36). Of importance, the hydrolyzed products such as oligosaccharides and low Mw polysaccharides

FIGURE 2 | Scheme for elucidation of polysaccharide structure based on degradation. Partial acid hydrolysis with low concentrations of TFA is generally used to remove degradable side chains of polysaccharides. Enzymatic hydrolysis with glycosidase is a more specific method for degradation of glycosyls. The released oligosaccharides and the degradation-resistant fraction can be separated by dialysis using dialysis bags with Mw cutoff < 5.0 kDa or size-exclusion columns such as Bio-Gel P4 or P6. The obtained products can be further analyzed by mass spectrometry, methylation analysis, and NMR experiments. TFA, trifluoroacetic acid; NMR, nuclear magnetic resonance.

can be further analyzed by mass spectrometry (MS). As reviewed previously, matrix-assisted laser desorption/ionization (MALDI)-MS and HPLC-MS/MS with a high sensitivity are utilized for the structural elucidation and quantification of oligosaccharides and polysaccharides with a low Mw (17, 18, 37).

The saccharide analysis can be carried out using electrospray ionization MS (ESI-MS) and MALDI-time of flight (MALDI-TOF) MS. Collision-induced dissociation is widely applied for detection of oligosaccharide (38). The ion fragments are informative for explaining the glycosyl linkages of carbohydrates, and the systematic nomenclature rules have been previously documented by Domon and Costello (39).

Of note, monosaccharide loss, migration, and rearrangement, during MS analysis is common due to the weak glycosidic bonds. Permethylation is an efficient method to improve the stability of glycans. Hydrophilic interaction chromatography coupled with mass spectrometric detection (HILIC-MS) is also used to sequence carbohydrates (40, 41). Moreover, HPLC-MS was recently used to detect the metabolites of polysaccharides as well as their interaction with proteins (42). Ionization efficiency, instability, and limited sensitivity of molecules with low Mw are the major factors that influence the application of MALDI-TOF mass spectrometry for the analysis of carbohydrates. The compound, 2-hydrazinoquinoline, can react with the reducing

end of carbohydrates with high stability and efficiency. This derivatization method can effectively improve the problems of MALDI-TOF mass spectrometry as mentioned above (43). Mass spectrometry imaging is a novel technique used for investigating the distribution of metabolites in plant tissues. For instance, MALDI-TOF MS imaging has been used to reveal the disaccharide distribution in onion bulb tissues and the chemical components of *C. sinensis* (44, 45). Of note, microarray in combination with MALDI-TOF mass spectrometry was recently developed for the detection of glycosphingolipid glycans (46).

STRUCTURAL CHARACTERISTICS OF *CORDYCEPS MILITARIS*-DERIVED POLYSACCHARIDES

The methods used for cultivation of *C. militaris* are shown in **Figure 3**. *C. militaris*-derived polysaccharides can be obtained from mycelia fermentation (mycelia and fermentation broth) and cultivated fruiting bodies. Fermentation broth can be used to obtain extracellular polysaccharide (exopolysaccharide), while mycelia and fruiting bodies of *C. militaris* are used to extract intracellular polysaccharide (endo-polysaccharide). The isolation and purification processes for preparation of *C. militaris*-derived polysaccharides are summarized in **Figure 4**. Generally, only polysaccharides with high purity are used for the analysis of structural characteristics. Most of the polysaccharides derived from *C. militaris* are consisted of glucose (Glc), galactose (Gal), and mannose (Man) (3). However, polysaccharides containing other monosaccharides, such as rhamnose, arabinose (Ara), xylose (Xyl), ribose, fucose, galacturonic acid (GalA), glucuronic acid (GlcA), and N-acetyl galactosamine, can also be isolated from *C. militaris* (3, 18).

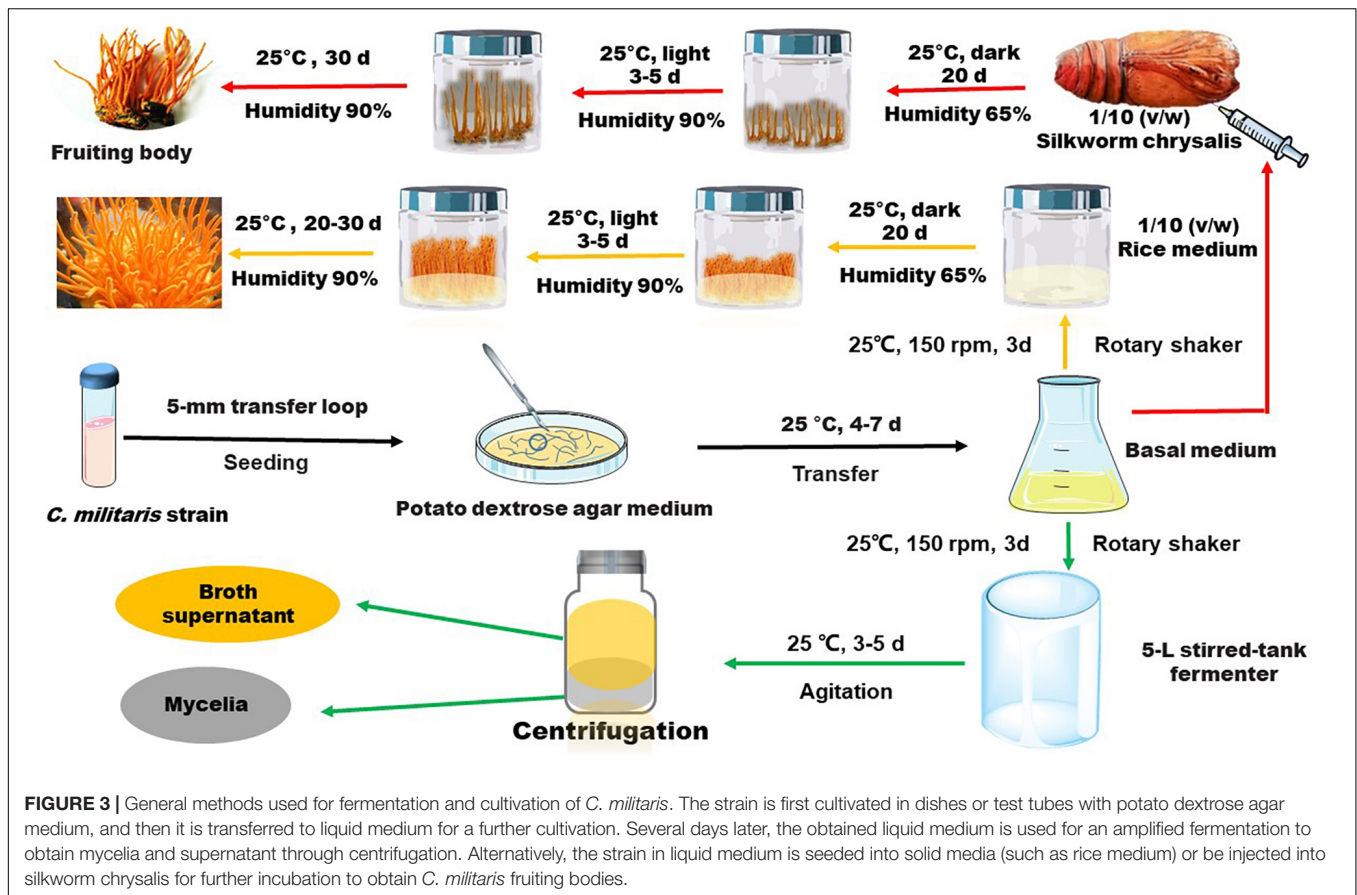## Mycelia Fermentation-Derived Polysaccharides

The general fermentation processes are summarized in **Figure 3**. The fermentation conditions and the proposed mechanisms for biosynthesis of exopolysaccharide in Cordyceps have been reviewed recently by Yang et al. (47). Repeated batch cultivation is reported to enhance exopolysaccharide production of *C. militaris* (48). UV light irradiation-induced mutagenesis is found to improve production of extracellular and intracellular polysaccharides by more than 120-fold (49, 50). Ionic conditions and pH of the culture media also have important effects on the structural characteristics of polysaccharides. Addition of metal ions is found to influence the production of exopolysaccharides, such as $Mg^{(2+)}$ and $Mn^{(2+)}$ can improve while $Ca^{(2+)}$ and $K^{(+)}$ may reduce the yield (51, 52). Addition of Na_2SO_4 may induce the presence of sulfate in polysaccharides obtained *via* fermentation (53). Furthermore, addition of metal ions in the culture medium may result in metal ion-enriched polysaccharides. For instance, addition of $FeSO_4$ solution can promote formation of polysaccharide-iron (III) complexes containing 2.73% of iron (54). The pH of the culture medium is reported to influence gene expression

of mycelia, thereby modulating structural characteristics of polysaccharides extracted from fermented mycelia (55). Of note, a weak alkaline (pH 8–9) culture medium is reported to increase production of β-(1→6)-glucan (55). Recently, gene engineering strategies have also been applied to modulate production of *C. militaris* polysaccharides. For instance, the combined overexpression of phosphoglucomutase and UDP-glucose 6-dehydrogenase genes can increase production of exopolysaccharides by 78.13% compared to that of wild-type strain (56). Furthermore, bacteria in sclerotia have been demonstrated to influence mycelium biomass and metabolites of *C. militaris* (57). A recent study showed that submerged fermentation with talc microparticles can promote polysaccharide production (58).

Based on the literature, we presumed some chemical structures of fermentation-derived *C. militaris* polysaccharides as shown in **Figure 5**. Two purified exopolysaccharides have been extracted from *C. militaris* strain (CICC 14015), and they have a similar Mw of more than 1,000 kDa. However, their monosaccharide composition and glycosidic linkages are completely different (59, 60). The exopolysaccharide obtained from *C. militaris* strain (CICC 14014) is different from that of CICC 14015. As reported, this heteropolysaccharide with a lower Mw has →4)-α-D-Glc*p* (1→ and →4,6)-α-D-Glc*p* (1→ glycosyls as its main chain (61). Another heteropolysaccharide mainly consisting of →2)-α-D-Man*p* (1→ and →6)-α-D-Man*p* (1→ glycosyls is obtained from *C. militaris* strain (KCTC 6064) (62). Most of the endo-polysaccharides obtained from the fermented mycelia are composed of at least three kinds of monosaccharides. Of note, most of them are mainly composed of glucose and have a backbone consisted of →4)-α-D-Glc*p* (1→ glycosyls (22, 63–65). The backbone of some heteropolysaccharides is found to be consisted of →2)-α-D-Man*p* (1→ glycosyls (8).

Structural Characteristics of Polysaccharides Obtained From the Fruiting Body of *Cordyceps militaris*

The general processes for cultivation of the fruiting body of *C. militaris* are shown in **Figure 3**. Many factors, such as light irradiation and intensity, can influence polysaccharide production of the fruiting bodies (50, 66). Spaying biotic elicitors, such as chitosan (1 mg/L), can increase yield of polysaccharide by 1.41-fold (67). Furthermore, culture time also affect the production of polysaccharides. Within 35–45 days, polysaccharide content increases gradually and declines with a prolonged culture time (68). Recently, a comprehensive transcriptomic analysis of *C. militaris* cultivated on germinated soybeans was carried out by Yoo et al. (69). The gene information obtained from the analysis is useful in modulating the production of metabolites. In this article, we summarize the presumed structures of the *C. militaris* fruiting body-derived polysaccharides that are provided by the related literature (**Figure 6**). We also presume some chemical structures of polysaccharides according to the descriptions in the literature as shown in **Figure 7**.

FIGURE 3 | General methods used for fermentation and cultivation of *C. militaris*. The strain is first cultivated in dishes or test tubes with potato dextrose agar medium, and then it is transferred to liquid medium for a further cultivation. Several days later, the obtained liquid medium is used for an amplified fermentation to obtain mycelia and supernatant through centrifugation. Alternatively, the strain in liquid medium is seeded into solid media (such as rice medium) or be injected into silkworm chrysalis for further incubation to obtain *C. militaris* fruiting bodies.

As Glc is the major component of the cell walls of *C. militaris*, polysaccharides mainly composed of Glc are the most documented carbohydrate complex. A recent study demonstrated that →4)-α-D-Glc*p* (1→ linked glucan is specific to Cordyceps caterpillar and can be used as a marker for Cordyceps (70). Indeed, many water-extracted polysaccharides of the fruiting body of *C. militaris* have →4)-α-D-Glc*p* (1→ glycosyls as their backbone (22, 62, 64, 71, 72). Furthermore, most of these polysaccharides are heteropolysaccharides. However, several groups isolated glucans from the fruiting body of *C. militaris* (14, 73). Our group obtained a linear →6)-β-D-Glc*p* (1→ glucan with a Mw of 18.2 kDa (14). Some heteropolysaccharides are found to contain →4)-β-D-Glc*p* (1→ and →6)-α-D-Glc*p* (1→ glycosyls (14, 72). Polysaccharides mainly consisting of →2)-α-D-Man*p* (1→ glycosyls are also found in the fruiting bodies of *C. militaris* (3, 19).

The alkaline extracted polysaccharides are also reported. For instance, an alkali-extracted polysaccharide is found to have →2)-α-D-Man*p* (1→ and →2,6)-α-D-Man*p* (1→ glycosyls as its backbone (74). The polysaccharide CMPB90-1 obtained *via* 0.3 mol/L of NaOH is mainly composed of →6)-α-D-Glc*p* (1→ and →3)-α-D-Glc*p* (1→ glycosyls (75). Our lab obtained a novel alkali-extracted polysaccharide which mainly composed of →4)-β-D-Man*p* (1→, →6)-β-D-Man*p* (1→, and →6)-α-D-Man*p* (1→ glycosyls (16). Of note, alkaline-extracted (5% KOH) polysaccharides can be further treated with a free-thawing

process, and the water insoluble fractions can be further treated with Me₂SO to obtain a β-(1→3)-D-glucan (76). Our team obtained a glucan with →4)-α-D-Glc*p* (1→ and →4,6)-β-D-Glc*p* (1→ glycosyls as the backbone as shown in **Figure 6** (15). Furthermore, one acidic-extractable polysaccharide is found to be consisted of Fuc (1.23%), Ribose (0.57%), Ara (0.29%), Xyl (2.12%), Man (2.73%), Gal (4.66%), and Glc (88.4%) (77).

BIOACTIVITIES OF *CORDYCEPS MILITARIS*-DERIVED POLYSACCHARIDES

The polysaccharides obtained from *C. militaris* have been demonstrated to have various biological activities, including antioxidant, immunoregulatory, anti-inflammatory, and anti-tumor activities (7, 12). In the following sections, we discuss the potential structure-activity relationship of these polysaccharides. Furthermore, we summarize the hypolipidemic, anti-diabetic, and anti-atherosclerotic functions of *C. militaris*-derived polysaccharides.

Anti-oxidation

The antioxidant activity and mechanisms of *C. militaris*-derived polysaccharides have been well documented previously in the literature (3), especially by Gu et al. (7). Here, we discuss the

FIGURE 4 | Scheme for Extraction and Purification of *C. Militaris*-Derived polysaccharides.
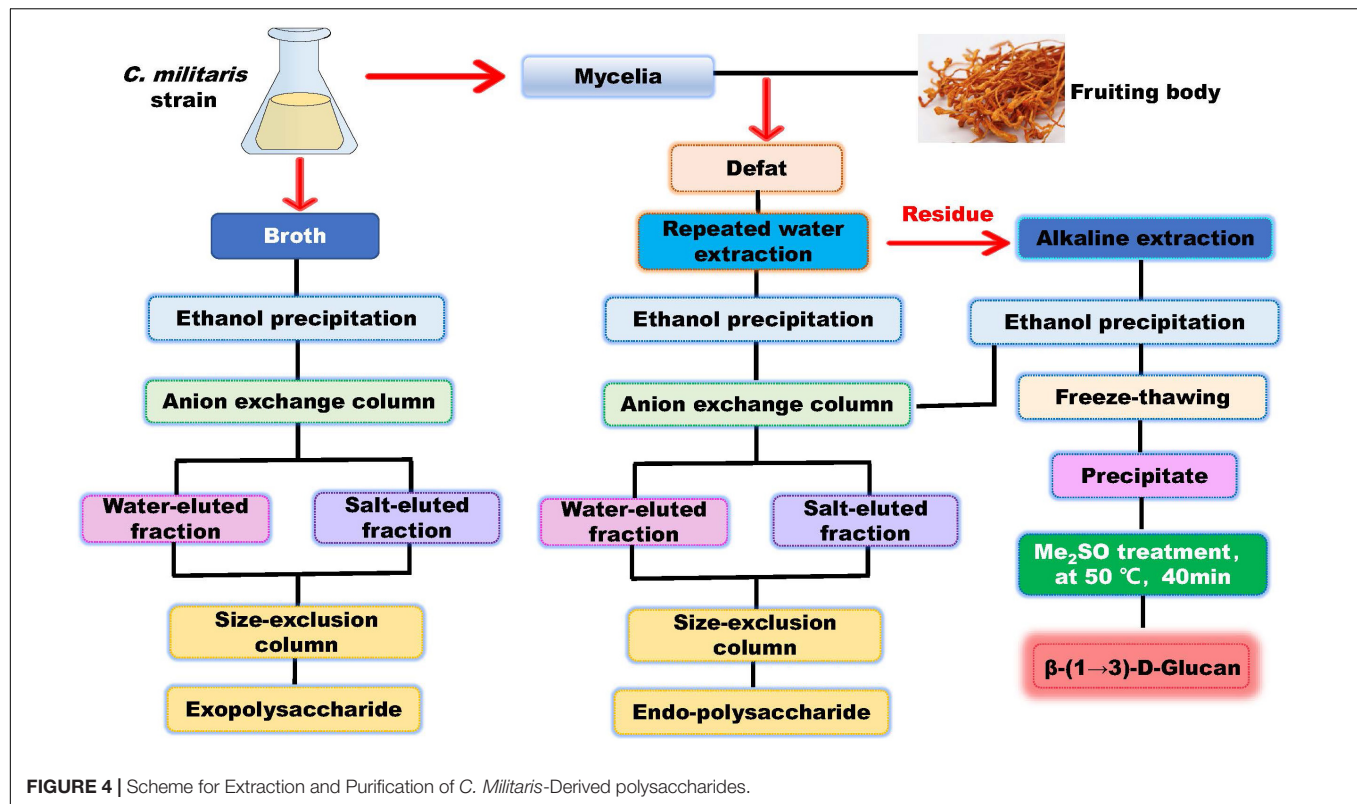
potential structure-activity relationship of these polysaccharides as antioxidants. Xu et al. demonstrated that the monosaccharide composition may significantly influence the antioxidant activity of polysaccharides (78). For instance, polysaccharides from the fruiting body of cultured *C. militaris* grown on silkworm pupae are reported to have better antioxidant activity than that grown on solid rice medium. The former has more Glc and the latter has more Man (79). The purified polysaccharide primarily consisting of Glc (47.5%), Man (34.3%), Gal (10.8%), and Ara (4.85%) in α-type glycosidic linkage can scavenge DPPH, hydroxyl, and superoxide radicals *in vitro* (80). The acidic-extractable heteropolysaccharide mostly composed of Glc (88.4%) not only scavenge free radicals *in vitro* but also improve the activity of antioxidant enzyme in type 2 diabetes mice (77). Furthermore, the mycelia polysaccharide obtained using a weak alkaline (pH 8–9) culture medium is reported to be rich in β-(1→6)-glucan, which has better antioxidant activity than that obtained from weak acidic conditions (pH 5–7) (55). These studies demonstrate that Glc and the β-configuration may enhance the antioxidant activity. Secondly, the ions contained in the polysaccharides may contribute to the antioxidant activity. The polysaccharide-iron (III) composed of →2)-β-D-Glc$p$ (1→ and highly branched →2,4)-α-D-Glc$p$ (1→ glycosyls shows antioxidant activity almost equal to that of vitamin C. This molecule can scavenge DPPH, hydroxyl, and superoxide anion radicals (54). Similarly, addition of sodium selenite can promote production of Se-polysaccharides with a better antioxidant activity than those without Se. Another study demonstrated that the Se-polysaccharide has better antioxidant activity with regard

to scavenging free radicals (81). *In vivo*, Se-polysaccharides can further promote the activity of superoxide dismutase (SOD) (82). Thirdly, the acidic groups may also support the antioxidant activity of these polysaccharides. The acidic polysaccharide mainly consisted of →6) Gal$p$ (1→, →4) Glc$p$ (1→, and →4,6) Glc$p$ (1→ glycosyls and GlcA and GalA can improve the activities of glutathione peroxidase and SOD, thereby reducing malondialdehyde concentration (83). Furthermore, sulfation may enhance the free radical-scavenging effect of polysaccharides as revealed *in vitro* (35). A recent study also indicated that polysaccharides with →2)-α-D-Man$p$ (1→ as the backbone exhibit good antioxidant activity (19). Therefore, glucosyls in β-configuration, →2)-α-D-Man$p$ (1→ linked backbone, metal ions, and acid groups, may contribute to the antioxidant activity of these polysaccharides.

Immune Enhancement

Immune response plays an importance role in host defense system. B-lymphocyte and T-lymphocyte specifically mediates humoral and cellular immunity, respectively. Polysaccharides from *C. militaris* exhibit mitogenic effects in mouse splenocytes and can promote differentiation of murine T-, B-lymphocytes, and neutrophiles. These polysaccharides also increase IgG function and production of cytokines, such as interleukin (IL)-1β, tumor necrosis factor (TNF)-α, interferon (IFN)-γ, and IL-6 (79, 84, 85). On the cell surface, pattern recognition receptors (PRRs), such as Toll-like receptor (TLR) 2, TLR4, and dectin-1, can trigger different signaling pathways including phosphoinositide-3-kinase/protein kinase B (PKB/AKT),
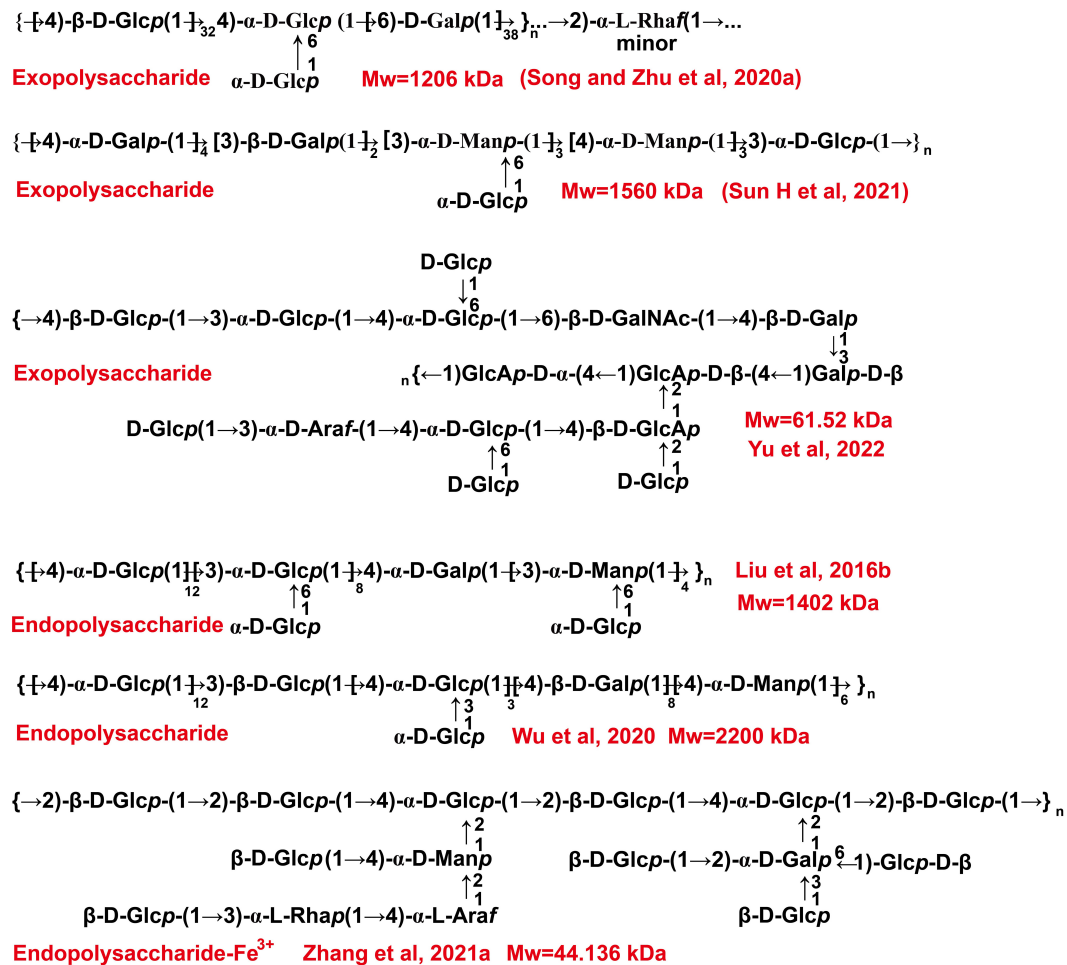
{[→4)-β-D-Glc*p*(1→]$_{32}$4)-α-D-Glc*p* (1→6)-D-Gal*p*(1→]$_{38}$}$_n$...→2)-α-L-Rha*f*(1→...

Exopolysaccharide   α-D-Glc*p*   **Mw=1206 kDa (Song and Zhu et al, 2020a)**   minor

{[→4)-α-D-Gal*p*-(1→]$_4$ [3)-β-D-Gal*p*(1→]$_2$ [3)-α-D-Man*p*-(1→]$_3$ [4)-α-D-Man*p*-(1→]$_3$3)-α-D-Glc*p*-(1→}$_n$

Exopolysaccharide   α-D-Glc*p*   **Mw=1560 kDa   (Sun H et al, 2021)**

D-Glc*p*

{→4)-β-D-Glc*p*-(1→3)-α-D-Glc*p*-(1→4)-α-D-Glc*p*-(1→6)-β-D-GalNAc-(1→4)-β-D-Gal*p*

Exopolysaccharide $_n${←1)GlcA*p*-D-α-(4←1)GlcA*p*-D-β-(4←1)Gal*p*-D-β

D-Glc*p*(1→3)-α-D-Ara*f*-(1→4)-α-D-Glc*p*-(1→4)-β-D-GlcA*p*   **Mw=61.52 kDa**

D-Glc*p*   D-Glc*p*   **Yu et al, 2022**

{[→4)-α-D-Glc*p*(1→]$_{12}$3)-α-D-Glc*p*(1→]$_8$4)-α-D-Gal*p*(1→]3)-α-D-Man*p*(1→]$_4$}$_n$ **Liu et al, 2016b**

Endopolysaccharide   α-D-Glc*p*   α-D-Glc*p*   **Mw=1402 kDa**

{[→4)-α-D-Glc*p*(1→]$_{12}$3)-β-D-Glc*p*(1→]4)-α-D-Glc*p*(1→]4)-β-D-Gal*p*(1→]$_8$4)-α-D-Man*p*(1→]$_6$}$_n$

Endopolysaccharide   α-D-Glc*p*   **Wu et al, 2020 Mw=2200 kDa**

{→2)-β-D-Glc*p*-(1→2)-β-D-Glc*p*-(1→4)-α-D-Glc*p*-(1→2)-β-D-Glc*p*-(1→4)-α-D-Glc*p*-(1→2)-β-D-Glc*p*-(1→}$_n$

β-D-Glc*p*(1→4)-α-D-Man*p*   β-D-Glc*p*-(1→2)-α-D-Gal*p*←1)-Glc*p*-D-β

β-D-Glc*p*-(1→3)-α-L-Rha*p*(1→4)-α-L-Ara*f*   β-D-Glc*p*

Endopolysaccharide-Fe^{3+} Zhang et al, 2021a   Mw=44.136 kDa

FIGURE 5 | The presumed chemical structures of polysaccharides derived from the fermentation broth of *C. militaris*.

mitogen-activated protein kinase (MAPK), and tyrosine kinases (86, 87). Lipopolysaccharide (LPS) and some polysaccharides can activate these cell surface receptors and exert their immune modulating functions. As recently reviewed by Lee et al. (10), polysaccharides of *C. militaris* are likely to cause type 1 immunity. They can increase TNF-α secretion in macrophages and enhance NK cell activity. The immune enhancement activity of *C. militaris*-derived polysaccharides has been recently reviewed by different groups (3, 7), and Phull et al. have reviewed the influence of monosaccharide composition and Mw on the immunomodulatory effect (12). Here, we consider the related signaling pathways as shown in **Figure 8** and discuss the potential structure-activity relationship by focusing on glycosidic linkage.

C. militaris-derived polysaccharides that are composed of Glc are reported to act on macrophages and increase production of NO, IL-1β, IL-6 *in vitro* (73). The marker polysaccharide of *C. militaris*, →4)-α-D-Glc*p* (1→ linked glucan, can promote production of NO and cytokines in RAW 264.7 macrophages (70). Mechanistically, this polysaccharide is highly selective for the TLR4/MyD88/p38 axis as demonstrated in TLR4-deficient mice (88). The polysaccharide mainly composed of →4)-α-D-Glc*p* (1→ (~70%), →4,6)-α-D-Man*p* (1→, and →2,6)-α-D-Gal*p* (1→ glycosyls could promote macrophage phagocytosis and secretion of NO, TNF-α, and IL-6, *via* up-regulation of the MAPK/nuclear factor kappa-B (NF-κB) pathway, including phosphorylation of extracellular regulated kinase (ERK), p-38, and C-Jun Kinase (JNK) (71). The acidic exopolysaccharide mainly composed of →4)-α-D-Glc*p* (1→ can promote cytokine secretion by increasing the phosphorylation of ERK, p-38, and JNK (61). Furthermore, the alkali-extracted polysaccharide CMPB90-1 mainly composed of →6)-α-D-Glc*p* (1→ and →3)-α-D-Glc*p* (1→ glycosyls, is reported to improve macrophage M1 polarization through the activation of TLR2/MAPK/NF-κB signaling pathway (75). These data demonstrate that →4)-α-D-Glc*p* (1→ and →6)-α-D-Glc*p* (1→ glycosyls play key roles in immune enhancement by *C. militaris*-derived polysaccharide *via* the up-regulation of PRRs/MAPK/NF-κ B signaling.

Of note, the *C. militaris*-derived glucogalactomannan, whose backbone is composed of →2) Man*p* (1→ and →6) Man*p* (1→ glycosyls, can also interact with PRRs, such as TLR2, TLR4, and dectin-1, and promotes the downstream MAPK/NF-κB

→4)-β-D-Glc*p*(1→2)-α-D-Man*p*(1→2)-α-D-Man*p*(1→2)-α-D-Man*p*(1→4)β-D-Glc*p*(1→4)β-D-Glc*p*(1→
↑6 ↑6 ↑6
1 CH₃ 1
[α-D-Man*p*]ₐ [β-D-Gal*f*]_b
↑2 ↑2
1 1
α-D-Man*p* β-D-Gal*f*

CM1: Mw=700 kDa
（Hu et al, 2019）

α-D-Glc-1{→6)-β-D-Glc*p*-(1→)ₙ6-β-DGlc*p*
Mw=18.2 kDa (Hu et al, 2019)

→3)-β-D-Glc*p*-(1→
(Smiderle et al., 2014)

(6←1)-β-L-Rha*p*-(3←1)-α-D-Glc*p*
↑ Mw=4.3 kDa
{→4)-α-D-Glc-(1→4)-α-D-Glc-(1→6)-α-D-Glc-(1→}ₙ (Jing et al, 2014)

(6←1)-α-L-Man-(2←1)-α-L-Man
↑
{→3)-α-D-Gal-(1→3)-α-D-Gal-(1→3)-α-D-Gal-(1→}ₙ Mw=9.3 kDa
(Jing et al, 2015)
Man-L-α-(1→5)-Ara-L-α-(1→6) (6←1)-β-L-Ara-(3←1)-α-L-Man

{→4)-β-D-Man*p*(1→6)-β-D-Man*p*(1→6)-α-D-Man*p*(1→4)-β-D-Man*p*(1→6)-β-D-Man*p*(1→6)-α-D-Man*p*(1→4)-β-D-Man*p*(1→}ₙ
↑4 ↑4
1 1
β-D-Gal*p*(1→2)-α-D-Man*p* β-D-Gal*f*→2)-β-D-Gal*f* Mw=25.2 kDa
↑6 or (Wang et al, 2021a)
CH₃ β-D-Gal*p*

{→4)-α-D-Glc*p*(1→4)-α-D-Glc*p*(1→4)-β-D-Glc*p*(1→4)-α-D-Glc*p*(1→4)-α-D-Glc*p*(1→}ₙ Mw=856.9 kDa
↑6 (Yang et al, 2021)
1
α-D-Glc*p*

{→4)-β-D-Man*p*(1→6)-β-D-Man*p*(1→6)-α-D-Man*p*(1→4)-β-D-Man*p*(1→6)-α-D-Man*p*(1→4)-β-D-Man*p*(1→6)-β-D-Man*p*(1→6)-α-D-Man*p*(1→}ₙ
↑4 ↑2 ↑4
1 1 1
α-D-Gal*f* β-D-Gal*p* β-D-Gal*p*
or or Mw=19.1kDa
β-D-Gal*f*(1→2)β-D-Gal*f* β-D-Gal*p*(1→2)-β-D-Gal*f* →4)-β-D-Glc*p* (Yang et al, 2021)
↑6
CH₃

[→2)-α-D-Man*p*-(1]ₐ→2)-α-D-Man*p*-(1→]_b (6←1)-β-D-Man*p*-(4←1)-β-D-Gal*p*
↑6
R {→3)-α-D-Glc*p*(1→6)-α-D-Glc*p*(1→3)-α-D-Glc*p*(1→}ₙ
R= [→2)-β-D-Gal*f*-(1]ₙ→G or [→6)-α-D-Man*p*-(1]ₙ→G ↓ Mw=5.8 kDa
G= α-D-Gal*f*1→ or α-D-Gal*p*(1→ (Bi et al, 2018)
a:b=5:3 Mw=19.3 kDa (Zhang et al, 2020) Gal*p*-D-β-(1←6)-Glc*p*-D-α-(1←6)
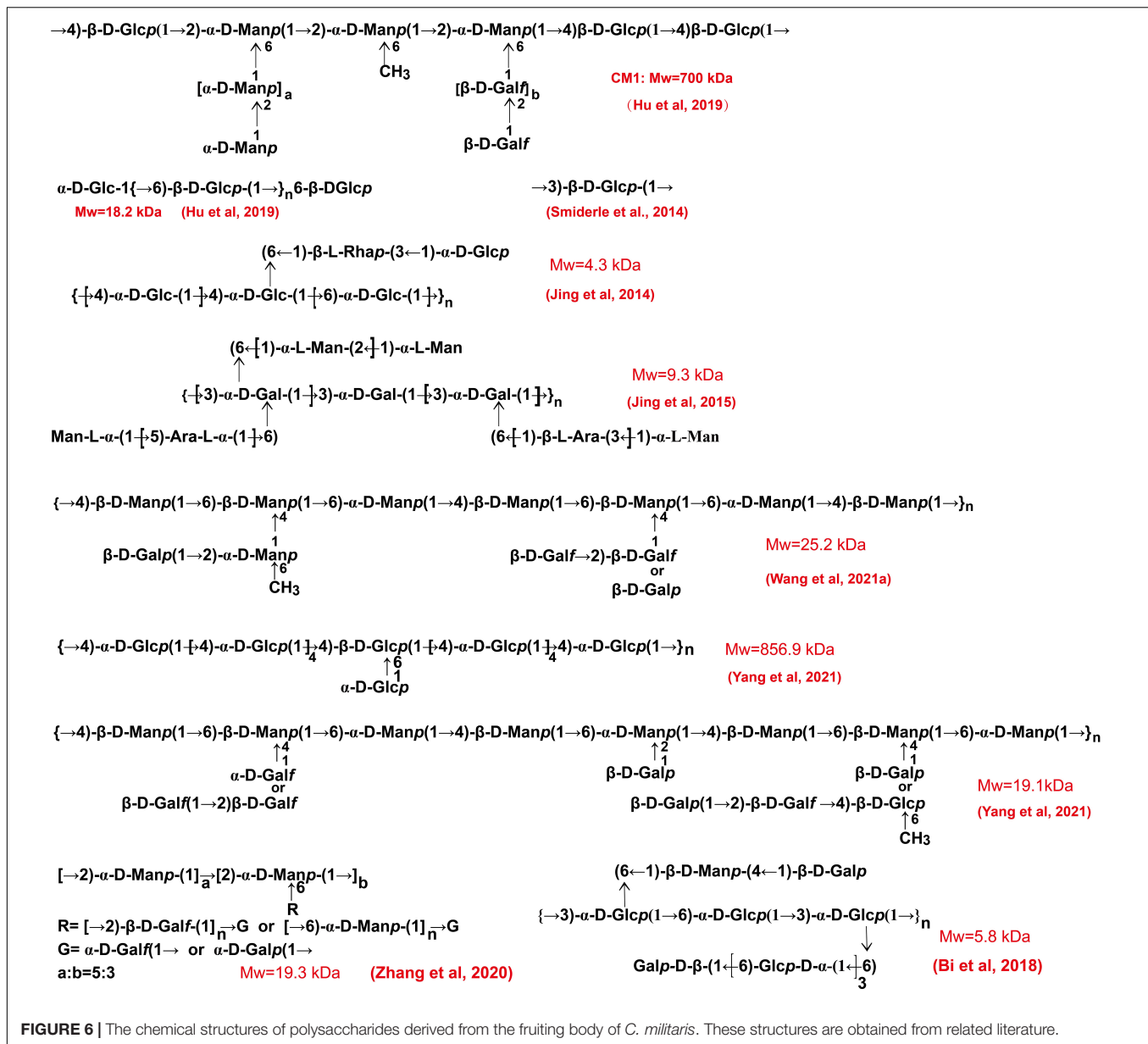3

FIGURE 6 | The chemical structures of polysaccharides derived from the fruiting body of *C. militaris*. These structures are obtained from related literature.

signaling pathway, thereby increasing production of NO, reactive oxygen species, and TNF-α, and enhancing phagocytic activity of RAW264.7 macrophages (13, 62, 86). In line with this study, the polysaccharide with →2)-α-D-Man*p* (1→ as its backbone shows immunomodulatory activity by promoting secretion of inflammatory factors by macrophages and inducing macrophage M1 polarization (19). Furthermore, the arabinogalactan-type polysaccharide obtained from the fruiting body of *C. militaris* can promote dendritic cell maturation through activation of TLR4, downstream MAPK signaling (phosphorylation of ERK, p38, and JNK) and NF-κB p50/p65, thereby increasing the expression of IL-12, IL-1β, TNF-α, and IFN-α/β (89). The acidic arabinogalactan-type polysaccharide consists of →5)-Ara*f*-(1→, →4)-Gal*p*-(1→, →4)-GalA*p*-(1→, and Ara*f* (1→ glycosyls can also enhance secretion of inflammatory cytokines and

improve production of nitric oxide (NO) by up-regulating the expression of inducible nitric oxide synthase in macrophages (90). Additionally, *C. militaris*-derived β-glucan can enhance macrophage activation and phagocytosis by increasing protein phosphorylation of Lyn, Syk, and MAPK (91).

Anti-inflammation

The recent review by Phull et al. largely reviewed the immune enhancement activity of *C. militaris*-derived polysaccharides rather than the anti-inflammatory effects (12). Here, we review the anti-inflammatory activity of these polysaccharides based on an analysis of the literature. Some polysaccharides of *C. militaris* are found to suppress secretion of eotaxin, IL-4, IL-5, IL-13, and IFN-γ, and reduce serum IgE level, inflammatory cell infiltration, and goblet cell hyperplasia by inhibiting transforming growth
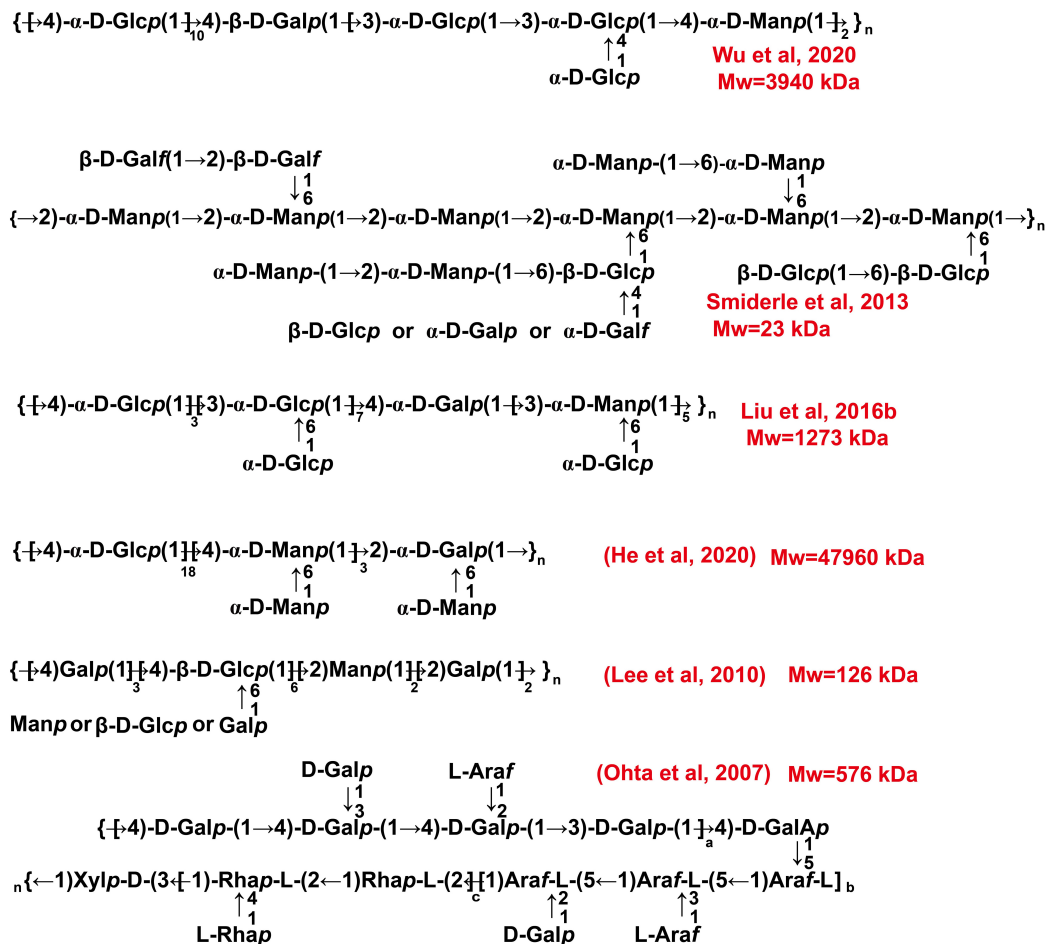
FIGURE 7 | The chemical structures of polysaccharides derived from the fruiting body of *C. militaris*. We presumed these structures according to the descriptions in the literature.

factor β1 (TGF-β1) and the phosphorylation of Smad2/3 proteins in ovalbumin challenged asthmatic mice (92). A recent study demonstrated that cordyceps polysaccharide can reduce acute liver injury by promoting hepatocyte proliferation, liver vascular regeneration, and liver tissue repair in line with the upregulation of vascular endothelial growth factor (VEGF), stromal cell-derived factor-1α, proliferating cell nuclear antigen, and signal regulatory protein α1, and the reduction of IL-18 and caspase-1 (93). Se-rich polysaccharides can effectively reduce inflammation by reducing the mRNA expression of TNF-α and IL-6 as well as serum content of LPS-binding proteins in C57BL/6J mice fed a high-fat diet (94). *C. militaris*-derived β-(1→3)-D-glucan can also inhibit LPS-induced mRNA expression of IL-1β, TNF-α, and cyclooxygenase 2 in THP-1 macrophages and reduce formalin-induced nociceptive response and leukocyte migration (76). Of note, gut microbiota also plays a key role in modulating inflammation. For instance, *Akkermansia* prefers to ingest polysaccharides as its nutritional source, and *A. muciniphila* is reported to suppress intestinal inflammation and improve gut barrier function (95). *C. militaris*-derived polysaccharides can increase the population of *Akkermansia* and

Lachnospiraceae_Eubacterium, and decrease the abundance of *Bacteroides*, *Parabacteroides*, and *Blautia*, thereby suppressing inflammation (96). A recent study demonstrated that *C. militaris* treatment downregulates the mucosal levels of pro-inflammatory cytokines and upregulates the levels of anti-inflammatory cytokines *via* inhibiting TLR4/MyD88/NF-κB signaling in pigs. Furthermore, this treatment also modulates gut microbiota and increases the concentrations of acetate and butyrate, thereby improving intestinal barrier function (97). Another study demonstrated that Cordyceps improves inflammation *via* modulating the abundance of *Enterococcus cecorum* (98).

Anti-hyperlipidemia and Anti-atherosclerosis

Polysaccharides obtained from mycelia and fruiting body of *C. militaris* can decrease total cholesterol (TC), triglyceride (TG), and low-density lipoprotein (LDL) cholesterol (LDL-C) levels and increase high density lipoprotein cholesterol (HDL-C) in streptozotocin-induced diabetic mice (99, 100). Crude polysaccharides from the fruiting body of *C. militaris* can
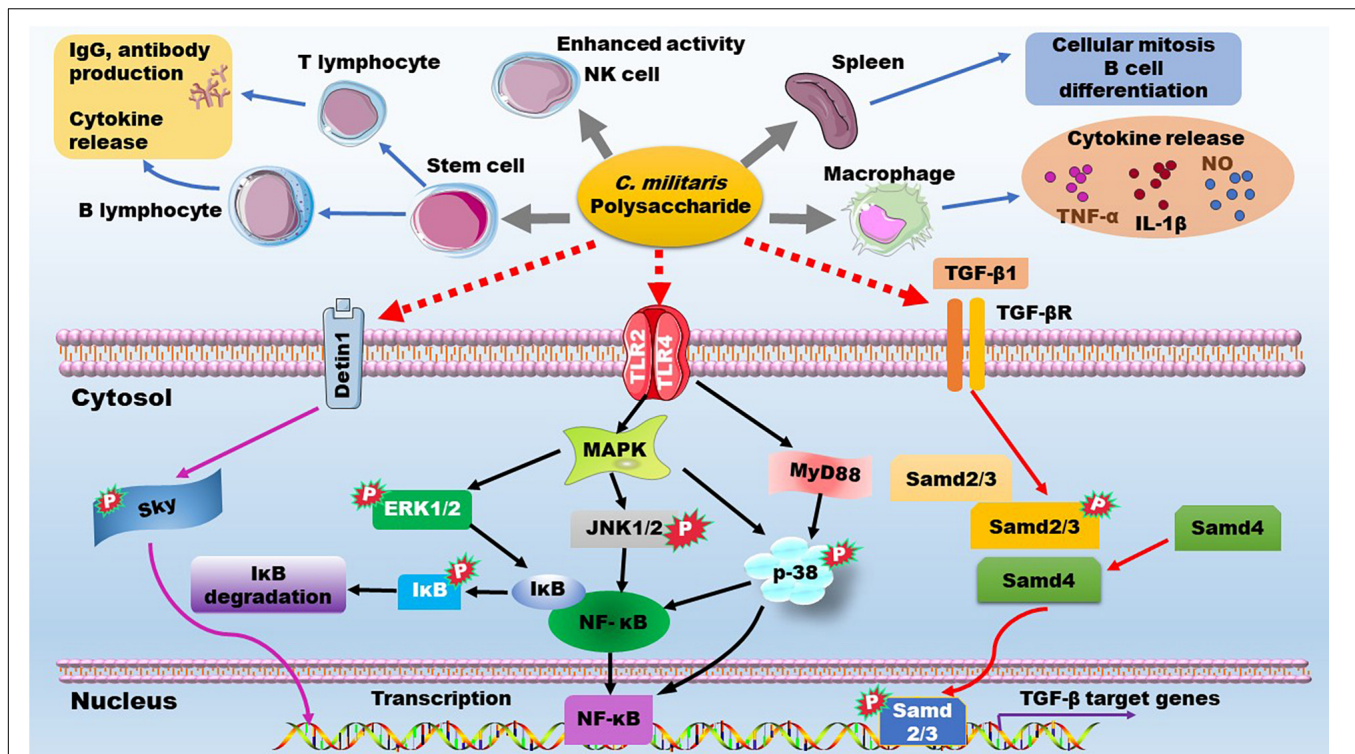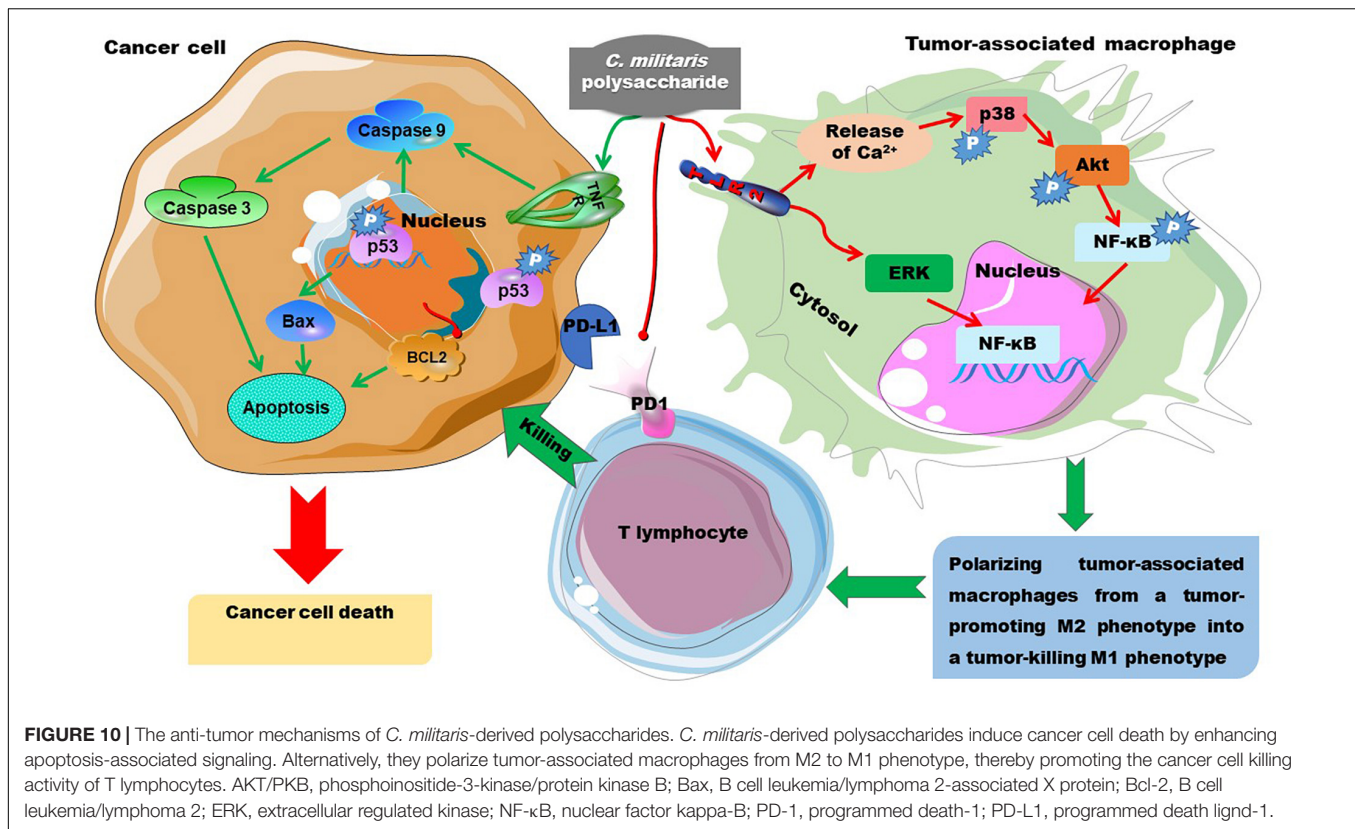
FIGURE 8 | The immune enhancement effects and the underlying mechanisms of *C. militaris*-derived polysaccharides. ERK, extracellular regulated kinase; IgG, immunoglobulin G; IL, interleukin; JNK, C-Jun Kinase; MAPK, mitogen-activated protein kinase; NF-κB, nuclear factor kappa-B; NK cell, natural killer cell; NO, nitric oxide; PRRs, pattern recognition receptors; TGF-β, transforming growth factor β; TGF-βR, TGR-β receptor; TLR, Toll-like receptor; TNF-α, tumor necrosis factor-α.

improve reverse cholesterol transport (RCT) in C57BL/6J mice (101). Furthermore, the →6)-β-D-Glc*p* (1→ linked glucan and the heteropolysaccharide (CM1) primarily consisting of →4)-β-D-Glc*p* (1→, →2)-α-D-Man*p* (1→, and →2,6)-α-D-Man*p* (1→ glycosyls, can improve cholesterol efflux *in vitro* (14). Recently, studies in our group demonstrated that CM1 can alleviate hyperlipidemia and adipocyte differentiation in LDLR$^{(\pm)}$ hamsters, whose lipid profiles are similar to human (102). Mechanistically, these polysaccharides are found to up-regulate genes and proteins related to RCT, such as liver X receptors and ATP-binding cassette (ABC) transporters (14, 15, 102). Low-density lipoprotein receptor (LDLR) plays a key role in the clearance of apolipoprotein (apo) B-containing lipoproteins in circulation, and proprotein convertase subtilisin/kexin-type 9 (PCSK9) plays a key role in post-translational degradation of LDLR (103). Our lab obtained a novel alkali-extracted polysaccharide from the fruiting body of *C. militaris* mainly composed of →4)-β-D-Man*p* (1→, →6)-β-D-Man*p* (1→, and →6)-α-D-Man*p* (1→ glycosyls, which can inhibit PCSK9 secretion in Huh7 cells (16). Additionally, Se-rich polysaccharide from *C. militaris* can effectively reduce serum TG and LDL-C by 51.5 and 44.1% in C57BL/6J mice, respectively (94). Mechanistically, this molecule can reduce adiponectin levels and decrease gut bacteria, such as *Dorea*, *Lactobacillus*, *Clostridium*, and *Ruminococcus*, that are negatively associated with obesity. Furthermore, it can increase mucosal beneficial

bacteria *Akkermansia*, and has no effect on the content of short-chain fatty acids (94, 104). A recent study demonstrated that Cordyceps may improve obesity *via* modulating the abundance of *Enterococcus cecorum* as well as bile acid metabolism (98). The lipid-lowering mechanisms of these polysaccharides are summarized in **Figure 9**.

Given that hyperlipidemia promotes the development of atherosclerosis, our group investigated the anti-atherosclerotic effects of the polysaccharides derived from *C. militaris*. As demonstrated in apoE$^{(-/-)}$ and LDLR$^{(-/-)}$ mice, the polysaccharide CM1 can significantly decrease atherosclerotic plaque formation in the aorta of these mice. Mechanistically, this molecule can improve the expression of RCT-related genes and proteins in the liver and small intestine of the mice (105). Integrated bioinformatics analysis suggested that these polysaccharides can modulate the expression of hundreds of genes. KEGG and GO enrichment demonstrated that these differentially expressed genes are associated with lipid metabolism, inflammation, oxidation, and shear stress (5). Of importance, these polysaccharides may modulate the lncRNA-miRNA-mRNA axis (6, 85). Additionally, the anti-atherosclerotic effect of these polysaccharides may also be attributed to their effect on the reduction of trimethylamine and oxidized trimethylamine *via* modulating gut bacteria (100). The mannan core and glycosyls in a β-configuration may play an important role in ameliorating atherosclerosis (105,

FIGURE 9 | The lipid-lowering mechanisms of *C. militaris*-derived polysaccharides. These polysaccharides are found to modulate multiple genes and proteins related to lipid absorption and metabolism in the plasma, small intestine, and liver, thereby improving hyperlipidemia and atherosclerosis. ABC, ATP-binding cassette; Apo, apolipoprotein; CRM, chylomicron remnant; FFA, free fatty acid; HSPG, heparan sulfate proteoglycan; IDL, intermediate density lipoprotein; LDL, low-density lipoprotein; LDLR, low-density lipoprotein receptor; LRP1, LDLR-related protein 1; LXRα, liver X receptor α; NPC1L1, Niemann-Pick C1-like protein 1; SR-B1, scavenger receptor B type 1; SREBP, sterol regulatory element-binding protein; VLDL, very low-density lipoprotein.

106). Of note, the TG-lowering effect of *C. militaris*-derived polysaccharides is better than their TC-lowering effect (5, 15, 102, 107). It is known that there is a positive correlation between plasma TG and cardiovascular disease (CVD) (108, 109). These data suggest that *C. militaris*-derived polysaccharides have a potential application in prevention of CVD as TG-lowering compounds.

Anti-diabetic Activity

In streptozotocin-induced diabetic mice, the mycelia polysaccharide increases body weight and thymus index and decreases fasting blood glucose, insulin resistance as well as secretion of pro-inflammatory cytokines (TNF-α and IL-6) and C-reactive protein (99). The purified polysaccharide CBPS-II with a Mw of 1,273 kDa can reduce blood Glc level in streptozotocin-induced diabetic mice (100). The acid-extracted heteropolysaccharide mainly composed of glucose (88.4%) also showed good hypoglycemic effect in type 2 diabetes mice that were induced by a high-fat diet and streptozotocin (77). Of note, the heteropolysaccharide that is primarily composed of →4)-α-D-Glc*p* (1→, →3,6)-α-D-Man*p* (1→, and →4)-α-D-Man*p* (1→ glycosyls can improve glucose tolerance in STZ-induced diabetic mice, and this activity may be related to an inhibitory effect on alpha-glucosidase (59). Several other labs have also demonstrated that polysaccharides from *C. militaris* can inhibit the activity of alpha-glucosidase (110). It seems that

polysaccharides from the fruiting bodies have a better effect on inhibition of alpha-glucosidase than those from fermentation mycelia (65). Furthermore, carboxymethylation and acetylation of these polysaccharides may enhance their inhibitory effects on alpha-glucosidase (111). *C. militaris*-derived polysaccharides can also protect diabetic nephropathy in mice by regulating cell autophagy (112). Additionally, the anti-hyperglycemic effect of *C. militaris*-derived polysaccharides can be partially attributed to its effect on promoting *Akkermansia*, a beneficial bacterium in the gut (96).

Antitumor Activity

The antitumor activity of *C. militaris*-derived polysaccharides has been summarized by Zhang et al. (3) and Gu et al. (7). Here, we have tried to elucidate the potential structure-activity relationship of these polysaccharides. Moreover, the potential antitumor mechanisms of these polysaccharides are summarized in **Figure 10**. Polysaccharides obtained from mycelia can attenuate doxorubicin-induced cytotoxic effects during chemotherapy (85). Polysaccharides from mycelia (CMPS-II) seem to have a better effect than that obtained from the fruiting body (CBPS-II). CMPS-II and CBPS-II can up-regulate the expression of apoptosis factors including Caspase-3, Caspase-9, and p53, and down-regulating proliferating cell nuclear antigen (64). These two 1,3-branched-galactomannoglucans with triple-helical chains have similar Mw (1.2–1.4 kDa) and the

FIGURE 10 | The anti-tumor mechanisms of *C. militaris*-derived polysaccharides. *C. militaris*-derived polysaccharides induce cancer cell death by enhancing apoptosis-associated signaling. Alternatively, they polarize tumor-associated macrophages from M2 to M1 phenotype, thereby promoting the cancer cell killing activity of T lymphocytes. AKT/PKB, phosphoinositide-3-kinase/protein kinase B; Bax, B cell leukemia/lymphoma 2-associated X protein; Bcl-2, B cell leukemia/lymphoma 2; ERK, extracellular regulated kinase; NF-κB, nuclear factor kappa-B; PD-1, programmed death-1; PD-L1, programmed death lignd-1.

same backbone of →4)-α-D-Glc$p$ (1→ glycosyls. However, CMPS-II has significantly more Glc than CBPS-II, suggesting that the branched →4)-α-D-Glc$p$ (1→ glycosyls may facilitate the antitumor activity of these polysaccharides. Our team recently demonstrated that the branched glucans primarily consisting of →4)-α-D-Glc$p$ (1→ glycosyls can inhibit the proliferation of tumor cells (113). A previous study also demonstrated that water-extracted *C. militaris* polysaccharide, largely composed of →4)-α-D-Glc$p$ (1→, →6)-β-D-Glc$p$ (1→, and →4)-β-D-Glc$p$ (1→ glycosyls, inhibits the proliferation of several tumor cell lines *in vitro* (72). Additionally, a recent study demonstrated that the alkaline-extracted polysaccharides mostly composed of →6)-α-D-Glc$p$ (1→ and →3)-α-D-Glc$p$ (1→ glycosyls shows anti-tumor effects though the modulation of tumor-associated macrophages, which inhibit the killing effect of T lymphocytes on tumor cells through the programmed death lignd-1/programmed death-1 axis (114). Mechanistically, this molecule binds to TLR2, causes release of Ca^{2+} and activation of p38, AKT, and NF-κB, thereby polarizing tumor-associated macrophages from a tumor-promoting M2 phenotype into a tumor-killing M1 phenotype (114). Furthermore, Se-polysaccharides with a backbone of →4) Glc$p$ (1→ glycosyl exhibit an appreciable antitumor effect *in vitro*, and the polysaccharides with a lower Mw (65 and 16 kDa) have better activity than the one with a higher Mw of 1,902 kDa (63). The above data indicate that the glucosyls in the α-D-configuration play a key role in the anti-tumor activity of *C. militaris*-derived polysaccharides.

Others

Addition of *C. militaris* in diet is reported to improve physical fatigue in mice (115). The crude polysaccharide derived from the fruiting body of *C. militaris* has good anti-fatigue activity (116). One exopolysaccharide exhibits hypouricemic effect in mice by decreasing urate production and the activity of xanthine oxidase (117). The presence of sulfate and polygalacturonic acids endow *C. militaris* polysaccharide with anti-angiogenesis activity *via* reducing the protein expression of VEGF in human umbilical vein endothelial cells (53). A acidic polysaccharide that mainly composed of →6)Gal$p$(1→, →4)Glc$p$ (1→, and →4,6)Glc$p$(1→ glycosyls can prevent Pb^{2+}-induced liver and kidney toxicity by activating nuclear factor erythroid 2-related factor 2 (Nrf2) signaling pathway and increasing bacterial diversity of gut microbiota (83). Mechanistically, it enhances the protein expression of Nrf2, Kelch-like ECH-associated protein-1, Heme oxygenase, and NAD(P)H: quinone oxidoreductase 1. Furthermore, this polysaccharide promotes the abundance of *Ruminococcaceae* and reduces the abundance of *Lachnospiraceae* families; it reduces *Roseburia* and increases *Bacteroides* genera (83). The exopolysaccharide Cs-HK1 with a high Mw can protect bifidobacterial cells against antibiotics through physical interactions (118). *C. militaris* is found to modulate the formation of short-chain fatty acids (97, 119). Additionally, the acidic arabinogalactan-type polysaccharide obtained from mycelia can reduce virus titer of mice infected with influenza A virus (90). *C. militaris* may also have a potential application for the treatment of mild-to-moderate COVID-19 disease (120).

Comparisons With Other Studies and What Does the Current Work Add to the Existing Knowledge

Recently, the research involving *C. militaris*-derived polysaccharides has increased rapidly, particularly in their structural characterization and pharmaceutical activities. The pharmaceutical effects of these polysaccharides including antioxidant, immunomodulatory, and anti-tumor activities have been widely reviewed (7, 12). However, the structural characteristics of polysaccharides and the related methods used for elucidating these polysaccharides have not been reviewed in the recent literature. Given that the structure of polysaccharide determines its bioactivity, we describe the methods used for elucidation of polysaccharide structure in this article. Of note, most of the chemical methods are described by presenting the detailed chemical reactions, which are helpful in understanding the principle behind the processes. The development of novel techniques including mass spectrometry are also discussed in this article. Of importance, we review the structural characteristics of *C. militaris*-derived polysaccharides in the format of presumed chemical structure and have discussed the potential structure-activity relationship. The mechanisms of action of these polysaccharides are presented by constructing the signaling pathways as seen in the figures. Furthermore, the anti-diabetic, anti-hyperlipidemic, anti-atherosclerotic, and gut microbiota modulatory effects that have not been elucidated well in previous reviews in the literature are also summarized in this article. This detailed review focuses on polysaccharide structure and bioactivity and makes it possible to discuss and understand the structure-activity relationship of *C. militaris*-derived polysaccharides. It is found that different glycosyls and functional groups may play distinct roles in the bioactive functions of these polysaccharides.

CONCLUSION AND FUTURE PERSPECTIVE

The widespread use of advanced analysis tools such as HPLC, MS, and NMR techniques has greatly improved the structural elucidation of *C. militaris*-derived polysaccharides. Most of the reported heteropolysaccharides have mannosyls, such as →2)-α-D-Man*p* (1→, →6)-α-D-Man*p* (1→, or →6)-β-D-Man*p* (1→ glycosyls, as their core. The obtained glucans are found to consist of →4)-α-D-Glc*p* (1→, →6)-α-D-Glc*p* (1→, or →3)-β-D-Glc*p* (1→ glycosyls as their backbone. Recently developed novel techniques, such as mass spectrometry imaging and the novel NMR methods, are definitely going to improve our understanding of the structure of *C. militaris*-derived polysaccharides in the future. *C. militaris*-derived polysaccharides can modulate multiple signaling pathways and have great potential for use as dietary supplements and health food products for the prevention and treatment of oxidation, inflammation, tumors, immune dysfunction, and metabolic syndrome. The glucosyls in a β-configuration, →2)-α-D-Man*p* (1→ linked backbone, metal ions, and acid groups, may all

contribute to the antioxidant activity of these polysaccharides. The α-D-glucosyls and α-D-mannosyls mainly contribute to the immune enhancing activity, while the β-D linked glycosyls and α-D-mannosyls may facilitate the hypolipidemic and anti-atherosclerotic effects. Additionally, the branched →4)-α-D-Glc*p* (1→, →6)-α-D-Glc*p* (1→, and →3)-α-D-Glc*p* (1→ glycosyls may enable the anti-tumor effect of *C. militaris*-derived polysaccharides.

The high-frequency degeneration of *C. militaris* during cultivation has limited the development of the *C. militaris* industry (9). Gene engineering strategies are expected to further improve the yield of *C. militaris*-derived polysaccharides. The structural characteristics, including Mw, monosaccharide composition, glycosyl linkage, glycosyl configuration, physicochemical properties, and even the animal models and cultivation conditions of *C. militaris* may influence their bioactivity. Therefore, standardized procedures are needed to guarantee the quality of *C. miliatris*-derived polysaccharides. The focus of the standardization procedures should be on cover strain preservation, cultivation conditions, extraction and purification methods, quality control, and impurity detection. The recent studies using purified polysaccharides have greatly improved our understanding of their structure-activity relationships. However, we still do not know the functional groups and/or bioactive domains due to lack of comparative studies. To improve this, researchers may design parallel experiments to evaluate the activity and/or the underlying mechanisms of polysaccharides of interest containing different backbones or differently digested polysaccharides with the same backbone or polysaccharides with different chemical modifications. Furthermore, given the large Mw of these polysaccharides, they may have little change of directly entering the circulation. One possible mechanism is that these molecules can exert their bioactivity *via* modulating gut microbiota and their metabolites, which can easily penetrate the intestinal barrier and then work within the circulation. Another possibility is that the polysaccharides digested by the gastric acid or gut microbiota with a lower Mw or the corresponding oligosaccharides may be directly absorbed by the intestine, thereby exerting their bioactivities in different organs. The polysaccharides that are resistant to degradation *in vivo* may either act directly on receptors in the gut or work through mechanisms involving physical binding. These ideas need to be investigated further in future studies.

AUTHOR CONTRIBUTIONS

MM, W-QY, YL, and Y-LS performed reference collection. MM, W-QY, and YL drew the figures. S-DG wrote and re-edited the manuscript. All authors contributed to the article and approved the submitted version.

FUNDING

REFERENCES

1. Olatunji OJ, Tang J, Tola A, Auberon F, Oluwaniyi O, Ouyang Z. The genus *Cordyceps*: an extensive review of its traditional uses, phytochemistry and pharmacology. *Fitoterapia.* (2018) 129:293–316. doi: 10.1016/j.fitote.2018.05.010

2. Wu X, Wu T, Huang A, Shen Y, Zhang X, Song W, et al. New insights into the biosynthesis of typical bioactive components in the traditional Chinese medicinal fungus *Cordyceps militaris*. *Front Bioeng Biotechnol.* (2021) 9:801721. doi: 10.3389/fbioe.2021.801721

3. Zhang J, Wen C, Duan Y, Zhang H, Ma H. Advance in *Cordyceps militaris* (Linn) link polysaccharides: isolation, structure, and bioactivities: a review. *Int J Biol Macromol.* (2019) 132:906–14. doi: 10.1016/j.ijbiomac.2019.04.020

4. Cao C, Yang S, Zhou Z. The potential application of *Cordyceps* in metabolic-related disorders. *Phytother Res.* (2020) 34:295–305. doi: 10.1002/ptr.6536

5. Lin P, Yin F, Shen N, Liu N, Zhang BH, Li Y, et al. Integrated bioinformatics analysis of the anti-atherosclerotic mechanisms of the polysaccharide CM1 from *Cordyceps militaris*. *Int J Biol Macromol.* (2021) 193:1274–85. doi: 10.1016/j.ijbiomac.2021.10.175

6. Li Y, Miao M, Yin F, Shen N, Yu WQ, Guo SD. The polysaccharide-peptide complex from mushroom *Cordyceps militaris* ameliorates atherosclerosis by modulating the lncRNA-miRNA-mRNA axis. *Food Funct.* (2022) 13:3185–97. doi: 10.1039/d1fo03285b

7. Gu C, Zhang D, Zhai W, Zhang H, Wang S, Lv S, et al. Research progress on *Cordyceps militaris* polysaccharides. *Food Biosci.* (2022) 45:101503. doi: 10.1016/j.fbio.2021.101503

8. Dong Y, Hu S, Liu C, Meng Q, Song J, Lu J, et al. Purification of polysaccharides from *Cordyceps militaris* and their anti-hypoxic effect. *Mol Med Rep.* (2015) 11:1312–7. doi: 10.3892/mmr.2014.2786

9. Lou H, Lin J, Guo L, Wang X, Tian S, Liu C, et al. Advances in research on *Cordyceps militaris* degeneration. *Appl Microbiol Biotechnol.* (2019) 103:7835–41. doi: 10.1007/s00253-019-10074-z

10. Lee CT, Huang KS, Shaw JF, Chen JR, Kuo WS, Shen G, et al. Trends in the immunomodulatory effects of *Cordyceps militaris*: total extracts, polysaccharides and cordycepin. *Front Pharmacol.* (2020) 11:575704. doi: 10.3389/fphar.2020.575704

11. Jędrejko KJ, Lazur J, Muszyńska B. *Cordyceps militaris*: an overview of its chemical constituents in relation to biological activity. *Foods.* (2021) 10:2634. doi: 10.3390/foods10112634

12. Phull AR, Ahmed M, Park HJ. *Cordyceps militaris* as a bio functional food source: pharmacological potential, anti-inflammatory actions and related molecular mechanisms. *Microorganisms.* (2022) 10:405. doi: 10.3390/microorganisms10020405

13. Luo X, Duan Y, Yang W, Zhang H, Li C, Zhang J. Structural elucidation and immunostimulatory activity of polysaccharide isolated by subcritical water extraction from *Cordyceps militaris*. *Carbohydr Polym.* (2017) 157:794–802. doi: 10.1016/j.carbpol.2016.10.066

14. Hu S, Wang J, Li F, Hou P, Yin J, Yang Z, et al. Structural characterisation and cholesterol efflux improving capacity of the novel polysaccharides from *Cordyceps militaris*. *Int J Biol Macromol.* (2019) 131:264–72. doi: 10.1016/j.ijbiomac.2019.03.078

15. Yang X, Lin P, Wang J, Liu N, Yin F, Shen N, et al. Purification, characterization and anti-atherosclerotic effects of the polysaccharides from the fruiting body of *Cordyceps militaris*. *Int J Biol Macromol.* (2021) 181:890–904. doi: 10.1016/j.ijbiomac.2021.04.083

16. Wang J, Wang Y, Yang X, Lin P, Liu N, Li X, et al. Purification, structural characterization, and PCSK9 secretion inhibitory effect of the novel alkali-extracted polysaccharide from *Cordyceps militaris*. *Int J Biol Macromol.* (2021) 179:407–17. doi: 10.1016/j.ijbiomac.2021.02.191

17. Zhao J, Xie J, Li SP. Advanced development in chemical analysis of *Cordyceps*. *J Pharmaceut Biomed Anal.* (2014) 87:271–89. doi: 10.1016/j.jpba.2013.04.025

18. Zhao J, Deng Y, Li SP. Advanced analysis of polysaccharides, novel functional components in food and medicine dual purposes Chinese herbs. *Trends Analyt Chem.* (2017) 96:138–50. doi: 10.1016/j.trac.2017.06.006

19. Zhang Y, Zeng Y, Cui Y, Liu H, Dong C, Sun Y. Structural characterization, antioxidant and immunomodulatory activities of a neutral polysaccharide from *Cordyceps militaris* cultivated on hull-less barley. *Carbohydr Polym.* (2020) 235:115969. doi: 10.1016/j.carbpol.2020.115969

20. Li Y, Liang J, Gao JN, Shen Y, Kuang HX, Xia YG. A novel LC-MS/MS method for complete composition analysis of polysaccharides by aldononitrile acetate and multiple reaction monitoring. *Carbohydr Polym.* (2021) 272:118478. doi: 10.1016/j.carbpol.2021.118478

21. Leontein K, Lindberg B, Lönngren J. Assignment of absolute configuration of sugars by g.l.c. of their acetylated glycosides from chiral alcohols. *Carbohydr Res.* (1978) 62:359–62. doi: 10.1016/s0008-6215(00)80882-4

22. Liu XC, Zhu ZY, Tang YL, Wang MF, Wang Z, Liu AJ, et al. Structural properties of polysaccharides from cultivated fruit bodies and mycelium of *Cordyceps militaris*. *Carbohydr Polym.* (2016) 142:63–72. doi: 10.1016/j.carbpol.2016.01.040

23. Galermo AG, Nandita E, Barboza M, Amicucci MJ, Vo T-TT, Lebrilla CB. Liquid chromatography-tandem mass spectrometry approach for determining glycosidic linkages. *Anal Chem.* (2018) 90:13073–80. doi: 10.1021/acs.analchem.8b04124

24. Novakovic M, Kupče Ē, Oxenfarth A, Battistel MD, Freedberg DI, Schwalbe H, et al. Sensitivity enhancement of homonuclear multidimensional NMR correlations for labile sites in proteins, polysaccharides, and nucleic acids. *Nat Commun.* (2020) 11:5317. doi: 10.1038/s41467-020-19108-x

25. Matsumori N, Kaneno D, Murata M, Nakamura H, Tachibana K. Stereochemical determination of acyclic structures based on carbon-proton spin-coupling constants. a method of configuration analysis for natural products. *J Org Chem.* (1999) 64:866–76. doi: 10.1021/jo981810k

26. Guo S, Mao W, Yan M, Zhao C, Li N, Shan J, et al. Galactomannan with novel structure produced by the coral endophytic fungus *Aspergillus ochraceus*. *Carbohydr Polym.* (2014) 105:325–33. doi: 10.1016/j.carbpol.2014.01.079

27. Gimeno A, Valverde P, Ardá A, Jiménez-Barbero J. Glycan structures and their interactions with proteins. a NMR view. *Curr Opin Struc Biol.* (2020) 62:22–30. doi: 10.1016/j.sbi.2019.11.004

28. Nokab MEHE, van der Wel PCA. Use of solid-state NMR spectroscopy for investigating polysaccharide-based hydrogels: a review. *Carbohydr Polym.* (2020) 240:116276. doi: 10.1016/j.carbpol.2020.116276

29. Chakraborty A, Deligey F, Quach J, Mentink-Vigier F, Wang P, Wang T. Biomolecular complex viewed by dynamic nuclear polarization solid-state NMR spectroscopy. *Biochem Soc Trans.* (2020) 48:1089–99. doi: 10.1042/BST20191084

30. Poulhazan A, Dichwella Widanage MC, Muszyński A, Arnold AA, Warschawski DE, Azadi P, et al. Identification and quantification of glycans in whole cells: architecture of microalgal polysaccharides described by solid-state nuclear magnetic resonance. *J Am Chem Soc.* (2021) 143:19374–88. doi: 10.1021/jacs.1c07429

31. Zhao W, Kirui A, Deligey F, Mentink-Vigier F, Zhou Y, Zhang B, et al. Solid-state NMR of unlabeled plant cell walls: high-resolution structural analysis without isotopic enrichment. *Biotechnol Biofuels.* (2021) 14:14. doi: 10.1186/s13068-020-01858-x

32. Reif B, Ashbrook AE, Emsley L, Hong M. Solid-state NMR spectroscopy. *Nat Rev Methods Primers.* (2021) 1:2. doi: 10.1038/s43586-020-00002-1

33. Zhao W, Fernando LD, Kirui A, Deligey F, Wang T. Solid-state NMR of plant and fungal cell walls: a critical review. *Solid State Nucl Magn Reson.* (2020) 107:101660. doi: 10.1016/j.ssnmr.2020.101660

34. Gao Y, Mortimer JC. Unlocking the architecture of native plant cell walls via solid-state nuclear magnetic resonance. *Methods Cell Biol.* (2020) 160:121–43. doi: 10.1016/bs.mcb.2020.05.001

35. Jing Y, Zhu J, Liu T, Bi S, Hu X, Chen Z, et al. Structural characterization and biological activities of a novel polysaccharide from cultured *Cordyceps militaris* and its sulfated derivative. *J Agric Food Chem.* (2015) 63:3464–71. doi: 10.1021/jf505915t

36. Wu DT, Cheong KL, Wang LY, Lv GP, Ju YJ, Feng K, et al. Characterization and discrimination of polysaccharides from different species of *Cordyceps* using saccharide mapping based on PACE and HPTLC. *Carbohydr Polym.* (2014) 103:100–9. doi: 10.1016/j.carbpol.2013.12.034

37. Xiao K, Han Y, Yang H, Lu H, Tian Z. Mass spectrometry-based qualitative and quantitative N-glycomics: an update of 2017-2018. *Anal Chim Acta.* (2019) 1091:1–22. doi: 10.1016/j.aca.2019.10.007

38. Zhou S, Dong X, Veillon L, Huang Y, Mechref Y. LC-MS/MS analysis of permethylated N-glycans facilitating isomeric characterization. *Anal Bioanal Chem.* (2017) 409:453–66. doi: 10.1007/s00216-016-9996-8

39. Domon B, Costello CE. A systematic nomenclature for carbohydrate fragmentations in FAB-MS/MS spectra of glycoconjugates. *Glycoconjugate J.* (1988) 5:397–409. doi: 10.1007/bf01049915

40. Wu J, Wei J, Chopra P, Boons GJ, Lin C, Zaia J. Sequencing heparan sulfate using HILIC LC-NETD-MS/MS. *Anal Chem.* (2019) 91:11738–46. doi: 10.1021/acs.analchem.9b02313

41. Pismennõi D, Kiritsenko V, Marhivka J, Kütt ML, Vilu R. Development and optimisation of HILIC-LC-MS method for determination of carbohydrates in fermentation samples. *Molecules.* (2021) 26:3669. doi: 10.3390/molecules26123669

42. Mustafa S, Mobashir M. LC-MS and docking profiling reveals potential difference between the pure and crude fucoidan metabolites. *Int J Biol Macromol.* (2020) 143:11–29. doi: 10.1016/j.ijbiomac.2019.11.232

43. Lin X, Xiao C, Ling L, Guo L, Guo X. A dual-mode reactive matrix for sensitive and quantitative analysis of carbohydrate by MALDI-TOF MS. *Talanta.* (2021) 235:122792. doi: 10.1016/j.talanta.2021.122792

44. Zhan L, Huang X, Xue J, Liu H, Xiong C, Wang J, et al. MALDI-TOF/TOF tandem mass spectrometry imaging reveals non-uniform distribution of disaccharide isomers in plant tissues. *Food Chem.* (2021) 338:127984. doi: 10.1016/j.foodchem.2020.127984

45. Liu QB, Lu JG, Jiang ZH, Zhang W, Li WJ, Qian ZM, et al. In situ chemical profiling and imaging of cultured and natural *Cordyceps sinensis* by TOF-SIMS. *Front Chem.* (2022) 10:862007. doi: 10.3389/fchem.2022.862007

46. Du H, Yu H, Yang F, Li Z. Comprehensive analysis of glycosphingolipid glycans by lectin microarrays and MALDI-TOF mass spectrometry. *Nat Protoc.* (2021) 16:3470–91. doi: 10.1038/s41596-021-00544-y

47. Yang S, Yang X, Zhang H. Extracellular polysaccharide biosynthesis in *Cordyceps. Crit Rev Microbiol.* (2020) 46:359–80. doi: 10.1080/1040841X.2020.1794788

48. Wang CC, Wu JY, Chang CY, Yu ST, Liu YC. Enhanced exopolysaccharide production by *Cordyceps militaris* using repeated batch cultivation. *J Biosci Bioeng.* (2019) 127:499–505. doi: 10.1016/j.jbiosc.2018.09.006

49. Huang SJ, Huang FK, Li YS, Tsai SY. The quality improvement of solid-state fermentation with *Cordyceps militaris* by UVB irradiation. *Food Technol Biotechnol.* (2017) 55:445–53. doi: 10.17113/ftb.55.04.17.5235

50. Huang SJ, Huang FK, Purwidyantri A, Rahmandita A, Tsai SY. Effect of pulsed light irradiation on bioactive, nonvolatile components and antioxidant properties of Caterpillar medicinal mushroom *Cordyceps militaris* (Ascomycetes). *Int J Med Mushrooms.* (2017) 19:547–60. doi: 10.1615/IntJMedMushrooms.v19.i6.60

51. Cui JD, Zhang YN. Evaluation of metal ions and surfactants effect on cell growth and exopolysaccharide production in two-stage submerged culture of *Cordyceps militaris. Appl Biochem Biotechnol.* (2012) 168:1394–404. doi: 10.1007/s12010-012-9865-7

52. Lin S, Liu ZQ, Baker PJ, Yi M, Wu H, Xu F, et al. Enhancement of cordyceps polysaccharide production via biosynthetic pathway analysis in Hirsutella sinensis. *Int J Bio Macromol.* (2016) 92:872–80. doi: 10.1016/j.ijbiomac.2016.08.002

53. Zeng Y, Han Z, Qiu P, Zhou Z, Tang Y, Zhao Y, et al. Salinity-induced anti-Angiogenesis activities and structural changes of the polysaccharides from cultured *Cordyceps militaris. PLoS One.* (2014) 9:e103880. doi: 10.1371/journal.pone.0103880

54. Zhang X, Zhang X, Gu S, Pan L, Sun H, Gong E, et al. Structure analysis and antioxidant activity of polysaccharide-iron (III) from *Cordyceps militaris* mycelia. *Int J Biol Macromol.* (2021) 178:170–9. doi: 10.1016/j.ijbiomac.2021.02.163

55. Liu Y, Li Y, Zhang H, Li C, Zhang Z, Liu A, et al. Polysaccharides from *Cordyceps miltaris* cultured at different pH: Sugar composition and antioxidant activity. *Int J Biol Macromol.* (2020) 162:349–58. doi: 10.1016/j.ijbiomac.2020.06.182

56. Wang Y, Yang X, Chen P, Yang S, Zhang H. Homologous overexpression of genes in *Cordyceps militaris* improves the production of polysaccharides. *Food Res Int.* (2021) 147:110452. doi: 10.1016/j.foodres.2021.110452

57. Luo L, Zhou J, Xu Z, Guan J, Gao Y, Zou X. Identification and functional analysis of bacteria in sclerotia of *Cordyceps militaris. Peer J.* (2021) 9:e12511. doi: 10.7717/peerj.12511

58. Tong LL, Wang Y, Yuan L, Liu MZ, Du YH, Mu XY, et al. Enhancement of polysaccharides production using microparticle enhanced technology by *Paraisaria dubia. Microb Cell Fact.* (2022) 21:12. doi: 10.1186/s12934-021-01733-w

59. Sun H, Yu X, Li T, Zhu Z. Structure and hypoglycemic activity of a novel exopolysaccharide of *Cordyceps militaris. Int J Biol Macromol.* (2021) 166:496–508. doi: 10.1016/j.ijbiomac.2020.10.207

60. Song Q, Zhu Z. Chemical structure and mechanism of polysaccharide on Pb(2+) tolerance of *Cordyceps militaris* after Pb(2+) domestication. *Int J Biol Macromol.* (2020) 165:958–69. doi: 10.1016/j.ijbiomac.2020.09.243

61. Yu Y, Wen Q, Song A, Liu Y, Wang F, Jiang B. Isolation and immune activity of a new acidic *Cordyceps militaris* exopolysaccharide. *Int J Biol Macromol.* (2022) 194:706–14. doi: 10.1016/j.ijbiomac.2021.11.115

62. Lee JS, Kwon JS, Won DP, Lee JH, Lee KE, Lee SY, et al. Study of macrophage activation and structural characteristics of purified polysaccharide from the fruiting body of *Cordyceps militaris. J Microbiol Biotechnol.* (2010) 20:1053–60. doi: 10.4014/jmb.0910.10022

63. Liu F, Zhu ZY, Sun X, Gao H, Zhang YM. The preparation of three selenium-containing *Cordyceps militaris* polysaccharides: characterization and anti-tumor activities. *Int J Biol Macromol.* (2017) 99:196–204. doi: 10.1016/j.ijbiomac.2017.02.064

64. Liu XC, Zhu ZY, Liu YL, Sun HQ. Comparisons of the anti-tumor activity of polysaccharides from fermented mycelia and cultivated fruiting bodies of *Cordyceps militaris* in vitro. *Int J Biol Macromol.* (2019) 130:307–14. doi: 10.1016/j.ijbiomac.2019.02.155

65. Wu L, Sun H, Hao Y, Zheng X, Song Q, Dai S, et al. Chemical structure and inhibition on alpha-glucosidase of the polysaccharides from *Cordyceps militaris* with different developmental stages. *Int J Biol Macromol.* (2020) 148:722–36. doi: 10.1016/j.ijbiomac.2020.01.178

66. Wu CY, Liang ZC, Tseng CY, Hu SH. Effects of illumination pattern during cultivation of fruiting body and bioactive compound production by the Caterpillar medicinal mushroom, *Cordyceps militaris* (Ascomycetes). *Int J Med Mushrooms.* (2016) 18:589–97. doi: 10.1615/intjmedmushrooms.v18.i7.40

67. Lin LZ, Wei T, Yin L, Zou Y, Bai WF, Ye ZW, et al. An efficient strategy for enhancement of bioactive compounds in the fruit body of Caterpillar medicinal mushroom, *Cordyceps militaris* (Ascomycetes), by spraying biotic elicitors. *Int J Med Mushrooms.* (2020) 22:1161–70. doi: 10.1615/IntJMedMushrooms.2020037155

68. Zhu L, Zhang H, Liu Y, Zhang JS, Gao X, Tang Q. Effect of culture time on the bioactive components in the fruit bodies of Caterpillar mushroom, *Cordyceps militaris* CM-H0810 (Ascomycetes). *Int J Med Mushrooms.* (2019) 21:1107–14. doi: 10.1615/IntJMedMushrooms.2019032704

69. Yoo CH, Sadat MA, Kim W, Park TS, Park DK, Choi J. Comprehensive transcriptomic analysis of *Cordyceps militaris* cultivated on germinated soybeans. *Mycobiology.* (2022) 50:1–11. doi: 10.1080/12298093.2022.2035906

70. Li LF, But GW, Zhang QW, Liu M, Chen MM, Wen X, et al. A specific and bioactive polysaccharide marker for *Cordyceps. Carbohydr Polym.* (2021) 269:118343. doi: 10.1016/j.carbpol.2021.118343

71. He BL, Zheng QW, Guo LQ, Huang JY, Yun F, Huang SS, et al. Structural characterization and immune-enhancing activity of a novel high-molecular-weight polysaccharide from *Cordyceps militaris. Int J Biol Macromol.* (2020) 145:11–20. doi: 10.1016/j.ijbiomac.2019.12.115

72. Jing Y, Cui X, Chen Z, Huang L, Song L, Liu T, et al. Elucidation and biological activities of a new polysaccharide from cultured *Cordyceps militaris. Carbohydr Polym.* (2014) 102:288–96. doi: 10.1016/j.carbpol.2013.11.061

73. Zhu L, Tang Q, Zhou S, Liu Y, Zhang Z, Gao X, et al. Isolation and purification of a polysaccharide from the caterpillar medicinal mushroom *Cordyceps militaris* (Ascomycetes) fruit bodies and its immunomodulation of RAW 264.7 macrophages. *Int J Med Mushrooms.* (2014) 16:247–57. doi: 10.1615/intjmedmushr.v16.i3.50

74. Smiderle FR, Sassaki GL, Van Griensven LJ, Iacomini M. Isolation and chemical characterization of a glucogalactomannan of the medicinal

mushroom *Cordyceps militaris*. *Carbohydr Polym.* (2013) 97:74–80. doi: 10.1016/j.carbpol.2013.04.049

75. Bi S, Jing Y, Zhou Q, Hu X, Zhu J, Guo Z, et al. Structural elucidation and immunostimulatory activity of a new polysaccharide from *Cordyces militaris*. *Food Funct.* (2018) 9:279–93. doi: 10.1039/c7fo01147d

76. Smiderle FR, Baggio CH, Borato DG, Santana-Filho AP, Sassaki GL, Iacomini M, et al. Anti-inflammatory properties of the medicinal mushroom *Cordyceps militaris* might be related to its linear (13)-beta-D-glucan. *PLoS One.* (2014) 9:e110266. doi: 10.1371/journal.pone.0110266

77. Zhao H, Lai Q, Zhang J, Huang C, Jia L. Antioxidant and hypoglycemic effects of acidic-extractable polysaccharides from *Cordyceps militaris* on type 2 diabetes mice. *Oxid Med Cell Longev.* (2018) 2018:9150807. doi: 10.1155/2018/9150807

78. Xu L, Wang F, Zhang Z, Terry N. Optimization of polysaccharide production from *Cordyceps militaris* by solid-state fermentation on rice and its antioxidant activities. *Foods.* (2019) 8:590. doi: 10.3390/foods8110590

79. Wu F, Yan H, Ma X, Jia J, Zhang G, Guo X, et al. Comparison of the structural characterization and biological activity of acidic polysaccharides from *Cordyceps militaris* cultured with different media. *World J Microbiol Biotechnol.* (2012) 28:2029–38. doi: 10.1007/s11274-012-1005-6

80. Chen X, Wu G, Huang Z. Structural analysis and antioxidant activities of polysaccharides from cultured *Cordyceps militaris*. *Int J Biol Macromol.* (2013) 58:18–22. doi: 10.1016/j.ijbiomac.2013.03.041

81. Zhu ZY, Liu F, Cao H, Sun H, Meng M, Zhang YM. Synthesis, characterization and antioxidant activity of selenium polysaccharide from *Cordyceps militaris*. *Int J Biol Macromol.* (2016) 93:1090–9. doi: 10.1016/j.ijbiomac.2016.09.076

82. Dong JZ, Lei C, Ai XR, Wang Y. Selenium enrichment on *Cordyceps militaris* link and analysis on its main active components. *Appl Biochem Biotechnol.* (2012) 166:1215–24. doi: 10.1007/s12010-011-9506-6

83. Song Q, Zhu Z. Using *Cordyceps militaris* extracellular polysaccharides to prevent Pb^{2+}-induced liver and kidney toxicity by activating Nrf2 signals and modulating gut microbiota. *Food Funct.* (2020) 11:9226–39. doi: 10.1039/d0fo01608j

84. Liu JY, Feng CP, Li X, Chang MC, Meng JL, Xu LJ. Immunomodulatory and antioxidative activity of *Cordyceps militaris* polysaccharides in mice. *Int J Biol Macromol.* (2016) 86:594–8. doi: 10.1016/j.ijbiomac.2016.02.009

85. Lin RK, Choong CY, Hsu WH, Tai CJ, Tai CJ. Polysaccharides obtained from mycelia of *Cordyceps militaris* attenuated doxorubicin-induced cytotoxic effects in chemotherapy. *Afr Health Sci.* (2019) 19:2156–63. doi: 10.4314/ahs.v19i2.40

86. Lee JS, Kwon DS, Lee KR, Park JM, Ha SJ, Hong EK. Mechanism of macrophage activation induced by polysaccharide from *Cordyceps militaris* culture broth. *Carbohydr Polym.* (2015) 120:29–37. doi: 10.1016/j.carbpol.2014.11.059

87. Liu N, Zhang B, Sun Y, Song W, Guo S. Macrophage origin, phenotypic diversity, and modulatory signaling pathways in the atherosclerotic plaque microenvironment. *Vessel Plus.* (2021) 5:43. doi: 10.20517/2574-1209.2021.25

88. Zhang Q, Liu M, Li L, Chen M, Puno PT, Bao W, et al. Cordyceps polysaccharide marker CCP modulates immune responses via highly selective TLR4/MyD88/p38 axis. *Carbohydr Polym.* (2021) 271:118443. doi: 10.1016/j.carbpol.2021.118443

89. Kim HS, Kim JY, Kang JS, Kim HM, Kim YO, Hong IP, et al. Cordlan polysaccharide isolated from mushroom Cordyceps militaris induces dendritic cell maturation through toll-like receptor 4 signaling. *Food Chem Toxicol.* (2010) 48:1926–33. doi: 10.1016/j.fct.2010.04.036

90. Ohta Y, Lee JB, Hayashi K, Fujita A, Park DK, Hayashi T. In vivo anti-influenza virus activity of an immunomodulatory acidic polysaccharide isolated from *Cordyceps militaris* grown on germinated soybeans. *J Agric Food Chem.* (2007) 55:10194–9. doi: 10.1021/jf0721287

91. Kwon HK, Jo WR, Park HJ. Immune-enhancing activity of C. militaris fermented with *Pediococcus* pentosaceus (GRC-ON89A) in CY-induced immunosuppressed model. *BMC Complement Altern Med.* (2018) 18:75. doi: 10.1186/s12906-018-2133-9

92. Zheng Y, Li L, Cai T. Cordyceps polysaccharide ameliorates airway inflammation in an ovalbumin-induced mouse model of asthma via TGF-beta1/Smad signaling pathway. *Respir Physiol Neurobiol.* (2020) 276:103412. doi: 10.1016/j.resp.2020.103412

93. Gu L, Yu T, Liu J, Lu Y. Evaluation of the mechanism of cordyceps polysaccharide action on rat acute liver failure. *Arch Med Sci.* (2020) 16:1218–25. doi: 10.5114/aoms.2020.94236

94. Yu M, Yue J, Hui N, Zhi Y, Hayat K, Yang X, et al. Anti-hyperlipidemia and gut microbiota community regulation effects of Selenium-rich *Cordyceps militaris* polysaccharides on the high-fat diet-fed mice model. *Foods.* (2021) 10:2252. doi: 10.3390/foods10102252

95. Thomas LV, Suzuki K, Zhao J. Probiotics: a proactive approach to health. A symposium report. *Br J Nutr.* (2015) 114:S1–15. doi: 10.1017/S0007114515004043

96. Lee BH, Chen CH, Hsu YY, Chuang PT, Shih MK, Hsu WH. Polysaccharides obtained from *Cordyceps militaris* alleviate hyperglycemia by regulating gut microbiota in mice fed a high-fat/sucrose diet. *Foods.* (2021) 10:1870. doi: 10.3390/foods10081870

97. Zheng H, Cao H, Zhang D, Huang J, Li J, Wang S, et al. *Cordyceps militaris* modulates intestinal barrier function and gut microbiota in a pig model. *Front Microbiol.* (2022) 13:810230. doi: 10.3389/fmicb.2022.810230

98. Wu GD, Pan A, Zhang X, Cai YY, Wang Q, Huang FQ, et al. Cordyceps improves obesity and its related inflammation via modulation of *Enterococcus cecorum* abundance and bile acid metabolism. *Am J Chin Med.* (2022) 10:1–22. doi: 10.1142/S0192415X22500343

99. Liu RM, Dai R, Luo Y, Xiao JH. Glucose-lowering and hypolipidemic activities of polysaccharides from *Cordyceps taii* in streptozotocin-induced diabetic mice. *BMC Complement Altern Med.* (2019) 19:230. doi: 10.1186/s12906-019-2646-x

100. Shang XL, Pan LC, Tang Y, Luo Y, Zhu ZY, Sun HQ, et al. (1)H NMR-based metabonomics of the hypoglycemic effect of polysaccharides from *Cordyceps militaris* on streptozotocin-induced diabetes in mice. *Nat Prod Res.* (2020) 34:1366–72. doi: 10.1080/14786419.2018.1516216

101. Guo SD, Cui YJ, Wang RZ, Wang RY, Wu WX, Ma T. Separation, purification and primary reverse cholesterol transport study of *Cordyceps militaris* polysaccharide. *Zhongguo Zhong Yao Za Zhi.* (2014) 39:3316–20.

102. Yu WQ, Yin F, Shen N, Lin P, Xia B, Li YJ, et al. Polysaccharide CM1 from *Cordyceps militaris* hinders adipocyte differentiation and alleviates hyperlipidemia in LDLR(+/-) hamsters. *Lipids Health Dis.* (2021) 20:178. doi: 10.1186/s12944-021-01606-6

103. Guo SD, Xia XD, Gu HM, Zhang DW. Proprotein convertase subtilisin/kexin-type 9 and lipid metabolism. *Adv Exp Med Biol.* (2020) 1276:137–56. doi: 10.1007/978-981-15-6082-8_9

104. Dao MC, Everard A, Aron-Wisnewsky J, Sokolovska N, Prifti E, Verger EO, et al. *Akkermansia muciniphila* and improved metabolic health during a dietary intervention in obesity: relationship with gut microbiome richness and ecology. *Gut.* (2016) 65:426–36. doi: 10.1136/gutjnl-2014-308778

105. Ciecierska A, Drywień ME, Hamulka J, Sadkowski T. Nutraceutical functions of beta-glucans in human nutrition. *Rocz Panstw Zakl Hig.* (2019) 70:315–24. doi: 10.32394/rpzh.2019.0082

106. Korolenko TA, Bgatova NP, Ovsyukova MV, Shintyapina A, Vetvicka V. Hypolipidemic effects of β-glucans, mannans, and fucoidans: mechanism of action and their prospects for clinical application. *Molecules.* (2020) 25:1819. doi: 10.3390/molecules25081819

107. Yin F, Lin P, Yu WQ, Shen N, Li Y, Guo SD. The *Cordyceps militaris*-derived polysaccharide CM1 alleviates atherosclerosis in LDLR(-/-) mice by improving hyperlipidemia. *Front Mol Biosci.* (2021) 8:783807. doi: 10.3389/fmolb.2021.783807

108. Tokgözoğlu L, Libby P. The dawn of a new era of targeted lipid-lowering therapies. *Eur Heart J.* (2022) 2022:ehab841. doi: 10.1093/eurheartj/ehab841

109. Crea F. An update on triglyceride-rich lipoprotein and their remnants in atherosclerotic cardiovascular disease. *Eur Heart J.* (2021) 42:4777–80. doi: 10.1093/eurheartj/ehab844

110. Zhu ZY, Guo MZ, Liu F, Luo Y, Chen L, Meng M, et al. Preparation and inhibition on alpha-d-glucosidase of low molecular weight polysaccharide from *Cordyceps militaris*. *Int J Biol Macromol.* (2016) 93:27–33. doi: 10.1016/j.ijbiomac.2016.08.058

111. Ren YY, Sun PP, Ji YP, Wang XT, Dai SH, Zhu ZY. Carboxymethylation and acetylation of the polysaccharide from *Cordyceps militaris* and their alpha-glucosidase inhibitory activities. *Nat Prod Res.* (2020) 34:369–77. doi: 10.1080/14786419.2018.1533830

112. Chen DD, Xu R, Zhou JY, Chen JQ, Wang L, Liu XS, et al. *Cordyceps militaris* polysaccharides exerted protective effects on diabetic nephropathy in mice via regulation of autophagy. *Food Funct.* (2019) 10:5102–14. doi: 10.1039/c9fo00957d

113. Ji C, Zhang Z, Zhang B, Chen J, Liu R, Song D, et al. Purification, characterization, and in vitro antitumor activity of a novel glucan from the purple sweet potato *Ipomoea Batatas (L.)* Lam. *Carbohydr Polym.* (2021) 257:117605. doi: 10.1016/j.carbopol.2020.117605

114. Bi S, Huang W, Chen S, Huang C, Li C, Guo Z, et al. *Cordyceps militaris* polysaccharide converts immunosuppressive macrophages into M1-like phenotype and activates T lymphocytes by inhibiting the PD-L1/PD-1 axis between TAMs and T lymphocytes. *Int J Biol Macromol.* (2020) 150:261–80. doi: 10.1016/j.ijbiomac.2020.02.050

115. Zhong L, Zhao L, Yang F, Yang W, Sun Y, Hu Q. Evaluation of anti-fatigue property of the extruded product of cereal grains mixed with *Cordyceps militaris* on mice. *J Int Soc Sports Nutr.* (2017) 14:15. doi: 10.1186/s12970-017-0171-1

116. Xu YF. Effect of polysaccharide from *Cordyceps militaris* (Ascomycetes) on physical fatigue induced by forced swimming. *Int J Med Mushrooms.* (2016) 18:1083–92. doi: 10.1615/IntJMedMushrooms.v18.i12.30

117. Ma L, Zhang S, Yuan Y, Gao J. Hypouricemic actions of exopolysaccharide produced by *Cordyceps militaris* in potassium oxonate-induced hyperuricemic mice. *Curr Microbiol.* (2014) 69:852–7. doi: 10.1007/s00284-014-0666-9

118. Mao YH, Song AX, Wang ZM, Yao ZP, Wu JY. Protection of Bifidobacterial cells against antibiotics by a high molecular weight exopolysaccharide of a medicinal fungus Cs-HK1 through physical interactions. *Int J Biol Macromol.* (2018) 119:312–9. doi: 10.1016/j.ijbiomac.2018.07.122

119. Omak G, Yilmaz-Ersan L. Effect of *Cordyceps militaris* on formation of short-chain fatty acids as postbiotic metabolites. *Prep Biochem Biotechnol.* (2022) 22:1–9. doi: 10.1080/10826068.2022.2033992

120. Alschuler L, Chiasson AM, Horwitz R, Sternberg E, Crocker R, Weil A, et al. Integrative medicine considerations for convalescence from mild-to-moderate COVID-19 disease. *Explore (NY).* (2022) 18:140–8. doi: 10.1016/j.explore.2020.12.005

Potential Use of Emerging Technologies for Preservation of Rice Wine and Their Effects on Quality: Updated Review

Jinjin Pei [1,2†], Zhe Liu [1†], Yigang Huang [1], Jingzhang Geng [1], Xinsheng Li [1],
Sisitha Ramachandra [3], Amali Alahakoon Udeshika [4*], Charles Brennan [5] and Yanduo Tao [2*]

[1] Shaanxi Key Laboratory of Bioresources, 2011 QinLing-Bashan Mountains Bioresources Comprehensive Development C. I. C., Qinba State Key Laboratory of Biological Resources and Ecological Environment, College of Bioscience and Bioengineering, Shaanxi University of Technology, Hanzhong, China, [2] Northwest Institute of Plateau Biology, Chinese Acadamy of Science, Xining, China, [3] School of Technology, Faculty of Engineering and Technology, Sri Lanka Technological Campus (SLTC), Padukka, Sri Lanka, [4] Department of Biosystems Technology, Faculty of Technology, University of Sri Jayewardenepura, Nugegoda, Sri Lanka, [5] Royal Melbourne Institute of Technology, Melbourne, VIC, Australia

Rice wine, a critical fermented alcoholic beverage, has a considerable role in different cultures. It contains compounds that may have functional and nutritional health benefits. Bacteria, yeasts, and fungi commonly found in rice wines during fermentation can induce microbial spoilage and deterioration of the quality during its distribution and aging processes. It is possible to control the microbial population of rice wines using different preservation techniques that can ultimately improve their commercial shelf life. This paper reviews the potential techniques that can be used to preserve the microbial safety of rice wines while maintaining their quality attributes and further highlights the advantages and disadvantages of each technique.

Keywords: rice wine, fermentation, microbial safety, preservation, technologies

INTRODUCTION

Rice wine is a world-renowned fermented product that plays a crucial role in the wine culture of different countries. The production of alcoholic beverages based on rice fermentation has been practiced in many Asian countries for a long time. It is called "rice wine" because its alcohol content is close to that of wine, and its appearance is a clear and transparent light yellow liquid (1). Rice wine is known under different names based on the manufacturing procedures and raw materials used in different regions. In China (and throughout Asia), Shaoxing rice wine is a widely consumed type of rice-based fermented beverage (2). In the Republic of Korea, *makgeolli* is a traditional and trendy alcoholic drink (3). In Japan, *sake* is the most popular alcoholic beverage, and its consumption is assumed to contribute to a healthy life since it reduces the stress response.

Rice wine is made by fermenting refined rice at a low temperature of 9–11°C for 20–25 days. In the fermentation stage, the first batch of bacteria was mainly nitrate-reducing bacteria, and the second batch was *Leuconostoc mesenteroides varsake and Lactilactobacillus sakei* and yeasts. Because the pH of alkaline syrup is too high, which is not conducive to the good growth of yeast or producing good taste, it is also essential to control the number of lactic acid bacteria (1). These microorganisms also act as the source of microbial spoilage that occurs during transportation and can ultimately restrict the quality of rice wine (4, 5). Thermal processes, such as pasteurization,

are widely utilized as sterilization techniques to improve the shelf life of rice wines. However, the heating of rice wine can also have a negative impact on its organoleptic properties, particularly the relationship between proteins, sugars and flavonoids. Non-thermal processing techniques can avoid these heat-induced quality changes, the addition of plant-based extracts such as seed extract from grapefruit and the addition of chitosan (5). This review summarizes recently published data on the potential technologies to preserve the microbial safety of rice wines and the positive or negative quality changes caused by each of these technologies in terms of the technological, sensory, and nutritional quality attributes. The development of rice wine preservation technology has been improving, and the processing methods described in some old documents need to be updated. We reviewed the literature after 2010, with rice wine, rice wine processing, rice wine preservation and rice wine quality as the key words. We searched the Google Academic, Web of Science, and Springer Nature databases as data sources.

FUNCTIONAL AND SPOILAGE BACTERIA PRESENT IN RICE WINE

Bacteria can usually be classified as functional bacteria and spoilage bacteria. Functional bacteria refer to the strains responsible for producing enzymes and flavor compounds; spoilage bacteria are strains that cause food spoilage (6, 7).

During the manufacture of rice wine, the carbohydrate components of the rice are converted to sugars and then fermented by microbial elements (yeasts and molds) into alcohol.

The general process of Chinese rice wine production is shown in **Figure 1**. In Chinese rice wine fermentation, wheat Qu may be used as a saccharifying agent with rice. The frequently used starter is yeast (*Saccharomyces cerevisiae*), facilitating simultaneous saccharification fermentation (8). *Nuruk* is a starter made of herbal extracts, and koji is used to produce Korean rice wine (*makgeolli*) (9).

Lv et al. (10) stated that bacteria are the primary microorganisms that are important in producing flavor-related compounds. It determines the overall acceptability of Chinese rice wines, whereas Nile (11) stated that the volatile compounds produced by yeasts are the leading cause of the organoleptic properties in *makgeolli* fermentation.

Fermentation with fungi and bacteria allows the saccharification of rice starch, which results in glucose, ethanol, and carbon dioxide production. **Table 1** depicts the fermented alcoholic beverages from various countries and the primary starter cultures used in each country. Some microorganisms in the starter tend to remain active during bottling and dispensing (17). Suppose that any microorganisms remain in the alcoholic beverages after bottling. In that case, this could cause a food safety risk since these microorganisms can spoil and degrade the quality of the rice wine, and their control postfermentation is of considerable interest (18). Several pathogenic bacteria, such as *Bacillus cereus, Campylobacter jejuni, Staphylococcus aureus, Escherichia coli* 0157:H7 and *Salmonella* sp., can exist in rice wine (19–22). For example, the spoilage bacteria in Chinese rice

wine mainly include *E. coli* and other foodborne pathogens, such as *Bacillus cereus, Campylobacter jejuni, Staphylococcus aureus* and *Salmonella sp.* The microorganism that causes the deterioration of Japanese *sake* is a bacterium called "hiochi"; Hiochi bacteria are generally composed of lactobacilli, namely, hiochi-lactobacilli and hiochi-bacilli. The former includes various kinds of lactic acid bacteria, including *Lacticaseibacillus casei, Lacticaseibacillus paracasei, Lacticaseibacillus rhamnosus, Limosilactobacillus fermentum, Lactiplantibacillus plantarum,* and *Lactobacillus hilgardii.* In contrast, the latter includes *Lactobacillus fructivorans and Lactobacillus homohiochi.* Because *hiochi-lactobacilli* are easily inactivated by pasteurization, it is considered that *hiochi-bacilli* are the actual spoilage bacteria of sake. The spoilage bacteria in *makgeolli* are *Escherichia coli, Bacillus cereus, Campylobacter jejuni, Clostridium perfringens, Escherichia coli* O157:H7, *Listeria monocytogenes, Salmonella sp., Staphylococcus aureus,* and *Yersinia enterocolitica* (12, 13, 23). Highly resistant endospores formed by *Bacillus cereus* are all active in the product or gastrointestinal tract. Keot et al. (14) detected the presence of harmful microorganisms, such as *Acidovorax, Herbaspirillum, Methylobacterium, Pantoea, Pseudomonas, Stenotrophomonas, Staphylococcus, Micrococcus, Acinetobacter, etc.,* in rice wine through Illumina technology. Kim et al. (19) suggested that *Bacillus cereus* contamination found during rice wine fermentation may come from rice and wheat flour. Kim et al. (19) stated that acetic acid bacteria promote the oxidation of sugars or ethanol and acetic acid production during rice wine fermentation. One of the main issues in the rice wine industry is finding effective techniques to preserve microbial safety while maintaining the nutritional and sensory attributes of the final products.

EFFECTS OF PLANT ADDITIVES ON THE PRESERVATION AND QUALITY OF RICE WINE

Increasing the health consciousness of consumers has prompted the use of natural food substitutes instead of synthetic food additives. Therefore, there is a growing demand for appropriate antimicrobial food additives that do not cause toxicity and maintain the sensory quality of fresh rice wines. In many countries, numerous locally available medicinal plants, herbs, and spices are added to the fermentation process of rice wine and rice beverages to inhibit the growth of harmful microorganisms in the final product. These plants can also provide specific nutrients for the starter cultures (24). The preservative effect of any spice and herb may be related to their composition of phytochemicals, antimicrobial compounds, and secondary metabolites, such as alkaloids and phenolics, which can modulate the growth of pathogenic bacteria (24). Herbs may help improve rice wine's sensory properties and give it some medical value (25). For instance, Murugan et al. (24) found that the fresh leaves and stems of the medicinal plants *Plumbagozeylanica* (Ceylon leadwort), *Thelypteris clarkei C.F. Reed* (Lady fern), *Clerodendrum D. Don* (Glory bower) *and Scoparia dulcis* (goat weed) resulted in elevated antimicrobial activity in fermented

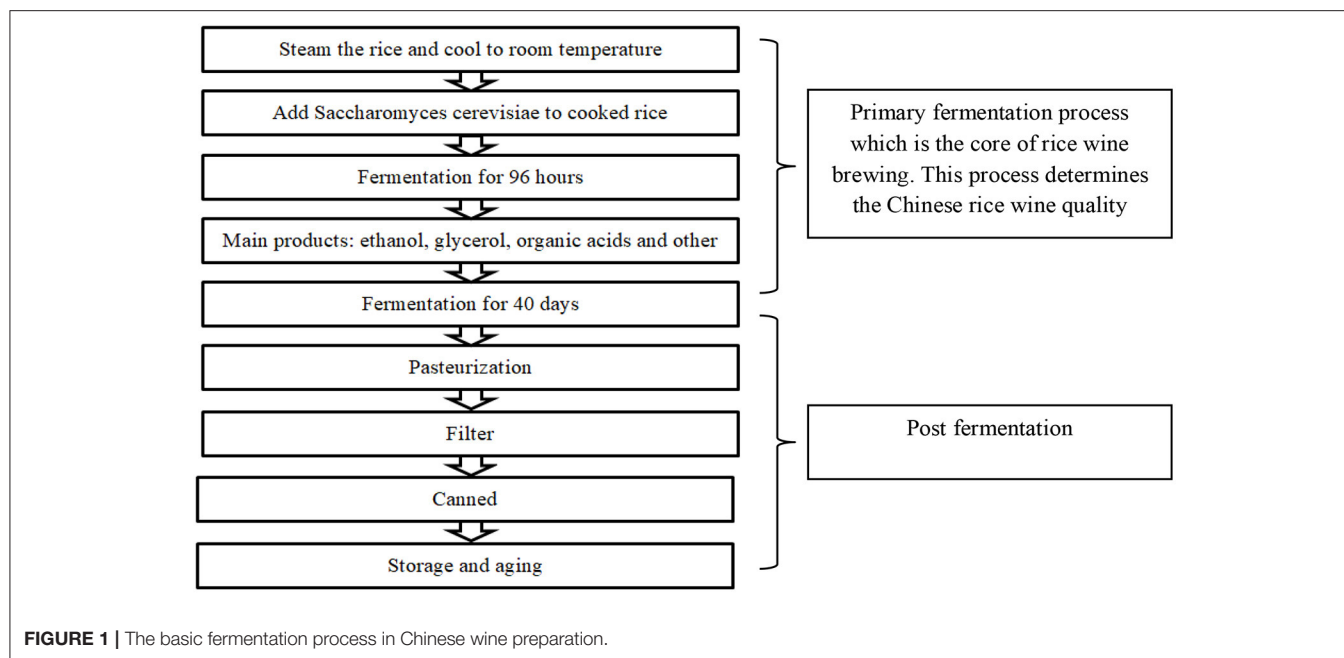**FIGURE 1** | The basic fermentation process in Chinese wine preparation.

TABLE 1 | Traditional rice wine in various countries, the starter cultures used in those rice wines, and the functional yeast and molds present in those starter cultures (12–16).

Country	Type of rice wine	Functional yeast and mold present in starter cultures
China	Mie-chiu, Shaohing, Huangjiu	*Saccharomyces cerevisiae, Wheat koji*
Japan	Sake	*A. Oryzae, A. awamorii, Saccharomyces cerevisiae,*
Korea	Yakju, Takju	*Yeast, Wheat barn koji, Nuruk (traditional natural starter with bacteria, yeast, and fungi) yeast, and fungi)*
India	Sonti	*Acidovorax, Herbaspirillum, Methylobacterium, Pantoea, Pseudomonas, Stenotrophomonas, Staphylococcus, Micrococcus, Acinetobacter*
Malaysia	Tapai	*Amylomyces rouxii, Rhizopus sp., Endomycopsis sp.*
Vietnam	Ruou Nep	*Mucor sp., Rhizopus sp., Aspergillus sp., Saccharomyces cerevisiae, Torulopsis candida*
Thailand	Sato, Krachae	*Mucor sp., Rhizopus sp., Candida sp., Saccharomyces sp.*
Phillipine	Tapuy	*Aspergillus sp., Endomycopsis sp., Hansenula sp., Rhodotorula glutinis, Candida parapsilosis*

rice beverages and the inhibition of *Staphylococcus aureus* in rice beverages. The presence of chemical constituents, such as flavonoids, alkaloids, tannins, carbohydrates, and glycosides, in these medicinal plants may have an antimicrobial effect (26). Zhou et al. (27) found that bamboo leaf extract had a significant effect on ethyl carbamate in compound microbially fermented rice wine. The addition of the primary leaf extract promoted the production of ethanol and amino acids in compound microbially fermented rice wine but inhibited the generation of aroma. Through sensory evaluation, it can be concluded that bamboo leaf extract can improve the comprehensive quality of rice wine.

In Northeast India, people add different plants and herbs to modulate the flavor of traditional rice wine. Some of these plants include *Albizia myriophylla* (Albezia) used in the state of Manipur, *Plumbago zeylanica* (leadwort), *Buddleja asiatica* (dog tail), *Gingiber officinale* (ginger) used in the state of Sikkim, and *Amomum aromaticum* used in Meghalaya. The Assam region also paid attention to the effect of adding banana (pineapple), jackfruit (jackfruit), *calotris gigantean* (giant milkeed), and Nagaland sprouted rice on rice wine. They found that bromelain, saponins, flavonoids, and polyphenols in pineapple are active compounds that control bacterial activity (28).

The physicochemical and microbial characteristics of *makgeolli* (Korean rice wines) incorporated with bananas have been investigated by Kim et al. (29) due to bananas' ability to add to the taste and nutritional value of the final product. Bananas also contain many secondary metabolites, such as phenolic compounds, which can act as antimicrobials.

Choi et al. (30) found that grape seed extracts influence the growth of both the brewing and spoilage of microorganisms in *makgeolli*. A concentration of 0.1–0.2% grape seed extract has been reported to prolong the shelf life of bottled fresh *makgeolli*

by decreasing the concentration of bacteria and yeast. In addition, grapefruit seed extract has been reported to possess natural antimicrobial properties due to antimicrobial compounds, including naringin, limonoid, quercetin, kaempferol, and citric acid. These seed extracts do not negatively affect rice wine color, smell, or overall acceptance (31).

Jeong et al. (3) found that *makgeolli* had the best antioxidant activity when 0.45% steaming and drying deodeok *(Codonopsis lanceolata)* was added. In general, plant extract additive is a natural and healthy preservative for rice wine, and it can also make rice wine obtain some beneficial substances attached to plants. However, plant additives often affect fermentation strains, resulting in a decline in rice wine quality. Improving the shelf life of rice wine and reducing the impact on the quality of rice wine are also problems to be solved in the future.

Table 2 illustrates the effects of a few plant-based and nonplant-based natural additives that have been used in different rice wines.

EFFECT OF HEAT TREATMENT ON THE PRESERVATION AND QUALITY OF RICE WINE

Thermal processes are well known as food preservation methods (34). These techniques are economically feasible and efficient for inactivating pathogenic microorganisms in rice wines. In some countries, commercial rice wine is distributed in two forms (pasteurized or unpasteurized). Rather than using high-temperature short-term pasteurization (80°C for 23 secs), rice wines (such as *makgeolli*) are often treated using low-temperature, long-term pasteurization. Low-temperature, long-term pasteurization (55–65°C for 10–15 mins) is reported to cause some issues in sensory attributes, such as a strong off-flavor that gives a burnt odor, a reduction in color, and a separation of the layers in the final product. Such treatments can result in a commercially stable shelf life of 14 to 50 days (35). However, high-temperature processing can cause a reduction in color and sedimentation and can produce a strong off-flavor. Thus, food manufacturers prefer to use the low-temperature long-term process.

Park et al. (35) reported changes in the volatile components of unpasteurized and pasteurized *makgeolli* during storage (30 days). They found that the odor-related compounds in pasteurized rice wine were not changed over the storage period compared to those in non-pasteurized rice wine. However, Li et al. (21) stated that high-temperature (75, 80, 85, 90, 95°C) sterilization affected the sugar content of rice wine, which is considered an important quality indicator.

Kim et al. (19) compared commercially available sterilized Korean rice wine (*makgeolli*) from different plants subjected to different temperature/time combinations for sterilization. They stated that rice wines subjected to high-temperature sterilization (95°C/<1 min) had the most significant bactericidal effect of decreasing the aerobic bacterial counts and the microbial numbers of *Clostridium jejuni*, *Clostridium perfringens*, *Escherichia coli 0157:H7*, *Listeria monocytogenes*, and *Staphylococcus aureus*. In addition, these treatment conditions were reported to either eliminate or significantly reduce the lactic acid bacteria, fungi, and acetic acid bacteria. The researchers reported that even with sterilization of wine at 85°C/1 min followed by 85°C/2 min, *Bacillus cereus* spores were present, but not the vegetative cells. Jeon (36) also reported the presence of *B. cereus* in 61% of sterilized products tested in Korean *makgeolli* and *yakju*. Lv et al. (13) illustrated the presence of *Bacillus cereus* cells in Chinese rice wine, increasing the heat treatment time to 60, 70, and 80°C, leading to a reduction in their value.

The most appropriate strategy to control *B. cereus* in rice wine would be to prevent the contamination of the rice wine rather than striving to eliminate the spores at a later stage (19). The processing factors (pH, water activity) can determine the heat resistance of the microorganisms. However, the duration of the exposure and temperature have a major impact on heat resistance (37). The medium's proteins and sugars act as a protective barrier to heat damage, while low water activity also provides protection (38). As Lv et al. (13) observed, the presence of protein and glucose in Chinese rice wines reduced the thermal sensitivity of *Bacillus cereus*. In contrast, the medium-high alcohol content and acidic pH increased the lethality. This could be attributed to disruption of the microbial cell wall due to the acidic pH and alcohol contents.

The other widely used thermal treatment for rice wines is conventional boiling (80–95°C for 15–30 min), which is considered a thermal sterilization method to kill bacteria, fungi, and other microorganisms. However, the drawbacks of this technique include the negative effect of temperature on the flavor characteristics, the low viscosity of the liquid, and the high energy usage, which limits the expansion of this method on an industrial scale (39).

It has been reported that conventional boiling has a bactericidal effect in the preparation of different rice wine types. Yang et al. (40) stated that thermal processing (90°C/15 min) could eliminate 99% of the microorganisms in rice wines. These authors further reported that conventional boiling at 90°C/15 min causes an unavoidable loss of volatile alcohols and aldehydes in Chinese rice wines, resulting in overall low acidity. In addition, this study showed that thermal treatment decreased the ethanol content in rice wine compared with non-treated wine due to the oxidation and esterification reactions caused by the thermal treatment. Thermal treatment reduces sugar content due to the Millard reaction, which reacts with sugar and free amino acids (41). In terms of the sensory characteristics of the rice wine, thermal boiling increased the loss of red pigments, and it tended to deteriorate the flavor.

According to the research conducted thus far, different sterilization parameters should be selected because different rice wine components and microbial survival rates are different to prevent adverse effects on the quality of rice wine. However, very few studies are available on determining the effects of rice wine composition on sterilization and the fundamental mechanisms of heat inactivation under different environments. For instance, Wu et al. (42) showed that Chinese rice wine should be sterilized at 85–95°C, as these rice wines have relatively high amounts

TABLE 2 | Effect of different plant-based and nonplant natural additives on the quality attributes of rice wines (3, 9, 26, 32, 33).

Rice wine type	Natural additives used	Quality characteristics	References
Plant-based additives			
Korean Takju	Natural honey (5%)	• Temperature, pH, acidity, and total sugar content showed no significant differences • Increase the flavor	Jung et al. (32)
Korean Takju	Codonopsis lanceolate (0,0.15%,0.3%,0.45%)	• The content of alcohol and polyphenols increased, while the content of reducing sugar decreased	Jeong et al. (3)
Chinese yellow rice wine	Bamboo leaves extract	• Enhanced antioxidant activity • Inhibit arginine metabolism • Prevent the reaction of urea and citrulline with ethanol	Zhou et al. (26)
Korean Yakju	Lotus leaves	• Lotus-leaf Yakjus containing fresh leaves and dried leaves were preferred to the others in color and flavor among Yakjus prepared with lotus leaves before cold storage.	Choi et al. (29)
Non-plant based additives			
Takju	0.001% of Chitosan	• Moderately decrease the viable microbial cells and yeasts • More stabilized in terms of turbidity during storage at 10°C for 12 days compared to untreated wine • Improved the sensory qualities compared to untreated wine	Kim et al. (33)
Makgeolli	Lysozyme 270ppm and glycine 0.27%, or Lysozyme 450 ppm and glycine 0.45%	• Suppressed the acid formation of wine • Increased the nucleotides contents of inosine monophosphate and inosine content • Improved the taste and palatability	Lee and Ahn (17)

of protein and the concentrations of sugar vary. Under certain conditions, the heating temperature should be carefully chosen to prevent melanoidin development from sugars and amino acids. For example, a Chinese rice wine that has been boiled at higher temperatures (90–95°C) will have a sugar content lower than 15.0 g/L, whereas semisweet and sweet Chinese rice wine that has a sugar content that is >40.0 g/L will have been boiled at 85–90°C (42, 43). Under the condition of heat sterilization, spores still exist in rice wine, which has always been a problem. However, achieving the maximum lethality of pathogenic microorganisms through excessive heating will reduce the sensory properties of yellow rice wine (21, 44). Therefore, either minimizing the intensity of the thermal treatment and the duration of exposure or substituting the thermal treatment with an appropriate non-thermal technology would be appropriate to preserve the quality without compromising safety (13).

EFFECTS OF ULTRAHIGH TEMPERATURE (UHT) ON THE PRESERVATION AND QUALITY OF RICE WINE

Ultrahigh-temperature (UHT) processing uses continuous-flow thermal processing for the sterilization process (45). UHT operates at ~130–150°C for a short duration to reduce microbial loading (46). Therefore, the advantage of UHT is to use a shorter processing time to retain the natural sensory and nutritional characteristics of food and reduce the loss of quality. Jin et al. (47) stated that UHT treatment (125°C/5 s) inactivated the yeast and total bacteria in Korean rice wines (*makgeolli*) while having no adverse effects on the pH, titratable acidity, or sugar contents of the rice wine during storage (at 15°C). However, the drawback was an increase in off-flavor development with an increase in

storage time, which might be attributed to sulfur-containing amino acid degradation by UHT treatment.

Yang et al. (40) also reported that UHT (125°C/5 s or 135°C/5 s) could eliminate the microorganisms in Chinese rice wines, resulting in above 99% lethality. Concerning the sensory and other quality attributes, the UHT treatment increased the total acidity of the rice wines after treatment. According to Tian et al. (48) this increase could be attributed to the production of aldehydes due to alcohol oxidation. These aldehydes later oxidize to acids, which tend to increase the total acidity of the rice wine. In addition, the UHT increased the Millard reaction in the rice wines, which caused a reduction in the sugar content of the final product. However, the UHT did affect the flavor of the rice wine with the short processing time (5 s). Therefore, ensuring the flavor of rice wine is one of the complex problems to be solved when UHT eliminates spoilage bacteria.

EFFECTS OF HIGH HYDROSTATIC PRESSURE PROCESSING (HHP) ON THE PRESERVATION AND QUALITY OF RICE WINE

Consumer demand for healthy and nutritious food has driven people to seek new food processing alternatives. It is expected that the use of these new techniques may produce safer food while retaining fresh-like quality, even though a few challenges still exist. The high hydrostatic pressure used in a refrigeration room or at a moderate temperature is believed to reduce/inactivate spoilage and pathogenic bacteria in the food. Compared to conventional heating, HHP prevents negative consequences on the quality of rice wine (49). The shorter processing time that

HHP technology requires would be useful to maintain the quality of the food products in contrast to the foods treated by conventional methods. The main principle of the HHP treatment involves subjecting the food to water pressure (100–900 MPa) by placing the packaged food inside a pressure vessel. Rendueles et al. (50) stated that microbial inactivation by HHP is caused by changes in the cellular functions and the integrity of the microflora membrane. Cell death of the microflora is believed to occur due to any moderations in ion exchange, changes in the fatty acid composition, denaturation of cell proteins, or processes affecting enzyme activity. Several studies have observed that HHP can decrease the initial numbers of bacteria, yeasts, and mold in rice wine. Buzrul (51) found that HHP at 500 MPa pressure for ≤30 min has antimicrobial effects on rice wine. Xu et al. (15) found that adding calcium and magnesium ions during extrusion can give yellow rice wine a high phenol content and antioxidant activity. Jin et al. (47) declared that the HHP treatment (400 MPa for 10 min) of Korean rice wine (*makgeolli*) resulted in a reduction in total bacterial, lactic acid bacteria and yeast counts in sterilized *makgeolli* during storage. Yang et al. (40) also reported that HHP treatment (200, 400, and 600 MPa for 10 and 20 min) could eliminate the total aerobic bacteria in rice wines, and the lethal rate was reported to be > 99%. Ha et al. (52) illustrated that lactic acid bacteria and yeast were not observed immediately after HHP at 400 MPa for 5 min because they were decreased under the detection limit. However, this study further found white wrinkly shaped bacteria in the samples even after HHP treatment, confirmed as *Bacillus amyloliquefaciens*. These findings suggest that although HHP inactivates most of the bacterial growth conditions that support the growth of Bacillus, Bacillus can still compete with other strains. Bañuelos et al. (53) noted that ultrahigh-pressure sterilization can eliminate local microorganisms in grape juice and effectively inactivate oxidase, reducing browning and improving sensory quality.

However, it is crucial to select the best HHP treatment conditions that can positively impact the sensory attributes of rice wines. The study of Jin et al. (47) which used HHP treatment at 400 MPa for 10 min for *makgeolli,* maintained pH stability and total acidity during storage (15°C/20 weeks). In contrast, those with untreated *makgeolli* decreased over time. Apart from that, HHP could maintain a desirable color, flavor, taste, and overall sensory qualities in rice during storage. Yang et al. (40) reported that HHP treatment increased the reducing sugar content of rice wines, which might be due to the increased activity of the enzymes, and the activation of the Saccharomyces enzymes as a result of the HHP treatment may be the factor that affects reducing the sugars overall. HHP also increased the free amino acid contents due to the proteolysis promoted by HHP. Even though HHP may promote the Maillard reaction, the speed is lower than that of proteolysis. Moreover, the HHP treatment (>200 MPa) resulted in more flavor compounds than the non-HHP-treated rice wine. However, the pressure and time involved in the HHP treatment play a vital role, suggesting 600 MPa/10 min, which accelerates the oxidation and esterification processes in the rice wines. At the same time, 600 MPa is excessive for the rice wine flavor in this study.

Ha et al. (52) showed that 400 MPa HHP treatment promoted an increase in reducing sugars in *makgeolli*, while the reducing sugar content of *makgeolli* not treated with HHP decreased. The researchers examined *makgeolli*, which was treated with HHP and stored at 25 °C for 6 days, and found that HHP could slow the increase in alcohol content, pH and acidity. The research shows that HPP can prolong the shelf life of *makgeolli* by inactivating lactic acid bacteria and yeast.

Tian et al. (48) showed that as the storage time (at 10–15°C for 18 months) increased, HHP-treated (200/550 MPa for 30 min) hongqu rice wines showed a significant difference in some oenological properties, such as alcohol % and total solids. This study noted that the alcohol content in the HHP-treated rice wine rapidly decreased after 6 months of storage. The highest-pressure condition of 550 MPa tested in this study had a more rapid decrease in alcohol than the 200 MPa. Additionally, the 550 MPa treatment led to a rapid decrease in total solids after 3 months of storage due to the acceleration of sugar-amine condensation by the HHP treatment and a significant decrease in total free amino acids. This study showed that the Maillard and oxidation reactions in the HHP-treated wines were promoted due to the fast reduction in the total solid content, the reduced free amino acids, and the higher content of the ketones.

Therefore, rice wines treated with HHP may not be appropriate for long-term storage under certain conditions. HHP treatment can quickly deteriorate the sensory quality of wine, producing a higher bitterness and higher astringency level (48). Considering the above facts, it can be suggested to use only certain pressure conditions to facilitate maximum microbial safety while preserving nutritional and sensory attributes. Therefore, the problem of temporary storage after HHP treatment should be optimized in future research to obtain the maximum sensory and nutritional effect in any type of rice wine.

EFFECTS OF PULSED ELECTRIC FIELDS (PEFS) ON THE PRESERVATION AND QUALITY OF RICE WINE

Pulsed electric field processing is an emerging non-thermal food technology that can be used to treat liquid foods, such as fruit juices and rice wines (54, 55).

Pulsed electric field (PEF) technology is a short-term electric treatment that works (ns-ms) promptly with electric field strengths ranging from 100 to 300 V/cm to 20–80 kV/cm. At high electric fields (> 20 kV/cm), the PEF can act as a substitute for conventional thermal processing to inactivate pathogenic bacteria and enzymes. PEF has an advantage over traditional thermal processing because it can retain the sensory, nutritional, or health-promoting ingredients of liquid food products (56).

Recently, PEF technology has been explored as a preservation technology to eliminate spoilage bacteria in wines. A few studies have been conducted to test whether PEF technology can control spoilage in the microflora in grape wine and beer (57). However, the inactivation efficacy of different microbial species by PEF treatment is primarily related to their different susceptibility levels. Therefore, the inactivation efficiency depends on the genetic characteristics of the specific microorganism (58).

Huang et al. (54) used PEF to control the spoilage microorganisms in Chinese rice wines. PEF was applied at an electric field strength of 12–21 kV/cm (treatment duration 30–180 μs, monopolar square pulses) to investigate the inactivation efficiency of PEF to inactivate the spoilage yeast *Saccharomyces cerevisiae* in this study. The decrease in the number of yeasts has been supported by finding the PEF-induced destruction of the cell membrane structure. The highest inactivation was observed with PEF at 21 kV/cm and 180 μs, suggesting that the high intensity of the PEF causes higher inactivation. Thus, the complete inactivation of the microorganisms could be achieved with PEF at an adequate treatment intensity. However, for each microorganism, the optimum conditions need to be found. Therefore, the required amount of energy could be calculated without wasting too much unwanted energy and affecting the quality of the rice wine.

However, the efficiency of microbial inactivation via PEF treatment is also closely related to the treatment temperature. Microbial sensitivity to PEF increases with increasing temperature. Huang et al. (54) illustrated that PEF applied at different temperatures had a different antimicrobial potency. This study further showed a higher inactivation rate (2.05 log-cycles) of the yeasts in the Chinese rice wine that was treated at a higher initial temperature for the PEF treatment (18 kV/cm, 150 ms at 25°C).

The lethality is also based on the composition of the rice wine, basically, the concentration of ethanol. Puertolas et al. (59) stated that the lethal influence of PEF treatment on the microbes in rice wine is increased due to the high ethanol concentration present in the wine. Moreover, Milani et al. (60)investigated the impact of PEF treatment (45 kV/cm, 46.3 pulses, and 70 ms) on the inactivation of *Saccharomyces cerevisiae* spores in beer and found that beer samples with the highest log reduction had the highest alcohol concentration. These results suggested that the use of PEF for samples with a high alcohol concentration can result in higher microbial inactivation.

Apparently, PEF processing does not have a considerable negative effect on rice wine sensory and other quality attributes. Shen et al. (61) showed that micro oxygen combined with electric field treatment could greatly improve the flavor intensity of yellow rice wine. Huang et al. (54) found that PEF treatment at 12–21 kV/cm did not cause changes in the soluble solids, pH, or color during the post-PEF treatment period or storage at 22°C. However, finding treatment conditions suitable for most microorganisms is also a complicated problem that must be overcome in the future. Further investigation is needed to study the feasibility of the use of PEF in microbial inactivation before promoting the use of PEF on a commercial scale.

EFFECTS OF UV-C IRRADIATION AND ELECTRON BEAM IRRADIATION (EB) ON THE PRESERVATION AND QUALITY OF YELLOW RICE WINE

Ultraviolet (UV) irradiation has been used to process liquid foods (34). It is used as a substitute for thermal processing.

Reducing microbial corruption will have a negative impact on the sensory characteristics of liquid food. UV radiation technology can inhibit the reproductive function of other cells by destroying the DNA of microorganisms. The penetration and effectiveness of UV-C depend on the absorbance, density, color, soluble solids and density of beverages (62).

The principle of electric beam irradiation (EBI) is the generation of electrons from a cathode using commercial electricity in a vacuum environment. These electrons are subsequently emitted from an electron gun in sequence, creating a beam of electrons (63). EBI can directly or indirectly damage the metabolism and cell chemical reactions of microorganisms or cause consequent microbial cell death (63).

However, based on a review of the literature, only a few studies are available on the use of UV-C and EBI to enhance the microbial safety or sensory quality of rice wines. Kim et al. (29) showed the impact of UV-C and EBI on the different quality attributes of the *makgeolli* during storage (at 4°C for 15 days). This investigation stated that EBI (at 0.5, 1, 2, and 3 kGy) effectively controlled the microorganisms in the *makgeolli* compared with the UV-C treatment. However, there are certain drawbacks involved with using both of these treatments on the quality of the *makgeolli* related to an increase in the pH of the wine over the storage time. EBI tended to have a higher acidity in the wine than UV-C-treated rice wine. However, further studies are recommended to determine how to minimize the quality deterioration in rice wines during storage after UV-C or EBI treatment.

Jin et al. (47) reported that UV sterilization (15 W germicidal lamp for 10 min) completely inactivated the yeasts and the total bacteria in *makgeolli*. This treatment did not significantly affect the pH or the titratable acidity, nor did it reduce the sugar content during storage (at 15°C for 20 weeks). This might be attributed to the inactivation of the majority of the microorganisms by sterilization. Therefore, the pH and the titratable acidity of the wines are not affected. On the other hand, this study showed that UV treatment could maintain the color of *makgeolli* during storage. To use irradiation as an alternative approach for thermal treatments, further studies on the effect of irradiation at different doses on various spoilage microorganisms should be conducted while directing attention to the other quality attributes. In addition, the available information on UV-C or EB radiation is not enough to conclude that the potential application of these technologies in commercial rice wine production will be beneficial.

EFFECT OF NANOMATERIALS ON THE PRESERVATION OF RICE WINE

In recent years, nanotechnology has developed rapidly in the food industry and can be used in food production, packaging and transportation. The application of nanomaterials in food preservation can improve the microbial pollution of food and improve the bioavailability of nutrients. Moreover, aerosols using water nanostructures can also kill foodborne pathogens such as *Salmonella aureus, Escherichia coli,* and *Bacillus atrophaeus* (64). The unique physical, chemical, and biological properties of

nanoparticles disrupt enzyme activity and destroy intracellular organelles. Therefore, metal oxide nanoparticles have attracted much attention as antibacterial agents. According to González-Arenzana et al. (58) silver nanoparticles have an inhibitory effect on all microbial populations in the wine used for testing. Before adding sulfur dioxide and silver nanoparticles, the author analyzed the white wine samples collected after 1 day and 30 days, respectively, and then analyzed the red wine polluted by Breton for 15, 30, and 60 days. Finally, the results show that silver nanoparticles are used as antibacterial agents and have more potential than SO_2 in controlling lactic acid bacteria (LAB), acetic acid bacteria (AAB), and yeast. However, the safety of nanosilver ions after entering the human body is not apparent. Pachnowska et al. (16) believe that silica nanospheres can replace sulfur dioxide to stabilize microorganisms in wine. It is worth noting that the author's experiment is tested on one strain. This experiment is in the laboratory stage. Whether it is effective for other bacteria must be further studied. In short, nano preservation technology has become a hot topic in the food industry in recent years; however, its application in rice wine preservation is slightly scarce, and whether nanomaterials, such as nanosilver ions, nano silicon and nano clay, are harmful to the human body needs further research.

CONCLUSION AND FUTURE PERSPECTIVES

Even though several sterilization methods can be used for food processing, each method has specific opportunities and drawbacks. Therefore, the most appropriate method should be selected according to the sterilization purpose and food. For example, heat treatment is widely used to preserve rice wine worldwide. However, some studies still show that due to the specific adverse effects on the final sensory quality of rice wine, the deterioration of the quality of rice wine should be limited during these heat treatments. Although heat treatment has clarified its beneficial role in protecting the microbial safety of products, commercial rice wine producers are still looking for the most effective choice to obtain nutritionally and sensorily acceptable rice wine. Therefore, the primary concern of the rice wine industry is to find an effective process to ensure the microbial safety of rice wine and minimize quality defects. For example, compared with pasteurization, plant additives not only do not reduce the sensory quality of rice wine but also bring some unique flavor to plants. However, we need to further explore the safety of plant additives and their impact on the fermentation process. UHT can kill some bacteria that cannot be killed by pasteurization in terms of the sterilization

effect, but its impact on product flavor is also difficult to solve. Compared with pasteurization and UHT, HHP can well ensure the sensory quality of rice wine, but the problem that rice wine cannot be preserved for a long time is highlighted. Compared with the above sterilization methods, PEF and UV-C irradiation and electron beam irradiation (EB) technology can package the sensory quality of rice wine and prolong its storage period. However, PEF requires different processing conditions for different microorganisms and obviously cannot be used in factories. Finding a method suitable for most microorganisms is a complex problem that must be overcome. Nanotechnology is one of the rapidly developing food preservation, transportation and processing technologies in recent years, but its application in rice wine is little known, and we need to explore it.

Emerging technologies, such as plant additives, HHP, UHT and pulsed electric field treatment, can be effectively used to produce commercial yellow rice wine. However, further research is needed to immediately eliminate different spoilage microorganisms in rice wine after treatment and during storage at different temperatures. In addition, before implementing these processes in the yellow rice wine industry, more research is needed to determine the safety of these compounds and the toxicity problems related to different technologies and their impact on human health.

AUTHOR CONTRIBUTIONS

JP: conceptualization, design of the work, visualization, resources, funding acquisition, and writing—review and editing. ZL and YH: acquisition, resources, investigation, and formal analysis. JG, XL, and SR: supervision, conception or design of the work, resources, and investigation. AA: data acquisition, formal analysis, conceptualization, and writing—review and editing. CB and YT: supervision and review. All authors contributed to the article and approved the submitted version.

FUNDING

REFERENCES

1. Kwon DY, Nyakudya E, Jeong YS. *Fermentation: Food Products*. (2014), p. 113–123.
2. Shen F, Yang D, Ying Y, Li B, Zheng Y, Jiang T. Discrimination between Shaoxing wines and other Chinese rice wines by near-infrared spectroscopy and chemometrics. *Food Bioprocess Technol*. (2012) 5:786–95. doi: 10.1007/s11947-010-0347-z
3. Jeong M, Lee KY, Lee HG. Effects of steaming and drying processing on Korean rice wine (Makgeolli) with deodeok (Codonopsis lanceolate). *Korean J Food Sci Technol*. (2021) 53:85–91. doi: 10.9721/KJFST.2021.53.1.85

4. Bak JS. Effective inactivation of *Saccharomyces cerevisiae* in minimally processed Makgeolli using low pressure homogenization-based pasteurization. *SpringerPlus* . (2015) 4:160–9. doi: 10.1186/s40064-015-0936-4

5. Choi JS, Lee YR, Ha YM, Seo HJ, Kim YH, Park SM, et al. Antibacterial effect of grapefruit seed extract (GSE) on Makgeolli-brewing microorganisms and its application in the preservation of fresh Makgeolli. *J Food Sci.* (2014) 79:1159–67. doi: 10.1111/1750-3841.12469

6. Dung NTP, Rombouts FM, Nout MJR. Characteristics of some traditional Vietnamese starch-based rice wine fermentation starters (men). *LWT—Food Sci. Technol.* (2007) 40:130–5. doi: 10.1016/j.lwt.2005.08.004

7. Xie GF, Li WJ, Lu J, Cao Y, Fang H, Zou HJ. Isolation and identification of representative fungi from Shaoxing rice wine wheat qu using a polyphasic approach of culture-based and molecular-based methods. *J Institute Brew.* (2007) 113:272–9. doi: 10.1002/j.2050-0416.2007.tb00287.x

8. Chen S, Xu Y. Effect of 'wheat Qu' on the fermentation processes and volatile flavor-active compounds of Chinese rice wine (Huangjiu). *J Instit Brew.* (2013) 119:71–7. doi: 10.1002/jib.59

9. Lee MY, Sung SY, Kang HK, Byun HS, Jung SM, Song JH, et al. Quality characteristics and physiological functionality of traditional rice wines in Chungnam province of Korea. *Korean J Microbiol Biotechnol.* (2010) 38:177–82. doi: 10.1017/S0952836901000036

10. Lv, X-C., Huang, X-L., Zhang W, Rao, et al., Ni. L. Yeast diversity of traditional alcohol fermentation starters for Hong Qu glutinous rice wine brewing, revealed by culture-dependent and culture-independent methods. *Food Control.* (2013) 31:183–90. doi: 10.1016/j.foodcont.2013.04.020

11. Nile SH. The nutritional, biochemical and health effects of makgeolli—a traditional Korean fermented cereal beverage. *J Instit Brewing.* (2015) 121:457–63. doi: 10.1002/jib.264

12. Kim NH, Jun SH, Lee SH, Hwang IG, Rhee MS. Microbial diversities and potential hazards of Korean turbid rice wines (makgeolli): Multivariate analyses. *Food Microbiol.* (2018) 76:466–72. doi: 10.1016/j.fm.2018.07.008

13. Lv R, Chantapakul T, Zou M, Li M, Zhou J, Ding T, et al. Thermal inactivation kinetics of *Bacillus cereus* in Chinese rice wine and in simulated media based on wine components. *Food Control.* (2018) 89:308–13. doi: 10.1016/j.foodcont.2018.01.029

14. Keot J, Bora SS, Das Kangabam R, Barooah M. Assessment of microbial quality and health risks associated with traditional rice wine starter Xaj-pitha of Assam, India: a step toward defined and controlled fermentation. *Biotech.* (2020) 10:1–14. doi: 10.1007/s13205-020-2059-z

15. Xu E, Wu Z, Chen J, Tian J, Cheng H, Li D, et al. Calcium—lactate-induced enzymatic hydrolysis of extruded broken rice starch to improve Chinese rice wine fermentation and antioxidant capacity. *LWT.* (2020) 118:108803. doi: 10.1016/j.lwt.2019.108803

16. Pachnowska K, Cendrowski K, Stachurska X, Nawrotek P, Augustyniak A, Mijowska E. Potential use of silica nanoparticles for the microbial stabilization of wine: an in vitro study using Oenococcus oeni as a model. *Foods.* (2020) 9:1338. doi: 10.3390/foods9091338

17. Lee, S-J., Ahn, B-H. Sensory profiling of rice wines made with nuruks using different ingredients. *Korean J Food Sci Technol.* (2010) 42:119–23.

18. Delsart C, Grimi N, Boussetta N, Sertier CM, Ghidossi R, Peuchot MM, et al. Comparison of the effect of pulsed electric field or high voltage electrical discharge for the control of sweet white must fermentation process with the conventional addition of sulfur dioxide. *Food Res Int.* (2015) 77:718–24. doi: 10.1016/j.foodres.2015.04.017

19. Kim SA, Yun SJ, Jeon SH, Kim NH, Kim HW, Cho T, et al. Microbial composition of turbid rice wine (Makgeolli) at different stages of production in a real processing line. *Food Control.* (2015) 53:1–8. doi: 10.1016/j.foodcont.2015.01.002

20. Kim B, Bang J, Kim H, Kim Y, Beuchat LR, Ryu, et al. Bacillus cereus and Bacillus thuringiensis spores in Korean rice: Prevalence and toxin production as affected by production area and degree of milling. *Food Microbiol.* (2014) 42:89–94. doi: 10.1016/j.fm.2014.02.021

21. Li XM, Wang PH, Wu DH, Lu J. Effects of sterilization temperature on the concentration of ethyl carbamate and other quality traits in Chinese rice wine. *J Instit Brew.* (2014) 120:512–5. doi: 10.1002/jib.169

22. Liu SP, Mao J, Liu YY, Meng XY, Ji ZW, Zhou ZL, et al. Bacterial succession and the dynamics of volatile compounds during the fermentation of Chinese rice wine from Shaoxing region. *World Journal of Microbiology and Biotechnology.* (2015) 31:1907–1921. doi: 10.1007/s11274-015-1931-1

23. Suzuki K, Asano S, Iijima K, Kitamoto K. Sake and beer spoilage lactic acid bacteria—a review. *J Instit Brew.* (2008) 114:209–23. doi: 10.1002/j.2050-0416.2008.tb00331.x

24. Murugan NB, Mishra BK, Paul B. Antibacterial activity of indigenous fermented rice beverage of West Garo Hills, Meghalaya, India. *Int J Ferment Foods.* (2018) 7:39–44. doi: 10.30954/2321-712X.01.2018.5

25. Das AJ, Deka SC, Miyaji T. Methodology of rice beer preparation and various plant materials used in starter culture preparation by some tribal communities of north-east India: a survey. *Int Food Res J.* (2012) 19:101–7.

26. Zulfiker AHM, Ahmed D, Alam MB, Saha MR, Saha SK, Khalil MI, et al. Phenolic content and in vitro antioxidant potential of selected medicinal plants of Bangladesh. *J Pharm Res.* (2011) 4:1991–8.

27. Zhou W, Hu J, Zhang X, Chen Q. Application of bamboo leaves extract to Chinese yellow rice wine brewing for ethyl carbamate regulation and its mitigation mechanism. *Food Chemistr.* (2020) 319:126554. doi: 10.1016/j.foodchem.2020.126554

28. Deka D, Sarma GC. Traditionally used herbs in the preparation of rice-beer by the Rabha tribe of Goalpara district, Assam. *Indian Journal of Traditional Knowledge.* (2010) 9:459–62. doi: 10.1007/s10658-010-9609-x

29. Kim E, Chang YH, Ko JY, Jeong Y. Physicochemical and microbial properties of the korean traditional rice wine, makgeolli, supplemented with banana during fermentation. *Prevent Nutri Food Sci.* (2013) 18:203–9. doi: 10.3746/pnf.2013.18.3.203

30. Choi, J-S., Yeo, S-H., Choi, H-S., et al. Quality characteristics of Yakju containing pretreated lotus leaves. *Korean J Food Preserv.* (2016) 23:204–10. doi: 10.11002/kjfp.2016.23.2.204

31. Jang SA, Shin YJ, Song KB. Effect of rapeseed protein–gelatin film containing grapefruit seed extract on 'Maehyang' strawberry quality. *Int J Food Sci Technol.* (2011) 46:620–5. doi: 10.1111/j.1365-2621.2010.02530.x

32. Chim C, Erlinda ID, Elegado FB, Hurtada AW, Chakrya N, Raymundo CL. Traditional dried starter culture (Medombae) for rice liquor production in Cambodia. *Int Food Res J.* (2015) 22:1642–50.

33. Jung SJ, Shin TS, Kim JM. Improvement of Takju quality by a ripening-fermentation process using honey and extension of shelf life by control of takju mash sediment. *J Life Sci.* (2012) 22:80–6. doi: 10.5352/JLS.2012.22.1.80

34. Rawson A, Patras A, Tiwari BK, Noci F, Koutchma T, Brunton N. Effect of thermal and nonthermal processing technologies on the bioactive content of exotic fruits and their products: review of recent advances. *Food Res Int.* (2011) 44:1875–87. doi: 10.1016/j.foodres.2011.02.053

35. Park, H-J., Lee SM, Song SH, Kim, Y-S. Characterization of volatile components in *makgeolli*, a traditional Korean rice wine, with or without pasteurization, during storage. *Molecules* (2013) 18:5317–25. doi: 10.3390/molecules18055317

36. Jeon SH. *Microbiota composition of fermented alcoholic beverages products including beer, Cheongju, fruit wine, Makgeolli, Yakju consumed in Korea. (A thesis for the degree of master).* Korea University, Seoul, South Korea (2012).

37. Esteban MD, Huertas, J-P., Fernández PS, Palop A. Effect of the medium characteristics and the heating and cooling rates on the nonisothermal heat resistance of Bacillus sporothermodurans IC4 spores. *Food Microbiol.* (2013) 34:158–63. doi: 10.1016/j.fm.2012.11.020

38. Hereu A, Bover-Cid S, Garriga M, Aymerich T. High hydrostatic pressure and biopreservation of dry-cured ham to meet the Food Safety Objectives for *Listeria monocytogenes. Int J Food Microbiol.* (2012) 154:107–12. doi: 10.1016/j.ijfoodmicro.2011.02.027

39. Jiao A, Xu X, Jin Z. Research progress on the brewing techniques of new-type rice wine. *Food Chemistr.* (2017) 215:508–15. doi: 10.1016/j.foodchem.2016.08.014

40. Yang Y, Xia Y, Wang G, Tao L, Yu J, Ai L. Effects of boiling, ultrahigh temperature and high hydrostatic pressure on free amino acids, flavor characteristics and sensory profiles in Chinese rice wine. *Food Chemistr.* (2019) 275:407–16. doi: 10.1016/j.foodchem.2018.09.128

41. Guan, Y-G., Lin H, Han Z, Wang J, Yu, et al., Zeng, X-A., Liu YY, Xu, C-H., Sun, W-W. Effects of pulsed electric field treatment on a bovine serum albumin–dextran model system, a means of promoting the Millard reaction. *Food Chemistr.* (2010) 123:275–80. doi: 10.1016/j.foodchem.2010.04.029

42. Wu HM, Chen L, Pan GS, Tu CY, Zhou XP, Mo LY. Study on the changing concentration of ethyl carbamate in yellow rice wine during production and storage by gas chromatography/mass spectrometry. *Euro Food Res Technol.* (2012) 235:779–82. doi: 10.1007/s00217-012-1807-7

43. Xia XL, Zhang QW, Zhang B, Zhang WJ, Wang W. Insights into the biogenic amine metabolic landscape during industrial semidry Chinese rice wine fermentation. *J Agricult Food Chemistr.* (2016) 64:7385–93. doi: 10.1021/acs.jafc.6b01523

44. Wu, P.G., Cai CG, Shen XH, Wang LY, Zhang J, Tan, Y. et al. Formation of ethyl carbamate and changes during fermentation and storage of yellow rice wine. *Food Chemistr.* (2014) 152:108–12. doi: 10.1016/j.foodchem.2013.11.135

45. Lewis MJ. Heat treatment of foods: ultra-high-temperature treatments. *Encycloped Food Microbiol.* (2014) 14:187–92. doi: 10.1016/B978-0-12-384730-0.00158-0

46. Phinney DM, Feldman A, Heldman D. Modeling high protein liquid beverage fouling during pilot scale ultrahigh temperature (UHT) processing. *Food Bioproduct Process.* (2017) 106:43–52. doi: 10.1016/j.fbp.2017.08.007

47. Jin, T.-Y., Saravanakumar K, Wang, M-H. Effect of different sterilization methods on physicochemical and microbiological properties of rice wine. *Beni-Suef Univ J Basic Appl Sci.* (2018) 7:487–91. doi: 10.1016/j.bjbas.2018.05.002

48. Tian Y, Huang J, Xie T, Huang L, Zhuang W, Zheng Y, et al. Oenological characteristics, amino acids and volatile profiles of Hongqu rice wines during pottery storage: Effects of high hydrostatic pressure processing. *Food Chemistr.* (2016) 203:456–64. doi: 10.1016/j.foodchem.2016.02.116

49. Balasubramaniam VM, Martínez-Monteagudo SI, Gupta R. Principles and application of high pressure–based technologies in the food industry. *Ann Rev Food Sci Technol.* (2015) 6:435–62. doi: 10.1146/annurev-food-022814-015539

50. Rendueles E, Omer MK, Alvseike O, Alonso-Calleja C, Capita R, Prieto M. Microbiological food safety assessment of high hydrostatic pressure processing: a review. *LWT—Food Sci Technol.* (2011) 44:1251–60. doi: 10.1016/j.lwt.2010.11.001

51. Buzrul S. High hydrostatic pressure treatment of beer and wine: a review. *Innovat Food Sci Emerg Technol.* (2012) 13:1–12. doi: 10.1016/j.ifset.2011.10.001

52. Ha SJ, Kim YJ, Oh SW. Effect of high hydrostatic pressure (HHP) treatment on chemical and microbiological properties of *Makgeolli*. *J Korean Soc Appl Biol Chemistr.* (2013) 56:325–9. doi: 10.1007/s13765-013-3003-2

53. Bañuelos MA, Loira I, Guamis B, Escott C, Del Fresno JM, Codina-Torrella, et al. Morata A. White wine processing by UHPH without SO2. elimination of microbial populations and effect in oxidative enzymes, colloidal stability and sensory quality. *Food Chemistr.* (2020) 332:127417. doi: 10.1016/j.foodchem.2020.127417

54. Huang K, Yu L, Liu D, Gai L, Wang J. Modeling of yeast inactivation of PEF-treated Chinese rice wine: effects of electric field intensity, treatment time and initial temperature. *Food Res Int.* (2013) 54:456–67. doi: 10.1016/j.foodres.2013.07.046

55. Niu D, Zeng XA, Ren EF, Xu FY, Li J, Wang MS, et al. Review of the application of pulsed electric fields (PEF) technology for food processing in China. *Food Res Int.* (2020) 137:109715. doi: 10.1016/j.foodres.2020.109715

56. Sánchez-Vega R, Elez-Martínez P, Martín-Belloso O. Effects of high-intensity pulsed electric fields processing parameters on the chlorophyll content and its degradation compounds in broccoli juice. *Food Bioprocess Technol.* (2014) 7:1137–48. doi: 10.1007/s11947-013-1152-2

57. Walkling-Ribeiro M, Rodríguez-González O, Jayaram SH, Griffiths MW. Processing temperature, alcohol and carbonation levels and their impact on pulsed electric fields (PEF) mitigation of selected characteristic microorganisms in beer. *Food Res Int.* (2011) 44:2524–33. doi: 10.1016/j.foodres.2011.01.046

58. González-Arenzana L, Portu J, López R, López N, Santamaría P, Garde-Cerdán T, et al. Inactivation of wine-associated microbiota by continuous pulsed electric field treatments. *Innovat Food Sci Emerg Technol.* (2015) 29:187–92. doi: 10.1016/j.ifset.2015.03.009

59. Puértolas E, López N, Condón S, Raso J, Álvarez I. Pulsed electric fields inactivation of wine spoilage yeast and bacteria. *Int J Food Microbiol.* (2009) 130:49–55. doi: 10.1016/j.ijfoodmicro.2008.12.035

60. Milani EA, Alkhafaji S, Silva FVM. Pulsed electric field continuous pasteurization of different types of beers. *Food Control.* (2015) 50:223–9. doi: 10.1016/j.foodcont.2014.08.033

61. Shen C, Zhu H, Zhu W, Zhu Y, Peng Q, Elsheery, et al. The sensory and flavor characteristics of Shaoxing Huangjiu (Chinese rice wine) were significantly influenced by micro-oxygen and electric field. *Food Sci Nutri.* (2021) 9:6006–19. doi: 10.1002/fsn3.2531

62. Silva FV, van Wyk S. Emerging nonthermal technologies as alternative to SO2 for the production of wine. *Foods.* (2021) 10:2175. doi: 10.3390/foods10092175

63. Lung H-M, Cheng Y-C, Chang Y-H, Yang BB, Wang C-Y. Microbial decontamination of food by electron beam irradiation. *Trends Food Sci Technol.* (2015) 44:66–78. doi: 10.1016/j.tifs.2015.03.005

64. Chaturvedi S, Dave PN. "Application of nanotechnology in foods and beverages," in *Nanoengineering in the Beverage Industry*. London: Academic Press (2020). pp. 137–62 .

Identification and Characterization of the Stability of Hydrophobic Cyclolinopeptides From Flaxseed Oil

Adnan Fojnica[1], Hans-Jörg Leis[2] and Michael Murkovic[1]*

[1] Institute of Biochemistry, Graz University of Technology, Graz, Austria, [2] Department of Pediatrics and Adolescent Medicine, Medical University of Graz, Graz, Austria

Flaxseed (linseed) is a cultivar of the spring flowering annual plant flax (*Linum usitatissimum*) from the Linaceae family. Derivatives of this plant are widely used as food and as health products. In recent years, cyclic peptides isolated from flaxseed and flaxseed oil, better known as cyclolinopeptides (CLPs), have attracted the attention of the scientific community due to their roles in the inhibition of osteoclast differentiation or their antimalarial, immunosuppressive, and antitumor activities, as well as their prospects in nanotechnology and in the biomedical sector. This study describes the detection, identification, and measurement of CLPs in samples obtained from nine different flaxseed oil manufacturers. For the first time, Q Exactive Hybrid Quadrupole-Orbitrap Mass Spectrometer was used for CLP identification together with RP-HPLC. The routine analyses were performed using RP chromatography, measuring the absorption spectra and fluorescence detection for identifying tryptophan-containing peptides using the native fluorescence of tryptophan. In addition, existing protocols used for CLP extraction were optimized and improved in a fast and cost-efficient way. For the first time, 12 CLPs were separated using methanol/water as the eluent with RP-HPLC. Finally, the stability and degradation of individual CLPs in the respective flaxseed oil were examined over a period of 60 days at different temperatures. The higher temperature was chosen since this might reflect the cooking practices, as flaxseed oil is not used for high-temperature cooking. Using HPLC–MS, 15 CLPs were identified in total in the different flaxseed oils. The characterization of the peptides *via* HPLC–MS highlighted two types of CLP profiles with a substantial variation in the concentration and composition of CLPs per manufacturer, probably related to the plant cultivar. Among the observed CLPs, CLP-O, CLP-N, and CLP-B were the least stable, while CLP-C and CLP-A were the most stable peptides. However, it is important to highlight the gradual degradation of most of the examined CLPs over time, even at room temperature.

Keywords: flaxseed oil, cyclolinopeptides, characterization, stability, Orbitrap MS-RP HPLC

INTRODUCTION

Flaxseed (linseed) is a cultivar of the spring flowering annual plant flax (*Linum usitatissimum*) from the Linaceae family (1). Flax was first domesticated in approximately 8,000 B.C. in southwest Asia (Turkey, Iran, Jordan, and Syria) and is native to Algeria, Egypt, Tunisia, Greece, Italy, Spain, and Asia Minor (2). It is primarily used for direct consumption or as a salad oil and as an ingredient in traditional medicine (3). Currently, flaxseed is cultivated in more than 50 countries, including Canada, the United States, Brazil, India, China, and Ethiopia (4). Canada is the leading producer and exporter of oil-type flaxseed, producing on average 1,260,000 tons of flaxseed for oil, meal, and fiber, representing 43% of world production (5). The United States produces 224,000 tons of linseed annually (5). In Europe, the main producers of flax are the Czech Republic, Slovakia, France, Germany, Italy, Belgium, and Ireland (6). The plant is primarily cultivated to produce fibers for linen production, while plants grown for oilseed are of the same species but belong to a different cultivar (6).

Major constituents of flaxseed on average are 41% fat, 28% fiber, 20% protein, 7.7% moisture, and 3.4% ash, indicating that the percentage varies depending on the cultivar, growing conditions, and seed processing (7). Other components that are commonly found in flaxseed are cyclolinopeptides (CLPs), lignans, phenols, phytic acid, cyanogenic glycosides, trypsin inhibitor, linatine, and condensed tannins (8, 9).

Cyclolinopeptides, also called orbitides or linusorbs, represent a group of cyclic, hydrophobic peptides composed of eight (octapeptides), nine (non-apeptides), or even ten (decapeptides) amino acids, with molecular weights in the range of 950–2,300 Da (10, 11). CLPs are homomono-cyclopeptides and belong to the type VI (Caryophyllaceae) cyclopeptides (12).

The first cyclopeptide ever identified was cyclolinopeptide A, extracted in 1959 by Kaufmann and Tobschirbel (13) from the deposited sediments of crude flaxseed oil. Subsequently, each newly discovered cyclic peptide from flaxseed was named after the next letter in the alphabet. In total, 39 cyclolinopeptides were identified in flaxseed oil, roots, and seeds (10, 11), while 15 cyclolinopeptides are abundantly found in flaxseed oil, including peptides from CLP-A to CLP-O (14). Novel nomenclature was proposed by Shim et al. (10). However, the results described in this manuscript use the nomenclature commonly found in the literature with three-letter codes (8, 9, 13, 15–18). The CLPs detected in this study are shown in **Table 1**.

The natural function CLPs have in plants is still unknown. However, an increasing number of biological activities of hydrophobic CLPs have been examined, and diverse effects of CLPs have been identified, such as immunosuppressive, antimalarial, cancer-inhibiting, tumor-inhibiting, and osteoclast differentiation inhibiting effects (8, 9, 20–22). As each CLP has a unique biological activity, the potential treatment with flaxseed oil will depend on the presence of the respective peptide and its concentration in the oil.

To better understand CLPs and optimize their application, the development of an efficient extraction method would be a prerequisite step. Due to the complexity and structural similarity, protocols in the past had difficulties in CLP separation and detection, where using methanol/water as eluent, only five CLPs could be identified and separated (23, 24). Due to frequent encounters with unpleasant and bitter flavors during flaxseed oil consumption, a lack of consumer acceptance of flaxseed oil is apparent. Research conducted in previous years revealed that CLPs (primarily methionine oxidized variants of CLPs) contribute to the bitterness of the oil (23, 25, 26). Additional effort should be made to examine commercially available flaxseed oils and the levels of oxidation taking place in them. Furthermore, the stability of individual CLPs in flaxseed oil at room temperature (25°C) has not been reported in the literature to our knowledge. In 2007, Brühl and his team tried to visualize the effect of storage on the development of bitter taste in flaxseed oil. For this purpose, they examined flaxseed oil over a period of 30 weeks at −18 and 22°C (23). In 2014, Lao and his group examined the forced aging of a fresh flaxseed oil sample at 68°C using the Schaal oven test (17). The most extensive work on CLP stability was performed in 2013 by Aladedunye and his group (24). They examined the stability of flaxseed oil at 65°C for 30 days, evaluated the storage of CLP extracts for 25 h and 1 month at 4°C, and finally examined CLP concentrations in flax meals stored at room temperature for up to 48 months (24).

The objective of this study was to develop an efficient, novel, rapid, and cost-efficient extraction method as a prerequisite step for a better understanding of CLPs. Additionally, we aimed to find an appropriate high-resolution HPLC column for optimal separation of the CLPs among various C18 columns. Furthermore, an examination of different flaxseed oils, commonly found on the shelves of grocery stores in Central Europe, aimed to observe different patterns of CLPs and their oxidation. The next objective was to use a Q Exactive Hybrid Quadrupole-Orbitrap Mass Spectrometer coupled with RP-HPLC for the first time to detect and identify CLPs. Finally, the behaviors of 11 individual CLPs was examined over a period of 60 days at room temperature, and the effects of higher temperatures on the CLPs were investigated.

MATERIALS AND METHODS

Flaxseed Oil Samples and Chemicals

Abbreviations were used for flaxseed oil samples, and only the authors of this publication are familiar with the exact names of manufacturers. Cold-pressed flaxseed oil samples were acquired from the "AN" (Darmstadt, Germany), "VD" (Vienna, Austria), "ES" (Graz, Austria), "DM" (Karlsruhe, Germany), "BL" (Wels, Austria), "PB" (Spittal an der Drau, Austria), "GA" (Slovenska Bistrica, Slovenia), "SP" (Salzburg, Austria), and "FA" (Pöllau, Austria). Flaxseed oil samples were packaged in 250-ml dark bottles and stored at 4°C. All samples were freshly procured from local markets, except that flaxseed oil from the "GA" manufacturer was purchased in 2015 and was used multiple times before this experiment.

The HPLC grade deionized water, ethanol, and methanol were supplied by ChemLab Analytical (Zedelgem, Belgium).

TABLE 1 | CLPs in flaxseed oil extract detected using Hybrid Quadrupole-Orbitrap Mass Spectrometer-RP HPLC.

Type	Sequence	Chemical formula (MW + H$^+$)	References	Oils in which CLPs are detected
CLP-A	Ile-Leu-Val-Pro-Phe-Phe-Leu-Ile	$C_{57}H_{85}N_9O_9$ (1,040.6543)	(13)	"AN," "BL," "SP," "DM," "ES," "FA," "GA," "PB," and "VD"
CLP-B	Met-Leu-Ile-Pro-Pro-Phe-Phe-Val-Ile	$C_{56}H_{83}N_9O_9S$ (1,058.6107)	(8)	"BL," SP," "DM," "ES," "FA," "PB," and "VD"
CLP-C	Mso-Leu-Ile-Pro-Pro-Phe-Phe-Val-Ile	$C_{56}H_{83}N_9O_{10}S$ (1,074.6056)	(19)	"AN," "BL," "SP," "DM," "ES," "FA," "GA," "PB," and "VD"
CLP-D	Mso-Leu-Leu-Pro-Phe-Phe-Trp-Ile	$C_{57}H_{77}N_9O_8S$ (1,064.5638)	(19)	"AN," "BL," "SP," "DM," "ES," "FA," "GA," "PB," and "VD"
CLP-E	Mso-Leu-Val- Phe- Pro-Leu-Phe-Ile	$C_{51}H_{77}N_8O_9S$ (977.5529)	(19)	"AN," "BL," "SP," "DM," "ES," "FA," "GA," "PB," and "VD"
CLP-F	Mso-Leu-Mso-Pro-Phe-Phe-Trp-Val	$C_{55}H_{73}N_9O_{10}S_2$ (1,084.4995)	(15)	"AN," "BL," "SP," "DM," "ES," "FA," "GA," "PB," and "VD"
CLP-G	Mso-Leu-Mso-Pro-Phe-Phe-Trp-Ile	$C_{56}H_{75}N_9O_{10}S_2$ (1,098.5151)	(15)	"AN," "BL," "SP," "DM," "ES," "FA," "GA," "PB," and "VD"
CLP-I	Met-Leu-Mso-Pro-Phe-Phe-Trp-Val	$C_{55}H_{73}N_9O_9S_2$ (1,068.5045)	(9)	"DM" and "ES"
CLP-K	Msn-Leu-Ile-Pro-Pro-Phe-Phe-Val-Ile	$C_{56}H_{83}N_9O_{11}S$ (1,090.6006)	(16)	"GA"
CLP-L	Met-Leu-Val-Phe-Pro-Leu-Phe-Ile	$C_{51}H_{76}N_8O_8S$ (961.5580)	(16)	"SP," "DM," "ES," "FA," and "VD"
CLP-M	Met-Leu-Leu-Pro-Phe-Phe-Trp-Ile	$C_{57}H_{83}N_9O_8S$ (1,048.5689)	(16)	"BL," "SP," "DM," "ES," "FA," "PB," and "VD"
CLP-N	MET-Leu-Met-Pro-Phe-Phe-Trp-Val	$C_{55}H_{73}N_9O_8S_2$ (1,052.5096)	(16)	"BL," "SP," "DM," "ES," "FA," and "VD"
CLP-O	Met-Leu-Met-Pro-Phe-Phe-Trp-Ile	$C_{56}H_{75}N_9O_8S_2$ (1,066.5253)	(16)	"BL," "SP," "DM," "ES," "FA," and "VD"
CLP-P	Met-Leu-Mso-Pro-Phe-Phe-Trp-Ile	$C_{56}H_{75}N_9O_9S_2$ (1,082.5202)	(16)	"BL," "SP," "DM," "ES," "FA," "PB," and "VD"
CLP-T	Mso-Leu-Met-Pro-Phe-Phe-Trp-Val	$C_{55}H_{73}N_9O_9S_2$ (1,068.5045)	(17)	"BL," "SP," "DM," "ES," "FA," and "VD"

*Ile, isoleucine; Leu, leucine; Val, valine; Pro, proline; Phe, phenylalanine; Trp, tryptophan; Met, methionine; Msn, methionine sulfone; Mso, methionine sulfoxide.

Extraction of Cyclolinopeptides

Cyclolinopeptides were isolated from flaxseed oil using both liquid–liquid extraction methods and sonication-assisted methanol extraction (SAME). Both methods were previously reported to be used in 2013 and 2014, and their optimized versions are reported here (17, 24). Additionally, for the first time during liquid–liquid extraction, a novel method was introduced where a simple, additional step of using a methanol-water mixture preheated at 90°C was added before the extraction. In a liquid–liquid extraction method, an aliquot of 700 µl of flaxseed oil was added to a 700 µl methanol/ethanol + water mixture, followed by vortexing for 10 min and centrifugation for 10 min at 14,000 rpm. After centrifugation, the supernatant was used for analysis. Ratios of 60:40, 70:30, and 80:20 methanol–water mixtures were tested. In addition to liquid–liquid extraction, SAME was applied, for which 1 ml of flaxseed oil was added to 1 ml of methanol, vortexed for 10 mins, and sonicated at 30°C for 1 h. The mixture was centrifuged at 14,000 rpm for 10 mins, and the supernatant containing the peptides was analyzed by RP-HPLC. Variations in methanol volume (3, 5, 7, and 10 ml) and temperature (50 and 70°C) were also investigated.

As some CLPs are more prone to heat and oxidation, normal liquid–liquid extraction without a preheating step was used for all other experiments.

CLPs Separation Using RP-HPLC

High-performance liquid chromatography was conducted using an Agilent1100 series HPLC system. This comprised a quaternary pump, a degasser, a thermostated autosampler, and a diode array detector. The samples were separated using four different columns: Grace^{TM} Vydac (5 µm; 250 × 4.6 mm; 300 Å; Hichrom, Lutterworth, United Kingdom), Gemini^{TM} C18 (3 µm; 150 × 3 mm; 110 Å; Phenomenex, Aschaffenburg, Germany), Kinetex^{TM} C18 (5 µm; 150 × 3 mm; 100 Å; Phenomenex, Aschaffenburg, Germany), and Kinetex^{TM} C18 (2.6 µm; 100 × 3 mm; 100 Å; Phenomenex, Aschaffenburg, Germany). The separation was performed using an isocratic mobile phase of 70% methanol (A), 30% water, and 5% methanol (B) at 25°C with a flow rate of 0.5 ml/min. The column compartment temperature was 25°C for all experiments. The run time was set to 15 min with an injection volume of 5 µl. The detection was performed at a wavelength of 214 nm for the determination of the peptide

TABLE 2 | CLP extraction methods and their efficiencies.

CLPs	Methanol-water extraction (mAU)[a]	Hot methanol-water extraction (mAU)[a]	Ethanol-water extraction (mAU)[a]	SAME (mAU)[a]	Methanol-water extraction (mAU)[b]	Hot methanol-water extraction (mAU)[b]
CLP-F	125 ± 1[a]	173± 1[b]	106 ± 2[c]	99 ± 2[d]	3 ± 0[e]	4 ± 1[e]
CLP-G	314 ± 1[a]	452 ± 2[b]	274 ± 4[c]	264 ± 1[d]	13 ± 1[e]	16 ± 1[f]
CLP-C	314 ± 1[a]	403 ± 1[b]	280 ± 1[c]	266 ± 1[d]	66 ± 2[e]	82 ± 1[f]
CLP-D	100 ± 1[a]	113 ± 2[b]	88 ± 1[c]	96 ± 3[d]	N.A.	N.A.
CLP-E	181 ± 1[a]	212 ± 1[b]	178 ± 2[c]	181 ± 1[d]	N.A.	N.A.
CLP-A	296 ± 1[a]	283 ± 2[b]	325 ± 1[c]	322 ± 1[d]	403 ± 4[e]	474 ± 1[f]
CLP-M	33 ± 1[a]	7± 1[b]	25 ± 1[c]	23 ± 1[d]	261 ± 1[e]	303 ± 1[f]
CLP-T	N.A.	N.A.	N.A.	N.A.	29 ± 1[e]	40 ± 1[f]
CLP-P	N.A.	N.A.	N.A.	N.A.	118 ± 1[e]	140 ± 1[f]
CLP-N	N.A.	N.A.	N.A.	N.A.	65 ± 1[e]	76 ± 1[f]
CLP-B	N.A.	N.A.	N.A.	N.A.	307 ± 2[e]	348 ± 1[f]
CLP-O	N.A.	N.A.	N.A.	N.A.	177 ± 4[e]	203 ± 3[f]

Values are given as height with the standard deviation of three experiments.
[a] "PB", sample; [b] "FA", sample; N.A., not available. Different letters in each line reflect a significant difference of the ANOVA test of the analyses.

bonds, while 280 and 260 nm were used for tryptophan and phenylalanine detection, respectively. As the quantitation of CLP content was not the focus of this project, the injection of CLP extracts was intended to determine the presence, levels, and patterns of cyclic peptides. As the content of the CLPs is proportional to the peak height (mAU) of the detector, the response at 214 nm was used to evaluate the stability.

CLP Patterns of Nine Different Flaxseed Oil Manufacturers

The CLP levels, presence, and pattern differ among manufacturers due to different flaxseed varieties and oil processing techniques. Each sample was analyzed separately and compared. Aliquots of 700 μl were taken from each oil. To each tube containing flaxseed oil, 700 μl of a methanol–water mixture (70:30; *v/v*) was added. The combined mixture was vortexed for 10 min and centrifuged for 10 mins at 14,000 rpm and 4°C. The peptides were found in the supernatant, while the lower phase was discarded. In addition to individual measurements of each oil using RP-HPLC, 150 μl of each CLP extract was combined in one Eppendorf tube and further analyzed by RP-HPLC coupled with a Q Exactive Hybrid Quadrupole-Orbitrap Mass Spectrometer.

Cyclolinopeptide Detection and Identification Using Q Exactive Hybrid Quadrupole-Orbitrap Mass Spectrometer

High-resolution mass spectrometry (HRMS) spectra were recorded using a high-resolution Q Exactive Hybrid Quadrupole-Orbitrap Mass Spectrometer (Thermo Scientific) coupled with RP-HPLC. Q Exactive Orbitrap MS was used together with a Thermo Scientific Accela Open Autosampler, Thermo Scientific

Accela 1,250 Pump, MayLab MistraSwitch New Generation (NG) System Solution, and Phenomenex Kinetex 2.6 μm C18 100 Å, LC 150 × 3 mm. The parameters of HPLC–MS were as follows: 45 min of stop time; scan range: 150–2,000 m/z, resolution: 140,000 (MS1) and 35,000 (MS2); positive polarity; data-dependent MS² peak apex triggering (15 s); LC-flow rate: 0.5 ml/min, and an injection volume of 10 μl.

CLP Stability in Flaxseed Oil Over a Period of 60 Days at Room Temperature and 90°C

The stability and behavior of CLPs were examined at room temperature and 90°C. In general, biochemical stability and structural rigidity are notable features of cyclic peptides, and no significant change would be expected at lower temperatures (27). Additionally, the primary structure and number of amino acids of CLPs significantly differ and impact many properties of CLPs, including biological activity. Therefore, the stability of individual CLPs was expected to vary depending on their primary structure. As flaxseed oil is not used for cooking at high temperatures (e.g., frying and roasting) but could be added during boiling, the high temperature of 90°C was chosen as the simulation for the boiling process.

For this experiment, flaxseed oil samples from the "PB" and "FA" manufacturers were used. Aliquots of 700 μl were prepared for day 1, day 5, day 10, day 20, day 40, and day 60 and heated over a defined period in an Eppendorf Thermomixer at 300 rpm. Additional time points of 30 min, 1 h, 2 h, 4 h, and 6 h were incubated at 90°C. To test the stability at 25°C (as suggested by IUPAC), the same experimental setup was used. All samples were prepared at least in duplicate.

RESULTS AND DISCUSSION

CLP Extraction Methods and Efficiency of Extraction

For the purpose of examining CLP extraction methods, moderately aged flaxseed oil "PB" was used in this experiment, but the extraction methods for the "FA" sample are shown as well. There was a significant difference in CLP extraction using the liquid–liquid, hot methanol, and SAME methods, as shown in **Table 2**.

All tested methods showed good reproducibility. Overall, the most efficient method for most CLPs is the hot methanol–water extraction method. This is a simple and fast protocol reported for the first time. Five of the seven cyclolinopeptides were significantly extracted more efficiently in the hot methanol/water mixture compared to the other methods for the "PB" sample. For the "FA" oil, the extraction was improved for all CLPs, including CLP-A and CLP-M.

It is important to stress here that even though there was no momentous improvement in CLPs extraction efficiency in the examined methanol and water ratios used during liquid–liquid extraction, the 70:30 methanol ratio was the most efficient in
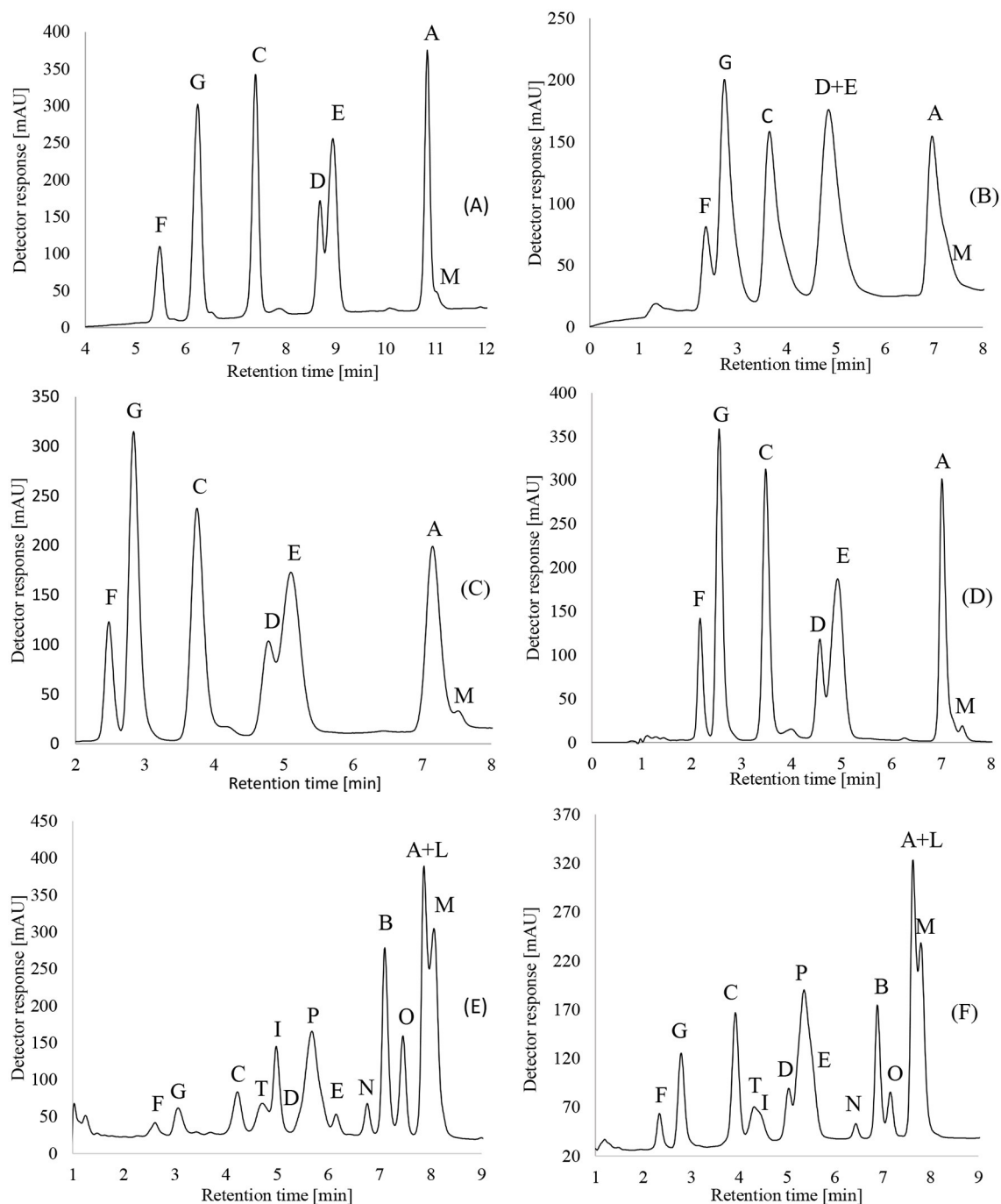
FIGURE 1 | RP-HPLC separations of CLPs from a moderately aged flaxseed oil sample using **(A)** GeminiTM C18, 3 μm column, **(B)** VydacTM C18, 5 μm column, **(C)** KinetexTM C18, 5 μm column, and **(D)** KinetexTM C18, 2.6 μm column and application of KinetexTM C18, 2.6 μm column for separations of CLPs from fresh flaxseed oil sample, "DM" manufacturer **(E)** and combined flaxseed oil samples **(F)**. The following settings were used: 0.5 ml/min flow rate; methanol and water isocratic elution as described in the "Methods" section. Liquid–liquid extraction was used for the extraction.

terms of CLP levels obtained. Additionally, for SAME, sonication at different temperatures (30, 50, and 70°C) gave almost identical results. Increasing the methanol content resulted in higher extraction of triglycerides.

In 2010, Marr et al. (28) reported a 5-fold increase in CLP recovery using liquid–liquid extraction compared to silica column extraction. However, the use of silica columns for the extraction for CLP isolation is a common approach used over the

FIGURE 2 | RP-HPLC detection and separations of CLPs from **(A)** "AN," **(B)** "BL," **(C)** "SP," **(D)** "DM," **(E)** "ES," **(F)** "FA," **(G)** "GA," **(H)** "PB," and **(I)** "VD" using a Kinetex™ C18 2.6 μm column. Eluent settings were used: 0.5 ml/min flow rate; methanol and water isocratic elution as described in the "Methods" section. Liquid–liquid extraction was used as the extraction method.
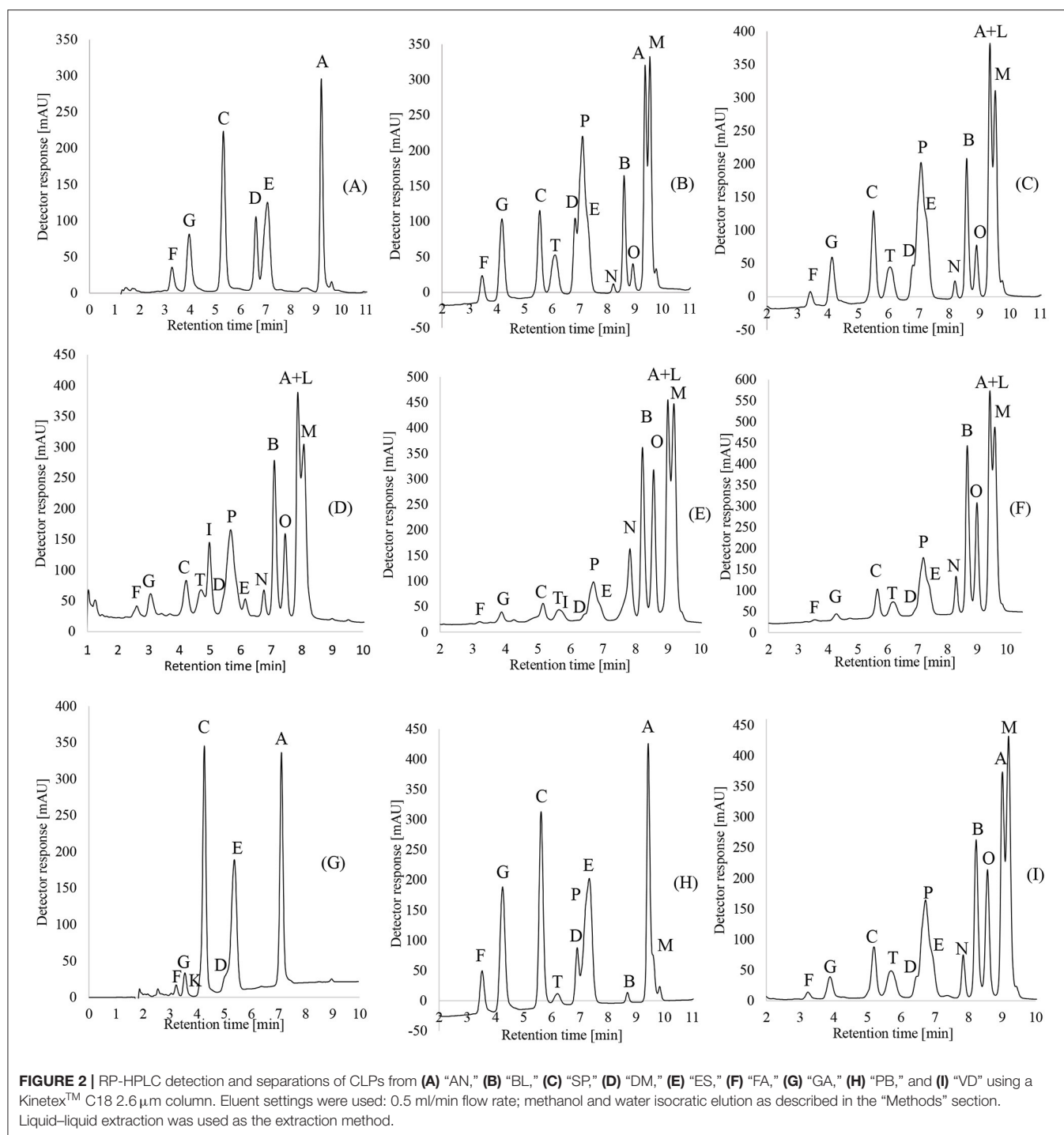
years (14, 23, 29, 30). In 2013, Aladedunye et al. reported SAME to be a more efficient method compared to silica column or solvent extraction conducted in 2010 and 2011 (24, 28, 31). As the exact concentration of the CLPs is unknown in the experiments conducted here, only the UV absorption of the CLPs could be

compared. This was especially useful for the very stable CLP-A. Based on CLP levels reported in their protocols, the optimized methods gave slightly better results compared to most previous protocols. However, the injection volume they used was higher than the injection volume used in our experiments.

TABLE 3 | Oxidative pathways of CLPs [according to Lao et al. (17)].

	0 Met	1 Met			2 Met			
0 Mso	CLP-A ILVPPFFLI	CLP-B MLIPPFFVI	CLP-L MLVFPLFI	CLP-M MLLPFFWI	CLP-N MLMPFFWV		CLP-O MLMPFFWI	
		↓	↓	↓	↗	↘	↗	↘
1 Mso		CLP-C **Mso**LIPPFFVI	CLP-E **Mso**LVFPLFI	CLP-D **Mso**LLPFFWI	CLP-T **Mso**LMPFFWV	CLP-I ML**Mso**PFFWV	CLP-H **Mso**LMPFFWI	CLP-P ML**Mso**PFFWI
					↘	↙	↘	↙
2 Mso		↓	↓		CLP-F **Mso**L**Mso**PFFWV		CLP-G **Mso**L**Mso**PFFWI	
1 Msn		CLP-K **Msn**LIPPFFVI	CLP-J **Msn**LVFPLFI					

The oxidation of the methionine thiol results in the formation of sulfoxide (Mso) or sulfone (Msn).
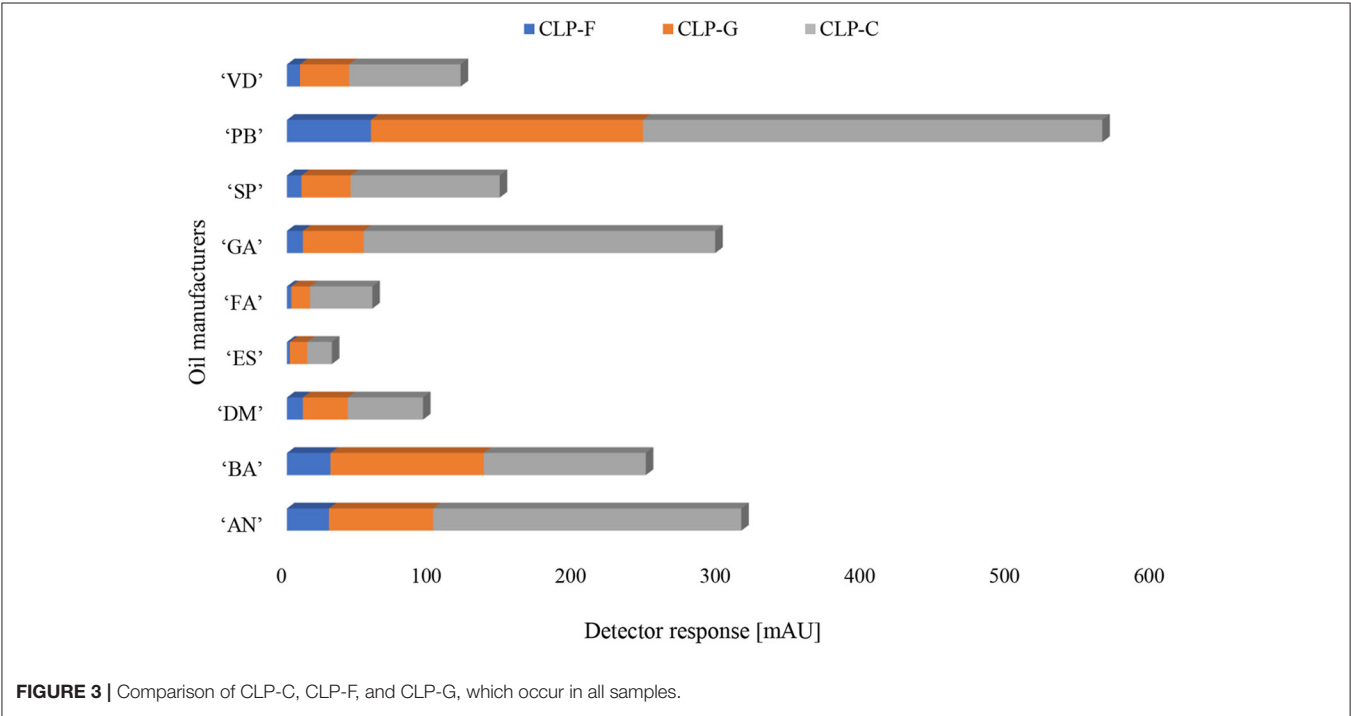
FIGURE 3 | Comparison of CLP-C, CLP-F, and CLP-G, which occur in all samples.

Comparison of the RP-HPLC Separation of Cyclolinopeptides Using Four Different Columns

The chromatographic performance of the two Kinetex™ reversed-phase HPLC columns with different particle sizes was compared to that of reversed-phase HPLC columns from Gemini™ and Vydac™ to evaluate their capability for CLP mixture separation. The optimized method was used for routine analyses as well as the MS experiments. An identical gradient, flow, and temperature were used for each of the described columns as previously described in the methods, with no further need for additional optimization. The good chromatographic separation of the CLPs allowed the use of UV detection for the determination of the major CLPs. MS was only used for unambiguous identification of the cyclic peptides. For the

routine analyses, UV detection (214 nm for determination of the peptide bond, 260 nm for phenylalanine residues, and 280 nm for tryptophan residues) could be used. In **Figure 1**, RP-HPLC separation of the CLPs is shown.

The overall retention time of the peptides was lower on the Kinetex™ and Vydac™ columns than on the Gemini™ column. The Gemini™ and Kinetex™ C18 columns with particle diameters of 3 and 2.6 μm performed better than the columns with a particle size of 5 μm (Vydac™ and Kinetex™), and separation was better for both the column and the CLP levels detected. Even though the Vydac™ column is generally used for proteins and peptides, it seems that columns with smaller particle sizes, such as Kinetex™ and Gemini™ C18 columns, are more suitable for the separation of octa- and non-apeptides. Additionally, the Kinetex™ C18 column with a particle diameter
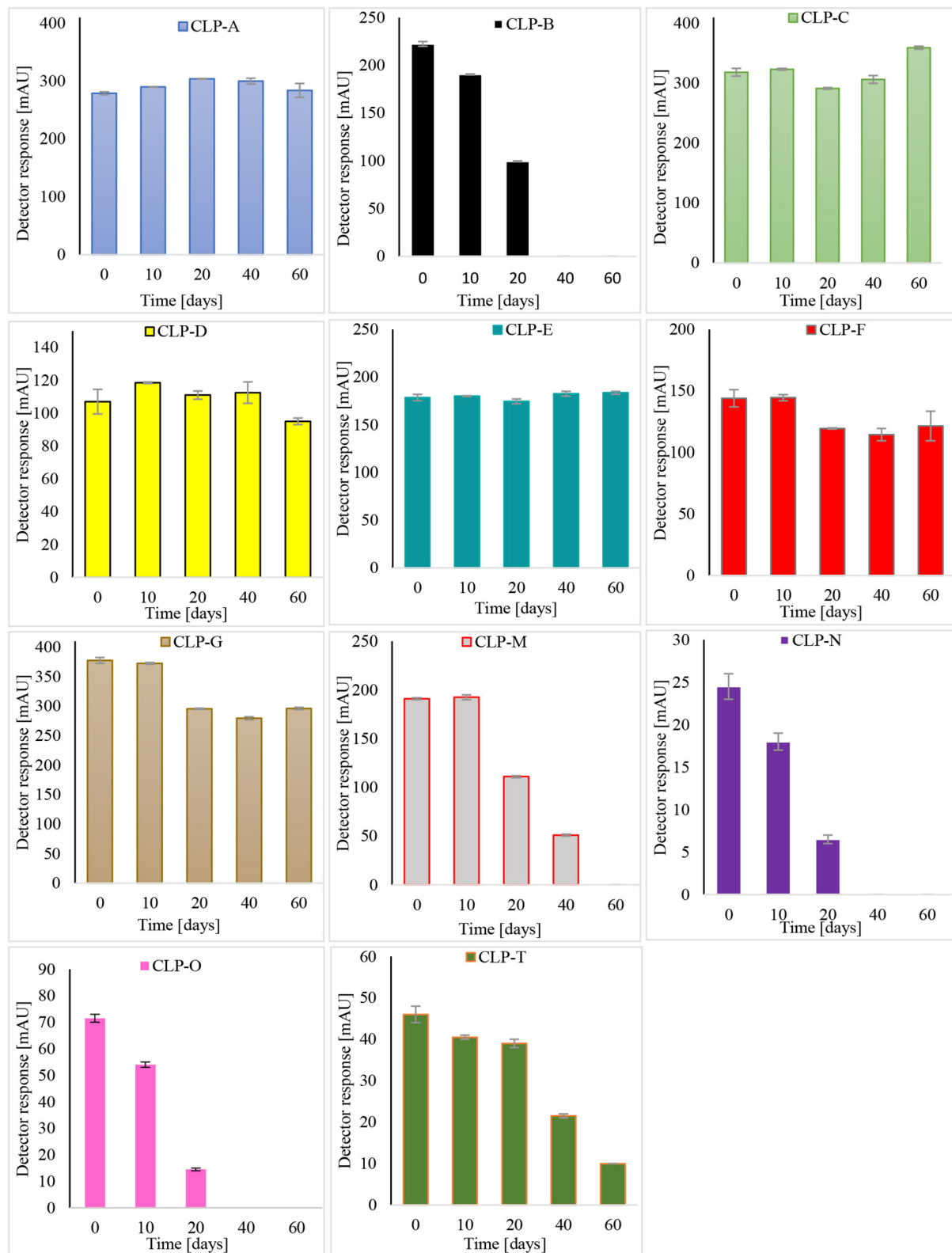
FIGURE 4 | Stability of CLPs at room temperature.

of 5 μm had a better separation, resulting in higher peaks of the CLPs compared to the Vydac™ column.

For the "PB" sample using Kinetex™ C18 columns, 7 peaks could be identified and separated, which are CLP-F, CLP-G, CLP-C, CLP-D, CLP-E, CLP-A, and CLP-M, similar to the Gemini™ C18 column. Using the Vydac™ C18 column, 7 peaks could also be identified. However, the separation of the pairs CLP-D and CLP-E, CLP-A, and CLP-M was not possible. The Kinetex™ C18 column with a particle size of 2.6 μm had the best overall separation and was used for further experiments, including CLP identification with Orbitrap MS-RP HPLC. For the fresh sample, using a Kinetex™ C18 column with a 2.6 μm particle size, up to 14 cyclolinopeptides could be detected, and 12 of them were effectively separated, CLP-F, CLP-G, CLP-C, CLP-T, CLP-I, CLP-D, CLP-P, CLP-E, CLP-N, CLP-B, CLP-O, CLP-A, CLP-L, and CLP-M. Efficient separation of CLP-A and CLP-L was not achieved.

In previous studies of chromatographic conditions for CLP separation, Brühl et al. (23) separated 5 CLPs using a LiChrospher 100 RP-18 column and methanol/water eluent. In 2012, Bo Gui et al. (14) managed to separate 6 CLPs using a ZORBAX Eclipse XDB-C18 column and acetonitrile/water eluent. In 2012, 7 cyclolinopeptides were separated using ZORBAX Eclipse XDB-C18 and Chromolith columns, again using acetonitrile-water as an eluent (29). In 2014, Lao et al. (17) separated up to 10 CLPs using a Kinetex™ phenyl-hexyl column and an acetonitrile-water gradient with RP-HPLC. Using a fast and cost-efficient approach with methanol-water as the eluent, we were able to detect 14 CLPs in freshly prepared flaxseed oil (e.g., "DM" manufacturer), while separation was efficient for up to 12 CLPs using RP-HPLC. Detection and separation of CLPs were achieved within 10 min using a flow of 0.5 ml/min. Additionally, it is important to mention that some other groups managed to separate 11 and 12 CLPs using RP-HPLC. However, applying time-consuming and expensive approaches for extraction and elution, where gradients of acetonitrile-water were used, with flows of 2 and 16 ml/min (30, 32). A potential limitation of using methanol as the eluent would be an occasional drift in the baseline, which was also reported in other publications (24).

CLP Patterns in Nine Different Flaxseed Oil Manufacturers

Levels of oxidation of freshly analyzed flaxseed oil samples from "AN," "BL," "DM," "ES," "FA," "PB," "SP," and "VD" were compared to the aged flaxseed oil sample from the "GA" manufacturer, produced in 2015. "GA" flaxseed oil was used as the reference for an oxidation pattern and oil with an unappealing content. All the above-mentioned manufacturers are commonly found on the shelves of grocery stores in Central Europe, especially Austria and Germany. The degree of oxidation of CLPs is considered to be a key element in the assessment of flaxseed oil quality (23, 24). Additionally, the bitterness of the flaxseed oil would depend mostly on the concentration of CLP-E in the oil (23, 24). There are many factors that affect the degree of oxidation of the oil, namely, the quality and level of oxidation of seeds, the methods used during flaxseed oil pressing and extraction, and

the handling of the oil during packaging. The samples shown below are measurements of fresh flaxseed oil, aiming to avoid prolonged deterioration and oxidation (**Figure 2**). The pathways of CLP oxidation are shown in **Table 3**.

The presence of methionine-containing peptides and the absence of methionine sulfoxide, as well as methionine sulfone-containing peptides, is a prerequisite for high-quality flaxseed oil. The complete absence of doubly oxidized CLP-F and CLP-G or their presence in low levels would be highly desirable and a good indication of high oil quality. The CLP patterns and their levels of oxidation in different flaxseed oil samples are shown in **Figure 2**.

The CLP patterns in flaxseed oil from nine different manufacturers showed that most oil samples have low levels of methionine sulfoxide, which is an indication of high oil quality. There was no detection of the peptides containing methionine sulfone, except for the "GA" sample from 2015, where CLP-K was detected, as would be expected for this aged sample. Additionally, CLP-E (indicator of bitterness) had the highest levels in the "GA" manufacturer, as it was forecasted in comparison to the other manufacturers. "AN" was the manufacturer with the second highest levels of oxidized CLP-E. Interestingly, doubly oxidized CLP-F and CLP-G had the highest levels in "PB." The levels of CLP-E in this sample were the third highest among the manufacturers. "BL" manufacturer was flaxseed oil with the second highest levels of CLP-F and CLP-G. Among all the examined manufacturers, "ES," "FA," and "DM" samples had the highest levels of methionine-containing CLPs and the lowest levels of oxidized peptides CLP-F and CLP-G, as well as the lowest levels of "bitter peptide" CLP-E. Additionally, example data demonstrating important comparisons between all samples are shown in **Figure 3**. CLP-C, CLP-F, and CLP-G are compared in all samples.

CLP Stability at Room Temperature and 90°C Over a Period of 60 Days

The stability of 11 CLPs was examined over a period of 60 days in two flaxseed oil samples, namely, "PB" and "FA." CLP-B, CLP-N, CLP-M, CLP-O, and CLP-T were observed in the "FA" sample, while the remaining CLPs were observed in the mild-aged aliquot of the "PB" flaxseed oil sample. The oxidation and behavior of CLPs were observed at room temperature (25°C) and 90°C. The stability of CLPs at room temperature is shown in **Figure 4**.

The least stable CLP at room temperature was CLP-O, where 80% of it degraded during the first 20 days, followed by CLP-N and CLP-B. All three CLPs were completely converted into their isomers, CLP-G, CLP-F, and CLP-C, within 40 days. CLP-M and CLP-T were also among the unstable CLPs. The levels of CLPs decreased by 45% and 80% over 40 days, whereas CLP-M was completely converted to CLP-D within 60 days. CLP-A, CLP-C, and CLP-E did not oxidize over a period of 60 days. Slight degradation of CLP-F and CLP-G was observed. It is important to mention here that in the case of the "FA" sample, CLP-B, CLP-N, CLP-M, CLP-O, and CLP-T would degrade over time, and peptides C, D, F, and G would increase accordingly. As the oxidation of peptides B, N, M, O, and T has already taken place in the case of the "PB" sample, this conversion would
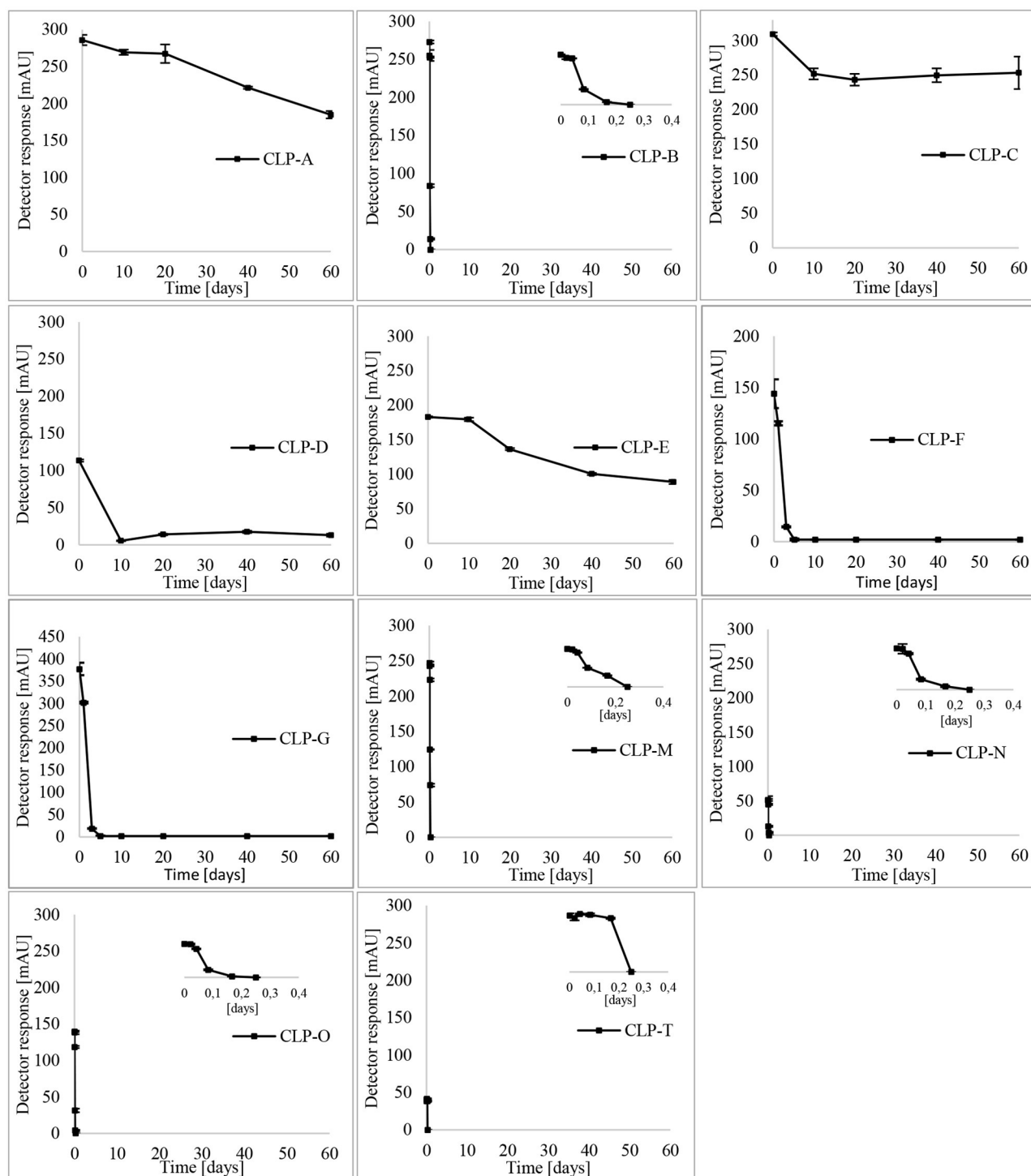
FIGURE 5 | Degradation of 11 CLPs at 90°C from a mild-aged mixture of "PB" and fresh "FA" oil sample.

not be observed. Therefore, in the sample "PB," the oxidation of peptides would not interfere with the examined temperature influence, and this oil is more suitable for the examination of the individual stability of the peptides C, D, F, and G. "FA" would be

the sample of choice for the examination of the dynamics of CLPs at specific temperatures.

Interestingly, Aladedunye et al. observed almost constant CLP levels in flaxseed meals over extended periods of several
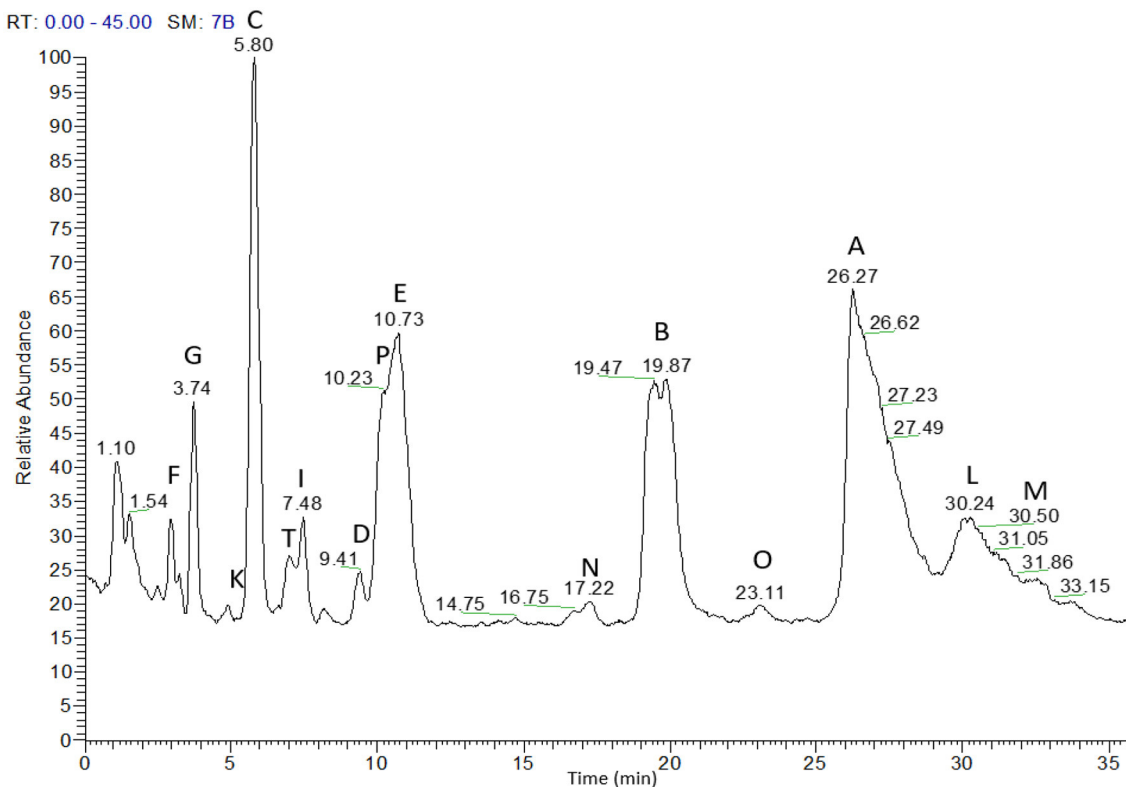
FIGURE 6 | RP-HPLC-Orbitrap MS analysis of flaxseed oil extract using a Kinetex™ C18 column.

months. A possible explanation for this could be the presence of an antioxidative system in flaxseed meals (24). Here, we report the complete evanescence of three CLPs within 40 days at 25°C.

Significant changes were expected to occur at 90°C, even during the very first hours of heat exposure. Due to the accelerated oxidation during the very first hours, a different graphical representation compared to room temperature was used to observe changes in the very first hours of heat exposure (**Figure 5**).

After half an hour of heat exposure, CLP-O, CLP-B, and CLP-N showed identical degradation. However, after 2 h, CLP-O showed the highest rate of oxidation, where 80% of degradation was observed, following the degradation of CLP-N and CLP-B with 75% and 70% decreases in the levels of CLPs. The levels of CLP-M decreased by 50% after 2 h and by 67% after 4 h. The above-mentioned CLPs degraded after 6 h. CLP-T was stable for 4 h, with no indication of oxidation, and after 6 h, the CLPs were degraded completely. Even though the trends of CLP-F, CLP-G, and CLP-C stability shown here are from the "PB" sample, in the "FA" sample, these peptides would increase accordingly with the degradation of CLP-B, CLP-N, CLP-M, CLP-O, and CLP-T and reach their peak after 6 h of heating, after which the degradation phase starts. This increase in the concentration of primary oxidation products was only observed in "FA" and not in "PB," as in "PB," the oxidation process had already taken place. After

3 days, CLP-F decreased by 90% and remained constant at lower levels, while CLP-G was reduced by 95% and remained constant later. CLP-D was stable in the first several days. However, 5 days after heat treatment, the amount of CLP-D decreased by 90%. In a period of 5 days, CLP-C was reduced by 20%, CLP-E by 25%, and CLP-A by approximately 7%. Interestingly, after prolonged periods, CLP-C remained at reduced levels, while CLP-E and CLP-A deteriorated further. Over a period of 60 days, CLP-C was more stable than CLP-A. The order of the stability of the CLPs is as follows: O < N < B < T < M < G < F < D < E < C < A.

In a publication from 2013, CLP-N, CLP-O, CLP-B, and CLP-L were observed to be the fastest degrading peptides (24). They also reported CLP-A to be the most stable peptide, together with CLP-C and CLP-E (24). Overall, the group used lower temperatures, resulting in significantly lower oxidation rates compared to our results. However, a similar pattern for almost all CLPs was observed (24).

Detection of Major CLPs in Flaxseed Oil Extracts Using High-Resolution MS

Detection of the major CLPs in a mixture of moderately aged and fresh flaxseed oil extracts was examined using a Q Exactive Hybrid Quadrupole-Orbitrap Mass Spectrometer coupled with RP-HPLC (**Figure 6**).

In total, 15 cyclic peptides could be identified with elution orders F, G, K, C, T, I, D, P, E, N, B, O, A, L, and M. Aladedunye

et al. (24) identified 14 CLPs in flaxseed oil, F, G, C, E, I, D, H, N, B, L, A, J, M, and K, using a Kinetex Column and HPLC Exactive Orbitrap MS. Lao and his group identified 15 CLPs, F, G, C, E, T, H, D, I, P, B, A, L, N, O, and M, using a Kinetex^{TM} phenyl-hexyl column and MALDI quadrupole/TOF prototype mass spectrometry (17). In 2021, in the CLP isolation experiment, 15 CLPs were identified using a Kinetex^{TM} phenyl hexyl column with a TripleTOF 5600 mass analyzer (32). Other groups identified up to 7 CLPs using Hybrid Quadrupole-TOF MS/MS with monolithic and microparticulate columns (29).

The phenomenon of peak splitting was previously reported in 2013 and 2014 for the peptides CLP-I and CLP-P (17, 24), while peak splitting for CLP-B was observed in this study. Usually, peak splitting was observed only in freshly prepared flaxseed oil on columns with higher separation efficiency (17).

CONCLUSION

Complete separation of 12 CLPs was achieved using a fast and economical approach within just 10 min, using RP-HPLC with a standard Kinetex^{TM} C18 column and methanol/water as the eluent. Most of the CLPs ever separated using a methanol eluent are reported in this study. A Vydac^{TM} C18 5 μm column, which is an industrial standard for peptides and proteins, was examined for separation purposes. However, better separation was observed for Gemini^{TM} and Kinetex^{TM} columns. A novel method has been introduced, where the extraction of CLPs was significantly improved with the simple heating of a methanol–water mixture before liquid–liquid extraction. The presence of CLPs was confirmed using Hybrid Quadrupole Orbitrap Mass Spectrometer coupled with RP-HPLC, and a total of 15 CLPs could be identified. Levels of peptide oxidation, presence of the bitter compound "CLP-E," and degree of oil deterioration would significantly vary in flaxseed oils commonly found on shelves in grocery markets. "GA," "AN," and "PB" had the highest levels

of CLP-E. Among all examined manufacturers, "ES," "FA," and "DM" samples had the highest levels of methionine-containing CLPs, the lowest levels of oxidized peptides, and lower levels of the "bitter" peptide CLP-E.

The pattern of CLP oxidation was examined at room temperature and 90°C, and the conversion of methionine-containing peptides into methionine sulfoxide-containing peptides was followed over a period of 60 days. At room temperature, the least stable CLP was CLP-O, where 80% of it degraded during the first 20 days, followed by the unstable CLP-N and CLP-B. All three peptides were completely converted into their isomers within 40 days. The same degradation pattern is observed at 90°C. However, with significantly faster oxidation, the abovementioned peptides were degraded in just 4 h. The order of stability of the CLPs is as follows: O < N < B < T < M < G < F < D < E < C < A.

DATA AVAILABILITY STATEMENT

The raw data supporting the conclusions of this article will be made available by the authors, without undue reservation.

AUTHOR CONTRIBUTIONS

AF conceived the main work on chromatography and stability experiments. H-JL performed the MS experiments. MM was responsible for the experimental design. All authors contributed to the writing of the manuscript. All authors contributed to the article and approved the submitted version.

ACKNOWLEDGMENTS

REFERENCES

1. Kole C, editor. *Genomic Designing of Climate-smart Oilseed Crops*. New York, NY: Springer Publishing (2019).

2. Oomah BD. Flaxseed as a functional food source. *J Food Sci Technol.* (2001) 81:889–94. doi: 10.1002/jsfa.898

3. Watson RR, Preedy VR, editors. *Bioactive Food as Dietary Interventions for Diabetes*. London: Academic Press (2019).

4. Mishra DK, Awasthi H. Quality evaluation of flaxseed obtained from different locations. *MDPI.* (2020) 4:70. doi: 10.3390/IECPS2020-08754

5. Wrigley CW, Corke H, Seetharaman K, Faubion J, editors. *Encyclopedia of Food Grains*. London: Academic Press (2015).

6. Bemiller JN, Whistler RL, Barkalow DG, Chen CC. *Aloe, Chia, Flaxseed, Okra, Psyllium Seed, Quince Seed, and Tamarind Gums*. London: Academic Press (1993).

7. Daun JK, Barthet VJ, Chornick TL, Duguid S. *Structure, Composition, and Variety Development of Flaxseed*. Urbana: ACOS (2003).

8. Morita H, Shishido A, Matsumoto T, Takeya K, Itokawa H, Hirano T, et al. A new immunosuppressive cyclic nonapeptide, cyclolinopeptide B from Linum usitatissimum. *Bioorg Med Chem Lett.* (1997) 7:1269–72. doi: 10.1016/S0960-894X(97)00206-0

9. Matsumoto T, Shishido A, Morita H, Itokawa H, Takeya K. Cyclolinopeptides F–I, cyclic peptides from linseed. *Phytochemistry.* (2001) 57:251–60. doi: 10.1016/S0031-9422(00)00442-8

10. Shim YY, Young LW, Arnison PG, Gilding E, Reaney MJ. Proposed systematic nomenclature for orbitides. *J Nat Prod.* (2015) 78:645–52. doi: 10.1021/np500802p

11. Shim YY, Song Z, Jadhav PD. Reaney MJ. Orbitides from flaxseed (*Linum usitatissimum* L): a comprehensive review. *Trends Food Sci Technol.* (2019) 93:197–211. doi: 10.1016/j.tifs.2019.09.007

12. Tan NH, Zhou J. Plant cyclopeptides. *Chem Rev.* (2006) 106:840–95. doi: 10.1021/cr040699h

13. Kaufmann HP, Tobschirbel A. Über ein oligopeptid aus leinsamen. *Chem Ber.* (1959) 92:2805–9. doi: 10.1002/cber.19590921122

14. Gui B, Shim YY, Reaney MJ. Distribution of cyclolinopeptides in flaxseed fractions and products. *J Agri Food Chem.* (2012) 60:8580–9. doi: 10.1021/jf3023832

15. Stefanowicz P. Detection and sequencing of new cyclic peptides from linseed by electrospray ionization mass spectrometry. *Acta Biochim.* (2001) 48:1125–9. doi: 10.18388/abp.2001_3877

16. Stefanowicz P. Electrospray mass spectrometry and tandem mass spectrometry of the natural mixture of cyclic peptides from linseed. *Eur J Mass Spectrom.* (2004) 10:665–71. doi: 10.1255/ejms.657

17. Lao YW, Mackenzie K, Vincent W, Krokhin OV. Characterization and complete separation of major cyclolinopeptides in flaxseed oil by reversed-phase chromatography. *J Sep Sci.* (2014) 37:1788–96. doi: 10.1002/jssc.201400193

18. Morita H, Takeya K. Bioactive cyclic peptides from higher plants. *Heterocycles.* (2010) 80:739–64. doi: 10.3987/REV-09-SR(S)7

19. Morita H, Shishido A, Matsumoto T, Itokawa H, Takeya K. Cyclolinopeptides B-E, new cyclic peptides from *Linum usitatissimum. Tetrahedron.* (1999) 55:967–76. doi: 10.1016/S0040-4020(98)01086-2

20. Kaneda T, Yoshida H, Nakajima Y, Toishi M, Nugroho AE, Morita H. Cyclolinopeptides, cyclic peptides from flaxseed with osteoclast differentiation inhibitory activity. *Bioorg Med Chem Lett.* (2016) 26:1760–1. doi: 10.1016/j.bmcl.2016.02.040

21. Zimecki M, Kaczmarek K. Effects of modifications on the immunosuppressive properties of cyclolinopeptide A and its analogs in animal experimental models. *Molecules.* (2021) 26:2538. doi: 10.3390/molecules26092538

22. Taniguchi Y, Yamamoto N, Hayashi K, Takeuchi A, Miwa S, Igarashi K, et al. Anti-tumor effects of cyclolinopeptide on giant-cell tumor of the bone. *Anticancer Res.* (2019) 39:6145–53. doi: 10.21873/anticanres.13822

23. Brühl L, Matthäus B, Fehling E, Wiege B, Lehmann B, Luftmann H, et al. Identification of bitter off-taste compounds in the stored cold pressed linseed oil. *J Agri Food Chem.* (2007) 55:7864–8. doi: 10.1021/jf071136k

24. Aladedunye F, Sosinska E, Przybylski R. Flaxseed cyclolinopeptides: analysis and storage stability. *J Am Oil Chem' Sco.* (2013) 90:419–28. doi: 10.1007/s11746-012-2173-0

25. Lang T, Frank O, Lang R, Hofmann T, Behrens M. Activation spectra of human bitter taste receptors stimulated with cyclolinopeptides corresponding to fresh and aged linseed oil. *J Agri Food Chem.* (2022) 70:4382–90. doi: 10.1021/acs.jafc.2c00976

26. Wu S, Wang X, Qi W, Guo Q. Bioactive protein/peptides of flaxseed: a review. *Trends Food Sci Technol.* (2019) 92:184–93. doi: 10.1016/j.tifs.2019.08.017

27. Joo SH. Cyclic peptides as therapeutic agents and biochemical tools. *Biomol Therap.* (2012) 20:19–26. doi: 10.4062/biomolther.2012.20.1.019

28. Marr J, Tremblay P, Picard P, Auger S, Burnett PG, Okinyo Owiti DP, et al. High throughput cyclolinopeptide and triacylglycerol (TAG) profiling of *Linum usitatissimum* using LDTD-MS/MS. In: *Paper presented at The American Society for Mass Spectrometry (ASMS) conference,* Salt Lake City, Utah (2010).

29. Olivia CM, Burnett PG, Okinyo-Owiti DP, Shen J, Reaney MJ. Rapid reversed-phase liquid chromatography separation of cyclolinopeptides with monolithic and microparticulate columns. *J Chromatogr B.* (2012) 904:128–34. doi: 10.1016/j.jchromb.2012.07.037

30. Sharav O, Shim YY, Okinyo-Owiti DP, Sammynaiken R, Reaney MJ. Effect of cyclolinopeptides on the oxidative stability of flaxseed oil. *J Agri Food chem.* (2014) 62:88–96. doi: 10.1021/jf4037744

31. Bagonluri MT, Okinyo-Owiti DP, Burnett PG, Olivia C, Gui B, Reaney MJ. High throughput HPLC analysis of cyclolinopeptides in flax seeds. In: *Paper presented at the CAOCS conference,* Edmonton. (2011).

32. Liu X, Cai ZZ, Lee WJ, Lu XX, Reaney MJ, Zhang JP, et al. A practical and fast isolation of 12 cyclolinopeptides (linusorbs) from flaxseed oil via preparative HPLC with phenyl-hexyl column. *Food Chem.* (2021) 30:351–129318. doi: 10.1016/j.foodchem.2021.129318

Check for
updates

Microencapsulation of Plant Phenolic Extracts Using Complex Coacervation Incorporated in Ultrafiltered Cheese Against AlCl$_3$-Induced Neuroinflammation in Rats

Tarek N. Soliman[1], Dina Mostafa Mohammed[2], Tamer M. El-Messery[1], Mostafa Elaaser[1], Ahmed A. Zaky[3]*, Jong-Bang Eun[4], Jae-Han Shim[5]* and Marwa M. El-Said[1]*

[1] Dairy Department, Food Industries and Nutrition Research Institute, National Research Centre, Cairo, Egypt, [2] Department of Nutrition and Food Sciences, Food Industries and Nutrition Research Institute, National Research Centre, Cairo, Egypt, [3] Department of Food Technology, Food Industries and Nutrition Research Institute, National Research Centre, Cairo, Egypt, [4] Department of Food Science and Technology, Chonnam National University, Gwangju, South Korea, [5] Natural Products Chemistry Laboratory, Biotechnology Research Institute, Chonnam National University, Gwangju, South Korea

Plant-derived phenolic compounds have numerous biological effects, including antioxidant, anti-inflammatory, and neuroprotective effects. However, their application is limited because they are degraded under environmental conditions. The aim of this study was to microencapsulate plant phenolic extracts using a complex coacervation method to mitigate this problem. Red beet (RB), broccoli (BR), and spinach leaf (SL) phenolic extracts were encapsulated by complex coacervation. The characteristics of complex coacervates [zeta potential, encapsulation efficiency (EE), FTIR, and morphology] were evaluated. The RB, BR, and SL complex coacervates were incorporated into an ultrafiltered (UF) cheese system. The chemical properties, pH, texture profile, microstructure, and sensory properties of UF cheese with coacervates were determined. In total, 54 male Sprague–Dawley rats were used, among which 48 rats were administered an oral dose of AlCl$_3$ (100 mg/kg body weight/d). Nutritional and biochemical parameters, including malondialdehyde, superoxide dismutase, catalase, reduced glutathione, nitric oxide, acetylcholinesterase, butyrylcholinesterase, dopamine, 5-hydroxytryptamine, brain-derived neurotrophic factor, and glial fibrillary acidic protein, were assessed. The RB, BR, and SL phenolic extracts were successfully encapsulated. The RB, BR, and SL complex coacervates had no impact on the chemical composition of UF cheese. The structure of the RB, BR, and SL complex coacervates in UF cheese was the most stable. The hardness of UF cheese was progressively enhanced by using the RB, BR, and SL complex coacervates. The sensory characteristics of the UF cheese samples achieved good scores and were viable for inclusion in food systems. Additionally, these microcapsules improved metabolic strategies and neurobehavioral systems and enhanced the protein biosynthesis of rat brains. Both forms failed to

induce any severe side effects in any experimental group. It can be concluded that the microencapsulation of plant phenolic extracts using a complex coacervation technique protected rats against AlCl3-induced neuroinflammation. This finding might be of interest to food producers and researchers aiming to deliver natural bioactive compounds in the most acceptable manner (i.e., food).

INTRODUCTION

Recently, plants have garnered considerable research attention. They contain metabolites and compounds such as phenolics, flavonoids, alkaloids, anthocyanins, glycosides, and peptides. These compounds have a number of pharmacological effects, including immunomodulatory, antinociceptive, anti-inflammatory, antioxidant, antibacterial, anticarcinogenic, antiulcer, gastroprotective, antifungal, antispasmodic, antiviral, aphrodisiac, emergency contraception, hepatoprotective, antihyperglycemic, antilipidemic, nephroprotective, and antiamnesic effects (1–3).

However, these compounds become unstable under oxidation, light, heating, and moisture (4). Furthermore, the usefulness of bioactive constituents is inextricably linked to their bioavailability, which means that they must be properly digested in the stomach and then transported through the blood before reaching the target cells. However, they may be destroyed by pH changes in the gastrointestinal tract (5).

Microencapsulation technology is used to maintain delicate substances in harsh environmental conditions. This technology can also facilitate regulated release and disguise undesirable sensory characteristics of certain substances (6, 7). Encapsulation using complex coacervation is an approach related to the interaction of two oppositely charged particles in the aqueous phase, in which an interaction between the shell components (typically proteins and carbohydrates) takes place around the bioactive compounds (8). These coacervates are used to encapsulate different products, such as vitamins, sugars, and phenolics (9–12).

Many recent studies have illustrated the relevance of cheese as an excellent source of critical nutrients for the human body. As a result, adding cheese to the food system may encourage the consumption of herbs, fruits, and vegetables compared to diets not including cheese (13, 14).

Combining the aforementioned elements with cheese has garnered substantial attention in human health and disease control research by supplying health-promoting aspects and increasing overall nutrient consumption, thereby improving diet quality. Aluminum (Al) is a neurotoxic chemical that has been found in contaminated food and water and is also subject to particle inhalation by people in certain environments and experimental animals (15–17). Aluminum has been linked to the pathologic progression of a variety of brain diseases and was reported to be among the factors that cause neuroinflammation and deficits in cognitive functions. Neuroinflammation alters the density of dendritic spines, thereby contributing to cognitive impairment and neurodegenerative diseases (18, 19). Numerous *in vitro*, experimental, and human investigations have shown that Al leads to oxidative stress in the brain (20, 21). Manufacturing reactive oxygen species deplete antioxidant systems and promote lipid peroxidation, mutagenesis, and protein alteration, along with other issues (22, 23). Moreover, Al causes impairment in long-term memory (24) and hippocampal long-term potentiation (25). The verification of neuroprotective therapies is of particular importance, given that there are currently no cures for neurodegenerative diseases (26).

To our knowledge, no research has used encapsulated phenolic extracts [spinach leaf (SL), broccoli (BR), and red beet (RB)] for neuroinflammation, particularly their integration into UF cheese. Furthermore, phenolic extracts and cheese are good delivery vehicles for bioactive compounds, particularly phenolic compounds. As a result, this study integrated encapsulation, phenolic extracts, and UF cheese to preserve key bioactive components and also investigated the effects of these extracts on experimental rats against AlCl3-induced neuroinflammation.

MATERIALS AND METHODS

Materials

The Animal Production Research Institute, Agriculture Research Center, Dokki, Egypt, supplied fresh ultrafiltration buffalo cream retentate. Gaglio Star (Spain) provided the fungal rennet powder (RENIPLUS) derived from Mucor miehei. RB (*Beta vulgaris*), BR (*Brassica oleracea var. italica*), and SL (*Spinach oleracea*) were acquired in a vegetable market in Giza. The analytical- and laboratory-grade chemicals and solvents utilized in the investigation were purchased from Sigma chemicals company (St. Louis, United States).

Methods

Extraction of Phenolic Compounds

RB, BR, and SL were chosen for lack of flaws and then cleaned under flowing water. A measure of 10 g of each plant sample was added to 200 mL of ethanol (80%) and placed in an ultrasonicator for 1 min at room temperature. The samples were centrifuged, and the supernatant was separated. The extraction procedure was conducted three times. The solvent was evaporated by using a rotary evaporator (Büchi R20, Switzerland), and the residue was powdered using a freeze dryer (Labconco cooperation, Kansas City, United States) at −52°C for 48 h under 0.1 mPa and stored at −18°C (27).

High-Performance Liquid Chromatography

An Agilent 1260 series was used for high-performance liquid chromatography (HPLC) analysis. An Eclipse C18 column (4.6250 mm i.d., 5 m) was utilized for the separation. At a flow rate of 1 mL min G1, the mobile phase was composed of water (A) and 0.05% trifluoroacetic acid in acetonitrile (B). The mobile phase was set in the following order: 0 min (82% A), 0–5 min (80% A), 5–8 min (60% A), 8–12 min (60% A), 12–15 min (85% A), and 15–16 min (82% A). The multiwavelength detector was monitored at 280 nm. For each of the sample solutions, the injection volume was 10 L. The temperature in the column was kept constant at 35°C.

Preparation of Complex Coacervate Microcapsules

Cilek et al. (28) and El-Messery et al. (29) clarified that microcapsules of RB, BR, and SL powdered extracts can be prepared using a complex coacervation technique utilizing gum arabic (GA) and whey protein concentrate (WPC). We initially dissolved 3% (w/w) WPC in distilled water (40°C) once it became a homogeneous mixture. Then, we dissolved 1% (w/w) GA in distilled water at 25°C. The microcapsules were prepared by dissolving the powdered extract in the WPC solution at a ratio of 1:10, followed by diluting three to four times with distilled water at 50°C. The previous mixture (powdered extract and WPC) was mixed with the GA solution and centrifuged at 800 rpm. To generate electrostatic contact between WPC and GA, the pH of this combination was changed to 3.75 by infusion of 1% citric acid (added dropwise). The microencapsulation strategy was conducted at 25°C and then cooled to $5°C\ h^{-1}$. Last, the resultant complex was powdered using a freeze dryer (Labconco cooperation, Kansas City, United States) at –52°C for 48 h under 0.1 mPa.

Characterization of Microcapsules

ζ-Potential

To assess zeta potential, a dynamic light scattering instrument (Nano ZS, Malvern Instruments, Worcestershire, United Kingdom) was employed.

Total Phenolic Content

The total phenolic content (TPC) of the samples was evaluated according to the technique described in Zaky et al. (30). Folin–Ciocalteu reagent (100 μL) was used, followed by the addition of 1.58 mL of DW, and 20 μL of the sample. After 3 min, 300 μL of Na2CO3 (20%) was added. The mixture was left to stand at room temperature for 30 min. Then, the absorbance was estimated at 765 nm using a spectrophotometer (Cary 60 UV–Vis, Agilent Technologies, United States). The findings are presented as milligrams of gallic acid equivalent per gram.

Surface Phenolic Content

The Surface Phenolic Content (SPC) of the complex coacervates was determined according to the method described by Saénz et al. (31). A total of 100 mg of microcapsules was dispersed in 1 mL of ethanol–methanol mixture (1:1, *v/v*) for 1 min. The amounts of surface phenolic compounds were measured and quantified using the same method described in the TPC section.

Encapsulation Efficiency

The following equation (32) was used to calculate the EE of microcapsules:

$$EE = (TPC - SPC)/\ TPC \times 100$$

Morphology

A scanning electron microscope (Quanta FEG 250 SEM) (Thermo Fisher Scientific, Oregon, United States) was used to characterize the particle structure of RB, BR, and SL microcapsules.

Fourier Transform Infrared Spectroscopy

Hu et al. (33) suggested a technique to identify chemical structures using an fourier transform infrared spectroscopy (FT-IR) spectrophotometer (Nicolet iS10, Thermo Fisher Scientific Co., Ltd., Waltham, Massachusetts, United States). In a ceramic mortar, the powdered sample was mixed with KBr powder and crushed into pellets. The FT-IR spectrum of the sample was obtained at a frequency of 4 cm^{-1} in the transmission mode in a wavelength range of 500–4,000 cm^{-1}.

Preparation of Ultrafiltration Soft Cheese

UF cheese was prepared as per the method of Hala et al. (13). Fresh UF full cream retentate was used to make UF soft cheese, which was pasteurized at 72°C for 15 s, cooled and adjusted to 42°C, and then split into four batches. The first batch served as a control, and the other three batches were mixed separately with the RB, BR, and SL complex coacervates (equivalent to 100 mg of phenolic content in each microcapsule). Rennet was added and packed in plastic cups (100 mL) and then incubated (42°C) until full coagulation (40 min). The cheese samples were stored at a low (5 ± 2°C) temperature. Three duplicates from separate batches were prepared and examined.

Chemical Analysis

The chemical properties of UF cheese formulations were evaluated as described in AOAC (34). A pH meter (Jenway 3510) was utilized to determine the pH of the UF cheese samples.

Texture Profile Analysis

The parameters of texture assessment (cohesion, hardness, springiness, gumminess, and chewiness) for UF cheese samples were examined utilizing the dual stress test (TMS-Pro Texture Analyzer, United States) (35).

Sensory Evaluation

As indicated by Clark et al. (36), the UF cheese samples were analyzed for sensory qualities at 5 ± 2°C. A total of 10 panelists from the Dairy Department, National Research Centre, assessed the cheese samples for color and appearance, body and texture, and flavor (50, 40, and 10, respectively).

Experimental Animals

A total of 54 male Sprague–Dawley rats between 7 and 9 weeks of age and weighing 200–250 g were obtained from the National Care Unit, NRC, Cairo, Egypt. The animals were fed a basic balanced diet and water for 7 days before the study to enable acclimatization and ensure normal development and behavior. Individualized solid bottom cages were used to acclimate the rats

in a temperature-regulated (23°C) environment at 40–60 g/100 g relative moisture, were lighted artificially (12 h dark/light cycle), and were free of contaminants. All rats were handled in accordance with the Animal Experimental Guidelines approved by the Ethical Committee of Medical Research, National Research Centre, Egypt, and the National Legislation on Lab Animal Rescue and Usage.

Diet Formulation

The basic balanced diet consisted of casein (150 g/kg), unsaturated fat (100 g/kg), sucrose (220 g/kg), maize starch (440 g/kg), cellulose (40 g/kg), salt mixture (40 g/kg), and vitamin mixture (10 g/kg) (37, 38). The salt and vitamin mixture was created using the AIN-93 M diet as a guide (39).

Induction of AlCl$_3$ Neuroinflammation

AlCl$_3$ solution was prepared for oral administration. AlCl$_3$ was solubilized in distilled water and given orally at a dosage of 100 mg/kg body weight [BW]/d) (1 mL/rat/d for 4 weeks) (40).

Experimental Design

This study used 54 rats divided into nine groups (six rats each) described as follows:

- **Negative control:** Normal rats fed a basic balanced diet.
- **Positive control:** Rats with AlCl$_3$-induced neuroinflammation were orally administered anhydrous AlCl$_3$ daily for 4 weeks.
- **Group (1):** Rats with AlCl$_3$-induced neuroinflammation were fed daily and orally administered the RB complex coacervate for 4 weeks (300 mg/kg BW/d) (41) 1 h before AlCl$_3$ induction.
- **Group (2):** Rats with AlCl$_3$-induced neuroinflammation were fed daily and orally administered the BR complex coacervate for 4 weeks (1.5 g/kg BW/d) (42) 1 h before AlCl$_3$ induction.
- **Group (3):** Rats with AlCl$_3$-induced neuroinflammation were fed daily and orally administered the SL complex coacervate for 4 weeks (400 mg/kg BW/d) (43) 1 h before AlCl$_3$ induction.
- **Group (4):** Rats with AlCl$_3$-induced neuroinflammation were fed UF cheese for 4 weeks 1 h before AlCl$_3$ induction.
- **Group (5):** Rats with AlCl$_3$-induced neuroinflammation were fed UF cheese supplemented with the RB complex coacervate (45 mg/2.25 g UF/rat/d) for 4 weeks 1 h before AlCl$_3$ induction.
- **Group (6):** Rats with AlCl$_3$-induced neuroinflammation were fed UF cheese supplemented with the BR complex coacervate (0.3/2.25 g UF/rat/d) for 4 weeks 1 h before AlCl$_3$ induction.
- **Group (7):** Rats with AlCl$_3$-induced neuroinflammation were fed UF cheese supplemented with the SL complex coacervate (60 mg/2.25 g UF/rat/d) for 4 weeks 1 h before AlCl$_3$ induction.

During the experiment, the rats were fed a well-balanced diet. Food consumption was tracked on a daily basis. The total food intake, BW gain, and feed efficiency ratio were determined. All animal groups were starved for 12 h before being euthanized by cervical dislocation. They were sedated with

ketamine hydrochloride (35 mg/kg IM) after a 4-week research period before euthanasia.

Biochemical Parameters

Preparation of Brain Homogenates.. Brain tissues were dissected from each animal, placed on ice, and stored in 10% saline. The brain tissues were homogenized in PBS (pH 7.4) and subjected to high-speed centrifugation at 4,000 rpm for 20 min (4°C). The resultant supernatant was used for the biochemical analysis. All rat brain homogenates were promptly assessed for malondialdehyde (MDA) (44, 45), superoxide dismutase (SOD) (46), CAT (47), glutathione peroxidase (GPx) (48), reduced glutathione (GSH) (49), nitric oxide (NO) (50), acetylcholinesterase (AChE) (51), and butyrylcholinesterase (52). Additionally, dopamine (DA), 5-hydroxytryptamine (5-HT; serotonin), brain-derived neurotrophic factor (BDNF), and glial fibrillary acidic protein (GFAP) levels were determined by an enzyme-linked immunosorbent assay with ELISA kits (Sunlong Biotech, China).

Statistical Analyses.. SPSS (IBM® SPSS®, 2017) was used to analyze data (mean values and standard deviation, or mean values and standard error). Differences at 5% significance were assessed using ANOVA and Duncan's multiple range tests ($P < 0.05$; $P < 0.005$). All of the tests were repeated three times, and the analysis was performed in triplicate (53).

RESULTS AND DISCUSSION

High-Performance Liquid Chromatography Analysis of Phenolic Extracts

The HPLC profiles of RB, BR, and SL were analyzed for 17 phenolic compounds, including gallic acid, chlorogenic acid, methyl gallate, caffeic acid, syringic acid, pyrocatechol, rutin, ellagic acid, coumaric acid, vanillin, ferulic acid, naringenin, daidzein, quercetin, cinnamic acid, apigenin, kaempferol, and hesperetin. The quantitative results are shown in **Table 1**. The total amount of phenolics in the SL extract was the greatest, followed by the BR extract and the RB extract (12801.16, 4923.08, and 541.77 μg/g, respectively). For the RB extract, six major phenolics were observed with concentrations of 11.67, 252.04, 9.68, 51, 79.14, and 38.24 μg/g for gallic acid, chlorogenic acid, syringic acid, daidzein, kaempferol, and hesperetin, respectively. Although chlorogenic and gallic acids had the highest concentrations in the BR extract (1506.3 and 1241.6 g/g, respectively), the phenolic compound with the lowest concentration was caffeic acid (13.24 μg/g). From the results in **Table 1**, it is clear that the highest concentration of phenolic compounds in the SL extract was observed for daidzein, followed by quercetin (3984.8 and 2836.7 μg/g, respectively).

Complex Coacervate Characterization
ζ-Potential Analysis

The ζ-potential values of the RB, BR, and SL complex coacervates are shown in **Figure 1**. The colloidal molecules interact depending on their ζ-potential; therefore, determining

TABLE 1 | Phenolic compound profile (µg/g) of red beet, broccoli, and spinach leaf extracts using HPLC.

Phenolic compounds conc. (µg/g)	Red beet	Broccoli	Spinach leaves
Gallic acid	111.67	1241.57	453.84
Chlorogenic acid	252.04	1506.33	646.86
Methyl gallate	0	783.47	62.88
Caffeic acid	0	13.24	100.88
Syringic acid	9.68	84.13	865.14
Pyro catechol	0	21.25	0
Rutin	0	158.55	400.82
Ellagic acid	0	167.37	1621.3
Coumaric acid	0	66.34	92.07
Vanillin	0	62.2	219.24
Ferulic acid	0	54.21	684.19
Naringenin	0	365.18	805.31
Daidzein	51	207.37	3984.79
Quercetin	0	85.65	2836.71
Apigenin	0	21.95	0
Kaempferol	79.14	0	23.21
Hesperetin	38.24	84.27	3.92
Total	**541.77**	**4923.08**	**12801.16**

the ζ-potential explains possible repulsive interactions between charged molecules (54). The RB, BR, and SL complex coacervates had −11.55 ± 0.64, −10.75 ± 0.78, and −11.90 ± 0.57 mV ζ-potentials, respectively. Because of the higher WPC and GA weights in solution, the ζ-potential of the RB, BR, and SL complex particles was always negatively charged. The RB, BR, and SL complex coacervates had ζ-potential values close to zero, indicating that electrostatic interactions neutralize the charges of biopolymers, as predicted in the complex coacervation technique (12). Aggregations were caused primarily by a shortage of electrostatic interactions among biomolecules, which resulted in the development of insoluble microcapsule coacervates (55). However, a ζ-potential of approximately 30 mV suggested a steady diffusion system because of the dominance of electrostatic interparticle interactions (56). The ζ-potential values assisted in determining the total charge of the microcapsules included in the diffusion GA/WPC, indicating charge neutralization through electrostatic interactions.

Encapsulation Efficiency

Figure 2 shows the encapsulation efficiency of the RB, BR, and SL complex coacervates. However, the greatest EE (81.3%) was reported for the RB complex coacervate, followed by the EEs of both the BR and SL complex coacervates. This is in agreement with the findings of El-Messery et al. (57), who reported that orange peel polyphenol extract was maintained and included in functional yogurt because of the encapsulation of this extract in WPC and GA. Additionally, the WPC was used for polyphenol encapsulation as an encapsulated material in oat bran biotechnology studies (58). The EE was 95.28% when WPC and MD were used at a ratio of 60:40. Furthermore, spray-drying monomeric anthocyanins in whey protein isolates, according to Flores et al. (59), resulted in an encapsulation effectiveness of

70%. Ong et al. (60) reported that anthocyanins extracted from the peel of sour cherries were successfully packaged in a whey protein isolate, with a 70.30 ± 2.20% encapsulation efficiency. Overall, encapsulation efficiency depends on the interaction between phenolics and protein to form the phenolic–protein complex. This interaction is based on strong hydrophobic and hydrogen bonds. Therefore, the red beet phenolic extract may contain a phenolic group that acts as an excellent hydrogen donor. When interacting with protein, the phenolic group will form a strong hydrogen bond with the carboxyl group in protein.

Morphology

Figure 3 demonstrates the WPC/GA ratio, which provides a protective coating for the RB, BR, and SL phenolic extracts. The particles containing the RB, BR, and SL phenolic extracts were examined by scanning electron microscopy. It was observed that the microcapsules had smoother and fewer wrinkles on the surface, presumably because of the presence of the extracts in microparticles, which decreased evaporation from the surface and increased the particle moisture content. This feature of the microcapsules was caused by the rapid sublimation of ice water from the wall component, resulting in the formation of a hollow in a crystallite surface without enough time for wrinkles to form (61). These findings demonstrate that using a WPC/GA ratio of 60:40 as the wall material can microencapsulate phenolics with the lowest particle diameter (321–338 nm), which is consistent with previous findings (57, 58, 62).

FTIR Spectroscopy

The FTIR spectra of the powdered extract, its microcapsules (RB, BR, and SL), and the raw materials utilized to make the microcapsules in this investigation are presented in **Figure 4**. These formulations were studied in their solid phases to avoid the influence of water absorption. In the FTIR spectrum of pure GA, OH stretching, which is typical of the glycosidic ring vibration of hydroxyl groups, contributed to the presence of a broad band at 3,274 cm^{-1}, whereas GA revealed a signal for the dilation of C–H at 2,971 cm^{-1}. Furthermore, the COO-symmetric stretching of GA yielded a prominent signal at 1,637 cm^{-1}. The peaks at 1,454 cm^{-1} were related to the asymmetric dilation of COO−, whereas the peaks at 1,254–1,029 cm^{-1} were the fingerprint of carbohydrates. However, the FTIR spectrum of WPC was 1,648 and 1,453 cm^{-1}. The peaks of the phenolic OH groups were at 3,258, 3,279, and 2,359 cm^{-1} in the raw material FTIR spectra of pure BR, RB, and SL powdered extracts, respectively. The other phenolic compounds from the extracts were capped on the surface of the produced nanoparticles, stabilizing them, as shown by the presence of the other distinctive peaks of extracts in the FTIR spectrum of the WPC. There were significant changes in peak positions in the bands because of hydrogen bonding between phenolics and proteins. The interactions of WPC with several monophenolic, diphenolic, and polyphenolic chemicals are clarified in **Figures 4A–C** (57). The interaction between phenolics in WPC was studied using FTIR, which revealed the formation of certain complex hydrogen bonds. Furthermore, electrostatic interactions are important in the stabilization of the peptide by phenolic compounds. Phenolic
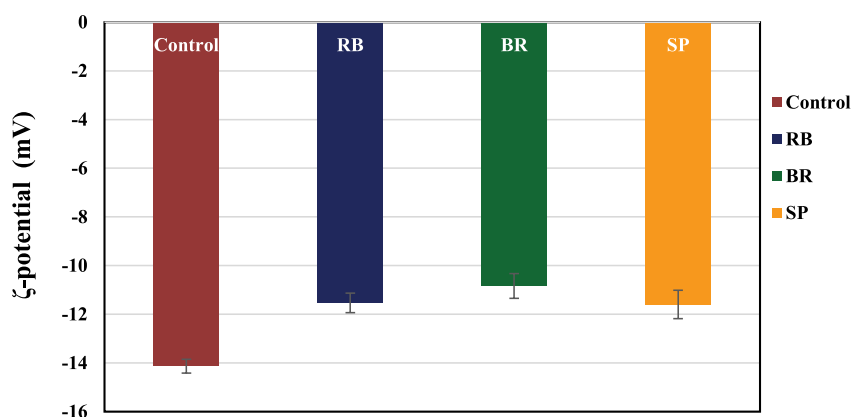
FIGURE 1 | ζ-Potential of control (without phenolic extract), red beet (RB), broccoli (BR), and spinach leaf (SL) complex coacervate microcapsules.
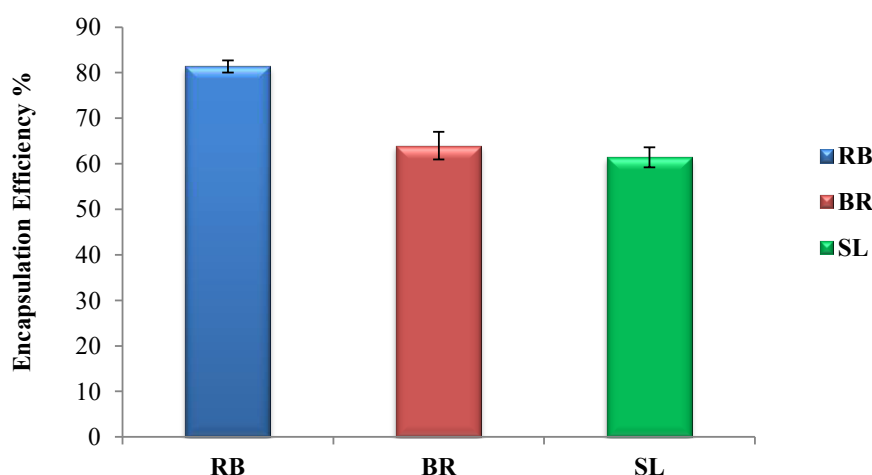

FIGURE 2 | Encapsulation efficiency (EE %) of the red beet (RB), broccoli (BR), and spinach leaf (SL) complex coacervate microcapsules.

compounds were strategically placed near the peptide side chain groups. The active groups para-OH (p-OH), meta-OH (m-OH), and COOH of phenolics are postulated to act as hydrogen bond donors/acceptors for various amino acid side chain groups (63).

Chemical Composition of Cheese

Table 2 shows the chemical composition of cheese fortified with the RB, BR, and SL extract complex coacervates on the day of processing. As shown in **Table 2**, there was no significant variation in composition ($P < 0.05$) of free complex coacervates of cheese and the fortified cheese samples of the RB, BR, and SL complex coacervates (except for pH). This implies that, in this experiment, fortifying cheese with the RB, BR, and SL complex coacervates did not negatively influence the chemical analysis of UF cheese. As indicated in **Table 2**, there was a minor change in pH values between the control cheese and cheese fortified with the RB, BR, and SL complex coacervates. The control cheese had the highest pH, whereas the cheese fortified with the BR complex coacervate had the lowest pH. Adding tomato extract microcapsules to Queso Blanco cheese caused a comparable

decrease in cheese pH in the study by Jeong et al. (64). The acidic pH of these compounds may explain the lowering of the pH of the medium to which bioactive compounds were introduced. This finding is similar to the findings of the HPLC analysis for the RB, BR, and SL extracts, which showed that the BR extract had approximately three times the phenolic content of the SL extract and nine times that of the RB extract.

Texture Analysis

Texture profile analysis (TPA) is a useful measure of the textural quality of a cheese product that corresponds well with sensory characteristics (60). The texture profile analysis of all cheese samples was performed in this study for chewiness, hardness, cohesiveness, gumminess, and adhesiveness, as provided in **Table 3**. The chewiness, hardness, cohesiveness, gumminess, and adhesiveness of the fortified UF cheese containing the RB, BR, and SL extract complex coacervates differed slightly ($P < 0.05$), as seen in **Table 3**. Ionic entities crosslinked by covalent bonds to casein strands were protonated during cheese formation when the pH dropped. As a result, the connection between casein
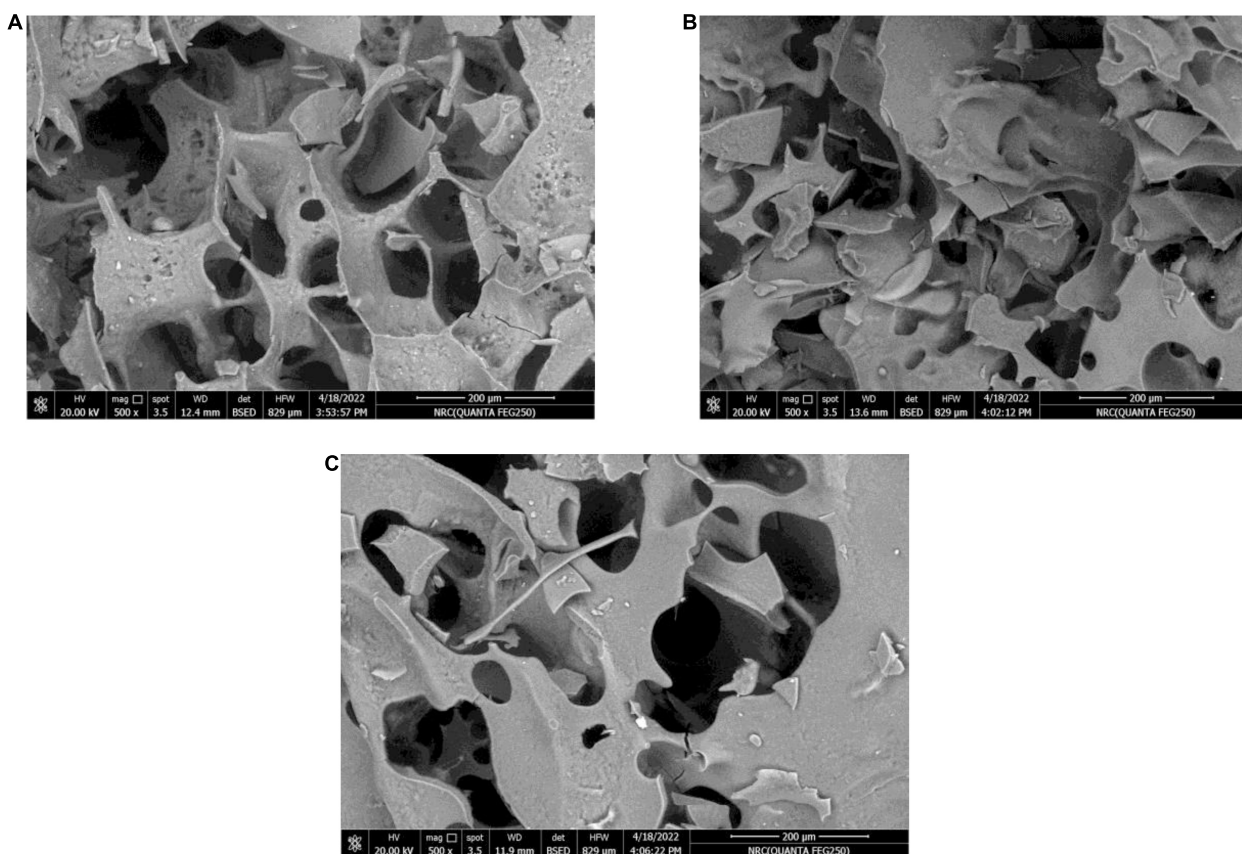
FIGURE 3 | Scanning electron microscope (SEM) images of the red beet (RB) **(A)**, broccoli (BR) **(B)**, and spinach leaf (SL) **(C)** complex coacervate microcapsules (after freeze-drying).

micelles strengthened, forming tough curds (65). In this respect, Ong et al. (60) found that curds manufactured with rennin at pH 6.5 were tougher than curds manufactured with renin at pH 6.1. This finding was also true in the present investigation, in which the pH of the UF cheese samples fortified with RB, BR, and SL complex coacervates was higher than that of the control cheese. As a result, the presence of the RB, BR, and SL complex coacervates in the current investigation could be one of the factors contributing to the increase in hardness, cohesiveness, and gumminess of the fortified cheese (BR > SL > RB).

Sensory Evaluation

Sensory evaluation of cheese is crucial to the feasibility of an industrial manufacturing approach to food organoleptic properties (66). The total sensory scores of UF cheese comprise color, appearance, body, texture, and flavor, as illustrated in **Table 4**. The sensory score of UF cheese fortified with the RB, BR, and SL extract complex coacervates was somewhat higher than that of the control cheese. These results could be attributed to the favorable impact of RB, BR, and SL extract complex coacervate fortification on the UF cheese compared to the control cheese; they enhanced the flavor and appearance scores. These findings are consistent with those of our previous study (57), in which we found that fortifying processed cheese

with a phenolic extract from the mandarin peel in the form of liposomes had little influence on sensory characteristics, which remained acceptable. The current findings are congruent with those of Farrag et al. (67). Cheese supplemented with polyphenol capsules had higher overall rankings and improved flavor, body, texture, and acceptance.

Nutritional Parameters

Table 5 shows the initial and final body weights, body weight gain, total food intake, and food efficiency of the negative control, $AlCl_3$-induced neuroinflammation (positive control), $AlCl_3$-induced neuroinflammation + UF cheese (gp. 4), and all treated groups (groups 1, 2, 3, 5, 6, and 7), which were examined in a 4-week trial. There were no significant variations ($P > 0.05$) in initial body weights; total food intake and food efficiency did not differ in all treated groups, including RB, BR, and SL extracts; and UF cheese containing the RB, BR, and SL complex coacervates represented as 1, 2, 3, 5, 6, and 7 when compared to the $AlCl_3$-induced neuroinflammation (positive control) and $AlCl_3$-induced neuroinflammation + UF cheese (gp. 4) groups. The same result was observed in the $AlCl_3$-induced neuroinflammation + UF cheese group (gp. 4) compared to the $AlCl_3$-induced (positive) group, and the $AlCl_3$-induced (positive) group compared to the negative control group. This result agreed

FIGURE 4 | FTIR spectrum of the red beet (RB) **(A)**, broccoli (BR) **(B)**, and spinach leaf (SL) **(C)** powdered extracts encapsulated with different wall materials. WPC, whey protein concentrate; GA, gum arabic.
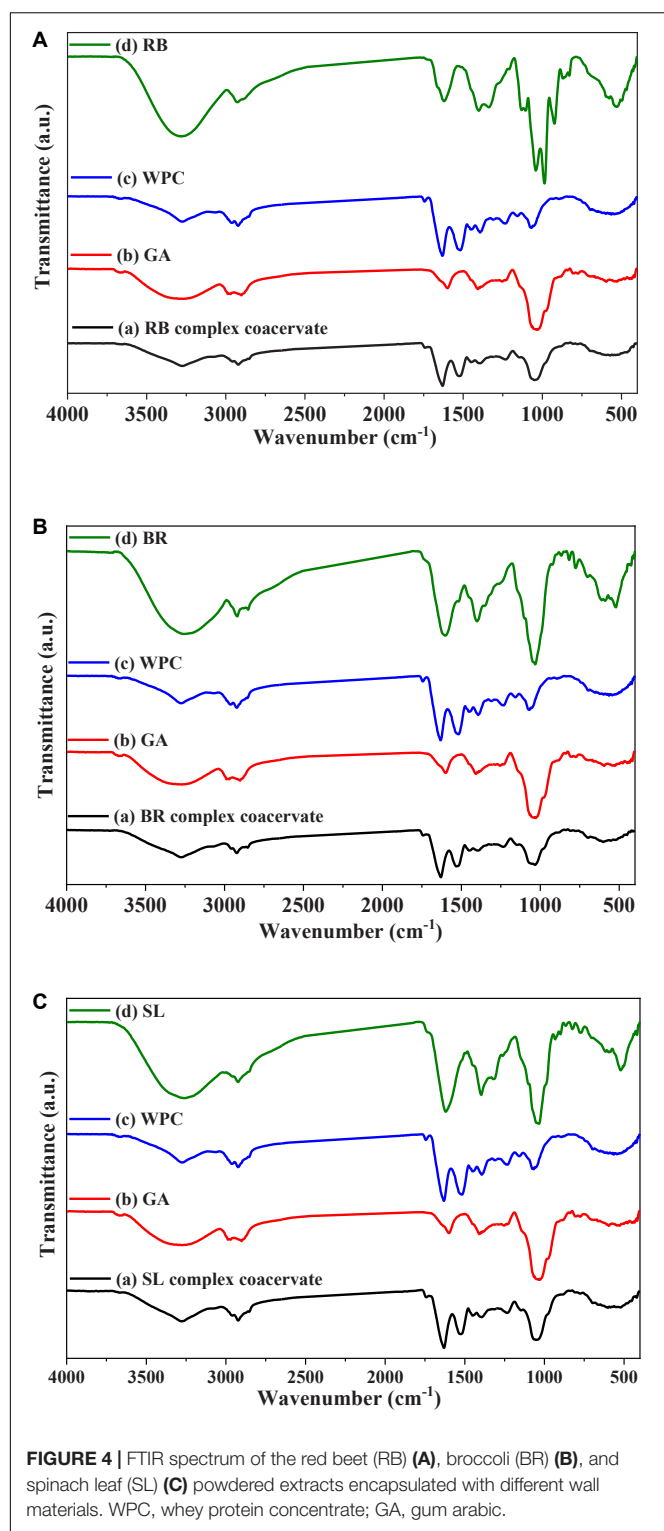
with that of several studies (68, 69). In contrast, a significant reduction ($P \leq 0.05$) in body weight was detected in the AlCl$_3$-induced neuroinflammation (positive) and AlCl$_3$-induced neuroinflammation + UF cheese (gp. 4) groups compared to the negative control (70). A significant elevation in body weight

occurred in all treated groups (1, 2, 3, 5, 6, and 7) compared to the AlCl$_3$-induced neuroinflammation (positive) and AlCl$_3$-induced neuroinflammation + UF cheese (gp. 4) groups.

Biochemical Parameters

AlCl$_3$ is toxic and enters the food chain through drinking water and food (71). It crosses the blood–brain barrier (BBB) and aggregates in the brain, mainly in the hippocampus, which is responsible for memory and cognition. AlCl$_3$ induced biochemical changes and oxidative stress in a rat brain model and may evoke neuronal disorders in human. Aluminum accumulates in the brain over time, causing neuroinflammation in the form of neurofibrillary tangles and amyloid aggregates. As a result, elucidating the specific mechanism of AlCl$_3$-induced neuroinflammation is critical. This prompted us to investigate the impact of the RB, BR, and SL extracts and UF cheese containing complex coacervates of the RB, BR, and SL extracts in the AlCl$_3$-induced rat model.

Acetylcholine is a cholinergic neurotransmitter that is controlled by acetylcholinesterases (AChE and BChE), the main enzymes that break down acetylcholine. In **Table 6**, it is shown that AlCl$_3$ administration to the rats led to a significant elevation in AChE and BChE in AlCl$_3$-induced neuroinflammation (positive) and AlCl$_3$-induced neuroinflammation + UF cheese groups compared to the negative control (72). AlCl$_3$ can trigger an imbalance in neurotransmitter levels (73). Additionally, the rats treated with the RB, BR, and SL extracts showed a significant reduction similar to rats treated with UF cheese containing complex coacervates of the RB, BR, and SL extracts in AlCl$_3$-treated rats and suppressed AChE and BChE activities. This result is consistent with that of previous studies. Similarly, the mode of action of the RB, BR, and SL extracts can be utilized in the treatment of neurodegenerative diseases and memory-deficit disorders, with benefits attributed to their modulatory impacts on acetylcholinesterase action, which can enhance learning and memory (74, 75). These extracts are considered the most promising in improving the neuronal damage and memory dysfunction triggered by AlCl$_3$ injection, along with the advancement of cholinergic activity in the brain tissue and cholinergic neurotransmission in rats with memory impairment (76–78).

As seen in **Table 6**, the brain (hippocampus and cortex homogenate) neurotransmitters (5-HT and DA) significantly decreased in the AlCl$_3$-induced neuroinflammation (positive) and AlCl$_3$-induced neuroinflammation + UF cheese groups (gp. 4) compared to the negative control. This could be the reason for the development of some neurodegenerative and neuropsychiatric diseases. However, the administration of the RB, BR, and SL extracts and UF cheese containing complex coacervates of the RB, BR, and SL extracts significantly elevated these neurotransmitters compared to the AlCl$_3$-induced neuroinflammation (positive) and AlCl$_3$-induced neuroinflammation + UF cheese groups. The preventive effect of the RB, BR, and SL extracts against the depletion of neurotransmitters is caused by their polyphenolic and flavonoid contents, which are involved in elevating brain dopamine levels by suppressing monoamine oxidase-B action, which is effective

TABLE 2 | Chemical analysis of UF cheese with the RB, BR, and SL complex coacervates.

Parameters	Control	RB	BR	SL
Moisture, %	69.17 ± 0.34[a]	68.53 ± 0.40[a]	68.52 ± 0.38[a]	68.52 ± 0.42[a]
Total solids, %	30.83 ± 0.34[a]	31.48 ± 0.40[a]	31.48 ± 0.38[a]	31.49 ± 0.42[a]
Fat, %	10.53 ± 0.04[a]	10.54 ± 0.02[a]	10.54 ± 0.01[a]	10.53 ± 0.03[a]
Protein, %	10.95 ± 0.14[a]	11.30 ± 0.11[a]	11.32 ± 0.16[a]	11.32 ± 0.13[a]
pH	6.73 ± 0.02[a]	6.64 ± 0.01[b]	6.62 ± 0.01[c]	6.68 ± 0.01[ab]

All the values are the mean ± Stdv. [a,b,c]Within rows, the means with different letters were significantly different ($P < 0.05$). Control: UF cheese without a complex coacervate; RB: UF cheese with a red beet complex coacervate; BR: UF cheese with a broccoli complex coacervate; and SL: UF cheese with a spinach leaf complex coacervate.

TABLE 3 | Texture parameters of UF cheese with the RB, BR, and SL complex coacervates.

Samples	Hardness (N)	Springiness (mm)	Cohesiveness	Gumminess (N)	Chewiness (N*mm)
Control	10.405 ± 0.19[c]	0.76 ± 0.05[a]	0.65 ± 0.01[c]	6.68 ± 0.07[c]	5.14 ± 0.49[a]
RB	11.56 ± 0.25[b]	0.82 ± 0.04[a]	0.74 ± 0.01[ab]	7.26 ± 0.11[b]	5.22 ± 0.35[a]
BR	12.73 ± 0.60[a]	0.77 ± 0.02[a]	0.73 ± 0.01[b]	8.36 ± 0.11[a]	6.12 ± 0.42[a]
SL	12.02 ± 0.13[ab]	0.77 ± 0.03[a]	0.76 ± 0.01[a]	6.93 ± 0.13[c]	6.09 ± 0.28[a]

All the values are the mean ± Stdv. [a,b,c]Within a column, the means with different letters were significantly different ($P < 0.05$). Control: UF cheese without a complex coacervate; RB: UF cheese with a red beet complex coacervate; BR: UF cheese with a broccoli complex coacervate; and SL: UF cheese with a spinach leaf complex coacervate.

in avoiding aging-associated cognitive impairments. BDNF plays a vital role in nerve cell survival and synaptic plasticity and participates in a number of neurological deficits (79). GFAP is the major filament in the astrocytic cytoskeleton and has long been utilized as a biomarker for neurotoxicity and astrocyte activation (80). The results in **Table 6** demonstrate that there was a significant decrease in BDNF and a significant increase in GFAP levels in both the AlCl₃-induced neuroinflammation (positive) and AlCl₃-induced neuroinflammation + UF cheese groups compared to the negative control group. The RB, BR, and SL extracts and UF cheese containing complex coacervates of the RB, BR, and SL extracts exhibited a significant elevation in BDNF and a significant reduction in GFAP levels compared to AlCl₃-induced neuroinflammation (positive control) and AlCl₃-induced neuroinflammation + UF cheese groups. In the central nervous system, flavonoids target astrocytes and promote BDNF release while inhibiting GFAP expression (81). This may explain the ability of the RB, BR, and SL extracts to elevate BDNF and reduce GFAP levels following AlCl₃ exposure in our present research.

The brain is a susceptible organ to oxidative stress owing to its high oxygen consumption, low mitotic rate, and low antioxidant levels. Neuronal injury is caused by extensive oxidative damage caused by AlCl₃ toxicity, which disrupts the antioxidant defense mechanism of the brain (82) by promoting the buildup of reactive oxygen species in cells that can eventually result in the elevated expression of genes encoding antioxidant enzymes (83).

SOD is a pioneering antioxidant enzyme that neutralizes singlet oxygen and spontaneously dismutates superoxide radicals to hydrogen peroxide. CAT is a naturally produced cellular antioxidant that is responsible for reducing oxidative stress. CAT effectively decomposes hydrogen peroxide and therefore avoids lipid peroxidation (84). GPx enhances hydrogen peroxide and

lipid peroxide reduction, whereas GR stimulates the NADPH-driven conversion of GSSG to GSH (85). The reduction among these antioxidant enzymes and molecules may be linked to an excessive buildup of hydrogen peroxide, which inhibits neuronal antioxidant defenses (86). AlCl₃ reduced the activities of GPx, SOD, and GR. Both MDA as a lipid peroxidation marker and NO as an inflammatory marker in the brain (cerebrum, cerebellum, and midbrain) are essential for neuronal cells that are considerably susceptible to oxidative stress and inflammation; thus, they require an effectual steady supply of powerful antioxidants to neutralize the lipid peroxidation chain reaction that causes free radical destruction (87).

According to **Table 7**, AlCl₃ administration caused oxidative stress, which was reflected in a significant increase in CAT, MDA, and NO and a significant reduction in SOD, glutathione peroxidase, and glutathione in both the AlCl₃-induced neuroinflammation (positive) and AlCl₃-induced neuroinflammation + UF cheese groups in comparison with the

TABLE 4 | Sensory characteristics of UF cheese fortified with the RB, BR, and SL complex coacervates.

Samples	Color and appearance	Body and texture	Flavor
Control	18.50 ± 1.00[a]	43.17 ± 1.26[a]	32.00 ± 1.50[a]
RB	14.67 ± 1.53[b]	44.00 ± 1.00[a]	26.50 ± 1.80[b]
BR	14.00 ± 2.00[b]	40.00 ± 2.00[b]	21.33 ± 1.53[c]
SL	14.00 ± 2.00[b]	44.00 ± 1.00[a]	20.00 ± 1.00[c]

All the values are the mean ± Stdv. [a,b,c]Within the same column, the means with different letters were significantly different ($P < 0.05$). Control: UF cheese without a complex coacervate; RB: UF cheese with a red beet complex coacervate; BR: UF cheese with a broccoli complex coacervate; and SL: UF cheese with a spinach leaf complex coacervate.

TABLE 5 | Effects of the RB, BR, and SL complex coacervates and UF cheese with coacervates on body weight, body weight gain, total food intake, and food efficiency.

Groups	Initial body weight (g)	Final body weight (g)	Body weight gain (g)	Total food intake (g)	Food efficiency*
Negative control	205.2 ± 2.65	253.7 ± 3.18	48.5 ± 0.53	3536.5 ± 2.22	0.014 ± 0.24
Positive control	207.3 ± 3.21[a]	244.9 ± 4.06[a]	37.6 ± 0.85[a]	3525.5 ± 2.15[a]	0.011 ± 0.4[a]
Group (1)	206.2 ± 3.37[b]	249 ± 3.91[b]	42.8 ± 0.54[b]	3533.5 ± 2.31[b]	0.012 ± 0.23[b]
Group (2)	206.1 ± 3.43[b]	249.5 ± 3.9[c]	43.4 ± 0.47[c]	3531.4 ± 2.33[b]	0.012 ± 0.2[b]
Group (3)	205.2 ± 3.53[b]	251.9 ± 4.31[d]	46.7 ± 0.78[d]	3534.6 ± 2.41[b]	0.013 ± 0.32[b]
Group (4)	204.9 ± 3.25[ab]	243.6 ± 3.78[ab]	38.7 ± 0.53[ab]	3525.5 ± 2.27[ab]	0.011 ± 0.23[ab]
Group (5)	205.1 ± 3.12[b]	247.9 ± 3.57[e]	42.8 ± 0.45[e]	3533.4 ± 2.32[b]	0.012 ± 0.19[b]
Group (6)	204.2 ± 3.63[b]	247.8 ± 4.36[f]	43.6 ± 0.73[f]	3531.2 ± 2.43[b]	0.012 ± 0.3[b]
Group (7)	204.9 ± 3.55[b]	251.3 ± 4.11[g]	46.4 ± 0.56[g]	3534.5 ± 2.28[b]	0.013 ± 0.25[b]

*Values are the mean ± SE (n = 6). The same letters in each column reflect a non-significant difference across treatments, whereas different letters reflect a significant difference (P ≤ 0.05, P ≤ 0.005). *Food efficiency, body weight gain/total food intake.*

TABLE 6 | Effects of the RB, BR, and SL complex coacervates and UF cheese with these complex coacervates on biochemical parameters.

Groups	Acetylcholinesterase (ng/g tissue)	Butyrylcholinesterase (U/g tissue)	Dopamine (μ g/g tissue)	5-hydroxytryptamine (μ g/g tissue)	BDNF (pg/g tissue)	GFAP (pg/g tissue)
Negative control	0.99 ± 0.08	310.64 ± 7.42	449.64 ± 2.12	44.34 ± 1.32	24.13 ± 0.34	243.34 ± 1.67
Positive control	2.34 ± 0.06[a]	611.32 ± 8.13[a]	231.42 ± 2.33[a]	27.32 ± 1.43[a]	11.19 ± 0.23[a]	539.89 ± 1.92[a]
Group (1)	1.76 ± 0.07[b]	405.43 ± 15.04[b]	325.13 ± 2.14[b]	32.23 ± 1.19[b]	17.45 ± 0.19[b]	315.63 ± 1.34[b]
Group (2)	1.45 ± 0.07[c]	402.32 ± 16.11[c]	332.35 ± 2.16[c]	33.39 ± 1.21[c]	18.21 ± 0.23[c]	302.39 ± 1.26[c]
Group (3)	1.38 ± 0.07[d]	398.43 ± 13.25[d]	395.42 ± 2.21[d]	39.48 ± 1.16[d]	21.13 ± 0.16[d]	296.22 ± 1.21[d]
Group (4)	2.29 ± 0.06[a]	602.12 ± 8.18[a]	235.49 ± 2.43[a]	27.12 ± 1.37[a]	12.08 ± 0.22[a]	535.73 ± 1.84[a]
Group (5)	1.74 ± 0.07[e]	403.23 ± 14.64[e]	322.14 ± 2.11[e]	31.53 ± 1.29[e]	17.12 ± 0.19[e]	311.23 ± 1.32[e]
Group (6)	1.43 ± 0.07[f]	401.32 ± 15.71[f]	327.31 ± 2.12[f]	32.67 ± 1.21[f]	18.11 ± 0.23[f]	300.67 ± 1.27[f]
Group (7)	1.34 ± 0.07[g]	396.33 ± 13.68[g]	390.37 ± 2.17[g]	37.38 ± 1.16[g]	20.97 ± 0.16[g]	299.61 ± 1.23[g]

Values are represented as the mean ± SE (n = 6). The same letter in each column reflects a non-significant difference across treatments, whereas different letters reflect a significant difference (P ≤ 0.05, P ≤ 0.005).

TABLE 7 | Effects of the RB, BR, and SL complex coacervates and UF cheese with complex coacervates on biochemical parameters.

Groups	Superoxide Dismutase (U/g tissue)	Catalase (μ mol/g tissue)	Glutathione peroxidase (U/g tissue)	Reduced glutathione (μ mol/g tissue)	Malonaldehyde (nmol/g tissue)	Nitric oxide (nmol/g tissue)
Negative control	7.48 ± 0.49	3.63 ± 0.24	4.84 ± 0.74	13.56 ± 0.78	5.23 ± 0.39	1.99 ± 0.29
Positive control	4.19 ± 0.33[a]	7.82 ± 0.42[a]	3.32 ± 0.64[a]	9.89 ± 0.49[a]	14.97 ± 0.81[a]	3.89 ± 0.23[a]
Group (1)	5.41 ± 0.35[b]	4.32 ± 0.32[b]	4.12 ± 0.72[b]	10.82 ± 0.32[b]	11.21 ± 0.72[b]	2.41 ± 0.22[b]
Group (2)	6.48 ± 0.28[c]	4.21 ± 0.28[c]	4.33 ± 0.68[c]	11.71 ± 0.58[c]	10.43 ± 0.69[c]	2.38 ± 0.21[c]
Group (3)	6.93 ± 0.27[d]	3.82 ± 0.31[d]	4.62 ± 0.71[d]	12.98 ± 0.51[d]	9.49 ± 0.61[d]	2.11 ± 0.19[d]
Group (4)	4.23 ± 0.33[a]	7.63 ± 0.41[a]	3.41 ± 0.65[a]	9.76 ± 0.48[a]	13.86 ± 0.82[a]	3.65 ± 0.24[a]
Group (5)	5.42 ± 0.34[e]	4.31 ± 0.33[e]	4.07 ± 0.71[e]	10.75 ± 0.31[e]	11.55 ± 0.74[e]	2.52 ± 0.23[e]
Group (6)	6.43 ± 0.28[f]	4.19 ± 0.29[f]	4.26 ± 0.67[f]	11.63 ± 0.54[f]	10.62 ± 0.64[f]	2.46 ± 0.22[f]
Group (7)	6.91 ± 0.27[g]	3.93 ± 0.34[g]	4.58 ± 0.71[g]	12.72 ± 0.51[g]	9.51 ± 0.67[g]	2.19 ± 0.19[g]

Values are represented as the mean ± SE (n = 6). The same letters in each column reflect a non-significant difference across treatments, whereas different letters reflect a significant difference (P ≤ 0.05).

negative control. There is a disturbance in redox homeostasis and an imbalance between oxidative stress and antioxidant defenses that occur when free radicals accumulate excessively in the body, causing damage to biological macromolecules, which leads to brain damage and severe cognitive impairment (88–91). The RB, BR, and SL extracts and UF cheese containing complex coacervates of the RB, BR, and SL extracts induced a significant elevation of SOD and glutathione peroxidase and reduced glutathione with a significant reduction in the CAT, MDA, and NO levels compared to AlCl$_3$-induced neuroinflammation (positive) and AlCl$_3$-induced neuroinflammation + UF cheese groups. The results in **Table 7** are compatible with those of

FIGURE 5 | Effects of the RB, BR, and SL complex microcapsules and UF cheese with complex coacervates on the brain weight of rats.
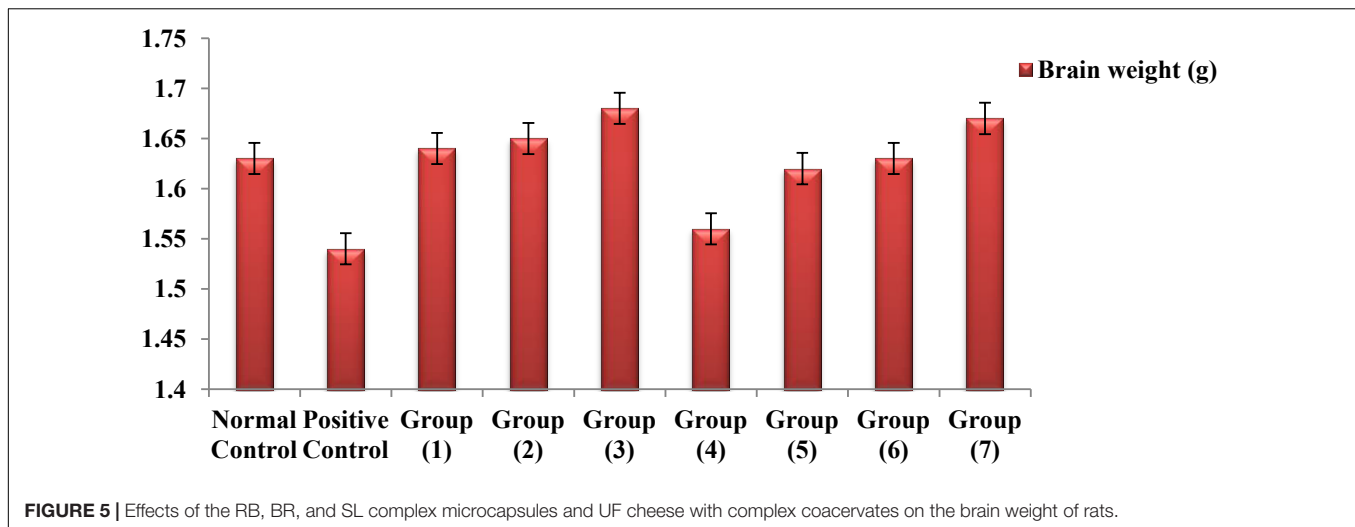
prior studies that revealed that the administration of RB, BR, and SL extracts and UF cheese containing complex coacervates of the RB, BR, and SL extracts was linked to the prevention of oxidative reactions *via* prooxidant inhibition and endogenous antioxidant system activation (92). This prevents tissue damage by inhibiting enzyme leakage *via* neuronal cell membranes (79) in rats. A potential process between the lowered enzyme activities examined and the effect of RB, BR, and SL extracts could be a synergetic effect between the antioxidant activity of the phenolic and flavonoid compounds and endogenous antioxidants, which maintains redox homeostasis after AlCl$_3$ administration (93). These findings may explain why RB, BR, and SL treatments mitigated the overall severity of rat brain tissue damage, demonstrating their therapeutic effects against AlCl$_3$-induced impairments (94). Hence, the antioxidant activity of RB, BR, and SL as neuroprotective drugs against AlCl$_3$-induced neuroinflammation in rat models was further supported by our findings.

Numerous study results have shown that, if chemical toxins are not treated, they cause significant brain weight loss in rats (95–97). According to **Figure 5**, the observed reduction results for the brain weights of both the AlCl$_3$-induced neuroinflammation and AlCl$_3$-induced neuroinflammation + UF cheese groups compared to the negative control, which could have occurred because of nutrient depletion, modification of physiological functions or pathways, and protein denaturation (97). The administration of the RB, BR, and SL extracts and UF cheese containing complex coacervates of the RB, BR, and SL extracts significantly elevated the brain weight of rats to the normal level because of their polyphenolic and flavonoid contents. This could lead to a significant reduction in the oxidative markers caused by both antioxidant and anti-inflammatory properties (98). The overall findings confirmed the ability of the RB, BR, and SL extracts and UF cheese containing the RB, BR, and SL complex coacervates to improve metabolic and neurobehavioral strategies and enhance the protein biosynthesis of the brain (99).

CONCLUSION

Based on our findings, the complex coacervation technique is an excellent alternative for encapsulating the RB, BR, and SL phenolic extracts. Although the addition of the encapsulated phenolic extract complex coacervates to UF cheese decreased the pH, it did not considerably influence the composition and texture profile of the UF cheese. UF cheese with encapsulated phenolic extracts improved metabolic activities, neurobehavioral function, and protein synthesis in the brain through mechanisms that contribute to its antioxidant property, acetylcholinesterase suppression, lipid peroxidation inhibition, and anti-inflammatory and neurobehavioral restorative properties mediated by the regulation of AChE activity. Additionally, it increased BDNF, decreased GFAP, inhibited prooxidant (NO), and enhanced the cortical endogenous antioxidant substances (GSH, GPx, GR, SOD, and CAT). These findings support the use of encapsulated phenolic extracts from the RB, BR, and SL complex coacervates against AlCl$_3$-induced neuroinflammation in rats. The efficient production of functional UF cheese, including encapsulated phenolic extract complex coacervates, revealed in this research could be of interest to both food producers and academics seeking to provide natural bioactive substances in the most suitable way (i.e., food).

DATA AVAILABILITY STATEMENT

The original contributions presented in this study are included in the article/supplementary material, further inquiries can be directed to the corresponding author/s.

ETHICS STATEMENT

The animal study was reviewed and approved by the Ethical Committee of Medical Research at Egypt's National Research Centre.

AUTHOR CONTRIBUTIONS

REFERENCES

1. Hrichi S, Chaabane-Banaoues R, Giuffrida D, Mangraviti D, Oulad El Majdoub Y, Rigano F, et al. Effect of seasonal variation on the chemical composition and antioxidant and antifungal activities of *Convolvulus althaeoides* L. leaf extracts. *Arab J Chem.* (2020) 13:5651–68. doi: 10.1016/j.arabjc.2020.04.006

2. Zaky AA, Simal-Gandara J, Eun J-B, Shim J-H, Abd El-Aty AM. Bioactivities, applications, safety, and health benefits of bioactive peptides from food and by-products: a review. *Front Nutr.* (2022) 8:815640. doi: 10.3389/fnut.2021.815640

3. Zaky AA, Chen Z, Qin M, Wang M, Jia Y. Assessment of antioxidant activity, amino acids, phenolic acids and functional attributes in defatted rice bran and rice bran protein concentrate. *Progr Nutr.* (2020) 22:1–9. doi: 10.23751/pn.v22i4.8971

4. Massounga Bora AF, Ma S, Li X, Liu L. Application of microencapsulation for the safe delivery of green tea polyphenols in food systems: review and recent advances. *Food Res Int.* (2018) 105:241–9. doi: 10.1016/j.foodres.2017.11.047

5. Soltanzadeh M, Peighambardoust SH, Ghanbarzadeh B, Mohammadi M, Lorenzo JM. Chitosan nanoparticles as a promising nanomaterial for encapsulation of pomegranate (*Punica granatum* L.) peel extract as a natural source of antioxidants. *Nanomaterials.* (2021) 11:1439. doi: 10.3390/nano11061439

6. Soltanzadeh M, Peighambardoust SH, Ghanbarzadeh B, Amjadi S, Mohammadi M, Lorenzo JM, et al. Active gelatin/cress seed gum-based films reinforced with chitosan nanoparticles encapsulating pomegranate peel extract: preparation and characterization. *Food Hydrocolloids.* (2022) 129:107620. doi: 10.1016/j.foodhyd.2022.107620

7. Soltanzadeh M, Peighambardoust SH, Ghanbarzadeh B, Mohammadi M, Lorenzo JM. Chitosan nanoparticles encapsulating lemongrass (*Cymbopogon commutatus*) essential oil: physicochemical, structural, antimicrobial and in-vitro release properties. *Int J Biol Macromol.* (2021) 192:1084–97. doi: 10.1016/j.ijbiomac.2021.10.070

8. De Kruif CG, Weinbreck F, de Vries R. Complex coacervation of proteins and anionic polysaccharides. *Curr Opin Colloid Interface Sci.* (2004) 9:340–9. doi: 10.1016/j.cocis.2004.09.006

9. Alvim ID, Grosso CRF. Microparticles obtained by complex coacervation: influence of the type of reticulation and the drying process on the release of the core material. *Ciência e Tecnologia de Alimentos.* (2010) 30:1069–76.

10. Nori MP, Favaro-Trindade CS, Matias de Alencar S, Thomazini M, de Camargo Balieiro JC, Contreras Castillo CJ. Microencapsulation of propolis extract by complex coacervation. *LWT Food Sci Technol.* (2011) 44:429–35. doi: 10.1016/j.lwt.2010.09.010

11. Comunian TA, Monterrey-Quintero ES, Thomazini M, Balieiro JCC, Piccone P, Pittia P, et al. Assessment of production efficiency, physicochemical properties and storage stability of spray-dried chlorophyllide, a natural food colourant, using gum Arabic, maltodextrin and soy protein isolate-based carrier systems. *Int J Food Sci Technol.* (2011) 46:1259–65. doi: 10.1111/j.1365-2621.2011.02617.x

12. Rocha-Selmi GA, Bozza FT, Thomazini M, Bolini HMA, Fávaro-Trindade CS. Microencapsulation of aspartame by double emulsion followed by complex coacervation to provide protection and prolong sweetness. *Food Chem.* (2013) 139:72–8. doi: 10.1016/j.foodchem.2013.01.114

13. Hala MF, Ebtisam IG, Sanaa MA, Gad AS, El-Said MM. Total phenolic compounds, radical scavenging and ferric reducing activity of low fat UF-soft cheese supplemented with thyme extract. *J Appl Sci Res.* (2012) 8:2335–41.

14. El-Sayed SM, Youssef AM. Potential application of herbs and spices and their effects in functional dairy products. *Heliyon.* (2019) 5:e01989. doi: 10.1016/j.heliyon.2019.e01989

15. Dórea JG. Exposure to mercury and aluminum in early life: developmental vulnerability as a modifying factor in neurologic and immunologic effects. *Int J Environ Res Public Health.* (2015) 12:1295–313. doi: 10.3390/ijerph120201295

16. Igbokwe IO, Igwenagu E, Igbokwe NA. Aluminium toxicosis: a review of toxic actions and effects. *Interdisciplin Toxicol.* (2019) 12:45. doi: 10.2478/intox-2019-0007

17. Wang M, Chen JT, Ruan DY, Xu YZ. The influence of developmental period of aluminum exposure on synaptic plasticity in the adult rat dentate gyrus *in vivo*. *Neuroscience.* (2002) 113:411–9. doi: 10.1016/s0306-4522(02)00193-8

18. Radtke FA, Chapman G, Hall J, Syed YA. Modulating neuroinflammation to treat neuropsychiatric disorders. *BioMed Res Int.* (2017) 2017:1–21.

19. Rather MA, Thenmozhi AJ, Manivasagam T, Bharathi MD, Essa MM, Guillemin GJ. Neuroprotective role of Asiatic acid in aluminium chloride induced rat model of Alzheimer's disease. *Front Biosci Scholar.* (2018) 10:262–75. doi: 10.2741/s514

20. Said MM, Abd Rabo MM. Neuroprotective effects of eugenol against aluminiuminduced toxicity in the rat brain. *Arh Hig Rada Toksikol.* (2017) 68:27–36. doi: 10.1515/aiht-2017-68-2878

21. Yuan CY, Lee YJ, Hsu GS. Aluminum overload increases oxidative stress in four functional brain areas of neonatal rats. *J Biomed Sci.* (2012) 19:1–9. doi: 10.1186/1423-0127-19-51

22. Al-Amin M, Chowdury M, Amin I, Saifullah AR, Alam MN, Jain P, et al. Levocarnitine improves AlCl3-induced spatial working memory impairment in Swiss albino mice. *Front Neurosci.* (2019) 13:278. doi: 10.3389/fnins.2019.00278

23. Wahby MM, Mohammed DS, Newairy AA, Abdou HM, Zaky A. Aluminum-induced molecular neurodegeneration: the protective role of genistein and chickpea extract. *Food Chem Toxicol.* (2017) 107:57–67. doi: 10.1016/j.fct.2017.05.044

24. Zhang H, Yang X, Qin X, Niu Q. Caspase-3 is involved in aluminum-induced impairment of long-term potentiation in rats through the Akt/GSK-3β pathway. *Neurotoxicity Res.* (2016) 29:484–94. doi: 10.1007/s12640-016-9597-5

25. Hendriks HS, Koolen LA, Dingemans MM, Viberg H, Lee I, Leonards PE, et al. Effects of neonatal exposure to the flame retardant tetrabromobisphenol-A, aluminum diethylphosphinate or zinc stannate on long-term potentiation and synaptic protein levels in mice. *Arch Toxicol.* (2015) 89:2345–54. doi: 10.1007/s00204-014-1366-8

26. Bilgic Y, Demir EA, Bilgic N, Dogan H, Tutuk O, Tumer C. Detrimental effects of chia (*Salvia hispanica* L.) seeds on learning and memory in aluminum chloride-induced experimental Alzheimer's disease. *Acta Neurobiol Exp Wars.* (2018) 78:322–31.

27. El-Messery TM, El-Said MM, Salama HH, Mohammed DM, Ros G. Bioaccessibility of encapsulated mango peel phenolic extract and its application in milk beverage. *Int J Dairy Sci.* (2021) 16:29–40.

28. Cilek B, Luca A, Hasirci V, Sahin S, Sumnu G. Microencapsulation of phenolic compounds extracted from sour cherry pomace: effect of formulation, ultrasonication time and core to coating ratio. *Eur Food Res Technol.* (2012) 235:587–96.

29. El-Messery TM, Mwafy EA, Mostafa AM, El-Din HM, Mwafy A, Amarowicz R, et al. Spectroscopic studies of the interaction between isolated polyphenols from coffee and the milk proteins. *Surf Interfaces.* (2020) 20:100558.

30. Zaky AA, Chen Z, Liu Y, Li S, Jia Y. Preparation and assessment of bioactive extracts having antioxidant activity from rice bran protein hydrolysates. *J Food Measurement Characterization.* (2019) 13:2542–8. doi: 10.1007/s11694-019-00174-9

31. Saénz C, Tapia S, Chávez J, Robert P. Microencapsulation by spray drying of bioactive compounds from cactus pear (*Opuntia ficus-indica*). *Food Chem.* (2009) 114:616–22.

32. Ydjedd S, Bouriche S, Loìpez-Nicolaìs R, Saìnchez-Moya T, Frontela-Saseta C, Ros-Berruezo G, et al. Effect of *in vitro* gastrointestinal digestion on encapsulated and nonencapsulated phenolic compounds of carob (*Ceratonia siliqua* L.) pulp extracts and their antioxidant capacity. *J Agric Food Chem.* (2017) 65:827–35. doi: 10.1021/acs.jafc.6b05103

33. Hu Y, Li Y, Zhang W, Kou G, Zhou Z. Physical stability and antioxidant activity of citrus flavonoids in arabic gum-stabilized microcapsules: modulation of whey protein concentrate. *Food Hydrocolloids.* (2018) 77:588–97.

34. Association of Official Analytical Chemists [AOAC]. *Official Methods of Analysis, Benjamin Franklin Station Washington, D.C., USA.* 18th ed. Washington DC: AOAC (2007).

35. Zheng Y, Liu Z, Mo B. Texture profile analysis of sliced cheese in relation to chemical composition and storage temperature. *J Chem.* (2016) 2016:8690380.

36. Clark S, Costello M, Drake M, Bodyfelt F (eds). *The Sensory Evaluation of Dairy Products.* Berlin: Springer Science & Business Media (2009).

37. Association of Official Analytical Chemists [AOAC]. *Official Methods of Analysis, Benjamin Franklin Station Washington, D.C., USA.* 12th ed. Washington DC: AOAC (1990).

38. Ezzat A, Abdelhamid AO, El Awady MK, Abd El Azeem AS, Mohammed DM. The biochemical effects of nano tamoxifen and some bioactive components in experimental breast cancer. *Biomed Pharmacother.* (2017) 95:571–6. doi: 10.1016/j.biopha.2017.08.099

39. Reeves PG, Nielsen FH, Fahey GC Jr. AIN-93 purified diets for laboratory rodents: final report of the American Institute of Nutrition ad hoc writing committee on the reformulation of the AIN-76A rodent diet. *J Nutr.* (1993) 123:1939–51. doi: 10.1093/jn/123.11.1939

40. Shunan D, Yu M, Guan H, Zhou Y. Neuroprotective effect of Betalain against AlCl3-induced Alzheimer's disease in Sprague Dawley Rats via putative modulation of oxidative stress and nuclear factor kappa B (NF-κB) signaling pathway. *Biomed Pharmacother.* (2021) 137:111369. doi: 10.1016/j.biopha.2021.111369

41. Albasher G, Alsaleh AS, Alkubaisi N, Alfarraj S, Alkahtani S, Farhood M, et al. Red beetroot extract abrogates chlorpyrifos-induced cortical damage in rats. *Oxid Med Cell Longev.* (2020) 2020:2963020. doi: 10.1155/2020/2963020

42. Khalaj L, Chavoshi Nejad S, Mohammadi M, Sarraf Zadeh S, Hossein Pour M, Ashabi G, et al. Assessing competence of broccoli consumption on inflammatory and antioxidant pathways in restraint-induced models: estimation in rat hippocampus and prefrontal cortex. *BioMed Res Int.* (2013) 2013:590379. doi: 10.1155/2013/590379

43. Pezeshki-Nia S, Asle-Rousta M, Mahmazi S. *Spinacia oleracea* L. extract attenuates hippocampal expression of TNF-α and IL-1β in rats exposed to chronic restraint stress. *Med J Islamic Republic Iran.* (2020) 34:10. doi: 10.34171/mjiri.34.10

44. Jain SK, McVie R, Duett J, Herbst JJ. Erythrocyte membrane lipid peroxidation and glycosylated hemoglobin in diabetes. *Diabetes.* (1989) 38:1539–43.

45. Ohkawa H, Ohishi N, Yagi K. Assay for lipid peroxides in animal tissues by thiobarbituric acid reaction. *Analytical Biochem.* (1979) 95:351–8.

46. Marklund S, Marklund G. Involvement of the superoxide anion radical in the autoxidation of pyrogallol and a convenient assay for superoxide dismutase. *Eur J Biochem.* (1974) 47:469–74. doi: 10.1111/j.1432-1033.1974.tb03714.x

47. Aebi HBTM. Oxygen radicals in biological systems. *Methods Enzymol.* (1984) 105:121–6.

48. Paglia DE, Valentine WN. Studies on the quantitative and qualitative characterization of erythrocyte glutathione peroxidase. *J Lab Clin Med.* (1967) 70:158–69.

49. Aykaç G, Uysal M, Yalçin AS, Koçak-Toker N, Sivas A, Öz H. The effect of chronic ethanol ingestion on hepatic lipid peroxide, glutathione, glutathione peroxidase and glutathione transferase in rats. *Toxicology.* (1985) 36:71–6. doi: 10.1016/0300-483x(85)90008-3

50. Tracey WR, Nakane M, Basha F, Carter G. *In vivo* pharmacological evaluation off two novel type II (inducible) nitric oxide synthase inhibitors. *Can J Physiol Pharmacol.* (1995) 73:665–9.

51. Ellman GL, Courtney KD, Andres V, Featherstone RM. A new and rapid colorimetric determination of acetylcholinesterase activity. *Biochem Pharmacol.* (1961) 7:88–95.

52. Vaisi-Raygani A, Rahimi Z, Kharazi H, Tavilani H, Aminiani M, Kiani A, et al. Determination of butyrylcholinesterase (BChE) phenotypes to predict the risk of prolonged apnea in persons receiving succinylcholine in the healthy population of western Iran. *Clin Biochem.* (2007) 40:629–33. doi: 10.1016/j.clinbiochem.2007.01.018

53. Jotarkar PS, Panjagari NR, Singh AK, Arora S. Effect of whey protein−iron based edible coating on the quality of Paneer and process optimisation. *Int J Dairy Technol.* (2018) 71:395–407.

54. Moschakis T, Murray BS, Biliaderis CG. Modifications in stability and structure of whey protein-coated o/w emulsions by interacting chitosan and gum arabic mixed dispersions. *Food Hydrocolloids.* (2010) 24:8–17.

55. Souza FN, Gebara C, Ribeiro MC, Chaves KS, Gigante ML, Grosso CR. Production and characterization of microparticles containing pectin and whey proteins. *Food Res Int.* (2012) 49:560–6.

56. Cabuk M, Yavuz M, Unal HI. Electrokinetic, electrorheological and viscoelastic properties of Polythiophene-graft-Chitosan copolymer particles. *Colloids Surf Physicochem Eng Aspects.* (2016) 510:231–8.

57. El-Messery TM, El-Said MM, Shahein NM, El-Din HF, Farrag A. Functional yoghurt supplemented with extract orange peel encapsulated using coacervation technique. *Pak J Biol Sci PJBS.* (2019) 22:231–8. doi: 10.3923/pjbs.2019.231.238

58. Bannikova A, Rasumova L, Evteev A, Evdokimov I, Kasapis S. Protein−loaded sodium alginate and carboxymethyl cellulose beads for controlled release under simulated gastrointestinal conditions. *Int J Food Sci Technol.* (2017) 52:2171–9.

59. Flores FP, Singh RK, Kong F. Physical and storage properties of spray-dried blueberry pomace extract with whey protein isolate as wall material. *J Food Eng.* (2014) 137:1–6.

60. Ong L, Dagastine RR, Kentish SE, Gras SL. The effect of pH at renneting on the microstructure, composition and texture of Cheddar cheese. *Food Res Int.* (2012) 48:119–30.

61. Smrdel P, Bogataj M, Zega A, Planinšek O, Mrhar A. Shape optimization and characterization of polysaccharide beads prepared by ionotropic gelation. *J Microencapsul.* (2008) 25:90–105.

62. Ursache FM, Andronoiu DG, Ghinea IO, Barbu V, Ioniţă E, Cotârleţ M, et al. Valorizations of carotenoids from sea buckthorn extract by microencapsulation and formulation of value-added food products. *J Food Eng.* (2018) 219:16–24.

63. Mehanna NS, Hassan ZM, El-Din HM, Ali AA, Amarowicz R, El-Messery TM. Effect of interaction phenolic compounds with milk proteins on cell line. *Food Nutr Sci.* (2014) 5:2130.

64. Jeong HJ, Lee YK, Ganesan P, Kwak HS, Chang YH. Physicochemical, microbial, and sensory properties of queso blanco cheese supplemented with powdered microcapsules of tomato extracts. *Korean J Food Sci Anim Resour.* (2017) 37:342. doi: 10.5851/kosfa.2017.37.3.342

65. Lawrence RC, Creamer LK, Gilles J. Texture development during cheese ripening. *J Dairy Sci.* (1987) 70:1748–60.

66. Nottagh S, Hesari J, Peighambardoust SH, Rezaei-Mokarram R, Jafarizadeh-Malmiri H. Effectiveness of edible coating based on chitosan and Natamycin on biological, physico-chemical and organoleptic attributes of Iranian ultra-filtrated cheese. *Biologia.* (2020) 75:605–11.

67. Farrag AF, Zahran H, Al-Okaby MF, El-Sheikh MM, Soliman TN. Physicochemical properties of white soft cheese supplemented with encapsulated olive phenolic compounds. *Egyptian J Chem.* (2020) 63:2921–31.

68. Astiz M, de Alaniz MJ, Marra CA. The oxidative damage and inflammation caused by pesticides are reverted by lipoic acid in rat brain. *Neurochem Int.* (2012) 61:1231–41. doi: 10.1016/j.neuint.2012.09.003

69. Abdel Moneim A. The neuroprotective effects of purslane (*Portulaca oleracea*) on rotenone-induced biochemical changes and apoptosis in brain of rat. *CNS Neurol Disord Drug Targets (Formerly Curr Drug Targets CNS Neurol Disord).* (2013) 12:830–41. doi: 10.2174/18715273113129990081

70. Taïr K, Kharoubi O, Taïr OA, Hellal N, Benyettou I, Aoues A. Aluminium-induced acute neurotoxicity in rats: treatment with aqueous extract of Arthrophytum (*Hammada scoparia*). *J Acute Dis.* (2016) 5:470–82.

71. Bolognin S, Messori L, Drago D, Gabbiani C, Cendron L, Zatta P. Aluminum, copper, iron and zinc differentially alter amyloid-Aβ1−42 aggregation and toxicity. *Int J Biochem Cell Biol.* (2011) 43:877–85. doi: 10.1016/j.biocel.2011.02.009

72. Kaizer RR, Corrêa MC, Spanevello RM, Morsch VM, Mazzanti CM, Gonçalves JF, et al. Acetylcholinesterase activation and enhanced lipid peroxidation after long-term exposure to low levels of aluminum on different mouse brain

regions. *J Inorganic Biochem.* (2005) 99:1865–70. doi: 10.1016/j.jinorgbio.2005.06.015

73. Gulya K, Rakonczay Z, Kasa P. Cholinotoxic effects of aluminum in rat brain. *J Neurochem.* (1990) 54:1020–6.

74. Akram M, Nawaz A. Effects of medicinal plants on Alzheimer's disease and memory deficits. *Neural Regenerat Res.* (2017) 12:660.

75. Li Y, Lein PJ, Ford GD, Liu C, Stovall KC, White TE, et al. Neuregulin-1 inhibits neuroinflammatory responses in a rat model of organophosphate-nerve agent-induced delayed neuronal injury. *J Neuroinflamm.* (2015) 12:1–3. doi: 10.1186/s12974-015-0283-y

76. Hajihosseini S, Setorki M. The antioxidant activity of Beta vulgaris leaf extract in improving scopolamine-induced spatial memory disorders in rats. *Avicenna J Phytomed.* (2017) 7:417.

77. Mokhtari S, Rabiei Z, Shahrani M, Rafieian-Kopaei M. The ameliorating effect of beta vulgaris extract on memory and learning impairment induced by Lesions of the nucleus basalis of meynert in rat. *J Clin Diagnostic Res.* (2017) 11:9–14.

78. Sacan O, Yanardag R. Antioxidant and antiacetylcholinesterase activities of chard (*Beta vulgaris L. var. cicla*). *Food Chem Toxicol.* (2010) 48:1275–80. doi: 10.1016/j.fct.2010.02.022

79. Okail HA, Ibrahim AS, Badr AH. The protective effect of propolis against aluminum chloride-induced hepatorenal toxicity in albino rats. *J Basic Appl Zool.* (2020) 81:34.

80. Brenner M. Role of GFAP in CNS injuries. *Neurosci Lett.* (2014) 565:7–13.

81. Matias I, Buosi AS, Gomes FC. Functions of flavonoids in the central nervous system: astrocytes as targets for natural compounds. *Neurochem Int.* (2016) 95:85–91.

82. Parekh KD, Dash RP, Pandya AN, Vasu KK, Nivsarkar M. Implication of novel bis-imidazopyridines for management of Alzheimer's disease and establishment of its role on protein phosphatase 2A activity in brain. *J Pharm Pharmacol.* (2013) 65:1785–95. doi: 10.1111/jphp.12149

83. Michiels C, Raes M, Toussaint O, Remacle J. Importance of Se-glutathione peroxidase, catalase, and Cu/Zn-SOD for cell survival against oxidative stress. *Free Radical Biol Med.* (1994) 17:235–48. doi: 10.1016/0891-5849(94)90079-5

84. AlBasher G, Alfarraj S, Alarifi S, Alkhtani S, Almeer R, Alsultan N, et al. Nephroprotective role of selenium nanoparticles against glycerol-induced acute kidney injury in rats. *Biol Trace Element Res.* (2020) 194:444–54. doi: 10.1007/s12011-019-01793-5

85. Al-Olayan EM, El-Khadragy MF, Omer AS, Shata TMM, Kassab BR, Abdel Moneim EA. The beneficial effect of cape gooseberry juice on carbon tetrachloride-induced neuronal damage. *CNS Neurol Disord Drug Targets (Formerly Curr Drug Targets CNS Neurol Disord).* (2016) 15:344–50. doi: 10.2174/1871527314666150821112051

86. Mahmoud SM, Abdel Moneim AE, Qayed MM, El-Yamany NA. Potential role of N-acetylcysteine on chlorpyrifos-induced neurotoxicity in rats. *Environ Sci Pollut Res.* (2019) 26:20731–41. doi: 10.1007/s11356-019-05366-w

87. Abushouk AI, Negida A, Ahmed H, Abdel-Daim MM. Neuroprotective mechanisms of plant extracts against MPTP induced neurotoxicity: future applications in Parkinson's disease. *Biomed Pharmacother.* (2017) 85:635–45. doi: 10.1016/j.biopha.2016.11.074

88. Auti ST, Kulkarni YA. Neuroprotective effect of cardamom oil against aluminum induced neurotoxicity in rats. *Front Neurol.* (2019) 10:399. doi: 10.3389/fneur.2019.00399

89. Kweon S, Park KA, Choi H. Chemopreventive effect of garlic powder diet in diethylnitrosamine-induced rat hepatocarcinogenesis. *Life Sci.* (2003) 73:2515–26. doi: 10.1016/s0024-3205(03)00660-x

90. Pradeep K, Mohan CV, Gobianand K, Karthikeyan S. Silymarin modulates the oxidant–antioxidant imbalance during diethylnitrosamine induced oxidative stress in rats. *Eur J Pharmacol.* (2007) 560:110–6. doi: 10.1016/j.ejphar.2006.12.023

91. Sivaramakrishnan V, Shilpa PN, Kumar VR, Devaraj SN. Attenuation of N-nitrosodiethylamine-induced hepatocellular carcinogenesis by a novel flavonol—Morin. *Chem Biol Interact.* (2008) 171:79–88. doi: 10.1016/j.cbi.2007.09.003

92. Adedara IA, Rosemberg DB, de Souza D, Farombi EO, Aschner M, Souza DO, et al. Neurobehavioral and biochemical changes in Nauphoeta cinerea following dietary exposure to chlorpyrifos. *Pesticide Biochem Physiol.* (2016) 130:22–30. doi: 10.1016/j.pestbp.2015.12.004

93. Sadri H, Goodarzi MT, Salemi Z, Seifi M. Antioxidant effects of biochanin A in streptozotocin induced diabetic rats. *Braz Arch Biol Technol.* (2017) 60:e17160741.

94. Liu X, Morris MC, Dhana K, Ventrelle J, Johnson K, Bishop L, et al. Mediterranean-DASH Intervention for Neurodegenerative Delay (MIND) study: rationale, design and baseline characteristics of a randomized control trial of the MIND diet on cognitive decline. *Contemporary Clin Trials.* (2021) 102:106270. doi: 10.1016/j.cct.2021.106270

95. Farombi EO, Awogbindin IO, Farombi TH, Oladele JO, Izomoh ER, Aladelokun OB, et al. Neuroprotective role of kolaviron in striatal redo-inflammation associated with rotenone model of Parkinson's disease. *Neurotoxicology.* (2019) 73:132–41. doi: 10.1016/j.neuro.2019.03.005

96. Oladele J, Oyewole O, Bello O, Oladele O. Assessment of protective potentials of Ficus exasperata leaf on arsenate-mediated dyslipidemia and oxidative damage in rat's brain. *J Basic Appl Res Biomed.* (2017) 3:89–94.

97. Oyewole OI, Oladele JO. Changes in activities of tissues enzymes in rats administered Ficus exasperata leaf extract. *Int J Biol Chem Sci.* (2017) 11:378–86.

98. El-Abbadi NH, Dao MC, Meydani SN. Yogurt: role in healthy and active aging. *Am J Clin Nutr.* (2014) 99:1263S–70S. doi: 10.3945/ajcn.113.073957

99. Ano Y, Nakayama H. Preventive effects of dairy products on dementia and the underlying mechanisms. *Int J Mol Sci.* (2018) 19:1927.

Chemistry of Protein-Phenolic Interactions Toward the Microbiota and Microbial Infections

Hilal Yilmaz[1], Busra Gultekin Subasi[2,3], Hasan Ufuk Celebioglu[1], Tugba Ozdal[4] and Esra Capanoglu[5]*

[1] Department of Biotechnology, Faculty of Science, Bartin University, Bartin, Turkey, [2] Division of Food and Nutrition Science, Chalmers University of Technology, Gothenburg, Sweden, [3] Hafik Kamer Ornek MYO, Sivas Cumhuriyet University, Sivas, Turkey, [4] Department of Food Engineering, Faculty of Engineering and Natural Sciences, Istanbul Okan University, Istanbul, Turkey, [5] Department of Food Engineering, Faculty of Chemical and Metallurgical Engineering, Istanbul Technical University, Istanbul, Turkey

Along with health concerns, interest in plants as food and bioactive phytochemical sources has been increased in the last few decades. Phytochemicals as secondary plant metabolites have been the subject of many studies in different fields. Breakthrough for research interest on this topic is re-juvenilized with rising relevance in this global pandemics' era. The recent COVID-19 pandemic attracted the attention of people to viral infections and molecular mechanisms behind these infections. Thus, the core of the present review is the interaction of plant phytochemicals with proteins as these interactions can affect the functions of co-existing proteins, especially focusing on microbial proteins. To the best of our knowledge, there is no work covering the protein-phenolic interactions based on their effects on microbiota and microbial infections. The present review collects and defines the recent data, representing the interactions of phenolic compounds -primarily flavonoids and phenolic acids- with various proteins and explores how these molecular-level interactions account for the human health directly and/or indirectly, such as increased antioxidant properties and antimicrobial capabilities. Furthermore, it provides an insight about the further biological activities of interacted protein-phenolic structure from an antiviral activity perspective. The research on the protein-phenolic interaction mechanisms is of great value for guiding how to take advantage of synergistic effects of proteins and polyphenolics for future medical and nutritive approaches and related technologies.

Keywords: food phenolics, protein-phenolic interaction, antiviral, antioxidant activity, phytochemicals, microbial protein (MP)

INTRODUCTION

Phenolic compounds are secondary metabolites that are synthesized through the shikimic acid and phenylpropanoid pathways found in most plant tissues, including fruits and vegetables. Even though they are not one of the major nutrients, they provide many bioactive properties including antioxidant, anti-cancer, anti-inflammatory, antimicrobial properties. Their bioactive properties provide many health-protective effects including prevention of cancer, cardiovascular diseases, diabetes, and stroke (1).

Protein-phenolic interactions take place in two different mechanisms, which include either covalent or non-covalent interactions. Covalent bonding between two molecules of proteins and phytochemicals is accomplished by two mechanisms, enzymatic and non-enzymatic reaction mechanisms; on the other hand, non-covalent interactions include hydrogen bonding, hydrophobic interactions, electrostatic interactions, and van der Waals binding forces that are reversible reactions. Additionally, some internal factors including characteristics of proteins, types of phytochemicals, protein/phytochemical ratio and external factors including temperature, pH, ionic strength, additional reagents, and other food components influence these interactions (2).

The reciprocal interactions between phenolic compounds and proteins result in various nutritional, functional, and structural changes in both sides. Among these properties, antioxidant activities are of significant importance in terms of organic chemistry, as well as health and nutrition. Mainly, all antioxidative compounds take the action throughout some particular mechanisms which are scavenging of the free radicals in the media, inhibition of enzymes causing free radical formation, chelating the existing metallic ions, induction of endogenous antioxidant enzymes, preventing the lipid peroxidation, DNA damage, protein modification, and/or sugar degradation (3). All these mechanisms are attributed with many diseases within the living organisms; hence, dietary antioxidants have crucial importance to be a part of the diet (4). Dietary phenolic compounds, due to their antioxidant potentials besides their other benefits have been investigated extensively. In one-step further, reaction of dietary phenolic compounds with protein structures might increase the antioxidative properties of phenolics (5). Particularly, flavonoids and phenolic acids have been subjected to extensive studies in order to clarify the reaction mechanisms with protein structures and the consequences of these interactions in terms of biological activities.

Oxidative stress induced by viruses is well established. The viral infection interferes with the body's important metabolic processes in addition to participating in the replication of the virus (6). In this sense, not only the antioxidant properties but also the antiviral activities of phenolic compounds have great significance especially during the recent pandemics of viral diseases. Phenolic compounds have potential to inhibit viral replication by regulating viral adsorption, binding to cell receptors, inhibition of virus penetration into the host cell and by competing for pathways of activation of intracellular signals (7). However, the existing studies have focused on the antiviral effects of phenolics alone; thus, the antiviral mechanisms of the protein-phenol conjugates are not fully elucidated. Similarly, it is known that dietary phenolic compounds affect both physiology and gene expressions of gut microorganisms. These effects can result from interactions of phenolic compounds with bacterial proteins.

To the best of our knowledge, there is no recent study framing the chemistry of food protein - phenolic interactions playing roles in their antioxidant and antimicrobial activities. Thus, the present review collects and defines the recent data, representing the interactions of phenolic compounds, mainly flavonoids and phenolic acids with food proteins and explores how these molecular-level interactions account for the human health directly and/or indirectly, such as increased antioxidative properties, altering physiology of gut microorganisms and antimicrobial capabilities. As antimicrobial mechanism of food protein-phenol conjugates is not clear with the existing literature, we focused on the microbial protein– dietary phenol interactions in the present review to better understand the chemistry of protein-phenolic binding.

CHEMISTRY OF PROTEIN-PHENOLIC INTERACTIONS

Protein-phenolic interactions take place as covalent and non-covalent interactions (8, 9). Covalent interaction mechanisms are defined as the establishment of irreversible binding between molecules under specific conditions such as availability of phenolic oxidases or alkaline conditions. Non-covalent interactions are defined as the reversible forces including electrostatic interactions, hydrogen bonding, hydrophobic interactions, and ionic bonds (8, 10). These reciprocal actions between proteins and phenolics result in a change in the nutritional, functional, and biological characteristics of both proteins and phenolics.

Covalent bonding between two molecules of proteins and phytochemicals is accomplished by two reaction mechanisms: Enzymatic and non-enzymatic reaction mechanisms. Enzymatic reaction mechanisms mostly use phenolic oxidase such as laccase and tyrosinase. In enzymatic reaction mechanisms, non-enzymatic processes are used to convert phenolics to semiquinone or quinone intermediates. These semiquinone and quinone intermediates are then assailed by nucleophilic side chains and produce C–S or C–N covalent bonds between molecules (10, 11). For non-enzymatic protein-phenolic reaction mechanisms, the free radical grafting and alkaline reaction are two extensively utilized procedures. Phenolic compounds are susceptible to oxidation while in contact with air under alkaline conditions. When they are oxidized, they turn into semiquinones and then to quinones. Covalent cross linkages are formed between proteins-phenolic compounds by reaction of nucleophilic amino acid residues such as Lys, Try, Met and Cys with these extremely reactive products (12, 13). Hydrogen peroxide (H_2O_2) and ascorbic acid are frequently used as a redox pair in the free-radical grafting method. They produce hydroxyl radicals, and these radicals oxidize amino acids on the side chain of the proteins. Then, they react with phenolic compounds and generate cross-linked conjugates (14, 15).

Non-covalent interactions include reversible reactions and they contain hydrogen bonding, hydrophobic interactions, electrostatic interactions, and van der Waals binding forces (8, 9). Firstly, phenolic compounds are recognized as hydrogen donors that can produce hydrogen bonds with protein carboxyl groups. Hydrogen bonding occur between hydroxyl groups of phenolics and the oxygen or nitrogen, specifically hydroxyl and amino groups of proteins (10, 16). Specifically, associations between compounds non-polar aromatic ring of the phenolic and hydrophobic regions of the protein molecules are the

main reason of hydrophobic interactions (11). Furthermore, electrostatic interactions occur between the hydroxyl groups of phenolics and charged groups on the proteins. In general, a non-covalent protein-phenolic complex is the consequence of a combination of some foregoing relationships, with hydrogen bonding and hydrophobic interactions serving as the primary driving forces. According to the literature, most of the interactions between protein and phenolic compounds occur as non-covalent interactions in nature. Despite its instability, the non-covalent protein-phenolic interaction has a significant influence on the establishment and enhancement of associated food systems in the food industry (17).

In comparison with the non-covalent interactions, covalent interactions are irreversible and more stable in food processes. However, both covalent and non-covalent interactions affect the chemical structure of proteins and phenolic compounds that also change their nutritional, functional, and biological characteristics (11).

FACTORS AFFECTING PROTEIN-PHENOLIC INTERACTIONS

The factors affecting protein-phenolic interactions are classified as internal factors (characteristics of proteins, types of phytochemicals, protein/phytochemical ratio) and external factors (temperature, pH, ionic strength, additional reagents, and other food components). The parameters that influence protein-phenolic interactions must be studied in order to investigate relevant applications.

Internal Factors
Characteristics of Proteins
Dietary proteins' propensity to interact with phenolics is influenced by several factors, including their hydrophobicity, molecular weight (MW), conformational configurations, amino acid composition and amino acid sequence (9). According to strong hydrophobic interactions, hydrophobicity supports a strong binding between proteins and phenolics (18). Proteins with more basic amino acids and proline, as well as a bigger, more conformationally open and flexible structure, have a better chance of interacting with polyphenols (9). Furthermore, protein properties such as surface structure, total charges, and secondary structures have been found to have varying degrees of correlation with the non-covalent binding of dietary proteins to specific phenolic substances (9, 10).

Types of Phytochemicals
Occurrence of functional groups such as glycosyl, hydroxyl and methyl groups, as well as molecular weight, hydrophobicity, structural flexibility are the key determinants impacting phenolics' binding capabilities (19). It was reported that high molecular weight polyphenols in tea exhibited a stronger prosperity for interaction with milk proteins attributed to the fact that bigger polyphenols having more binding sites (20). Besides, it was reported in several studies that binding efficiency of tea catechins ((-)-epigallocatechin gallate (EGCG) > epicatechin gallate > epicatechin > catechin) to β-lactoglobulin

was related with their molecular size (21, 22). Molecular flexibility of tannins also increase the interactions and binding bonds on proteins (23). In general, it was also reported in several studies that while hydroxylation of flavonoids at ring A and B (**Figure 1**) increase their interactions to whole milk proteins, methoxylation and methylation decrease the binding affinity and strength (24). Depending on sugar moieties and conjugation sites glycosylation also affect the interaction of phenolics with γ-globulin and hemoglobin. Moreover, hydrogenation of double bond between C2 and C3 also lower the binding affinity of phenolics (19, 24). By the way, hydroxylation of phenolic acids at the 3-position increases their binding affinity to BSA. However, their hydroxylation at the 2-/4-positions decrease their binding affinity. Individually, for increasing the binding strength, the hydroxy groups can be replaced with methoxy groups (4-position) or methyl groups (3-position) (25). Seczyk et al. (26) studied the interactions of pure phenolic compounds (gallic acid, ferulic acid, chlorogenic acid, quercetin, apigenin, and catechin) and phenolics from plant extracts including green tea and green coffee, with protein fractions including albumins and globulins of white bean. They have measured the physicochemical properties of complexes. Their results showed that, in most cases, phenolic type significantly affected the protein-phenolic interactions and measured properties (26).

Protein/Phenolic Ratio
Protein/phenolic ratio is another important factor that could affect the interactions between phenolic compounds and proteins. Multidentate and monodentate mechanisms can be involved at differing protein/phenolic ratio (27). The multidentate process requires a lower phenolic/protein ratio because phenolic chemicals operate as multi-site ligands by binding with several protein molecules or sites. In order to achieve cross linking of proteins to produce dimers or oligomers, phenolics should have large size. In the monodentate process, many phenolics bind with a single protein molecule, necessitating a significantly greater phenolic concentration (11). In complex phenolic combinations, synergistic or antagonistic actions between phenolics toward protein binding might occur, which should be taken into account when working with complex food matrices (28).

External Factors
Temperature
Temperature can alter interactions by changing protein structures, ligand solubility, and the strength of certain non-covalent linkages. Thermal denaturation of proteins has been shown to affect phenolics' binding affinities to proteins on both sides: (1) by exposing previously buried hydrophobic sites by protein unfolding, and on the other hand, (2) by reducing interactions by forming aggregates with limited surface area (29, 30). Thermal modification of protein-phenolic interactions can result in structures due to phenolic oxidation into semiquinone and quinone intermediates (31). The binding affinities of proteins can be measured using fluorescence quenching analysis and It is possible to discern the key driving forces (9). Acknowledging the
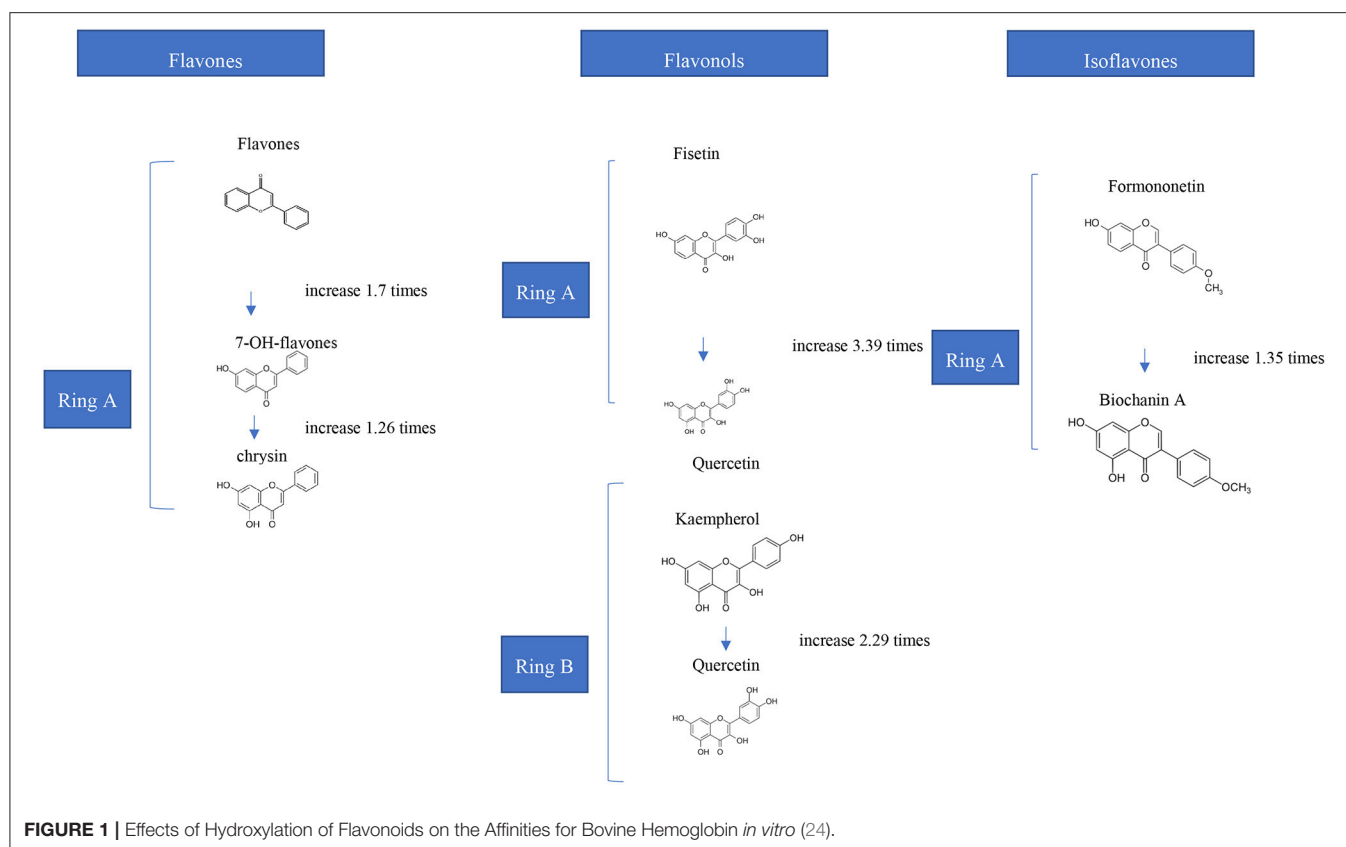
FIGURE 1 | Effects of Hydroxylation of Flavonoids on the Affinities for Bovine Hemoglobin *in vitro* (24).

temperature-dependent relationships of such protein-phenolic combinations might aid in the development of functional food products.

pH

Protein conformational structures, as well as the binding properties of phenolics, may be significantly changed by pH. The tendency of phenolics, such as those found in berries and tea, to precipitate proteins has been shown to be pH-sensitive, especially at the isoelectric points of proteins, indicating that hydrophobic forces are involved in the interactions (32). Due to various reduced binding sites produced by protein secondary structural changes, increasing the pH from acidic to neutral values lowered the affinities of ferulic and chlorogenic acid to BSA (33). Abdollahi et al. (34) studied the interactions between β-lactoglobulin, and ferulic acid at ambient temperature temperature in relation to the dimer, and monomer forms of the protein at pH 7.3 and 2.4, respectively. They have reported that pH affects the binding site and strength of ferulic acid – β-lactoglobulin interaction and binding affinity was found to be higher when β-lactoglobulin was in monomer form (34). Non-covalent binding of dietary polyphenol extracts (tea, coffee, and cocoa) to β-lactoglobulin has been observed to alter with rising pH, probably due to differently charged states of constitutive components at different pH (35). Since the phenolics were auto-oxidized to quinones/semiquinones, which might interact with protein side-chain groups through covalent bonds, further rising

the pH to alkaline conditions with oxygen would form covalent protein-phenolic complexes (13, 14, 36).

Moreover, Seczyk et al. (26) studied the interactions of pure phenolic compounds (gallic acid, ferulic acid, chlorogenic acid, quercetin, apigenin, and catechin) and phenolics from plant extracts including green tea and green coffee, with protein fractions including albumins and globulins of white bean, also determining the effect of ionic strength and pH on protein-phenolic interactions. It was reported that protein-phenolic interactions were affected by pH according to the results of relative protein solubility. The relative protein solubility was increased gradually as alkalinity increased from pH 5.0 to pH 11.0 (26).

Other Factors (Ionic Strength, Additional Reagents, Other Food Components)

Salt concentration in food products also affects the protein-phenolic interactions as it increases the ionic strength. The binding affinities of quercetin to BSA were reduced when ionic strength was raised by adding NaCl, probably due to a stronger hydration hull of the proteins with dissolved electrostatic connections (33). On the other hand, increased ionic strength in a buffering system improved the interactions between chlorogenic acid and BSA, which were largely mediated by hydrophobic forces (37). Furthermore, binding of EGCG to β-lactoglobulin in the presence of $CaCl_2$ resulted in a bigger network of electrostatic calcium–EGCG bridging, resulting in greater levels of EGCG

remaining in the complexes (38). Moreover, the increase of phenolic oxidase or free radicals such as OH radicals affect protein-phenolic interactions through oxidation of phenolics with irreversible covalent bonds. On the other hand, due to the suppression of enzyme activity, reducing substances such as Na_2SO_3 and ascorbic acid significantly decreased the oxidase-mediated connections (15, 39). Additionally, other macro nutrients including carbohydrates and fats also interact with proteins, however their potential for interfering with dietary protein-phenolic interactions is rarely examined (8).

IMPLICATIONS OF DIETARY PROTEIN-PHENOLIC INTERACTIONS

In general, it is considered that the reciprocal interactions in between food phenolics and proteins had a negative effect on the desired properties of both compounds such as functional properties and/or bioavailabilities (40), yet the improvements of varying techniques and approaches in recent years led to opposite results -in terms of boosted functional properties of proteins and bioavailability/antioxidant capacities of phenolic compounds-might also be possible and strictly dependent on the types of the compounds (5).

Dietary phenolics and proteins might interact following different mechanisms, which are dependent on the type of protein and phenolic compound, composition of food matrix, processing conditions as well as the digestion (9). Those interactions (**Figure 2**) were revealed having either covalent bonds as conjugates (chemical bonds) (**Figure 2A**) or non-covalent bonds as complexes (physical bonds), which have varying effects on techno-functional properties of the compounds but particularly the health promoting properties of both phenolic compounds and the food proteins. As explained in the previous part, food protein-phenolic conjugates occur either with free radical induction or under alkaline conditions while protein-phenolic complexes might comprise even as a result of a forced turbulence such as mixing/vortex action (41). Conjugates-covalent bonds mostly have resistant and irreversible interactions in between the molecules, on the other hand the complexes-non-covalent bonds are comprised of reversible hydrophobic interactions (**Figure 2B**), hydrogen bonds (**Figure 2C**), as well as ionic bonds which indicate that both types of food protein- phenolic compounds interaction might easily be generated by food processing and digestion periods. However, very few of research in the literature provided an insight about the type of protein-phenolic interaction mechanism in the matrix and most of the studies rather prefer to focus on the reciprocal consequences of the interactions, instead of the mechanisms. Depending on the prevalence of non-covalent interactions compared with the covalent bond formations during food processing and/or throughout the digestive tract after consumption, all reported protein-phenolic interactions in the food systems are assumed as "complexes," unless other specified (9, 17). Consequently, the interaction in between the protein-phenolic compounds in food matrices are dynamic processes lasting until the digestion is completed and

resulting distinctive indirect health promoting activities such as improved antioxidant capacities, *in vivo/in vitro* bioavailabilities for phenolics and better digestibility and nutritional levels for proteins. Furthermore, it was critically reviewed in a recent study that multistep interactions in between the ingested phenolic compounds and further derived functional proteins in the body such as enzymes, transporters, receptors and transcription factors are also matter of facts (42). Engineering the phenolic compounds as well as proteins to boost their varying range of health-attributed properties with increased retentions/stabilities are considered as one of the major factors to design and produce novel functional food products (43).

Since the stability and bioaccessibility of phenolic compounds were induced with protein interactions, phenolic compounds protect their antioxidative properties for longer times, with being less affected by external processing/environmental conditions and/or digestion periods (44). This protection effect was considered to increase the antioxidative potential of phenolic compounds indirectly throughout the whole digestion process. In this section, the latest studies covering the flavonoid and phenolic acid interactions with food proteins are reviewed for a positive health effect point of view, but the focus is mainly on the improved antioxidant activities. Only very recent papers (in the last 2 years) are covered to present the most novel outcomes.

Flavonoid-Protein Interactions

Covalently structured soy protein isolates and black rice anthocyanins were exposed to *in vitro* gastrointestinal digestion, and it was indicated that the conjugated protein-anthocyanin structure had a higher degree of hydrolysis by around 20%, increased antioxidant capacity by 30 nmol/mg by DPPH assay and 1.5 nmol/mg by $ABTS^{+\cdot}$ assay (Trolox equivalent) compared to the control sample, however a decrease by 13% was reported for transepithelial transport of peptides across Caco-2 cell monolayer (45). Complex and conjugate forms of soybean protein isolate (5 mg/ml) and EGCG (0.2 mM) were investigated for the differences of protein digestibility as well as the antioxidant capacities following the *in vitro* digestion. It was observed that the protein digestibility of non-covalent complexes decreased to 59.14-65.71% compared with the control which was also higher than that of the covalent conjugates. Likewise, antioxidant activities by both $ABTS^{+\cdot}$ and FRAP assays were greater than the control sample in varying ranges for all stages of digestions for both interactions however, $ABTS^{+\cdot}$ trend was consistent for non-covalent structure with a promising scavenging activity increase from 29.02 to 360.51 µg Trolox/g protein (46). In another study with a similar approach, soybean protein isolate-EGCG complexes were used to fabricate alginate hydrogel beads in order to obtain higher antioxidant activities from the core material during the digestion process. It was indicated that 2:1 soy protein:EGCG covalent compounds enabled to produce 20% more stable and highly bioaccessible alginate beads by 20%, while non-covalent complexes enabled this ratio as around 10% (47). On the other hand, lentil protein isolates conjugated with quercetin were indicated in another study as to increase the radical scavenging activity with DPPH

FIGURE 2 | Mechanisms of protein-phenolic compounds interactions as conjugation via covalent bond **(A)**, complexation via hydrophilic interactions **(B)** and hydrogen bonds **(C)** [Adapted from (113)].
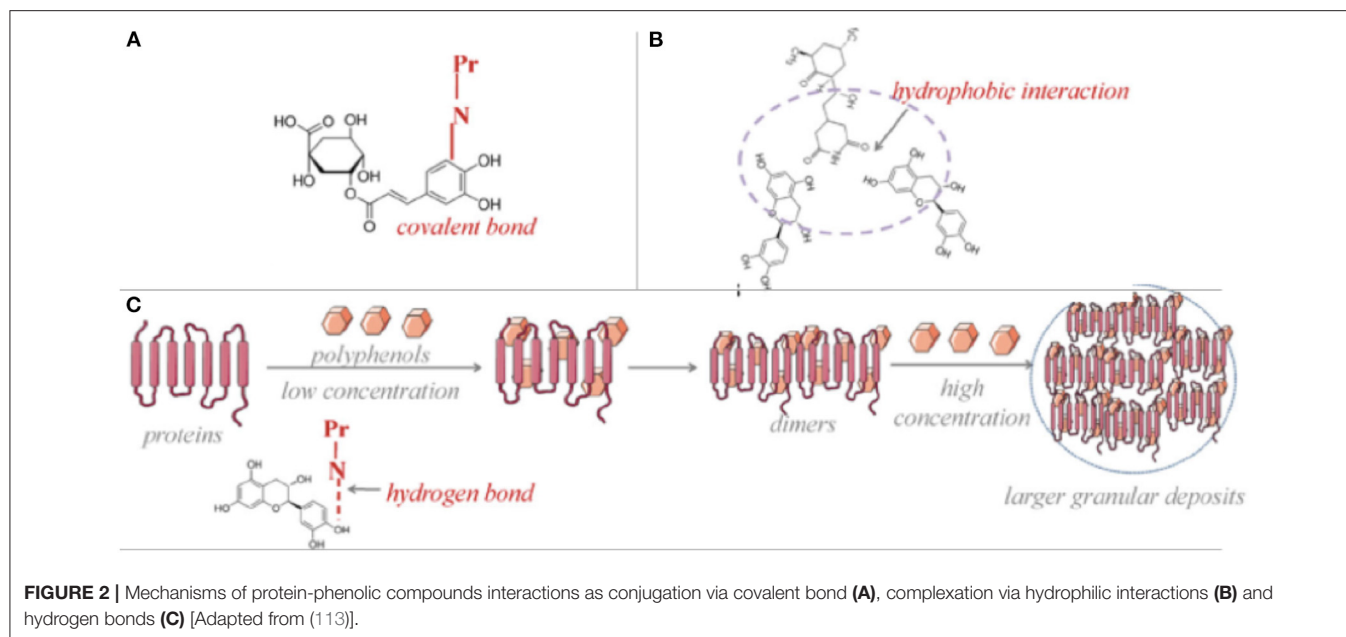
and FRAP assays by 66 and 46%, compared to the phenolic alone, respectively (48).

In a study mainly focusing on the polyphenol stability during a storage period (12 days at 37°C), strawberry polyphenol extract (dominating by flavonols and phenolic acids) was used to make non-covalent complexes with canola protein extract. Degradation rate of the compounds such as pelargonidin-3-O-glucoside, cyanidin-3-O-glucoside, pelargonidin-3-O-rutinoside, pelargonidin-3-O-malonylglucoside, kaempferol-3-O-malonylglucoside were found to decrease significantly in a range of 17–44%. However, no significant difference was observed for total antioxidant activity of defined phenolic compounds after complexation with canola protein extract (49).

Bioaccessibility of coffee beverage phenolics was observed to increase by applying different protein sources as skimmed milk or soy proteins. Total bioaccessibility of coffee phenolics increased with skimmed milk and soy protein application by 37.01–64.21% and 24.74–47.32%, respectively while individual phenolics bioaccessibility *in vitro* increased by 4.40–27.29% and 12.02–28.61% under heat treatment (25, 90, 121°C). An antioxidant activity analysis was not conducted however, the study was observed to have the potential to increase the antioxidative properties (50).

Besides the antioxidative property improvement potentials of the phenolic interactions with food proteins, their capability to decrease the allergen effects of particular food proteins is another research interest of protein-phenolic interaction, with a growing attention. The potential of covalent and non-covalent interactions between the major milk proteins (α-casein and β-lactoglobulin) and cyanidin-3-O-glucoside were investigated aiming to reduce/mask the allergenic activity of milk proteins. Covalent conjugated forms significantly reduced the digestibility of milk proteins (a decrease range 5–11% with varying phenolic:protein ratios as 20, 30, 50) for both proteins,

while showing lower IgE binding properties compared with the non-covalent complex forms as a decrease by 54 and 88% for α-casein and β-lactoglobulin conjugates (when the phenolic:protein ratio is 50), respectively (16). Similar promising results were presented by Pu et al. (51) who intended to examine the allergen reduction potentials of six different flavonoids such as EGCG, naringenin, quercetin, kaempferol, myricetin, and phloretin non-covalent complexations with β-lactoglobulin. Molar ratios of protein and phenolics were applied as 1:1–1:5. All phenolic complexations were indicated to perform antigenic inhibition for β-lactoglobulin in a descending order; 72.6, 68.4, 59.7, 52.3, 51.4, and 40.8% for EGCG, phloretin, naringenin, myricetin, kaempferol, and quercetin (51). Due to the promising results of existing antigenic factor inhibition studies for varying food proteins with distinctive types of phenolic compounds, the research interest on this area has been growing (52).

Phenolic Acid-Protein Interactions

According to the literature, it is a very well know issue that the phenolic acid interactions with varying food proteins have a significant potential to increase their antioxidant activities as well as improvements in many other reciprocal techno-functional properties. For instance, the non-covalent interactions of whey protein isolate and casein with chlorogenic acid (240 μmol/g protein) were evaluated in terms of the interaction effect on the protein digestibility. It was observed that at the end of 2 h, degree of hydrolysis was increased by 7.7 and 5.3% for casein and whey protein isolate, respectively compared with the samples without phenolic interactions. The same samples also yielded a significant antioxidant capacity increase by 460 and 400% for casein and whey protein isolate, respectively based on the $ABTS^{+\cdot}$ assay (53). A different study focused on the type of complexations in β-lactoglobulin (150 μM) and chlorogenic acid (1.5 mM) under different thermal conditions as well as the

alteration of antioxidant capacities. It was indicated that, with the temperatures below 60°C, the interactions were observed as non-covalent however, above that temperature covalent interactions started to be established. Both interactions retarded the loss of antioxidant capacities based on ABTS and FRAP assays. Non-covalent complexations had no significant increase on antioxidant capacity by ABTS assay, however covalent conjugates showed increased capacities (the highest increase as 56.18% at 121°C). Based on FRAP assay, both interactions increased the antioxidant capacities but the highest one (23.36%) was observed for 85°C conjugates (54).

In another study, covalent crosslinking effect of soy protein isolate (12%, w/v) on the antioxidant capacity of tannic acid (29, 58, 88, 117, 146 μmol/g protein) was investigated with DPPH, FRAP, and ABTS$^{+.}$ assays. It was indicated that 146 μmol/g protein tannic acids yielded the highest antioxidant capacity in terms of all three assays in a pH (9.0–11.0) dependent manner (55). Soy protein isolate was covalently interacted with chlorogenic acid (20, 40, 60, 80, 100 μmol/g protein) and based on the ABTS and DPPH assays, an antioxidant capacity increase by 10.87% and 33.08 μmol Trolox/g protein was observed for the chlorogenic acid concentration of 100 μmol/g protein (56). Another plant-based material, pea protein isolate was studied in case of non-covalent complexations with chlorogenic acid (50 μmol/g protein). The main interaction in between the phenolic acid and protein sample was declared as electrostatic interactions. Degree of hydrolysis as an indicator for *in vitro* digestion for pea protein was found to increase by around 5% (57).

Consequently, protein-phenolic interactions are of significant techno-functional reactions ending up with crucial biological activities such as significant antioxidative properties, varying dependent on the types of the compounds, processing conditions and physical media. However, further in-depth research is still required for better tailoring and designing for novel functional foods with boosted health promoting factors.

IMPLICATIONS OF DIETARY POLYPHENOLS-VIRAL PROTEIN INTERACTIONS

In recent years, the pandemic of viral diseases caused serious economic losses and community associated infections, which forced the scientific community to investigate less toxic antiviral phytomolecules instead of using nucleic acid analogs, protease inhibitors or other toxic synthetic molecules as antiviral therapeutics. Although the use of natural antimicrobial agents for food preservation is a trend that is followed by both consumers and food manufacturers, the studies on the antimicrobial activity of phenolic–protein conjugates are very limited (58). On the other hand, there are few studies on the antibacterial activity of protein-phenolic conjugates (59, 60), and the antiviral mechanisms of the conjugates are still unclear until now. The existing studies have focused on the antiviral effect of phytochemicals alone (7). Most of the studied plant-derived secondary metabolites were polyphenolic compounds. They have three main modes of action in treating/preventing viral diseases.

(1) They can bind to the various non-structural proteins (enzymes) to replicate the virus itself, thus inhibit early and late phase of viral replication.
(2) They can bind to structural protein (spike protein) of virus itself, thus inhibit the virus from binding and penetration to the host cells.
(3) They can bind to cell receptor proteins and inhibit virus penetration into the cell.

Since antiviral mechanism of food protein-phenolic conjugates is not clear with the existing literature, we focused on the viral protein-phenolic interactions in this review to better understand the chemistry of protein-phenolic binding.

In the literature there are many natural product-derived phytochemicals investigated as potential agents against viruses. The majority have been classified as polyphenols among the most promising small molecules identified as virus inhibitors. Most studies interpret whether phytochemicals have an antiviral effect based on changes in virus numbers, but they do not show that this antiviral effect is related to the binding between phytochemical and virus protein. We have not included the details on such studies investigating the antiviral activity of numerous phytochemicals in this review. Rather, our aim is to explain the antiviral effect of polyphenols by focusing on their binding properties with viral proteins through the most studied viruses in the literature.

Recently, molecular docking studies have become popular and provided detailed information about ligand-protein binding properties. According to the results, protein-phenolic interactions have direct effect on viral inhibition. These interactions generally occur between phytochemical and non-structural proteins of the viruses, but binding with structural viral protein was also available though.

Corona Viruses

Novel corona-virus (SARS-CoV-2 or COVID-19) has structural and non-structural proteins, which are the key viral molecules, involved in attachment, replication and reproduction of viral particle in the human host cells. SARS-CoV spike glycoprotein (S protein) is the surface protein (structural protein) that is mainly responsible for the initial attachment with the host cells receptor, Angiotensin-converting enzyme (ACE2) (61). SARS-CoV-2 chymotrypsin-like main protease (3CLpro or Mpro, corresponding to Nsp5), papain like protease (PLpro, a domain within Nsp3) are non-structural viral proteins which facilitates viral assembly by cleaving polyproteins (62). RNA dependent RNA polymerase (RdRp) is another nonstructural protein that is vital for viral life cycle (63). These viral protein molecules serve as a novel target to inhibit the viral lifecycle in human host cells.

Basu et al. (64) mentioned that the phytochemical hesperidin (flavonoid) can bind to ACE2 protein. It can also interact with the bound structure of ACE2 protein and spike protein of SARS-CoV2 (64). The binding sites of ACE2 protein for spike protein and hesperidin, are located in different parts of ACE2 protein. Molecular dynamics and docking studies confirmed the conformational change in three-dimensional structure of protein ACE2 due to ligand spike protein. This compound modulates the

binding energy of bound structure of ACE2 and spike protein. After all, in the presence of hesperidin, the bound structure of ACE2 and spike protein fragment becomes unstable and lost its viral activity in SARS-CoV-2 infection.

Moreover, natural flavonoids, quercetin, epigallocatechin gallate and gallocatechin gallate (GCG) showed good inhibition properties by binding to the 3CLpro active site and the 3-OH galooyl group, which was required for SARS-CoV inhibitory activity (65). Green tea polyphenols also have SARS-CoV-2 interaction with catalytic residues of major protease (Mpro). Green tea EGCG binds to spike protein by having the highest affinity to SARS-CoV-2 (66). Catechin is another possible therapeutic phenolic compound able to bind to the viral spike protein and ACE2 of the host (67).

In another study, binding of flavonoids, herbacetin, isobavachalcone, quercetin 3-β-d-glucoside and helichristine was studied by the fluorescence spectroscopy. As a result, flavonols were found to bind to the Middle East Respiratory Syndrome Coronavirus (MERS-CoV) 3CLpro catalytic site and inhibit the virus (68). Chen et al. (69) studied the binding of quercetin-3-β-galactoside to SARS-CoV 3CLpro and found its protease inhibition role (69). Di Petrillo et al. (70) have schematized the interaction between quercetin-3-β-galactoside and the SARS-CoV-2 protease in **Figure 3** (70).

The interaction of flavonoids presents in *Galla chinensis* extract to the structural protein of SARS-CoV was studied by Wang and Liu (71). They observed that the flavonoids could bind to the surface of the spike protein of the virus and prevent their penetration to the cell (71). A recent study with phytochemicals used for the inhibition of SARS-CoV-2 Mpro enzyme indicated that the flavonoid, 5,7-dimethoxyflavanone-4-*O*-β-d-glucopyranoside, interacts with the target enzyme and this interaction is strengthened by the establishment of five hydrogen bonds with a contribution of hydrophobic interaction, too (72). A flavonolignan, silybin (73) and a phenol phytocompound, 6-gingerol (74) have exhibited higher binding affinity and hydrogen bond interaction with non-structural protein targets in SARS-CoV-2 in comparison to currently used repurposed drugs against SARS-CoV-2. Gingerol also exhibited good binding affinity with SARS-CoV-2 spike glycoprotein. Gingerol formed hydrogen-bonded interaction with those viral proteins but with different amino acid residues. There was also a hydrophobic interaction between them (74). The electronic distribution (DFT study) also provided a clear picture of SARS CoV-2 protein-gingerol interactions and supported the molecular docking results.

Glycyrrhiza (liquorice) active compounds against spike (glycoprotein) and non-structural protein of SARS-CoV-2 were investigated (17, 75). Glyasperin A (flavonoid) had a high interaction with endoribonuclease (NS protein) and a high binding ability with the protein receptor cavity. A covalent binding of luteolin-7-*O*-glucuronide and chlorogenic acid (phenol) present in *O. sanctum* to Cys145 of Mpro of SARS-CoV-2 have been mentioned *in silico* analysis, so this may hinder the virus enzymes (76). Kumar et al. (77) recently reported novel natural metabolites namely, ursolic acid, carvacrol and oleanolic acid as the potential inhibitors against main protease (Mpro) of SARS-CoV-2 by using integrated molecular modeling approaches. They found that three ligands were bound to protease and these chemical molecules had stable and favorable energies causing strong binding with binding site of Mpro protein (77).

Lastly, Singh et al. (78) analyzed the binding affinity of 586 phytochemicals to the viral proteins (glycoprotein spike, Papain-protease, and protease main) and host proteins (ACE2, Importin-subunit a-5, and b-1). Their hydrogen bonds and hydrophobic interaction, as well as the binding energies and interactive amino acid residues, were categorized. **Figure 4** shows the binding energy of the most potent phytochemicals. Hetisinone (alkaloid) showed the highest binding energy among all selected phytochemicals. Hetisinone formed 6 H-bonds whereas, control drug, hydroxychloroquine (HCQ), formed 4 H-bonds. This means that the interaction by hydrogen bonds between hetisinone and ACE2 represented a strong interaction than the control drug molecule. The viral-host interaction was disturbed by HCQ binding to the ACE2 receptor (allosteric region), which can inhibit the viral penetration to the human cell (78).

Hepatitis Virus

Manvar et al. (79) identified the anti-Hepatitis C virus (HCV) activity of four different compounds obtained from crude extract of *Eclipe alba*. These are 3,4-dihydroxybenzoic acid (1), 4-hydroxybenzoic acid (2), luteolin (3), wedelolactone (4) and apigenin (5). They used fluorescence spectroscopy technique and quenching the fluorescence emission of the non-structural HCV protein NS5B (an RNA-dependent RNA polymerase) indicating their ability to bind with the enzyme. In addition to the fluorescence quenching technique, they used cell culture system and found that compounds 3, 4 and 5 bound to the enzyme HCV replicase which resulted with the inhibition of HCV replication (79). In fact, the results showed that these compounds have a dose-dependent synergistic inhibitory effect on the enzyme activity, which confirms that HCV replicase have five different binding sites for small molecules that might bind and block enzyme activity (80). The observed synergistic or additive effect of these compounds against HCV replication suggesting that these compounds are more beneficial when used together in the crude extract (79).

Recently, the possible interaction of quercetin with HCV's non-structural protein was identified *in vitro* (70). Molecular docking study of Zhong et al. (81) provided that quercetin derivates can interact with NS5B (non-structural protein 5B in HCV) by two magnesium ions as well as establish coordination with residues at the active site (81). Another molecular docking study showed that quercetin can bind and inhibit the NS2 (non-structural protein 2) protease of HCV (82). Its interacting ability with different proteases causes virus replication blocking and reduces HCV-induced reactive oxygen and nitrogen species (ROS/RNS) generation in replicating cells.

Furthermore, quercetin extracted from *Guiera senegalensis* demonstrated a high anti-Hepatitis B virus (HBV) potential. Data showed that quercetin binds the active site of HBV Polymerase by forming nine hydrogen bonds that stabilizes the quercetin-polymerase complex with an estimated free
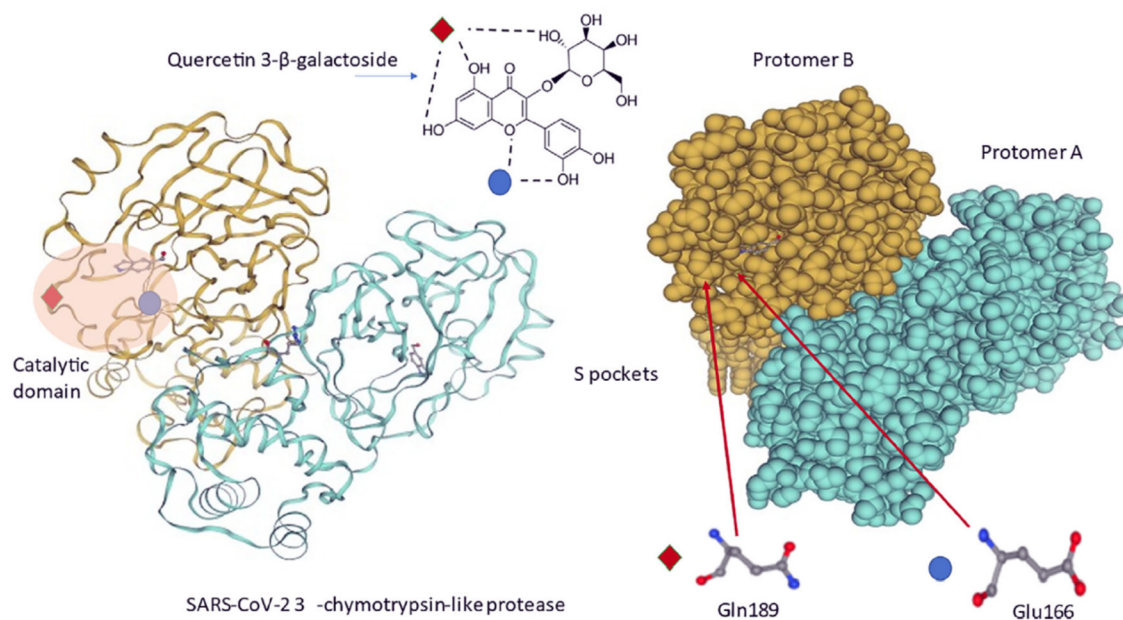
FIGURE 3 | Molecular interactions between quercetin-3-β-galactoside and SARS-CoV-2 3CLpro. Quercetin-3-β-galactoside forms hydrogen bonds specifically with Gln189 and Glu166 amino acids located inside a specific pocket hollowed in 3CLpro surface (70).
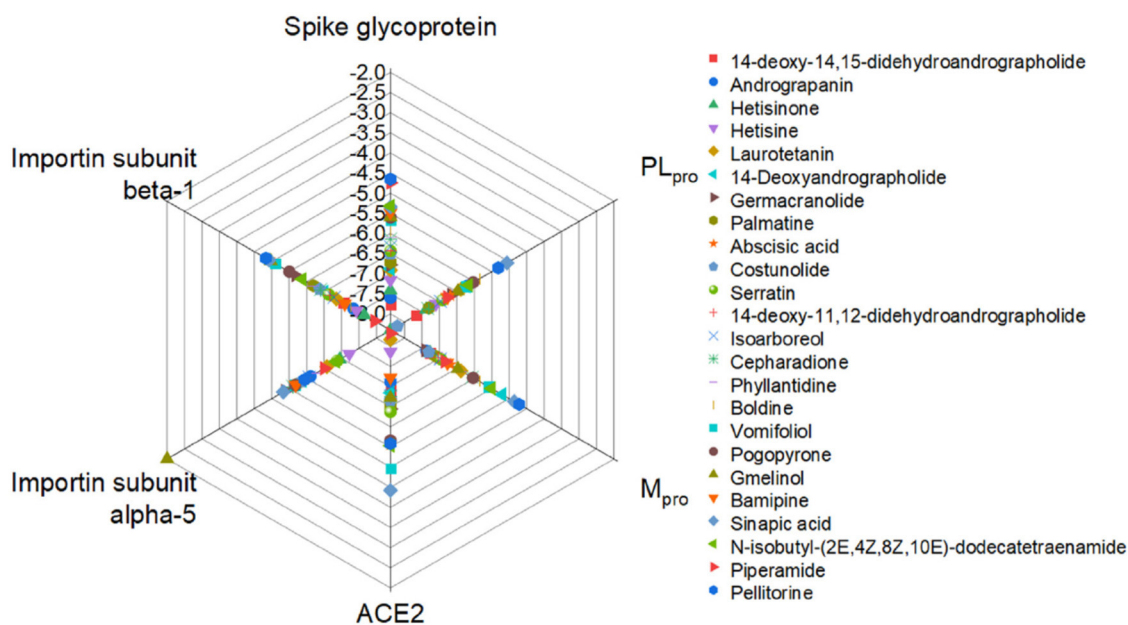

FIGURE 4 | Relative binding energies of phytochemicals with the viral and host proteins (78).

energy of 7.4 kcal/mol (83). These interactions have important contributions for stabilization of the complexes. Another research suggested that quercetin and its derivatives exert their action by interacting with the M2-1 protein, involved in genome replication and transcription by forming the complex RNA-dependent RNA polymerase (84). Caffeic acid was also found to inhibit HBV by binding to non-structural proteins of the virus (85).

Dengue Virus

Dengue, a mosquito-borne disease, has appeared as a major infectious disease globally. In the study of ul Qamar et al. (86) different phytochemicals were used against the non-structural protein of Dengue virus (DENV), which is the NS2B/NS3 protease having the ability to cleave viral proteins (86). As a phytochemical source, garcinia is a genus of flowering plants in the family *Clustaceae* native to Asia, America, Australia, tropical and southern Africa, and Polynesia. With the help of molecular docking, (-)-gossypol (polyphenol), mangostenone C (prenylated xanthones), garcidepsidone A (aromatic), 4-hydroxyacetophenone4-*O*-(6'-*O*-beta-D-apiofuranosyl)-beta-D-glucopyranoside, demethylcalabaxanthone (flavone glycosides), and mangostanin (natural xanthonoid) were found to be bound deeply inside the active site of DENV NS2B/NS3 protease. They had hydrophobic interactions with catalytic triad of the protease enzyme. Thus, it can be concluded from the study that these gracinia phytochemicals could serve as important inhibitors to inhibit the viral replication inside the host cell.

In addition, cyanidin 3-glucoside, dithymoquinone, and glabridin were predicted to be potent inhibitors against the NS3 protease according to their binding affinity. These ligands showed several non-covalent interactions, including hydrogen bond, hydrophobic interaction, electrostatic interaction, pi-sulfur interactions (**Figure 5**). After interaction, the C terminal region of NS3 tends to form a helical structure. This deviation from the initial structure resulted in enzyme inhibition (87).

In the other study, kushenol W and kushenol K flavonoids showed not only strong hydrogen binding but also hydrophobic and non-covalent interactions with structurally and functionally active site of dengue proteases (88). At last, kushenol W and kushenol K disrupted non-structural DV protein functions crucial for viral replication, thereby inhibiting DENV infectivity. Moreover, baicalin has a good binding ability with the NS3/NS2B protein of DENV. Recently, Loaizo-cano et al. (6) reviewed 20 different phenolic compounds against DENV and their good binding affinity to viral particles and proteins but didn't mention the interaction mechanism and types of bindings (6).

Other Viruses

Currently novaccines to prevent Zika virus (ZIKV) infection is available. In the work of Byler et al. (89), potential anti-Zika viral agents from 2263 plant-derived secondary metabolites have been investigated in *in-silico* molecular docking studies. Most of them were polyphenolic compounds (total 1043 of aurones, chalcones, chromones, coumarins, flavonoids, isoflavonoids, lignans, stilbenoids, xanthones, and miscellaneous phenolics). It was shown that the main antiviral molecule targets are several ZIKV non-structural proteins, typically the various enzymes to replicate the virus itself, such as NS2B-NS3 protease, helicase, NS5 methyltransferase. The best binding phytochemical ligands were the polyphenolics with generally two phenolic groups with flexible links to have strong connection to several of the protein targets. For example, rosemarinic acid, cimiphenol, and cimiracemate B showed relatively strong binding energies, thus they inhibit the replication of the virus. They also mentioned that

the poorest enzyme binding ligands were found as terpenoids due to their small size, and their paucity of functional groups (89).

Many phenolic compounds have also been related to antiviral activity against many viruses, such as Herpes simplex virus (HSV), influenza virus (IV), RSV, measles, and rotavirus. These studies demonstrates that flavonoids could be one of the most active compounds against different types of viruses with multiple inhibition mechanisms, such as the inhibition of virus adsorption, entry, binding, and replication by binding both viral and host cell proteins (6). For example, quercetin showed high binding activity on cap-binding site of the PB2 (polymerase basic 2) of influenza viral RNA polymerase. Moreover, it could interact with influenza NA protein (virus surface glycoprotein neuraminidase) and block virus entry at the initial step (90). Flavonoids have non-covalent binding to reverse transcriptase and block RNA synthesis of HSV (7). EGCG also inhibits HSV by binding to their gB, gD, or other envelope proteins (91).

IMPLICATIONS OF DIETARY PHENOLIC ON MICROBIOTA AND MICROBIAL PROTEINS

Human gastrointestinal tract (GIT) is the home for hundreds of different microorganism species and this microbiota plays crucial roles for healthy human homeostasis, including immune and digestive systems (92). The GIT microbiota is not homogenous but very variable through different part of the system; however, it is one of the most populated microbial habitats on the earth (93, 94). All the commensal microorganisms reside within the mucosal layer of the GIT, except pathogenic ones, which go into epithelial layer by digesting the mucosa (95). The GIT microbiota is shaped by the host factors, one of the most important is the diet (96). The members of GIT microbiota are able to metabolize sugars, especially the indigestible ones (97). Not only the sugars, but also they can metabolize other ingredients of the diet. For instance, dietary phenolic compounds can be transformed by GIT microbiota before absorption and this transformation can modulate their biological activities (98). Very small portion (5–10%) of these phenolic compounds taken with the foods are directly absorbed through the small intestine, while most are transported to the large intestine, especially colon, and there they are metabolized by the microbiota (99). However, the transformation of the phenolics is dependent on the nature of the phenolic compound, as well as the microbial species (100). For example, one of the most-studied and very-well known phenolic compounds, resveratrol, is metabolized by human GIT microbiota, shown both *in vitro* and *in vivo* (101). In the study of Bode et al., fecal samples of different volunteers were used to investigate *in vitro* metabolism of trans-resveratrol. They showed fecal samples completely degraded trans-resveratrol and then metabolites were detected after 2–24 h of fermentation. Furthermore, in the same study, a separate human *in vivo* study with 12 volunteers was conducted and trans-resveratrol was given orally to the volunteers. After 24 h, a subsequent proportion of trans-resveratrol was found to be metabolized by GIT microbiota and same metabolites found in *in vitro* study were also detected in the urine samples, which confirms that trans-resveratrol
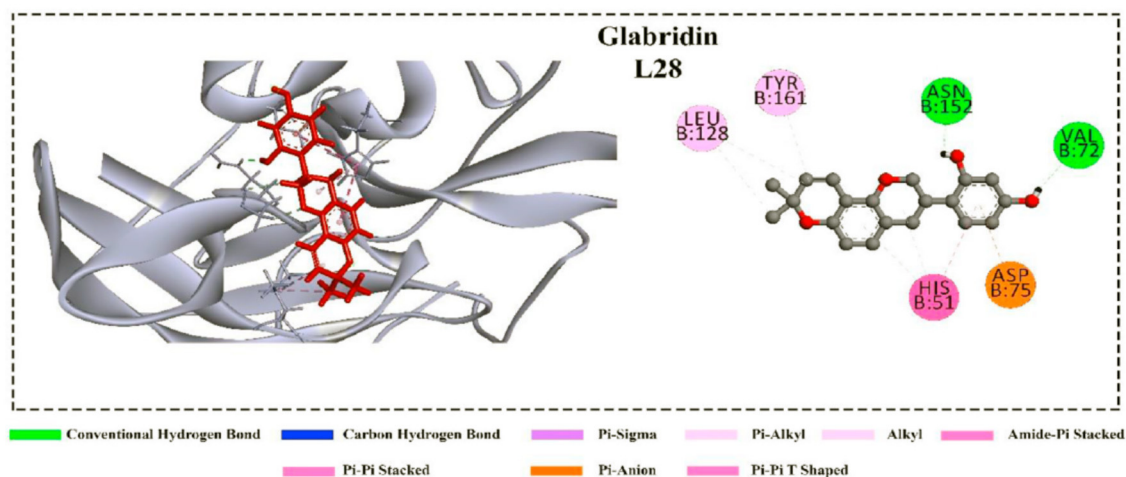
FIGURE 5 | Non-covalent interactions of the glabridin with the NS3 protease (87).
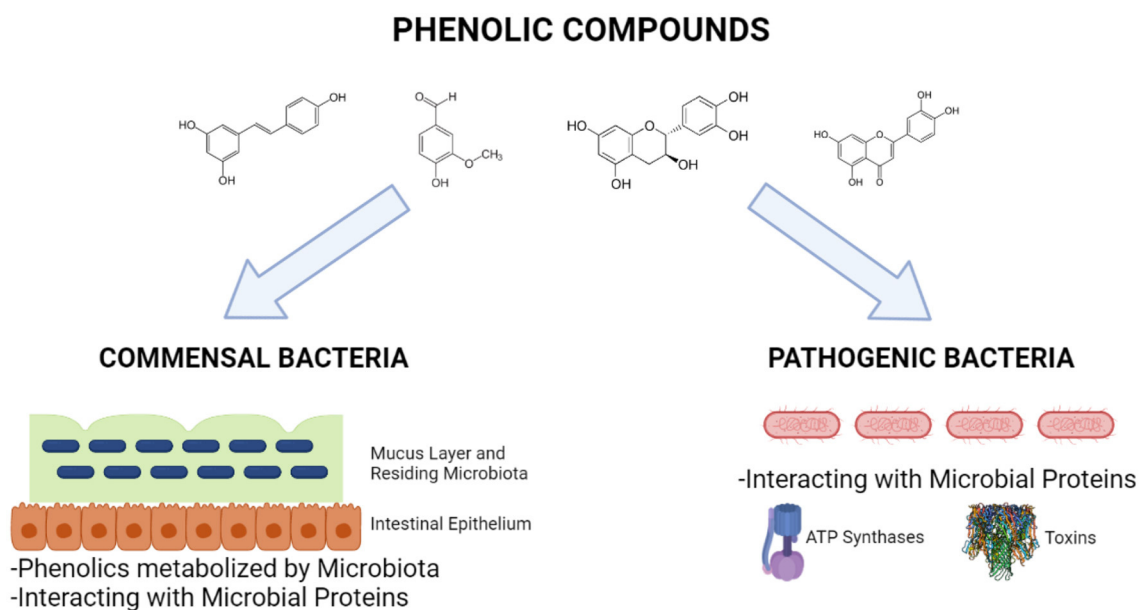

FIGURE 6 | Interactions of phenolic compounds with commensal and pathogenic bacteria (Created with BioRender.com).

was metabolized into three metabolites, main ones being dihydroresveratrol and lunularin. This study also confirmed the interindividual differences of resveratrol metabolism by GIT microbiota as microbiota can differ between the individuals (101). A pure-culture study investigated the metabolism and transformation of different but related glycosylated phenolic compounds using *Lactobacillus acidophilus* NCFM (102). They showed that *Lactobacillus acidophilus* NCFM can use such phenolic compounds and other phytochemicals as carbon source. In this mentioned study, eleven plant glycosides, including salicin, rutin, vanillin, and arbutin, were used and esculin, fraxin, and salicin supplemented to the growth were completely utilized

by the bacterium. Vanillin was almost completely utilized and the growth of the bacterium in these phytochemicals reached 0.3 to 1.3 (OD_{600}) in 200-μl cultures in 96-well plates. Furthermore, it is very-well known that dietary phenolic compounds affect both physiology and gene expressions of gut microorganisms. Thus, these effects can result from interactions of phenolic compounds with microbial macromolecules, including proteins. As the phenolic compounds usually interact with food proteins or host proteins, these conjugated complexes should further affect the gut microbiota. Theilmann et al. used transcriptomics to examine which genes are affected by these phytochemicals. Genes related with carbohydrate metabolism were differentially regulated in

the phytochemical-supplemented group, with respect to control in which glucose was used as carbon source. In addition, the genes encoding the proteins related with mucus, fibrinogen, and epithelial cell adhesion were also upregulated (102). These proteins may have roles in adhesion to the host components and this upregulation may lead to higher adhesion, which means better colonization in the GIT. Previously, it has been also showed that polyphenols affect the proteome profile of this bacterium, as well as its adhesion to mucus and host cells (103). These studies suggest that plant phenolic compounds can interact either directly to the probiotic proteins or indirectly by altering the gene expressions.

Phenolic compounds can interact not only commensal microorganisms residing in the GIT or probiotics but also pathogen microorganisms so that they exert antimicrobial activities (**Figure 6**). These compounds especially affect proteins of such organisms, thus inhibiting crucial proteins and microbial growth, leading to antimicrobial activity. The microbial proteins affected by phenolic compounds belong to membrane (efflux system, cell envelope metabolism, and ATP synthase system), anabolic and catabolic reactions, pathogenic and antibiotic-resistance mechanisms, such as toxins and virulence factors transporters and antibiotic-inactivating enzymes, virulence factors, biofilm, and DNA metabolisms. Bacterial cell membrane is a complex system that plays roles as barrier between outside and inside of the cell, regulator of the osmotic, energy, and lipid systems, as well as cell wall maintenance (104). The major antibiotics, including penicillins, cephalosporins, and polymixins, target the bacterial membrane and cell wall, thus disrupting their functions and leading to bacterial death. The studies showed that some phenolic compounds, especially flavonoids can inhibit the efflux pumps present in the bacterial membranes and having roles in drug modulation (105, 106). A study done by Sinsinwar et al. showed that catechin treatment of *Staphylococcus aureus* led to decreases in the activities of superoxide dismutase and catalase enzymes, which are responsible for anti-oxidant system of the bacteria (107).

Bacterial energetics is mainly driven by ATPase activity, which is a complex protein structures responsible for ATP production. Other than some known antibiotics or antibacterial compounds, phenolics can also be inhibiting agents of ATPase system. For example, resveratrol, piceatannol, quercitrin, and quercetin inhibit ATPase belonging to *Escherichia coli* but in different degrees (108). Among these, the ATPase activity was completely inhibited by piceatannol, thus can lead to bacterial death; however, this study was performed *in vitro* using purified ATPase or membrane. Furthermore, Chinnam et al. also investigated the inhibitory effect of flavonoids on *E. coli* ATPase (109). In their study, seventeen polyphenols were used and *E. coli* growth, as well as inhibitory effect on purified ATPase activity were investigated. They found polyphenols used in the study caused complete, partial, slight, or no inhibition on ATPase activity. For instance, morin, silymarin, baicalein, silibinin, epicatechin, rimantadine HCl, and amantidin completely inhibited the ATPase activity, while hesperidin, chrysin, kaempferol, diosmin, apigenin, genistein, and rutin led to partial inhibition. On the other hand, luteolin, daidzein, and galangin showed insignificant

inhibition. The authors stated that presence of number of hydroxyl groups can be important for the inhibition (109).

Pathogenic bacteria produce virulence factors, which are various molecules promoting disease state by invading and attacking host cells. They include endotoxins (found within the cell) or exotoxin (released to the outside of the cells). Some phenolic compounds target and inhibit such virulence factors. For example, flavone and luteolin, which are flavonoids, were found to reduce production of staphyloxantin, a carotenoid pigment produced by some strains of *Staphylococcus aureus*, and acting as a virulence factor (110). Furthermore, flavone also inhibited gene expression of α-hemolysin, causing red blood cell lysis by disrupting the cell membrane, investigated using qRT-PCR technique (110). Another study done by Stockovic et al. showed that methanolic extract of *Phlomis fruticosa* L. (Jerusalem sage) inhibited the expression of staphyloxantin (111). Another common pathogen is *Listeria monocytogenes*, which produces a virulence factor called listeriolysin O. This bacterium causes gastroenteritis, meningitis, and abortions and listeriolysin allows this bacterium to escape phagocytosis by the host immune system and also disrupt the vacuole of the host cells. A study done by Wang et al. indicated that fisetin, a plant flavonol present in many plants including strawberries, apples, persimmons, onions and cucumbers, inhibits listeriolysin O–induced hemolysis, suggesting that fisetin antagonizes the hemolytic activity and protects the red blood cells by directly or indirectly interacting with the toxin (112). Furthermore, fisetin also facilitates the elimination of *L. monocytogenes* by macrophages by blocking bacterial escape into the cytosol. These studies implicated that those phenolic compounds inhibit the pathogenic bacteria by interacting with their proteins that are crucial for bacterial growth or pathogenesis. However, more molecular investigations are required to enlighten how exactly phenolic compounds interact and inhibit microbial proteins.

Concluding Remarks

Phenolic compounds are abundant bioactive compounds in human diet and used as natural colorants and preservatives in foods. Despite the valuable biological activities of phenolics, such as antioxidant, antimicrobial, anticancer, antiallergenic, and anti-inflammatory effects, little is known about the health-related activity of phenolic-protein conjugates. Thus, in the last decade there is a growing interest on the functionalization of proteins with phenolic compounds. The interaction of food polyphenolics and proteins, as well as its effect on the functional properties including antioxidant and antimicrobial properties related to the chemistry of their binding, are reviewed in this paper.

Protein-phenolic interactions take place as covalent and non-covalent interactions. Protein interaction with polyphenolics-flavonoids and phenolic acids is influenced by their hydrophobicity, molecular weight, conformational configurations, amino acid composition and sequence. Type of phenolics has also significant effect on the protein-phenolic interactions and biological properties. However, very few studies in the literature provided an insight about the type of protein-polyphenolic interaction mechanism in the matrix and most of the studies focused only on the reciprocal consequences of

the interactions, instead of the mechanisms. These reciprocal interactions between proteins and phenolics result in a change in the nutritional, functional, biological characteristics of both proteins and polyphenolics, and thus needs to be deeply investigated.

The main interaction mechanism between the phenolic acids and proteins was the electrostatic attraction. Depending on the temperature, both non-covalent complexations and covalent conjugates can lead to increased antioxidant capacity. Moreover, covalent conjugated forms significantly reduce the digestibility of some food proteins, therefore have an indirect effect on allergen activity. On the other hand, protein-phenolic interactions have direct effect on viral inhibition. These interactions are generally of non-covalent origin and occur between phenolic and non-structural proteins of the viruses. Many phenolics form hydrogen-bonded interactions with those viral proteins and increased number hydrogen bonds result in more stable proteins, which leads to more effective antiviral capacity. In addition to the antioxidant and antiviral activity, dietary phenolic compounds affect both physiology and gene expressions

of gut microorganisms as a result of the interaction with microbial proteins. This interaction is not only with commensal microorganism in the gastrointestinal track but also with pathogen microorganisms; so that, they exert antimicrobial activities by inhibiting crucial proteins and microbial growth of such organisms.

Overall, studies on the antioxidant and antimicrobial activities of protein-phenolic conjugates are very limited. Due to the altered structures of both proteins and phenolics, systematic structure-functionality relationships of various conjugates should be investigated together with *in vitro* and *in vivo* studies to fully evaluate the biological activities of protein- phenolic conjugates.

AUTHOR CONTRIBUTIONS

HY and BS: conceptualization and methodology. HY, BS, HC, and TO: writing—original draft preparation. HY, BS, HC, and EC: writing—review and editing. EC: supervision. All authors have read and agreed to the published version of the manuscript.

REFERENCES

1. Laura A, Moreno-Escamilla JO, Rodrigo-García J, Alvarez-Parrilla E. Phenolic compounds.In: *Postharvest physiology and biochemistry of fruits and vegetables*. Sawston: Woodhead Publishing. (2019). p. 253–271.

2. Ozdal T, Yalcinkaya IE, Toydemir G, Capanoglu E. Polyphenol-Protein Interactions and Changes in Functional Properties and Digestibility In: Melton L, Shahidi F, Varelis PBT-E of FC, editors. Oxford: Academic Press (2019). p. 566–77.

3. Carocho M, Morales P, Ferreira ICFR. Antioxidants: reviewing the chemistry, food applications, legislation and role as preservatives. *Trends Food Sci Technol.* (2018) 71:107–20. doi: 10.1016/j.tifs.2017.11.008

4. Grosso G. Dietary antioxidants and prevention of non-communicable diseases. *Antioxidants.* (2018) 7:94. doi: 10.3390/antiox7070094

5. Cianciosi D, Forbes-Hernández TY, Regolo L, Alvarez-Suarez JM, Navarro-Hortal MD, Xiao J, et al. The reciprocal interaction between polyphenols and other dietary compounds: impact on bioavailability, antioxidant capacity and other physico-chemical and nutritional parameters. *Food Chem.* (2022) 375:131904. doi: 10.1016/j.foodchem.2021.131904

6. Loaiza-Cano V, Monsalve-Escudero LM, Filho C da SMB, Martinez-Gutierrez M, Sousa DP de. Antiviral role of phenolic compounds against dengue virus: a review. *Biomolecules.* (2020) 11:11. doi: 10.3390/biom11010011

7. Kapoor R, Sharma B, Kanwar SS. Antiviral phytochemicals: an overview. *Biochem Physiol.* (2017) 6:7. doi: 10.4172/2168-9652.1000220

8. Jakobek L. Interactions of polyphenols with carbohydrates, lipids and proteins. *Food Chem.* (2015) 175:556–67. doi: 10.1016/j.foodchem.2014.12.013

9. Zhang Q, Cheng Z, Wang Y, Fu L. Dietary protein-phenolic interactions: characterization, biochemical-physiological consequences, and potential food applications. *Crit Rev Food Sci Nutr.* (2021) 61:3589–615. doi: 10.1080/10408398.2020.1803199

10. Quan TH, Benjakul S. Sae-leaw T, Balange AK, Maqsood S. Protein–polyphenol conjugates: Antioxidant property, functionalities and their applications. *Trends Food Sci Technol.* (2019) 91:507–17. doi: 10.1016/j.tifs.2019.07.049

11. Chu Q, Bao B, Wu W. Mechanism of interaction between phenolic compounds and proteins based on non-covalent and covalent interactions. *Med Res.* (2018) 2:180014. doi: 10.21127/yaoyimr20180014

12. Liu F, Ma C, Gao Y, McClements DJ. Food-grade covalent complexes and their application as nutraceutical delivery systems: a review. *Compr Rev Food Sci Food Saf.* (2017) 16:76–95. doi: 10.1111/1541-4337.12229

13. Sui X, Sun H, Qi B, Zhang M, Li Y, Jiang L. Functional and conformational changes to soy proteins accompanying anthocyanins: focus on covalent and non-covalent interactions. *Food Chem.* (2018) 245:871–8. doi: 10.1016/j.foodchem.2017.11.090

14. He W, Xu H, Lu Y, Zhang T, Li S, Lin X, et al. Function, digestibility and allergenicity assessment of ovalbumin–EGCG conjugates. *J Funct Foods.* (2019) 61:103490. doi: 10.1016/j.jff.2019.103490

15. Wu S, Zhang Y, Ren F, Qin Y, Liu J, Liu J, et al. Structure–affinity relationship of the interaction between phenolic acids and their derivatives and β-lactoglobulin and effect on antioxidant activity. *Food Chem.* (2018) 245:613–9. doi: 10.1016/j.foodchem.2017.10.122

16. Zhang Q, Cheng Z, Chen R, Wang Y, Miao S, Li Z, et al. Covalent and non-covalent interactions of cyanidin-3-: O -glucoside with milk proteins revealed modifications in protein conformational structures, digestibility, and allergenic characteristics. *Food Funct.* (2021) 12:10107–20. doi: 10.1039/D1FO01946E

17. Sinha SK, Prasad SK, Islam MA, Gurav SS, Patil RB, AlFaris NA, et al. Identification of bioactive compounds from Glycyrrhiza glabra as possible inhibitor of SARS-CoV-2 spike glycoprotein and non-structural protein-15: a pharmacoinformatics study. *J Biomol Struct Dyn.* (2021) 39:4686–700. doi: 10.1080/07391102.2020.1779132

18. Ren C, Xiong W, Li J, Li B. Comparison of binding interactions of cyanidin-3-O-glucoside to β-conglycinin and glycinin using multi-spectroscopic and thermodynamic methods. *Food Hydrocoll.* (2019) 92:155–62. doi: 10.1016/j.foodhyd.2019.01.053

19. Xiao J, Kai G. A. review of dietary polyphenol-plasma protein interactions: characterization, influence on the bioactivity, and structure-affinity relationship. *Crit Rev Food Sci Nutr.* (2012) 52:85–101. doi: 10.1080/10408398.2010.499017

20. Dubeau S, Samson G, Tajmir-Riahi HA. Dual effect of milk on the antioxidant capacity of green, Darjeeling, and English breakfast teas. *Food Chem.* (2010) 122:539–45. doi: 10.1016/j.foodchem.2010.03.005

21. Kanakis CD, Hasni I, Bourassa P, Tarantilis PA, Polissiou MG, Tajmir-Riahi HA. Milk β-lactoglobulin complexes with tea polyphenols. *Food Chem.* (2011) 127:1046–55. doi: 10.1016/j.foodchem.2011.01.079

22. Chanphai P, Bourassa P, Kanakis CD, Tarantilis PA, Polissiou MG, Tajmir-Riahi HA. Review on the loading efficacy of dietary tea

polyphenols with milk proteins. *Food Hydrocoll.* (2018) 77:322–8. doi: 10.1016/j.foodhyd.2017.10.008

23. Dobreva MA, Green RJ, Mueller-Harvey I, Salminen JP, Howlin BJ, Frazier RA. Size and molecular flexibility affect the binding of ellagitannins to bovine serum albumin. *J Agric Food Chem.* (2014) 62:9186–94. doi: 10.1021/jf502174r

24. Xiao JB, Huo JL, Yang F, Chen XQ. Noncovalent interaction of dietary polyphenols with bovine hemoglobin in vitro: Molecular structure/property–affinity relationship aspects. *J Agric Food Chem.* (2011) 59:8484–90. doi: 10.1021/jf201536v

25. Wu X, Lu Y, Xu H, Lin D, He Z, Wu H, et al. Reducing the allergenic capacity of β-lactoglobulin by covalent conjugation with dietary polyphenols. *Food Chem.* (2018) 256:427–34. doi: 10.1016/j.foodchem.2018.02.158

26. Seczyk Ł, Swieca M, Kapusta I, Gawlik-Dziki U. Protein–phenolic interactions as a factor affecting the physicochemical properties of white bean proteins. *Molecules.* (2019) 24:408. doi: 10.3390/molecules24030408

27. Haslam E. *Plant Polyphenols: Vegetable Tannins Revisited.* Cambridge: CUP Archive, pp.154–195. (1989).

28. García-Estévez I, Ramos-Pineda AM, Escribano-Bailón MT. Interactions between wine phenolic compounds and human saliva in astringency perception. *Food Funct.* (2018) 9:1294–309. doi: 10.1039/C7FO02030A

29. Yildirim-Elikoglu S, Erdem YK. Interactions between milk proteins and polyphenols: Binding mechanisms, related changes, and the future trends in the dairy industry. *Food Rev Int.* (2018) 34:665–97. doi: 10.1080/87559129.2017.1377225

30. Zhan F, Yang J, Li J, Wang Y, Li B. Characteristics of the interaction mechanism between tannic acid and sodium caseinate using multispectroscopic and thermodynamics methods. *Food Hydrocoll.* (2018) 75:81–7. doi: 10.1016/j.foodhyd.2017.09.010

31. Buchner N, Krumbein A, Rohn S, Kroh LW. Effect of thermal processing on the flavonols rutin and quercetin. *Rapid Commun Mass Spectrom.* (2006) 20:3229–35. doi: 10.1002/rcm.2720

32. Xu H, Zhang T, Lu Y, Lin X, Hu X, Liu L, et al. Effect of chlorogenic acid covalent conjugation on the allergenicity, digestibility and functional properties of whey protein. *Food Chem.* (2019) 298:125024. doi: 10.1016/j.foodchem.2019.125024

33. Rawel HM, Meidtner K, Kroll J. Binding of selected phenolic compounds to proteins. *J Agric Food Chem.* (2005) 53:4228–35. doi: 10.1021/jf0480290

34. Abdollahi K, Ince C, Condict L, Hung A, Kasapis S. Combined spectroscopic and molecular docking study on the pH dependence of molecular interactions between β-lactoglobulin and ferulic acid. *Food Hydrocoll.* (2020) 101:105461. doi: 10.1016/j.foodhyd.2019.105461

35. Stojadinovic M, Radosavljevic J, Ognjenovic J, Vesic J, Prodic I, Stanic-Vucinic D, et al. Binding affinity between dietary polyphenols and β-lactoglobulin negatively correlates with the protein susceptibility to digestion and total antioxidant activity of complexes formed. *Food Chem.* (2013) 136:1263–71. doi: 10.1016/j.foodchem.2012.09.040

36. Pham LB, Wang B, Zisu B, Adhikari B. Covalent modification of flaxseed protein isolate by phenolic compounds and the structure and functional properties of the adducts. *Food Chem.* (2019) 293:463–71. doi: 10.1016/j.foodchem.2019.04.123

37. Prigent SVE, Gruppen H, Visser AJWG, Van Koningsveld GA, De Jong GAH, Voragen AGJ. Effects of non-covalent interactions with 5-O-caffeoylquinic acid (chlorogenic acid) on the heat denaturation and solubility of globular proteins. *J Agric Food Chem.* (2003) 51:5088–95. doi: 10.1021/jf021229w

38. Carnovale V, Britten M, Couillard C, Bazinet L. Impact of calcium on the interactions between epigallocatechin-3-gallate and β-lactoglobulin. *Food Res Int.* (2015) 77:565–71. doi: 10.1016/j.foodres.2015.08.010

39. Le Bourvellec C, Renard C. Interactions between polyphenols and macromolecules: Quantification methods and mechanisms. *Crit Rev Food Sci Nutr.* (2012) 52:213–48. doi: 10.1080/10408398.2010.499808

40. Kamiloglu S, Tomas M, Ozdal T, Capanoglu E. Effect of food matrix on the content and bioavailability of flavonoids. *Trends Food Sci Technol.* (2021) 117:15–33. doi: 10.1016/j.tifs.2020.10.030

41. Baba WN, McClements DJ, Maqsood S. Whey protein–polyphenol conjugates and complexes: Production, characterization, and applications. *Food Chem.* (2021) 365:130455. doi: 10.1016/j.foodchem.2021.130455

42. Guan H, Zhang W, Sun-Waterhouse D, Jiang Y, Li F, Waterhouse GIN, Li D. Phenolic-protein interactions in foods and post ingestion: Switches empowering health outcomes. *Trends Food Sci Technol.* (2021) 118:71–86. doi: 10.1016/j.tifs.2021.08.033

43. Li Y, He D, Li B, Lund MN, Xing Y, Wang Y, et al. Engineering polyphenols with biological functions via polyphenol-protein interactions as additives for functional foods. *Trends Food Sci Technol.* (2021) 110:470–82. doi: 10.1016/j.tifs.2021.02.009

44. Shahidi F, Senadheera R. Encyclopedia of food chemistry: protein–phenol interactions. *Encycl Food Chem.* (2018) 2:532–8. doi: 10.1016/B978-0-08-100596-5.21485-6

45. Jiang L, Liu Y, Li L, Qi B, Ju M, Xu Y, et al. Covalent conjugates of anthocyanins to soy protein: Unravelling their structure features and *in vitro* gastrointestinal digestion fate. *Food Res Int.* (2019) 120:603–9. doi: 10.1016/j.foodres.2018.11.011

46. Zhou SD, Lin YF, Xu X, Meng L, Dong MS. Effect of non-covalent and covalent complexation of (–)-epigallocatechin gallate with soybean protein isolate on protein structure and in vitro digestion characteristics. *Food Chem.* (2020) 309:125718. doi: 10.1016/j.foodchem.2019.125718

47. Hu M, Du X, Liu G, Huang Y, Qi B, Li Y. Sodium alginate/soybean protein-epigallocatechin-3-gallate conjugate hydrogel beads: evaluation of structural, physical, and functional properties. *Food Funct.* (2021) 12:12347–61. doi: 10.1039/D1FO03099J

48. Parolia S, Maley J, Sammynaiken R, Green R, Nickerson M, Ghosh S. Structure – Functionality of lentil protein-polyphenol conjugates. *Food Chem.* (2022) 367:130603. doi: 10.1016/j.foodchem.2021.130603

49. Hanuka Katz I, Okun Z, Parvari G, Shpigelman A. Structure dependent stability and antioxidant capacity of strawberry polyphenols in the presence of canola protein. *Food Chem.* (2022) 385:132630. doi: 10.1016/j.foodchem.2022.132630

50. Qie X, Cheng Y, Chen Y, Zeng M, Wang Z, Qin F, et al. *In vitro* phenolic bioaccessibility of coffee beverages with milk and soy subjected to thermal treatment and protein–phenolic interactions. *Food Chem.* (2022) 375:131644. doi: 10.1016/j.foodchem.2021.131644

51. Pu P, Zheng X, Jiao L, Chen L, Yang H, Zhang Y, et al. Six flavonoids inhibit the antigenicity of β-lactoglobulin by noncovalent interactions: a spectroscopic and molecular docking study. *Food Chem.* (2021) 339:128106. doi: 10.1016/j.foodchem.2020.128106

52. Pan T, Wu Y, He S, Wu Z, Jin R. Food allergenic protein conjugation with plant polyphenols for allergenicity reduction. *Curr Opin Food Sci.* (2022) 43:36–42. doi: 10.1016/j.cofs.2021.10.002

53. Jiang J, Zhang Z, Zhao J, Liu Y. The effect of non-covalent interaction of chlorogenic acid with whey protein and casein on physicochemical and radical-scavenging activity of in vitro protein digests. *Food Chem.* (2018) 268:334–41. doi: 10.1016/j.foodchem.2018.06.015

54. Qie X, Chen W, Zeng M, Wang Z, Chen J, Goff HD, et al. Interaction between β-lactoglobulin and chlorogenic acid and its effect on antioxidant activity and thermal stability. *Food Hydrocoll.* (2021) 121:107059. doi: 10.1016/j.foodhyd.2021.107059

55. Guo Y, Bao YH, Sun KF, Chang C, Liu WF. Effects of covalent interactions and gel characteristics on soy protein-tannic acid conjugates prepared under alkaline conditions. *Food Hydrocoll.* (2021) 112:106293. doi: 10.1016/j.foodhyd.2020.106293

56. Guo K, Zhou G, Lok US, Wang X, Jiang L. Improving interface-related functions and antioxidant activities of soy protein isolate by covalent conjugation with chlorogenic acid. *J Food Meas Charact.* (2022) 16:202–13. doi: 10.1007/s11694-021-01148-6

57. Hao L, Sun J, Pei M, Zhang G, Li C, Li C, et al. Impact of non-covalent bound polyphenols on conformational, functional properties and *in vitro* digestibility of pea protein. *Food Chem.* (2022) 383:132623. doi: 10.1016/j.foodchem.2022.132623

58. Liu J, Yong H, Yao X, Hu H, Yun D, Xiao L. Recent advances in phenolic–protein conjugates: Synthesis, characterization, biological

activities and potential applications. *RSC Adv.* (2019) 9:35825–40. doi: 10.1039/C9RA07808H

59. Fu S, Wu C, Wu T, Yu H, Yang S, Hu Y. Preparation and characterisation of chlorogenic acid-gelatin: a type of biologically active film for coating preservation. *Food Chem.* (2017) 221:657–63. doi: 10.1016/j.foodchem.2016.11.123

60. Ali M, Keppler JK, Coenye T, Schwarz K. Covalent whey protein–rosmarinic acid interactions: a comparison of alkaline and enzymatic modifications on physicochemical, antioxidative, and antibacterial properties. *J Food Sci.* (2018) 83:2092–100. doi: 10.1111/1750-3841.14222

61. Nag A, Banerjee R, Chowdhury RR, Krishnapura Venkatesh C. Phytochemicals as potential drug candidates for targeting SARS CoV 2 proteins, an in silico study. *VirusDisease.* (2021) 32:98–107. doi: 10.1007/s13337-021-00654-x

62. Mengist HM, Fan X, Jin T. Designing of improved drugs for COVID-19: Crystal structure of SARS-CoV-2 main protease Mpro. *Signal Transduct Target Ther.* (2020) 5:1–2. doi: 10.1038/s41392-020-0178-y

63. Elfiky AA. SARS-CoV-2 RNA dependent RNA polymerase (RdRp) targeting: an in silico perspective. *J Biomol Struct Dyn.* (2021) 39:3204–12. doi: 10.1080/07391102.2020.1761882

64. Basu A, Sarkar A, Maulik U. Molecular docking study of potential phytochemicals and their effects on the complex of SARS-CoV2 spike protein and human ACE2. *Sci Rep.* (2020) 10:1–15. doi: 10.1038/s41598-020-74715-4

65. Nguyen NK, Nguyen PB, Nguyen HT, Le PH. Screening the optimal ratio of symbiosis between isolated yeast and acetic acid bacteria strain from traditional kombucha for high-level production of glucuronic acid. *LWT Food Sci Technol.* (2015) 64:1149–55. doi: 10.1016/j.lwt.2015.07.018

66. Ghosh R, Chakraborty A, Biswas A, Chowdhuri S. Evaluation of green tea polyphenols as novel corona virus (SARS CoV-2) main protease (Mpro) inhibitors–an in silico docking and molecular dynamics simulation study. *J Biomol Struct Dyn.* (2021) 39:4362–74. doi: 10.1080/07391102.2020.1779818

67. Jena AB, Kanungo N, Nayak V, Chainy GBN, Dandapat J. Catechin and curcumin interact with S protein of SARS-CoV2 and ACE2 of human cell membrane: insights from computational studies. *Sci Rep.* (2021) 11:1–14. doi: 10.1038/s41598-021-81462-7

68. Jo S, Kim H, Kim S, Shin DH, Kim M. Characteristics of flavonoids as potent MERS-CoV 3C-like protease inhibitors. *Chem Biol Drug Des.* (2019) 94:2023–30. doi: 10.1111/cbdd.13604

69. Chen L, Li J, Luo C, Liu H, Xu W, Chen G, et al. Binding interaction of quercetin-3-β-galactoside and its synthetic derivatives with SARS-CoV 3CLpro: Structure–activity relationship studies reveal salient pharmacophore features. *Bioorg Med Chem.* (2006) 14:8295–306. doi: 10.1016/j.bmc.2006.09.014

70. Di Petrillo A, Orrù G, Fais A, Fantini MC. Quercetin and its derivates as antiviral potentials: a comprehensive review. *Phyther Res.* (2022) 36:266–78. doi: 10.1002/ptr.7309

71. Wang X, Liu Z. Prevention and treatment of viral respiratory infections by traditional Chinese herbs. *Chin Med J (Engl).* (2014) 127:1344–50. doi: 10.3760/cma.j.issn.0366-6999.20132029

72. Gurung AB, Ali MA, Lee J, Farah MA, Al-Anazi KM. Unravelling lead antiviral phytochemicals for the inhibition of SARS-CoV-2 Mpro enzyme through in silico approach. *Life Sci.* (2020) 255:117831. doi: 10.1016/j.lfs.2020.117831

73. Pandit M, Latha N. *In silico* studies reveal potential antiviral activity of phytochemicals from medicinal plants for the treatment of COVID-19 infection. *Res Sq.* (2020) 1:22687. doi: 10.21203/rs.3.rs-22687/v1

74. Rathinavel T, Palanisamy M, Palanisamy S, Subramanian A, Thangaswamy S. Phytochemical 6-Gingerol–A promising Drug of choice for COVID-19. *Int J Adv Sci Eng.* (2020) 6:1482–9. doi: 10.29294/IJASE.6.4.2020.1482-1489

75. Gupta S, Singh AK, Kushwaha PP, Prajapati KS, Shuaib M, Senapati S, et al. Identification of potential natural inhibitors of SARS-CoV2 main protease by molecular docking and simulation studies. *J Biomol Struct Dyn.* (2021) 39:4334–45. doi: 10.1080/07391102.2020.1776157

76. Anand AV, Balamuralikrishnan B, Kaviya M, Bharathi K, Parithathvi A, Arun M, et al. Medicinal plants, phytochemicals, and herbs to combat viral pathogens including SARS-CoV-2. *Molecules.* (2021) 26:1775. doi: 10.3390/molecules26061775

77. Kumar A, Choudhir G, Shukla SK, Sharma M, Tyagi P, Bhushan A, et al. Identification of phytochemical inhibitors against main protease of COVID-19 using molecular modeling approaches. *J Biomol Struct Dyn.* (2021) 39:3760–70. doi: 10.1080/07391102.2020.1772112

78. Singh P, Chauhan SS, Pandit S, Sinha M, Gupta S, Gupta A, et al. The dual role of phytochemicals on SARS-CoV-2 inhibition by targeting host and viral proteins. *J Tradit Complement Med.* (2022) 12:90–9. doi: 10.1016/j.jtcme.2021.09.001

79. Manvar D, Mishra M, Kumar S, Pandey VN. Identification and evaluation of anti hepatitis C virus phytochemicals from Eclipta alba. *J Ethnopharmacol.* (2012) 144:545–54. doi: 10.1016/j.jep.2012.09.036

80. Hang JQ, Yang Y, Harris SF, Leveque V, Whittington HJ, Rajyaguru S, et al. Slow binding inhibition and mechanism of resistance of non-nucleoside polymerase inhibitors of hepatitis C virus. *J Biol Chem.* (2009) 284:15517–29. doi: 10.1074/jbc.M808889200

81. Zhong D, Liu M, Cao Y, Zhu Y, Bian S, Zhou J, et al. Discovery of metal ions chelator quercetin derivatives with potent anti-HCV activities. *Molecules.* (2015) 20:6978–99. doi: 10.3390/molecules20046978

82. Sajitha Lulu S, Thabitha A, Vino S, Mohana Priya A, Rout M. Naringenin and quercetin–potential anti-HCV agents for NS2 protease targets. *Nat Prod Res.* (2016) 30:464–8. doi: 10.1080/14786419.2015.1020490

83. Parvez MK, Rehman MT, Alam P, Al-Dosari MS, Alqasoumi SI, Alajmi MF. Plant-derived antiviral drugs as novel hepatitis B virus inhibitors: cell culture and molecular docking study. *Saudi Pharm J.* (2019) 27:389–400. doi: 10.1016/j.jsps.2018.12.008

84. Teixeira TSP, Caruso ÍP, Lopes BRP, Regasini LO, de Toledo KA, Fossey MA, et al. Biophysical characterization of the interaction between M2-1 protein of hRSV and quercetin. *Int J Biol Macromol.* (2017) 95:63–71. doi: 10.1016/j.ijbiomac.2016.11.033

85. Wang GF, Shi LP, Ren YD, Liu QF, Liu HF, Zhang RJ, et al. Anti-hepatitis B virus activity of chlorogenic acid, quinic acid and caffeic acid *in vivo* and *in vitro. Antiviral Res.* (2009) 83:186–90. doi: 10.1016/j.antiviral.2009.05.002

86. ul Qamar T, Mumtaz A, Ashfaq UA, Azhar S, Fatima T, Hassan M, et al. Computer aided screening of phytochemicals from Garcinia against the dengue NS2B/NS3 protease. *Bioinformation.* (2014) 10:115. doi: 10.6026/97320630010115

87. Rahman MM, Biswas S, Islam KJ, Paul AS, Mahato SK, Ali MA, et al. Antiviral phytochemicals as potent inhibitors against NS3 protease of dengue virus. *Comput Biol Med.* (2021) 134:104492. doi: 10.1016/j.compbiomed.2021.104492

88. Tahir ul Qamar M, Maryama A, Muneer I, Xing F, Ashfaq UA, Khan FA, et al. Computational screening of medicinal plant phytochemicals to discover potent pan-serotype inhibitors against dengue virus. *Sci Rep.* (2019) 9:1–16. doi: 10.1038/s41598-018-38450-1

89. Byler KG, Ogungbe IV, Setzer WN. *In-silico.* screening for anti-Zika virus phytochemicals. *J Mol Graph Model.* (2016) 69:78–91. doi: 10.1016/j.jmgm.2016.08.011

90. Gansukh E, Nile A, Kim DH, Oh JW, Nile SH. New insights into antiviral and cytotoxic potential of quercetin and its derivatives–a biochemical perspective. *Food Chem.* (2021) 334:127508. doi: 10.1016/j.foodchem.2020.127508

91. Isaacs CE, Wen GY, Xu W, Jia JH, Rohan L, Corbo C, et al. Epigallocatechin gallate inactivates clinical isolates of herpes simplex virus. *Antimicrob Agents Chemother.* (2008) 52:962–70. doi: 10.1128/AAC.00825-07

92. Sekirov I, Russell SL, Antunes LCM, Finlay BB. Gut microbiota in health and disease. *Physiol Rev.* (2010) 90:859–904. doi: 10.1152/physrev.00045.2009

93. Hakansson A, Molin G. Gut microbiota and inflammation. *Nutrients.* (2011) 3:637–82. doi: 10.3390/nu3060637

94. Whitman WB, Coleman DC, Wiebe WJ. Prokaryotes: the unseen majority. *Proc Natl Acad Sci.* (1998) 95:6578–83. doi: 10.1073/pnas.95.12.6578

95. Thursby E, Juge N. Introduction to the human gut microbiota. *Biochem J.* (2017) 474:1823–36. doi: 10.1042/BCJ20160510

96. Donaldson GP, Lee SM, Mazmanian SK. Gut biogeography of the bacterial microbiota. *Nat Rev Microbiol.* (2016) 14:20–32. doi: 10.1038/nrmicro3552

97. Zoetendal EG, Raes J, Van Den Bogert B, Arumugam M, Booijink CCGM, Troost FJ, et al. The human small intestinal microbiota is driven by rapid

uptake and conversion of simple carbohydrates. *ISME J.* (2012) 6:1415–26. doi: 10.1038/ismej.2011.212

98. Selma M V, Espin JC, Tomas-Barberan FA. Interaction between phenolics and gut microbiota: role in human health. *J Agric Food Chem.* (2009) 57:6485–501. doi: 10.1021/jf902107d

99. Cardona F, Andrés-Lacueva C, Tulipani S, Tinahones FJ, Queipo-Ortuño MI. Benefits of polyphenols on gut microbiota and implications in human health. *J Nutr Biochem.* (2013) 24:1415–22. doi: 10.1016/j.jnutbio.2013.05.001

100. D'Archivio M, Filesi C, Varì R, Scazzocchio B, Masella R. Bioavailability of the polyphenols: status and controversies. *Int J Mol Sci.* (2010) 11:1321–42. doi: 10.3390/ijms11041321

101. Bode LM, Bunzel D, Huch M, Cho GS, Ruhland D, Bunzel M, et al. *In vivo* and *in vitro* Metab trans-resveratrol by Hum gut microbiota. *Am J Clin Nutr.* (2013) 97:295–309. doi: 10.3945/ajcn.112.049379

102. Theilmann MC, Goh YJ, Nielsen KF, Klaenhammer TR, Barrangou R, Abou Hachem M. Lactobacillus acidophilus metabolizes dietary plant glucosides and externalizes their bioactive phytochemicals. *MBio.* (2017) 8:e01421–17. doi: 10.1128/mBio.01421-17

103. Celebioglu HU, Delsoglio M, Brix S, Pessione E, Svensson B. Plant polyphenols stimulate adhesion to intestinal mucosa and induce proteome changes in the probiotic Lactobacillus acidophilus NCFM. *Mol Nutr Food Res.* (2018) 62:1700638. doi: 10.1002/mnfr.201700638

104. Donadio G, Mensitieri F, Santoro V, Parisi V, Bellone ML, De Tommasi N, et al. Interactions with microbial proteins driving the antibacterial activity of flavonoids. *Pharmaceutics.* (2021) 13:660. doi: 10.3390/pharmaceutics13050660

105. Maia GL de A, Falcão-Silva V, dos S, Aquino PGV, Araújo-Júnior JX de, Tavares JF, et al. Flavonoids from Praxelis clematidea RM King and Robinson modulate bacterial drug resistance. *Molecules.* (2011) 16:4828–35. doi: 10.3390/molecules16064828

106. Farooq S, Wahab A, Fozing CDA, Rahman A, Choudhary MI. Artonin I inhibits multidrug resistance in S taphylococcus aureus and potentiates the action of inactive antibiotics in vitro. *J Appl Microbiol.* (2014) 117:996–1011. doi: 10.1111/jam.12595

107. Sinsinwar S, Vadivel V. Catechin isolated from cashew nut shell exhibits antibacterial activity against clinical isolates of MRSA through ROS-mediated oxidative stress. *Appl Microbiol Biotechnol.* (2020) 104:8279–97. doi: 10.1007/s00253-020-10853-z

108. Dadi PK, Ahmad M, Ahmad Z. Inhibition of ATPase activity of Escherichia coli ATP synthase by polyphenols. *Int J Biol Macromol.* (2009) 45:72–9. doi: 10.1016/j.ijbiomac.2009.04.004

109. Chinnam N, Dadi PK, Sabri SA, Ahmad M, Kabir MA, Ahmad Z. Dietary bioflavonoids inhibit Escherichia coli ATP synthase in a differential manner. *Int J Biol Macromol.* (2010) 46:478–86. doi: 10.1016/j.ijbiomac.2010.03.009

110. Lee JH, Park JH, Cho MH, Lee J. Flavone reduces the production of virulence factors, staphyloxanthin and α-hemolysin, in *Staphylococcus aureus*. *Curr Microbiol.* (2012) 65:726–32. doi: 10.1007/s00284-012-0229-x

111. Stojković D, Gašić U, Drakulić D, Zengin G, Stevanović M, Rajčević N, et al. Chemical profiling, antimicrobial, anti-enzymatic, and cytotoxic properties of Phlomis fruticosa L. *J Pharm Biomed Anal.* (2021) 195:113884. doi: 10.1016/j.jpba.2020.113884

112. Wang J, Qiu J, Tan W, Zhang Y, Wang H, Zhou X, et al. Fisetin inhibits Listeria monocytogenes virulence by interfering with the oligomerization of listeriolysin O. *J Infect Dis.* (2015) 211:1376–87. doi: 10.1093/infdis/jiu520

113. Shahidi F, Pan Y. Influence of food matrix and food processing on the chemical interaction and bioaccessibility of dietary phytochemicals: a review. *Crit Rev Food Sci Nutr.* (2021) 113:1–25. doi: 10.1080/10408398.2021.1901650

Check for updates

Verification of autoclaving-cooling treatment to increase the resistant starch contents in food starches based on meta-analysis result

Didah Nur Faridah[1,2]*[†], Rhoito Frista Silitonga[1,3][†], Dias Indrasti[1,2][†], Frendy Ahmad Afandi[4][†], Anuraga Jayanegara[5][†] and Maria Putri Anugerah[1][†]

[1]Department of Food Science and Technology, Faculty of Agricultural Engineering Technology, IPB University, Bogor, Indonesia, [2]Southeast Asia Food and Agricultural Science and Technology (SEAFAST) Center, Lembaga Penelitian dan Pengabdian Kepada Masyarakat, Institut Pertanian Bogor University, Bogor, Indonesia, [3]Center for Agro-Based Industry, Ministry of Industry, Bogor, Indonesia, [4]Deputy Ministry for Food and Agribusiness, Coordinating Ministry for Economic Affairs Republic of Indonesia, Jakarta, Indonesia, [5]Department of Nutrition and Feed Technology, Faculty of Animal Science, Institut Pertanian Bogor University, Bogor, Indonesia

Autoclaving-cooling is a common starch modification method to increase the resistant starch (RS) content. The effect of this method varies depending on the type of crop and treatment condition used. The objectives of this study were to verify the autoclaving-cooling treatment based on a meta-analysis result and to evaluate the physicochemical properties of modified starches. The meta-analysis study used 10 articles from a total of 1,293 that were retrieved using the PRISMA approach. Meta-analysis showed that the optimal treatments of autoclaving-cooling process that increase the RS content significantly, was in starch samples from the cereal group (corn, oats, rice) (SMD: 19.60; 95% CI: 9.56−29.64; $p < 0.001$), with water ratio 1:4 (SMD: 13.69; 95% CI: 5.50−21.87; $p < 0.001$), using two cycles of autoclaving-cooling (SMD: 16.33; 95% CI: 6.98−25.67; $p < 0.001$) and 30 min of autoclaving heating (SMD: 12.97; 95% CI: 1.97−23.97; $p < 0.001$) at 121°C (SMD: 12.18; 95% CI: 1.88−22.47; $p < 0.001$). Verification using corn flour and corn starch showed a significant increase in RS contents from 15.84 to 27.78% and from 15.27 to 32.53%, respectively, and a significant decrease in starch digestibility from 67.02 to 35.74% and from 76.15 to 28.09%, respectively. Treated sample also showed the pasting profile that was stable under heating and stirring.

KEYWORDS

autoclaving-cooling, cereal, meta-analysis, resistant starch, starch modification

Introduction

Resistant starch (RS) are any starch fractions that cannot be absorbed in the small intestine but can be fermented in the large intestine (1). It is recognized to impact gut bacteria, act as pre- and probiotics, has a role in preventing colon cancer, and help to overcome gastrointestinal dysfunction (2). RS is known to have a hypoglycemic effect,

which can lower fasting blood glucose levels, increase insulin secretion and improve insulin sensitivity (3). According to Kumar et al. (4) and Lemlioglu-Austin et al. (5), the higher the content of RS in the sample, the lower the glycaemic index value produced. RS is classified into 5 types (RS 1, RS2, RS3, RS4, and RS5) with RS3 being the RS generated by retrograded amylose (2, 3). Various types of RS have been produced commercially, including Hi-maze® whole grain corn flour (RS1 and RS2), Hi-maze 260 corn starch (RS2), Fibersym® RW (RS4 Resistant Wheat Starch), and Novelose® 330 (RS3).

A modification process can increase the amount of RS content in a material, and autoclaving-cooling is one of the methods that is widely used. This modification does not use chemicals, so it does not produce by-products in the final product. However, this modification process requires equipment such as an autoclave that can provide high temperature and pressure. It involves heating a starch sample suspended in water in an autoclave, then cooling it to produce retrograded amylose (6). The application of higher temperature along with higher pressure causes faster retrogradation rate, while cooling temperature leads to better retrogradation. The technical conditions used affect the gelatinization and retrogradation processes, which subsequently influence the amount of RS produced (7). In autoclaving-cooling, RS can be increased by adjusting processing conditions such as source of sample, heating and cooling temperature and time, also number of heating-cooling cycles (8). One example of a commercial RS product produced through a retrogradation process is Novelose® 330.

Several studies stated that the more cycles used, the higher the RS content increase (1, 9–11). However, Ratnaningsih et al. (12) reported that autoclaving-cooling 1 cycle resulted in higher RS content than autoclaving-cooling with 3 cycles and 5 cycles. Rahmawati et al. (13) reported that the addition of cycles in the autoclaving-cooling process did not significantly affect the content of RS. Various studies have also been conducted to investigate differences in the use of heating time during the autoclaving process. Variations of autoclaving time used include 15, 30, 60, and 120 min. These variations have different effects on the of RS content (14–16).

The findings of studies did not clearly describe the effect of autoclaving-cooling treatment on RS contents. Therefore, a meta-analysis study needs to be carried out to evaluate the effect of the treatment used. Meta-analysis is a quantitative scientific synthesis of various research results that have been used in many scientific fields. Meta-analysis aids in the practice of evidence-based research and the resolution of conflicting study findings. The meta-analysis extracts one or more study outcomes in terms of effect sizes. The purpose of effect sizes is to put the results of a large number of research on the same scale by employing a number of metrics such as oddity and risk ratios, standardized mean differences, transformed correlation coefficients and logarithmic response ratios (17,

18). The effectiveness of hydrothermal starch modification such as heat moisture treatment (HMT) and annealing has been conducted (19, 20). However, the effectiveness of autoclaving-cooling modification and its physicochemical properties of the modified starch has not been done. The objectives of this study were to verify the autoclaving-cooling treatment based on a meta-analysis result and to evaluate the physicochemical properties of modified starches. This study provides the optimal treatment of the autoclaving-cooling process to achieve a significant increase in RS content, especially RS 3, which can be applied as functional food ingredients.

Materials and methods

Materials

Materials for meta-analysis study were articles obtained from several reputable online journal databases and published from 2000 to 2020. Corn flour and corn starch for verification are obtained from commercial products in Indonesia, under the brands "Mugo Tepung Jagung" and "Maizena 328," respectively.

Meta-analysis study

The studies were retrieved using PRISMA (Preferred Reporting Items for Systematic Reviews and Meta-Analysis) statement guidelines (21). Several reputable online journal databases, such as ProQuest, Science Direct, PubMed, Wiley Online Library, and Google Scholar were used to search and identify studies. Studies were limited to articles published from 2000 to 2020 and searched with appropriate keywords, for instance "autoclaving cooling starch," "autoclaving cooling resistant starch" and "autoclaving cooling modification starch." In order to identify relevant articles, keywords were combined with Boolean operators and advanced search tools.

Based on inclusion and exclusion criteria, studies were selected through screening and eligibility stages. Research articles from international journals indexed by Scopus (Q1–Q3) and web of science published from 2000 to 2020 were used as inclusion criteria. Articles also have to include sufficient data, namely source of starch, the value of RS from native (as control) and from autoclaving-cooling process (as experiment), standard deviation or standard error, and number of replications. Exclusion criteria included studies from books or patents, studies with raw materials other than starch, and studies with other treatments or multiple modifications.

Data were extracted and inputted into a worksheet developed by Afandi et al. (22) using the calculation +formula from Palupi et al. (23) and Borenstein et al. (17). The following information was gathered: source of starch, water ratio, number of autoclaving-cooling cycles, heating time, temperature of

heating and cooling, mean and standard deviation of RS (control and experiment), and number of replications.

Verification and characterization of physicochemical properties

Verification of the autoclaving-cooling treatments was carried out based on the results of the meta-analysis. Sample (fineness 100 mesh) was weighed as much as 60 g, then suspended with distilled water in a ratio (sample:water, 1:4). The sample was put into an autoclave for 30 min at a temperature of 121°C. The sample then continued was cooled in a refrigerator at 4°C for 24 h. The autoclaving-cooling was repeated once again, so that the total cycle is two times. The samples obtained were then dried in an oven at 50°C for 24 h. After that, the sample was mashed and shieved (100 mesh) for further characterization. Native and modified samples were analyzed for moisture, ash, protein and fat content according to AOAC (24). The RS content (25), starch digestibility (26) and gelatinization profile (using Rapid Visco Analyzer) of the samples were also determined. Starch morphology was observed using a light microscope, polarizing microscope and scanning electron microscopy (SEM) (27) while the crystalline analysis was carried out using Fourier Transform Infrared (FTIR) (28, 29).

Statistical analysis

The meta-analysis data were analyzed by the effect size value using Hedges'd (standardized mean difference/SMD), with 95% CI (confidence interval) pooled through a random-effects model (22, 23) to assess the effect of autoclaving-cooling on RS content. A forest plot was used to evaluate the individual study and pooled effect sizes. The value of CI that did not include zero determined the significance of the autoclaving-cooling effect (30). Heterogeneity test was assessed using the I^2 value (31), while publication bias was determined by funnel plot and Egger's regression test. The subgroup analysis of crop type, water ratio, number of cycles, heating time and temperature of autoclaving were performed to analyze the subset of included studies. The meta-analysis process was performed using Meta-Essentials 1.5 software (32). The characterization data was analyzed by comparison of the native and treated sample using the paired t-test. The analysis was carried out at a significance level of 5% (95% CI) using SPSS 26 software.

Results and discussion

Autoclaving-cooling treatments to increase the resistant starch content based on meta-analysis

Included study analysis

A total of 1,293 studies were initially retrieved and screened by the search strategy. Then, 135 full articles were evaluated, with 125 studies being excluded, leaving 10 studies for meta-analysis (**Figure 1**). These studies were excluded for several reasons, including studies published in journals not indexed Scopus, as well as studies that did not have the required completeness of data, such as number of replication, standard
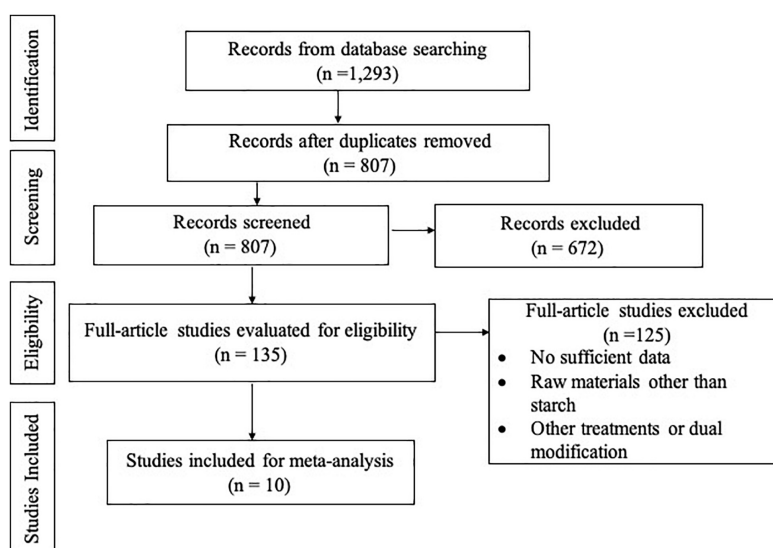

FIGURE 1
Schematic representation (PRISMA flow chart) of the literature review process.

deviation values, or data treatment (total cycle, temperature of autoclaving, and temperature of cooling) The required data information was extracted from the selected studies, resulting in 21 data (Table 1).

In autoclaving-cooling process, heating above the gelatinization temperature resulted in the dissociation of hydrogen bonds from the double helix structure of amylopectin, melting of crystallites and the release of the amylose fraction from the granules (7, 8, 33). The amylose fraction then binds to form a double helix structure and binds to other double helix structures to form crystallite, so that amylose recrystallizes and forms RS3 (34).

The forest plot of individual studies was shown in Figure 2. The CI value from combined effect size (SMD 4.04; 95% CI: −4.06 to 12.13; $p = 0.149$) included zero. It is revealed that single modification by autoclaving-cooling process statistically had no significant effect on increasing the RS content. This insignificant outcome may be due to the numerous variations used in the autoclaving-cooling process.

The heterogeneity (I^2) among studies is 89.70% and classified as high heterogeneity (greater than 75%) (31). The starch source of crop and treatment conditions (such as number of autoclaving cycles and heating time) can contribute to this high heterogeneity value of RS change (35). To evaluate the effect of these variants on changes of RS, the subgroup analysis was performed. Subgroup analysis was conducted to groups with $n \geq 2$.

Subgroup analysis based on type of crop

Analysis of RS content based on type of crop consist of 2 types of crops, namely cereal and legume (Figure 3). The autoclaving-cooling treatment enhanced the RS content in cereal group (SMD: 19.60; 95% CI: 9.56–29.64; $p < 0.001$) but did not significantly affect the legume group (SMD: −7.09; 95% CI: −15.68 to 1.50; $p < 0.001$). The amounts of RS are closely linked to the levels of amylopectin and amylose contained in a substance. In general, the higher amylose/amylopectin ratio, the more RS is present. This is because the chain structure of amylose is small and easy to orient and regenerate, while amylopectin has a dendritic structure and is difficult to orient (43).

Figure 3 also showed a negative value (decrease of RS) from the legume group. This decrease may be related to the destruction of RS1 and RS2 during the autoclave process, where the amount of RS1 and RS2 degraded was more than the RS3 formed by an incomplete starch retrogradation (44). The destruction of RS1 and RS2 in a more open structure with fragmented starch chains of varying lengths. After gelatinization, these flexible linear amylose molecules align themselves into tight linear configurations, forming helices, rendering the α-1,4 glycosidic linkages inaccessible to amylase (45).

The subgroup of cereal sample types was investigated to determine which type of sample had the highest effect on increasing levels of RS for laboratory verification (Figure 4). There were three groups of samples analyzed, namely corn, oats and rice. Based on the results of the analysis, the sample groups of corn, oats and rice had a significant effect in increasing the levels of RS. The highest effect size value was corn (SMD 46.38; 95% CI: 20.80–71.96), followed by rice (SMD 27.72; 95% CI: 20.69–34.76) and oats (SMD 10.91; 95% CI: 3.89–17.94).

The higher effect in corn samples could be attributed to the higher amylose content when compared to rice and oat samples. The amylose content in normal corn is 30%, in oats is 28%, and in normal rice is 20–22% (46, 47). The higher the amylose content, the faster starch retrogrades, and increases the formation of RS (8). Punia et al. (48) also stated that the retrogradation rate of corn starch was higher than that of oat starch.

The rate of retrogradation is also affected by the unit-chain length distribution of amylopectin. Srichuwong et al. (27) stated that there is a positive correlation between the distribution of DP (degree of polymerization) 16–26 and the rate of retrogradation, while the DP 8–12 (short chain) has a negative correlation. The more composition of DP 16–26, the rate of retrogradation will be faster, conversely the more unit-chain DP 8–12, the rate of retrogradation will be slower. Corn starch and rice starch are known to have the unit-chain length distribution of DP 13–24 by 56.7 and 52.1%, and the unit-chain length distribution of DP 9–12 by 31.4 and 34.5%, respectively (27). The distribution of the unit-chain DP 13–24 in oat starch ranged from 54.78 to 57.83% while the DP 6–12 ranged from 27.53 to 32.07% (49).

Subgroup analysis based on water ratio

Based on water ratio, the studies were sub grouped into 3 groups, namely the ratio of 1:3.5; 1:4 and 1:5 (Figure 5). The analysis results showed that ratio (sample:water) of 1:4 had a significant effect on increasing the RS content (SMD: 13.69; 95% CI: 5.50–21.87; $p < 0.001$), while the ratio 1:3.5 (SMD: 51.01; 95% CI: −58.59 to 160.62; $p < 0.001$) and 1:5 (SMD: −5.80; 95% CI: 15.24–3.64; $p < 0.001$) had no significant effect. The higher water content during gelatinization increases starch gelatinization and retrogradation enthalpy. This value is associated with the amount of single and double helical structures (50).
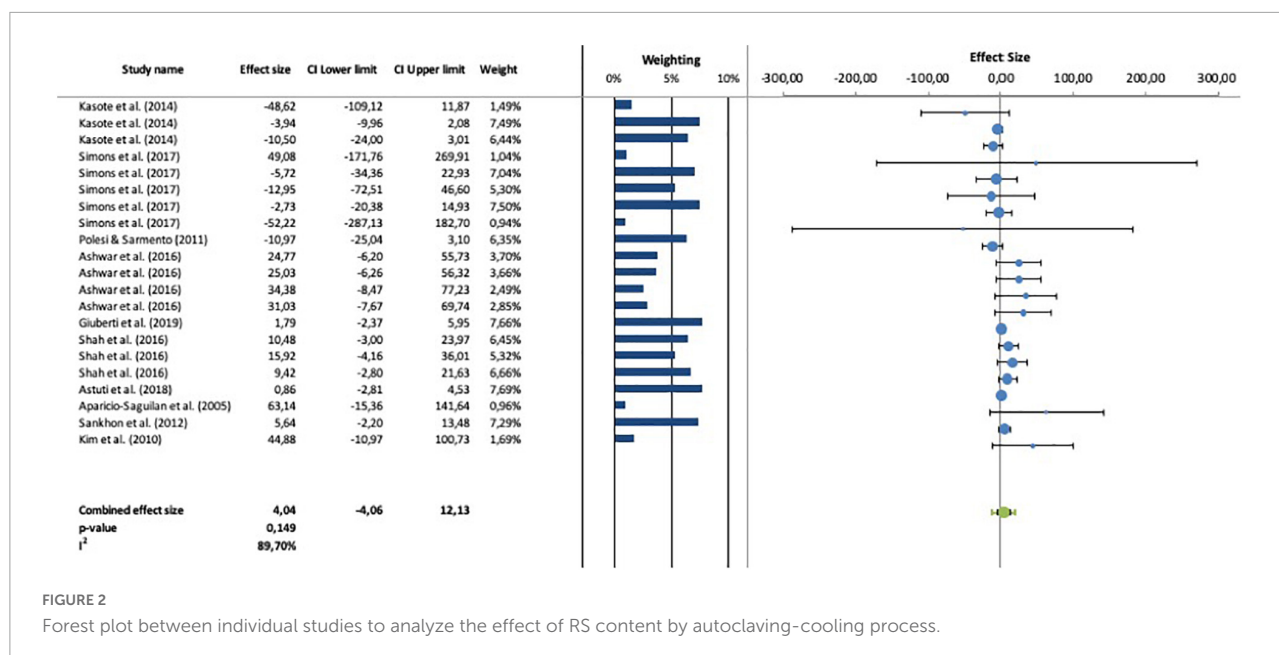
Subgroup analysis based on number of autoclaving-cooling cycles

Based on the number of autoclaving-cooling cycles, the studies were sub grouped into 4 groups (AC 1 cycle, 2 cycles, 3 cycles, and 4 cycles) and presented in the forest plot SMD, 95% CI (Figure 6). The analysis result showed that autoclaving-cooling 2 cycles had a significant effect on increasing the RS content (SMD: 16.33; 95% CI: 6.98–25.67; $p < 0.001$), while autoclaving-cooling 1 cycle (SMD: −7.94; 95% CI: −17.58 to

TABLE 1 Characteristic of included studies.

No	Study	Source of starch	Water ratio	AC cycle	Heating time (minutes)	Temperature (°C)		n	RS (% w/w)		Change of RS (%)
						Heating	Cooling		C (X ± SD)	E (X ± SD)	
1	Shah et al. (15)	Rice SR-1	1:4	2	30	121	4	3	4.42 ± 0.88	30.31 ± 0.79	585.75
2	Shah et al. (15)	Rice SR-2	1:4	2	30	121	4	3	8.26 ± 0.86	35.80 ± 0.90	333.41
3	Shah et al. (15)	Rice Pusa	1:4	2	30	121	4	3	5.91 ± 0.61	32.56 ± 0.63	450.93
4	Shah et al. (15)	Rice Jhelum	1:4	2	30	121	4	3	10.94 ± 0.59	38.65 ± 0.82	253.29
5	Sankhon et al. (36)	Parkia seed	1:4	4	120	110	5	3	28.96 ± 2.00	43.06 ± 2.00	48.69
6	Astuti et al. (37)	Arrowroot	1:5	3	15	121	4	3	22.56 ± 0.43	24.21 ± 2.14	7.31
7	Kim et al. (38)	Corn	1:3.5	4	60	121	4	3	0.30 ± 0.00	12.20 ± 0.30	3966.67
8	Giuberti et al. (39)	Sorghum grain	1:4	2	30	121	4	3	43.70 ± 5.89	56.90 ± 5.89	30.21
9	Shah et al. (15)	Oat Sabzaar	1:4	2	30	121	4	3	23.90 ± 1.27	38.88 ± 1.00	62.68
10	Shah et al. (15)	Oat SK020	1:4	2	30	121	4	3	17.39 ± 0.57	29.14 ± 0.61	67.57
11	Shah et al. (15)	Oat S090	1:4	2	30	121	4	3	17.14 ± 0.06	25.81 ± 1.04	50.58
12	Kasote et al. (40)	Pigeon pea	1:5	1	60	120	4	3	16.86 ± 0.26	3.96 ± 0.15	−76.51
13	Kasote et al. (40)	Green gram	1:5	1	60	120	4	3	11.60 ± 2.42	3.16 ± 0.16	−72.76
14	Kasote et al. (40)	Black gram	1:5	1	60	120	4	3	11.35 ± 0.77	4.07 ± 0.15	−64.14
15	Simons et al. (16)	Corn	1:5	1	15	110	4	2	0.12 ± 0.08	8.38 ± 0.11	6883.33
16	Simons et al. (16)	Great northern bean	1:5	1	15	110	4	2	40.83 ± 3.11	18.33 ± 0.67	−55.11
17	Simons et al. (16)	Pinto bean	1:5	1	15	110	4	2	43.86 ± 1.56	17.13 ± 0.59	−60.94
18	Simons et al. (16)	Black bean	1:5	1	15	110	4	2	30.52 ± 4.62	14.86 ± 0.41	−51.31
19	Simons et al. (16)	Lima bean	1:5	1	15	110	4	2	60.28 ± 0.64	14.88 ± 0.29	−75.32
20	Polesi and Sarmento (41)	Chickpea	1:10	1	30	121	4	3	31.87 ± 1.35	16.35 ± 0.86	−48.70
21	Aparicio-Saguilán et al. (42)	Banana	1:3.5	3	60	121	4	3	1.51 ± 0.10	16.02 ± 0.24	960.93

n, number of replications; RS, resistant starch; X, mean; SD, standard deviation; C, control (native); E, experiment (treated starch).

Forest plot between individual studies to analyze the effect of RS content by autoclaving-cooling process.

1.71; $p < 0.001$), 3 cycles (SMD: 29.33; 95% CI: −364.91 to 423.52; $p < 0.001$) and 4 cycles (SMD: 23.15; 95% CI: −224.69 to 271.0; $p < 0.001$) had no significant effect.

Many studies applied autoclaving-cooling starch modification with varying numbers of cycles. The addition of cycles is expected to increase the formation of short chain amylose fraction and increase the amount of retrograded amylose, resulting in more RS (51). Setiarto et al. (11) modified taro flour by autoclaving-cooling 1 cycle and 2 cycles. The RS produced by a 2 cycles process was increased 169.98%, higher than the RS produced by a single cycle process (91.77%). Likewise, the increasing RS content produced from 3 cycles autoclaving-cooling on purple water yam (48.92%), yellow water yam (75.86%) and white water yam (73.51%) were higher than increasing RS from 2 cycles (37.87%; 54.43%; 58.35%) and 1 cycle (7.5%; 27.09%; 4.03%), respectively (51). The number of autoclaving-cooling cycles, on the other hand, can increase the depolymerization of long-chain amylose into short-chain fractions (51, 52), as well as the breaking of amylose chains into simple sugars. The presence of these simple sugar components is known to slow down the retrogradation process, thereby affecting the formation of RS (53). Autoclaving-cooling cycle is closely related to retrogradation kinetics. The significance of the autoclaving-cooling 2 cycles could be influenced by its retrogradation kinetics that higher than in other cycles.

Subgroup analysis based on heating time

Analysis for subgroups based on heating time of autoclaving was shown in Figure 7. Heating time 30 min (SMD: 12.97; 95% CI: 1.97–23.97; $p < 0.001$) has a significant effect on increasing the RS content compared to heating time 60 min (SMD: 2.82; 95% CI: −44.14 to 49.78; $p < 0.001$). Meanwhile, heating time

15 min (SMD: −3.86; 95% CI: −17.01 to 9.29; $p < 0.001$) has no significant effect on decreasing the RS content. The application of heat to a certain temperature and time is required to confirm that the starch is gelatinized fully thus it will undergo retrogradation later.

Subgroup analysis based on autoclaving temperature

Analysis based on temperature of autoclaving showed that autoclaving at 121°C has significant effect on increasing the RS content (SMD: 12.18; 95% CI: 1.88–22.47; $p < 0.001$) compared to autoclaving at 110°C (SMD: −2.99; 95% CI: −20.41 to 14.43; $p < 0.001$) and 120°C (SMD: −11.86; 95% CI: 53.49–29.76; $p < 0.001$) (Figure 8). Aside from the number of autoclaving-cooling cycles, the temperature in the autoclaving process influences the degree of retrogradation, which affects the RS content (54). The temperature of 121°C is higher than the temperature of traditional gelatinization. Therefore, it leads to better gelatinization. Gelatinization at lower temperatures might require a longer time period. Right combination of temperature and time is needed for retrogradation. The cooling temperature of the process was not analyzed further because almost all data used the cooling temperature at 4°C (only 1 data used 5°C).

Publication bias

The funnel plot and Egger's test were used to assess the publication bias of included studies, with $p < 0.05$ being statistically significant for publication bias (22). The publication bias analysis (Figure 9) showed a funnel plot with symmetric data points. It indicated that the data is not affected by bias (32, 55). It is also demonstrated by the results of the analysis using the Egger's test where the p-value is greater than 0.05
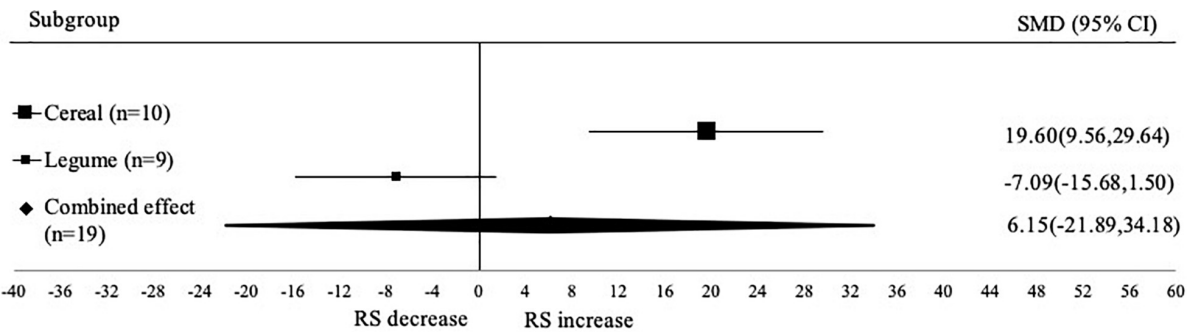
FIGURE 3
Forest plot from subgroup analysis based on type of crop. A positive value indicates the increase of RS content, while negative value indicates the decrease of RS.
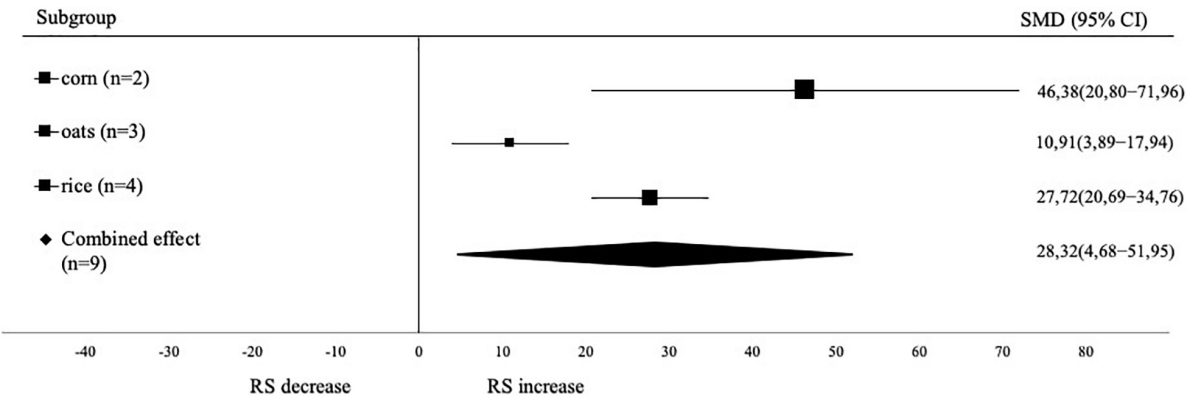

FIGURE 4
Forest plot from subgroup analysis based on cereal sample. A positive value indicates the increase of RS content, while negative value indicates the decrease of RS.
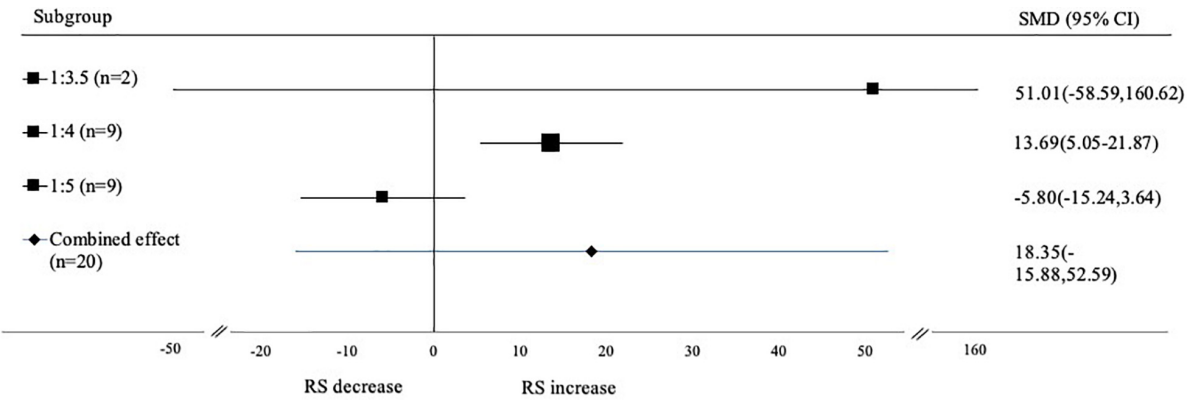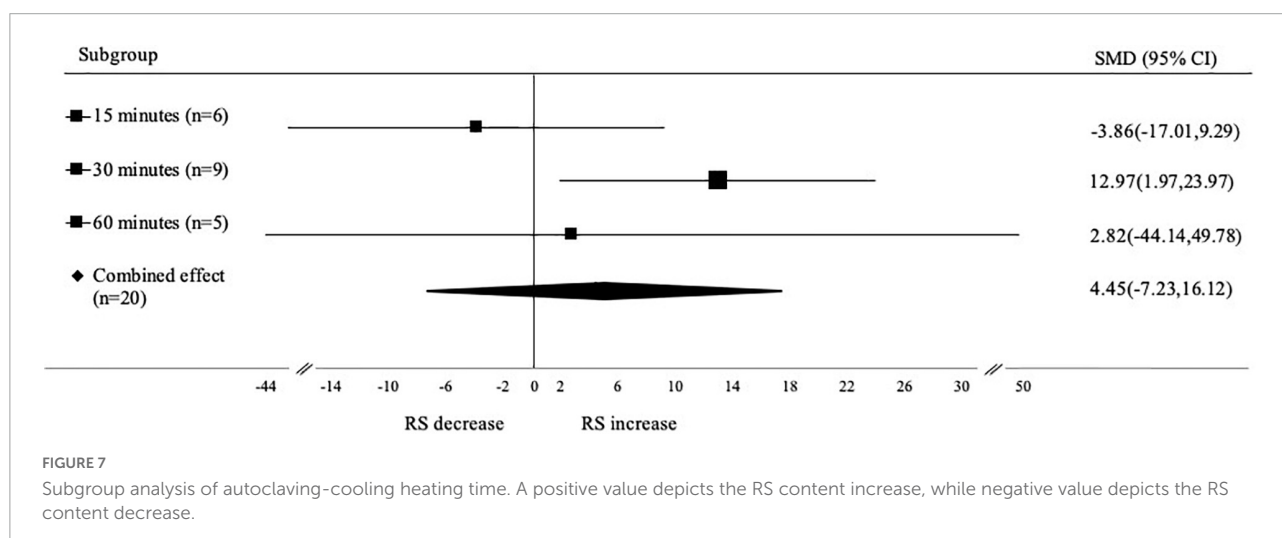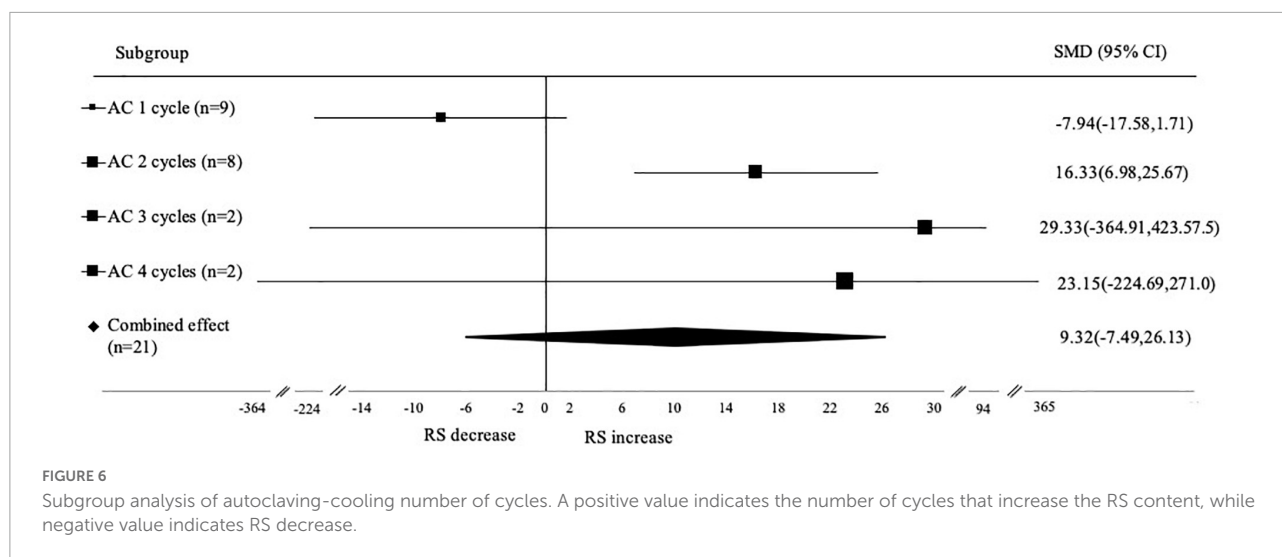

FIGURE 5
Forest plot from subgroup analysis based on water ratio. A positive value indicates the increase of RS content, while negative value indicates the decrease of RS.

FIGURE 6
Subgroup analysis of autoclaving-cooling number of cycles. A positive value indicates the number of cycles that increase the RS content, while negative value indicates RS decrease.

FIGURE 7
Subgroup analysis of autoclaving-cooling heating time. A positive value depicts the RS content increase, while negative value depicts the RS content decrease.

and being statistically not significant for publication bias. This study has limitations, including the small sample size and heterogeneity among studies that may affect the reliability of the results. Larger sample sizes are needed to confirm the current results.

Physicochemical properties

Chemical properties

Verification was carried out based on the results of the meta-analysis, namely using corn samples, which were treated by 2 cycle of autoclaving-cooling, with (sample:water) ratio 1: 4 and autoclaving for 30 min at 121°C. The samples used were in the form of starch and flour from corn. Corn flour is also used as a sample so that it can be used as a comparison for use in application, because corn flour is easier to obtain than corn starch which requires an extraction stage. The chemical

properties of native and treated samples are presented in Table 2.

In corn flour, all parameters showed significant changes from native and treated samples, while in cornstarch, the ash content, protein content, and amylose content did not change significantly. The moisture of each sample is at a low value, which is below 12%. Low moisture is needed especially for samples in the form of flour, to increase the shelf life of the product. The ash content in the corn flour decreased from 0.6 to 0.14%, while in cornstarch, the ash content value did not change. The decrease in ash content in the sample after treatment indicates that the autoclaving-cooling process in this experiment resulted in a cleaner sample (56). Autoclaving decreases the number of low melting point during ashing. In flour samples the amount of volatile mineral elements is higher than that in starch samples. The protein content of cornstarch decreased from 0.41 to 0.31%. The decrease of protein after the autoclaving-cooling process also reportedly occurred due to the heating process

FIGURE 8
Subgroup analysis of autoclaving temperature.
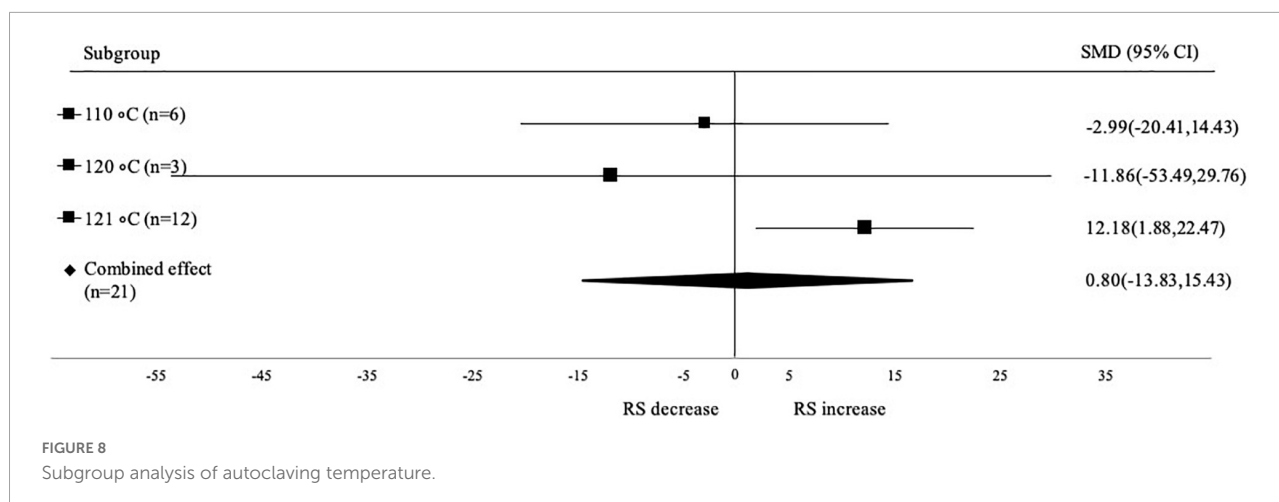
at high temperatures during the autoclaving-cooling process which resulted in the protein structure being damaged (14, 42, 51). However, from **Table 2**, there was an increase in protein content in the corn flour after treatment from 6.86 to 7.32%. Similar results also occurred in the samples of potatoes (57) and black beans (44) from the autoclaving-cooling treatment, which showed an increase in protein content from 0.13 to 0.43% and from 7.54 to 13.47%. Denaturation leads to changes in the three-dimensional structure of protein. It happens during the application of thermal treatments. It causes the decrease

FIGURE 9
Publication bias analysis of included studies.

of protein solubility due to aggregation and precipitation. This phenomenon resulted in the increase of protein content in modified samples (44). The autoclaving-cooling process was also seen to reduce the fat content of each sample. These results are in accordance with the results obtained by Aparicio-Saguilán et al. (42) and Rosida et al. (51).

Characterization of the samples was also carried out through analysis of amylose content, RS content and starch digestibility. In **Table 2**, there was a decrease in the amylose content of the corn flour, from 32.47 to 30.35%, while the amylose content of the cornstarch sample did not change significantly. A decrease in amylose levels was also seen in a study conducted by Shah et al. (15). In this research, the amylose content of the two cycles of autoclaving-cooling samples decreased in three types of oat samples, namely Sabzaar oats (from 26.97 to 25.91%), SKO20 oats (from 26.13 to 25, 43%) and SKO90 oats (from 25.81 to 25.45%). The decrease in amylose content in the sample after autoclaving-cooling treatment can occur due to hydrolysis of long-chain amylose molecules to short-chain molecules because of the gelatinization under pressure (52). This process could break the amylose chain into simple sugars, such as dextrin. The dextrin could not form blue complex with iodine during the amylose analysis therefore the observed amylose concentration was lower.

A significant increase in the levels of RS was seen in corn flour and cornstarch after treatment (**Table 2**). This result is in accordance with the results of the meta-analysis that the autoclaving-cooling process in corn samples can significantly increase the levels of RS. The RS content in the corn flour increased by 75.38% (from 15.84 to 27.78%) while in cornstarch increased by 113.03% (from 15.27 to 32, 53%). The increase in RS levels in corn flour was lower than in cornstarch. Flour consists of other components such as fiber, protein and lipid, therefore the retrogradation rate becomes slower. The fat content (especially free fatty acids) in starch is known to have the potential to form amylo-lipid complexes (RS type 5),
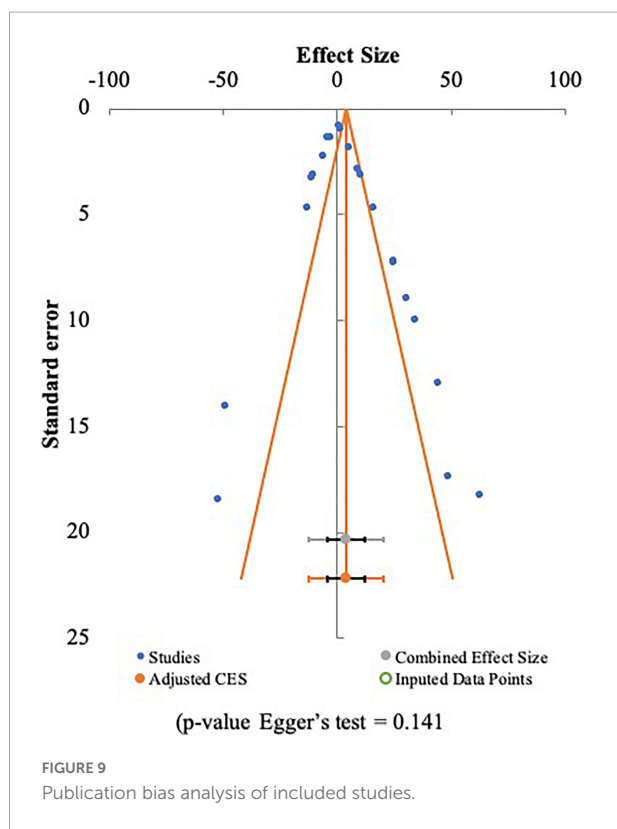
TABLE 2 Chemical properties of native and modified samples.

Parameter(% db)	Sample			
	Corn flour		Cornstarch	
	Native	Treated	Native	Treated
Moisture	12.72 ± 0.12	9.43 ± 0.04*	11.93 ± 0.12	11.63 ± 0.04*
Ash	0.64 ± 0.02	0.14 ± 0.01*	0.16 ± 0.01	0.16 ± 0.01
Protein	6.86 ± 0.19	7.32 ± 0.34*	0.41 ± 0.03	0.37 ± 0.06
Fat	2.56 ± 0.05	0.41 ± 0.01*	0.12 ± 0.01	0.04 ± 0.01*
Carbohydrate (by difference)	89.55 ± 1.48	92.13 ± 0.35*	99.31 ± 0.04	99.43 ± 0.06*
Amylose	32.47 ± 0.34	30.35 ± 0.67*	39.75 ± 0.53	38.37 ± 1.69
Resistant starch	15.84 ± 0.28	27.78 ± 1.28*	15.27 ± 3.79	32.53 ± 3.97*
Starch digestibility	67.02 ± 2.37	35.74 ± 2.67*	76.15 ± 6.24	28.09 ± 3.48*

Values expressed are mean ± standard deviation (number of replications = 4).

*There is significant difference between native and treated sample.

while the presence of protein can interfere with the process of incorporating starch molecules (54).

The value of RS content in treated cornstarch (32.53%) was higher than in the corn flour (27.78%). This could be caused by the amylose content of the cornstarch (39.75%) which was higher than in the corn starch (32.47%). The higher the amylose content in a material, the higher the RS content produced (58–60). High amylose content in a material affects the formation of RS during the autoclaving-cooling process. The starch retrogradation process that occurs in autoclaving-cooling is mainly caused by amylose interactions, because hydrogen bonds between amylose are easily formed. The more amylose fractions that came out of the starch granules during the gelatinization process, resulted in the formation of more retrograded starch during the cooling process, thereby increasing the formation of RS (51). Changes in RS content are not only affected by amylose content, but associated with other factors, such as crystalline type, amylose:amylopectin ratio, length of amylopectin chain and autoclaving-cooling conditions. The RS content of the treated corn flour and cornstarch was categorized as very high, namely 27.78 and 32.53% (above 15%) (25). This value is close to the commercial retrogradation resistant starch (RS3) (Novelose 330), which is 37.0% (42).

The digestibility of starch in the treated corn flour decreased by 46.67% (from 67.02 to 35.74%), while the maize starch sample decreased by 63.11% (from 76.15 to 28.09%). The decrease in starch digestibility in the corn flour was also in line with the smaller increase in RS content when compared to the cornstarch. In autoclaving-cooling process, there is a rearrangement of starch molecules, both between amylose-amylose and amylose-amylopectin, so that it can strengthen starch bonds which make starch more difficult to digest (6). The amylose fraction which has a linear structure is also known to facilitate the formation of cross-links in the presence of hydrogen bonds, thus forming a more compact amylose

structure that is difficult to hydrolyze by enzymes (42, 61). Apart from proportions and structure of amylose and amylopectin, the digestibility of starch also influenced by the starch granule (its morphology, surface features, molecular composition and supramolecular structures), proteins and lipids content. The presence of endogenous protein attached to the starch granule surfaces could reduce the granular swelling and restrict the access to digestive enzymes (62). The digestibility of starch from corn flour and cornstarch treated by autoclaving-cooling (35.74 and 28.09%, respectively) was lower than the digestibility of starch from commercial starch products Novelose 330 which was 33.33% (63). This proves that samples of corn flour and corn starch treated by autoclaving-cooling have the potential to be used as raw materials for functional food.

Crystallinity properties

Crystallinity properties were seen through changes in crystalline and amorphous regions in the starch structure before and after treatment through FTIR. FTIR can determine the level of helical arrangement of starch to see changes in starch due to gelatinization, retrogradation or storage processes. Polysaccharides in starch can be absorbed at a wave number of 800–1,200 cm^{-1}, which is a fingerprint of

TABLE 3 Changes in crystalline and amorphous regions of corn flour and cornstarch based on FTIR analysis.

Sample	Crystalline	Amorphous
	A_{1045}/A_{1022}	A_{1022}/A_{995}
Corn flour native	0.9289 ± 0.0037	1.0249 ± 0.0007
Corn flour treated	1.0213 ± 0.0126	0.8759 ± 0.0062
Cornstarch native	0.9682 ± 0.0339	1.0302 ± 0.0030
Cornstarch treated	1.0376 ± 0.0023	0.8164 ± 0.0065

Values expressed are mean ± standard deviation (number of replications = 2).

the conformation and hydration of starch. Wave numbers 1,045–1,047 cm^{-1} and 1,020–122 cm^{-1} are bands for the crystalline region and amorphous region in starch granules. The ratio 1,045 cm^{-1}/1,022 cm^{-1} indicates the arrangement of the crystalline regions, while the ratio 1,022 cm^{-1}/995 cm^{-1} indicates the arrangement of the amorphous regions (29, 64). The changes in crystalline and amorphous regions from native and treated samples are presented in Table 3.

Table 3 shows that there is an increase of the crystalline region and a decrease of the amorphous region in each of the treated samples. The crystalline region of corn flour native was 0.9289 and increased to 1.0213 due to the autoclaving-cooling treatment, as well as the amorphous region, which decreased from 1.0249 to 0.8759. Likewise, the native cornstarch experienced an increase in the crystalline region from 0.9682 to 1.0376 and a decrease in the amorphous region from 1.0302 to 0.8164. The ratio intensity of 1,045 cm^{-1}/1,022 cm^{-1} also expresses the degree of order in starch (15). Increase of 1,045 cm^{-1}/1,022 cm^{-1} ratio exhibits that crystallites at the granule surface of treated samples were better organized (39). This ratio intensity may differ depending on the modification treatment and the source of the sample. Maize starch treated with annealing increased the ratio intensity of 1,045 cm^{-1}/1,022 cm^{-1}, while heat-moisture treatment decreased the ratio (64).

Amylose content strongly affects the crystallization during retrogradation, which reduces the access of digestive enzymes. Thus increasing RS content (65). The application of autoclaving cooling was also observed to reorder double helices in the crystalline lamellae. This phenomenon is affected by amylopectin branch length as well. Longer amylopectin branch resulted in more packed double helices structure (66). It was also observed in annealing modification (67).

Morphology properties

Morphological changes of starch granules were observed using a polarizing microscope and a light microscope (Figure 10) also using SEM (Figure 11).

Figure 10 showed that the native starch granules were still intact and had an oval shape. This indicates that the granule structure of the native starch has not been damaged in comparison to the treated starch. The native samples in Figure 10 also still exhibit birefringence and intact maltose cross pattern, as indicated by a clear blue-yellow color pattern. The presence of this birefringence indicates that the starch has not been gelatinized. Meanwhile, the birefringence properties of the treated starch were not observed.

Figure 11 showed that the autoclaving-cooling treatment causes the structure change of corn flour and cornstarch. This result is similar to that of Herawati et al. (68) and Faridah et al. (19), who performed an analysis on tacca starch and rice starch treated with autoclaving-cooling. The granules of treated samples become shapeless or irregular shapes. This irregular shape of crystalline was formed because of granules being damaged and swollen during the gelatinization and retrogradation in the autoclaving-cooling process. The crystalline form is largely responsible for its resistance to digestive enzyme (14, 68).

Gelatinization profile

Gelatinization profile of corn flour and cornstarch using Rapid Visco Analyser (RVA) are shown in Table 4 and Figure 11. There is a decrease in peak viscosity in each sample after the autoclaving-cooling treatment. The peak viscosity value indicates the ability of starch granules to bind water and maintain swelling during the heating process. There was no peak viscosity (Supplementary Figure 1) in
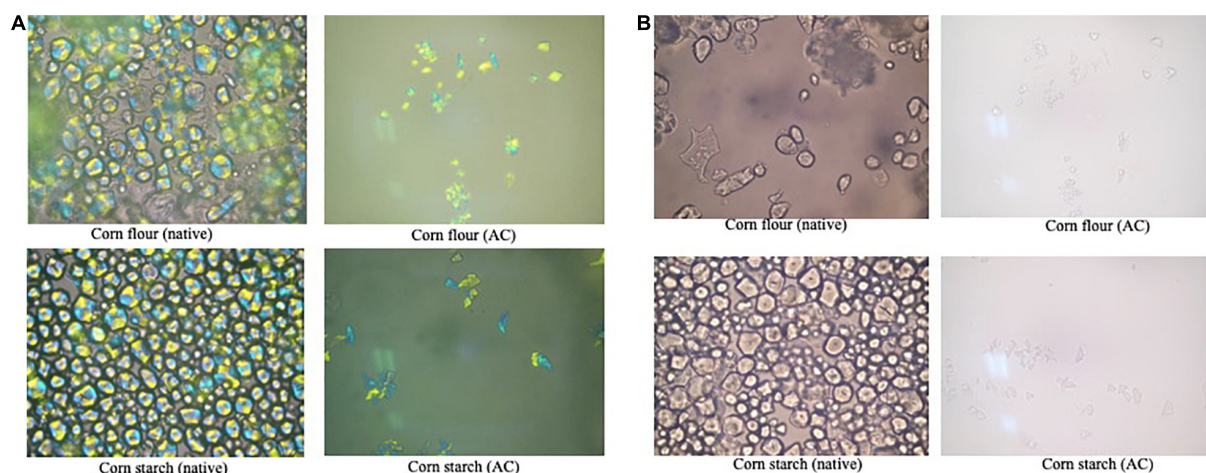

FIGURE 10
Morphological analysis of starch granules using a polarizing microscope (A) and a light microscope (B) (magnification × 1,000).
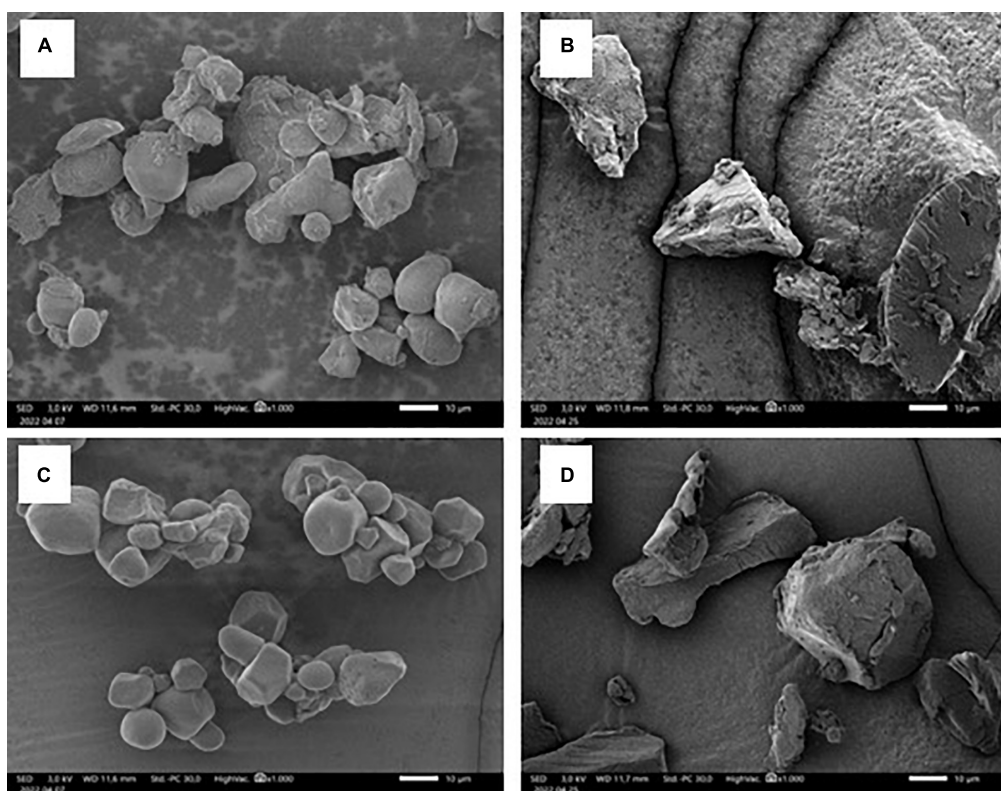
FIGURE 11
Scanning electron microscopy of native corn flour **(A)**, treated corn flour **(B)**, native cornstarch **(C)** and treated cornstarch **(D)** with 1,000 × magnification.

TABLE 4   Gelatinization profile.

Parameter	Sample			
	Corn flour		Corn starch	
	Native	Treated	Native	Treated
Peak viscosity (cP)	3301.50 ± 70.00	638.50 ± 0.71	3939.50 ± 6.36	976.50 ± 10.61
Breakdown viscosity (cP)	1808.00 ± 209.30	193.50 ± 37.48	1815.00 ± 18.38	5.00 ± 5.66
Setback viscosity (cP)	3400.00 ± 103.24	592.00 ± 31.11	1879.00 ± 8.49	366.50 ± 103.94
Final viscosity (cP)	4893.50 ± 242.54	1250.00 ± 308.30	4003.50 ± 20.51	1338.00 ± 98.99
Time (min)	8.13 ± 0.00	8.30 ± 0,14	8.04 ± 0.05	11.94 ± 1.51
Temperature (°C)	74.30 ± 0.28	–	73.22 ± 0.03	–

–, undetected until 95°C.
Values expressed are mean ± standard deviation (number of replications = 2).

the treated sample due to the decrease of peak viscosity value after autoclaving-cooling treatment. The decrease in the peak viscosity value in the treated sample was caused by the hydrothermal treatment and high pressure during the autoclaving process, which resulted in the granule structure being destroyed thereby reducing the viscosity value (9, 38, 69). **Supplementary Figure 1** also shows that the treated starch exhibits a very low viscosity which remains almost

constant regardless of temperature changes. During the autoclave process, starch is hydrothermally treated under high pressure conditions. As a result, the starch is gelatinized and its granular structure is disturbed, resulting in a decrease in peak viscosity in the modified sample (38). The peak viscosity of the corn flour was smaller than the viscosity of the cornstarch. This could be due to the presence of other components such as ash, fat, and protein in the corn flour

which were larger than in the cornstarch, thus affecting the gelatinization process.

The final viscosity value in each sample also decreased. The final viscosity indicates the ability of the starch paste to form a gel after the heating or cooling process and the resistance of the paste to the stirring process. The gelatinization temperature of the treated sample decreased in the corn flour. The decrease in gelatinization temperature also occurred in arrowroot tuber samples that were treated with autoclaving-cooling (37). The gelatinization temperature of the treated cornstarch was not detected by RVA analysis at a maximum temperature capacity of 95°C. This indicates that the starch was gelatinized during the autoclaving-cooling process at 121°C. The gelatinization profile of the corn flour and cornstarch in this study was the same as the profile in the experiment using oat samples conducted by Shah et al. (15). The results of the RVA analysis of the treated oat samples from autoclaving-cooling two cycles showed a decrease in the value of peak viscosity, breakdown viscosity, setback viscosity, final viscosity and gelatinization temperature. Based on the gelatinization profile presented above, corn flour and cornstarch treated with autoclaving-cooling from meta-analysis results were found to be stable to heating and stirring processes. The properties of these materials are suitable to be used as ingredients for food products, especially those that require a cooking process at high temperatures, such as corn-based bakery products and canned food.

Gelatinization and retrogradation occur during the autoclaving-cooling and result in RS type 3. The retrogradation rate in cereal starch is higher than those of tuber due to higher precipitation rate of the cereal starch. Thus, the RS content increases significantly in cereal starch. Based on analysis, autoclaving-cooling on corn flour and cornstarch caused the decrease of amylose content and starch digestibility and the increase of RS content. Morphological changes were also observed after autoclaving-cooling. There was crystalline formation due to retrogradation.

Conclusion

Meta-analysis study found that RS content significantly increased after autoclaving-cooling treatment using a sample:water ratio of 1:4, two cycles of autoclaving-cooling, and 30 min of autoclaving at 121°C. This RS increase was significant in cereal (corn, oat and rice) with corn as the type of sample that has the highest effect size value. Verification using corn flour and cornstarch showed a significant increase in RS contents and a significant decrease in starch digestibility. Treated sample also showed the pasting profile that was stable under heating and stirring. This study can provide the optimal treatment of autoclaving-cooling process to achieve a significant increase in RS content for research treatment or industrial purpose.

Data availability statement

The raw data supporting the conclusions of this article will be made available by the authors, without undue reservation.

Author contributions

DF: content, methodology, and schema research. RS: writing – original draft and processing data. DI: review manuscript. FA, AJ, and MA: processing data. All authors contributed to the article and approved the submitted version.

Funding

Conflict of interest

The authors declare that the research was conducted in the absence of any commercial or financial relationships that could be construed as a potential conflict of interest.

Publisher's note

All claims expressed in this article are solely those of the authors and do not necessarily represent those of their affiliated organizations, or those of the publisher, the editors and the reviewers. Any product that may be evaluated in this article, or claim that may be made by its manufacturer, is not guaranteed or endorsed by the publisher.

Supplementary material

The Supplementary Material for this article can be found online at: https://www.frontiersin.org/articles/10.3389/fnut.2022.904700/full#supplementary-material

SUPPLEMENTARY FIGURE 1
Gelatinization profile of corn flour and cornstarch.

References

1. Zhao XH, Lin Y. Resistant starch prepared from high-amylose maize starch with citric acid hydrolysis and its simulated fermentation in vitro. *Eur Food Res Technol.* (2009) 228:1015–21. doi: 10.1007/s00217-009-1012-5

2. Lockyer S, Nugent AP. Health effects of resistant starch. *Nutr Bull.* (2017) 42:10–41. doi: 10.1111/nbu.12244

3. Zhang L, Li HT, Shen L, Fang QC, Qian LL, Jia WP. Effect of dietary resistant starch on prevention and treatment of obesity-related diseases and its possible mechanisms. *Biomed Environ Sci.* (2015) 28:291–7.

4. Kumar A, Sahoo U, Baisakha B, Okpani OA, Ngangkham U, Parameswaran C, et al. Resistant starch could be decisive in determining the glycemic index of rice cultivars. *J Cereal Sci.* (2018) 79:348–53. doi: 10.1016/j.jcs.2017.11.013

5. Lemlioglu-Austin D, Turner ND, McDonough CM, Rooney LW. Effects of sorghum [*Sorghum bicolor* (L.) moench] crude extracts on starch digestibility, estimated glycemic index (EGI), and resistant starch (RS) contents of porridges. *Molecules.* (2012) 17:11124–38. doi: 10.3390/molecules170911124

6. Pratiwi M, Faridah DN, Lioe HN. Structural changes to starch after acid hydrolysis, debranching, autoclaving-cooling cycles, and heat moisture treatment (HMT): A review. *Starch/Staerke.* (2018) 70:1700028. doi: 10.1002/star.201700028

7. Fuentes-Zaragoza E, Riquelme-Navarrete MJ, Sánchez-Zapata E, Pérez-Álvarez JA. Resistant starch as functional ingredient: a review. *Food Res Int.* (2010) 43:931–42. doi: 10.1016/j.foodres.2010.02.004

8. Sajilata MG, Singhal RS, Kulkarni PR. Resistant starch – a review. *Compr Rev Food Sci Food Saf.* (2006) 5:1–17. doi: 10.1111/j.1541-4337.2006.tb00076.x

9. Dundar AN, Gocmen D. Effects of autoclaving temperature and storing time on resistant starch formation and its functional and physicochemical properties. *Carbohydr Polym.* (2013) 97:764–71. doi: 10.1016/j.carbpol.2013.04.083

10. Lee KY, Lee S, Lee HG. Influence of storage temperature and autoclaving cycles on slowly digestible and resistant starch (RS) formation from partially debranched rice starch. *Starch/Staerke.* (2013) 65:694–701. doi: 10.1002/star.201200186

11. Setiarto RHB, Jenie BSL, Faridah DN, Saskiawan I, Sulistiani. Effect of lactic acid bacteria fermentation and autoclaving-cooling for resistant starch and prebiotic properties of modified taro flour. *Int Food Res J.* (2018) 25:1691–7.

12. Ratnaningsih N, Suparmo, Harmayani E, Marsono Y. Physicochemical properties, in vitro starch digestibility, and estimated glycemic index of resistant starch from cowpea (*Vigna unguiculata*) starch by autoclaving-cooling cycles. *Int J Biol Macromol.* (2020) 142:191–200. doi: 10.1016/j.ijbiomac.2019.09.092

13. Rahmawati A, Murdiati A, Marsono Y, Anggrahini S. Changes of complex carbohydrates on white jack bean (*Canavalia ensiformis*) during autoclaving-cooling cycles. *Curr Res Nutr Food Sci.* (2018) 6:470–80. doi: 10.12944/CRNFSJ.6.2.21

14. Ashwar BA, Gani A, Wani IA, Shah A, Masoodi FA, Saxena DC. Production of resistant starch from rice by dual autoclaving-retrogradation treatment: Invitro digestibility, thermal and structural characterization. *Food Hydrocoll.* (2016) 56:108–17. doi: 10.1016/j.foodhyd.2015.12.004

15. Shah A, Masoodi FA, Gani A, Ashwar BA. In-vitro digestibility, rheology, structure, and functionality of RS3 from oat starch. *Food Chem.* (2016) 212:749–58. doi: 10.1016/j.foodchem.2016.06.019

16. Simons CW, Hall C, Vatansever S. Production of resistant starch (RS3) from edible bean starches. *J Food Process Preserv.* (2017) 42:1–6. doi: 10.1111/jfpp.13587

17. Borenstein M, Hedges LV, Higgins JP, Rothstein HR. *Introduction to Meta-Analysis.* 1st Ed. Hoboken, NJ: John Wiley & Sons, Ltd (2009). doi: 10.1002/9780470743386

18. Gurevitch J, Koricheva J, Nakagawa S, Stewart G. Meta-analysis and the science of research synthesis. *Nature.* (2018) 555:175–82. doi: 10.1038/nature25753

19. Faridah DN, Damaiyanti S, Indrasti D, Jayanegara A, Afandi FA. Effect of heat moisture treatment on resistant starch content among carbohydrate sources: a meta-analysis. *Int J Food Sci Technol.* (2021) 57:1965–74. doi: 10.1111/ijfs.15276

20. Faridah DN, Anugerah MP, Hunaefi D, Afandi FA, Jayanegara A. The effect of annealing on resistant starch content of different crop types: a systematic review and meta-analysis study. *Int J Food Sci Technol.* (2021) 57:2026–38. doi: 10.1111/ijfs.15388

21. Moher D, Liberati A, Tetzlaff J, Altman DG, Grp P. Preferred reporting items for systematic reviews and meta-analyses: the PRISMA statement (reprinted from annals of internal medicine). *Phys Ther.* (2009) 89:873–80. doi: 10.1093/ptj/89.9.873

22. Afandi FA, Wijaya CH, Faridah DN, Suyatma NE, Jayanegara A. Evaluation of various starchy foods: a systematic review and meta-analysis on chemical properties affecting the glycemic index values based on in vitro and in vivo experiments. *Foods.* (2021) 10:364. doi: 10.3390/foods10020364

23. Palupi E, Jayanegara A, Ploeger A, Kahl J. Comparison of nutritional quality between conventional and organic dairy products: a meta-analysis. *J Sci Food Agric.* (2012) 92:2774–81. doi: 10.1002/jsfa.5639

24. Aoac. *Official Methods of Analysis.* Vol. 18. Maryland, MD: AOAC International (2005).

25. Goñi I, García-Diz L, Mañas E, Saura-Calixto F. Analysis of resistant starch: a method for foods and food products. *Food Chem.* (1996) 56:445–9. doi: 10.1016/0308-8146(95)00222-7

26. Anderson AK, Guraya HS, James C, Salvaggio L. Digestibility and pasting properties of rice starch heat-moisture treated at the melting temperature (Tm). *Starch/Staerke.* (2002) 54:401–9. doi: 10.1002/1521-379X(200209)54:9<401::AID-STAR401>3.0.CO;2-Z

27. Srichuwong S, Sunarti TC, Mishima T, Isono N, Hisamatsu M. Starches from different botanical sources I: contribution of amylopectin fine structure to thermal properties and enzyme digestibility. *Carbohydr Polym.* (2005) 60:529–38. doi: 10.1016/j.carbpol.2005.03.004

28. Lopez-Rubio A, Flanagan BM, Shrestha AK, Gidley MJ, Gilbert EP. Molecular rearrangement of starch during in vitro digestion: toward a better understanding of enzyme resistant starch formation in processed starches. *Biomacromolecules.* (2008) 9:1951–8. doi: 10.1021/bm800213h

29. Sevenou O, Hill SE, Farhat IA, Mitchell JR. Organisation of the external region of the starch granule as determined by infrared spectroscopy. *Int J Biol Macromol.* (2002) 31:79–85. doi: 10.1016/S0141-8130(02)00067-3

30. Hak T, van Rhee H, Suurmond R. How to interpret results of meta-analysis. *SSRN Electron J.* (2018) 1–21.

31. Jin ZC, Wu C, Zhou XH, He J. A modified regression method to test publication bias in meta-analyses with binary outcomes. *BMC Med Res Methodol.* (2014) 14:132. doi: 10.1186/1471-2288-14-132

32. Suurmond R, van Rhee H, Hak T. Introduction, comparison, and validation of meta-essentials: a free and simple tool for meta-analysis. *Res Synth Methods.* (2017) 8:537–53. doi: 10.1002/jrsm.1260

33. Zabar S, Shimoni E, Bianco-Peled H. Development of nanostructure in resistant starch type III during thermal treatments and cycling. *Macromol Biosci.* (2008) 8:163–70. doi: 10.1002/mabi.200700183

34. Mutungi C, Rost F, Onyango C, Jaros D, Rohm H. Crystallinity, thermal and morphological characteristics of resistant starch type iii produced by hydrothermal treatment of debranched Cassava starch. *Starch/Staerke.* (2009) 61:634–45. doi: 10.1002/star.200900167

35. Zavareze EDR, Dias ARG. Impact of heat-moisture treatment and annealing in starches: a review. *Carbohydr Polym.* (2011) 83:317–28. doi: 10.1016/j.carbpol.2010.08.064

36. Sankhon A, Yao W-R, Wang H, Qian H, Sangare M. The yield improvement of resistant starches from africa locust (*Parkia biglobosa*): the influence of heat-moisture, autoclaving-cooling and cross-linking treatments. *Am J Food Technol.* (2012) 7:386–97. doi: 10.3923/ajft.2012.386.397

37. Astuti RM, Widaningrum, Asiah N, Setyowati A, Fitriawati R. Effect of physical modification on granule morphology, pasting behavior, and functional properties of arrowroot (*Marantha arundinacea* L) starch. *Food Hydrocoll.* (2018) 81:23–30. doi: 10.1016/j.foodhyd.2018.02.029

38. Kim NH, Kim JH, Lee S, Lee H, Yoon JW, Wang R, et al. Combined effect of autoclaving-cooling and crosslinking treatments of normal corn starch on the resistant starch formation and physicochemical properties. *Starch/Staerke.* (2010) 62:358–63. doi: 10.1002/star.200900237

39. Giuberti G, Marti A, Gallo A, Grassi S, Spigno G. Resistant starch from isolated white sorghum starch: functional and physicochemical properties and resistant starch retention after cooking. a comparative study. *Starch/Staerke.* (2019) 71:1–9. doi: 10.1002/star.201800194

40. Kasote DM, Nilegaonkar SS, Agte VV. Effect of different processing methods on resistant starch content and in vitro starch digestibility of some common Indian pulses. *J Sci Ind Res (India).* (2014) 73:541–6.

41. Polesi LF, Sarmento SBS. Structural and physicochemical characterization of RS prepared using hydrolysis and heat treatments of chickpea starch. *Starch/Staerke.* (2011) 63:226–35. doi: 10.1002/star.201000114

42. Aparicio-Saguilán A, Flores-Huicochea E, Tovar J, García-Suárez F, Gutiérrez-Meraz F, Bello-Pérez LA. Resistant starch-rich powders prepared by autoclaving of native and lintnerized banana starch: Partial characterization. *Starch/Staerke.* (2005) 57:405–12. doi: 10.1002/star.200400386

43. Tian S, Sun Y. Influencing factor of resistant starch formation and application in cereal products: a review. *Int J Biol Macromol.* (2020) 149:424–31. doi: 10.1016/j.ijbiomac.2020.01.264

44. Escobedo A, Loarca-Piña G, Gaytan-Martínez M, Orozco-Avila I, Mojica L. Autoclaving and extrusion improve the functional properties and chemical composition of black bean carbohydrate extracts. *J Food Sci.* (2020) 85:2783–91. doi: 10.1111/1750-3841.15356

45. Eyaru R, Shrestha AK, Arcot J. Effect of various processing techniques on digestibility of starch in Red kidney bean (*Phaseolus vulgaris*) and two varieties of peas (*Pisum sativum*). *Food Res Int.* (2009) 42:956–62. doi: 10.1016/j.foodres.2009.06.007

46. Morrison WRR, Law RVV, Snape CEE. Evidence for inclusion complexes of lipids with V-amylose in maize, rice and oat starches. *J Cereal Sci.* (1993) 18:107–9. doi: 10.1006/jcrs.1993.1039

47. Vilaplana F, Hasjim J, Gilbert RG. Amylose content in starches: toward optimal definition and validating experimental methods. *Carbohydr Polym.* (2012) 88:103–11. doi: 10.1016/j.carbpol.2011.11.072

48. Punia S, Sandhu KS, Dhull SB, Siroha AK, Purewal SS, Kaur M, et al. Oat starch: physico-chemical, morphological, rheological characteristics and its applications – a review. *Int J Biol Macromol.* (2020) 154:493–8. doi: 10.1016/j.ijbiomac.2020.03.083

49. Xu J, Kuang Q, Wang K, Zhou S, Wang S, Liu X, et al. Insights into molecular structure and digestion rate of oat starch. *Food Chem.* (2017) 220:25–30. doi: 10.1016/j.foodchem.2016.09.191

50. Ding L, Zhang B, Tan CP, Fu X, Huang Q. Effects of limited moisture content and storing temperature on retrogradation of rice starch. *Int J Biol Macromol.* (2019) 137:1068–75. doi: 10.1016/j.ijbiomac.2019.06.226

51. Rosida, Harijono, Estiasih T, Sriwahyuni E. Physicochemical properties and starch digestibility of autoclaved-cooled water yam (*Dioscorea Alata* L.) flour. *Int J Food Prop.* (2015) 19:1659–70. doi: 10.1080/10942912.2015.1105818

52. Zheng M-z, Xiao Y, Yang S, Liu H-m, Liu M-h, Yaqoob S, et al. Effects of heat–moisture, autoclaving, and microwave treatments on physicochemical properties of proso millet starch. *Food Sci Nutr.* (2020) 8:735–43. doi: 10.1002/fsn3.1295

53. Wang S, Li C, Copeland L, Niu Q, Wang S. Starch retrogradation: a comprehensive review. *Compr Rev Food Sci Food Saf.* (2015) 14:568–85. doi: 10.1111/1541-4337.12143

54. Dupuis JH, Liu Q, Yada RY. Methodologies for increasing the resistant starch content of food starches: a review. *Compr Rev Food Sci Food Saf.* (2014) 13:1219–34. doi: 10.1111/1541-4337.12104

55. Bowden J, Jackson C. Weighing evidence "Steampunk". style via the meta-analyser. *Am Stat.* (2016) 70:385–94. doi: 10.1080/00031305.2016.1165735

56. Gunorubon J, Kekpugile K. Modification of cassava starch for industrial uses. *Int J Eng Technol.* (2012) 2:913–9.

57. Babu AS, Parimalavalli R. Effect of autoclaving on chemical, functional and morphological. *J Root Crop.* (2013) 39:78–83.

58. Yuliwardi F, Syamsira E, Hariyadi P, Widowati S. Pengaruh Dua Siklus Autoclaving-Cooling Terhadap Kadar Pati Resisten Tepung Beras dan Bihun yang Dihasilkannya. *Pangan.* (2014) 23:43–51.

59. Yadav BS, Sharma A, Yadav RB. Studies on effect of multiple heating/cooling cycles on the resistant starch formation in cereals, legumes and tubers. *Int J Food Sci Nutr.* (2009) 60(Suppl. 4):258–72. doi: 10.1080/09637480902970975

60. Vatanasuchart N, Niyomwit B, Wongkrajang K. Resistant starch content, in vitro starch digestibility and physico-chemical properties of flour and starch from Thai bananas. *Maejo Int J Sci Technol.* (2012) 6:259–71.

61. Lehmann U, Jacobasch G, Schmiedl D. Characterization of resistant starch type III from banana (*Musa acuminata*). *J Agric Food Chem.* (2002) 50:5236–40. doi: 10.1021/jf0203390

62. Toutounji MR, Farahnaky A, Santhakumar AB, Oli P, Butardo VM, Blanchard CL. Intrinsic and extrinsic factors affecting rice starch digestibility. *Trends Food Sci Technol.* (2019) 88:10–22. doi: 10.1016/j.tifs.2019.02.012

63. Liu S, Reimer M, Ai Y. In vitro digestibility of different types of resistant starches under high-temperature cooking conditions. *Food Hydrocoll.* (2020) 107:105927. doi: 10.1016/j.foodhyd.2020.105927

64. Chung HJ, Liu Q, Hoover R. Impact of annealing and heat-moisture treatment on rapidly digestible, slowly digestible and resistant starch levels in native and gelatinized corn, pea and lentil starches. *Carbohydr Polym.* (2009) 75:436–47. doi: 10.1016/j.carbpol.2008.08.006

65. Raungrusmee S, Anal AK. Effects of lintnerization, autoclaving, and freeze-thaw treatments on resistant starch formation and functional properties of pathumthani 80 rice starch. *Foods.* (2019) 8:558. doi: 10.3390/foods8110558

66. Li J, Han W, Zhang B, Zhao S, Du H. Structure and physicochemical properties of resistant starch prepared by autoclaving-microwave. *Starch/Staerke.* (2018) 70:1800060. doi: 10.1002/star.201800060

67. Anugerah MP, Faridah DN, Afandi FA, Hunaefi D, Jayanegara A. Annealing processing technique divergently affects starch crystallinity characteristic related to resistant starch content: a literature review and meta-analysis. *Int J Food Sci Technol.* (2022) 57:2535–44. doi: 10.1111/ijfs.15628

68. Herawati ER, Ariani D, Nurhayati R, Miftakhussolikhah M, Na'imah H, Marsono Y. Effect of autoclaving-cooling treatments on chemical characteristic and structure of Tacca (*Tacca leontopetaloides*). *Starch.* (2020) 194:169–72. doi: 10.2991/aer.k.200325.034

69. Reddy CK, Suriya M, Haripriya S. Physico-chemical and functional properties of resistant starch prepared from red kidney beans (*Phaseolus vulgaris*.L) starch by enzymatic method. *Carbohydr Polym.* (2013) 95:220–6. doi: 10.1016/j.carbpol.2013.02.060

Check for updates

Reduction in residual cyantraniliprole levels in spinach after various washing and blanching methods

Minsoo Park, Hyeonjun Kim, Myungheon Kim and Moo-hyeog Im*

Department of Food Engineering, Daegu University, Gyenogsan, South Korea

Pesticides are used to protect crops from pests and diseases. However, as many pesticides are toxic to humans, it is necessary to assess methods that can remove pesticide residues from agricultural products before human consumption. Spinach is consumed immediately after a relatively simple washing and heating process in the Republic of Korea. Cyantraniliprole is used as a systemic insecticide during spinach cultivation, which means it might remain in the crop after processing. Consequently, it is important to assess whether residues can be reduced to levels that are harmless to the human body after processing. This study investigated lowering the residual cyantraniliprole levels in spinach after washing and blanching. The amount of cyantraniliprole residue in the spinach samples sprayed with cyantraniliprole during cultivation was analyzed using ultrahigh-performance liquid chromatography-tandem mass spectrometry (UHPLC–MS/MS). The time of each washing and blanching method was set at 1, 3, and 5 min. The residual levels of cyantraniliprole decreased by 15.1−54.6% and 60.1−93.5% based on the washing and blanching methods employed. The most effective washing method to lower residual cyantraniliprole levels was steeping with a neutral detergent, resulting in cyantraniliprole reduction by 42.9−54.6%. When spinach was blanched after steeping washing with a neutral detergent, the largest removal rates of 77.9 and 91.2% were observed after 1 and 3 min of blanching, respectively. Blanching for 5 min after steeping and running washing exhibited the highest reduction rate of 93.5%. Therefore, a considerable amount of cyantraniliprole residue in spinach could be removed by washing or blanching. Based on the results of this study, blanching after steeping washing can be implemented as an effective method of lowering pesticide concentrations in spinach and other crops, thereby reducing their potential toxicity to humans upon consumption.

Introduction

Spinach is an annual crop belonging to the *Chenopodioideae* subfamily; it is an alkaline vegetable rich in various vitamins, iron, and calcium (1). In the Republic of Korea, the cultivation period of spinach is decided based on the variety; Chinese spinach is sown in autumn, and English spinach is sown in spring and summer. Hybrid spinach with the characteristics of both Chinese and English spinach is cultivated throughout the year (2). In 2019, spinach production in the Republic of Korea was 70,844 tons, with Gyeonggi-do, Gyeongsangnam-do, and Jeollanam-do producing 24,196 (∼34%), 15,873 (∼22%), and 8,038 (∼11%) tons, respectively (3). The average daily intake of spinach in the Republic of Korea in 2018 was 5.24 g/day per person; this was the 15th highest among all vegetables consumed in the Republic of Korea (4). Pesticide usage in spinach is essential because it is susceptible to diseases, such as mosaic and fusarium wilt, and pests, such as turnip moth and *Spodoptera litura* (5). Consequently, when pesticides are not used, the productivity and quality of crops decrease (6). However, as pesticides are toxic, spray standards and pesticide residue management should be strictly implemented (7). An analysis of hazards in domestic agricultural products— conducted by the Ministry of Food and Drug Safety (MFDS), Republic of Korea—revealed that 24 pesticides exceeded the maximum residue limit (MRL) in spinach (8). The patterns of residual pesticides vary depending on their physical and chemical properties, crop types, pesticide formulations, spray method, and environmental conditions. Sufficient knowledge and understanding of pesticides are required for their use (9). Removal of pesticide residues to acceptable levels through washing and blanching technologies may be a viable approach to enhance public health by minimizing ingestion of toxic contaminants. In a consumer perception survey regarding factors that can harm agricultural safety, pesticides were voted as the highest threat (45.7%), followed by heavy metals (31.8%) and chemical fertilizers (7.3%) (10). A survey on food safety hazards reported pesticides to be one of the hazards affecting human health. These surveys indicate that consumers are concerned about pesticide use and its associated detrimental effects (11).

To provide safe agricultural products to consumers, the Korean government implements good agricultural practices (GAPs) to manage the use of pesticides that are possibly retained during the harvesting, storage, packaging, processing, and distribution of agricultural products (12). In addition, the MRL is established for each agricultural product to a level that does not affect the human body, even if pesticides retained in agricultural products are consumed every day for the rest of the person's life (13). In the case of pesticides without a set MRL, the positive list system that applies the uniform standard (0.01 mg/kg) is taken into consideration to safely manage pesticide use at the level of non-detection (14). Pesticide residues are assessed in agricultural products that are imported, distributed, and produced during their raw material stage. However, people consume agricultural products in the form of processed foods that are washed and processed (15). As the amount of most pesticide residues in agricultural products can be reduced by pyrolysis and volatilization by washing and heating during the processing stages, it is very important to determine the residual level or pesticide properties after processing (16).

Among the pesticides used in spinach, insecticides include abamectin, chlorfenapyr, tebufenozide, cyantraniliprole, and fungicides, including azoxystrobin, pyraclostrobin and cyazofamid (17). In the Republic of Korea, the MRL has been set for 124 types of pesticides in spinach, and the MRL for cyantraniliprole use in spinach is set at 3.0 mg/kg (18). Cyantraniliprole is a diamide insecticide that passes from the xylem of crops, penetrates the leaf layer and roots, and causes muscle paralysis, coma, and lethargy in pests (19, 20). Diamide pesticides are safe and selective pesticides that exhibit high insecticidal activity and low toxicity to mammals (21). Cyantraniliprole is a systemic insecticide that has medium lipophilicity (log K_{ow} of 1.94), has a low water solubility of 14.2 mg/L and is non-volatile (V_p of 5.13×10^{-12} mPa at 20°C). These properties could be major indicators to understand the reduction of residual pesticides in agricultural products (22–24).

In the Republic of Korea, various studies on cyantraniliprole and spinach have been conducted, e.g., the development of an analytical method for cyantraniliprole residues in Welsh onion (20), residual properties and risk assessment of cyantraniliprole in some minor crops (21), and evaluation of cyantraniliprole residues observed in lettuce, spinach, and radish (25). A study on spinach sprayed with chlorpyrifos revealed a decrease of 33.4% in the pesticide residue when spinach was immersed twice in tap water for 30 s and a decrease of 57.6% when spinach was blanched without washing for 1 min (26). A study was performed on the change in the residual level of triazole fungicides during the cultivation and cooking of spinach; spinach sprayed with metconazole showed a reduction in the residue by 78.4% when it was immersed in tap water for 1 min and washed (27). After washing and blanching of lettuce, azoxystrobin residual levels were reduced by 38.9–75.3% and 73.6%, respectively (28). Based on these studies, it is confirmed that washing and blanching are effective in lowering residual pesticides. To the best of our knowledge, studies assessing the reduction in cyantraniliprole residue levels in spinach after washing and blanching are non-existent in the Republic of Korea.

Unlike other agricultural products, spinach is consumed immediately after a relatively simple washing and heating process in the Republic of Korea. Moreover, cyantraniliprole is a systemic insecticide, which means it might not easily be removed even after processing. Therefore, it is important to accurately determine the reduction in levels of residual cyantraniliprole introduced by washing and heating and whether it can be removed to an extent where it is harmless to the human body.

This study focused on the reduction of residual cyantraniliprole in spinach according to practical washing and blanching methods at home and identified the most effective washing and blanching method. The reduction in the residual pesticide during washing and blanching may differ depending on the amount of water, washing and blanching time, and use of detergent. Accordingly, various washing and blanching methods are needed to determine how to effectively lower residual cyantraniliprole. In this study, we aimed to investigate the reduction in cyantraniliprole residue levels in spinach after subjecting it to various washing and blanching methods.

Materials and methods

Materials

Cyantraniliprole (98.7%), formic acid (≥98%), sodium hydrogenate sesquihydrate (99%), sodium citrate (99%), magnesium sulfate (99.5%), and sodium chloride (99.5%) were from Sigma–Aldrich (St Louis, MO, USA), acetonitrile and methanol (both HPLC grade) were from Fisher J. T. Baker (Center Valley, PA, USA), and primary secondary amine (PSA) was purchased from Agilent Technologies (Santa Clara, CA, USA).

Pesticide application

This experiment was performed in Chilgok, Gyeongsangbuk-do Province in the Republic of Korea. Furthermore, our protocol was designed in accordance with the GAPs of the country. Cyantraniliprole 5% DC (TORICH®, NongHyup Chemical, Seongnam, Republic of Korea) was diluted 1,000 times (200 L/1,000 m^2) and sprayed twice on spinach 14 days before harvesting. The spinach samples were then collected. Samples were processed using a predetermined washing and blanching method, homogenized with a household mixer (Grinmic gold-DA10000G, DAESUNG ARTLON, Paju, Republic of Korea), and frozen at −20°C until analysis.

Washing and blanching methods

Various washing and blanching methods were employed to assess the reduction in residual cyantraniliprole levels in spinach. With respect to the washing methods, the wash time was set at 1, 3, or 5 min referring to household wash to assess the reduction in the residual levels (29). The following washing methods were used:

1. Running washing (RW): spinach (150 g) was washed for 1, 3, or 5 min while lightly shaking with running water at a flow rate of 2 L/min. The flow rate was selected within the range that does not damage spinach leaves.

2. Steeping washing (SW): spinach (150 g) was steeped in 3 L water for 1, 3, or 5 min while stirring lightly.

3. Steeping and running washing (SRW): spinach (150 g) was steeped in 3 L water for 1, 3, or 5 min while stirring lightly and washed for 3 min while lightly shaking with running water at a flow rate of 2 L/min.

4. Running washing with neutral detergent (RWND): Three milliliters of neutral detergent (EVERMIRACLE®, EM, Jeonju, Republic of Korea) were mixed with 3 L of water (1 mL/L). Spinach (150 g) was steeped in this mixture, lightly stirred for 1, 3, or 5 min and then rinsed with running water at a flow rate of 2 L/min for 5 min to remove all neutral detergent.

5. Steeping washing with neutral detergent (SWND): Three milliliters of neutral detergent were mixed with 3 L water (1 mL/L), and spinach (150 g) was steeped in this mixture and lightly stirred for 1, 3, or 5 min and then steeped three times in the same amount of fresh water for 3 min to remove all neutral detergent.

The washed spinach was placed in a strainer and dried at room temperature for 4 h until no visible water was present on the surface of the leaves. Following this, the spinach was homogenized using a household mixer, and dry ice was added to avoid pyrolysis of the pesticide. Approximately 20 g of dry ice was placed in the mixer, and then 150 g of spinach was added. The sample was subsequently ground until it became a form of powder and then stored at −20°C.

With respect to the blanching methods, the blanching time was set at 1, 3, and 5 min according to the study of Ling (30) to assess the reduction in the residual pesticide levels. The following blanching methods were used:

1. Blanching without washing (BW): spinach (150 g) was added to 1.5 L boiling water and blanched for 1, 3, or 5 min.

2. Running washing and blanching (RB): spinach (150 g) was washed with running water at a flow rate of 2 L/min for 3 min, added to 1.5 L boiling water and blanched for 1, 3, or 5 min.

3. Steeping washing and blanching (SB): spinach (150 g) was steeped in 3 L tap water for 3 min while stirring lightly, added to 1.5 L boiling water and blanched for 1, 3, or 5 min.

4. Blanching after steeping and running washing (BSR): spinach (150 g) was steeped in 3 L tap water for 3 min while stirring lightly and washed with running water at a flow rate of 2 L/min for 3 min. Then, the spinach samples were added to 1.5 L boiling water and blanched for 1, 3, or 5 min.

5. Blanching after running washing with neutral detergent (BRND): Three milliliters of neutral detergent were mixed with 3 L tap water (1 mL/L), and spinach (150 g) was steeped in this mixture for 3 min and rinsed by lightly

stirring with running water at a flow rate of 2 L/min for 5 min to remove all neutral detergent. The washed spinach was added to 1.5 L boiling water and blanched for 1, 3, or 5 min.

6. Blanching after steeping washing with neutral detergent (BSND): Three milliliters of neutral detergent were mixed with 3 L tap water (1 mL/L), and spinach (150 g) was steeped in this mixture for 3 min and steeped in the same amount of fresh water three times for 3 min to remove all neutral detergent. The washed spinach was added to 1.5 L boiling water and blanched for 1, 3, or 5 min.

The blanched spinach was placed in a strainer and dried at room temperature for 4 h until no visible water was present on the surface of the leaves. Following this, the spinach was homogenized and stored at −20°C.

Analysis of the pesticide residue

The pesticide residues in the spinach samples were analyzed using the second protocol described in the multiresidue methods of the Korea Food Code (31). A part of the purification process described in the protocol was modified for suitability considering the pigment and impurities in spinach. Briefly, acetonitrile (10 mL) was added to the homogenized spinach sample (10 g)—placed in a 50 mL conical tube—and the mixture was shaken at 2,000 rpm for 5 min at room temperature (∼20°C). Next, 4 g magnesium sulfate, 1 g sodium chloride, 1 g sodium citrate, and 0.5 g sodium hydrogen citrate sesquihydrate were added to the mixture, followed by shaking at 2,000 rpm for 5 min at ∼20°C. Then, the mixture was centrifuged at 4,160 × g for 10 min at 4°C. One milliliter of supernatant was collected, and 150 mg magnesium sulfate and 50 mg PSA were added to it. The mixture was vigorously shaken for 30 s and centrifuged at 2,000 × g for 5 min at ∼20°C. The supernatant was filtered using a 0.2-μm syringe filter and analyzed using UHPLC–MS/MS.

UHPLC–MS/MS analysis

An Agilent 1290 Infinity II UHPLC coupled with an Agilent 6470 triple quadrupole mass spectrometer (Agilent Technologies, Santa Clara, CA, USA) was used for the analysis. Methanol with 0.1% formic acid and deionized water with 0.1% formic acid were used as mobile phases A and B. The mobile phase gradients (A and B) started at 80:20 for 0–1 min, ramped to 30:70 for 1–7.5 min, maintained at 30:70 for 7.5–9 min, changed to 1:99 for 9–9.1 min, held at 1:99 for 9.1–15 min, ramped to 80:20 for 15–15.10 min, and maintained at 80:20 for 15.10–20 min. An Agilent Eclipse Plus C18 (100 × 2.1 mm × 1.8 μm) was used as the analytical column. The

flow rate was 0.2 mL/min, the column temperature was 40°C, and the injection volume was 5 μL. The following UHPLC–MS/MS conditions were used for analyzing cyantraniliprole: electrospray ionization and positive mode using multiple reaction monitoring (MRM). The capillary voltage was 3,500 V, and the drying gas flow and temperature were 9 L/min and 300°C, respectively. The sheath gas flow and temperature were 11 L/min and 350°C, respectively. MRM transitions were used as follows. The precursor ion m/z 473 and product ion m/z 284 were used for quantitative analysis, and the precursor ion m/z 442 and product ion m/z 177 m/z were used for qualitative analysis.

Method validation for cyantraniliprole

The cyantraniliprole standard was dissolved in acetonitrile to prepare a stock solution with a concentration of 1,000 mg/L. The working solutions were prepared by diluting the stock solutions to a concentration of 100 mg/L using acetonitrile. The working solution of the cyantraniliprole standard was diluted with the spinach sample matrix to concentrations of 0.001, 0.003, 0.005, 0.010, 0.030, 0.050, and 0.100 mg/L to plot matrix-matched calibration curves. To verify the reproducibility, the cyantraniliprole standard solution with a concentration of 0.030 mg/L was continuously injected into the UHPLC–MS/MS system 10 times to assess the coefficient of variation of retention time and m/z in the chromatogram. The limit of quantification (LOQ) was calculated by considering the minimum detection mass (ng), sample weight (g), injection volume (μL), and final solution volume (mL). In addition, the recovery test was conducted with blank samples to validate the analytical method. The spinach sample was mixed with cyantraniliprole at three different concentrations, i.e., LOQ (0.003 mg/kg), 10 × LOQ (0.030 mg/kg), and 50 × LOQ (0.150 mg/kg).

$$LOQ \left(\frac{mg}{kg} \right) = \frac{minimum\ detection\ mass\ (ng) \times final\ solution\ volume\ (mL)}{injection\ volume\ (uL) \times sample\ weight\ (g)}$$

Statistical analysis

Each sample analysis was repeated three times, and the obtained data were statistically evaluated using one-way analysis of variance (ANOVA) with the Statistical Analysis System software (SAS version 9.3). Duncan's multiple range test was performed in cases of significant differences ($P < 0.05$) to confirm the differences among mean values.

TABLE 1 Recovery of cyantraniliprole in spinach.

Compound	Fortification (mg/kg)	Recovery ± SD[a] (%)	CV[b] (%)	LOQ[c] (mg/kg)
Cyantraniliprole	0.003	97.6 ± 4.51	4.62	0.030
	0.030	96.8 ± 1.17	1.21	
	0.150	109 ± 1.83	1.67	

[a]Standard deviation.
[b]Coefficient of variation.
[c]Limit of quantitation.

Results and discussion

Method validation

The linearity of the matrix-matched calibration curves had an acceptable correlation coefficient $r > 0.999$. The coefficient of variation was 5.09% after 10 injections, and reproducibility was verified. The limit of detection (LOD) and LOQ used to analyze cyantraniliprole were 0.001 and 0.003 mg/kg, respectively. When the matrix samples of spinach were mixed with cyantraniliprole at concentrations of 0.003, 0.030, and 0.150 mg/kg, the recovery rate was 97.6–109%, and the coefficient of variation was 1.21–4.62% (Table 1). The analytical method was suitable for analyzing cyantraniliprole, exhibiting a recovery rate of 70–120% and a coefficient of variation within 10% of that specified in the guidelines of the Codex Alimentarius Commission (32).

Lowering the residual cyantraniliprole levels in spinach after washing methods

The changes in the level of residual cyantraniliprole according to the washing time are listed in Table 2. The initial level of residual cyantraniliprole in spinach was 4.43 mg/kg. After RW, SW, SRW, RWND, and SWND for 1, 3, and 5 min, the residual cyantraniliprole levels were 3.76, 3.40, and 2.61; 3.56, 3.33, and 2.59; 3.22, 3.13, and 2.53; 2.82, 2.47, and 2.38; and 2.53, 2.10, and 2.01 mg/kg, respectively. Upon using most washing methods, the residual cyantraniliprole levels tended to decrease as the washing time increased. However, no significant differences ($P > 0.05$) were observed between 1 and 3 min SRW (residual cyantraniliprole levels 3.22 and 3.13 mg/kg; a reduction of 27.3 and 29.4%) and between 3 and 5 min RWND (2.47 and 2.38 mg/kg; a reduction of 44.2 and 46.3%).

A comparison of the residual cyantraniliprole levels in spinach according to each washing method is provided in Table 3. After 1 min of washing, the residual cyantraniliprole levels after SWND, RWND, SRW, SW, and RW were 2.53, 2.82, 3.22, 3.56, and 3.76 mg/kg, with reductions of 42.9, 36.3, 27.3, 19.6, and 15.1%, respectively. Among all washing methods, SWND was the most effective at reducing the residual

TABLE 2 Changes in residual cyantraniliprole levels in spinach based on washing time.

Washing time (min)	Raw spinach Residue amount (mg/kg) Mean ± SD	RW Residue amount (mg/kg) Mean ± SD	RW % Removed[1]	SW Residue amount (mg/kg) Mean ± SD	SW % Removed	SRW Residue amount (mg/kg) Mean ± SD	SRW % Removed	RWND Residue amount (mg/kg) Mean ± SD	RWND % Removed	SWND Residue amount (mg/kg) Mean ± SD	SWND % Removed
1	4.43 ± 0.140	3.76 ± 0.070[a]	15.1	3.56 ± 0.010[a]	19.6	3.22 ± 0.090[a]	27.3	2.82 ± 0.040[a]	36.3	2.53 ± 0.060[a]	42.9
3		3.40 ± 0.100[b]	23.3	3.33 ± 0.110[b]	24.8	3.13 ± 0.030[a]	29.4	2.47 ± 0.120[b]	44.2	2.10 ± 0.040[b]	52.6
5		2.61 ± 0.160[c]	41.1	2.59 ± 0.140[c]	41.5	2.53 ± 0.130[b]	42.9	2.38 ± 0.170[b]	46.3	2.01 ± 0.020[c]	54.6

Washing method

[1]% Removed: 100 – (processing residue/raw product residue) × 100.
RW, running washing; SW, steeping washing; SRW, steeping and running washing; RWND, running washing with neutral detergent; SWND, steeping washing with neutral detergent.
Values followed by the same letter in the same column are not significantly different (P < 0.05).

TABLE 3 Comparison of the residual cyantraniliprole levels in spinach based on the washing method.

Washing method	Washing time (min)					
	1		3		5	
	Residue amount (mg/kg) Mean ± SD	% Removed	Residue amount (mg/kg) Mean ± SD	% Removed	Residue amount (mg/kg) Mean ± SD	% Removed
Raw spinach	4.43 ± 0.140					
RW	3.76 ± 0.070[a]	15.1	3.40 ± 0.100[a]	23.3	2.61 ± 0.160[a]	41.1
SW	3.56 ± 0.010[b]	19.6	3.33 ± 0.110[a]	24.8	2.59 ± 0.140[a]	41.5
SRW	3.22 ± 0.090[c]	27.3	3.13 ± 0.030[b]	29.4	2.53 ± 0.130[a]	42.9
RWND	2.82 ± 0.040[d]	36.3	2.47 ± 0.120[c]	44.2	2.38 ± 0.170[a]	46.3
SWND	2.53 ± 0.060[e]	42.9	2.10 ± 0.040[d]	52.6	2.01 ± 0.020[b]	54.6

Values followed by the same letter in the same column are not significantly different ($P < 0.05$).

cyantraniliprole levels (reduction rate, 42.9%). SW resulted in a more effective reduction in the residual cyantraniliprole levels than RW (19.6 vs. 15.1%). Ko et al. (33) showed that the diazinon reduction rate in lettuce was 33.7% after SW and 24.7% after RW; therefore, SW was more effective than RW in reducing the levels of residual diazinon. SRW (27.3%) was more effective than SW and RW (19.6 and 15.1%, respectively) at reducing the levels of residual cyantraniliprole. The reduction rates of residual cyantraniliprole levels after RWND (36.3%) and SWND (42.9%) were higher than those after RW (15.1%) and SW (19.6%). Consequently, cyantraniliprole levels tended to decrease more effectively when washed with a neutral detergent. Kwon et al. (34) reported a decrease of 3–4% in chlorpyrifos levels when lettuce was washed with tap water and a decrease of 12–31% when it was washed with a neutral detergent. Lee et al. (35) reported that the levels of chlorpyrifos-methyl sprayed on perilla leaves decreased by 44.3 and 81.5% after washing with tap water and neutral detergent, respectively. Our results are consistent with those of these studies because chlorpyrifos and cyantraniliprole are fat-soluble, and their levels were considerably reduced when a neutral detergent was used.

After 3 min of washing, the residual cyantraniliprole levels after SWND, RWND, SRW, SW, and RW were 2.10, 2.47, 3.13, 3.33, and 3.40 mg/kg, with reductions of 52.6, 44.2, 29.4, 24.8, and 23.3%, respectively. Among all washing methods, SWND exhibited the highest reduction rate in residual cyantraniliprole levels (52.6%). The reduction rate in cyantraniliprole levels after RW (24.8%) was slightly higher than that after SW (23.3%); however, the difference was not significant. The levels of residual cyantraniliprole decreased to a greater extent after SRW (29.4%) than after RW (24.8%) and SW (23.3%). The rates of reduction in residual cyantraniliprole levels after RWND (44.2%) and SWND (52.6%) were significantly higher than those after RW (23.3%) and SW (24.8%). Therefore, cyantraniliprole levels tended to decrease more effectively when the spinach was washed with a neutral detergent (compared to when it was washed with water).

After 5 min of washing, the residual cyantraniliprole levels after SWND, RWND, SRW, SW, and RW were 2.01, 2.38, 2.53, 2.59, and 2.61 mg/kg, with reductions of 54.6, 46.3, 42.9, 41.5, and 41.1%, respectively. Among all washing methods, SWND was the most effective at reducing cyantraniliprole levels (rate, 54.6%). No significant difference was observed in the levels of residual cyantraniliprole among RW, SW, SRW, and RWND.

Based on the overall results, it can be observed that residual cyantraniliprole can be lowered considerably by washing even though its water solubility is low (14.2 mg/L). The reason is assumed to be that residual cyantraniliprole remains more abundant on the surface of spinach than in its inner tissues because cyatraniliprole is relatively non-polar (log K_{ow} of 1.94) and interacts with plant epicuticular wax on the surface (36). Tahir et al. (37) reported that although cypermethrin has low solubility in water (0.01 mg/L), the reduction rate in washed vegetables was 6–100%. Klinhom et al. (38) showed that methomyl, which is a systemic pesticide, decreased by 37.90% in leafy Chinese-Kale after washing. These studies show that pesticides that have a low solubility in water or are systemic pesticides can be lowered by washing as a result of the study. The use of detergent solution is more effective in lowering residual cyantraniliprole than tap water. Due to the surfactant component of the neutral detergent, it seems that detergent solution has more influence than tap water on the reduction of cyantraniliprole. With respect to SW and RW, SW showed a higher reduction rate than RW. The reason is presumed to be that the amount of water that touches the surface of spinach during SW is higher than that of RW.

Lowering the residual cyantraniliprole levels in spinach after blanching methods

The changes in the level of residual cyantraniliprole according to the blanching time are shown in Table 4. After

TABLE 4 Changes in the residual cyantraniliprole levels in spinach based on blanching time.

Blanching time	Raw spinach	BW		RB		SB		BSR		BRND		BSND	
	Residue amount (mg/kg) Mean ± SD	Residue amount (mg/kg) Mean ± SD	% Removed	Residue amount (mg/kg) Mean ± SD	% Removed	Residue amount (mg/kg) Mean ± SD	% Removed	Residue amount (mg/kg) Mean ± SD	% Removed	Residue amount (mg/kg) Mean ± SD	% Removed	Residue amount (mg/kg) Mean ± SD	% Removed
													Blanching time
1	4.43 ± 0.140	1.77 ± 0.080[a]	60.1	1.28 ± 0.070[a]	71.1	1.00 ± 0.080[a]	77.4	1.05 ± 0.060[a]	76.3	1.01 ± 0.010[a]	77.2	0.980 ± 0.060[a]	77.9
3		1.02 ± 0.020[b]	77.0	0.610 ± 0.030[b]	86.2	0.630 ± 0.050[b]	85.8	0.400 ± 0.030[b]	91.0	0.490 ± 0.040[b]	88.9	0.390 ± 0.050[b]	91.2
5		0.800 ± 0.080[c]	81.9	0.350 ± 0.050[c]	92.1	0.300 ± 0.020[c]	93.2	0.290 ± 0.010[c]	93.5	0.370 ± 0.030[c]	91.7	0.330 ± 0.020[b]	92.6

BW, blanching without washing; RB, running washing and blanching; SB, steeping washing and blanching; BSR, blanching after steeping washing and running washing; BRND, blanching after running washing with neutral detergent; BSND, blanching after steeping washing with neutral detergent.

Values followed by the same letter in the same column are not significantly different (P < 0.05).

BW for 1, 3, and 5 min, the residual cyantraniliprole levels were 1.77, 1.02, and 0.800 mg/kg, with reduction rates of 60.1, 77.0, and 81.9%, respectively. This confirmed that a considerable amount of cyantraniliprole was removed just by blanching. Ryu (39) showed that when Korean cabbage sprayed with hexaconazole was blanched for 30 s without washing, the rate of hexaconazole reduction was 80.63%, i.e., more than 50% of the pesticide residue was removed only by blanching. After RB, SB, BSR, BRND, and BSND for 1, 3, and 5 min, the residual cyantraniliprole levels were 1.28, 0.610, and 0.350; 1.00, 0.630, and 0.300; 1.05, 0.400, and 0.290; 1.01, 0.490, and 0.370; and 0.980, 0.390, and 0.330 mg/kg, respectively. In most blanching methods, the residual cyantraniliprole levels tended to decrease as the blanching time increased. This is consistent with the results of Kim (40), who showed that the levels of procymidone residues in spinach decreased by 68.95–85.46% as the blanching time increased from 15, 30 s, and 1–3 min. However, no significant difference was observed in the residual cyantraniliprole levels after BSND for 3 and 5 min (0.390 and 0.330 mg/kg with a reduction of 91.2 and 92.6%, respectively).

A comparison of the levels of residual cyantraniliprole in spinach according to each blanching method is provided in Table 5. After 1 min of blanching, the residual cyantraniliprole levels after BSND, BRND, SB, BSR, RB, and BW were 0.980, 1.01, 1.00, 1.05, 1.28, and 1.77 mg/kg, with reduction rates of 77.9, 77.2, 77.4, 76.3, 71.1, and 60.1%, respectively. Among all blanching methods, BSND was the most efficient at reducing cyantraniliprole levels (77.9%); however, no significant difference was observed among the reduction rates obtained using BSND, BRND, BSR, and SB after 1 min of blanching. Consequently, the reduction in the levels of cyantraniliprole residues was similar after 1 min of blanching after BSND, BRND, BSR, and SB. Comparing the blanching methods after washing (BSND, BRND, SB, BSR, and RB), we found that the reduction in residual cyantraniliprole levels was the lowest after RB (71.1%). This was similar to the result obtained for the washing methods where RW resulted in the lowest reduction in residual cyantraniliprole levels among all washing methods after 1 min of washing. BW resulted in a reduction rate of 60.1%, which was considerably lower than those obtained with all blanching methods. Consequently, washing before blanching was more effective than BW with respect to reducing cyantraniliprole levels.

After 3 min of blanching, the residual cyantraniliprole levels after BSND, BSR, BRND, RB, SB, and BW were 0.390, 0.400, 0.490, 0.610, 0.630, and 1.02 mg/kg, with reductions of 91.2, 91.0, 88.9, 86.2, 85.8, and 77.0%, respectively. Among all blanching methods, BSND was the most effective at reducing the residual cyantraniliprole levels (91.2%); however, this was not significant compared with the reduction rate obtained with BSR (91.0%). BW

TABLE 5 Changes in the residual cyantraniliprole levels in spinach based on the blanching method.

Blanching method	Blanching time					
	1		3		5	
	Residue amount (mg/kg) Mean ± SD	% Removed	Residue amount (mg/kg) Mean ± SD	% Removed	Residue amount (mg/kg) Mean ± SD	% Removed
Raw spinach	4.43 ± 0.140					
BW	1.77 ± 0.080[a]	60.1	1.02 ± 0.020[a]	77.0	0.800 ± 0.080[a]	81.9
RB	1.28 ± 0.070[b]	71.1	0.610 ± 0.030[b]	86.2	0.350 ± 0.050[bc]	92.1
SB	1.00 ± 0.080[c]	77.4	0.630 ± 0.050[b]	85.8	0.300 ± 0.020[bc]	93.2
BSR	1.05 ± 0.060[c]	76.3	0.400 ± 0.030[d]	91.0	0.290 ± 0.010[c]	93.5
BRND	1.01 ± 0.010[c]	77.2	0.490 ± 0.040[c]	88.9	0.370 ± 0.030[b]	91.7
BSND	0.980 ± 0.060[c]	77.9	0.390 ± 0.050[d]	91.2	0.330 ± 0.020[bc]	92.6

Values followed by the same letter in the same column are not significantly different (P < 0.05).

resulted in the lowest reduction in residual cyantraniliprole levels (77.0%) among all blanching methods. Therefore, a considerable difference was observed in the residual cyantraniliprole levels with and without washing before blanching.

After 5 min of blanching, the residual cyantraniliprole levels after BSR, SB, BSND, RB, BRND, and BW were 0.290, 0.300, 0.330, 0.350, 0.370, and 0.800 mg/kg, with reductions of 93.5, 93.2, 92.6, 92.1, 91.7, and 81.9%, respectively. It was confirmed that washing before blanching was the most effective at removing most of the cyantraniliprole residue. This was consistent with the results of a previous study (41), where the reduction rates of pymetrozine and difenoconazole were 99.5 and 100%, respectively, when water celery was washed for 2 min and blanched for 1 min. The rate of reducing cyantraniliprole levels was the highest after BSR (93.5%) among all blanching methods; however, the difference was not significant among the rates after BSR, SB, BSND, and RB. Therefore, these methods were similarly effective at removing cyantraniliprole after 5 min of blanching. BW resulted in the lowest reduction rate (81.9%) among all blanching methods.

Based on the overall results, residual cyantraniliprole appeared to be considerably lowered by blanching; nevertheless, it is non-volatile (V_p of 5.13×10^{-12} mPa at 20°C). The reason is supposed to be that residual cyantraniliprole is lowered by not only volatilization but also hydrolysis due to leaching during blanching (42). Blanching is effective in lowering residual cyantraniliprole even without washing, and it is more effective with washing. In this context, Kim et al. (43) reported that pyridaben, which has low volatility (V_p of 1.0×10^{-2} at 20°C), decreased by 85.1–90.5 in pepper leaves following washing and blanching. Consequently, to lower residual cyantraniliprole as much as possible, washing should be employed before blanching.

Limitations of the study

This study was conducted under laboratory conditions. Consequently, the results do not represent all cases of washing and blanching spinach. Reduction of cyantraniliprole residue in spinach would vary depending on washing and blanching conditions such as the amount of water, flow rate of running water, number of washes, blanching times, type of detergent, and water temperature. Future studies should include these variables in the methodology to identify more effective measures for reducing pesticides in human foods. Furthermore, while washing with tap water is effective for polar pesticides, neutral detergents are more effective than tap water for non-polar chemicals, and the detergent solution may remain on the surface of the spinach, introducing another potential toxin to the human body. Therefore, ensuring that all detergent solution is removed after washing is important. Ascertaining the amounts of detergent that remains after washing with this solution and how much this decreases after washing may be part of a future study.

Conclusions

The rate of reduction in cyantraniliprole levels was 42.9–54.6% after SWND, which was the most effective at reducing the levels of the cyantraniliprole residue among all the washing methods. Among the blanching methods, the highest efficiency of removing cyantraniliprole residue was observed for BSND (reduction rate of 77.9%), SB (77.4%), BSR (76.3%), and BRND (77.2%) after 1 min of blanching (though these were similar); for BSND (91.2%) and BSR (91.0%) after 3 min of blanching; and for BSR (93.5%), SB (93.2%), RB (92.1%), and BSND (92.6%) after 5 min of blanching. Since all amounts of residual

cyantraniliprole after washing and blanching methods were below the MRL, residual cyantraniliprole in spinach can be removed to an extent that is harmless to the human body after washing and blanching. In summary, it was confirmed that a considerable amount of cyantraniliprole residue in spinach can be removed by washing or blanching. Blanching after steep washing was the most efficient method that removed up to 93.5% of the cyantraniliprole residue from spinach. These results can be considered a viable approach to enhance public health by minimizing the ingestion of residual cyantraniliprole. Furthermore, it can be utilized to predict the reduction tendency of residual cyantraniliprole in the food industry.

Data availability statement

The raw data supporting the conclusions of this article will be made available by the authors, without undue reservation.

Author contributions

MP, HK, MK, and M-hI conceptualized this study. MP, HK, and MK investigated all information needed for this study, were responsible for washing, blanching the spinach, and analyzing the cyantraniliprole residue present in the spinach samples obtained. M-hI supervised this study and reviewed and edited it. MP wrote the original draft. All authors contributed to the article and approved the submitted version.

Conflict of interest

The authors declare that the research was conducted in the absence of any commercial or financial relationships that could be construed as a potential conflict of interest.

Publisher's note

All claims expressed in this article are solely those of the authors and do not necessarily represent those of their affiliated organizations, or those of the publisher, the editors and the reviewers. Any product that may be evaluated in this article, or claim that may be made by its manufacturer, is not guaranteed or endorsed by the publisher.

References

1. Mi HL, Jae SH, Nobuyuki K, Takahisa M. Physicochemical characteristics of commercial spinach produced in autumn. *J East Asian Soc Diet Life.* (2005) 15:306–14.

2. Kim KK. *Agricultural Technology Guide.* Jeonju: Rural Development Administration (2018).

3. Statistics Korea. The amount of vegetables produced. (2019). https://kostat.go.kr/wnsearch/search.jsp (Accessed September 11, 2021)

4. Korea Health Industry Development. *Intake by Food.* Institute (2018). Available online at: https://www.khidi.or.kr/kps/dhraStat/result2?menuId=MENU01653&year=2018 (accessed September 24, 2021).

5. National Crop Pest Management System. *Information on Pests in Spinach.* Available online at: https://ncpms.rda.go.kr/npms/ImageSearchDtlR4.np?kncrCode=VC021008&kncrNm=%EC%8B%9C%EA%B8%88%EC%B9%98&upperNm=%EC%B1%84%EC%86%8C&flagCode=S&queryFlag=V&nextAction=%2Fnpms%2FImageSearchDtlR4.np (accessed September 26, 2021).

6. Kim JE, Kim JH, Lee YD, Im CH, Heo JH, Jung YH, et al. *The Latest Pesticide Science.* Seoul: Sigmapress (2020). p. 5–12.

7. Kim JH. Toxicity and acceptable daily intake of pesticide. *Safe Food.* (2007) 2:51−7.

8. Jung BS. *Food Safety Management Guidelines.* Cheongju: Ministry of Food and Drug Safety (2021).

9. Lee HJ, Choe WJ, Lee JY, Cho DH, Kang CS, Kim WS. Monitoring of ergosterol biosynthesis inhibitor (EBI) pesticide residues in commercial agricultural products and risk assessment. *J Kor Soc Food Sci Nutr.* (2009) 38:1779–84. doi: 10.3746/jkfn.2009.38.12.1779

10. Park HS. *Studies on Consumer Recognition for Agricultural Products.* Jeonju: Rural Development Administration (2007).

11. Yoon YM, Kim KJ. Consumers' knowledge on 10 food hazards. *Cons Policy Educ Rev.* (2015) 11:79–99. doi: 10.15790/cope.2015.11.4.079

12. Nam MJ, Chung DY, Shim WB, Chung DH. Hazard analysis for the application of good agricultural practices (GAP) on paprika during cultivation. *J Food Hyg S Afr.* (2011) 26:273–82.

13. Pesticides and Veterinary Drugs Information. *Safety Management of Residual Pesticides.* (2015). Available online at: http://www.foodsafetykorea.go.kr/residue/contents/view.do?contentsKey=4 (accessed September 30, 2021).

14. Moon KE. *Monitoring pesticide residue in agricultural products for comparison before and after applying the positive list system.* (MS thesis). Korea University, South Korea (2017).

15. Yoon HJ. *Method Validation and Monitoring of Pesticide Residues in Agricultural Products.* Cheonju: Ministry of Food and Drug Safety (2020).

16. Im MH, Ji YJ. A review on processing factors of pesticide residues during fruits processing. *J Appl Biol Chem.* (2016) 59:189–201. doi: 10.3839/jabc.2016.034

17. Pesticide Safety Information System. *Pesticide Safety Information System.* (2020). Available online at: https://psis.rda.go.kr/psis/index.ps (accessed October 12, 2021).

18. Ministry of Food and Drug Safety. *Pesticide MRLs*. (2021). Available online at: https://www.foodsafetykorea.go.kr/foodcode/02_02_01.jsp?food_code=ap106010005&s_option=KR&s_type=6 (accessed October 12, 2021).

19. Foster SP, Denholm I, Rison JL, Portillo HE, Margaritopoulis J, Slater R. Susceptibility of standard clones and European field populations of the green peach aphid, *Myzus persicae*, and the cotton aphid, *Aphis gossypii* (Hemiptera: Aphididae), to the novel anthranilic diamide insecticide cyantraniliprole. *Pest Manag Sci.* (2012) 68:629–33. doi: 10.1002/ps.2306

20. Do JA, Lee MY, Chang MI, Hong JH, Oh JH. Development of analytical method for cyantraniliprole residues in Welsh onion (*Allium species*). *Anal Sci Technol.* (2015) 28:175–81. doi: 10.5806/AST.2015.28.3.175

21. Lee JW. *Residual properties and risk assessment of cyantraniliprole on some minor crops* (MS thesis). Kangwon University, South Korea (2019).

22. Barry JD, Portillo HE, Annan IB, Cameron RA, Clagg DG, Dietrich RF, et al. Movement of cyantraniliprole in plants after foliar applications and its impact on the control of sucking and chewing insects. *Pest Manag Sci.* (2014) 71:395–403. doi: 10.1002/ps.3816

23. Zhang Y, Lorsbach BA, Castetter S, Lambert WT, Kister J, Wang NX, et al. Physicochemical property guidelines for modern agrochemicals. *Pest Manag Sci.* (2018) 74:1979–91. doi: 10.1002/ps.5037

24. Gong W, Jiang M, Zhang T, Zhang W, Liang G, Li B, et al. Uptake and dissipation of metalaxyl-M, fludioxonil, cyantraniliprole and thiamethoxam in greenhouse chrysanthemum. *Environ Pollut.* (2020) 257:113499. doi: 10.1016/j.envpol.2019.113499

25. Yoon JH, Lee SW, Lim DJ, Kim SW, Kim IS. Evaluation of cyantraniliprole residues translocated by lettuce, spinach and radish. *Kor J Environ Agric.* (2021) 40:335–44. doi: 10.5338/KJEA.2021.40.4.38

26. Seo JM, Ha DR, Lee HH, Oh MS, Park JJ, Shin HW, et al. The degradation patterns of two pesticides in spinach by cultivation, storage and washing. *J Food Hyg S Afr.* (2010) 25:91–9.

27. Jung HH. *Residual characteristics of triazole pesticides in spinach during cultivation and cooking process* (MS thesis). Kyungpook University, South Korea (2016).

28. Kim JA, Seo JA, Lee HS, Im MH. Residual characteristics and processing factors of azoxystrobin during eggplant and lettuce processing. *J Appl Biol Chem.* (2020) 63:51–60. doi: 10.3839/jabc.2020.007

29. Chung SW. How effective are common household preparations on removing pesticide residues from fruit and vegetables? A review. *J Sci Food Agric.* (2018) 95:2857–5870. doi: 10.1002/jsfa.8821

30. Ling Y, Wang H, Yong W, Zhang F, Sun L, Yang ML, et al. The effects of washing and cooking on chlorpyrifos and its toxic metabolites in vegetables. *Food Control.* (2011) 22:54–8. doi: 10.1016/j.foodcont.2010.06.009

31. The Korea Food Code. *Multiresidue Methods for Pesticide Residues*. (2022). Available online at: https://www.foodsafetykorea.go.kr/foodcode/01_03.jsp?idx=404 (accessed October 15, 2021).

32. Joint FAO/WHO Codex Alimentarius Commission. *CODEX. Guidelines on Performance Criteria for Methods of Analysis for the Determination of Pesticide Residues in Food and Feed, CODEX ALIMENTARIUS, CXG 90–2017*. Rome: Food and Agriculture Organization of the United Nations (2017).

33. Ko BS, Jeon TH, Jung KS, Lee SK. Removal effects of organic-phosphorus pesticide residue in lettuce by washing methods. *Kor J Rural.* (1996) 21:159–71.

34. Kwon HY, Kim TK, Hong SM, Kim CS, Baeck MK, Kim DH, et al. Removal of pesticide residues in field-sprayed leafy vegetables by different washing method. *Kor J Pestic Sci.* (2013) 17:237–43. doi: 10.7585/kjps.2013.17.4.237

35. Lee JM, Lee HR, Nam SM. Removal rate of residual pesticides in Perilla leaves with various washing methods. *Kor J Food Sci Technol.* (2003) 35:586–90.

36. Ku KM. Development of lab curriculum for teaching role of surfactant on waxy leaf surface and contact angle measurement using smartphone application and its educational efficacy analysis. *Trends Agric Life Sci.* (2019) 57:33–45. doi: 10.29335/tals.2019.57.33

37. Tahir S, Anwar T, Ahmad I, Khan D. Effects on washing on concentration of residual pesticides in salad vegetables. *Int J Biol Biotech.* (2014) 11:655–9.

38. Klinhom P, Halee A, Methawiwat S. The effectiveness of household chemiclas in residue removal of methomyl and carbaryl pesticides on Chinese-Kale. *Kasetsart J (Nat Sci).* (2008) 42:136–43.

39. Ryu JS. *Residual characteristics of triazole fungicides during cultivation period and processing of Korean cabbage* (MS thesis). Kyungpook University, South Korea (2017).

40. Kim HJ. *Changes in contents of residual pesticides in spinach during washing and cooking* (MS thesis). Konkuk University, South Korea (2006).

41. Kim SH. *Residual characteristics and processing factors of difenoconazole and pymetrozine in water celery* (MS thesis). Chungbuk University, South Korea (2013).

42. Lee MG, Jung D. Processing factors and removal ratios of select pesticides in hot pepper leaves by a successive process of washing, blanching, and drying. *Food Sci Biotechnol.* (2009) 18:1076–82.

43. Kim SW, El-Aty AM, Rahman MM, Choi JH, Choi OJ, Rhee GS, et al. Detection of pyridaben residue levels in hot pepper fruit and leaves by liquid chromatography-tandem mass spectrometry: effect of household process. *Biomed Chromatogr.* (2015) 29:990–7. doi: 10.1002/bmc.3383

Cruciferous vegetables as a treasure of functional foods bioactive compounds: Targeting p53 family in gastrointestinal tract and associated cancers

Saikat Mitra[1], Talha Bin Emran[2,3]*, Deepak Chandran[4], B. M. Redwan Matin Zidan[1], Rajib Das[1], Sukamto S. Mamada[5], Ayu Masyita[5], Mirnawati Salampe[6], Firzan Nainu[5], Mayeen Uddin Khandaker[7], Abubakr M. Idris[8,9]* and Jesus Simal-Gandara[10]*

[1]Department of Pharmacy, Faculty of Pharmacy, University of Dhaka, Dhaka, Bangladesh, [2]Department of Pharmacy, BGC Trust University Bangladesh, Chittagong, Bangladesh, [3]Department of Pharmacy, Faculty of Allied Health Sciences, Daffodil International University, Dhaka, Bangladesh, [4]Department of Veterinary Sciences and Animal Husbandry, Amrita School of Agricultural Sciences, Amrita Vishwa Vidyapeetham University, Coimbatore, Tamil Nadu, India, [5]Faculty of Pharmacy, Hasanuddin University, Makassar, Indonesia, [6]Sekolah Tinggi Ilmu Farmasi Makassar, Makassar, Indonesia, [7]Centre for Applied Physics and Radiation Technologies, School of Engineering and Technology, Sunway University, Subang Jaya, Selangor, Malaysia, [8]Department of Chemistry, College of Science, King Khalid University, Abha, Saudi Arabia, [9]Research Center for Advanced Materials Science (RCAMS), King Khalid University, Abha, Saudi Arabia, [10]Nutrition and Bromatology Group, Department of Analytical Chemistry and Food Science, Faculty of Science, Universidade de Vigo, Ourense, Spain

In the past few years, phytochemicals from natural products have gotten the boundless praise in treating cancer. The promising role of cruciferous vegetables and active components contained in these vegetables, such as isothiocyanates, indole-3-carbinol, and isothiocyanates, has been widely researched in experimental *in vitro* and *in vivo* carcinogenesis models. The chemopreventive agents produced from the cruciferous vegetables were recurrently proven to affect carcinogenesis throughout the onset and developmental phases of cancer formation. Likewise, findings from clinical investigations and epidemiological research supported this statement. The anticancer activities of these functional foods bioactive compounds are closely related to their ability to upregulate p53 and its related target genes, e.g., p21. As the "guardian of the genome," the p53 family (p53, p63, and p73) plays a pivotal role in preventing the cancer progression associated with DNA damage. This review discusses the functional foods bioactive compounds derived from several cruciferous vegetables and their use in altering the tumor-suppressive effect of p53 proteins. The association between the mutation of p53 and the incidence of gastrointestinal malignancies (gastric, small intestine, colon, liver, and pancreatic cancers) is also discussed. This review contains crucial information about the use of cruciferous vegetables in the treatment of gastrointestinal tract malignancies.

Introduction

Our cells are always exposed to a wide array of cellular stresses, such as ionizing radiation, oncogenes, and oxidative stress. Following the exposure of these stresses, genomic aberration and instability may occur which could lead to cancer development. Therefore, a proper and delicate mechanism is required for detecting any DNA damage and protecting cells from malignancies. It has been known that the role of the p53 family (p53, p63, and p73 proteins) in suppressing the development of cancerous cells is indispensable. More than 50% of human cancers are closely linked to the mutation or deletion of p53 which indicates the pivotal role of this transcription factor (1, 2). Once cellular stressors, such as ionizing radiation, are exposed to cells, p53 is activated. This activation could lead to cell cycle arrest and apoptosis. While the former is aimed to repair the damage occurring in DNA due to the stressors exposure, the latter is activated if the damage cannot be repaired.

Of several cancers, gastrointestinal-related cancers, such as colorectal cancer, have been attracting big interest as their malignancies are associated with a high figure of death. In the United States, colorectal cancer-related death is placed in second place. From ∼148,000 cases of colorectal cancer in the United States in 2020, the death was estimated at the rate of almost 35% (3). Surprisingly, from this figure, ∼18,000 cases were detected in individuals under 50 years old (3).

The efforts conducted to discover and develop novel anticancer candidates from various sources, including from cruciferous vegetables, are still ongoing. These vegetables are a member of Brassicaceae (Cruciferae). It has been known that consumption of cruciferous vegetables, such as broccoli and cauliflower, is correlated with the lower incidence of chronic diseases, including cancer (4, 5). In addition to their nutritive contents (e.g., proteins, carbohydrates, vitamins, and minerals) (6), these vegetables also contain a number of metabolites that can promote health e.g., glucosinolates, isothiocyanates, methyl cysteine sulfoxide, terpenes, anthocyanins, and flavonoids (7–10). Some studies have reported the anticarcinogenic activity of several metabolites found in cruciferous vegetables. For example, glucosinolates, a secondary metabolite mainly found in cruciferous plants, display activity in preventing the development and progression of gastrointestinal cancers as well as in treating these cancers (11). To date, the existence of more than 130 glucosinolates has been reported which can be classified into three major structural groups i.e., aliphatic, indole, and aromatic glucosinolates (12). Biologically, the parent glucosinolate possesses negligible activity in preventing cancer progression. However, once it is converted into its derivatives, such as isothiocyanates, thiocyanates, nitriles, and indoles, the biological activity becomes potent. This conversion is mediated by the action of myrosinases during the mechanical digestion (e.g., chewing and cutting) of the vegetables (13). The anticancer activity of the cruciferous metabolites might be associated with several proposed mechanisms of action. It has been suggested that isothiocyanates and indoles play a pivotal role in regulating cell growth and cell cycle arrest which is essential in repairing the damaged DNA so that this prevents DNA alteration. The pro-apoptotic activity of these metabolites has also been reported. Other putative mechanisms include their activity in modulating oxidative stress and preventing the occurrence of angiogenesis (7). Anticancer activities of these metabolites are closely linked to their ability in upregulating p53 and its related target genes, e.g., p21 (14–16).

This review summarizes the metabolites obtained from various cruciferous vegetables and their potential uses in modifying the tumor-suppressive action of p53 proteins. Further, the correlation between the incidence of gastrointestinal cancers (gastric, small intestine, colon, liver, and pancreatic cancers) and the mutation of p53 is also described. This review provides information that is important for those who are interested in investigating further utilization of cruciferous vegetables in tackling cancers developed in the gastrointestinal system.

Functional bioactive compounds from cruciferous vegetables

Cruciferous vegetables, often called Brassicaceae or mustard family, are commonly consumed globally in the human diet (17, 18). Brassica genus is the most popular among the Brassicaceae family and consists of 37 different species (19). *Brassica oleracea* are the principal Brassica vegetable species including cabbages, broccoli, brussels sprouts, kale, cauliflower, and others. Their cultivars are classified into seven main groups based on morphology and developmental forms: *B. oleracea* "capitata group" (cabbages), alboglabra group (Chinese broccoli or Kai-lan), acephala group (kale and collard greens), botrytis group (broccoflower, cauliflower, and Romanesco broccoli,), italica group (broccoli), gongylodes group (kohlrabi), and gemmifera group (Brussels sprouts) (17). *Brassica rapa* includes turnip, Asian greens, bok choy, Japanese mustard spinach, mizuna, rapini and napa cabbage are also consumed (Nikolov, 2019). Other species of Brassica are *Brassica hirta* (white mustard), *Nasturtium officinale* (watercress), *Amoracia rusticana* (horseradish), *Eruca vesicaria* (arugula), *Lepidium sativum* (garden cress), *Raphanus sativus* (radish), and *Wasabia japonica* (wasabi) (17). Cruciferous vegetables are high in nutrients and secondary metabolites such as sulfur-containing compounds, phenolic compounds, carotenoids, and others, known to have beneficial health properties.

Nutrients

Cruciferous vegetables have high macronutrients and micronutrients (20). Macronutrients are the nutritive components that provide energy and are required to maintain

body functions. The macronutrients of different Brassica vegetables is shown in Table 1. Water is the main component of these vegetables, with ranges 89–92%, while the fiber and fat content are relatively low (6, 8). Brussels sprouts possess high carbohydrates compared to other vegetables (21).

Moreover, cruciferous vegetables are also rich of micronutrients (Table 2) such as minerals (calcium, potassium, magnesium, iron, phosphorus, sulfur, chlorine, sodium, zinc, and selenium) and vitamins (thiamine, riboflavin, niacin, folate, and tocopherol) (22). These vegetables contain calcium in the range of 22–150 mg/100 g. Kale is an important mineral source especially potassium, magnesium, calcium, and iron. On the other hand, kale also contains a high level of vitamin C and folates (19, 23). Broccoli and brussels sprouts comprise potentially useful amounts of nutritionally important minerals. In a fresh state, these vegetables also consist of catalase, peroxidase, and superoxide dismutase enzymes. However, the nutritional constituent of Brassica vegetables depends on diversity, growth environment, time of harvest, processing, and cooking conditions (11).

Sulfur-containing compounds

Among the bioactive compounds in brassica vegetables, sulfur-containing compounds such as glucosinolates are the major constituents (24). Glucosinolates are found in these vegetables in high quantities of 1,500–2,000 μg/g, especially in broccoli, brussels sprouts, and cabbage (19). Glucosinolates are responsible for their spicy taste and pungent odor (25). These compounds are water-soluble anions with the basic structure consisting of a β-D-glucopyranose moiety and β-thioglucoside N-hydroxysulfate with a variable side chain derived from amino acids (26). The glucosinolates are biosynthesized in brassica plants by major three steps of naturally occurring chemical reactions namely, side chain modification, side chain elongation and glucone biosynthesis (8). A small change in the side chain determines its classification, such as aliphatic (e.g., glucobrassicanapin, glucoalyssin, glucoraphanin, glucocapparin, dehydroerucin, glucoerucin, epi-progoitrin, glucoiberin, glucoerysolin, glucolepidin, progoitrin, and sinigrin), aromatic aryl (e.g., glucobarberin, glucotropaeolin, gluconasturtiin, glucosinalbin, and glucosibarin), and aromatic indoles (neoglucobrassicin, glucobrassicin, 4-methoxyglucobrassicin, and 4-hydroxyglucobrassicin) (27, 28). The hydrolysis pathways of glucosinolate can be seen in Figure 1.

Glucosinolates are chemically and thermally stable, but not biologically active until they are hydrolyzed (Figure 1) by the β-thioglucosidase or myrosinase enzymes. This enzyme is released after damage in the plant by chewing or processing such as cutting, chopping, and mixing (19). Upon the plant cells are injured, the thioglucosidic bond breaks down, β-thioglucoside yields a β-D-glucose molecule and thiohydroximate-O-sulfonate

(an unstable aglycone) (29). Then, some breakdown products are formed depending on the pH level and other conditions (30). Hydrolysis of glucosinolates can also occur by gut microbiota action (25, 31). Both glucosinolates and their breakdown products play a large role in the health benefits of cruciferous vegetables. The more common breakdown products (Figure 1) include isothiocyanates (ITC), thiocyanate, amines, epithionitriles, indolic alcohols, nitriles, and oxazolidinethions (Figure 2) (12). The type and concentration of glucosinolates depends on cultivar, cultivation site, genotype, growth conditions, storage conditions, plant stage, preparation and cooking techniques (32). For example in cooking methods, glucosinolate levels were maximized in steaming compared to microwaving, boiling, and pressure cooking (33). Moreover, Casajús et al. found that the content of aliphatic glucosinolates decreased after storing broccoli in the darkness (34).

In a study by Hanschen et al., the formation of glucosinolates and their hydrolysis products of the five *Brassica oleracea* varieties including broccoli, cauliflower, and white, red, as well as savoy cabbages were determined. They reported that broccoli and red cabbage contains highest level of 4-(methylsulfinyl) butyl glucosinolate (glucoraphanin), whereas cauliflower, white cabbage and savoy cabbage mainly rich in 2-propenyl (sinigrin) and 3-(methylsulfinyl) propyl glucosinolate (glucoiberin). The sprouts of white cabbage is a rich source of the hydrolysis products such as epithionitriles or nitriles with 1-cyano-2,3-epithio propane with up to 5.7 μmol/g fresh weight. They also figured out that mini vegetable heads contained the highest concentrations of isothiocyanate (35). Similarly, Bhandari et al. evaluated the profiles of nine Brassica crops (baemuchae, broccoli, cabbage, Chinese cabbage, cauliflower, kale, leaf mustard, pakchoi, and radish) in various tissues: seeds, sprouts, mature roots, and shoots. Their results showed that total glucosinolate levels in most Brassica crops were highest in seeds and lowest in shoots. Aliphatic, indole, and aromatic glucosinolates were highest in the seeds, shoots, and roots tissues in most of the crops, respectively. The highest total glucosinolate levels were observed in seed and sprout of broccoli (110.76 and 162.19 μmol/g), whereas radish exhibited the lowest total glucosinolate levels across all tissues examined. On the other hand, leaf mustard showed the highest total concentration of glucosinolate in shoots (61.76 μmol/g) and roots (73.61 μmol/g) (36).

Carotenoids and tocopherols

Carotenoids are highly pigmented constituents (red, yellow, or orange) and also responsible for the appearance of the cruciferous vegetables (37, 38). These phytochemicals are classified as symmetrical tetraterpenes that possess a C40 backbone structure with conjugated double bonds. A wide range of carotenoids are observed in these vegetables including lutein

TABLE 1   Macronutrients of cruciferous vegetables per 100 g.

Species	Cultivar	Common name	Energy (kcal)	Water (g)	Carbohydrates (g)	Proteins (g)	Fats (g)	Fiber (g)
Brassica oleracea	var. *italica*	Broccoli	34	89.30	6.64	2.82	0.37	2.60
	var. *gemmifera*	Brussels sprouts	43	86	8.95	3.38	0.30	3.80
	var. *capitata*	Cabbage	25	92.18	5.80	1.28	0.10	2.50
	var. *botrytis*	Cauliflower	25	92.07	4.97	1.92	0.28	2.00
	var. *viridis*	Collard greens	32	89.62	5.42	3.02	0.61	4.00
	var. *achepala*	Kale	35	89.63	4.42	2.92	1.49	4.10
Brassica juncea	var. *rugosa* (or *integrifolia*)	Mustard greens	27	90.70	4.67	2.86	0.42	3.20
Brassica rapa	ssp. *rapa*	Turnip	28	91.87	6.43	0.90	0.10	1.80
	ssp. *parachinensis*	Rapini, broccoli rabe	22	92.55	2.85	3.17	0.49	2.70
Raphanus sativus	-	Radish	16	95.30	3.40	0.70	0.10	1.60

TABLE 2   Micronutrients of cruciferous vegetables per 100 g.

Cruciferous plant	Edible part	Minerals (mg)				Vitamins	
		K	Ca	Mg	Fe	C (mg)	B9 (µg)
Broccoli	Inflorescence	316	47	21	0.7	89.2	63
Brussels sprouts	Buds	389	42	23	1.4	85	61
Cabbage	Leaves	170	40	12	0.5	36.6	43
Cauliflower	Inflorescence	299	22	15	0.4	48.2	57
Collard greens	Leaves	-	232	27	-	35.30	-
Kale	Leaves	491	150	47	1.5	120	141
Mustard greens	Leaves	384	115	32	1.64	70	12
Turnip	Root	191	30	11	0.3	21	15
Rapini, broccoli rabe	Leave, stem, flower buds	-	108	0.39	-	20.20	-
Radish	Root	233	25	10	0.3	14.8	25
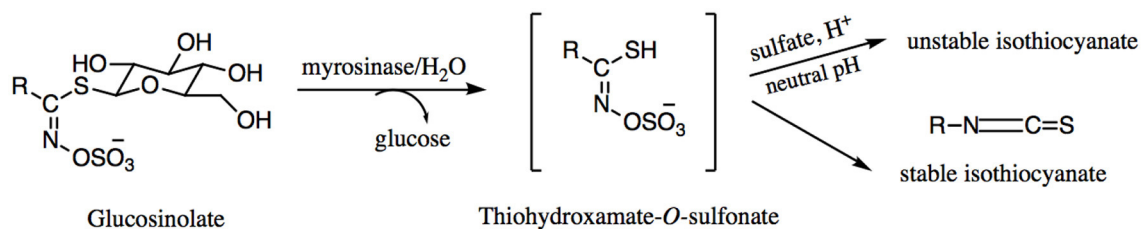
FIGURE 1
Enzymatic hydrolysis pathways of glucosinolate.

(Figure 3) and β-carotene as the predominant ones, followed by α-carotene, γ-carotene, β-cryptoxanthin, and lycopene presenting an antioxidant activity (39). Other carotenoids such as zeaxanthin, cryptoxanthin, neoxanthin, and violaxanthin have also been found in variable amounts (21, 40, 41).

Among the cruciferous vegetables, kale is considered the richest source of carotenoids, exceeding cabbage in about 40 times (18, 42). The main carotenoids present in kale are zeaxanthin and lutein, but important differences were identified among several cultivars of kale (41, 43, 44). Similarly to glucosinolates, the carotenoid accumulations in the brassica family are regulated by the developmental stage, environment, and tissue type (45). Tocopherols and tocotrienols (vitamin E) are lipid-soluble compounds present in cruciferous vegetables
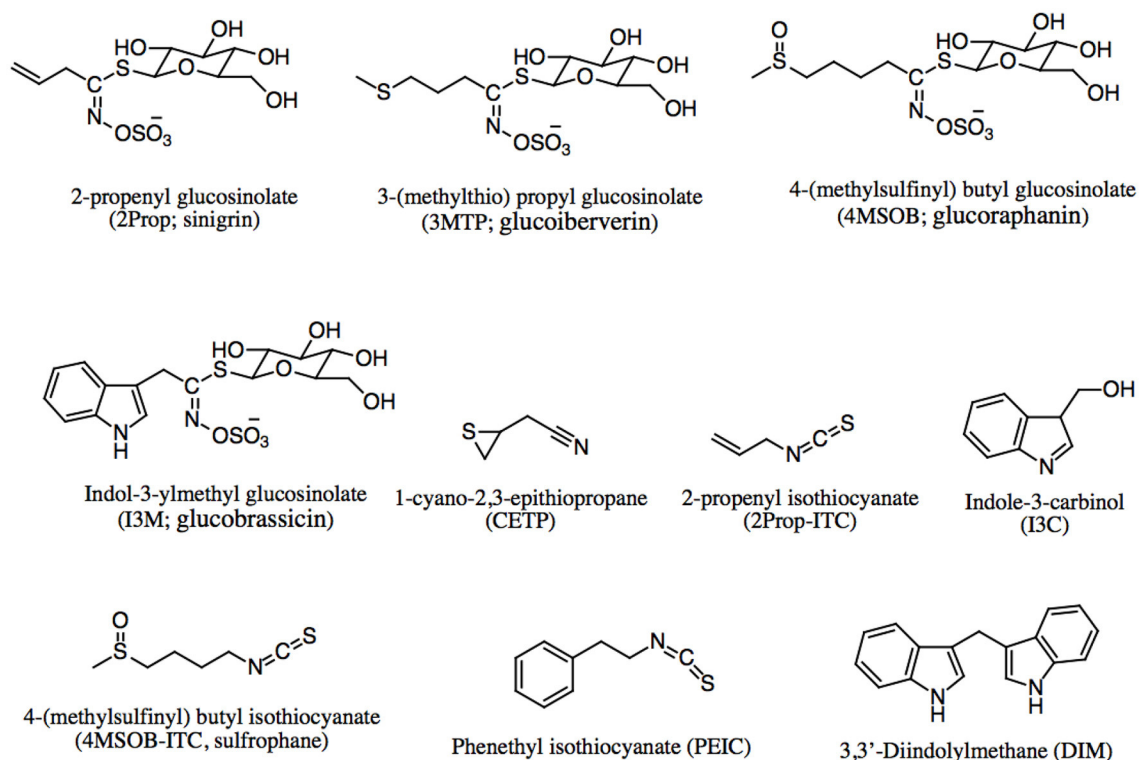
FIGURE 2
Chemical structures of glucosinolate and their breakdown products.

(39). Regarding the main tocopherols, α-tocopherol has been reported, but γ-tocopherols and δ-tocopherols are also detected (46, 47).

Phenolic compounds

Phenolic compounds are ubiquitously distributed bioactive compounds found in most plant tissues, including cruciferous vegetables (10, 48). These compounds are characterized by having at least one aromatic ring and one or more hydroxyl groups bonded directly to the former, showing diversity of structures (49). Their categorized based on the number and arrangement of carbon atoms in flavonoids (flavones, flavonols, flavanones, flavan-3-ols, isoflavones, and anthocyanidins) and non-flavonoids (phenolic acids, hydroxycinnamates, and stilbenes) (48, 50–52). Cruciferous vegetables possess antioxidant activity attributes to the high contents of phenolic compounds (53, 54). The most important phenolic constituents (Figure 4) present in cruciferous vegetables are the hydroxycinnamic acids and the flavonoids such as kaempferol, isorhamnetin, quercetin, and rutin (11, 18).

The profile of phenolic compounds vary significantly among species. In studies carried out by Upadhyay et al.,

red cabbage presented high contents of rutin (102.14 μg/g of fresh weight) compared to green cabbage (1.34 μg/g of fresh weight) and cauliflower (39.07 μg/g of fresh weight). The sinapic acid content of red cabbage, broccoli, cauliflower, and green cabbage are 30.20, 7.37, 4.66, and 3.52 μg/g of fresh weight, respectively. They also detected that broccoli had a high content of gentisic acid (83.17 μg/g of fresh weight), followed by cauliflower and green cabbage with values of 35.50 and 2.50 μg/g of fresh weight, respectively (55). Furthermore, Li et al. identified 74 phenolic compounds of 12 different cruciferous vegetables, including 58 flavonoids and 16 hydroxycinnamic acids and their derivatives using ultra-high performance liquid chromatography-quadrupole time-of-flight mass spectrometry (UHPLC-Q-TOF-MS/MS). Among the flavonoids, the main compounds found were kaempferol, isorhamnetin, and glycosylated quercetin. The main hydroxycinnamic acids were caffeic, ferulic, sinapic, and p-coumaric acids. Emphasizing that the cauliflower and cabbage presented high contents of flavonoids (5.70 mg/g dry weight) and hydroxycinnamic acids (46.02 mg/g of dry weight) (48, 56, 57).

Another group of phenolic compounds frequently detected in Brassicaceae vegetables is anthocyanins (18). They are responsible for pigmentations of red cabbage and purple
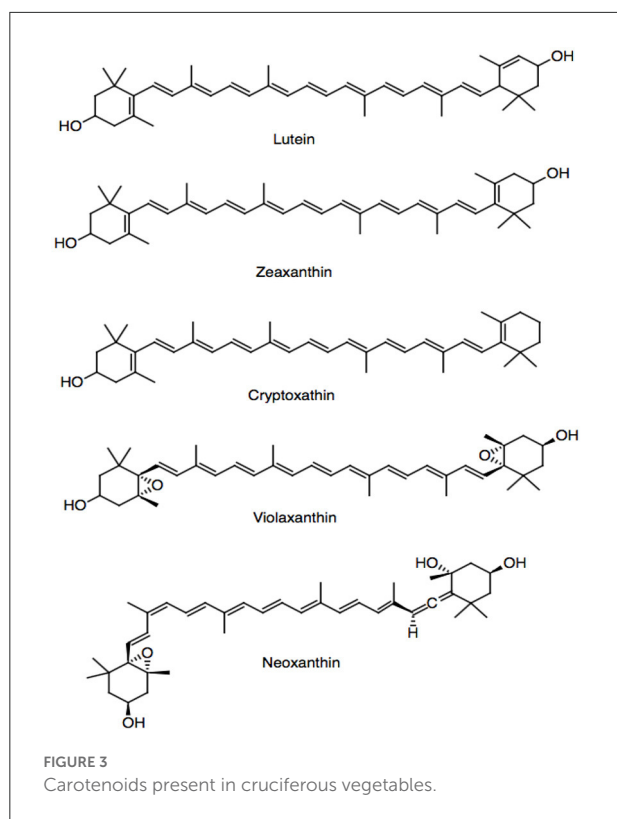
cauliflower. The common anthocyanins in Brassica crops are cyanidin, delphinidin, pelargonidin, petunidin, peonidin, and malvidin (21, 58). Broccoli sprouts and red cabbage contain mainly cyanidin glucosides derivatives (59). Red radish contains mainly cyanidin and peonidin anthocyanins acylated with aromatic acids (60).

Others

Phytosterols are other compounds found in cruciferous vegetables (21). They are steroid alcohols with a molecular nucleus of 17 carbon atoms and a characteristic three-dimensional arrangement of four rings. *Brassica napus* L., known as rapeseed, is the rich source of phytosterols among cruciferous vegetables, with yields of up to 9.79 g/kg oil (18, 61). In addition, *Brassica juncea* is also the most abundant natural source of phytosterols (62).

Brassicaceae family containing phytoalexins possess an indolic ring with C3 substitutions with N and S atoms (63, 64). Phytoalexins are produced from brassinin, which confers a unique structure among other vegetables (64). They have been identified in *Brassica juncea, Brassica napus, Brassica oleracea, Sinapis alba, Raphanus sativus, and Wasabi japonica* (18, 65). Furthermore, fatty acids such as palmitic, stearic, oleic, linoleic,

linolenic, eicosenoic, erucic, arachidic, arachidonic, and behenic acid also present in the oil extracted from Brassica crops (66).

Pathophysiology of p53 family in gastrointestinal cancers: Current status

As the "guardian of the genome," the p53 family (p53, p63, and p73) plays a critical role in preventing the development of cancers associated with DNA damage (67). Following the activation of the p53 family by a number of cellular stress (e.g., oncogenes, oxygen deficiency in the blood, radiation, and oxidative stress), several mechanisms are activated as the mitigating system toward the affected DNA i.e., cell cycle arrest, apoptosis, and senescence (68). Given the crucial role of p53 in suppressing cancer development, mutations causing dysfunctionality of p53 put the body in danger. Mutations occurring in the p53 family have been found in more than half of human cancers (1). Of this figure, p53 family-related mutations are detected in more than 50% of gastrointestinal cancer cases (69). It has been demonstrated that most p53 mutations are identified as missense mutations with DNA-binding domain (DBD) as the main site for the mutations (67).

The three members of the p53 family are encoded by p53, p63, and p73 genes located in different chromosomes i.e., 17p13, 3q27-29, and 1p36, respectively (69). Nevertheless, they share the high identity of amino acid sequence in the main three structural domains namely transactivation (TAD), DBD, and oligomerization domains (OD) (68). The former domain is responsible for regulating the transcription activity of p53 by providing the binding sites for either positive or negative regulators of p53. Further, as the central domain, the DBD is important for binding to response elements of various target genes. Finally, the latter domain acts as the main site for DNA alternative splicing and post-translational modification. In the normal physiological condition, the expression of p53 in the cell is very low. Upon the exposure of the aforementioned cellular stress to the cells, p53 upregulates the expression of its main negative regulator namely murine/human double minute 2 (MDM2) which provides a negative feedback mechanism to maintain the minute levels of p53 in normal cells (68).

p53 and apoptosis

As stated above, activation of p53 could induce apoptosis through either the intrinsic or extrinsic pathways. While the former pathway involves the role of mitochondria, the latter apoptotic pathway is induced by death receptors (DRs) (70). Molecularly, the intrinsic pathway of apoptosis is initiated by the upregulation of several B-cell lymphoma-2 (Bcl-2) pro-apoptotic proteins (e.g., Bax, Bak, Noxa, and PUMA) and
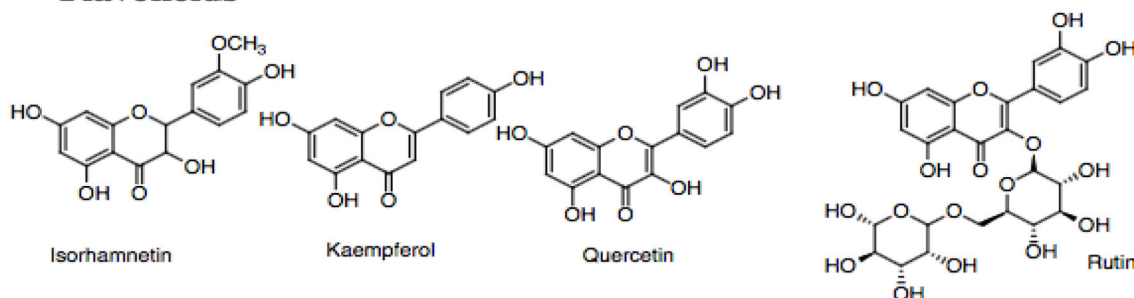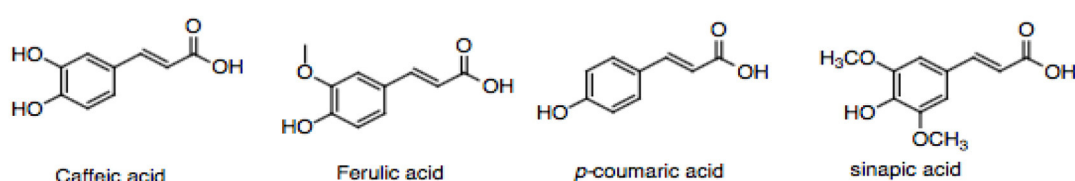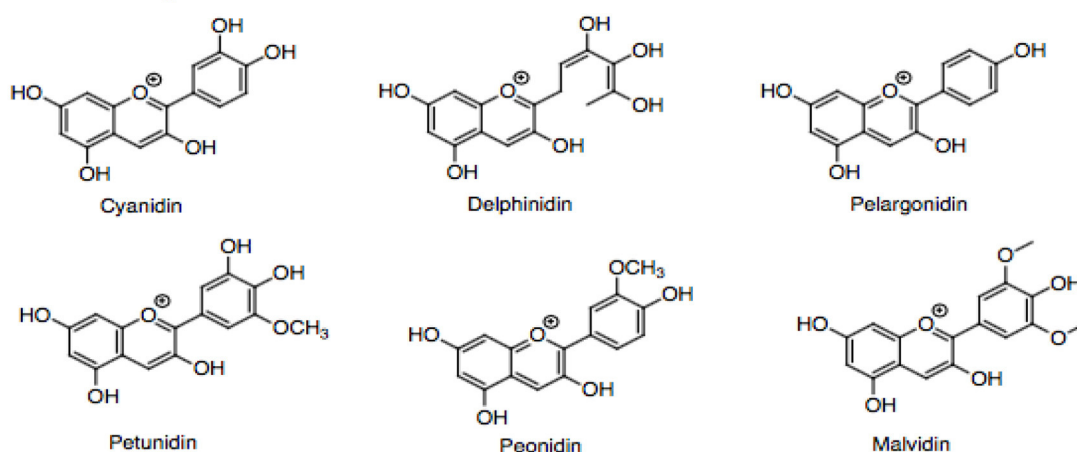
FIGURE 4
Phenolic compounds present in cruciferous vegetables.

downregulation of Bcl-2 pro-survival proteins (e.g., Bcl-2, Bcl-w, and Bcl-XL) (71). Upon cellular stress, Bax and Bak experience oligomerization leading to the release of cytochrome c from the intermembrane space of mitochondria to the cytosol (72). As a response to the release of cytochrome c, oligomerization of the apoptotic protease activating factor-1 (APAF-1) occurs followed by the formation of apoptosome complex. This complex recruits and activates pro-caspase-9, an initiator caspase of the intrinsic apoptotic pathway, which is subsequently followed by the induction of several executioner caspases, mainly caspase-3 (73).

The extrinsic pathway of apoptosis involves the role of the superfamily of tumor necrosis factor receptors (TNFRs), also known as DRs, such as TNFR1, DR3, DR6, CD4 (TRAIL-R1), CD5 (TRAIL-R2), and CD95 (67, 74, 75). These receptors are characterized by the presence of the "death domain" in their structure located in the cytoplasmic region. Upon binding of the appropriate ligand to the DRs, several adaptor proteins are activated followed by the recruitment of the caspase-8 and caspase-10 known as the initiator caspases. Eventually, this cascade activates caspase-3 resulting in the occurrence of apoptotic events (74).

p53 and cell cycle arrest

Another mechanism exerted by p53 as a response to cellular stress is the activation of cell cycle arrest. This mechanism acts as the checkpoint in which the cell is evaluated, checked, and repaired if there is damage, before moving to the other phases in the cell cycle. It has been known that the cell cycle is delicately regulated by cyclins. These proteins exert their actions on controlling the cell cycle through their interaction with another protein belonging to the cyclin-dependent kinases (CDKs) family (68). The activation of these proteins is essential for driving the cell cycle. Conversely, the inhibition of the CDKs could stop the cell cycle so that no cellular duplication and division occurs which is important in blocking the progression of cancer cells. At this point, the involvement of p21 is crucial as this protein could inhibit the CDKs. It has been demonstrated that p53 could induce the activation of p21 following cellular stress exposure. In addition to p21, other target genes of p53 are involved in facilitating cell cycle arrest. Some of those genes are 14-3-3σ, GADD45, and retinoblastoma protein (Rb) (67).

p53 and senescence

Senescence is a form of cell cycle arrest that can be induced upon exposure to various stimuli either exposed endogenously or exogenously (76). The senescent cells can be characterized by their bigger size, a significant abundance of nucleoli and vacuoles compared to the normal cells (77). Cellular senescence could also be induced following the activation of p53 through several related target genes e.g., p21, p16-Rb, and BTG2 (67, 76, 78). Compared to the previously described p53-related mechanisms, apoptosis and cell cycle arrest, senescence also plays a pivotal role in preventing the progression of cancerous cells.

Other p53 mechanisms in preventing cancerous events

In addition to these three main mechanisms of p53, other functions of p53 have also been deciphered. Those functions include p53 involvement in preventing cancer migration and metastasis, angiogenesis, cellular metabolism, oxidative stress, drug resistance, inducing autophagy, and promoting genomic stabilization (67, 79–84). Taken together, all of these mechanisms are crucial for preventing the genome from being cancerous.

p53 mutations in gastrointestinal tract and associated cancers

As stated above, p53 mutations are found as the most mutated gene in many types of cancers, including cancers

TABLE 3　Several common codons that are vulnerable to cellular stress leading to missense mutations (68).

Exon (Codon)	Missense mutation	Amino acid change
5 (175)	Guanine → Adenine	Arginine → Histidine
7 (245)	Guanine → Adenine	Glycine → Serine
	Guanine → Adenine	Glycine → Aspartic acid
7 (248)	Cytosine → Thymine	Arginine → Tryptophan
	Guanine → Adenine	Arginine → Glutamine
8 (273)	Cytosine → Thymine	Arginine → Cysteine
	Guanine → Adenine	Arginine → Histidine
8 (282)	Cytosine → Thymine	Arginine → Tryptophan

developed in the gastrointestinal tract, such as colorectal cancer (85, 86). p53 mutations can be detected in 34% of colon cancers occurring in the proximal area and in 45% of those occurring in the distal area of the colon (87). In addition to p53 genes, a number of other genes also experience mutations in colorectal cancer. However, a study conducted by Wood and co-workers indicated four other commonly mutated genes i.e., KRAS, APC, PIK3CA, and FBXW7 (86).

Furthermore, p53 mutations in colorectal cancer mainly occur in exon 5 to exon 8 in the DBD (p53 has 11 exons and 10 introns) (88). Throughout these vulnerable exons, several codons have been identified as the preferred sites of mutations (Table 3). For example, in exon 5, a missense mutation in codon 175 causes the failure to produce arginine. As a result, the codon is translated into histidine. This mutation occurs as codon CGC is changed into CAC. Another example is exhibited by missense alteration occurring in codon 282 in exon 8 where codon CGG (arginine) is changed into TGG (tryptophan) (68). Some other codons that are commonly vulnerable to mutations are codons 245, 248, and 273.

These data emerge other interesting questions. For example, why these exons and codons become the preferred sites of p53 mutations and why specific amino acid (e.g., arginine) seems to have higher vulnerability over the other amino acids (68). It has been demonstrated that p53 mutations are closely associated with several events leading to the malignancies. p53 mutations have a clear association with the emergence and development of cancer. Lopez et al. found that p53 mutations can be detected in more than 50% of colorectal cancer occurring sporadically (89). Not only, colorectal cancer, p53 mutations are also identified in high percentage in other types of gastrointestinal cancers. It is estimated that p53 mutations are involved in up to 77% of stomach cancer (90).

In addition, as in the other cancers, p53 mutations also show a close correlation with the progression and invasiveness of gastrointestinal cancer. One example is given by Russo et al. found that p53 mutations were closely linked to the invasiveness of colorectal cancer which is related to its ability to reach

lymphatic and blood circulation providing a great chance to be metastatic to the other parts of the body (87).

p53 limits the effectiveness of anticancer drugs

Most importantly, p53 mutation could diminish the effectiveness of chemotherapeutic agents (e.g., doxorubicin, temozolomide, tamoxifen, and gemcitabine) (80). Several mechanisms have been proposed to explain the emergence of this drug resistance (91, 92). p53 mutation could inhibit the entry of the chemotherapeutics so that the intracellular level of the drugs is inefficient in exerting their anticarcinogenic activities. Another proposed mechanism is related to the overexpression of ABC transporters, such as ABCB1 (p-glycoprotein) in cancerous cells, making the efflux of the drugs occurs extensively. The increased drug metabolism is also observed in p53 mutation which eventually causes extensive inactivation of the chemotherapeutics (91). Another study found that this effect was associated with the failure of the mutant p53 in upregulating PUMA expression (93). Although this study was only focused on colon cancer, this finding might correlate with the other types of cancer and provide a new insight for tackling mutant p53-related chemoresistance.

Molecularly, the involvement of the Wnt signaling pathway and epithelial-mesenchymal transition (EMT) in mediating pro-carcinogenic effects of the mutated p53 have attracted much interest. It has been found that proliferation, invasiveness, and development of colorectal cancer are facilitated by the upregulation of Wnt and EMT genes (94, 95). In the normal states, p53, in collaboration with microRNA-34, acts as a suppressor of the Wnt signaling pathway (94). A more recent study carried out *in vivo* investigating gastric cancer suggested that dysfunctionality of the wild-type p53 was accompanied by induction of Wnt and EMT. Also, this study found that loss of p53 function was negatively correlated with cyclooxygenase-2 (COX-2) levels indicating the role of inflammation in the progression of gastrointestinal cancer (96). In sum, the inhibition of these pathways (Wnt, EMT, and COX-2) might be useful in the effort of developing new chemotherapeutic agents.

Drug candidates acting in p53 pathways

MDM2 inhibitors

Several drug candidates have been developed with promising potency in tackling the pro-carcinogenic effects of the mutated p53, especially in gastrointestinal cancers. The candidates working in inhibiting MDM2 activity may be the most attractive approach (97). As previously stated, MDM2 is the negative regulator of p53. It binds to the N-terminal of p53 initiating ubiquitination of the protein resulting in p53 degradation. It

means that the excessive activity of MDM2 could lead to the significant inhibition of p53. As a result, this affects the tumor-suppressive function of p53. Conversely, inhibition of MDM2 could stabilize p53 protein (98).

Recently, several candidates with anti-MDM2 activities have been found and developed. Of those, MI-43 and nutlins are the most potent candidates. It has been reported that the former candidate has the ability to antagonize the action of MDM2 on p53. As a result, MI-43 could induce p53 accumulation leading to the activation of its target genes, such as p21, Noxa, and PUMA (99). A study reported that MI-43 could induce cell cycle arrest and apoptosis in colon cancer (100). Nutlins also have the ability to stabilize p53 by inhibiting MDM2 activity. Among the other Nutlins, Nutlin-3 activity in antagonizing MDM2 has been reported in the literature. In colorectal cancer, Nutlin-3 binds to the MDM2 pocket so that it disturbs the interaction between MDM2 and p53. As a result, p53 is stabilized and its downstream target genes are activated. However, it is noteworthy that Nutlin-3 has a great affinity only in MDM2, but not in the other members of the MDM family, such as MDMX. Consequently, cancer cells expressing abundant MDMX cannot be an appropriate target for Nutlin-3 (101).

Another MDM2 inhibitor with potential use in suppressing the growth of colon cancer is RITA (reactivation of p53 and induction of tumor cell apoptosis). Unlike the other MDM2 inhibitors that have been described above, this candidate binds directly to p53 instead of MDM2. This binding leads to the conformational change of p53 resulting in the interference with MDM2-p53 interaction (102).

Candidates targeting p63 and p73 genes

As stated previously, in addition to p53, the p53 family has two other proteins, p63 and p73. It has been demonstrated that targeting these members of the p53 family could be a promising strategy in developing anticancer drugs. For example, a derivative of ellipticine (a plant alkaloid), NSC176327, could kill the cancerous cells of colorectal cancer which is independent of p53 status. Also, this derivative could activate p73 and the target genes of the p53 family (e.g., p21 and DR5). Further, the loss of the p73 function plays a significant role in the emergence of chemoresistance (47).

Reactivator of mutant p53

Reactivation of mutant p53 is another strategy developed in the effort of seeking anticancer drugs. PRIMA-1 (p53-reactivation and induction of massive apoptosis-1) is an example of drugs utilizing this strategy (103). Reactivation of the mutated p53 by PRIMA-1 is linked to its covalent binding in DBD resulting in the restoration of a certain sequence in the core domain (104). Eventually, activation of p53 target genes in the cancer cells occurs. A more recent study reported the use of polysaccharides isolated from Ganoderma lucidum as an agent

for restoration of the suppressive action of the mutated p53 in colorectal cancer (105).

Relationship between compounds of cruciferous vegetables and p53 family in gastrointestinal tract and associated cancers

Many biological activities, such as DNA repair, cell cycle arrest, and apoptosis, depend on the tumor suppressor p53 (106). Approximately 50% of all malignancies in humans have p53 mutations (106). The majority of p53 mutations occur in the central core DNA-binding domain (DBD), which substantially impairs p53's ability to bind DNA and prevent tumor growth. Mutant p53 reduces the DNA-damage response and increases the resistance of tumor cells to drug-induced apoptosis (107). Additionally, there is evidence that suggests mutant p53 causes cancer by gaining function by transactivating genes related to growth or by silencing particular target genes (107). Increased tumorigenicity in nude mice and improved soft agar plating efficiency are both results of mutant p53 overexpression in deficient cells (107). In addition, p53 point mutation-carrying animals develop tumors and spread them more frequently than p53-deficient mice (108). Li-Fraumeni Syndrome, a germ-line p53 mutation, dramatically raises the chance of developing cancer in humans (108). Therefore, eliminating mutant p53 may present a viable strategy for cancer therapy and prevention. Cruciferous vegetables compounds have the capacity to arrest the cell cycle or induce apoptosis in cells by activating p53. For instance, carotene promotes the production of p53, p21, and BAX in cancer cells, which are all tumor suppressors (109). Activation of p53 and its targets p21, BAX, and RPRM led to the observation of the induction of cell cycle arrest when combined with bixin and canthaxanthin (110, 111). Apoptosis was seen in breast and bladder cancer cells after treatment with beta-carotene, phenethyl isothiocyanate, and allicin (112–114). The activation of BAX, Bcls, SAS, PERP, and LRDD resulted in this apoptosis, which was dependent on the protein p53. Natural compounds may be used to target these signaling pathways, ultimately halting the growth of cancer. For instance, astaxanthin, lycopene, and isothiocyanates, individually, have been found to induce p53-mediated apoptosis. The ERK, PI3K/Akt, and p21WAF1 pathways were activated in order to do this (115–117). Pharmacologically, therefore, MDM2 inhibition has become a promising mechanism utilized by a drug to exert its anticancer activity (118). Growth factors also play a crucial role in the development of cancer, including insulin-like growth factor (IGF), PDGF, EGF, tumor growth factor (TGF), FGF, and colony-stimulating factor (CSF). These substances stimulate signaling pathways, which in turn promote increased cell proliferation, block apoptosis, and allow cancer cells to invade healthy cells. Numerous downstream signaling pathways,

including PI3K-AKT, Ras-MAPK, and others, are activated as a result of growth factor receptor activation (119). Additionally, it has been shown that isothiocyanates interact with the bladder epithelium and activate the cytoprotective enzymes GST and NQO1, which are known to detoxify carcinogens. Curiously, NQ01 has also been demonstrated to stabilize the p53 tumor suppressor. Additionally, it was shown that the bladder is one of the most receptive tissues to the activation of these enzymes by broccoli sprout extracts, suggesting that it may be particularly useful for guarding the bladder against the development of cancer (108). On the other side, angiogenesis makes cancer cells more resistant to the effects of chemotherapy and radiation while also playing a crucial role in the development, spread, and starts of cancer. In HUVEC, capillary tubes' ability to survive, migrate, and develop was diminished by both quercetin and benzyl isothiocyanate (120, 121). They also have success reducing the expression of angiogenic and metastatic markers. Additionally, it has been shown in a number of malignancies that methylation of the promoter regions of tumor-suppressor genes silences those genes (122). In addition, methylation of certain genes has been linked to resistance to radiation and chemotherapy (119). The suppression and reversal of the DNA methylation process may be one of the mechanisms by which natural substances exert their chemopreventive impact. In order to repair damaged DNA, it has been suggested that fucoxanthin and sulforaphane may inhibit and reverse DNA methylation, increase histone acetylation, and modify the structure of chromatin (123, 124). In summary, Crusiferous vegetable chemicals led to an increase in the tumor suppressor p53 protein level and transcriptional activity, which was accompanied by an increase in the levels of p21WAF1 and Bax, two of p53's transcriptional targets. Despite the fact that p21 is increased during p53-mediated G1 arrest, this occurrence does not lead to p53-induced apoptosis. The Bax/Bcl-2 ratio was altered by the p53-dependent increase in Bax expression, which also coincided with the activation of caspases 9 and 3 and PARP cleavage (109). Bax siRNA transfection of cells reversed these effects and prevented death, but it had no impact on the buildup of G1 cells. In conclusion, we suggest that p53-dependent pathways play a major role in cruciferous vegetable compound-mediated growth arrest and apoptosis. The area of the current investigation was to determine the function of p53 in cancer prevention and to clarify how it contributes to cell cycle arrest and apoptosis caused by Cruciferous vegetables compounds.

Functional ingredients as therapeutics against gastrointestinal tract and associated cancers (pre-clinical findings)

Gastrointestinal (GIT) cancers, including those of the esophagus, stomach and colon, are closely associated with

lifestyle factors, particularly diet (125). Dietary variables are thought to be responsible for one-third of all cancer deaths. A diet high in cruciferous vegetables like brussels sprouts and broccoli is linked to a lower risk of several cancers of gastro-intestinal tract (GIT). It has been found that cruciferous vegetables protect against GIT cancers more effectively than a diet rich in fruits and vegetables. p53 is a transcription factor that inhibits tumor growth and suppresses tumor growth. This protein regulates a wide range of physiological processes, including cell signaling, DNA damage response, genomic integrity, cell cycle regulation, and apoptosis. To stop cancerous or damaged cells from multiplying, p53 activates genes such as p21WAF1 and Bax, which in turn activate the apoptotic pathway. A lack of p21, a regulator of cell division, is caused by a failure of p53 to bind DNA, and lead to unchecked cell proliferation resulting in tumors (126). The tumor suppresses p53 during cancer cell growth (either silenced or mutated). In order to control cancer cell development, angiogenesis, and cancer cell migration, p53 must be expressed in cancer cells (127).

Gastric cancer

Isothiocyanates (ITCs), a hydrolysis product of glucosinolates present in cruciferous vegetables, are chemoprotective compounds synthesized by the enzyme myrosinase. Gastric cancer may benefit from the use of potential ITCs such as PEITC (phenethyl isothiocyanate), BITC (benzyl isothiocyanate), and SFN (sulforaphane) (128, 129). An anticancer possibility for gastric cancer has been examined using the nontoxic indole derivative 3,3'-Diindolylmethane (DIM) from cruciferous vegetables (130). It was observed that DIM inhibits gastric cancer growth *in vitro* and *in vivo*, depending on the dose, by Ye et al. (131). By stimulating the Hippo signaling system, DIM slowed the growth of gastric cancers in a xenograft mouse model, according to Li et al. Reduced synthesis of CDKs (cyclin-dependent kinases) 2, 4 and 6, as well as cyclin D1, allowed for G1 cell cycle arrest while increasing levels of p53 protein (132). Studies on laboratory animals have shown that carotenoids (lycopene, lutein, and β-carotene) prevent the formation and growth of chemotherapeutically produced gastric tumors (133, 134). There was an investigation into the effects of oral lycopene supplements in ferrets by Liu et al., who found that the p53 gene, its target genes (p21Waf1/Cip1 and Bax-1), and gastric mucosal cell proliferation and apoptosis were all affected by lycopene supplementation (135). Bax (Bcl-2 family member) and P21waf1/cip1 (CDK inhibitor) are both critical for apoptosis and G1 cell cycle arrest, respectively. p21waf1/cip1 and Bax-1 act together as mediators for the enhancement of p53-dependent necrosis (136). There was a 9-week experiment in which ferrets were exposed to cigarette smoke and given either modest or high dosages of lycopene

supplementation. Ferrets given lycopene alone had significantly more lycopene in their gastrointestinal mucosa than ferrets given lycopene, and exposed to smoke, a finding that was dose-related (Figure 5). Lycopene dramatically reduced both the smoke-induced total p53 and phosphorylated p53 levels in ferrets that had recently been exposed to smoke, regardless of the level of total p53 and phosphorylated p53. In ferrets exposed to smoke alone, cell death indicators such p21 (Waf1/Cip1), Bax-1, and cleaved caspase 3 were significantly reduced, whereas lycopene dose-dependently mitigated the effects of smoke on these same markers as well as cyclin D1 and PCNA (Table 4) (135). Reactive oxygen species (ROS)-induced phosphorylation of p53 at serine 15 improves p53 accumulation and activation to prevent stomach cancer (159). It is possible to induce apoptosis in gastric cancer cells by activating p53 and upregulating the transcription of key target genes such as p21 (which is involved in cell cycle arrest) and pro-apoptotic BH3-only Bcl-2 family proteins, such as Bad, Noxa, BH3 interacting domain death agonist (Bid), and Bcl-2-like protein 11 (Bim; activator of BH3). Anti-apoptotic proteins like Bcl-2 and Bcl-2xL can be rendered inactive by the BH3 protein, a BH3-only sensitizer. There is a competition for the binding of BH3-only proteins like Bax and Bak, which results in their displacement from anti-apoptotic proteins like Bax and Bak (160).

Small intestine cancer

The presence of ITCs, particularly BITC, has been linked to a lower risk of small intestine cancers or cancer consequences in people who eat cruciferous vegetables. Cruciferous vegetables may contain ITCs that may be useful in the treatment of small intestinal malignancies, including BITC, PEITC, and SFN (128, 129). Thioredoxin reductase (TR), a selenoprotein that lowers thioredoxin and controls cell development by providing the reducing power for p53 and the redox cycling of endogenous antioxidants including vitamin C, lipoic acid, and niacin, can be made more active by ITCs and carotenoids present in cruciferous vegetables (Figure 4) (141). Apoptosis of cancer cells can be induced by increasing the expression and stability of the cell-killing protein p53, as well as PEITC and sulforaphane's role in p53 stabilization and nuclear localization (141, 142). Jang et al. and Shin et al. reported that carotene can promote apoptosis in intestinal cellular epithelium by boosting p53 and lowering Bcl-2, which is anti-apoptotic (Figure 5) (133, 161). Kim et al. conducted an *in vitro* investigation to evaluate the mechanism of astaxanthin's anticancer effects on small intestine carcinoma cell lines. Astaxanthin slowed down the growth of small intestinal cancer cells. The phosphorylation of extracellular signal-regulated kinase (ERK) was suppressed, and the expression of p53 was shown to rise as a result (Table 4) (117).
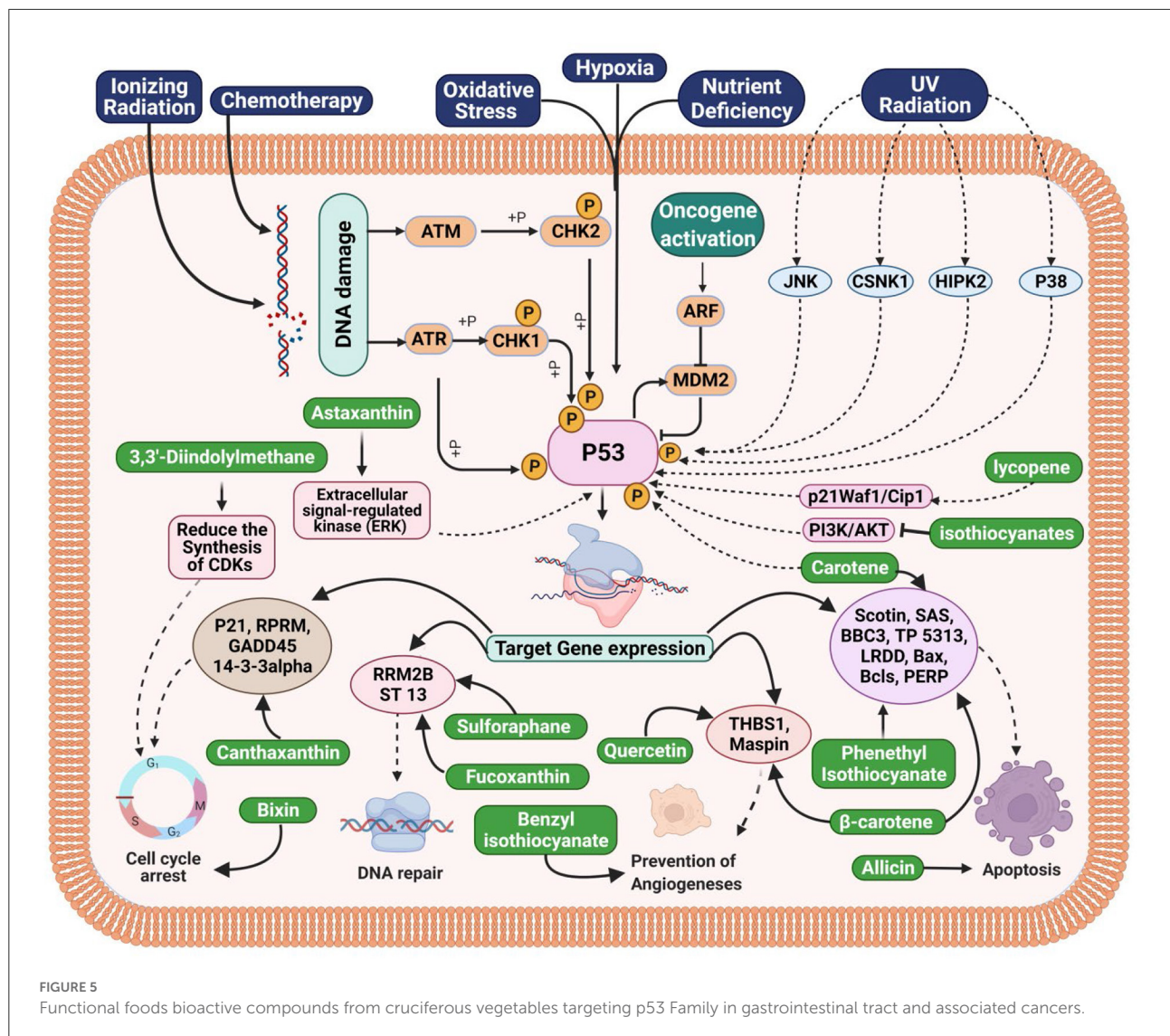
TABLE 4 Functional ingredients from cruciferous vegetables in gastrointestinal tract and associated cancers.

Gastrointestinal cancer types	Functional ingredients	Study model	Doses	Findings	References
Gastric cancer	Curcumin	*In vitro* (SGC7901, BGC823, MGC803 and MKN1 cell line)	50–100 µM	Efficient chemo sensitizing effect and also inhibits viability, proliferation, and migration of gastric cancer cells mainly	(137)
	Quercetin	Human model	3.89–6.02 mg/day	Inhibited cell growth and induced apoptosis, necrosis, and autophagy	(121)
	Allicin	*In vitro* (SGC-7901 cancer cells)	15–120 µg/ml	Apoptotic activity	(112)
	β-carotene	Human cell line	0–6.2 µg/dl	Reduced risk of gastric cancer	(113)
	Isothiocyanate	Human model	0.1 µmol/L.	Effective in protecting against gastric cancer, particularly among those who were lack of genes GSTMI (glutathione S-transferase M1) and GSTTI (glutathione S-transferase T1)	(138)
	Sulforaphane	Gastric cancer stem cells (CSCs)	0, 1, 5, 10 µM	Inhibitory action of sulforaphane on gastric CSCs *via* suppressing Sonic Hh pathway	(139)
	Thioredoxin reductase (TR)	Human model	7.34 U/mL	Threshold of TrxR activity was distinctive in the diagnosis of different tumor types	(140)
	Astaxanthin	Human gastric adenocarcinoma cell lines (AGS, KATO-III, MKN-45, and SNU-1)	0, 10, 50, and 100 µM	Astaxanthin inhibits proliferation by interrupting cell cycle progression in KATO-III and SNU-1 gastric cancer cells	(117)
	Benzyl isothiocyanate	AGS human gastric cancer cells	0, 0.25 and 0.5 mM	Inhibit migration and invasion of human gastric cancer AGS cells	(120)
Small Intestine cancer	Phenyl isothiocyanate	Human model	0.2–25 mmol/L	Isothiocyanate exposure may reduce the risk of colorectal cancer	(114)
	Thioredoxin reductase (TR)	Human model	-	Controls cell development by providing the reducing power for p53 and the redox cycling of endogenous antioxidants	(141)
	Sulforaphane	GC cell lines	0–22.5 µM	Role in p53 stabilization and nuclear localization	(142)
	Astaxanthin	Small intestine carcinoma cell lines	0, 10, 50, and 100 µM	Interrupting cell cycle progression	(117)
	Curcumin	Mice model	1,000 mg/kg	Suppressed Nrf2-Dependent Genes in Small Intestine	(143)
	Quercetin	Mice model	2% in diet	Anti-tumor activity in the small intestine	(144)
	Benzyl isothiocyanate (BITC)	Rat Model	400 P.P.M	Promising chemopreventive agents for human intestinal neoplasia	(145)
	Sulforaphane	Mice model	300 and 600 p.p.m.	Developed significantly less and smaller polyps with higher apoptotic and lower proliferative indices in their small intestine	(146)
Colon cancer	Isothiocyanate	Colon cancer cell lines	2.5 mM	Block the (PI3K)/AKT-dependent survival pathway of colon cancer cell lines, while stimulating the p53 pathway	(116)
	BITC	HCT-116 cells	50 µM	Capable of ameliorating the inflammation associated with colon cancer	(116)
	Sulforaphane	HCT116 colon cancer cells		DNA repair protein causes DNA damage in colon cancer cells	(123)

(Continued)

TABLE 4 Continued

Gastrointestinal cancer types	Functional ingredients	Study model	Doses	Findings	References
	PEITC	HT29 colon cancer cells	10–50 μM	Have anti-metastatic and anti-inflammatory effects against colon cancer	(147)
	3,3′-diindolylmethane (DIM),	Colon cancer HT29 cells	100 μM	Cytotoxic effects	(148)
	β-carotene	Human models	-	Increase Bax and P53 levels in malignant colon cells while decreasing Bcl-2 levels	(149)
	Astaxanthin	HCT-116 colon cancer cells	5–25 μg/ml	Increase of p53, p21WAF-1/CIP-1 and p27 expression (220, 160, 250%, respectively) was observed, concomitantly with a decrease of cyclin D1 expression (58%) and AKT phosphorylation (21%).	(150)
	Bixin	CRC cell lines	0-80 μM	Inhibit the CRC cell proliferation and survival	(111)
	β-cryptoxanthin	Human models	-	Enhances the antitumoral activity of oxaliplatin through δnp73 negative regulation in colon cancer	(151)
	Lycopene	Colon cancer HT-29 cells	2, 5, 10 μM	Inhibited cell proliferation in human colon cancer HT-29 cells	(115)
Hepatic and Pancreatic cancer	Bixin	Hep3B cell	5-50 μg/ml	Cell growth inhibition	(110)
	Quercetin	PANC-1	0, 10, 25, 50, 100, or 200 μM	Shows significant pro-apoptotic effects	(152)
	Curcumin	Hepatic cancer human models	-	Inhibited MMP-9 secretion in HCC (CBO140C12) cells, and repressed the adhesion and migration of fibronectin and laminin	(153)
	β-cryptoxanthin	Human models	-	Decreased significantly with increased prevalence of Leiden mutation (as a genetic factor) in patients before the clinical manifestation of histologically different GI cancer	(154)
	Lycopene	Hep3B human hepatoma c	-	Induced G0/G1 arrest and S phase block and inhibited cell growth in a dose-dependent manner by almost 40%	(155)
	Astaxanthin	HepG2 hepatoma cells	25 and 42 μM	Arrest induction at G0/G1 phase	(156)
	Fucoxanthin	Mice models	488.8 mg Fx/kg bw	Mediates the suppression of the CCL21/CCR7 axis, BTLA, tumor microenvironment, epithelial mesenchymal transition, and adhesion	(124)
	Isothiocyanate sulforaphane	MIA PaCa-2 and PANC-1.	10 μmol/L sulforaphane.	Sulforaphane Suppressed Growth and Triggered Activation of Caspase-3- and Caspase-8-Dependent Cell Death	(157)
	BITC	Mice model	0.5 μmol/L in plasma	BITC-treated mice showed 43% less tumor growth	(158)

FIGURE 5
Functional foods bioactive compounds from cruciferous vegetables targeting p53 Family in gastrointestinal tract and associated cancers.

Colon cancer

Oncogenes including K-ras and adenomatous polyposis coli (APC), as well as tumor suppressor genes like Smad4 and p53, have a critical role in colon cancer formation (162, 163). PI3K/AKT/mTOR pathway and p53 pathway abnormalities are the most prevalent anomalies in most colon cancer cells (164, 165). Blocking the phosphatidylinositol-3-kinases (PI3K/AKT) pathways while activating the p53 pathway; slows the growth of cancer cells. These pathways affect glucose metabolism, apoptosis, cell proliferation, and migration (166). ITCs present in cruciferous vegetables such as BITC, PEITC and sulforaphane have antimetastatic properties against colon cancer. These ITCs block the (PI3K)/AKT-dependent survival pathway of colon cancer cell lines, while stimulating the p53 pathway. In addition, they increase apoptosis-related proteins due to activation of

p53-family genes, while decreasing metastasis-related proteins. Because of all these reasons, BITC, PEITC and sulforaphane were capable of ameliorating the inflammation associated with colon cancer (116, 167). In HT29 colon cancer cells, BITC and PEITC have been demonstrated to have anti-metastatic and anti-inflammatory effects against colon cancer, and it slowed the migration of colon cancer cells through the activation of p53 pathway (147, 168, 169). Sulforaphane (SFN)-induced acetylation of a DNA repair protein causes DNA damage in colon cancer cells (Figure 5) (123). The p53-stimulated apoptosis of colon cancer cells is induced by activation of detoxifying enzymes, the release of cytochrome c, and the stimulation of poly(ADP-ribose) polymerase (PARP) proteolysis (170–172). Apoptosis occurs as a result of cell cycle arrest (173). Using human colorectal cancer cells as a model, Myzak et al., found that sulforaphane decreased histone deacetylase (HDAC)

activity while simultaneously increasing histone acetylation (174). HDAC inhibition has been linked to an increase in the transcription of p53 gene, which is a tumor-suppressor gene. Lycopene and canthaxanthin are two carotenoids that inhibited colon carcinoma cell proliferation by altering the cell cycle (175). As a result of cell cycle arrest due to activation of p53 pathway, astaxanthin was demonstrated to reduce cell proliferation and trigger death in cancer cells (Table 4) (117). The study by Palozza et al., found that *Haematococcus pluvialis* reduced cyclin D1 levels in colon cancer cells while increasing p53 and p21WAF-1/CIP1 levels in the cells (117). As a result of these findings, it can be concluded that the G1-phase cell cycle is blocked. In addition, β-carotene extracted from cruciferous vegetable has been demonstrated to increase Bax and P53 levels in malignant colon cells while decreasing Bcl-2 levels (149, 176).

Hepatic and pancreatic cancer

Anti-apoptotic genes overexpressed and tumor suppressor genes mutated, such as p53, are the first signs of tumor formation in the liver and pancreatic (158, 177). Several carotenoids in cruciferous vegetables, including bixin, β-cryptoxanthin, lutein, lycopene, astaxanthin, and fucoxanthin, have been examined for their function in triggering apoptosis in hepatic and pancreatic cancer cells through ROS generation. When the anti-apoptotic Bcl-2 and xL proteins, as well as proteins associated with B-cell lymphoma 2 (Bcl-2), are inhibited and pro-apoptotic proteins like p21, p27, and p53 are activated, hepato-pancreatic cancer cells might undergo apoptosis (149, 178). Dietary lutein raised the mRNA expression of proapoptotic genes p53 and Bax, decreased the expression of antiapoptotic gene Bcl-2, and increased the Bax:Bcl-2 ratio in hepato-pancreatic cancers (Figure 5). Activation of the p53 tumor suppressor gene causes apoptosis, DNA damage tolerance, and DNA repair (Table 4) (179). Further studies have demonstrated that the cruciferous vegetable isothiocyanates stimulate the GST and NQO1 enzymes renowned for their ability to remove carcinogens from the cells of the hepatic and pancreatic epithelial tissue. NQ01 appears to stabilize the tumor suppressor p53, according to certain research results. Liver and pancreas are the tissues susceptible to the stimulation of these enzymes by broccoli sprout extracts, which may be particularly effective in protecting these organs against the onset of cancer (119, 180).

Current progress toward clinical applications

The ability of cruciferous bioactive chemicals to suppress cancers in experimental animals has been documented in numerous studies. At the same time, the research studies conducted on human beings are very less. Isothiocyanates, indole-3-carbinol, and phytoalexins are among the bioactive chemicals in cruciferous vegetables studied for prevention of cancer of gastro-intestinal tract and other associated cancers (181). Cell cycle, apoptosis, genomic integrity, and DNA repair in human beings are all controlled by the tumor suppressor gene p53. Angiogenesis inhibition, cell cycle inhibition, and genetic stability come from the activation of particular genes by activated p53 gene (19). In addition, active p53 can operate as both a transactivator and a transrepressor at the same time. Activating p53 by the bioactive chemicals present in cruciferous vegetables may cause cell cycle arrest or death in cancerous cells of gastro-intestinal tract (129, 182). Carotenoids, for example, activates p53 and its targets p21 and Bax in gastric and colon cancer cells (183). Cell cycle arrest and apoptosis were both induced by lutein, which also activated the p53 gene's targets, including p21, Bax and PUMA (p53-upregulated modulator of apoptosis). Using ITCs, human gastric and colon cancer cells were able to apoptosis through the p53-dependent BAX induction. Apoptosis and ROS (reactive oxygen species) generation are two ways that ITCs limit tumor growth in body tissues of human beings. As ITCs and β-carotene activates p53's mitochondrial translocation, it has been shown to incite cell death through p53-mediated mechanisms. There are two closely related proteins in mammalian cells that when stimulated can cause apoptosis, similar to p53 protein, which are known as p63 and p73 (149). Indole-3-carbinol and phytoalexins have been found to induce apoptosis and cell cycle arrest in HT-29 human colon cancer cells (8). DNA damage checkpoints are essential for genome integrity because they stop the progression of the cell cycle when DNA damage or incomplete replication occurs, and the arrest of the G1 checkpoint occurs in mammalian cells because p53 protein mediates the action (182). Li et al. investigated the effects of indole-3-carbinol extracted from cruciferous vegetables on p53 protein induction. Indole-3-carbinol therapy enhanced the p53 protein level in human gastric cancer cell lines, causing cell cycle arrest in the G1 phase (132). By modifying the amounts of proteins that control cell cycle progression, indole-3-carbinol prevented human gastric cancer cells from entering the G1 phase. Glucosinolate compounds present in seeds of cruciferous vegetables, such as sinigrin, have been demonstrated to dramatically suppress hepatotumor cell proliferation when administered through the p53 pathway. Sinigrin, a major glucosinolate in cruciferous vegetable seeds, has been shown to suppress the growth of human liver cancer cells in a way that is dependent on the p53 signaling pathway (184, 185). More research studies should be conducted in the near future to attain further more development with regard to clinical applications of bioactive compounds available from cruciferous vegetables in human beings.

Concluding remarks and futuristic vision

A synopsis of the cancer-preventive potential of numerous Brassicaceae family members has been reported in this review. Even though there is a strong correlation between the prevention of carcinogenesis and consumption of cruciferous vegetables, it must be emphasized that many more studies are needed to fully understand the influence of these functional foods bioactive compounds on the human body. The upcoming experiments must specifically address the questions of bioavailability, stability, transport, and metabolism. These substances may have synergistic effects. It needs to be confirmed in further studies. In terms of the cancer-preventive characteristics of phytochemicals included in these veggies, the additional effects of typical food preparation techniques constitute another component that has yet to be fully investigated. Numerous studies aided in the acceptance of dietary agents as cancer treatment options. Due to their anti-tumorigenic and anti-proliferative competences, cruciferous vegetables are abundant with many functional bioactive compounds that have noteworthy inhibitory effects on different pathways of cancer cells. These veggies are advantageous because they are precursors to glucosinolates, which are precursors to isothiocyanates like sulforaphane and indoles like indole-3-carbinol. HDAC and DNMT overexpression, as well as miRNA misexpression, are common features of most malignancies. I3C, SFN, and I3C are regulators and inhibitors of these processes, and their usage causes malignant cell lines to seem more normal and healthier. With the inclusion of SFN and I3C, an increase in programmed cell death, as well as substantial reductions in uncontrolled cell proliferation, have been observed. Studies showed that functional bioactive compounds from cruciferous vegetables are potential candidates to fight cancer. Future research will likely focus on determining the epigenetic events influenced by the bioactive components of cruciferous vegetables and their importance in not just cancer prevention but also a variety of other biological systems.

Author contributions

SM, DC, and TE conceptualized and designed the manuscript, participating in drafting the article and/or acquisition of data, and/or analysis and interpretation of data. SM, BZ, RD, SSM, AM, MS, and FN participating in drafting the article and prepared the figures and tables. SM, TE, MK, AI, and JS-G wrote, edited, and revised the manuscript critically. TE and JS-G revised the final written. All authors critically revised the manuscript concerning intellectual content and approved the final manuscript.

Funding

Conflict of interest

The authors declare that the research was conducted in the absence of any commercial or financial relationships that could be construed as a potential conflict of interest.

Publisher's note

All claims expressed in this article are solely those of the authors and do not necessarily represent those of their affiliated organizations, or those of the publisher, the editors and the reviewers. Any product that may be evaluated in this article, or claim that may be made by its manufacturer, is not guaranteed or endorsed by the publisher.

References

1. Ozaki T, Nakagawara A. Role of p53 in cell death and human cancers. *Cancers.* (2011) 3:994–1013. doi: 10.3390/cancers3010994

2. Mitra S, Lami MS, Ghosh A, Das R, Tallei TE, Islam F, et al. Hormonal therapy for gynecological cancers: how far has science progressed toward clinical applications? *Cancers.* (2022) 14:759. doi: 10.3390/cancers14030759

3. Siegel RL, Miller KD, Goding Sauer A, Fedewa SA, Butterly LF, Anderson JC, et al. Colorectal cancer statistics, 2020. *CA Cancer J Clin.* (2020) 70:145–64. doi: 10.3322/caac.21601

4. Morrison MEW, Joseph JM, McCann SE, Tang L, Almohanna HM, Moysich KB. Cruciferous vegetable consumption and stomach cancer: a case-control study. *Nutr Cancer.* (2020) 72:52–61. doi: 10.1080/01635581.2019.1615100

5. Mitra S, Anjum J, Muni M, Das R, Rauf A, Islam F, et al. Exploring the journey of emodin as a potential neuroprotective agent: novel therapeutic

insights with molecular mechanism of action. *Biomed Pharmacother.* (2022) 149:112877. doi: 10.1016/j.biopha.2022.112877

6. Mitra S, Paul S, Roy S, Sutradhar H, Emran T, Nainu F, et al. Exploring the immune-boosting functions of vitamins and minerals as nutritional food bioactive compounds: a comprehensive review. *Molecules.* (2022) 27:20555. doi: 10.3390/molecules27020555

7. Esteve M. Mechanisms underlying biological effects of cruciferous glucosinolate-derived isothiocyanates/indoles: a focus on metabolic syndrome. *Front Nutr.* (2020) 7:111. doi: 10.3389/fnut.2020.00111

8. Manchali S, Chidambara Murthy KN, Patil BS. Crucial facts about health benefits of popular cruciferous vegetables. *J Funct Foods.* (2012) 4:94–106. doi: 10.1016/j.jff.2011.08.004

9. Mitra S, Lami MS, Uddin TM, Das R, Islam F, Anjum J, et al. Prospective multifunctional roles and pharmacological potential of dietary flavonoid narirutin. *Biomed Pharmacother.* (2022) 150:112932. doi: 10.1016/j.biopha.2022.112932

10. Mitra S, Tareq AM, Das R, Emran T, Nainu F, Chakraborty AJ, et al. Polyphenols: a first evidence in the synergism and bioactivities. *Food Rev Int.* (2022) 2022:1–23. doi: 10.1080/87559129.2022.2026376

11. Melim C, Lauro MR, Pires IM, Oliveira PJ, Cabral C. The role of glucosinolates from cruciferous vegetables (Brassicaceae) in gastrointestinal cancers: from prevention to therapeutics. *Pharmaceutics.* (2022) 14:10190. doi: 10.3390/pharmaceutics14010190

12. Connolly EL, Sim M, Travica N, Marx W, Beasy G, Lynch GS, et al. Glucosinolates from cruciferous vegetables and their potential role in chronic disease: investigating the preclinical and clinical evidence. *Front Pharmacol.* (2021) 12:767975. doi: 10.3389/fphar.2021.767975

13. Kissen R, Rossiter JT, Bones AM. The "mustard oil bomb": Not so easy to assemble?! Localization, expression and distribution of the components of the myrosinase enzyme system. *Phytochem Rev.* (2009) 8:69–86. doi: 10.1007/s11101-008-9109-1

14. Fimognari C, Nüsse M, Berti F, Iori R, Cantelli-Forti G, Hrelia P. Cyclin D3 and p53 mediate sulforaphane-induced cell cycle delay and apoptosis in non-transformed human T lymphocytes. *Cell Mol Life Sci.* (2002) 59:2004–12. doi: 10.1007/PL00012523

15. Fimognari C, Nüsse M, Cesari R, Iori R, Cantelli-Forti G, Hrelia P. Growth inhibition, cell-cycle arrest and apoptosis in human T-cell leukemia by the isothiocyanate sulforaphane. *Carcinogenesis.* (2002) 23:581–6. doi: 10.1093/carcin/23.4.581

16. Matsui TA, Murata H, Sakabe T, Sowa Y, Horie N, Nakanishi R, et al. Sulforaphane induces cell cycle arrest and apoptosis in murine osteosarcoma cells *in vitro* and inhibits tumor growth *in vivo*. *Oncol Rep.* (2007) 18:1263–8. doi: 10.3892/or.18.5.1263

17. Šamec D, Salopek-Sondi B. Cruciferous (brassicaceae) vegetables. *Nonvitamin Nonmineral Nutr Suppl.* (2018) 8:195–202. doi: 10.1016/B978-0-12-812491-8.00027-8

18. Ramirez D, Abellán-Victorio A, Beretta V, Camargo A, Moreno DA. Functional ingredients from brassicaceae species: overview and perspectives. *Int J Mol Sci.* (2020) 21:61998. doi: 10.3390/ijms21061998

19. Saban GM. The benefits of brassica vegetables on human health. *J Hum Heal Res.* (2018) 1:104.

20. Tiwari JN, Tiwari RN, Kim KS. Zero-dimensional, one-dimensional, two-dimensional and three-dimensional nanostructured materials for advanced electrochemical energy devices. *Prog Mater Sci.* (2012) 57:724–803. doi: 10.1016/j.pmatsci.2011.08.003

21. Favela-González KM, Hernández-Almanza AY, De la Fuente-Salcido NM. The value of bioactive compounds of cruciferous vegetables (Brassica) as antimicrobials and antioxidants: a review. *J Food Biochem.* (2020) 44:13414. doi: 10.1111/jfbc.13414

22. Kmiecik W, Lisiewska Z, Korus A. Retention of mineral constituents in frozen brassicas depending on the method of preliminary processing of the raw material and preparation of frozen products for consumption. *Eur Food Res Technol.* (2007) 224:573–9. doi: 10.1007/s00217-006-0337-6

23. Cartea ME, Francisco M, Soengas P, Velasco P. Phenolic compounds in Brassica vegetables. *Molecules.* (2011) 16:251–80. doi: 10.3390/molecules16010251

24. Miekus N, Marszałek K, Podlacha M, Iqbal A, Puchalski C, Swiergiel AH. Health benefits of plant-derived sulfur and organosulfur compounds. *Molecules.* (2020) 25:173804. doi: 10.3390/molecules25173804

25. Barba FJ, Nikmaram N, Roohinejad S, Khelfa A, Zhu Z, Koubaa M. Bioavailability of glucosinolates and their breakdown products: impact of processing. *Front Nutr.* (2016) 3:24. doi: 10.3389/fnut.2016.00024

26. Abbaoui B, Lucas CR, Riedl KM, Clinton SK, Mortazavi A. Cruciferous vegetables, isothiocyanates, and bladder cancer prevention. *Mol Nutr Food Res.* (2018) 62:79. doi: 10.1002/mnfr.201800079

27. Melrose J. The glucosinolates: a sulphur glucoside family of mustard anti-tumour and antimicrobial phytochemicals of potential therapeutic application. *Biomedicines.* (2019) 7:v2. doi: 10.20944/preprints201906.0042.v2

28. Wang M, Zhang Y, Leng C, Li X, Wang P, Gu Z, et al. Glucosinolates metabolism and redox state of rocket (*Eruca sativa* Mill) during germination. *J Food Process Preserv.* (2019) 43:14019. doi: 10.1111/jfpp.14019

29. Blažević I, Montaut S, Burčul F, Olsen CE, Burow M, Rollin P, et al. Glucosinolate structural diversity, identification, chemical synthesis and metabolism in plants. *Phytochemistry.* (2020) 169:112100. doi: 10.1016/j.phytochem.2019.112100

30. Bell L, Yahya HN, Oloyede OO, Methven L, Wagstaff C. Changes in rocket salad phytochemicals within the commercial supply chain: glucosinolates, isothiocyanates, amino acids and bacterial load increase significantly after processing. *Food Chem.* (2017) 221:521–34. doi: 10.1016/j.foodchem.2016.11.154

31. Luang-In V, Narbad A, Nueno-Palop C, Mithen R, Bennett M, Rossiter JT. The metabolism of methylsulfinylalkyl- and methylthioalkyl-glucosinolates by a selection of human gut bacteria. *Mol Nutr Food Res.* (2014) 58:875–83. doi: 10.1002/mnfr.201300377

32. Maina S, Misinzo G, Bakari G, Kim HY. Human, animal and plant health benefits of glucosinolates and strategies for enhanced bioactivity: a systematic review. *Molecules.* (2020) 25:163682. doi: 10.3390/molecules25163682

33. Shakour ZT, Shehab NG, Gomaa AS, Wessjohann LA, Farag MA. Metabolic and biotransformation effects on dietary glucosinolates, their bioavailability, catabolism and biological effects in different organisms. *Biotechnol Adv.* (2022) 54:107784. doi: 10.1016/j.biotechadv.2021.107784

34. Casajús V, Demkura P, Civello P, Gómez Lobato M, Martínez G. Harvesting at different time-points of day affects glucosinolate metabolism during postharvest storage of broccoli. *Food Res Int.* (2020) 136:109529. doi: 10.1016/j.foodres.2020.109529

35. Hanschen FS, Schreiner M. Isothiocyanates, nitriles, and epithionitriles from glucosinolates are affected by genotype and developmental stage in *Brassica oleracea* varieties. *Front Plant Sci.* (2017) 8:1095. doi: 10.3389/fpls.2017.01095

36. Bhandari SR, Jo JS, Lee JG. Comparison of glucosinolate profiles in different tissues of nine brassica crops. *Molecules.* (2015) 20:15827–41. doi: 10.3390/molecules200915827

37. Flakelar CL, Prenzler PD, Luckett DJ, Howitt JA, Doran G. A rapid method for the simultaneous quantification of the major tocopherols, carotenoids, free and esterified sterols in canola (*Brassica napus*) oil using normal phase liquid chromatography. *Food Chem.* (2017) 214:147–55. doi: 10.1016/j.foodchem.2016.07.059

38. Bahbah EI, Ghozy S, Attia MS, Negida A, Emran T, Mitra S, et al. Molecular mechanisms of astaxanthin as a potential neurotherapeutic agent. *Mar Drugs.* (2021) 19:40201. doi: 10.3390/md19040201

39. Lee HW, Zhang H, Liang X, Ong CN. Simultaneous determination of carotenoids, tocopherols and phylloquinone in 12 Brassicaceae vegetables. *LWT.* (2020) 130:109649. doi: 10.1016/j.lwt.2020.109649

40. Björkman M, Klingen I, Birch ANE, Bones AM, Bruce TJA, Johansen TJ, et al. Phytochemicals of Brassicaceae in plant protection and human health - influences of climate, environment and agronomic practice. *Phytochemistry.* (2011) 72:538–56. doi: 10.1016/j.phytochem.2011.01.014

41. Mitra S, Rauf A, Tareq AM, Jahan S, Emran T, Shahriar TG, et al. Potential health benefits of carotenoid lutein: an updated review. *Food Chem Toxicol.* (2021) 154:112328. doi: 10.1016/j.fct.2021.112328

42. Nilsson J, Olsson K, Engqvist G, Ekvall J, Olsson M, Nyman M, et al. Variation in the content of glucosinolates, hydroxycinnamic acids, carotenoids, total antioxidant capacity and low-molecular-weight carbohydrates in Brassica vegetables. *J Sci Food Agric.* (2006) 86:528–38. doi: 10.1002/jsfa.2355

43. Walsh RP, Bartlett H, Eperjesi F. Variation in carotenoid content of kale and other vegetables: a review of pre- and post-harvest effects. *J Agric Food Chem.* (2015) 63:9677–82. doi: 10.1021/acs.jafc.5b03691

44. Mageney V, Baldermann S, Albach DC. Intraspecific variation in carotenoids of *Brassica oleracea* var. sabellica. *J Agric Food Chem.* (2016) 64:3251–7. doi: 10.1021/acs.jafc.6b00268

45. Frede K, Schreiner M, Baldermann S. Light quality-induced changes of carotenoid composition in pak choi *Brassica rapa* ssp. Chinensis. *J Photochem Photobiol B Biol.* (2019) 193:18–30. doi: 10.1016/j.jphotobiol.2019.02.001

46. Mène-Saffrané L. Vitamin E biosynthesis and its regulation in plants. *Antioxidants.* (2018) 7:10002. doi: 10.3390/antiox7010002

47. Lu D, Yang Y, Li Y, Sun C. Analysis of tocopherols and tocotrienols in pharmaceuticals and foods: a critical review. *Curr Pharm Anal.* (2014) 11:66–78. doi: 10.2174/1573412910666140630170055

48. Li Z, Lee HW, Liang X, Liang D, Wang Q, Huang D, et al. Profiling of phenolic compounds and antioxidant activity of 12 cruciferous vegetables. *Molecules.* (2018) 23:51139. doi: 10.3390/molecules23051139

49. Cheynier V. Phenolic compounds: from plants to foods. *Phytochem Rev.* (2012) 11:153–77. doi: 10.1007/s11101-012-9242-8

50. Baenas N, Gómez-Jodar I, Moreno DA, García-Viguera C, Periago PM. Broccoli and radish sprouts are safe and rich in bioactive phytochemicals. *Postharvest Biol Technol.* (2017) 127:60–7. doi: 10.1016/j.postharvbio.2017.01.010

51. Vergun OM, Rakhmetov DB, Shymanska OV, Fishchenko V, Ivanisova E, Brindza J. Leaves extracts of selected crops. *Plant Introd.* (2019) 4:82–8. doi: 10.5281/zenodo.3566626

52. Islam MR, Islam F, Nafady MH, Akter M, Mitra S, Das R, et al. Natural small molecules in breast cancer treatment: understandings from a therapeutic viewpoint. *Molecules.* (2022) 27:72165. doi: 10.3390/molecules27072165

53. Avato P, Argentieri MP. Brassicaceae: a rich source of health improving phytochemicals. *Phytochem Rev.* (2015) 14:1019–33. doi: 10.1007/s11101-015-9414-4

54. Raiola A, Errico A, Petruk G, Monti DM, Barone A, Rigano MM. Bioactive compounds in brassicaceae vegetables with a role in the prevention of chronic diseases. *Molecules.* (2018) 23:10015. doi: 10.3390/molecules23010015

55. Upadhyay R, Sehwag S, Singh SP. Antioxidant activity and polyphenol content of *Brassica oleracea* varieties. *Int J Veg Sci.* (2016) 22:353–63. doi: 10.1080/19315260.2015.1048403

56. Mitra S, Islam F, Das R, Urmee H, Akter A, Idris AM, et al. Pharmacological potential of *Avicennia alba* leaf extract: an experimental analysis focusing on antidiabetic, anti-inflammatory, analgesic, and antidiarrheal activity. *Biomed Res Int.* (2022) 2022:1–10. doi: 10.1155/2022/7624189

57. Islam F, Mitra S, Nafady MH, Rahman MT, Tirth V, Akter A, et al. Neuropharmacological and antidiabetic potential of *Lannea coromandelica* (Houtt) merr leaves extract: an experimental analysis evidence-based complement. *Altern Med.* (2022) 2022:6144733. doi: 10.1155/2022/6144733

58. Rodríguez-García C, Sánchez-Quesada C, Toledo E, Delgado-Rodríguez M, Gaforio JJ. Naturally lignan-rich foods: a dietary tool for health promotion? *Molecules.* (2019) 24:50917. doi: 10.3390/molecules24050917

59. Moreno DA, Pérez-Balibrea S, Ferreres F, Gil-Izquierdo Á, García-Viguera C. Acylated anthocyanins in broccoli sprouts. *Food Chem.* (2010) 123:358–63. doi: 10.1016/j.foodchem.2010.04.044

60. Matera R, Gabbanini S, De Nicola GR, Iori R, Petrillo G, Valgimigli L. Identification and analysis of isothiocyanates and new acylated anthocyanins in the juice of *Raphanus sativus* cv. Sango sprouts. *Food Chem.* (2012) 133:563–72. doi: 10.1016/j.foodchem.2012.01.050

61. Gül MK, Seker M. Comparative analysis of phytosterol components from rapeseed (*Brassica napus* L) and olive (*Olea europaea* L) varieties. *Eur J Lipid Sci Technol.* (2006) 108:759–65. doi: 10.1002/ejlt.200600085

62. Sharma A, Rai PK, Prasad S. GC–MS detection and determination of major volatile compounds in *Brassica juncea* L. leaves and seeds. *Microchem J.* (2018) 138:488–93. doi: 10.1016/j.microc.2018.01.015

63. Ahuja I, Kissen R, Bones AM. Phytoalexins in defense against pathogens. *Trends Plant Sci.* (2012) 17:73–90. doi: 10.1016/j.tplants.2011.11.002

64. Klein AP, Sattely ES. Biosynthesis of cabbage phytoalexins from indole glucosinolate. *Proc Natl Acad Sci USA.* (2017) 114:1910–5. doi: 10.1073/pnas.1615625114

65. Pedras MSC, Okanga FI, Zaharia IL, Khan AQ. Phytoalexins from crucifers: synthesis, biosynthesis, and biotransformation. *Phytochemistry.* (2000) 53:161–76. doi: 10.1016/S0031-9422(99)00494-X

66. Cartea E, De Haro-Bailón A, Padilla G, Obregón-Cano S, Del Rio-Celestino M, Ordás A. Seed oil quality of *Brassica napus* and *Brassica rapa* germplasm from Northwestern Spain. *Foods.* (2019) 8:80292. doi: 10.3390/foods8080292

67. Pflaum J, Schlosser S, Müller M. P53 family and cellular stress responses in cancer. *Front Oncol.* (2014) 4:285. doi: 10.3389/fonc.2014.00285

68. Li XL, Zhou J, Chen ZR, Chng WJ. P53 mutations in colorectal cancer-molecular pathogenesis and pharmacological reactivation. *World J Gastroenterol.* (2015) 21:84–93. doi: 10.3748/wjg.v21.i1.84

69. Soussi T. The p53 tumor suppressor gene: From molecular biology to clinical investigation. *Ann N Y Acad Sci.* (2000) 910:121–39. doi: 10.1111/j.1749-6632.2000.tb06705.x

70. Ryan KM, Phillips AC, Vousden KH. Regulation and function of the p53 tumor suppressor protein. *Curr Opin Cell Biol.* (2001) 13:332–7. doi: 10.1016/S0955-0674(00)00216-7

71. Elkholi R, Floros K V, Chipuk JE. The role of BH3-only proteins in tumor cell development, signaling, and treatment. *Genes Cancer.* (2011) 2:523–37. doi: 10.1177/1947601911417177

72. Chipuk JE, Moldoveanu T, Llambi F, Parsons MJ, Green DR. The BCL-2 family reunion. *Mol Cell.* (2010) 37:299–310. doi: 10.1016/j.molcel.2010.01.025

73. Shakeri R, Kheirollahi A, Davoodi J. Apaf-1: regulation and function in cell death. *Biochimie.* (2017) 135:111–25. doi: 10.1016/j.biochi.2017.02.001

74. Guicciardi ME, Gores GJ. Life and death by death receptors. *FASEB J.* (2009) 23:1625–37. doi: 10.1096/fj.08-111005

75. Lavrik IN. Systems biology of death receptor networks: live and let die. *Cell Death Dis.* (2014) 5:160. doi: 10.1038/cddis.2014.160

76. Kumari R, Jat P. Mechanisms of cellular senescence: cell cycle arrest and senescence associated secretory phenotype. *Front Cell Dev Biol.* (2021) 9:645593. doi: 10.3389/fcell.2021.645593

77. Campisi J, D'Adda Di Fagagna F. Cellular senescence: when bad things happen to good cells. *Nat Rev Mol Cell Biol.* (2007) 8:729–40. doi: 10.1038/nrm2233

78. Mallette FA, Ferbeyre G. The DNA damage signaling pathway connects oncogenic stress to cellular senescence. *Cell Cycle.* (2007) 6:1831–6. doi: 10.4161/cc.6.15.4516

79. Beyfuss K, Hood DA. A systematic review of p53 regulation of oxidative stress in skeletal muscle. *Redox Rep.* (2018) 23:100–17. doi: 10.1080/13510002.2017.1416773

80. Hientz K, Mohr A, Bhakta-Guha D, Efferth T. The role of p53 in cancer drug resistance and targeted chemotherapy. *Oncotarget.* (2017) 8:8921–46. doi: 10.18632/oncotarget.13475

81. Teodoro JG, Evans SK, Green MR. Inhibition of tumor angiogenesis by p53: a new role for the guardian of the genome. *J Mol Med.* (2007) 85:1175–86. doi: 10.1007/s00109-007-0221-2

82. Yeo CQX, Alexander I, Lin Z, Lim S, Aning OA, Kumar R, et al. P53 maintains genomic stability by preventing interference between transcription and replication. *Cell Rep.* (2016) 15:132–46. doi: 10.1016/j.celrep.2016.03.011

83. Rauf A, Abu-Izneid T, Khalil AA, Imran M, Shah ZA, Bin Emran T, et al. Berberine as a potential anticancer agent: a comprehensive review. *Molecules.* (2021) 26:237368. doi: 10.3390/molecules26237368

84. Mitra S, Sarker J, Mojumder A, Shibbir TB, Das R, Emran T, et al. Genome editing and cancer: how far has research moved forward on CRISPR/Cas9? *Biomed Pharmacother.* (2022) 150:113011. doi: 10.1016/j.biopha.2022.113011

85. Kandoth C, McLellan MD, Vandin F, Ye K, Niu B, Lu C, et al. Mutational landscape and significance across 12 major cancer types. *Nature.* (2013) 502:333–9. doi: 10.1038/nature12634

86. Wood LD, Parsons DW, Jones S, Lin J, Sjöblom T, Leary RJ, et al. The genomic landscapes of human breast and colorectal cancers. *Science.* (2007) 318:1108–13. doi: 10.1126/science.1145720

87. Russo A, Bazan V, Iacopetta B, Kerr D, Soussi T, Gebbia N. The TP53 colorectal cancer international collaborative study on the prognostic and predictive significance of p53 mutation: influence of tumor site, type of mutation, and adjuvant treatment. *J Clin Oncol.* (2005) 23:7518–28. doi: 10.1200/JCO.2005.00.471

88. Saha MN, Qiu L, Chang H. Targeting p53 by small molecules in hematological malignancies. *J Hematol Oncol.* (2013) 6:23. doi: 10.1186/1756-8722-6-23

89. López I, Oliveira LL, Tucci P, Álvarez-Valín FA, Coudry R, Marín M. Different mutation profiles associated to P53 accumulation in colorectal cancer. *Gene.* (2012) 499:81–7. doi: 10.1016/j.gene.2012.02.011

90. Fenoglio-Preiser CM, Wang J, Stemmermann GN, Noffsinger A. TP53 and gastric carcinoma: a review. *Hum Mutat.* (2003) 21:258–70. doi: 10.1002/humu.10180

91. Cao X, Hou J, An Q, Assaraf YG, Wang X. Towards the overcoming of anticancer drug resistance mediated by p53 mutations. *Drug Resist Updat.* (2020) 49:100671. doi: 10.1016/j.drup.2019.100671

92. Rahman MM, Islam F, Afsana Mim S, Khan MS, Islam MR, Haque MA, et al. Multifunctional therapeutic approach of nanomedicines against inflammation in cancer and aging. *J Nanomater.* (2022) 2022:4217529. doi: 10.1155/2022/4217529

93. Huang Y, Liu N, Liu J, Liu Y, Zhang C, Long S, et al. Mutant p53 drives cancer chemotherapy resistance due to loss of function on activating transcription of PUMA. *Cell Cycle.* (2019) 18:3442–55. doi: 10.1080/15384101.2019.1688951

94. Kim NH, Kim HS, Kim NG, Lee I, Choi HS, Li XY, et al. p53 and microRNA-34 are suppressors of canonical Wnt signaling. *Sci Signal.* (2011) 4:2001744. doi: 10.1126/scisignal.2001744

95. Kim NH, Cha YH, Kang SE, Lee Y, Lee I, Cha SY, et al. p53 regulates nuclear GSK-3 levels through miR-34-mediated Axin2 suppression in colorectal cancer cells. *Cell Cycle.* (2013) 12:1578–87. doi: 10.4161/cc.24739

96. Ohtsuka J, Oshima H, Ezawa I, Abe R, Oshima M, Ohki R. Functional loss of p53 cooperates with the *in vivo* microenvironment to promote malignant progression of gastric cancers. *Sci Rep.* (2018) 8:1. doi: 10.1038/s41598-018-20572-1

97. Shen HG, Maki C. Pharmacologic activation of p53 by small-molecule MDM2 antagonists. *Curr Pharm Des.* (2011) 17:560–8. doi: 10.2174/138161211795222603

98. Micel LN, Tentler JJ, Smith PG, Eckhardt SG. Role of ubiquitin ligases and the proteasome in oncogenesis: novel targets for anticancer therapies. *J Clin Oncol.* (2013) 31:1231–8. doi: 10.1200/JCO.2012.44.0958

99. Sun SH, Zheng M, Ding K, Wang S, Sun Y. A small molecule that disrupts Mdm2-p53 binding activates p53, induces apoptosis and sensitizes lung cancer cells to chemotherapy. *Cancer Biol Ther.* (2008) 7:845–52. doi: 10.4161/cbt.7.6.5841

100. Shangary S, Ding K, Qiu S, Nikolovska-Coleska Z, Bauer JA, Liu M, et al. Reactivation of p53 by a specific MDM2 antagonist (MI-43) leads to p21-mediated cell cycle arrest and selective cell death in colon cancer. *Mol Cancer Ther.* (2008) 7:1533–42. doi: 10.1158/1535-7163.MCT-08-0140

101. Patton JT, Mayo LD, Singhi AD, Gudkov A V, Stark GR, Jackson MW. Levels of HdmX expression dictate the sensitivity of normal and transformed cells to Nutlin-3. *Cancer Res.* (2006) 66:3169–76. doi: 10.1158/0008-5472.CAN-05-3832

102. Issaeva N, Bozko P, Enge M, Protopopova M, Verhoef LGGC, Masucci M, et al. Small molecule RITA binds to p53, blocks p53-HDM-2 interaction and activates p53 function in tumors. *Nat Med.* (2004) 10:1321–8. doi: 10.1038/nm1146

103. Bykov VJN, Issaeva N, Shilov A, Hultcrantz M, Pugacheva E, Chumakov P, et al. Restoration of the tumor suppressor function to mutant p53 by a low-molecular-weight compound. *Nat Med.* (2002) 8:282–8. doi: 10.1038/nm0302-282

104. Lambert JMR, Gorzov P, Veprintsev DB, Söderqvist M, Segerbäck D, Bergman J, et al. PRIMA-1 reactivates mutant p53 by covalent binding to the core domain. *Cancer Cell.* (2009) 15:376–88. doi: 10.1016/j.ccr.2009.03.003

105. Jiang D, Wang L, Zhao T, Zhang Z, Zhang R, Jin J, et al. Restoration of the tumor-suppressor function to mutant p53 by *Ganoderma lucidum* polysaccharides in colorectal cancer cells. *Oncol Rep.* (2017) 37:594–600. doi: 10.3892/or.2016.5246

106. Hussain SP, Harris CC. Molecular epidemiology of human cancer: contribution of mutation spectra studies of tumor suppressor genes. *Cancer Res.* (1998) 58:4023–37.

107. Lorne J, HofsethNewton AC, Perwez Hussain P, Harris CC. P53: 25 years after its discovery. *Trends Pharmacol Sci.* (2004) 25:177–81. doi: 10.1016/j.tips.2004.02.009

108. Rao VA, Terzian T, Valentin-Vega YA, El-Naggar AK, Iwakuma T, Suh YA, et al. Gain of function of a p53 hot spot mutation in a mouse model of Li-Fraumeni syndrome. *Cell.* (2004) 119:861–72. doi: 10.1016/j.cell.2004.11.006

109. Hastak K, Agarwal MK, Mukhtar H, Agarwal ML. Ablation of either p21 or Bax prevents p53-dependent apoptosis induced by green tea polyphenol epigallocatechin-3-gallate. *FASEB J.* (2005) 19:1–19. doi: 10.1096/fj.04-2226fje

110. Kumar Y, Phaniendra A, Periyasamy L. Bixin triggers apoptosis of human Hep3B hepatocellular carcinoma cells: an insight to molecular and *in silico* approach. *Nutr Cancer.* (2018) 70:971–83. doi: 10.1080/01635581.2018.1490445

111. Qiu Y, Li C, Zhang B, Gu Y. Bixin prevents colorectal cancer development through AMPK-activated endoplasmic reticulum stress. *Biomed Res Int.* (2022) 2022:9329151. doi: 10.1155/2022/9329151

112. Yuan A. Allicin induces apoptosis in gastric cancer cells through activation of both extrinsic and intrinsic pathways. *Oncol Rep.* (2010) 24:1021. doi: 10.3892/or_00001021

113. Persson C, Sasazuki S, Inoue M, Kurahashi N, Iwasaki M, Miura T, et al. Plasma levels of carotenoids, retinol and tocopherol and the risk of gastric cancer in Japan: a nested case-control study. *Carcinogenesis.* (2008) 29:1042–8. doi: 10.1093/carcin/bgn072

114. Yang G, Gao YT, Shu XO, Cai Q, Li GL, Li HL, et al. Isothiocyanate exposure, glutathione S-transferase polymorphisms, and colorectal cancer risk. *Am J Clin Nutr.* (2010) 91:704–11. doi: 10.3945/ajcn.2009.28683

115. Tang FY, Shih CJ, Cheng LH, Ho HJ, Chen HJ. Lycopene inhibits growth of human colon cancer cells via suppression of the Akt signaling pathway. *Mol Nutr Food Res.* (2008) 52:646–54. doi: 10.1002/mnfr.200700272

116. Yang Q, Miyagawa M, Liu X, Zhu B, Munemasa S, Nakamura T, et al. Methyl-β-cyclodextrin potentiates the BITC-induced anti-cancer effect through modulation of the Akt phosphorylation in human colorectal cancer cells. *Biosci Biotechnol Biochem.* (2018) 82:2158–67. doi: 10.1080/09168451.2018.1514249

117. Kim JH, Park JJ, Lee BJ, Joo MK, Chun HJ, Lee SW, et al. Astaxanthin inhibits proliferation of human gastric cancer cell lines by interrupting cell cycle progression. *Gut Liver.* (2016) 10:369–74. doi: 10.5009/gnl15208

118. Vassilev LT. MDM2 inhibitors for cancer therapy. *Trends Mol Med.* (2007) 13:23–31. doi: 10.1016/j.molmed.2006.11.002

119. Gullett NP, Ruhul Amin ARM, Bayraktar S, Pezzuto JM, Shin DM, Khuri FR, et al. Cancer prevention with natural compounds. *Semin Oncol.* (2010) 37:258–81. doi: 10.1053/j.seminoncol.2010.06.014

120. Ho CC, Lai KC, Hsu SC, Kuo CL, Ma CY, Lin ML, et al. Benzyl isothiocyanate (BITC) inhibits migration and invasion of human gastric cancer AGS cells *via* suppressing ERK signal pathways. *Hum Exp Toxicol.* (2011) 30:296–306. doi: 10.1177/0960327110371991

121. Ekström AM, Serafini M, Nyrén O, Wolk A, Bosetti C, Bellocco R. Dietary quercetin intake and risk of gastric cancer: results from a population-based study in Sweden. *Ann Oncol.* (2011) 22:438–43. doi: 10.1093/annonc/mdq390

122. Poke F, Qadi A, Holloway A. Reversing aberrant methylation patterns in cancer. *Curr Med Chem.* (2010) 17:1246–54. doi: 10.2174/092986710790936329

123. Rajendran P, Kidane AI, Yu TW, Dashwood WM, Bisson WH, Löhr CV, et al. Turnover, CtIP acetylation and dysregulated DNA damage signaling in colon cancer cells treated with sulforaphane and related dietary isothiocyanates. *Epigenetics.* (2013) 8:612–23. doi: 10.4161/epi.24710

124. Murase W, Kamakura Y, Kawakami S, Yasuda A, Wagatsuma M, Kubota A, et al. Fucoxanthin prevents pancreatic tumorigenesis in c57bl/6j mice that received allogenic and orthotopic transplants of cancer cells. *Int J Mol Sci.* (2021) 22:413620. doi: 10.3390/ijms222413620

125. Chung MY, Lim TG, Lee KW. Molecular mechanisms of chemopreventive phytochemicals against gastroenterological cancer development. *World J Gastroenterol.* (2013) 19:984–93. doi: 10.3748/wjg.v19.i7.984

126. Aggarwal BB, Shishodia S. Molecular targets of dietary agents for prevention and therapy of cancer. *Biochem Pharmacol.* (2006) 71:1397–421. doi: 10.1016/j.bcp.2006.02.009

127. Soundararajan P, Kim JS. Anti-carcinogenic glucosinolates in cruciferous vegetables and their antagonistic effects on prevention of cancers. *Molecules.* (2018) 23:112983. doi: 10.3390/molecules23112983

128. Yamada H, Shinmura K, Okudela K, Goto M, Suzuki M, Kuriki K, et al. Identification and characterization of a novel germ line p53 mutation in familial gastric cancer in the Japanese population. *Carcinogenesis.* (2007) 28:2013–8. doi: 10.1093/carcin/bgm175

129. Ranjan A, Ramachandran S, Gupta N, Kaushik I, Wright S, Srivastava S, et al. Role of phytochemicals in cancer prevention. *Int J Mol Sci.* (2019) 20:204981. doi: 10.3390/ijms20204981

130. Hintze KJ, Keck AS, Finley JW, Jeffery EH. Induction of hepatic thioredoxin reductase activity by sulforaphane, both in Hepa1c1c7 cells and in male Fisher 344 rats. *J Nutr Biochem.* (2003) 14:173–9. doi: 10.1016/S0955-2863(02)00282-6

131. Ye Y, Fang Y, Xu W, Wang Q, Zhou J, Lu R. 3,3′-Diindolylmethane induces anti-human gastric cancer cells by the miR-30e-ATG5 modulating autophagy. *Biochem Pharmacol.* (2016) 115:77–84. doi: 10.1016/j.bcp.2016.06.018

132. Li XJ, Park ES, Park MH, Kim SM. 3,3'-Diindolylmethane suppresses the growth of gastric cancer cells *via* activation of the Hippo signaling pathway. *Oncol Rep.* (2013) 30:2419–26. doi: 10.3892/or.2013.2717

133. Shin J, Song MH, Oh JW, Keum YS, Saini RK. Pro-oxidant actions of carotenoids in triggering apoptosis of cancer cells: a review of emerging evidence. *Antioxidants.* (2020) 9:1–17. doi: 10.3390/antiox9060532

134. Liu C, Russell RM. Nutrition and gastric cancer risk: an update. *Nutr Rev.* (2008) 66:237–49. doi: 10.1111/j.1753-4887.2008.00029.x

135. Liu C, Russell RM, Wang XD. Lycopene supplementation prevents smoke-induced changes in p53, p53 phosphorylation, cell proliferation, and apoptosis in the gastric mucosa of ferrets. *J Nutr.* (2006) 136:106–11. doi: 10.1093/jn/136.1.106

136. El-Deiry WS. Regulation of p53 downstream genes. *Semin Cancer Biol.* (1998) 8:345–57. doi: 10.1006/scbi.1998.0097

137. Cai XZ, Wang J, Li XD, Wang GL, Liu FN, Cheng MS, et al. Curcumin suppresses proliferation and invasion in human gastric cancer cells by downregulation of PAK1 activity and cyclin D1 expression. *Cancer Biol Ther.* (2009) 8:1360–8. doi: 10.4161/cbt.8.14.8720

138. Moy KA, Yuan JM, Chung FL, Wang XL, Van Den Berg D, Wang R, et al. Isothiocyanates, glutathione S-transferase M1 and T1 polymorphisms and gastric cancer risk: a prospective study of men in Shanghai, China. *Int J Cancer.* (2009) 125:2652–9. doi: 10.1002/ijc.24583

139. Ge M, Zhang L, Cao L, Xie C, Li X, Li Y, et al. Sulforaphane inhibits gastric cancer stem cells *via* suppressing sonic hedgehog pathway. *Int J Food Sci Nutr.* (2019) 70:570–8. doi: 10.1080/09637486.2018.1545012

140. Peng W, Zhou Z, Zhong Y, Sun Y, Wang Y, Zhu Z, et al. Plasma activity of thioredoxin reductase as a novel biomarker in gastric cancer. *Sci Rep.* (2019) 9:6. doi: 10.1038/s41598-019-55641-6

141. McKenzie RC, Arthur JR, Beckett GJ. Selenium and the regulation of cell signaling, growth, and survival: molecular and mechanistic aspects. *Antioxidants Redox Signal.* (2002) 4:339–51. doi: 10.1089/152308602753666398

142. Wang Y, Wu H, Dong N, Su X, Duan M, Wei Y, et al. Sulforaphane induces S-phase arrest and apoptosis *via* p53-dependent manner in gastric cancer cells. *Sci Rep.* (2021) 11:2. doi: 10.1038/s41598-021-81815-2

143. Shen G, Xu C, Hu R, Jain MR, Gopalkrishnan A, Nair S, et al. Modulation of nuclear factor E2-related factor 2-mediated gene expression in mice liver and small intestine by cancer chemopreventive agent curcumin. *Mol Cancer Ther.* (2006) 5:39–51. doi: 10.1158/1535-7163.MCT-05-0293

144. Murakami A, Ashida H, Terao J. Multitargeted cancer prevention by quercetin. *Cancer Lett.* (2008) 269:315–25. doi: 10.1016/j.canlet.2008.03.046

145. Sugie S, Okamoto K, Okumura A, Tanaka T, Mori H. Inhibitory effects of benzyl thiocyanate and benzyl isothiocyanate on methylazoxymethanol acetate-induced intestinal carcinogenesis in rats. *Carcinogenesis.* (1994) 15:1555–60. doi: 10.1093/carcin/15.8.1555

146. Hu R, Khor TO, Shen G, Jeong WS, Hebbar V, Chen C, et al. Cancer chemoprevention of intestinal polyposis in ApcMin/+ mice by sulforaphane, a natural product derived from cruciferous vegetable. *Carcinogenesis.* (2006) 27:2038–46. doi: 10.1093/carcin/bgl049

147. Hu R, Kim BR, Chen C, Hebbar V, Kong ANT. The roles of JNK and apoptotic signaling pathways in PEITC-mediated responses in human HT-29 colon adenocarcinoma cells. *Carcinogenesis.* (2003) 24:1361–7. doi: 10.1093/carcin/bgg092

148. Gamet-Payrastre L, Lumeau S, Gasc N, Cassar G, Rollin P, Tulliez J. Selective cytostatic and cytotoxic effects of glucosinolates hydrolysis products on human colon cancer cells *in vitro*. *Anticancer Drugs.* (1998) 9:141–8. doi: 10.1097/00001813-199802000-00005

149. Al-Ishaq RK, Overy AJ, Büsselberg D. Phytochemicals and gastrointestinal cancer: cellular mechanisms and effects to change cancer progression. *Biomolecules.* (2020) 10:10105. doi: 10.3390/biom10010105

150. Palozza P, Torelli C, Boninsegna A, Simone R, Catalano A, Mele MC, et al. Growth-inhibitory effects of the astaxanthin-rich alga *Haematococcus pluvialis* in human colon cancer cells. *Cancer Lett.* (2009) 283:108–17. doi: 10.1016/j.canlet.2009.03.031

151. Millán CS, Soldevilla B, Martín P, Gil-Calderón B, Compte M, Pérez-Sacristán B, et al. β-Cryptoxanthin synergistically enhances the antitumoral activity of oxaliplatin through ΔNP73 negative regulation in colon cancer. *Clin Cancer Res.* (2015) 21:4398–409. doi: 10.1158/1078-0432.CCR-14-2027

152. Liu ZJ, Xu W, Han J, Liu QY, Gao LF, Wang XH, et al. Quercetin induces apoptosis and enhances gemcitabine therapeutic efficacy against gemcitabine-resistant cancer cells. [[i]]Anticancer Drugs[[/i]] (2020)

153. Shehzad A, Lee J, Lee YS. Curcumin in various cancers. *BioFactors.* (2013) 39:56–68. doi: 10.1002/biof.1068

154. Mózsik G, Rumi G, Dömötör A, Figler M, Gasztonyi B, Papp E, et al. Involvement of serum retinoids and Leiden mutation in patients with esophageal, gastric, liver, pancreatic, and colorectal cancers in Hungary. *World J Gastroenterol.* (2005) 11:7646–50. doi: 10.3748/wjg.v11.i48.7646

155. Seren S, Lieberman R, Bayraktar UD, Heath E, Sahin K, Andic F, et al. Lycopene in cancer prevention and treatment. *Am J Ther.* (2008) 15:66–81. doi: 10.1097/MJT.0b013e31804c7120

156. Faraone I, Sinisgalli C, Ostuni A, Armentano MF, Carmosino M, Milella L, et al. Astaxanthin anticancer effects are mediated through multiple molecular mechanisms: a systematic review. *Pharmacol Res.* (2020) 155:104689. doi: 10.1016/j.phrs.2020.104689

157. Pham NA, Jacobberger JW, Schimmer AD, Cao P, Gronda M, Hedley DW. The dietary isothiocyanate sulforaphane targets pathways of apoptosis, cell cycle arrest, and oxidative stress in human pancreatic cancer cells and inhibits tumor growth in severe combined immunodeficient mice. *Mol Cancer Ther.* (2004) 3:1239–48. doi: 10.1158/1535-7163.1239.3.10

158. Boreddy SR, Pramanik KC, Srivastava SK. Pancreatic tumor suppression by benzyl isothiocyanate is associated with inhibition of PI3K/AKT/FOXO pathway. *Clin Cancer Res.* (2011) 17:1784–95. doi: 10.1158/1078-0432.CCR-10-1891

159. Xie S, Wang Q, Wu H, Cogswell J, Lu L, Jhanwar-Uniyal M, et al. Reactive oxygen species-induced phosphorylation of p53 on serine 20 is mediated in part by polo-like kinase-3. *J Biol Chem.* (2001) 276:36194–9. doi: 10.1074/jbc.M104157200

160. Kale J, Osterlund EJ, Andrews DW. BCL-2 family proteins: changing partners in the dance towards death. *Cell Death Differ.* (2018) 25:65–80. doi: 10.1038/cdd.2017.186

161. Jang SH, Lim JW, Kim H. Mechanism of β-carotene-induced apoptosis of gastric cancer cells: involvement of ataxia-telangiectasia-mutated. *Ann N Y Acad Sci.* (2009) 1171:156–62. doi: 10.1111/j.1749-6632.2009.04711.x

162. Tomasetti C, Marchionni L, Nowak MA, Parmigiani G, Vogelstein B. Only three driver gene mutations are required for the development of lung and colorectal cancers. *Proc Natl Acad Sci USA.* (2015) 112:118–23. doi: 10.1073/pnas.1421839112

163. Rauf A, Ali Shariati M, Imran M, Bashir K, Ali Khan S, Mitra S. Comprehensive review on naringenin and naringin polyphenols as a potent anticancer agent. *Environ Sci Pollut Res Int.* (2022) 29:31025–41. doi: 10.1007/s11356-022-18754-6

164. LoPiccolo J, Blumenthal GM, Bernstein WB, Dennis PA. Targeting the PI3K/Akt/mTOR pathway: effective combinations and clinical considerations. *Drug Resist Updat.* (2008) 11:32–50. doi: 10.1016/j.drup.2007.11.003

165. Tse G, Eslick GD. Cruciferous vegetables and risk of colorectal neoplasms: a systematic review and meta-analysis. *Nutr Cancer.* (2014) 66:128–39. doi: 10.1080/01635581.2014.852686

166. Zhu M, Li W, Dong X, Chen Y, Lu Y, Lin B, et al. Benzyl-isothiocyanate induces apoptosis and inhibits migration and invasion of hepatocellular carcinoma cells *in vitro*. *J Cancer.* (2017) 8:240–8. doi: 10.7150/jca.16402

167. Lai KC, Huang ANC, Hsu SC, Kuo CL, Yang JS, Wu SH, et al. Benzyl Lsothiocyanate (BITC) inhibits migration and invasion of human colon cancer HT29 cells by inhibiting matrix metalloproteinase-2/-9 and urokinase plasminogen (uPA) through PKC and MAPK signaling pathway. *J Agric Food Chem.* (2010) 58:2935–42. doi: 10.1021/jf9036694

168. Lai KC, Hsu SC, Kuo CL, Ip SW, Yang JS, Hsu YM, et al. Phenethyl isothiocyanate inhibited tumor migration and invasion *via* suppressing multiple signal transduction pathways in human colon cancer HT29 cells. *J Agric Food Chem.* (2010) 58:11148–55. doi: 10.1021/jf102384n

169. Liu Y, Dey M. Dietary phenethyl isothiocyanate protects mice from colitis associated colon cancer. *Int J Mol Sci.* (2017) 18:91908. doi: 10.3390/ijms18091908

170. Parnaud G, Li PF, Cassar G, Rouimi P, Tulliez J, Combaret L, et al. Mechanism of sulforaphane-induced cell cycle arrest and apoptosis in human colon cancer cells. *Nutr Cancer.* (2004) 48:198–206. doi: 10.1207/s15327914nc4802_10

171. Jakubíková J, Sedlák J, Mithen R, Bao Y. Role of PI3K/Akt and MEK/ERK signaling pathways in sulforaphane- and erucin-induced phase II enzymes and MRP2 transcription, G2/M arrest and cell death in Caco-2 cells. *Biochem Pharmacol.* (2005) 69:1543–52. doi: 10.1016/j.bcp.2005.03.015

172. Martin SL, Kala R, Tollefsbol TO. Mechanisms for the inhibition of colon cancer cells by sulforaphane through epigenetic modulation of MicroRNA-21 and human telomerase reverse transcriptase (hTERT) down-regulation. *Curr Cancer Drug Targets.* (2017) 18:97–106. doi: 10.2174/1568009617666170206104032

173. Okonkwo A, Mitra J, Johnson GS Li L, Dashwood WM, Hegde ML, Yue C, et al. Heterocyclic analogs of sulforaphane trigger DNA damage and impede DNA repair in colon cancer cells: interplay of HATs and HDACs. *Mol Nutr Food Res.* (2018) 62:800228. doi: 10.1002/mnfr.201800228

174. Myzak MC, Karplus PA, Chung FL, Dashwood RH. A novel mechanism of chemoprotection by sulforaphane: inhibition of histone deacetylase. *Cancer Res.* (2004) 64:5767–74. doi: 10.1158/0008-5472.CAN-04-1326

175. Kim SM. Cellular and molecular mechanisms of 3,3'-diindolylmethane in gastrointestinal cancer. *Int J Mol Sci.* (2016) 17:711550. doi: 10.3390/ijms17071155

176. Pan JH, Abernathy B, Kim YJ, Lee JH, Kim JH, Shin EC, et al. Cruciferous vegetables and colorectal cancer prevention through microRNA regulation: a review. *Crit Rev Food Sci Nutr.* (2018) 58:2026–38. doi: 10.1080/10408398.2017.1300134

177. Kountouras J, Zavos C, Chatzopoulos D. Apoptotic and anti-angiogenic strategies in liver and gastrointestinal malignancies. *J Surg Oncol.* (2005) 90:249–59. doi: 10.1002/jso.20254

178. Arathi BP, Sowmya PRR, Kuriakose GC, Vijay K, Baskaran V, Jayabaskaran C, et al. Enhanced cytotoxic and apoptosis inducing activity of lycopene oxidation products in different cancer cell lines. *Food Chem Toxicol.* (2016) 97:265–76. doi: 10.1016/j.fct.2016.09.016

179. Bolhassani A, Khavari A, Bathaie SZ. Saffron and natural carotenoids: biochemical activities and anti-tumor effects. *Biochim Biophys Acta Rev Cancer.* (2014) 1845:20–30. doi: 10.1016/j.bbcan.2013.11.001

180. Zhou Y, Li Y, Zhou T, Zheng J, Li S, Li H. Dietary natural products for prevention and treatment of liver cancer. *Nutrients.* (2016) 8:30156. doi: 10.3390/nu8030156

181. Blanchet A, Bourgmayer A, Kurtz JE, Mellitzer G, Gaiddon C. Isoforms of the p53 family and gastric cancer: a ménage à trois for an unfinished affair. *Cancers.* (2021) 13:1–45. doi: 10.3390/cancers13040916

182. Kunst C, Haderer M, Heckel S, Schlosser S, Müller M. The p53 family in hepatocellular carcinoma. *Transl Cancer Res.* (2016) 5:632–8. doi: 10.21037/tcr.2016.11.79

183. Nakayama M, Oshima M. Mutant p53 in colon cancer. *J Mol Cell Biol.* (2019) 11:267–76. doi: 10.1093/jmcb/mjy075

184. Jie M, Cheung WM, Yu V, Zhou Y, Tong PH, Ho JWS. Anti-proliferative activities of sinigrin on carcinogen-induced hepatotoxicity in rats. *PLoS ONE.* (2014) 9:110145. doi: 10.1371/journal.pone.0110145

185. Mazumder A, Dwivedi A, Plessis J. Sinigrin and its therapeutic benefits. *Molecules.* (2016) 21:40416. doi: 10.3390/molecules21040416

†These authors have contributed equally to this work and share first authorship

Hapten designs based on aldicarb for the development of a colloidal gold immunochromatographic quantitative test strip

Hong Shen[1†], Yuping Wan[2,3†], Xiaosheng Wu[2,3], Yu Zhang[2,3], Jingwen Li[4], Tingting Cui[2,3], Han Sun[1], Haifeng Cui[2,3], Kailun He[1], Guangpeng Hui[2,3], Xu Chen[2,3], Guoqiang Liu[2,3] and Meihong Du[4*]

[1]Biological Inspection Department, Zhejiang Institute for Food and Drug Control, Hangzhou, China, [2]Beijing Kwinbon Biotechnology Co., Ltd., Beijing, China, [3]Beijing Engineering Research Centre of Food Safety Immunodetection, Beijing, China, [4]Beijing Center for Physical and Chemical Analysis, Institute of Analysis and Testing, Beijing Academy of Science and Technology, Beijing, China

The common carbamate insecticide aldicarb is considered one of the most acutely toxic pesticides. Herein, rational design was used to synthesize two haptens with spacers of different carbon chain lengths. The haptens were then used to immunize mice. The antibodies obtained were evaluated systematically, and a colloidal gold immunochromatographic strip was developed based on an anti-aldicarb monoclonal antibody. The 50% inhibition concentration and linear range of anti-aldicarb monoclonal antibody immunized with Hapten 1 were 0.432 ng/mL and 0.106−1.757 ng/mL, respectively. The cross-reactivities for analogs of aldicarb were all <1%. The limit of detection of the colloidal gold immunochromatographic strip was 30 μg/kg, and the average recoveries of aldicarb ranged from 80.4 to 110.5% in spiked samples. In the analysis of spiked samples, the test strip could accurately identify positive samples detected by the instrumental method in the GB 23200.112-2018 standard but produced some false positives for negative samples. This assay provides a rapid and accurate preliminary screening method for the determination of aldicarb in agricultural products and environments.

Introduction

Aldicarb, chemically known as [(*E*)-(2-methyl-2-methylsulfanylpropylidene)amino]*N*-methylcarbamate, is a carbamate insecticidal, acaricidal, and anti-nematodal compound that is widely used to treat cotton, peanut, corn, and many other crops (1). Although aldicarb is easily degraded, with a half-life of only 5–12 days, degradation products such as aldicarb sulfoxide and aldicarb sulfone have stronger water solubility and environmental toxicity than the parent substance, leading to long-term pollution after dissolution in water (2). Therefore, they can often be detected in soil, air, water, and agricultural products (3–6), which has attracted extensive attention in various countries. For example, in China, the maximum residue limit (MRL) for aldicarb in bulb vegetables, brassica vegetables, and leaf vegetables is 0.03 mg/kg (7). Japan and England have set MRLs of 0.01–0.5 mg/kg for aldicarb in crops and vegetables. Therefore, it is necessary to develop sensitive, accurate, and efficient detection methods for aldicarb in agricultural products and environments.

At present, various instrumental analysis methods, such as gas chromatography and high-performance liquid chromatography–mass spectrometry (HPLC–MS), have been widely used for the detection of aldicarb (8–10). These methods are highly sensitive and provide accurate quantification and simultaneous detection of multiple indicators. However, these methods require expensive instruments, ongoing maintenance, professional technicians, cumbersome sample processing, and long detection times and, furthermore, are unsuitable for on-site detection (11). Immunological techniques are simple, economical, and rapid and thus can circumvent the shortcomings of instrumental methods (12). However, because aldicarb is toxic and unstable in the environment, there are few studies on haptens based on aldicarb. The first aldicarb hapten and associated enzyme-linked immunosorbent assay (ELISA) were developed in 1988 by Brady et al. (13). The aldicarb oxime hapten was prepared from *trans*-(aminomethyl)-cyclohexanecarboxylate, had high selectivity and was detectable at a low level of 0.3 mg/kg. In 2003, Siew et al. (14) synthesized a hapten based on aldicarb oxime ethyl acetate and coupled it with the carrier proteins bovine serum albumin (BSA) and keyhole limpet hemocyanin (KLH) to form two kinds of immunogens. They obtained two different monoclonal antibodies, but their inhibitory activities were not high (IC_{50} = 200 ng/mL), and the detection limit of the national standard was not achieved. Zhang et al. (15) designed and synthesized a new aldicarb hapten, aldicarb oxime succinic ester, and coupled it with BSA to prepare a polyclonal antibody. However, further research using an ELISA was not carried out, and the corresponding monoclonal antibody was not obtained. Yao (16) used aldicarb oxime as a raw material in one-step and two-step reactions to prepare two aldicarb haptens, which were then used to produce a monoclonal antibody with an IC_{50} of 18.505 ng/mL. Dichloromethane, which is a highly

toxic solvent with a low boiling point, was used in the costly preparation process to purify the product (17). Although these antibodies have been used for the detection of actual samples, they all have certain limitations, and for samples with complex matrices, they need to be diluted substantially to exclude matrix interference. Liu et al. (18) developed a rapid, simple, and sensitive immunochromatographic strip test to detect aldicarb in cucumber samples. The cutoff limit of the test strip for aldicarb was 100 ng/mL; however, this did not meet the MRL specified in the GB 2763 standard (7). Therefore, it is necessary to further improve the sensitivity of immunoassays using aldicarb haptens.

An effective immunoassay method requires antibodies with high affinity and selectivity. To achieve this, a suitable hapten for the immunogen is needed. Aldicarb has a small relative molecular mass and no immunogenicity, and thus it must be conjugated to a macromolecular carrier with immunogenicity (19). To realize coupling to macromolecular substances, the aldicarb hapten molecule must have an active group (such as –NH$_2$, –COOH, –OH, and –SH) that can covalently bind to the carrier, and to enhance the performance of the resulting antibody, the spacer arms of the hapten should be of a certain length (20). Current studies have found that the length and composition of the spacer arm affect the ability of the antibody to recognize the analyte, that is, the affinity of the antibody for the analyte, because the spacer arm affects the properties and structures of small pesticide molecules in artificial antigen molecules (21–23).

In this study, two aldicarb haptens differing in the carbon chain length of the spacer arm were used to prepare highly specific and highly sensitive anti-aldicarb monoclonal antibodies with an IC_{50} of 0.432 ng/mL. Compared with other antibodies (13–16, 18), the prepared monoclonal antibodies have significantly improved sensitivities. The immunological properties of the two antibodies were compared. In addition, a simple, rapid colloidal gold immunochromatographic method was developed, and its sensitivity and accuracy were evaluated. Specifically, spiked samples were analyzed using both the immunochromatographic method and an instrumental method, and the results from both methods were statistically compared.

Materials and methods

Reagents and apparatus

BALB/c mice (license number: SCXK2019-0010) were procured from SPF Biotechnology Co., Ltd. (Beijing, China). Standard materials (aldicarb, aldicarb sulfone, aldicarb sulfoxide, thiofanox, oxamyl, methomyl, metolcarb, isoprocarb, and carbofuran) were acquired from Dr. Ehrenstorfer GmbH (Augsberg, Germany). Freund's complete adjuvant and Freund's incomplete adjuvant, phosphate buffered saline (PBS; 10×), KLH, ovalbumin (OVA), *N,N*-dimethylformamide

(DMF), 1-ethyl-(3-dimethylaminopropyl) carbodiimide (EDC), N-hydroxysuccinimide (NHS), and goat anti-mouse IgG secondary antibody were purchased from Sangon Biotech Co., Ltd. (Shanghai, China). A mouse monoclonal antibody subtype identification ELISA kit was purchased from Sino Biological Co., Ltd. (Beijing, China).

UPLC–MS (Acquity UPLC, Waters, Milford, MA, United States and QTRAP 4000, SCIEX, Framingham, MA, United States) was used to identify the hapten structure. Hydrogen nuclear magnetic resonance (^{1}H NMR; AVANCE III-600, Bruker, Germany) spectra were also obtained to identify the hapten structure. Ultraviolet–visible (UV–Vis; UV-3600, Shimadzu, Japan) spectra were used to verify the coupling of haptens to carrier proteins. Other equipment included a GT-810 colloidal gold reader (Beijing Kwinbon Biotechnology Co., Ltd., Beijing, China).

Preparation of aldicarb hapten

Because the length and composition of the spacer arm in the hapten structure determine the specificity and sensitivity of the resultant monoclonal antibodies, in this study, spacer arms with different carbon chain lengths at the same position on the aldicarb molecule were used to prepare two haptens (Hapten 1 and Hapten 2). The synthetic processes are illustrated in Figure 1. The MS and ^{1}H NMR data for these haptens are shown in Supplementary Figure 1.

2-Methyl-2-(methylsulfanyl)propanaldoxime (1.33 g) was dissolved in 20 mL of DMF, to which 1.94 g of N,N-carbonyldiimidazole was added. The mixture was then stirred, and the reaction occurred at room temperature for 2 h. Then, 5 mL of an aqueous solution containing 2.06 g of aminobutyric acid was added, and the mixture was stirred at room temperature for 4 h. After the reaction was completed, 200 mL of water was added, and the mixture was stirred and transferred to a separatory funnel. Then, 200 mL of ethyl acetate was added, and the mixture was shaken and allowed to stand still. The aqueous phase was separated, and the organic phase was evaporated to dryness to obtain a yellow oily substance, which was passed through a silica gel column (petroleum ether: ethyl acetate = 5:1). Finally, 1.72 g of the carboxy-aldicarb hapten product, Hapten 1, was obtained, and the yield was 65.65%. The product was characterized by ESI-MS and ^{1}H NMR. ESI-MS, m/z: 261.16 [M–H]$^-$; ^{1}H NMR (600 MHz, DMSO): δ12.07 (s, 1H), 7.62 (s, 1H), 3.37 (s, 5H), 3.08 (dd, J = 13.0, 6.6 Hz, 2H), 2.53–2.47 (m, 2H), 2.23 (t, J = 7.4 Hz, 2H), 1.94 (s, 3H), 1.67 (p, J = 7.2 Hz, 2H), 1.40 (s, 6H).

2-Methyl-2-(methylsulfanyl)propanaldoxime (1.33 g) was dissolved in 50 mL of pyridine, to which 1.29 g of succinic anhydride was added. The mixture was stirred, heated to 80°C, and allowed to react for 4 h. After the reaction was completed, the mixture was cooled to room temperature, and pyridine was

removed by rotary evaporation. The residue was dissolved in 200 mL of water and 8 mL of 1 M hydrochloric acid, and the pH of the mixture was adjusted to 6. Then, 150 mL of ethyl acetate was added, and the mixture was stirred and transferred to a separatory funnel. The aqueous phase was separated, and the organic phase was evaporated to dryness by rotary evaporation to obtain a crude product, which was passed through a silica gel column (dichloromethane:methanol = 10:1) to obtain 2.12 g of the aldicarb succinate hapten product, Hapten 2, with a yield of 90.99%. The product structure was confirmed by ESI-MS and ^{1}H NMR. ESI-MS, m/z: 232.26 [M–H]$^-$; ^{1}H NMR (600 MHz, DMSO): δ12.23 (s, 1H), 7.75 (s, 1H), 3.33 (s, 12H), 2.62 (dd, J = 7.4, 5.5 Hz, 2H), 2.52 (dd, J = 7.5, 5.5 Hz, 2H), 2.51–2.49 (m, 5H), 1.95 (s, 3H), 1.40 (s, 6H).

Preparation of artificial antigens

Using the active ester method (EDC/NHS) (24), the synthetized haptens were coupled to the carrier proteins KLH and OVA.

To synthesize the first immunogen, 1.74 mg of Hapten 1 was dissolved in 0.3 mL of DMF, to which 3.06 mg of NHS and 5.01 mg of EDC were added. The mixture was stirred at room temperature for 2 h. Then, 10 mg of KLH was dissolved in 1 mL of carbonate–bicarbonate (CB) buffer (0.1 M, pH 9.1), and the hapten reaction solution was slowly added. The mixture was stirred at room temperature for 4 h. After the reaction was completed, the mixture was placed into a dialysis bag for dialysis with 0.02 M PBS for 3 days. The medium was changed three times a day. The dialyzed mixture was centrifuged to obtain the immunogen Hapten 1-KLH, which was stored at –20°C. To synthesize the second immunogen, 1.54 mg of Hapten 2 was dissolved in 0.3 mL of DMF, to which 4.54 mg of NHS and 7.6 mg of EDC were added. The remaining steps were the same as the above operation, which was applied to obtain the immunogen Hapten 2-KLH.

To synthesize the coated hapten, Hapten 1 (11.65 mg) was dissolved in 1 mL of DMF, to which 21 mg of NHS and 35 mg of EDC were added. The mixture was stirred at room temperature for 2 h. Then, OVA (100 mg) was dissolved in 1 mL of CB buffer (0.1 M, pH 9.1). The remaining steps were the same as the above operations, which were applied to obtain Hapten 1-OVA. Similarly, to synthesize the second coated hapten, Hapten 2 (10.3 mg) was dissolved in 1 mL of DMF, to which 20.4 mg of NHS and 33.1 mg of EDC were added. The remaining steps were the same as the above operations, which were applied to obtain Hapten 2-OVA.

The aldicarb haptens, carrier proteins, and conjugates synthesized above were examined using UV spectrophotometry to determine whether the hapten was successfully coupled to the carrier protein.
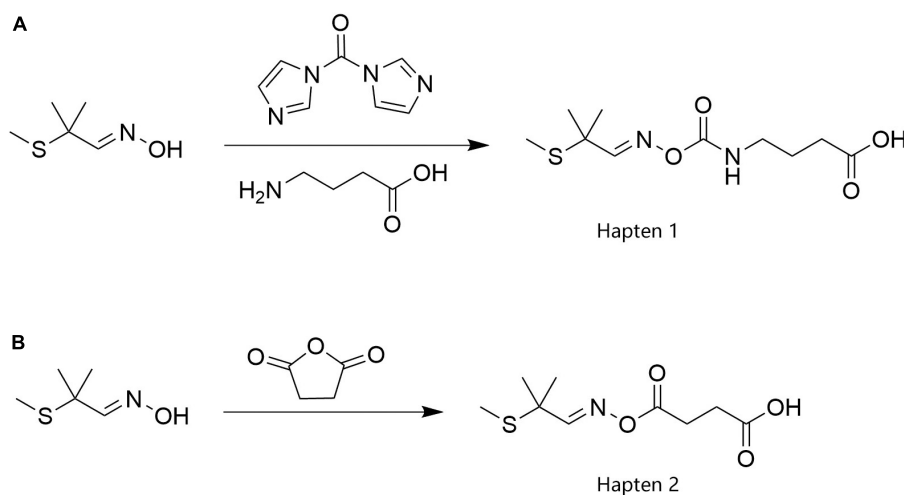
Preparation and titer detection of antiserum

Healthy 6–8-week-old female BALB/c mice were selected and immunized with the immunogens Hapten 1-KLH and Hapten 2-KLH at a dose of 200 μg. For the first immunization, an equal volume of Freund's adjuvant was used for emulsification. After emulsification was completed, subcutaneous injection was carried out on the back of the neck at multiple points. Thereafter, the dose was boosted and emulsified with Freund's incomplete adjuvant, and the mice were immunized once every 14 days for a total of 3 immunizations. On the seventh day after the fourth immunization, the blood of the mice was taken from the severed tail and centrifuged at 5,000 r/min for 5 min to obtain mouse serum. Serum titers were determined by indirect ELISA (25), and the spleen was selected for subsequent experiments.

Preparation of monoclonal antibodies and analysis of their immunological properties

Mouse spleen cells were fused with myeloma cells, and the cell lines that could stably secrete anti-aldicarb monoclonal antibodies were screened through cell culturing, screening, and other steps (26). Ascites antibodies were prepared by *in vivo* induction, and the anti-aldicarb monoclonal antibody was purified using octanoic acid and saturated sulfuric acid following the ammonium method (27).

A mouse monoclonal antibody subtype identification ELISA kit was used to identify the antibody subtype. Indirect competitive ELISA (icELISA) was used to determine the

50% inhibitory mass concentration (IC_{50}) of the monoclonal antibody against aldicarb, and IC_{50} was used to measure the sensitivity of the monoclonal antibody (28). Cross-reaction tests were used to determine specificity, in which aldicarb sulfone, aldicarb sulfoxide, thiofanox, oxamyl, methomyl, metolcarb, isoprocarb, and carbofuran were selected as inhibitors. The IC_{50} of each inhibitor was determined by icELISA, and the IC_{50} of the monoclonal antibody against aldicarb and the IC_{50} of the inhibitor were taken as the cross-reaction rate.

Sample preparation

Cabbage and leek samples obtained from local markets were confirmed to be negative for aldicarb using liquid chromatography (LC). The parameters for LC analysis are described in supplementary section 1.

The negative samples were mixed with an aldicarb standard solution to make positive cabbage and leek samples with aldicarb concentrations of 30 and 60 μg/kg, respectively. Each sample was extracted according to the following method. The cabbage and leeks were cut into 1-cm square pieces. The sample (2.00 ± 0.05 g) was mixed with 6 mL phosphate buffer (0.1 M, pH = 7.4), and the mixture was vortexed for 1 min and allowed to stand for 5 min. The upper liquid layer was tested.

Preparation of colloidal gold immunochromatographic test strips

Colloidal gold particles were prepared following the trisodium citrate reduction method (29), and the surface

TABLE 1   Results for mouse antiserum.

Immunogen	Negative OD$_{450}$	Positive OD$_{450}$	Potency	Inhibition rate (%)*
Hapten 1-KLH	1.925	0.807	10,000	58.1
Hapten 2-KLH	1.582	0.874	3,000	44.7

*Inhibition rate = (negative OD$_{450}$ − positive OD$_{450}$)/negative OD$_{450}$ × 100%. The concentrations of aldicarb used for determining the negative and positive OD$_{450}$ were 0 and 30 μg/L, respectively.

of the gold nanoparticles was labeled with the anti-aldicarb monoclonal antibody by referring to the method of Liu (30). Thereafter, 100 μL of anti-aldicarb monoclonal antibody-labeled colloidal gold was added to the microplate. The microplate was then treated for 3 h in a cold trap at −50°C and vacuum-dried for 15 h to obtain a lyophilized microporous reagent with anti-aldicarb monoclonal antibody-labeled colloidal gold, which was sealed.

The nitrocellulose (NC) membrane was coated with Hapten 1-OVA (1 mg/mL) as the test line (T line) and goat anti-mouse IgG antibody (0.5 mg/mL) as the control line (C line). The coated NC membrane was dried at 37°C for 16 h. The sample pad was immersed in working buffer for 2 h and dried at 37°C for 2 h.

The NC membrane coated with capture reagents was pasted in the center of the PVC backing plate and the sample pad, and the absorbent pad was laminated and pasted onto the backing plate. Finally, the plate was cut into 4-mm-wide strips.

Optimization of the test strip

The type of NC membrane and sample pad and the working buffer for the sample pad were optimized to improve the sensitivity of the immunoassay. The immunoassays were evaluated using the coefficient of the T/C value.

Use of test strips and evaluation of performance indicators

The test solution (100 μL) was pipetted into the lyophilized microwell with anti-aldicarb monoclonal antibody-labeled colloidal gold marker, which was slowly aspirated and fully mixed with the reagent in the microwell. Incubation occurred at 25°C for 3 min. Then, the liquid (100 μL) was dropped vertically into the sample hole of the test strip. Timing started when the liquid flowed, and the reaction was performed for 10 min. The color intensities of the T and C lines were read using a colloidal gold reader, and the T/C value was calculated.

The T/C value of the standard solution with aldicarb mass fractions of 0, 1.25, 2.5, 5, and 10 ng/mL was determined. Each mass fraction was tested 3 times in parallel, and the average value was calculated. A standard curve, with the aldicarb mass fraction

on the abscissa and the T/C value on the ordinate, was drawn. The sensitivity and linear range of the prepared test strips were obtained from the standard curve. Twenty negative vegetable samples were analyzed, and the corresponding concentration of each sample T/C value was calculated using the standard curve. The detection limit was reported as the average concentration of 20 samples plus 3 times the standard deviation (31).

The positive samples prepared in section "Sample preparation" were measured. Six parallel tests were conducted with three batches of test strips at each level, and the addition recovery and intra-assay coefficient of variation were calculated using the actual measured value of each added mass fraction to judge the test strip accuracy and precision.

Twenty vegetable samples, including samples that were negative and exceeded the standard, were prepared by mixing vegetables with an aldicarb standard solution. The samples were randomly assigned a number between 1 and 20. The samples were tested by aldicarb test strips and an instrumental method to determine the coincidence rate of positive samples. The instrument detection method was carried out with reference to the method of China National Standard GB 23200.112-2018 (32).

The test strips and the lyophilized microporous reagent with anti-aldicarb monoclonal antibody-labeled colloidal gold were stored at 4°C, room temperature, and 37°C, respectively. The test strips were tested on days 1, 3, 6, 9, 12, and 15. The T/C
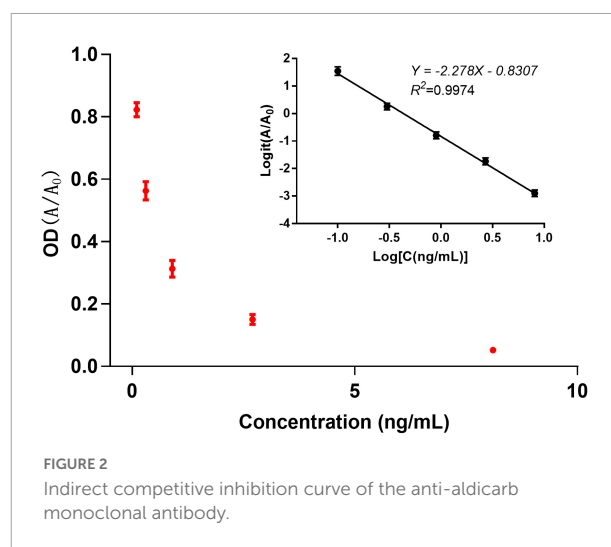

FIGURE 2
Indirect competitive inhibition curve of the anti-aldicarb monoclonal antibody.

values of cabbage samples with aldicarb concentrations of 0 and 30 µg/kg were investigated to evaluate the stability of the strip.

Results and discussion

Identification of artificial antigens

UV–Vis spectroscopy data were used to identify the coupling of the hapten to the carrier protein (**Supplementary Figure 2**). Obvious differences in the absorption wavelengths were observed among the conjugates and haptens. The hapten-to-protein molar ratios were estimated at 16.2 and 12.6 for haptens–KLHs and 5.2 and 4.1 for haptens–OVAs.

Titer detection of aldicarb antiserum
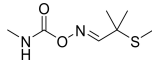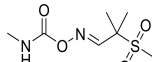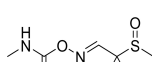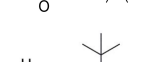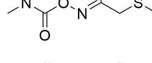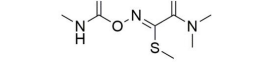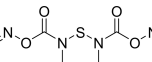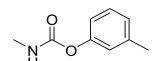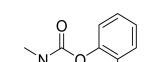
After the fourth immunization, the blood of the mice was taken from the severed tail and examined using indirect ELISA. The absorbance at 450 nm (OD_{450}) was measured using a microplate reader. The absorbance value of 0.8–1.2 was selected to calculate the inhibition rate, and the

corresponding dilution multiple was used as the antiserum efficacy value. As shown in **Table 1**, the potency of the antiserum produced by the immunogen Hapten 1-KLH was 10,000, and the inhibition rate was 58.1%. This value was relatively high because Hapten 1 retained the molecular structure of aldicarb, which allowed recognition by immune active cells to the greatest extent and thus stimulation of the body to produce a specific immune response and antibodies with high specificity for the test object (33). Therefore, the antiserum produced using the immunogen Hapten 1-KLH was selected for the next experiment.

Immunological characteristics of anti-aldicarb monoclonal antibody

Three mice were immunized with the immunogen Hapten 1-KLH, and three positive cell lines were obtained after three immunizations, one booster immunization, and fusion cloning. The subtypes of the three cell lines were identified as MC-28, MC-54, and MC-65, all of which were IgG1. Analysis of the supernatant showed that the MC-54 cell line had the highest inhibition rate (**Supplementary Table 2**). Therefore, the MC-54 antibody was selected to develop

TABLE 2 Cross-reactivity rates of anti-aldicarb monoclonal antibodies.

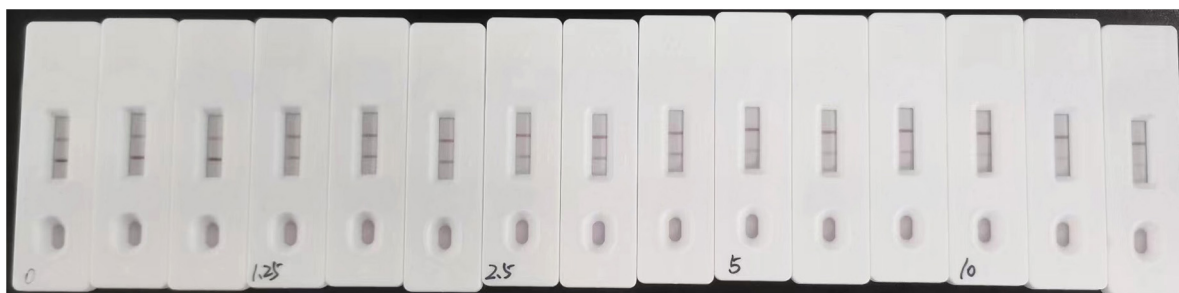| Compound	Chemical structure	Molecular formula	IC$_{50}$ (µg/L)	Cross-reaction rate (%)
Aldicarb		$C_7H_{14}N_2O_2S$	0.411	100
Aldicarb sulfone		$C_7H_{14}N_2O_4S$	>42	<0.978
Aldicarb sulfoxide		$C_7H_{14}N_2O_3S$	>42	<0.978
Thiofanox		$C_9H_{18}N_2O_2S$	>42	<0.978
Oxamyl		$C_7H_{13}N_3O_3S$	>42	<0.978
Methomyl		$C_5H_{10}N_2O_2S$	>42	<0.978
Metolcarb		$C_9H_{11}NO_2$	>42	<0.978
Isoprocarb		$C_{11}H_{15}NO_2$	>42	<0.978
Carbofuran		$C_{12}H_{15}NO_3$	>42	<0.978

FIGURE 3
Colloidal gold immunochromatography assay for aldicarb in standard solution.

colloidal gold immunochromatographic test strips in the subsequent experiments.

The sensitivity of the anti-aldicarb monoclonal antibody was determined using icELISA. An indirect competitive inhibition curve, with the logarithm of the standard concentration as the abscissa and the Logit value of the percent absorbance at 450 nm (A/A_0) as the ordinate, was drawn using GraphPad Prism 7.02 (**Figure 2**). The best fit had a correlation coefficient R^2 of >0.99. The IC_{50} of the anti-aldicarb monoclonal antibody was 0.432 ng/mL, and the linear range (IC_{20}–IC_{80}) was 0.106–1.757 ng/mL.

Antibody specificity is the ability of the antibody to bind to a specific antigen in preference over antigen analogs. The cross-reactivity rate is often used as an evaluation standard because an inverse relationship exists between the cross-reactivity rate and the specificity of the antibody. In this study, we selected aldicarb sulfone, aldicarb sulfoxide, thiofanox, oxamyl, methomyl, metolcarb, isoprocarb, and carbofuran, with chemical structures similar to that of aldicarb, for the specificity analysis. The results showed that the monoclonal antibody was specific to aldicarb and had no significant cross-reactivity with aldicarb sulfone, aldicarb sulfoxide, thiofanox, oxamyl, methomyl, metolcarb, isoprocarb, or carbofuran ($<1\%$) (**Table 2**).

Optimization of the test strip

Test strips were assembled with three different types of NC membranes (Milipore 90, Unisart CN 140, and Nupore 70) and used to detect the negative sample extract. The relative standard deviations (RSDs) of the T/C values were compared. Each NC membrane was tested 15 times. The RSD of Unisart CN 140 was lower than that of the other two membranes (**Supplementary Table 4**), and it was selected as the optimum NC membrane.

Similar experiments were performed to screen the working buffer for the sample pad. The lowest RSD was obtained with working buffer #5 (**Supplementary Table 5**). Therefore, the optimum working buffer for the sample pad was 0.02

M PBS (pH 7.4) containing 0.5% BSA, 0.05% Triton X-100, and 5.0% sucrose.

Next, sample pads prepared using different materials (nonwoven fabric, glass fiber, and whole blood filtration membrane) were treated with buffer #5 and used to assemble the test strip. Among these materials, the whole blood filtration membrane showed the fastest absorption rate for the sample solution (**Supplementary Table 6**). The glass fiber and nonwoven fabric had the same absorption rate, but the nonwoven fabric had the lowest RSD. Therefore, nonwoven fabric was selected as the best material for the sample pad.

Evaluation of performance indicators of colloidal gold immunochromatographic test strips

The sensitivity of the assay was investigated with a series aldicarb standards. **Figure 3** shows that the signal color on the test lines changed from strong (0 ng/mL) to weak and finally
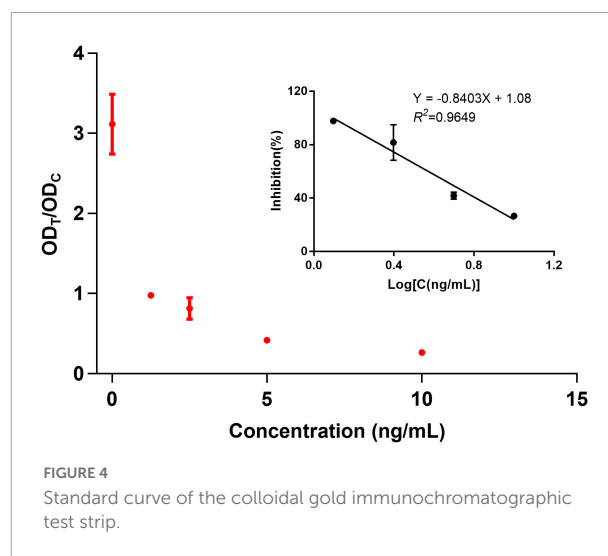

FIGURE 4
Standard curve of the colloidal gold immunochromatographic test strip.

TABLE 3 Test strip detection limit determination results (μg/kg).

	Leek				Cabbage		
Sample number	Measured value	Sample number	Measured value	Sample number	Measured value	Sample number	Measured value
1	5.6	11	12.2	1	13.6	11	2.1
2	1.8	12	6.1	2	4.7	12	9.5
3	0.2	13	5.5	3	0.8	13	6.7
4	11.3	14	9.4	4	2.6	14	21.6
5	2.7	15	7.8	5	11.9	15	0.0
6	4.9	16	22.4	6	0.0	16	1.7
7	20.6	17	1.5	7	6.1	17	24.6
8	0.0	18	3.9	8	15.2	18	8.8
9	8.2	19	14.8	9	7.3	19	4.5
10	3.5	20	6.6	10	5.8	20	10.6
Average value			7.45	Average value			7.90
Standard deviation			6.22	Standard deviation			6.83
Limit of detection			26.11	Limit of detection			28.39

disappeared completely at 10 ng/mL aldicab. In the quantitative assay, the color intensities of the T and C lines were read using a colloidal gold reader, and the T/C value was calculated. Then, an indirect competitive inhibition curve, with the logarithm of the standard concentration as the abscissa and the T/C value from the T- and C-line color intensity of the colloidal gold readout (OD_T/OD_C) as the ordinate, was drawn using GraphPad Prism 7.02 (Figure 4). There was a good linear relationship between the T/C value of the test strip and the logarithm of the aldicarb concentration in the range of 1.25–10 ng/mL (Figure 4). The linear equation of the best fit was Y = −0.8403X + 1.08, and

the correlation coefficient R^2 was 0.9649. The T/C values of the samples were determined using the same method, and the aldicarb concentration in each sample was calculated using the standard curve.

The detection limits of aldicarb in leek and cabbage samples were 26.11 and 28.39 μg/kg, respectively (Table 3). To ensure the accuracy and stability of the colloidal gold immunochromatographic method and to avoid false negatives, the detection limit of aldicarb in the vegetable samples was set to 30 μg/kg, which met the maximum residue limit specified in GB 2763 (7). The leek and cabbage samples were spiked with the aldicarb standard solution at final aldicard concentrations of 30 and 60 μg/kg. The spiked samples were analyzed with the test strip, and the results are summarized in Figure 5. Moreover, the aldicarb concentrations of the spiked samples were measured using a colloidal gold reader. As shown in Table 4, the average spiked recoveries of the leek and cabbage samples were 80.4%–110.5%, and the intra- and interassay relative standard deviations were <15%, indicating good accuracy and repeatability.

Among the 20 vegetable samples, eight samples were identified as positive by both the GB 23200.112-2018 standard method (32) and the test strip. Only sample 13 was identified as positive by the test strip (41.5 μg/kg) but negative by the instrumental method. Therefore, the test strip can accurately detect positive samples but with some false positives. This method could be applied to the detection and screening of aldicarb in vegetables, although the identification of positive samples needs to be confirmed by instrumental methods.

To evaluate the temperature stability, test strips were stored at 4°C, room temperature, and 37°C for 15 days.
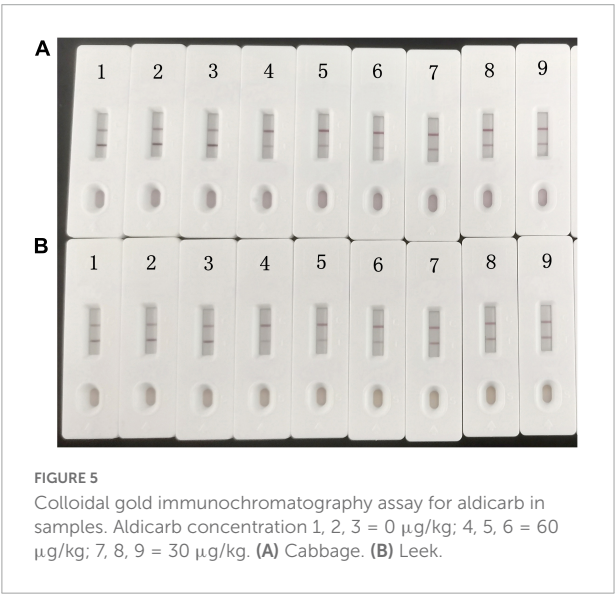

FIGURE 5
Colloidal gold immunochromatography assay for aldicarb in samples. Aldicarb concentration 1, 2, 3 = 0 μg/kg; 4, 5, 6 = 60 μg/kg; 7, 8, 9 = 30 μg/kg. (A) Cabbage. (B) Leek.

TABLE 4 Test strip accuracy and precision test results.

Sample	Add concentration (μg/kg)	Test strip batches	Recovery rate (%)	Intra-assay RSD ($n = 6$, %)	Average intra-assay RSD (%)	Inter-assay RSD ($n = 3$, %)
Leek	30	G-1	84.3/92.7/88.5/89.2/102.8/94.1	6.9	6.7	7.8
		G-2	96.4/82.9/90.3/91.6/85.2/85.6	5.7		
		G-3	94.7/110.5/95.6/89.7/95.5/103.5	7.6		
	60	G-1	100.5/108.3/92.7/103.1/101.9/105.8	5.3	6.7	8.6
		G-2	88.4/96.7/97.3/106.8/104.5/91.2	7.4		
		G-3	87.3/83.9/88.1/96.5/80.4/96.2	7.3		
Cabbage	30	G-1	85.6/93.1/86.4/85.9/100.4/81.7	7.6	7.9	9.5
		G-2	108.9/94.6/93.8/97.4/109.5/93.2	7.6		
		G-3	85.4/109.2/107.5/98.3/103.7/102.4	8.5		
	60	G-1	93.5/97.1/102.8/85.4/91.7/94.5	6.1	6.2	8.0
		G-2	105.1/99.6/106.2/89.5/100.3/108.6	6.7		
		G-3	88.2/82.9/92.3/93.7/84.4/95.1	5.7		

After storage, the test strips were used to analyze cabbage samples with aldicarb concentrations of 0 and 30 μg/kg. The T/C values obtained showed no significant changes (**Supplementary Figure 3**).

Conclusion

Aldicarb is a small molecule without immunogenicity and must be conjugated with carrier proteins to induce an appropriate immune response in animals. To synthesize complete antigens, haptens must be rationally designed to obtain high specificity (34). Two haptens, Hapten 1 and Hapten 2, with spacers of different carbon chain lengths were designed and synthesized using 2-methyl-2-(methylsulfanyl)propanaldoxime as the raw material. Hapten 1 retained more of the aldicarb molecular structure than Hapten 2, and from an analysis of the length of the introduced side chain, the distance of a chain of three carbon atoms ending in the -COOH group on the aldicarb molecule satisfied the distance for minimal interaction between each carrier protein. Effective coupling of aldicarb is required to expose the epitope of the aldicarb molecule, thus improving the specificity of the antibody (35). After immunizing the mice, we successfully obtained a highly specific and highly sensitive anti-aldicarb monoclonal antibody with an IC_{50} of 0.432 ng/mL and a linear range of 0.106–1.757 ng/mL, which showed no cross-reactivity with other structural analogs. Colloidal gold immunochromatography based on the prepared monoclonal antibody was demonstrated to be a rapid method for the detection of aldicarb residues in vegetables, with a detection limit of 30 μg/kg and a recovery rate of 80.4–110.5%. Moreover, the relative standard deviation between batches was less than 15%. Compared with instrumental analysis methods, colloidal gold immunochromatography has the advantages of simple operation, rapid detection, and low cost. However, owing to the technical limitations of colloidal gold immunochromatography, problems such as false positives may occur, and thus positive samples need to be confirmed through instrumental methods. Nevertheless, as a rapid screening method, this method can be widely used for the on-site screening and detection of aldicarb residues in vegetables and has important economic and social value.

Data availability statement

The original contributions presented in this study are included in the article/**Supplementary material**, further inquiries can be directed to the corresponding author.

Ethics statement

This animal study was reviewed and approved by the Beijing Kwinbon Biotechnology Co., Ltd. Written informed consent was obtained from the owners for the participation of their animals in this study.

Author contributions

MD and YW: conception and design of the study. HSh and YW: methodology. HSh, JL, HSu, and YZ: data curation. HC, XW, and KH: data statistical analysis. GH, XC, and GL: validation. TC: writing the first draft of the manuscript. All authors contributed

to manuscript revision, read, and approved the submitted version.

Conflict of interest

YW, XW, YZ, TC, HC, GH, XC, and GL were employed by the Beijing Kwinbon Biotechnology Co., Ltd.

The remaining authors declare that the research was conducted in the absence of any commercial or financial relationships that could be construed as a potential conflict of interest.

Publisher's note

All claims expressed in this article are solely those of the authors and do not necessarily represent those of their affiliated organizations, or those of the publisher, the editors and the reviewers. Any product that may be evaluated in this article, or claim that may be made by its manufacturer, is not guaranteed or endorsed by the publisher.

Supplementary material

The Supplementary Material for this article can be found online at: https://www.frontiersin.org/articles/10.3389/fnut.2022.976284/full#supplementary-material

References

1. Sajwan RK, Lakshmi GBVS, Solanki PR. Fluorescence tuning behavior of carbon quantum dots with gold nanoparticles *via* novel intercalation effect of aldicarb. *Food Chem.* (2020) 340:127835. doi: 10.1016/j.foodchem.2020.127835

2. Küster E, Altenburger R. Suborganismic and organismic effects of aldicarb and its metabolite aldicarb-sulfoxide to the zebrafish embryo (*Danio rerio*). *Chemosphere.* (2007) 68:751–60. doi: 10.1016/j.chemosphere.2006.12.093

3. Fisher IJ, Phillips PJ, Bayraktar BN, Chen S, McCarthy BA, Sandstrom MW, et al. Pesticides and their degradates in groundwater reflect past use and current management strategies, Long Island, New York, USA. *Sci Tot Environ.* (2020) 752:141895. doi: 10.1016/j.scitotenv.2020.141895

4. Li YB, Qin GF, He FR, Zou K, Zuo B, Liu R, et al. Investigation and analysis of pesticide residues in edible fungi produced in the mid-western region of China. *Food Control.* (2022) 136:108857. doi: 10.1016/j.foodcont.2022.108857

5. Boucaud-Maitre D, Ranabourg MO, Sinno-Tellier S, Puskarczyk E, Pineau X, Kammerer M, et al. Human exposure to banned pesticides reported to the French Poison Control Centers: 2012-2016. *Environ Toxicol Pharmacol.* (2019) 69:51–6. doi: 10.1016/j.etap.2019.03.017

6. Somashekar KM, Mahima MR, Manjunath KC. Contamination of water sources in Mysore City by pesticide residues and plasticizer – a cause of health concern. *Aquatic Proc.* (2015) 4:1181–8. doi: 10.1016/j.aqpro.2015.02.150

7. GB 2763-2021. *National Food Safety Standard—Maximum Residue Limits For Pesticides In Food.* Beijing: China Agricultural Press (2021).

8. Dai XL, Luan Y, Wang XY, Hua S, Hu C. Gas chromatographic determination of aldicarb and its metabolites in urine. *J Chromatogr A.* (1991) 542:526–30. doi: 10.1016/S0021-9673(01)88788-4

9. Nunes GS, Alonso RM, Ribeiro ML, Barceló D. Determination of aldicarb, aldicarb sulfoxide and aldicarb sulfone in some fruits and vegetables using high-performance liquid chromatography-atmospheric pressure chemical ionization mass spectrometry. *J Chromatogr A.* (2000) 888:113–20. doi: 10.1016/s0021-9673(00)00553-7

10. Totti S, Fernández M, Ghini S, Picó Y, Fini F, Mañes J, et al. Application of matrix solid phase dispersion to the determination of imidacloprid, carbaryl, aldicarb, and their main metabolites in honeybees by liquid chromatography-mass spectrometry detection. *Talanta.* (2006) 69:724–9. doi: 10.1016/j.talanta.2005.11.012

11. Wang YL, Xu JL, Qiu YL. Highly specific monoclonal antibody and sensitive quantum dot beads-based fluorescence immunochromatographic test strip for tebuconazole assay in agricultural products. *J Agric Food Chem.* (2019) 67:9096–103. doi: 10.1021/acs.jafc.9b02832

12. Esteve-Turrillas FA, Mercader JV, Agullo C, Abad-Somovilla A, Abad-Fuentes A. Highly sensitive monoclonal antibody-based immunoassays for boscalid analysis in strawberries. *Food Chem.* (2018) 267:2–9. doi: 10.1016/j.foodchem.2017.06.013

13. Brady JF, Fleeker JR, Wilson RA. Enzyme immunoassay for aldicarb. *Am Chem Soc.* (1988) 1021:262–84. doi: 10.1021/bk-1988-0382.ch021

14. Siew LK, Winger LA, Spoors JA, Dessi JL, Jennens L, Self CH, et al. Monoclonal antibodies useful in sensitive immunoassays for aldicarb in either laboratory or the field. *Int J Environ Anal Chem.* (2003) 83:417–26. doi: 10.1080/0306731031000099819

15. Zhang YF, Gao ZX, Zhang QM, Dai SG. A new hapten for immunoassay of aldicarb. *Chin Chem Lett.* (2006) 17:1021–4.

16. Yao LJ. *Development of rapid immunoassay of imidacloprid, acetamiprid, carbofuran and aldicarb.* Jiangsu: Jiangnan University (2017).

17. Zhang M, Yan H, Liu BF. Toxicity and bio-monitoring of dichloromethane: A review of recent studies. *J Environ Health.* (2015) 32:1108–12.

18. Liu LQ, Suryoprabowo S, Zheng QK, Song S, Kuang H. Rapid detection of aldicarb in cucumber with animmunochromatographic test strip. *Food Agric Immunol.* (2017) 28:427–38. doi: 10.1080/09540105.2017.1293015

19. Weltzien HU, Moulon C, Martin S, Padovan E, Hartmann U, Kohler J, et al. T cell immune responses to haptens. Structural models for allergic and autoimmune reactions. *Toxicology.* (1996) 107:141–51. doi: 10.1016/0300-483x(95)03253-c

20. Kim YJ, Cho YA, Lee HS, Lee YT. Investigation of the effect of hapten heterology on immunoassay sensitivity and development of an enzyme-linked immunosorbent assay for the organophosphorus insecticide fenthion. *Anal Chim Acta.* (2003) 494:29–40. doi: 10.1016/j.aca.2003.07.003

21. Kim YJ, Cho YA, Lee HS, Lee YT, Gee SJ, Hammock BD, et al. Synthesis of haptens for immunoassay of organophosphorus pesticides and effect of heterology in hapten spacer arm length on immunoassay sensitivity. *Anal Chim Acta.* (2003) 475:85–96. doi: 10.1016/S0003-2670(02)01037-1

22. Mari GM, Li HF, Dong BL, Yang H, Talpur A, Mi J, et al. Hapten synthesis, monoclonal antibody production and immunoassay development for direct detection of 4-hydroxybenzehydrazide in chicken, the metabolite of nifuroxazide. *Food Chem.* (2021) 355:129598. doi: 10.1016/j.foodchem.2021.129598

23. Esteve-Turrillas FA, Meracde JV, Agullo C, Abad-Somovilla A, Abad-Fuentes A. Site-heterologous haptens and competitive monoclonal antibody-based immunoassays for pyrimethanil residue analysis in foodstuffs. *LWT Food Sci Technol.* (2015) 63:604–11. doi: 10.1016/j.lwt.2015.03.074

24. Lee JK, Ahn KC, Stoutamire DW, Gee SJ, Hammock BD. Development of an enzyme-linked immunosorbent assay for the detection of the organophosphorus insecticide acephate. *J Agric Food Chem.* (2003) 51:3695–703. doi: 10.1021/jf021020i

25. Li YQ. Study on immunoassay of quinclorac and bensulfuron methyl. *Chin Acad Agric Sci Thesis.* (2021). doi: 10.27630/d.cnki.gznky.2021.000732

26. Shen H, Li C, Sun H, Chen W, Chen B, Yi Y, et al. Generation and characterization of an anti-diclazuril monoclonal antibody and development of a diagnostic ELISA for poultry. *Front Nutr.* (2022) 9:910876. doi: 10.3389/fnut.2022.910876

27. Kuang H, Xing C, Hao C, Liu L, Wang L, Xu C, et al. Rapid and highly sensitive detection of lead ions in drinking water based on a strip immunosensor. *Sensors.* (2013) 13:4214–24. doi: 10.3390/s130404214

28. Li PW, Zhou Q, Wang T, Zhou H, Zhang W, Ding X, et al. Development of an enzyme-linked immunosorbent assay method specific for the detection of G-group aflatoxins. *Toxins.* (2016) 8:1–11. doi: 10.3390/toxins8010005

29. Putalun W, Morinaga O, Tanaka H. Development of a one-step immunochromatographic strip test for the detection of sennosides A and B. *Phytochem Anal.* (2004) 15:112–6. doi: 10.1002/pca.752

30. Liu X, Xiang JJ, Tang Y, Zhang XL, Fu QQ, Zou JH, et al. Colloidal gold nanoparticle probe-based immunochromatographic assay for the rapid detection of chromium ions in water and serum samples. *Anal Chim Acta.* (2012) 745:99–105. doi: 10.1016/j.aca.2012.06.029

31. SN/T 2775-2011. *Methods for the evaluation of commercial test kits for food testing purpose.* China's General Administration of Quality Supervision, Inspection and Quarantine (2011).

32. GB 23200.112-2018. *National Food Safety Standard Determination Of 9 Carbamate Pesticides And Metabolites Residues In Foods Of Plant Origin Liquid Chromatography Post Column Derivatization Method.* Beijing: China Agricultural Press (2021).

33. Goodrow MH, Hammock BD. Hapten design for compound-selective antibodies: ELISAs for environmentally deleterious small molecules. *Anal Chim Acta.* (1998) 376:83–91. doi: 10.1016/S0003-2670(98)00433-4

34. Gefen T, Vaya J, Khatib S, Rapoport I, Lupo M, Barnea E, et al. The effect of haptens on protein-carrier immunogenicity. *Immunology.* (2015) 144:116–26. doi: 10.1111/imm.12356

35. Shelver WL, Smith DJ. Enzyme-linked immunosorbent assay development for the beta-adrenergic agonist zilpaterol. *Agric Food Chem.* (2004) 52:2159–66. doi: 10.1021/jf049919i

Residue, dissipation, and dietary intake evaluation of fenpyroximate acaricide in/on guava, orange, and eggplant under open field condition

Farag Malhat[1]*, Osama Abdallah[1], Chris Anagnostopoulos[2]*, Mohamed Hussien[3], Indra Purnama[4], Rania M. A. Helmy[1], Hanim Soliman[1] and Dalia El-Hefny[1]

[1]Pesticide Residues and Environmental Pollution Department, Central Agricultural Pesticide Laboratory, Agricultural Research Center, Giza, Egypt, [2]Benaki Phytopathological Institute, Department of Pesticides Control and Phytopharmacy, Laboratory of Pesticides Residues, Athens, Greece, [3]Department of Chemistry, Faculty of Science, King Khalid University, Abha, Saudi Arabia, [4]Department of Agrotechnology, Universitas Lancang Kuning, Pekanbaru, Indonesia

Fenpyroximate is a widely used acaricide applicable in many crops. In this study, the residue behavior of fenpyroximate on eggplant, orange, and guava was investigated. The chronic and acute dietary intake was calculated at several sampling points, and preharvest intervals (PHI) were proposed to ensure compliance with the existing maximum residue levels. A simple extraction protocol combined with ultrahigh-performance liquid chromatography−tandem mass spectrometry (UHPLC-MS/MS) was employed to quantify residue levels. The method was successfully validated according to the European Union (EU) guidelines, and a limit of quantification of 0.01 mg/kg was set. The dissipation patterns in all crops could be described by the first-order kinetics model with half-lives of 1.7, 2.2, and 1.9 days for eggplants, guavas, and oranges, respectively. The dietary risk assessment at the authorized or more critical application patterns was acceptable for the consumers. For oranges and eggplant, a PHI of 3 and 7 days, respectively, can be proposed; however, a proposal was not possible for guava due to the absence of maximum residue limits (MRLs) and quantitative residue findings at all sampling points tested. The current work not only contributes to the practical application of fenpyroximate related to residue management in dryland areas, such as Egypt, but can also be used to estimate the appropriate PHIs and support the authorization of plant protection products as supplementary information.

KEYWORDS

dissipation kinetics, citrus, eggplants, guava, residual behavior, risk assessment

Introduction

Pesticides are used to protect crops and increase agricultural yields (1), assuming that they will be applied according to authorized agricultural patterns. On the other hand, the misuse of pesticides may lead to high concentrations of residues in agricultural products, which has forced international agencies and governments to establish maximum residue limits (MRLs) to ensure that safe consumer products enter the market.

One widely used pesticide is fenpyroximate, an acaricide with an oxime-bearing pyrazole structure (**Figure 1**) developed in 1985 by the Nihon Noyaku Co. (2). It has high efficacy against larvae by inhibiting mitochondrial electron transport (3). Currently, fenpyroximate is widely used for the control of mites in orange, apple, peach, and pear orchards (4). Although fenpiroximate is applicable to many crops, in the current work, the extent of the scope of application was investigated in three additional crops of high economic significance in Egypt: guava, oranges, and eggplants.

Guava (*Psidium guajava L.*) is one of the most consumed edible fruits in tropical and subtropical climates worldwide. In a processed form, it is consumed as beverages, puree, jam, canned slices, syrup concentrate, and juices, with commercial importance in more than 50 countries worldwide (5). Egypt is one of the largest guava producers, with an annual production of 343.703 tons in 2016 (6, 7). In addition to guava, citrus is a major export product of Egypt, which currently exports fruit to the European Union (EU) and the Gulf States. Oranges represent approximately 65% of the Egyptian citrus production, with a total planted area of 162,000 ha (8). Egypt is the sixth-largest producer and the second-largest exporter of oranges globally (9). Eggplant (*Solanum melongena L.*) is a commercial vegetable crop with high demand for most farmers (10). Worldwide, eggplant production has been increasing, with the main producing countries being China, India, Egypt, Turkey, and Japan (11). Eggplant fruits contain a considerable amount of carbohydrates, proteins, and vitamins (12). In Egypt, it is one of the most important crops in the summer season and ranks third worldwide, with an annual production of 2.94% (over 1,180,240 tons) of the total world production (6).

Although field conditions are the ones that affect residue behavior, sensitive and reliable analytical methods are a default requirement for accurate and reliable estimations of residue patterns. Due to the high number of coextracts from the plant matrices, analyte extraction followed by cleanup is required before residue determination (13). The QuEChERS ("quick, easy, cheap, effective, rugged, and safe") methodology is an extraction protocol first developed by Anastassiades et al. (14) and Lehotay et al. (13, 15, 16). It is commonly used for the extraction of pesticide residues in fruit and vegetables with high water content, replacing conventional extraction techniques

(17), which use solvents that generate much hazardous waste or have time-consuming and laborious procedures (18). The coupling of ultrahigh-performance liquid chromatography (UHPLC) with tandem mass spectrometry (MS/MS) detectors is the utmost choice for pesticide residue determination at low levels (19). This combination increased the selectivity and sensitivity of the target analytes and simultaneously reduced the chromatographic run time compared with conventional HPLC techniques (20). However, as the matrix effect (ME) is a common problem for pesticide residue analysis, optimization of the sample preparation step gives more reliable results, minimizing interferences and instrument decay.

In this study, the dietary risk assessment was estimated by taking into consideration the residue levels and dissipation patterns of fenpyroximate in eggplant, orange, and guava cultivations. To ensure reliable measurements, a modified version of the QuEChERS extraction protocol was selected and revalidated according to the EU guidelines (21). Finally, based on the outcome results of the dietary risk assessment and the terminal residue levels found in the products, optimal preharvest intervals (PHIs) were suggested, and compliance with MRLs was checked.

Experimental

Chemicals and reagents

Acetonitrile and methanol (HPLC grade) and formic acid (LC–MS grade) were provided by Fisher Scientific Ltd. (Loughborough, United Kingdom). Anhydrous magnesium sulfate ($MgSO_4$) (purity, 98%) was purchased from Chem-Lab NV (Zedelgem, Belgium). Extra pure sodium chloride (NaCl) (purity, 99.5%) was acquired from Loba Chemie (Maharashtra, India). The reference standard of fenpyroximate (99.5%, purity) was obtained from Chem Service (West Chester, PA, United States). Fenpyroximate commercial formulation (Ortus®, 5% SC, suspension concentrate) (Nihon Nohyaku Co., Ltd., Tokyo, Japan) was secured from a local market. Ultra-pure deionized water was obtained from the Barnstead^{TM} Micro Purification system (Thermo Fisher Scientific, Budapest, Hungary).

Standard solutions

A stock standard solution of fenpyroximate (1,000 mg/L) was prepared in acetonitrile and stored at –20°C. The intermediate and working solutions were prepared by further dilution in acetonitrile. A solvent calibration curve (standard concentration vs. response) was constructed using acetonitrile, whereas matrix-matched calibration curves were
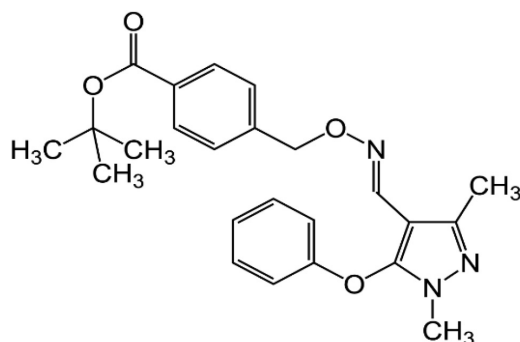
constructed using the extracts from blank guava, orange, and eggplant samples.

Field experiments, sample collection, and storage

To investigate the residue behavior, two kinds of trials were conducted. Trials (triplicates) estimate the dissipation rate according to the authorized agricultural pattern (1 × 25 g a.i./ha) and trials (triplicates) investigate the terminal residues according to more critical agricultural patterns (2–3 × 25–50 g a.i./ha, 14-day interval).

All trials were carried out under open field conditions during the growing season of 2019/2020. The experimental sites were in El Bhera governorate, an area in mainland Egypt with dry climatic conditions and extensive agricultural activity.

Guava and orange orchards were planted in rows with a row and plant-to-plant distance of 9 m. The experimental field was composed of three replicated plots, with three trees in each plot. To separate the plots with different treatments, a buffer area was maintained between each plot in the trial field. For eggplant, each experimental field consisted of three replicate plots with an area of 40 m^2 and was separated by irrigation channels.

The temperature of the experimental area ranged between 15 and 27°C during the eggplant, guava, and orange cultivation periods.

Fruit samples from all three plots were collected at 0 (2 h after the last application), 1, 3, 7, 10, 14, and 20 days for the dissipation rate trials and at 3, 7, and 14 days for the terminal residue trials. The size of the sample was at least 2 kg and in line with the guidelines from the Organization for Economic Co-operation and Development (22). Samples were transported to the laboratory, homogenized using a HOBART Food Processor (Hobart Corp., Troy, OH, United States) and stored for a maximum of 1 week in individual polyethylene bags and frozen at −20°C until analysis.

Pesticide residue analysis

Sample preparation and ultrahigh-performance liquid chromatography−tandem mass spectrometry analysis

A modified version of the QuEChERS protocol (23) was used for the extraction. The absorbent portion and the dilution rate were optimized in the current study to minimize the ME.

An aliquot of 10 g of the homogenized sample was weighed into a 50-ml centrifuge tube, to which 10 ml of acetonitrile was added. Then, a piece of a ceramic homogenizer was added, and the tube was manually shaken for 2 min. For the salting out step, a mixture of salts containing 4 g anhydrous magnesium sulfate and 1 g sodium chloride was added. After shaking vigorously for 30 s, the tube was centrifuged for 5 min at 5,000 rpm (ambient temperature). The upper layer extract was filtered through a PTFE 0.22 μm syringe filter (Millipore, Billerica, MA, United States), and then 0.05 ml was transferred into a vial, diluted 20 times using acetonitrile, and vortexed for 30 s before UPLC–MS/MS analysis.

Chromatographic separation and identification of fenpyroximate were achieved using a Dionex Ultimate 3000 RS ultrahigh-performance liquid chromatographic system (Dionex Softron GmbH, Germering, Germany) equipped with a TSQ Altis triple quadrupole mass spectrometer (Thermo Fisher Scientific, Austin, TX, United States). The separation was achieved using an Accucore RP-MS (2.1 × 100 mm, 2.6 μm) C$_{18}$ column (Thermo Fisher Scientific, Vilnius, Lithuania) at a constant temperature of 40°C.

Gradient elution comprised mobile phase A (water containing 0.1% formic acid v/v) and mobile phase B (methanol containing 0.1% formic acid v/v). The mobile-phase gradient program was 0–1 min 45% B, 1–4 min 90% B, 4–9 min 90% B, 9–9.1 min 45% B, and 9.1–14 min 45% B. A flow rate of 0.3 ml/min and an injection volume of 5 μl were used. Using this program, fenpyroximate was eluted at 8.5 min (SD 0.05%, $n = 10$).

The MS/MS analysis was performed in positive electron spray ionization (ESI$^+$) in the multiple reaction mode (MRM). For the optimization of the MS/MS conditions (Figure 2), 0.1 mg/L fenpyroximate was infused directly into the system using an infusion pump. The ion transfer tube temperature and vaporization temperature were set at 325 and 350°C, respectively. The capillary voltage was 3,800 V. The auxiliary and sheath gases were set at 10 and 40 bar. The LC–MS/MS parameters are presented in Table 1.

Method validation

The reliability of the method used was evaluated according to the EU guidelines (21), and the main evaluation criteria
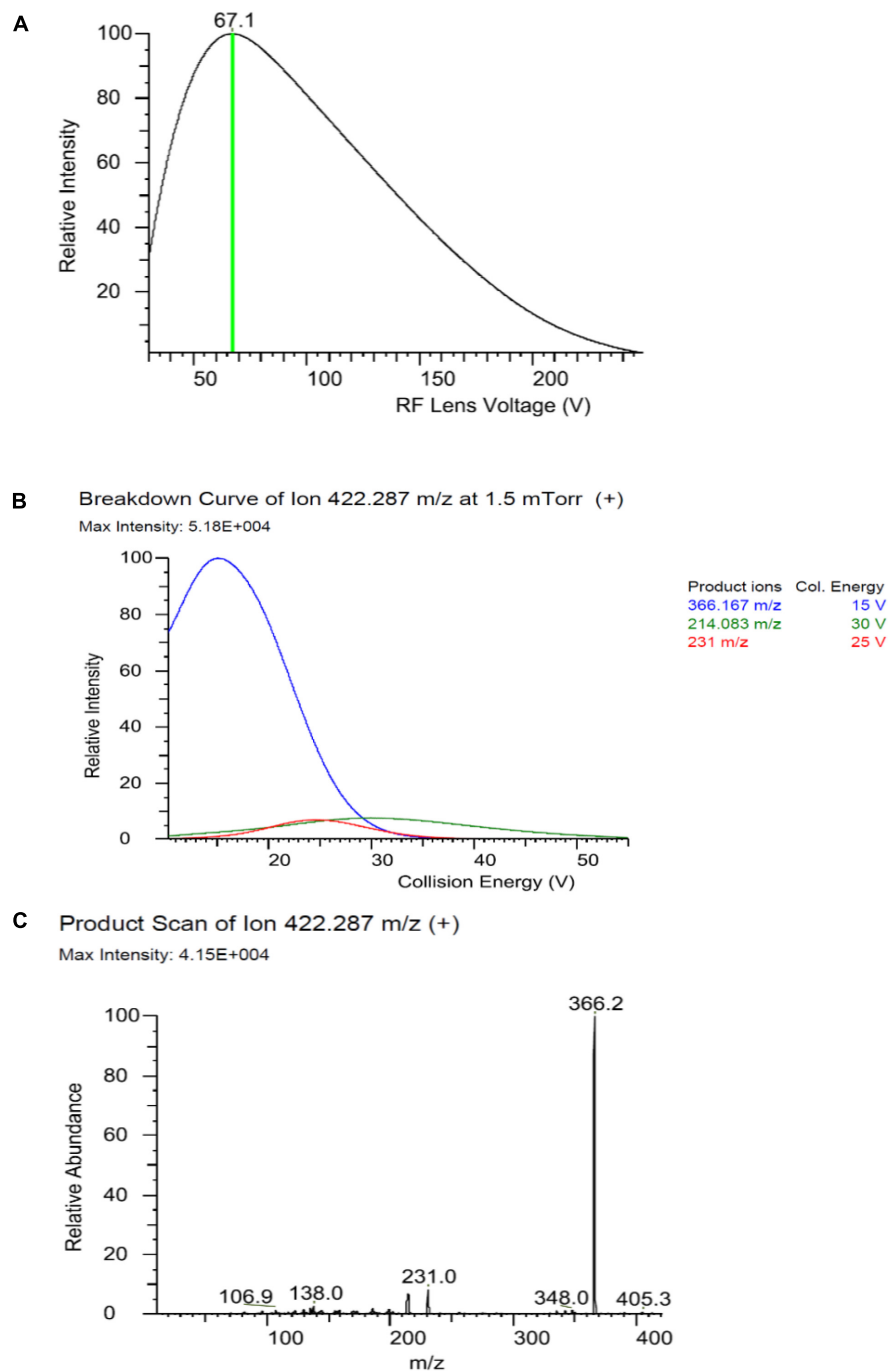
FIGURE 2
Optimizing Rf Lens voltage **(A)**, breakdown curve **(B)**, and product ion **(C)** of fenpyroximate precursor ion.

TABLE 1 Liquid chromatography–tandem mass spectrometry (LC–MS/MS) parameters for determination of fenpyroximate.

Pesticide	Retention time (min)	Precursor ion (m/z)	Product ion (m/z)	Collision energy (V)	Rf lens (V)	Dwell time (min)
Fenpyroximate	8.54	422.2	231	24	67	13.3
			366.2	15	67	13.3

were selectivity, linearity, accuracy, limit of quantitation (LOQ), and ME.

Selectivity is the ability of the method to distinguish between the analyte of interest and other molecules present in the matrix (21) and was tested by analyzing blank matrices previously known to be free of fenpyroximate and fortified matrices ($n = 5$, for each matrix) to establish the absence of signals at the elution time of fenpyroximate.

The limit of quantification (LOQ) was estimated as the lower concentration that provides a precision of 80–110% and a precision ≤20%. The default LOQ in the EU is 0.01 mg/kg; thus, this value was selected as the LOQ of the method.

Accuracy was evaluated in terms of trueness and precision. Trueness was studied by determining the recovery percentage. For each matrix, four sets of samples ($n = 7$, for each set) were spiked at levels of 0.01, 0.1, 1, and 4 mg/kg by adding appropriate volumes (not exceeding 200 μl) of fenpyroximate standard solution. Before the extraction step, the spiked samples in the tubes were vortexed for 30 s and allowed to settle for 1 h at room temperature. The spiking levels were chosen to cover the LOQ and concentrations 10, 100, and 400 times higher, thus covering a wide range of concentrations, which are exaggerated for trace analysis, such as residue determination.

Precision was assessed at 0.01 mg/kg in terms of interday repeatability ($n = 7$) and intraday reproducibility (three times with 7-day intervals, $n = 21$).

Linearity was evaluated by constructing calibration curves in acetonitrile and in extracts of each matrix (matrix-matched calibration standards) using ten calibration points between 0.00025 and 0.1 mg/L. In addition, calibration curves were used to estimate the ME by comparing the slopes of the constructed calibration curve in acetonitrile and in matrix-matched calibration standards.

Dissipation model

The dissipation behaviors and half-lives of fenpyroximate in eggplant, guava, and orange were calculated using the first-order kinetic equations (24); Eqs. 1 and 2:

$$C_t = C_0 e^{-kt} \tag{1}$$

$$t_{1/2} = ln2/k \tag{2}$$

where, C_t (mg/kg) is the residue levels of fenpyroximate at time t (days), C_0 (mg/kg) is the initial deposits and k is the rate constant (day^{-1}).

Microsoft Excel was used for statistical calculations.

Dietary exposure models

The risks that may result from the long-term intake for the Egyptian consumer were evaluated by using the following equations Eqs. 3 and 4 (24):

$$NEDI = \Sigma(STMRixFi)/bodyweight(bw) \tag{3}$$

$$RQ = NEDI/ADI(Eq. 4) \tag{4}$$

where, NEDI is the national estimated daily intake (mg/kg.bw) and STMRi is the median residue data from supervised trials; in our case, since we had three replicates, the mean was used. The ADI, Fi, and bw are the acceptable daily intake (ADI), food consumption data (kg/day), and body weight (kg), respectively. The average body weight is 60 kg for an Egyptian adult (25). Therefore, the risk quotient (RQ) is calculated by dividing the NEDI by the ADI. An RQ value less than 1 represents an acceptable risk for the consumer, while for values higher than 1, the risk is not acceptable. Data were statistically evaluated using one-way analysis of variance (ANOVA), and probability values $p < 0.5$ were considered significant.

In addition, since Europe is one of the main exporters of Egyptian products, to assess the long- and short-term intake for the European consumer, the deterministic EFSA PRIMo revision 3.1 model (26) was employed.

Results and discussion

Method development and validation

Evaluation of using adsorbent vs. dilution for the cleanup step

The use of adsorbents, such as PSA and GCB in the cleanup step and the effect of dilution at different rates, as a means of reducing the co-extractants in the final extract, were evaluated to minimize the ME, which in the case of LC–MS/MS can be translated into ion suppression in the electrospray source due to competition of the analyte ions with the ions of the coeluting compounds. The ME was considered non-significant if it ranged from −20 to +20%, since this variance value is considered acceptable in terms of repeatability between samples. The effect is considered medium if the value ranges from ±50 to ±20%, whereas the effect is considered strong if the value is below −50% and above +50% (27–29).

The results showed a medium signal suppression effect before the cleanup step. The orange sample extracts showed the highest signal suppression (47.9%) in comparison with eggplant (21.2%) and guava (33.9%) extracts. The addition of PSA at 25 mg/ml of extract or PSA + GCB (25 + 5 mg)/ml

of extract had a non-significant influence on the ME of eggplant and guava extracts. In contrast, a significant reduction was observed in the orange extract. When only PSA (25 mg/ml of extract) was used, the ME was reduced from 47.9 to 28.9%, and using the mixture of PSA + GCB reduced it to 12.3%.

To avoid the additional cost of adsorbent materials, extract dilution in solvent was also tested as a means to minimize the ME. In this context, four different dilution factors of 5-, 10-, 15-, and 20-fold for each matrix were tested. In eggplant and guava extracts, the ME was negligible at all tested dilution factors. In orange extract (**Figures 3**, **4**), fenpyroximate shows moderate signal suppression at a dilution factor of 5 and 10, possibly due to the presence of nobiletin and flavonoids in citrus peels, which are considered one of the prominent compounds of poly methoxy flavonoids in citrus fruits (30). Thus, a dilution factor of 20-fold was selected. To have a more robust estimation of the reduction of the ME, the slopes of the calibration curves (acetonitrile and the matrix-matched standards) were compared, *and non-significant (t-test)* matrix suppression effects of −8.3, −2.7, and −5.2% in orange, eggplant, and guava extracts, respectively, (**Table 2**), were observed.

A graphical presentation of the impact of adsorbents and sample dilution on the ME of fenpyroximate is presented in **Figure 5**.

Method validation

The selectivity results demonstrated that the matrix co-extractants present in the samples did not give false positives. Regarding linearity, as summarized in **Table 2**, the results showed a good response for all the tested matrices with a determination coefficient $R^2 \geq 0.998$ and residuals ≤19.8% in the range of 0.00025–0.1 mg/L (equivalent to 0.005–2 mg/kg), which shows very good linear regression. The LOQ was set at 0.01 mg/kg in all commodities, with recovery values ranging between 102.3 and 107.3% and relative standard deviation (RSD) ≤ 7.4%. The estimated LOQ value was equal, 50 times lower and 30 times lower than the corresponding lower available

MRLs of 0.01, 0.5, and 0.3 μg/kg for guava, orange, and eggplant, respectively.

Regarding precision, values for intraday repeatability were in the range of 4.4–7.4% and for interday repeatability between 10.1 and 15.4%. The higher interday values take into consideration the variability for different days and analysts.

Trueness was evaluated through a recovery study. The obtained recovery values were 93.7–107.3% for eggplant with RSDs of 4.1–8.6% for guava, 92.7–102.3% for eggplant with RSDs of 4.4–7.2% and 92.4–104.3% for orange with RSDs of 3.3–8.5%. The detailed validation results are presented in **Table 3**. In conclusion, the recovery values obtained for fenpyroximate for all commodities were within the acceptance criterion of 80–110% with a precision RSD of ≤20% (21), meaning the method performed well.

Pesticide residues

Dissipation curves and half-life for the studied pesticides

The initial deposits of fenpyroximate in/on eggplant, guava, and orange samples at 0 days (2 h) after application at the authorized dose of 25 g a.i./ha were at 1.64, 1.43, and 1.76 mg/kg, respectively, and exhibited different decreasing tendencies in the tested fruits up to 3 days of application. Approximately 64, 41, and 86% of the initial deposits dissipated, with residue values of 0.58, 0.83, and 0.24 mg/kg, respectively. The decrease was relatively equal up to 7 days after application in eggplant and orange samples. Fenpyroximate showed a lower dissipation rate tendency in guava samples overall to the sampling time compared with eggplant and orange samples (**Figure 6**). Saku et al. applying fenpyroximate in the authorized agricultural pattern in Egypt, showed that the degradation of 80% was observed after 21 days and 49.5% after 3 days (a half-life estimation was not performed) (31). This is consistent with the residue levels found at a PHI of 21 days but not at a PHI of 3 days.
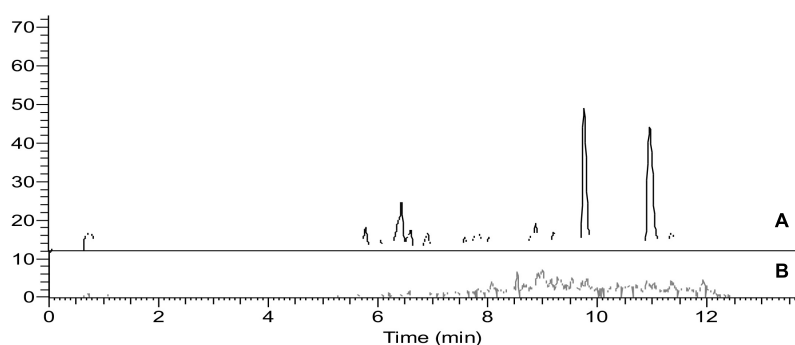

FIGURE 3

Representative chromatograms of blank orange final extract after 20× dilution. **(A)** Full scan mass spectrum **(B)** Single Ion monitoring of the parent ion 422.2 m/z of fenpyroximate.
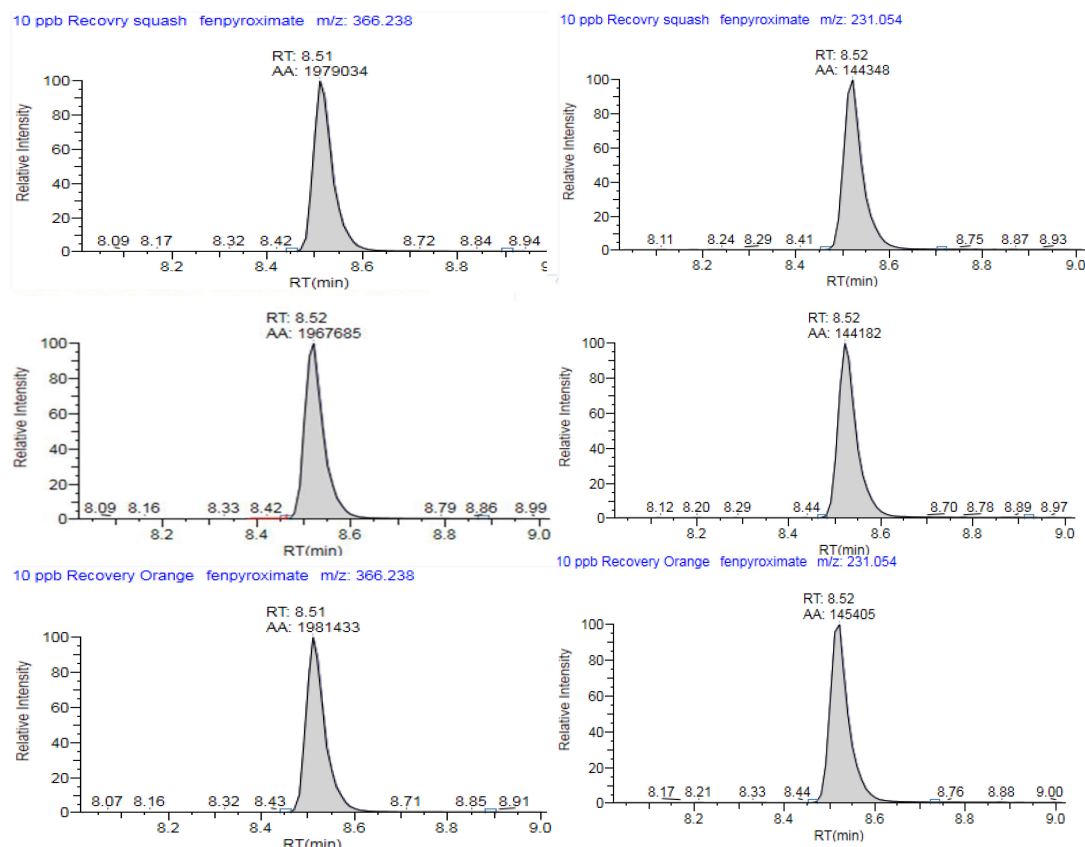
FIGURE 4

Representative multiple reaction monitoring (MRM) chromatogram of fenpyroximate, TIC for **(A)** m/z = 422.2 to 366.2 and **(B)** m/z = 422.2 to 231 in guava, eggplant, and orange final extract (20× dilution) spiked at 0.01 mg/kg.

TABLE 2 Linearity, reproducibility, and matrix effect (ME) results from the validation study of fenpyroximate in three commodities.

	Solvent	Eggplant	Guava	Orange
Linearity				
Linear range (mg/L)	0.00025–0.1			
Slope	271758	279106	285946	294366
Intercept	−485150	40200	−273498	−349840
R^2	0.9994	0.9987	0.9994	0.9981
Residual (%)	−16.3	−15.1	−19.8	−14.9
Reproducibility				
Intraday repeatability (RSD %) ($n = 7$)[a]	–	7.4	4.4	5.3
Interdays repeatability (RSD %) ($n = 21$)[a]	–	12.8	10.1	15.4
Matrix effect (ME)				
% Reduction compared to solvent	–	2.7	5.2	8.3

[a]Evaluated at the LOQ level of 0.01 mg/kg.

Despite the similarity of the application rates of fenpyroximate in the tested fruits, there were differences in the initial deposits that are attributed to the crops or the morphological characteristics of each crop or fruit. The outer surface of the orange fruit is rough compared with the smooth outer surface of eggplant and guava, which helps oranges retain a more significant amount of spray solution compared with eggplant and guava.

The dissipation kinetics of fenpyroximate residues in the studied crops are summarized in Table 4. The exponential function was the best descriptor among the other models, and it was found to be $C_t = 1.5991e^{-0.367t}$, $C_t = 1.8051e^{-0.222t}$, and
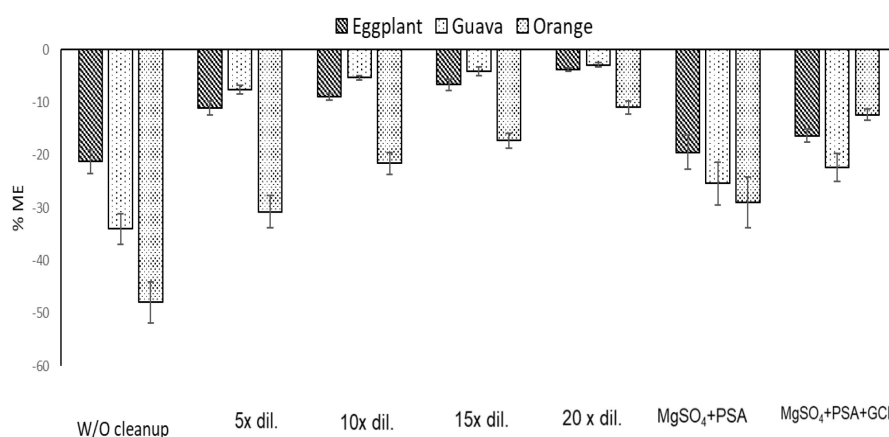
Estimation of the % matrix effect (ME) in eggplant, guava, and orange ($n = 3$) using four dilution and two cleanup, W/O Cleanup:% ME of matrix extracts without cleanup. 5× dilution:% ME of matrix extracts after five times dilution. 10× dilution:% ME of matrix extracts after 10 times dilution. 15× dilution:% ME of matrix extracts after 15 times dilution. 20× dilution:% ME of matrix extracts after 20 times dilution. MgSO4 + PSA:% ME of matrix extracts after cleanup with MgSO4 + PSA. MgSO4 + PSA + GCB:% ME of matrix extracts after cleanup with MgSO4 + PSA + GCB.

TABLE 3 Recovery of fenpyroximate in eggplant, guava, and orange samples ($n = 7$).

Level of fortification (mg/kg)	Eggplant		Guava		Orange	
	% Rec.	%RSD	% Rec.	%RSD	% Rec.	%RSD
0.01	107.3	7.4	102.3	4.4	104.3	5.3
0.1	96.1	4.1	98.6	7.2	95.9	3.3
1	94.5	5.2	97.8	6.7	92.4	8.5
4	93.7	8.6	92.7	6.1	96.8	7.9

$C_t = 1.1857e^{-0.305t}$ with R^2 values of 0.998, 0.914, and 0.932 for eggplant, guava, and orange, respectively, indicating that the dissipation behavior followed first-order kinetics.

The half-lives of fenpyroximate were 1.7, 2.2, and 1.9 days in eggplant, guava, and oranges, respectively.

Abd-Alrahman et al. observed almost similar half-lives ($t_{1/2}$) of 2.03, 1.56, 2.75, and 2.42 days for apples, grapefruits, grape leaves, and citrus, respectively, when applied at the authorized dose of 25 g a.i./ha [4]. Additionally, the half-life of fenpyroximate was 3.5 days in grapes [24]. The differences in the half-lives compared with previous studies might be explained by differences in fruit varieties and their masses, growth status, and the morphological structure of plants. In addition, environmental factors may be an explanation for the difference in half-lives and initial residue, such as temperature, sunlight, humidity, microorganisms, soil type, and other factors [32, 33].

Terminal residues

The final residual test of fenpyroximate in eggplant, guava, and orange samples was performed at the authorized (25 g a.i./ha) and double (50 g a.i./ha) dose rates at 2 or 3 application rates. Samples were collected after three sampling intervals (3, 7,

and 14 days after the last application). A summary of the results is presented in detail in Table 5.

The initial residues in eggplant and guava were similar (0.64–1.34 mg/kg in eggplant and 0.65–0.86 mg/kg in guava) and slightly lower than those in oranges (1.19–2.54 mg/kg). In all cases, the values of fenpyroximate residues decreased with the sampling interval, with a total degradation of 86–98% after 14 days.

By applying the authorized dose rate at 2 or 3 applications, residues ranged from 0.04 to 0.86 mg/kg, 0.07 to 0.8 mg/kg, and 0.03 to 1.37 mg/kg in eggplant, guava, and orange, respectively. The degradation of fenpyroximate between the 7th and 14th day after the application was 10–24% in all cases except in eggplant when the application was performed 3 times, in which the degradation was 33%. This difference is related to the fact that a lower degradation (63%) was observed after 7 days.

In the worst-case application pattern of double the dose rate and 2 or 3 applications, residues ranged from 0.04 to 1.34 mg/kg, 0.07 to 0.86 mg/kg, and 0.07 to 2.54 mg/kg at eggplant, guava, and orange, respectively. Similar to the previous trials, the degradation of fenpyroximate between the 7th and 14th day after the application was 16–28%; the exception, in this case, was in oranges when the application was performed two times, in
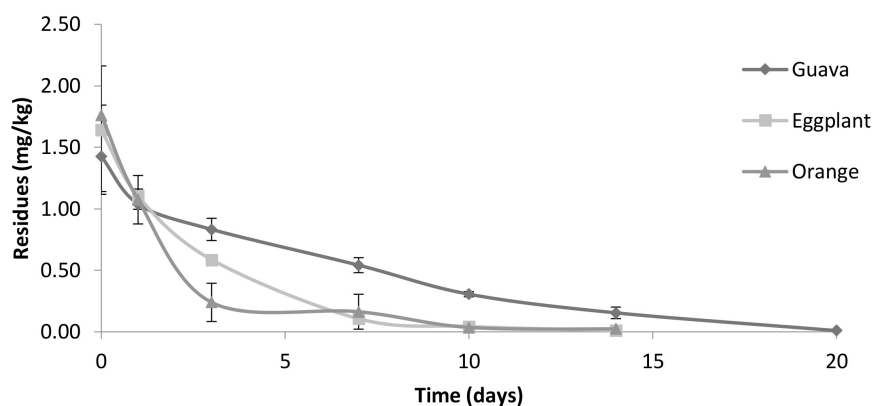
FIGURE 6
The dissipation behavior of fenpyroximate in eggplant, guava, and orange fruits. The residue concentrations (mg/kg) are expressed in semi-logarithmic scale.

TABLE 4   Fenpyroximate decline kinetics in eggplant, guava, and orange fruit.

Days after application	Eggplant	Guava	Orange
	Residue (mg/kg)[a] ± SD (decline%)	Residue (mg/kg) ± SD (decline%)	Residue (mg/kg) ± SD (decline%)
0	1.64 ± 0.52	1.42 ± 0.2	1.76 ± 0.084
1	1.1 ± 0.058 (32.7)	1.04 ± 0.044 (27.1)	1.07 ± 0.197 (38.9)
3	0.58 ± 0.006 (64.2)	0.83 ± 0.090 (41.6)	0.24 ± 0.155 (86.4)
7	0.11 ± 0.023 (93.5)	0.54 ± 0.061 (61.9)	0.16 ± 0.142 (90.7)
10	0.04 ± 0.006 (97.4)	0.31 ± 0.021 (78.5)	0.036 ± 0.002 (97.9)
14	0.011 ± 0.006 (99.4)	0.15 ± 0.047 (89.2)	0.024 ± 0.008 (98.6)
20	BDL[b]	0.01 ± 0.002(99.3)	BDL
Regression equation	$C_t = 1.59\,e^{-0.362t}$	$C_t = 1.79\,e^{-0.222t}$	$C_t = 1.18\,e^{-0.305t}$
Coefficient(R^2)	0.998	0.914	0.932
Half-life (days)	1.7	2.2	1.9

[a] Average of three replicates.
[b] Below the detection limit.

which the degradation was 58%. Additionally, in this case, the difference is related to the fact that a lower degradation (63%) was observed after 7 days.

Overall, a similarity in the degradation of fenpyroximate was observed in all three crops. Terminal residues at 7 days after the last application were degraded compared with 3 days by 31–37% in eggplant, 19–25% in guava, and 19–26% in oranges (except in one case where the degradation was up to 63%). Similarly, terminal residues at 14 days after the last application were degraded by 3–14%. Based on the results, neither the number of applications nor the dose rate affected the degradation pattern.

Consumer risk assessment

For the exposure calculations, as input values, the mean (three replicates) of fenpyroximate in eggplant, guava, and orange were used, except in the cases where residues were below the LOQ, for which the value of 0.01 mg/kg was used. The results

were compared with the ADI of 0.01 mg kg^{-1} bw/day in the case of long-term intake and with the acute reference dose (ARfD) of 0.02 mg kg^{-1} bw/day in the case of short-term intake (34).

For Egyptian consumers, following the RQ approach, the long-term exposure ranged from 5.24E^{-05}–5.18E^{-03} mg/kg bw for eggplant, 1.53E^{-05}–9.94E^{-04} mg/kg bw for guava, and 3.52E^{-05}–4.14E^{-03} mg/kg bw for orange. The corresponding RQs ranged from 0.01–0.52, 0.002–0.1, and 0.004–0.41, respectively. The results are summarized in Table 6. The dietary risk levels were found to be less than 1. Therefore, if fenpyroximate is applied according to the authorized and more critical application patterns and the fruits are harvested after the sampling times of 3, 7, and 14 days, the risks for the Egyptian consumer due to the long-term dietary intake are low, and the exposure for the consumer is acceptable.

As for the European consumer, as input data, the mean residue concentration measured from all agricultural patterns

TABLE 5   Terminal residues of fenpyroximate in eggplant, guava, and orange fruits.

Dosage (g.a.i/ha)	Number of times sprayed	Days after spraying	Residue (mg/kg)[a] ± SD		
			Eggplant	Guava	Orange
25	2	3	0.64 ± 0.01	0.65 ±0.04	1.19 ± 0.08
		7	0.19 ± 0.16	0.16 ± 0.03	0.23 ± 0.06
		14	0.09 ± 0.04	0.03 ± 0.02	0.03 ± 0.01
	3	3	0.86 ± 0.04	0.80 ± 0.06	1.37 ± 0.1
		7	0.32 ± 0.05	0.15 ± 0.03	0.36 ± 0.01
		14	0.04 ± 0.04	0.07 ± 0.03	0.03 ±0.01
50	2	3	0.87 ± 0.1	0.85 ± 0.05	1.28 ± 0.22
		7	0.27 ± 0.05	0.17 ± 0.06	0.81 ±0.12
		14	0.03 ± 0.02	0.03 ±0.01	0.15 ± 0.11
	3	3	1.34 ± 0.2	0.86 ±0.12	2.54 ± 0.49
		7	0.42 ± 0.11	0.21 ± 0.04	0.63 ±0.03
		14	0.04 ± 0.04	0.07 ± 0.01	0.07 ± 0.03

TABLE 6   Long-term exposure calculations of fenpyroximate in eggplant, guava, and orange fruits for the Egyptian consumer using the RQ approach.

Dosage (g a.i/ha)	Number of times sprayed	Days after spraying	Eggplant			Guava			Orange		
			Mean	NEDI	RQ	Mean	NEDI	RQ	Mean	NEDI	RQ
25	2	3	0.64	2.30E-03	0.23	0.65	7.07E-04	0.07	1.19	1.82E-03	0.18
		7	0.19	7.04E-04	0.07	0.16	1.73E-04	0.02	0.23	3.54E-04	0.04
		14	0.09	3.37E-04	0.03	0.03	3.28E-05	0.00	0.03	4.58E-05	0.00
	3	3	0.86	3.23E-03	0.32	0.8	8.63E-04	0.09	1.4	2.10E-03	0.21
		7	0.32	1.20E-03	0.12	0.15	1.65E-04	0.02	0.36	5.47E-04	0.05
		14	0.04	1.50E-04	0.01	0.07	7.57E-05	0.01	0.03	4.59E-05	0.00
50	2	3	0.87	3.25E-03	0.33	0.85	9.15E-04	0.09	1.3	1.96E-03	0.20
		7	0.27	1.03E-03	0.10	0.17	1.83E-04	0.02	0.81	1.24E-03	0.12
		14	0.03	1.12E-04	0.01	0.03	3.23E-05	0.00	0.15	2.30E-04	0.02
	3	3	1.3	5.02E-06	0.00	0.86	9.29E-04	0.09	2.5	3.88E-03	0.39
		7	0.42	1.56E-03	0.16	0.21	2.29E-04	0.02	0.63	9.68E-04	0.10
		14	0.04	1.50E-04	0.01	0.07	7.53E-05	0.01	0.07	1.07E-04	0.01

NEDI, national estimated daily intake; RQ, risk quotient.

and all PHIs was applied. In the case of oranges, a peeling factor of 0.24 was applied (35). The long-term exposure was calculated to be up to 5% of the ADI for eggplant, 0.5% for guavas, and 25% for oranges; thus, a chronic risk to the consumer is not observed. The short-term exposure was calculated to be up to 222% of the ARfD for eggplant, 157% for guava, and 404% of the ARfD for oranges. The results are summarized in Table 7.

In eggplant, for residues resulting from the agricultural patterns of 1 × 25 g a.i./ha, 0–1 day PHI; 3 × 25 g a.i./ha, 3 days PHI, and 2–3 × 50 g a.i./ha, 3 days PHI, an exceedance of the ARfD was observed. Similar to guava, for residues resulting from the agricultural patterns of 1 × 25 g a.i./ha, 0–1 day PHI. In oranges, the same applies to the agricultural patterns of 1 × 25 g a.i./ha, 0–1 day PHI; 2–3 × 25 g a.i./ha, 3 days PHI and 2–3 × 50 g a.i./ha, 3 and 7 days PHI. Thus, these agricultural

practices should not be used, and the information will be taken into consideration in the discussion of the proposal of the PHI.

Maximum residue limits and preharvest intervals

For fenpyroximate, the codex MRL in citrus fruits was set at 0.6 mg/kg, in eggplants at 0.3 mg/kg, and no value was set for guava. In the EU legislation, the EU MRLs (36) are set at 0.5 and 0.3 mg/kg for citrus fruits and eggplants, respectively, whereas for guava, the MRL is set at the LOQ of 0.01 mg/kg. In Egypt, national MRLs are not set; thus, the codex MRLs apply to ensure consumer safety. Based on the residue levels observed per agricultural pattern and the outcome of the consumer risk assessment, the following PHIs are proposed:

TABLE 7 Long-term and short-term exposure calculations of fenpyroximate in eggplant, guava, and orange fruits for the European consumer using the EFSA PRIMo revision 3.

Dosage (g a.i/ha)	Number of times sprayed	Days after spraying	Eggplant			Guava			Orange		
			Mean	Maximum ADI (%)	Maximum ARfD[a] (%)	Mean	Maximum ADI (%)	Maximum ARfD[a] (%)	Mean	Maximum ADI (%)	Maximum ARfD[a] (%)
25	1	0	1.64	5	**222**	1.42	0.5	**157**	1.76	17	**280**
		1	1.1	4	**149**	1.04	0.4	**115**	1.07	10	**170**
		3	0.58	2	73	0.83	0.3	92	0.24	2	38
		7	0.11	0.4	14	0.54	0.2	60	0.16	2	25
		10	0.04	0.1	5	0.31	0.1	34	0.036	0.3	6
		14	0.011	0	1	0.15	0.1	17	0.024	0.2	4
		20	< 0.01	0	1	0.01	0	1	<0.01	0.1	2
25	2	3	0.64	2.00	87.00	0.65	0.20	72.00	1.19	11.00	**189.00**
		7	0.19	0.60	36.00	0.16	0.1000	18.00	0.23	2.00	37.00
		14	0.09	0.30	12.00	0.03	0.00	3.00	0.03	0.30	5.00
	3	3	0.86	3.00	**116.00**	0.80	0.30	88.00	1.37	13.00	**218.00**
		7	0.32	1.00	43.00	0.15	0.10	17.00	0.36	3.00	57.00
		14	0.04	0.10	5.00	0.07	0.00	8.00	0.03	0.30	5.00
50	2	3	0.87	3.00	**118.00**	0.85	0.30	94.00	1.28	12.00	**204.00**
		7	0.27	0.90	37.00	0.17	0.10	19.00	0.81	8.00	**129.00**
		14	0.03	0.10	4.00	0.03	0.00	3.00	0.15	1.00	24.00
	3	3	1.34	4.00	**181.00**	0.86	0.30	95.00	2.54	25.00	**404.00**
		7	0.42	1.00	57.00	0.21	0.10	23.00	0.63	6.00	**100.00**
		14	0.04	0.10	5.00	0.07	0.00	8.00	0.07	0.70	11.00

[a]Bold are the values where an exceedance of the ARfD is observed.
ADI, acceptable daily intake; ARfD: acute reference dose.

For eggplant, a minimum PHI of 7 days is proposed if fenpyroximate is applied according to the authorized application pattern. In the case where the application is conducted with a more critical pattern, the PHI varies between 7 and 14 days depending on the residue levels. When fenpyroximate is applied at 2×25 or 50 g a.i./ha, a PHI of 7 days is proposed, and when fenpyroximate is applied at 3×25 or 50 g a.i./ha, a PHI of 14 days is proposed.

For guava, at all sampling points, quantitative residues were found. Since the EU MRL is set at the LOQ of 0.01 mg/kg, a PHI cannot be proposed, neither when fenpyroximate is applied according to the authorized nor a more critical pattern. However, after 20 days of the last application, when fenpyroximate was applied according to the authorized pattern, residues were at the LOQ (0.01 mg/kg), and according to the dissipation pattern in guava, residues below the LOQ were expected to be present after 25 days.

For oranges, a minimum PHI of 3 days is proposed if fenpyroximate is applied according to the authorized application pattern (1×25 g a.i./ha). In the case where the application is conducted with a more critical pattern, a PHI of 7 days is proposed if applied 2–3 times at the authorized dose rate (25 g a.i./ha) and 14 days if applied 2–3 times double the authorized dose rate (50 g a.i./ha).

Conclusion

An easy and effective approach using a modified QuEChERS pretreatment, with an additional 20-fold dilution step to minimize the MEs and combined with UPLC–MS/MS, was validated for the determination of fenpyroximate in eggplants, guavas, and oranges. The dissipation patterns in all crops could be described by the first-order kinetics model with half-lives of 1.7, 2.2, and 1.9 days for eggplants, guavas, and oranges, respectively. Additionally, the dietary risk assessment at the authorized or more critical application patterns was performed for Egyptian and European consumers, where exceedance of the ARfD were observed for residues at 0 and 1 day PHI for the authorized agricultural practices and at 3 and 7 days PHI for some more critical agricultural practices. In addition, in all cases, residues were not below the existing MRLs. Thus, setting a PHI is essential to avoid exceedances that have trade restrictions as a consequence or to ensure consumer safety. For oranges and eggplant, a PHI of 3 and 7 days, respectively, can be proposed if fenpyroximate is applied according to the authorized application pattern. For guava, due to the absence of MRLs and since quantitative levels were found in all cases, an accurate PHI cannot be proposed; however, based on the dissipation pattern, quantitative residues after 25 days are not expected.

The current work not only contributes to the practical application of fenpyroximate related to residue management in dryland areas, such as Egypt, but can also be used to estimate the appropriate PHIs and can support the authorization of plant protection products as supplementary information.

Data availability statement

The original contributions presented in the study are included in the article/supplementary material, further inquiries can be directed to the corresponding author/s.

Author contributions

Funding

Acknowledgments

Conflict of interest

The authors declare that the research was conducted in the absence of any commercial or financial relationships that could be construed as a potential conflict of interest.

Publisher's note

All claims expressed in this article are solely those of the authors and do not necessarily represent those of their affiliated organizations, or those of the publisher, the editors and the reviewers. Any product that may be evaluated in this article, or claim that may be made by its manufacturer, is not guaranteed or endorsed by the publisher.

References

1. Aktar W, Sengupta D, Chowdhury A. Impact of pesticides use in agriculture: their benefits and hazards. *Interdiscip Toxicol.* (2009) 2:1–12. doi: 10.2478/v10102-009-0001-7

2. Konno T, Kuriyama K, Hamaguchi H. "Fenpyroximate (NNI-850), a new acaricide," in *Proceedings of the Brighton Crop Protection Conference, Pests and Diseases.* (Vol. 1), (Farnham: British Crop Protection Council) (1990). p. 71–8.

3. Naik R, Kale V, Dethe M. Studies on residues of flufenzin and fenpyroximate on brinjal. *Int J Plant Protect.* (2009) 2:38–41.

4. Abd Al-Rahman SH, Almaz MM, Osama IA. Determination of degradation rate of acaricide fenpyroximate in apple, citrus, and grape by HPLC-DAD. *Food Anal Methods.* (2012) 5:306–11. doi: 10.1007/s12161-011-9243-z

5. Hassan TM, Abdel-Fattah FA, Farid AS, Kamel ER. Effect of feeding guava waste on growth performance, diet digestibility, carcass characteristics and production profitability of ossimi lambs. *Egypt J Nutr Feeds.* (2016) 19:461–72. doi: 10.21608/ejnf.2016.74985

6. FAOSTAT. *Food and Agriculture Organization of the United Nations.* (2019). Available online at: http://wwwfaoorg/faostat/en/#data/QC (accessed June 10, 2020).

7. Fernandez AEL, Obledo-Vazquez EN, Vivar-Vera MDLA, Ayerdi SGS, Montalvo-Gonzalez E. Evaluation of emerging methods on the polyphenol content, antioxidant capacity and qualitative presence of acetogenins in soursop pulp (*Annona muricata L.*). *Rev Bras Frutic.* (2017) 44:39. doi: 10.1590/0100-29452017358

8. Omer SA, Fakhre NA. Simultaneous determination of ternary mixture of carboxin, chlorpyrifos, and tebuconazole residues in cabbage samples using three spectrophotometric methods. *J Anal Methods Chem.* (2020) 2020:4912762. doi: 10.1155/2020/4912762

9. UFA Service. *GAIN Citrus Annual Report, Cairo, Egypt.* (2014). Available online at: http://gainfasusdagov/Recent%20GAIN%20Publications/Forms/Allltemsaspx. (accessed June 10, 2020).

10. Abdelbagi AO, Ismail REA, Ishag AESA, Hammad AMA. Pesticide residues in eggplant fruit from Khartoum State, Sudan. *J Health Pollut.* (2020) 10:200304. doi: 10.5696/2156-9614-10.25.200304

11. Oluoch M, Chadha M. "Evaluation of African eggplant for yield and quality characteristics," in *Proceedings of the I International Conference on Indigenous Vegetables and Legumes Prospectus for Fighting Poverty, Hunger and Malnutrition*, Hyderabad, India (2006) 752:303–6.

12. Rakha M. Growth, yield and fruit quality of eggplant (*Solanum melongena L.*) as affected by irrigation intervals and foliar application of some antitranspirants. *J Plant Prod.* (2014) 5:2069–83. doi: 10.21608/jpp.2014.64846

13. Lehotay SJ, Masiá A, Blasco C, Picó Y. Last trends in pesticide residue determination by liquid chromatography–mass spectrometry. *Trends Environ Anal Chem.* (2014) 2:11–24. doi: 10.1080/03601234.2022.2056393

14. Lehotay SJ, Anastassiades M, Lehotay SJ, Štajnbaher D, Schenck FJ. Fast and easy multiresidue method employing acetonitrile extraction/partitioning and "dispersive solid-phase extraction" for the determination of pesticide residues in produce. *J AOAC Int.* (2003) 86:412–31. doi: 10.1093/jaoac/86.2.412

15. Lehotay SJ. Quick, easy, cheap, effective, rugged, and safe approach for determining pesticide residues. In: Frenich AG, Vidal JLM editors. *Pesticide Protocols.* Berlin: Springer (2006). p. 239–61. doi: 10.1385/1-59259-929-X:239

16. Lehotay SJ, Kok AD, Hiemstra M, Bodegraven PV. Validation of a fast and easy method for the determination of residues from 229 pesticides in fruits and vegetables using gas and liquid chromatography and mass spectrometric detection. *J AOAC Int.* (2005) 88:595–614. doi: 10.1093/jaoac/88.2.595

17. Lam K-H, Wai H-Y, Leung KM, Tsang VW, Tang C-F, Cheung RY, et al. A study of the partitioning behavior of Irgarol-1051 and its transformation products. *Chemosphere.* (2006) 64:1177–84. doi: 10.1016/j.chemosphere.2005.11.006

18. Kaihara A, Yoshii K, Tsumura Y, Nakamura Y, Ishimitsu S, Tonogai Y. Multiresidue analysis of pesticides in fresh fruits and vegetables by supercritical fluid extraction and HPLC. *J Health Sci.* (2000) 46:336–42. doi: 10.1248/jhs.46.336

19. Lacina O, Urbanova J, Poustka J, Hajslova J. Identification/quantification of multiple pesticide residues in food plants by ultra-high-performance liquid chromatography-time-of-flight mass spectrometry. *J Chromatogr A.* (2010) 1217:648–59. doi: 10.1016/j.chroma.2009.11.098

20. Fernandes VC, Domingues VF, Delerue-Matos C, Mateus N. Determination of pesticides in fruit and fruit juices by chromatographic methods. An overview. *J Chromatogr Sci.* (2010) 49:715–30. doi: 10.1093/chrsci/49.9.715

21. European Commission. *Guidance Document on Analytical Quality Control and Method Validation Procedures for Pesticides Residues Analysis in Food and Feed (SANTE/12682/2019).* (2019). Available online at: https://eceuropaeu/food/sites/food/files/plant/docs/pesticides_mrl_guidelines_wrkdoc_2019-12682pdf (accessed June 10, 2020).

22. OECD. *Organisation for Economic Co-operation and Development. Test No. 509: Crop Field Trial.* Paris: OECD Publishing (2009).

23. European Standard EN 15662:2008. Foods of Plant Origin –Determination of Pesticide Residues using GC-MS and/or LC-MS/MS Following Acetonitrile Extraction/Partitioning and Clean-Up by Dispersive SPE –QuEChERS-Method. Brussels: European Committee for Standardization (2008).

24. Malhat F, El-Mesallamy A, Assy M, Madian W, Loutfy NM, Ahmed MT. Residues, half-life times, dissipation, and safety evaluation of the acaricide fenpyroximate applied on grapes. *Toxicol Environ Chem.* (2013) 95:1309–17. doi: 10.1080/02772248.2013.877245

25. World Health Organization. *GEMS/Food Regional Diets : Regional Per Capita Consumption of Raw and 409 Semi-Processed Agricultural Commodities / Prepared by The Global Environment Monitoring 410 System/Food Contamination Monitoring and Assessment Programme (GEMS/Food), Rev.411 ed.* World Health Organization. (2003). Available online at: https://apps.who.int/iris/handle/10665/42833 (accessed June 10, 2020).

26. European Food Safety Authority, Brancato A, Brocca D, Ferreira L, Greco L, Jarrah S, et al. Use of EFSA pesticide residue intake model (EFSA PRIMo revision 3). *EFSA J.* (2018) 16:e05147. doi: 10.2903/j.efsa.2018.5147

27. Kruve A, Künnapas A, Herodes K, Leito I. Matrix effects in pesticide multi-residue analysis by liquid chromatography–mass spectrometry. *J Chromatogr.* (2008) 1187:58–66. doi: 10.1016/j.chroma.2008.01.077

28. Hajšlová J, Zrostlíkova J. Matrix effects in (ultra) trace analysis of pesticide residues in food and biotic matrices. *J Chromatogr A.* (2003) 1000:181–97. doi: 10.1016/s0021-9673(03)00539-9

29. Wang L, Wang J, Fang L, Zheng Z, Zhi D, Wang S, et al. Anticancer activities of citrus peel polymethoxyflavones related to angiogenesis and others. *Bio Med Res Int.* (2014) 2014:453972. doi: 10.1155/2014/453972

30. Saku D, Bhatt C, Rai J, Rai MK, Goswami J, Goswami J, et al. Determination of fenpyroximate acaricide in vegetables, soil and water samples using UV-visible spectroscopy. *Asian J Chem.* (2020) 32:1991–5. doi: 10.14233/ajchem.2020.22766

31. Karageorgou E, Samanidou V. Youden test application in robustness assays during method validation. *J Chromatogr A.* (2014) 1353:131–9. doi: 10.1016/j.chroma.2014.01.050

32. Ferrer C, Lozano A, Agüera A, Girón AJ, Fernández-Alba A. Overcoming matrix effects using the dilution approach in multiresidue methods for fruits and vegetables. *J Chromatogr A.* (2011) 1218:7634–9. doi: 10.1016/j.chroma.2011.07.033

33. Cabras P, Spanedda L, Cabitza F, Cubeddu M, Martini MG, Brandolini V. Pirimicarb and its metabolite residues in lettuce. Influence of cultural environment. *J Agric Food Chem.* (1990) 38:879–82. doi: 10.1021/jf00093a061

34. European Food Safety Authority. Conclusion on the peer review of the pesticide risk assessment of the active substance fenpyroximate. *EFSA J.* (2013) 11:3493. doi: 10.2903/j.efsa.2013.3493

35. EFSA [European Food Safety Authority]. Reasoned opinion on the review of the existing maximum residue levels for fenpyroximate according to Article 12 of Regulation (EC) No 396/2005. *EFSA J.* (2016) 14:4382. doi: 10.2903/j.efsa.2016.4382

36. European Commission Regulation (EU). 2020/856 of 9 June 2020 amending Annexes II and III to Regulation (EC) No 396/2005 of the European Parliament and of the Council as regards maximum residue levels for cyantraniliprole, cyazofamid, cyprodinil, fenpyroximate, fludioxonil, fluxapyroxad, imazalil, isofetamid, kresoxim-methyl, lufenuron, mandipropamid, propamocarb, pyraclostrobin, pyriofenone, pyriproxyfen and spinetoram in or on certain products (Text with EEA relevance) C/2020/3608. *OJEU.* (2020) 17:9–51.

Assessment of the neuroprotective potential of d-cycloserine and l-serine in aluminum chloride-induced experimental models of Alzheimer's disease: *In vivo* and *in vitro* studies

Özlem Özdemir Tozlu[1], Hasan Türkez[2], Ufuk Okkay[3],
Onur Ceylan[4], Cemil Bayram[3], Ahmet Hacımüftüoğlu[3] and
Adil Mardinoğlu[5,6]*

[1]Department of Molecular Biology and Genetics, Erzurum Technical University, Erzurum, Turkey,
[2]Department of Medical Biology, Faculty of Medicine, Atatürk University, Erzurum, Turkey,
[3]Department of Medical Pharmacology, Faculty of Medicine, Atatürk University, Erzurum, Turkey,
[4]Department of Medical Pathology, Faculty of Medicine, Atatürk University, Erzurum, Turkey,
[5]Science for Life Laboratory, KTH-Royal Institute of Technology, Stockholm, Sweden, [6]Centre
for Host-Microbiome Interactions, Faculty of Dentistry, Oral & Craniofacial Sciences, King's College
London, London, United Kingdom

Alzheimer's disease (AD) is a neurodegenerative disease characterized by the accumulation of amyloid-β (Aβ) plaques and neurofibrillary tangles in the brain accompanied by synaptic dysfunction and neurodegeneration. No effective treatment has been found to slow the progression of the disease. Therapeutic studies using experimental animal models have therefore become very important. Therefore, this study aimed to investigate the possible neuroprotective effect of D-cycloserine and L-serine against aluminum chloride ($AlCl_3$)-induced AD in rats. Administration of $AlCl_3$ for 28 days caused oxidative stress and neurodegeneration compared to the control group. In addition, we found that aluminum decreases α-secretase activity while increasing β-secretase and γ-secretase activities by molecular genetic analysis. D-cycloserine and L-serine application resulted in an improvement in neurodegeneration and oxidative damage caused by aluminum toxicity. It is believed that the results of this study will contribute to the synthesis of new compounds with improved potential against $AlCl_3$-induced neurodegeneration, cognitive impairment, and drug development research.

KEYWORDS

Alzheimer's disease, aluminum, D-cycloserine, L-serine, neuroprotective, neuro-nutrient

Introduction

Alzheimer's disease is marked by a gradual loss of neuronal and synaptic functioning, resulting in memory and cognition problems. The major histological hallmarks of Alzheimer's disease are the deposition of amyloid beta peptides (Aβ) in neuronal cells and the creation of intracellular neurofibrillary tangles (1). The etiology of Alzheimer's disease is complex; the main pathogenic processes in the disease include oxidative stress, amyloidogenesis, and neuroinflammation (2).

Aluminum (Al), an environmental contaminant, has been implicated in the development of Alzheimer's disease (3, 4). Al has a neurotoxic-like effect on neuronal structure (5, 6), blood-brain barrier (BBB) permeability, and cholinergic/noradrenergic neurotransmission (7–9). Several investigations have shown that exposure to solid aluminum chloride and its decomposed form (ion metal Al^{3+}) can change the BBB, influence axonal transport, and cause inflammatory responses as well as synaptic structural abnormalities, resulting in significant memory loss (4, 7–9). Furthermore, the metal ion Al^{3+} hastens the dynamic process of Aβ aggregation, hence increasing neurotoxicity in neuronal cells as a result of significant changes in the biophysical characteristics of the Aβ peptide, which leads to its accumulation in the cortex and hippocampus (4, 9, 10).

Furthermore, Al causes cytoskeletal proteins to misfold, resulting in the production of amyloid plaques and neurofibrillary tangles in the brain (11, 12). As a result, using Al to induce neurodegenerative changes in animals to mimic Alzheimer's disease is generally recognized.

A disruption in glutamatergic neurotransmission *via* the N-methyl-D-aspartate (NMDA) subtype of glutamate receptors may be implicated in the etiology of Alzheimer's disease, according to many lines of evidence (13–15). NMDA receptors are diminished selectively and variably in parts of the brain associated with Alzheimer's disease (16, 17), suggesting that Alzheimer's disease may be linked to the loss of NMDA receptors in specific brain regions. Treatment with memantine, an NMDA receptor antagonist, was recently found to minimize clinical deterioration in moderate-to-severe Alzheimer's disease patients, implying a role for NMDA receptors in the pathogenesis of the disease (18). D-serine has been found to act as an endogenous ligand for the NMDA receptor's strychnine-insensitive glycine sites (19). Furthermore, free D-serine levels in the frontal cortex of Alzheimer's patients were comparable to those in the normal brain (20). D-cycloserine, a partial agonist of the NMDA receptor glycine site, has improved memory-related activities in Alzheimer's patients (21, 22). L-serine is a precursor of D-serine, the synaptic NMDAR's major coagonist, which is necessary for synaptic activity and plasticity. Therefore, it would be of great interest to clarify the potential contribution of L-serine and D-cycloserine to the pathophysiology of Alzheimer's disease. Along these lines, the current work focuses on the neuroprotective effects of L-serine

and D-cycloserine against $AlCl_3$-induced Alzheimer's disease *in vitro* and *in vivo*. It investigates the effects of L-serine and D-cycloserine on cognitive decline and oxidative stress in animals, as well as histopathological examinations. This research aids in slowing disease development and identifies viable therapeutic targets for treating Alzheimer's disease.

Materials and methods

Cell cultures and cellular differentiation

SH-SY5Y cells of human neuroblastoma origin were cultured in Dulbecco's modified Eagle medium F12 (Gibco®, New York, United States) supplemented with 10% fetal bovine serum (Gibco®, New York, United States), 1% penicillin and streptomycin at 37°C in 5% CO_2. Cells were seeded onto plates and passaged when they reached 70–80% confluence. For the differentiation of SH-SY5Y cells, the medium was replaced with DMEM: F12 medium containing 1% FBS and 10 µM retinoic acid (RA, Sigma–Aldrich®, Milan, Italy). The media of the cells were renewed every 3 days with a medium containing 1% FBS and 10 µM RA. The differentiation process of the cells was observed for 11 days with light microscopy (23).

In vitro treatments

WST-8 assay

Cell viability was measured by using a CVDK-8 (Ecotech Biotechnology®) kit according to the manufacturer's manual. Briefly, 1×10^4-1×10^5 cells were seeded in 96-well plates and kept under appropriate culture conditions (37°C, 5% CO_2) for 24 h for cell attachment. Then, the cells were incubated with different concentrations (0-800 µg/ml) of D-cycloserine (DCS) or L-serine (LS, Sigma–Aldrich, St. Louis, MO, United States) against $AlCl_3$ (200 µM) for 24 h. After incubation, CVDK-8 reagent was added to each well and incubated for 3 h. At the end of the incubation period, the absorbance of each sample was measured at 450 nm in a microplate reader (Synergy-HT; BioTek Winooski, VT, United States). As a positive control, cells were treated with 0.1% (*w/v*) Triton X-100.

LDH assay

Following the provider's instructions, the LDH assay was performed using the CytoSelect^TM LDH Cytotoxicity Assay Kit (Cell BioLabs, San Diego, CA, United States). Briefly, the cells were treated as mentioned above, and at the end of the culture period, 90 µL of supernatant was transferred to a new plate, and 10 µL of the reaction mixture was added to each well. The reaction was incubated for 30 min at room temperature in the dark. Eventually, the optical density was

measured at a wavelength of 450 nm in a microplate reader (Synergy-HT; BioTek Winooski, VT, United States). As a positive control, cells were treated with 0.1% (*w/v*) Triton X-100 (24).

Animals and *in vivo* experimental design

Adult male Wistar rats weighing 230 ± 20 g were procured from ATADEM, Ataturk University (Turkey). In the Experimental Animals Housing Unit facility in Atatürk University's Faculty of Pharmacy, animals were maintained at room temperature (25°C) with a 12-h light/dark cycle. Rats were given a regular pellet diet and had unlimited access to food and water *ad libitum*. Before starting the medication therapy, the rats were allowed to acclimatize for a week.

The animal ethics committee of Ataturk University authorized the experimental protocol for the care of experimental animals (approval number 77040475-000-E.1800140631-1851, date of approval 26 April 2018). Animal handling and all procedures were performed in accordance with and strictly adhered to the "Guide for the Care and Use of Laboratory Animals" 8th edition.

Chronic administration of $AlCl_3$ at various levels in mice has been utilized in various investigations to mimic the physiology of Alzheimer's disease (25). In our study, $AlCl_3$ was used at a dose of 5 mg/kg/i.p. for four weeks. This dosing regimen of $AlCl_3$ was selected based on previous reports because of the high rate of induction and low mortality (26, 27).

A total of 39 rats were randomly divided into six groups:

(1). **The control group (CG, *n* = 5)** received saline (1 mL/kg/day, i.p.) for four weeks.

(2). **The AD model group (*n* = 10)** was injected daily with $AlCl_3$ (5 mg/kg/day, i.p.) for four weeks.

(3). **DCS group (*n* = 6):** Rats in this group received DCS (3.6 mg/kg/day i.p.) for four weeks.

(4). **LS group (*n* = 6):** Rats in this group received LS (3.6 mg/kg/day i.p.) for four weeks.

(5). **$AlCl_3$ + DCS group (*n* = 6):** Rats in this group were induced with $AlCl_3$ and subsequently received DCS (3.6 mg/kg/day i.p.) for four weeks.

(6). **$AlCl_3$ + LS group (*n* = 6):** Rats in this group were induced with $AlCl_3$ and subsequently received LS (3.6 mg/kg/day i.p.) for four weeks.

Four days before the study's end date, rats were trained in the Morris water maze. On the last day of the study, animals received the last treatment dose, and the passive avoidance test was later performed. After 24 h, all animals were anesthetized with isoflurane and sacrificed. The blood samples were collected in both EDTA anticoagulant tubes and no anticoagulant tubes. The plasma was separated by centrifugation at 3000 rpm for 10 min at 4°C. The serum was separated from the blood. Whole blood samples were used for the hematological test, while plasma and serum samples were used for the biochemical analysis.

The brains were taken immediately, frozen in liquid nitrogen, and stored at –80°C. The brains were stored in neutral buffered formalin (pH-7.4) for histological investigations.

Neurobehavioral studies

Morris water maze

Morris water maze procedures were used to test rats' spatial memory and learning (28, 29). In this study, a circular swimming pool with a diameter of 150 cm and a height of 40 cm was divided into four quadrants (NW, NE, SE, and SW), with an escape platform located in the NW quadrant that remained 2 cm below the water level during the acquisition trials. External cues were set all over the pool and stayed the same throughout the trial. During the training days, the rats were taught to find this concealed platform by performing four acquisition trials each day for four days in a row (up to 90 seconds). The time needed for each rat to reach the platform was graphically recorded as the escape latency. Successful rats were permitted to stay on the platform for 10 s before being removed; however, if the rat did not find the platform within 60 s, it was gently directed to it and allowed to stay for another 15 s. The animals underwent four acquisition trials per day for four days in a row. The animal was placed in each quadrant during each experiment to remove quadrant effects. The trial time was reported as 2 min in the trials when the rats failed to reach the platform. On the fifth day, each rat was given a 90-s probe experiment in which the platform was withdrawn from the pool. The amount of time spent swimming in the target quadrant (within 90 s of the probe test time) was tracked.

Passive avoidance task

The passive avoidance task (PAT) is a widely used method for assessing the preservation of avoidance memory in mice. As reported in a prior study, a step-by-step PAT was carried out (30). The device had two bright and dark chambers, divided by an automatic door. The animal was placed in the light chamber for the acquisition session. The door was lifted after 30 s of acclimatization, and when the animal entered the dark compartment, a modest electric shock of 0.5 mA was provided for 3 s. After a 24 h acquisition trial, a retention trial was conducted using the same approach as the acquisition trial but without the use of electric shock. Each mouse's transfer latency time (sec) was collected in both the acquisition and retention trials. The test was stopped if the rat did not enter the dark room during the 5 min test period, and the step-through latency was recorded as 300 s (31).

Histopathological examination

Brain tissues of treated and control rats were fixed in 10% buffered formalin solution in labeled bottles. Tissues were

stained with hematoxylin-eosin (H-E) and examined under a microscopic imaging system (Leica Microsystems GmbH, Wetzlar, Germany).

Biochemical and hematological assays

An automated analyzer (Archem, BM240, Istanbul, Turkey) was used to assay for biochemical and hematological parameters.

Total oxidative stress and total antioxidant capacity analysis

Total antioxidant capacity (TAC) assays and total oxidant status (TOS) assays were conducted to measure antioxidative/oxidative capacity in the brain using commercially available TAC and TOS assay kits (Rel Assay Diagnostics®, Gaziantep, Turkey). Ascorbic acid (10 μM) and hydrogen peroxide (25 μM) from Sigma–Aldrich were used as positive control treatments to determine TAC and TOS levels, respectively (32).

Real-time PCR analysis

RNA isolation was performed by homogenizing brain tissues with a Pure Link^{TM} RNA Mini Kit (Invitrogen^{TM}, Carlsbad, CA, United States) following the provider's manual. Then, cDNA synthesis was conducted using 10 μL of RNA with a High-Capacity cDNA Reverse Transcription Kit (Applied Biosystems^{TM}, United States) following the provider's manual. qPCR was carried out using Sybr Green Master Mix (Applied Biosystems^{TM}, United States) on a Real-Time PCR Detection

System (Qiagen Rotor-Gene Q). The qPCR program was 50°C for 2 min, 95°C for 10 min x 40 cycles, 95°C for 15 s, and 60°C for 1 min (33). mRNA expression levels were normalized to ACTB mRNA expression levels. A list of the primers used is given in Supplementary Table 1.

Statistical analyses

Statistical analysis was conducted using the SPSS® 21.0 program. The results are given as the mean $\pm$ standard deviation. Duncan's test was used as a *post hoc* test followed by a one-way analysis of variance (ANOVA). $P < 0.05$ was set as the minimal level of significance.

Results

D-cycloserine and L-serine protect differentiated SH-SY5Y cells from damage induced by AlCl$_3$

The results of the WST-8 assay showed that the treatment of differentiated SH-SY5Y cells with DSC or LS at different concentrations (0-800 μg/ml) for 24 h had no significant effect on cell viability (data not shown). In differentiated SH-SY5Y cells, treatment with AlCl$_3$ at a concentration of 200 μg/ml dramatically reduced the cell viability rate ($P < 0.05$). Cotreatment with DCS or LS, on the other hand,
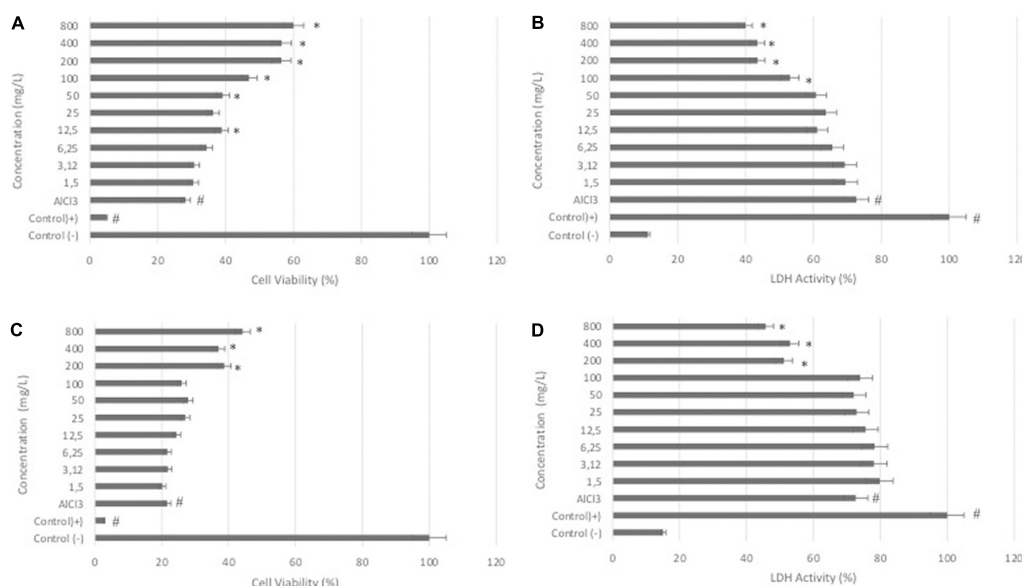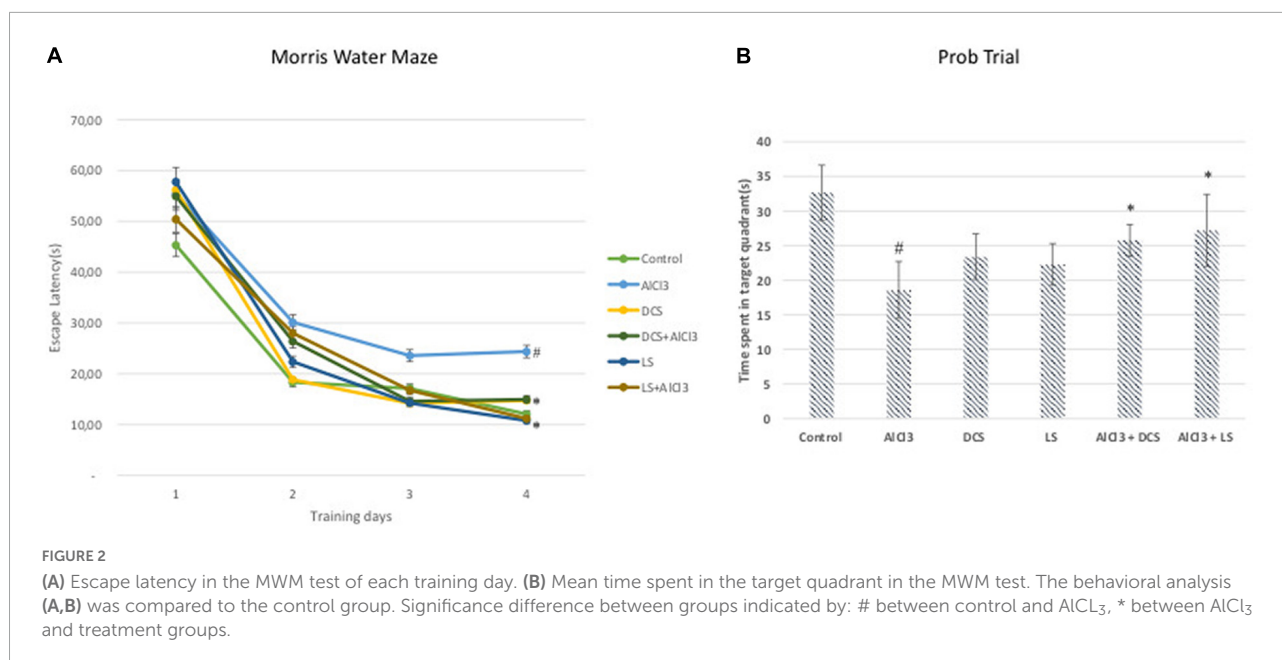

FIGURE 1
Effects of DCS and LS against AlCl$_3$-induced neurotoxicity in differentiated SHSY-5Y cells. **(A)** Viability of differentiated SHSY-5Y cells after 24 h of DCS (0-800 μg/ml) and AlCl$_3$ treatment. **(B)** LDH activity of cells after 24 h of DCS (0-800 μg/ml) and AlCl$_3$ treatment. **(C)** Viability of differentiated SHSY-5Y cells after 24 h of LS (0-800 μg/ml) and AlCl$_3$ treatment. **(D)** LDH activity of cells after 24 h of LS (0-800 μg/ml) and AlCl$_3$ treatment. All values are expressed as the mean $\pm$ standard deviation. Significance difference between groups indicated by: # between control and AlCl$_3$, * between AlCl$_3$ and treatment groups.

FIGURE 2

(A) Escape latency in the MWM test of each training day. **(B)** Mean time spent in the target quadrant in the MWM test. The behavioral analysis **(A,B)** was compared to the control group. Significance difference between groups indicated by: # between control and AlCL$_3$, * between AlCl$_3$ and treatment groups.

resulted in a substantial increase in percent cell viability, showing that DCS and LS have a neuroprotective impact (**Figures 1A,C**) ($P < 0.05$). The LDH assay confirmed the WST-8 results that demonstrated that cell membrane integrity was affected by ALCl$_3$ in a similar pattern. LDH activity was increased in the supernatant of AlCl$_3$-treated cells compared with untreated cells. The protective effect of DCS and LS against AlCl$_3$-induced toxic effects was also confirmed in the LDH assay (**Figures 1B,D**) ($P < 0.05$).

D-cycloserine and L-serine attenuated AlCl$_3$-induced learning and memory deficits

The AlCl3-treated group displayed a significantly ($P < 0.05$) longer escape latency than the untreated control group in the Morris water maze test. In contrast, when compared to the disease-control group, DCS or LS treatment significantly ($P < 0.05$) reduced the rise in escape latency brought on by aluminum chloride treatment (**Figure 2**).

The transfer delay for each mouse was assessed during the passive avoidance test for both the acquisition and retention phases. In the acquisition test, there was no noticeable difference in the transfer latency between any of the experimental groups, according to one-way ANOVA statistical analysis. However, in the retention test, the aluminum chloride-treated group showed a highly significant decline compared to the healthy control group. The DCS treatment demonstrated a considerable improvement in retention latency compared to the disease

control group. Compared to DCS, treatment with LS had more notable results (**Figure 3**).

D-cycloserine and L-serine attenuated the generation of neurofibrillary tangles in the AlCl$_3$-induced AD rat brain

Figure 4 displays the results of the histopathological tests performed on the brain tissues of the rats in the control and experimental groups using hematoxylin and eosin staining. The figure depicts the accumulation of neurofibrillary tangles in the brains of rats exposed to AlCl$_3$ (indicated by arrows). Recovery in the pathogenic alterations in the brain tissue was seen after treatment with DCS or LS.

D-cycloserine and L-serine attenuated aspartate aminotransferase, alanine aminotransferase, and creatine kinase levels

The toxicology results for the hematological parameters are shown in **Supplementary Table 2**. According to the findings, there was a statistically significant increase in aspartate aminotransferase (AST) and alanine aminotransferase (ALT) and a significant decrease in creatine kinase (CK) and uric acid values ($P < 0.05$) in AlCl$_3$-treated animals. Additionally, cotreatment with DCS or LS led to amelioration of these negative changes caused by AlCl$_3$ in rats.
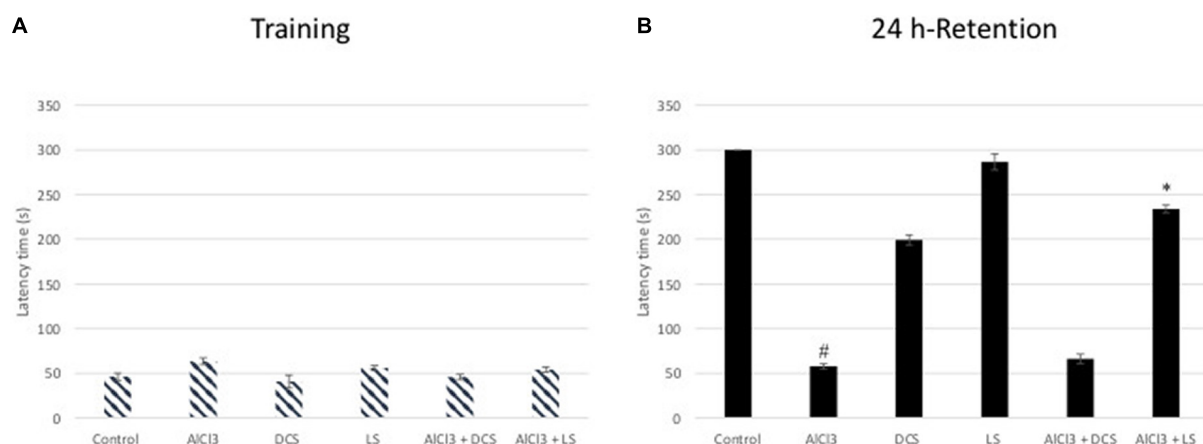
FIGURE 3

Performance in the passive avoidance test. The training latencies **(A)** and the retention latencies **(B)** to enter the dark chamber during sessions are shown. All values are expressed as the mean ± standard deviation. Significance difference between groups indicated by: # between control and $AlCl_3$, * between $AlCl_3$ and treatment groups.

D-cycloserine reduces $AlCl_3$-Induced inflammation

As depicted in **Supplementary Table 3**, $AlCl_3$ led to a significant increase in the level of neutrophils and a decrease in basophils compared to the control group ($P < 0.05$). Most importantly, DCS treatment opposed the effect of $ALCl_3$ and lowered neutrophil levels compared to the $AlCl_3$-treated group.

Additionally, the mRNA expression of TNF was markedly increased by $AlCl3$ incubation relative to the control group (**Figures 5C,D**). Compared with the $AlCl_3$-treated group, DCS and LS treatment significantly decreased the mRNA expression of TNF-a.

D-cycloserine and L-serine attenuated the decreased levels of TAC

Total antioxidant capacity and total oxidative status were measured in brain tissue samples from the rat groups, and the results are shown in **Figure 5**. The results revealed that both DCS and LS support TAC levels. As a positive control, DCS, LS and ascorbic acid (10 μM) increased TAC levels by approximately 2. 37-, 2.16- and 2.75-fold, respectively. At the TOS level, hydrogen peroxide (25 μM), used as a positive control, caused an approximately 3.12-fold increase, while $AlCl_3$ caused a 2.8-fold increase. However, the DCS- and LS-treated groups did not exhibit changes in TOS levels compared to the untreated group. The results showed that $AlCl_3$ exposure caused a significant ($P < 0.05$) decrease in TAC levels and an increase in TOS levels. In addition, it has been shown that the negative change in TAC levels caused by $ALCl_3$ is alleviated by DCS and

LS applications. LS was found to be more effective at alleviating oxidative stress induced by $AlCl_3$ than DCS.

D-cycloserine and L-serine decreased amyloid-beta production in the AD rat model

To further analyze the protective roles of DCS and LS against $AlCl3$-induced neurotoxicity, the levels of Aβ metabolism-related genes, such as APP, BACE 1, NCTSN, PSEN1, PS, ADAM10, and APH1A, were evaluated by RT–PCR. RT–PCR analysis revealed that exposure to $AlCl3$ significantly increased the mRNA expression of APP, BACE 1, NCTSN, and PSEN1 and inhibited the mRNA expression of ADAM10 relative to the control group ($P < 0.05$). Additionally, treatment with DCS or LS showed a significant ($P < 0.05$) beneficial effect in counteracting the effect of $AlCl3$ in the treated brain tissues (**Figure 6**).

Discussion

The current findings show that DCS and LS protect rats from $AlCl_3$-induced Alzheimer-like pathology. One of the most common clinical signs of Alzheimer's disease is cognitive loss, and aluminum causes most of the disease's symptoms (34–36). Aluminum causes behavioral, physiological, and neurochemical changes, which eventually contribute to cognitive impairment, as seen in Alzheimer's disease (37–39). We found that DCS and LS reduced behavioral, biochemical, and neurochemical
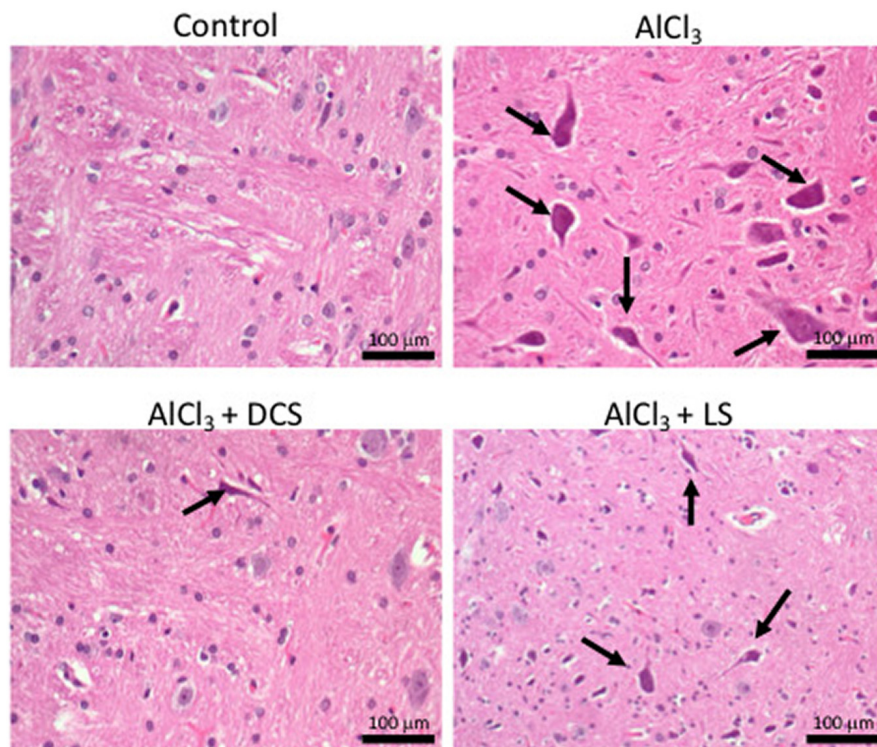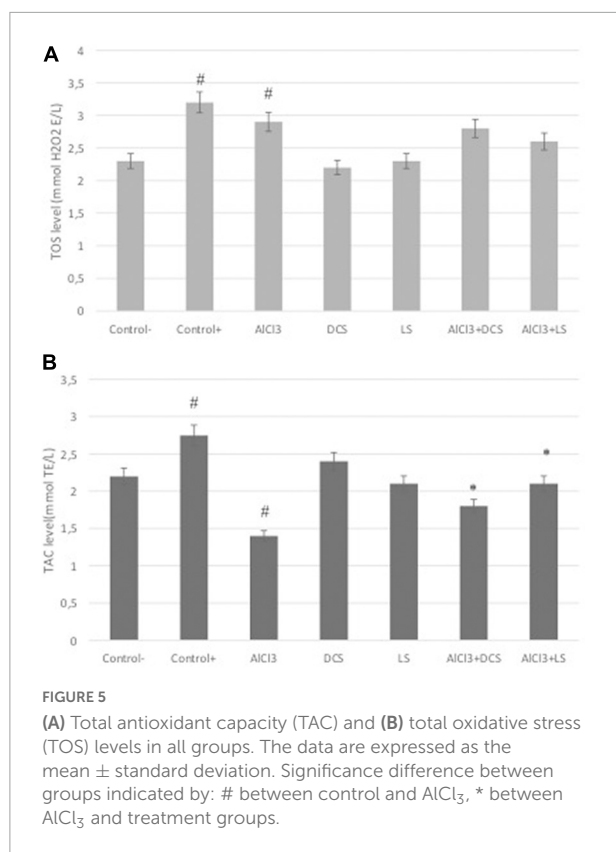
FIGURE 4

Representative histopathology images in the rat brain (n = 3) (hematoxylin-eosin, original magnification 200×) Arrows indicate neurofibrillary tangles.

abnormalities in AlCl$_3$-treated rats, indicating that they might have a neuroprotective function in Alzheimer's disease.

Chronic exposure to AlCl$_3$ resulted in a significant reduction in memory retention and spontaneous memory impairment as measured by passive avoidance and the Morris water maze (MWM) test, respectively. The results were in agreement with previous studies (26, 27). DCS or LS coadministration reduced the cognitive impairment caused by chronic AlCl$_3$ exposure, demonstrating that DCS and LS are powerful neurostimulators and memory enhancers. In the case of aluminum and oxidative stress, it has been established that oxidative damage is responsible for the etiology and cognitive dysfunctions in Alzheimer's disease (40). The total oxidant status (TOS) is usually used to estimate the overall oxidation state of the sample. Similarly, the total antioxidant status (TAS) is used to measure the overall antioxidant status of the sample. Because the measurement of different antioxidant molecules separately is not practical and their antioxidant effects are additive, we preferably measured the total antioxidant capacity and the total oxidant status (41). According to this study, chronic aluminum exposure reduces TAC levels in rat brain homogenates. It has been previously reported that aluminum treatment causes neurochemical changes in various brain areas as well as changes

in the brain's oxidative state, which is in line with our findings (42). Thus, prolonged aluminum exposure disrupts the balance between antioxidants and oxidative processes, a condition that is most likely responsible, at least in part, for the observed memory impairment in rats.

We then examined blood parameters to determine whether there were any changes in the hematological and biochemical systems. The value of CK was found to be significantly lower in AlCl$_3$-treated rats. Creatine kinase, which is vulnerable to oxidative damage and is significantly diminished in AD brains (43), causes a shift in glutamate concentrations and cellular toxicity. In contrast, oxidative damage to creatine kinase may affect energy equilibrium in the brain. The findings also revealed that DCS or LS therapy significantly increased CK activity, which was inhibited by AlCl$_3$ treatment. The reason could be the antioxidant characteristics of L-serine, as previously documented (44). L-serine is likely implicated in the cellular antioxidant defense system because its downstream metabolites glycine and cysteine are precursor amino acids necessary for the formation of the antioxidant glutathione (GSH), which shields cells from oxidative damage (45, 46) L-serine treatment has been found to have promising therapeutic benefits on brain damage and ischemic stroke in preclinical investigations (47, 48).

(A) Total antioxidant capacity (TAC) and **(B)** total oxidative stress (TOS) levels in all groups. The data are expressed as the mean ± standard deviation. Significance difference between groups indicated by: # between control and AlCl$_3$, * between AlCl$_3$ and treatment groups.

Alzheimer's disease is characterized pathologically by inflammation, and immune cells have been implicated in the pathophysiology of the disease. Neutrophils, well-known players of the immune system, perform a variety of tasks, such as producing reactive oxygen species (ROS), phagocytosis, degranulation, and releasing neutrophilic extracellular traps (NETs) (49–51). Neutrophils have a role in the pathophysiologic processes of AD, and the disease process itself may cause an increase in neutrophil count, according to a number of suggested pathways. Tumor necrosis factor-alpha (TNF-α) is a cytokine that is significantly increased in Alzheimer's disease (AD) and is closely associated with the development of neuropsychiatric symptoms (52). Additionally, it is known that TNF promotes neutrophil survival by releasing IL-9 through an NF-ß-dependent mechanism (53). This might be the reason why people with AD have higher neutrophil levels. Basophils express the high-affinity IgE receptor FcRI and contain histamine (54–56). Additionally, it has been shown that AD patients have higher quantities of histamine, a neurotransmitter with anti-inflammatory properties, in their brains and serum. However, it is still unclear how AD affects the quantity and functionality of basophils (57).

In previous investigations, NMDA neurotransmission enhancers have been shown to ameliorate behavior and memory symptoms (58, 59). However, there is disagreement regarding

whether D-cycloserine (a partial agonist of the NMDAR-glycine site) might enhance cognitive performance in dementia patients (21, 22, 60, 61). Clinical investigations have found that using significant amounts of D-serine and D-cycloserine as adjuvant therapy in schizophrenia patients can help with positive, negative, and cognitive symptoms (62, 63). Several studies have examined the link between AD and D-serine levels in serum or CSF. The outcomes were contentious. According to a previous study with a smaller sample size, d-serine serum levels in Alzheimer's patients were somewhat lower than those in normal controls (64). In more recent research, D-serine levels were shown to be increased in postmortem AD brains and CSF of probable AD patients, although the findings were not validated in other studies (65, 66). In contrast to previous studies that enrolled medicated AD patients, a newly published cohort study with a larger sample size that enrolled the entire clinical spectrum of drug-free AD patients revealed indistinguishable CSF and serum D-serine levels and D-serine/total serine ratios compared to controls (67).

The liver enzymes in the animal model of Alzheimer's disease showed significant elevations. The aminotransferases AST, OT1, and ALT (PT1), released into the bloodstream when the liver is damaged, are the most sensitive and widely used diagnostic liver enzymes. As a result, an increase in these enzymes indicates widespread hepatocyte death (hepatic necrosis), which is seen in many inflammatory illnesses (68, 69). In 90% of ischemia or toxic liver injury cases, high levels of aminotransferases have been observed (70). According to one study, blood AST levels increased 6–7 times in 98% of alcoholic hepatitis patients compared to normal values (71).

The amyloid cascade hypothesis establishes that aberrant Aβ aggregation in the brain is the primary cause of Alzheimer's disease, which arises when Aβ production and clearance are out of balance. In the amyloidosis route, Aβ1-42 is generated when APP is sequentially cleaved by β and γ secretases; however, in the non-amyloid pathway, APP is cleaved by α and γ secretases, which avoids Aβ production and seems to be a protective process (72). Previous studies have found that prolonged exposure to AlCl$_3$ increased the expression of APP, Aβ1-42, β and γ secretases, which accelerated Aβ formation and decreased its degradation (35, 73). Aluminum has been shown to accelerate Aβ production and aggregation, cause structural changes in Aβ, and promote the creation of Aβ oligomers (74–76). Exley (77) found that Al raises the Aβ burden in experimental animals by affecting Aβ anabolism or catabolism. The present study indicated that genes associated with Aβ metabolism, such as ADAM10, BACE1, PS1, and NCT, are involved in aluminum-induced neurotoxicity. It can be said that aluminum increases β-secretase and γ-secretase activities. Moreover, DCS or LS attenuated Al-induced Aβ toxicity by lowering the expression of APP, β- and γ -secretases.

The DAXX protein is associated with the FAS protein, which belongs to the tumor necrosis factor receptor superfamily
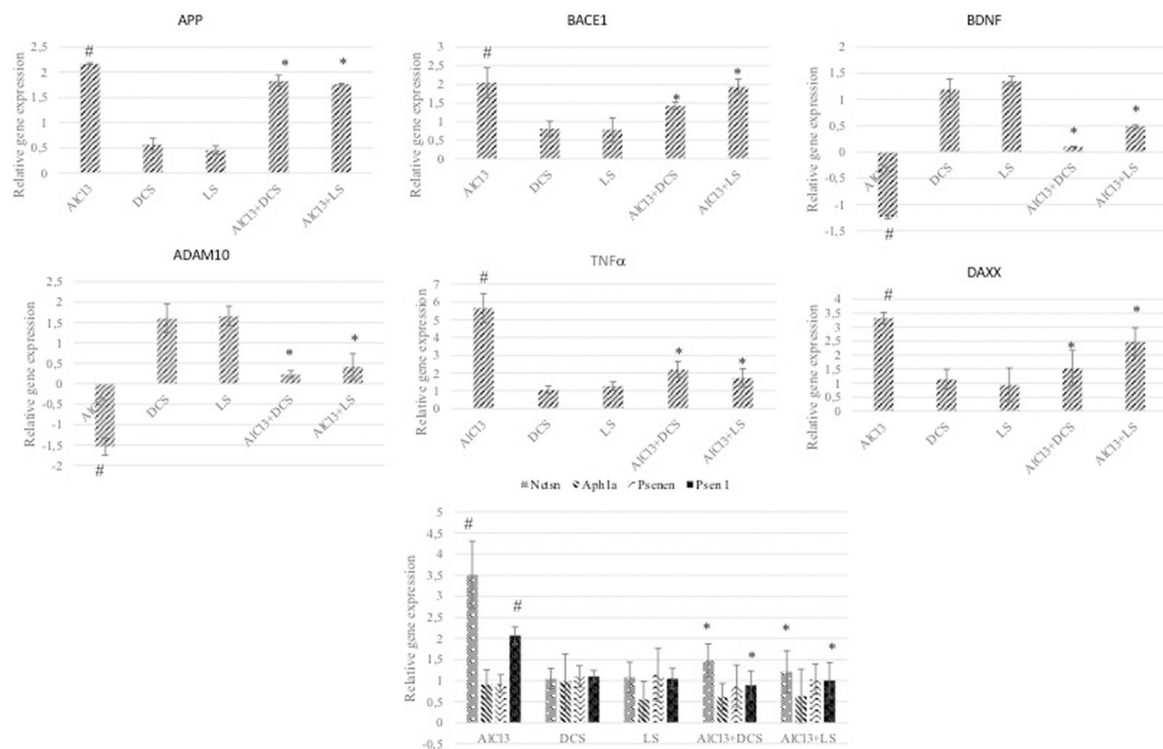
FIGURE 6
The graphs represent the relative expression levels of different genes related to Alzheimer's disease. The analyzed genes were APP, BACE1, BDNF, ADAM10, TNFα, DAXX, NCTSN, APH1A, PSENEN, and PSEN1. The data are expressed as the mean ± standard deviation. Significance difference between groups indicated by: # between control and $AlCl_3$, * between $AlCl_3$ and treatment groups.

and contains the death domain critical for apoptotic signaling. Overexpression of DAXX induces apoptosis, and its expression has been reported to be increased in the AD brain in previous studies (78). As shown in **Figure 6**, DAXX expression was increased in the $AlCl_3$-treated group compared to the control. In addition, DAXX expression decreased significantly due to DCS and LS applications. This finding shows that aluminum causes AD-related pathogenesis by causing apoptosis and that DCS and LS are protective against $AlCl_3$-induced apoptosis.

The failure of therapeutic tactics directed at a single component of Alzheimer's disease is apparent, and there is mounting evidence that the development of successful therapies for the disorder must consider this. In this context, the use of preventative medications, such as neuro-nutrients that can slow the progression of Alzheimer's disease is becoming more popular (79). This research supports this viewpoint, demonstrating that LS can have various therapeutic benefits and potentially contribute to current and future anti-AD treatments.

Data availability statement

The datasets presented in this study can be found in online repositories. The names of the repository/repositories and accession number(s) can be found in the article/**Supplementary material**.

Ethics statement

The animal study was reviewed and approved by the Animal Ethics Committee of Ataturk University.

Author contributions

ÖT, UO, and OC carried out the experiment. ÖT and CB wrote the manuscript with support from AH, AM, and HT conceived the original idea and supervised the project. All authors contributed to the article and approved the submitted version.

Funding

Conflict of interest

The authors declare that the research was conducted in the absence of any commercial or financial relationships that could be construed as a potential conflict of interest.

Publisher's note

All claims expressed in this article are solely those of the authors and do not necessarily represent those of their affiliated organizations, or those of the publisher, the editors and the reviewers. Any product that may be evaluated in this article, or claim that may be made by its manufacturer, is not guaranteed or endorsed by the publisher.

Supplementary material

The Supplementary Material for this article can be found online at: https://www.frontiersin.org/articles/10.3389/fnut.2022.981889/full#supplementary-material

References

1. Duyckaerts C, Delatour B, Potier MC. Classification and basic pathology of Alzheimer disease. *Acta Neuropathol.* (2009) 118:5–36. doi: 10.1007/s00401-009-0532-1

2. Cheignon C, Tomas M, Bonnefont-Rousselot D, Faller P, Hureau C, Collin F. Oxidative stress and the amyloid beta peptide in Alzheimer's disease. *Redox Biol.* (2018) 14:450–64. doi: 10.1016/j.redox.2017.10.014

3. Colomina MT, Peris-Sampedro F. Aluminum and Alzheimer's disease. *Adv Neurobiol.* (2017) 18:183–97. doi: 10.1007/978-3-319-60189-2_9

4. Sharma S, Wakode S, Sharma A, Nair N, Dhobi M, Wani MA, et al. Effect of environmental toxicants on neuronal functions. *Environ Sci Pollut Res.* (2020) 27:44906–21. doi: 10.1007/s11356-020-10950-6

5. Maya S, Prakash T, Goli D. Evaluation of neuroprotective effects of wedelolactone and gallic acid on aluminium-induced neurodegeneration: Relevance to sporadic amyotrophic lateral sclerosis. *Eur J Pharmacol.* (2018) 835:41–51. doi: 10.1016/j.ejphar.2018.07.058

6. Olawuyi TS, Akinola KB, Adelakun SA, Ogunlade BS, Akingbade GT. Effects of aqueous leaf extract of lawsonia inermis on aluminuminduced oxidative stress and adult wistar rat pituitary gland histology. *J Bras Reprod Assist.* (2019) 23:117–22. doi: 10.5935/1518-0557.20190024

7. Ferreira PC, De Abreu Tonani KA, Julião FC, Cupo P, Domingo JL, Segura-Muñoz SI. Aluminum concentrations in water of elderly people's houses and retirement homes and its relation with elderly health. *Bull Environ Contam Toxicol.* (2009) 83:565–9. doi: 10.1007/s00128-009-9791-8

8. Mocanu CS, Jureschi M, Drochioiu G. Aluminium binding to modified amyloid-β peptides: Implications for alzheimer's disease. *Molecules.* (2020) 25:4536. doi: 10.3390/molecules25194536

9. Mold MJ, O'Farrell A, Morris B, Exley C. Aluminum and neurofibrillary tangle co-localization in familial Alzheimer's disease and related neurological disorders. *J Alzheimer's Dis.* (2020) 78:139–49. doi: 10.3233/JAD-200838

10. Exley C. Aluminium and iron, but neither copper nor zinc, are key to the precipitation of β-sheets of Aβ42 in senile plaque cores in Alzheimer's disease. *J Alzheimer's Dis.* (2006) 10:173–7. doi: 10.3233/JAD-2006-102-305

11. Campbell A, Kumar A, La Rosa FG, Prasad KN, Bondy SC. Aluminum increases levels of β-amyloid and ubiquitin in neuroblastoma but not in glioma cells. *Proc Soc Exp Biol Med.* (2000) 223:397–402. doi: 10.1046/j.1525-1373.2000.22356.x

12. Kawahara M, Kato M, Kuroda Y. Effects of aluminum on the neurotoxicity of primary cultured neurons and on the aggregation of β-amyloid protein. *Brain Res Bull.* (2001) 55:211–7. doi: 10.1016/S0361-9230(01)00475-0

13. Liu J, Chang L, Song Y, Li H, Wu Y. The role of NMDA receptors in Alzheimer's disease. *Front Neurosci.* (2019) 13:43. doi: 10.3389/fnins.2019.00043

14. Kodis EJ, Choi S, Swanson E, Ferreira G, Bloom GSN. N-methyl-D-aspartate receptor–mediated calcium influx connects amyloid-β oligomers to ectopic neuronal cell cycle reentry in Alzheimer's disease. *Alzheimers Dement.* (2018) 14:1302–12. doi: 10.1016/j.jalz.2018.05.017

15. Paoletti P, Bellone C, Zhou Q. NMDA receptor subunit diversity: Impact on receptor properties, synaptic plasticity and disease. *Nat Rev Neurosci.* (2013) 14:383–400. doi: 10.1038/nrn3504

16. Procter AW, Wjong EHF, Stratmann GC, Lowe SL, Bowen DM. Reduced glycine stimulation of [3 H]MK-801 binding in Alzheimer's disease. *J Neurochem.* (1989) 53:698–704. doi: 10.1111/j.1471-4159.1989.tb11760.x

17. Sze C-I, Bi H, Kleinschmidt-DeMasters BK, Filley CM, Martin LJ. N-Methyl-d-aspartate receptor subunit proteins and their phosphorylation status are altered selectively in Alzheimer's disease. *J Neurol Sci.* (2001) 182:151–9. doi: 10.1016/S0022-510X(00)00467-6

18. Reisberg B, Doody R, Stöffler A, Schmitt F, Ferris S, Möbius HJ. Memantine in moderate-to-severe Alzheimer's disease. *N Engl J Med.* (2003) 348:1333–41. doi: 10.1056/NEJMoa013128

19. Panizzutti R, De Miranda J, Ribeiro CS, Engelender S, Wolosker H. A new strategy to decrease N-methyl-D-aspartate (n.d.) receptor coactivation: Inhibition of d-serine synthesis by converting serine racemase into an eliminase. *Proc Natl Acad Sci U.S.A.* (2001) 98:5294–9. doi: 10.1073/pnas.091002298

20. Nagata Y, Borghi M, Fisher GH, D'Aniello A. Free d-serine concentration in normal and Alzheimer human brain. *Brain Res Bull.* (1995) 38:181–3. doi: 10.1016/0361-9230(95)00087-U

21. Schwartz BL, Hashtroudi S, Herting RL, Schwartz P, Deutsch SI. d-Cycloserine enhances implicit memory in Alzheimer patients. *Neurology.* (1996) 46:420–4. doi: 10.1212/WNL.46.2.420

22. Tsai GE, Falk WE, Gunther J, Coyle JT. Improved cognition in Alzheimer's disease with short-term D-cycloserine treatment. *Am J Psychiatry.* (1999) 156:467–9. doi: 10.1176/ajp.156.3.467

23. Marinelli L, Fornasari E, Di Stefano A, Turkez H, Arslan ME, Eusepi P, et al. (R)-α-Lipoyl-Gly-l-Pro-l-Glu dimethyl ester as dual acting agent for the treatment of Alzheimer's disease. *Neuropeptides.* (2017) 66:52–8. doi: 10.1016/j.npep.2017.09.001

24. Dirican E, Turkez H. *In vitro* studies on protective effect of Glycyrrhiza glabra root extracts against cadmium-induced genetic and oxidative damage in human lymphocytes. *Cytotechnology.* (2014) 66:9–16. doi: 10.1007/s10616-012-9531-5

25. Saba K, Rajnala N, Veeraiah P, Tiwari V, Rana RK, Lakhotia SC, et al. Energetics of excitatory and inhibitory neurotransmission in aluminum chloride model of Alzheimer's disease: Reversal of behavioral and metabolic deficits by rasa sindoor. *Front Mol Neurosci.* (2017) 10:323. doi: 10.3389/fnmol.2017.00323

26. Khan KA, Kumar N, Nayak PG, Nampoothiri M, Shenoy RR, Krishnadas N, et al. Impact of caffeic acid on aluminium chloride-induced dementia in rats. *J Pharm Pharmacol.* (2013) 65:1745–52. doi: 10.1111/jphp.12126

27. Shuchang H, Qiao N, Piye N, Mingwei H, Xiaoshu S, Feng S, et al. Protective effects of gastrodia elata on aluminium-chloride-induced learning impairments and alterations of amino acid neurotransmitter release in adult rats. *Restor Neurol Neurosci.* (2008) 26:467–73.

28. Morris R. Developments of a water-maze procedure for studying spatial learning in the rat. *J Neurosci Methods.* (1984) 11:47–60. doi: 10.1016/0165-0270(84)90007-4

29. Vorhees CV, Williams MT. Morris water maze: Procedures for assessing spatial and related forms of learning and memory. *Nat Protoc.* (2006) 1:848–58. doi: 10.1038/nprot.2006.116

30. Tabrizian K, Yazdani A, Baheri B, Payandemehr B, Sanati M, Hashemzaei M, et al. Zinc chloride and lead acetate-induced passive avoidance memory retention

deficits reversed by nicotine and bucladesine in mice. *Biol Trace Elem Res.* (2016) 169:106–13. doi: 10.1007/s12011-015-0399-z

31. Prema A, Thenmozhi AJ, Manivasagam T, Essa MM, Akbar M, Akbar MD. Fenugreek seed powder nullified aluminium chloride induced memory loss, biochemical changes, Aβ burden and apoptosis *via* regulating Akt/GSK3β signaling pathway. *PLoS One.* (2016) 11:e0165955. doi: 10.1371/journal.pone.0165955

32. Turkez H, Togar B, Tatar A, Geyıkoglu F, Hacımuftuoglu A. Cytotoxic and cytogenetic effects of α-copaene on rat neuron and N2a neuroblastoma cell lines. *Biologia.* (2014) 69:936–42. doi: 10.2478/s11756-014-0393-5

33. Turkez H, Nóbrega FRD, Ozdemir O, Bezerra Filho CDSM, Almeida RN, Tejera E, et al. NFBTA: A potent cytotoxic agent against glioblastoma. *Molecules.* (2019) 24:2411. doi: 10.3390/molecules24132411

34. Bhattacharjee S, Zhao Y, Hill JM, Percy ME, Lukiw WJ. Aluminum and its potential contribution to Alzheimer's disease (AD). *Front Aging Neurosci.* (2014) 6:62. doi: 10.3389/fnagi.2014.00062

35. Mathiyazahan DB, Justin Thenmozhi A, Manivasagam T. Protective effect of black tea extract against aluminium chloride-induced Alzheimer's disease in rats: A behavioural, biochemical and molecular approach. *J Funct Foods.* (2015) 16:423–35. doi: 10.1016/j.jff.2015.05.001

36. Giorgianni CM, D'arrigo G, Brecciaroli R, Abbate A, Spatari G, Tringali MA, et al. Neurocognitive effects in welders exposed to aluminium. *Toxicol Ind Health.* (2014) 30:347–56. doi: 10.1177/0748233712456062

37. Walton JR. Evidence for participation of aluminum in neurofibrillary tangle formation and growth in Alzheimer's disease. *J Alzheimer's Dis.* (2010) 22:65–72. doi: 10.3233/JAD-2010-100486

38. Garcia T, Esparza J, Nogués MR, Romeu M, Domingo J, Gómez M. Oxidative stress status and RNA expression in hippocampus of an animal model of Alzheimer's disease after chronic exposure to aluminum. *Hippocampus.* (2010) 20:218–25. doi: 10.1002/hipo.20612

39. Bondy SC. Prolonged exposure to low levels of aluminum leads to changes associated with brain aging and neurodegeneration. *Toxicology.* (2014) 315:1–7. doi: 10.1016/j.tox.2013.10.008

40. Kamat PK, Kalani A, Rai S, Swarnkar S, Tota S, Nath C, et al. Mechanism of oxidative stress and synapse dysfunction in the pathogenesis of Alzheimer's disease: Understanding the therapeutics strategies. *Mol Neurobiol.* (2016) 53:648–61. doi: 10.1007/s12035-014-9053-6

41. Woodford FP, Whitehead TP. Is measuring serum antioxidant capacity clinically useful? *Ann Clin Biochem.* (1998) 35:48–56. doi: 10.1177/000456329803500105

42. Nampoothiri M, John J, Kumar N, Mudgal J, Nampurath GK, Chamallamudi MR. Modulatory role of simvastatin against aluminium chloride-induced behavioural and biochemical changes in rats. *Behav Neurol.* (2015) 2015:210169. doi: 10.1155/2015/210169

43. Butterfield DA, Hensley K, Cole P, Subramaniam R, Aksenov M, Aksenova M, et al. Oxidatively induced structural alteration of glutamine synthetase assessed by analysis of Spin label incorporation kinetics: Relevance to Alzheimer's disease. *J Neurochem.* (2002) 68:2451–7. doi: 10.1046/j.1471-4159.1997.68062451.x

44. Zhang C, Bjornson E, Arif M, Tebani A, Lovric A, Benfeitas R, et al. The acute effect of metabolic cofactor supplementation: a potential therapeutic strategy against non-alcoholic fatty liver disease. *Mol Syst Biol.* (2020) 16:e9495.

45. Bosley JR, Björnson E, Zhang C, Turkez H, Nielsen J, Uhlen M, et al. Informing pharmacokinetic models with physiological data: oral population modeling of L-serine in humans. *Front Pharmacol.* (2021) 12:643179. doi: 10.3389/fphar.2021.643179

46. Yang H, Mayneris-Perxachs J, Boqué N, del Bas JM, Arola L, Yuan M, et al. Combined metabolic activators decrease liver steatosis by activating mitochondrial metabolism in hamsters fed with a high-fat diet. *Biomedicines.* (2021). 9:1440.

47. Ren TJ, Qiang R, Jiang ZL, Wang GH, Sun L, Jiang R, et al. Improvement in regional CBF by L-Serine contributes to its neuroprotective effect in rats after focal cerebral ischemia. *PLoS One.* (2013) 8:e67044. doi: 10.1371/journal.pone.0067044

48. Wang GH, Jiang ZL, Chen ZQ, Li X, Peng LL. Neuroprotective effect of L-serine against temporary cerebral ischemia in rats. *J Neurosci Res.* (2010) 88:2035–45. doi: 10.1002/jnr.22365

49. Zenaro E, Pietronigro E, Bianca VD, Piacentino G, Marongiu L, Budui S, et al. Neutrophils promote Alzheimer's disease-like pathology and cognitive decline *via* LFA-1 integrin. *Nat Med.* (2015) 21:880–91. doi: 10.1038/nm.3913

50. Sayed A, Bahbah EI, Kamel S, Barreto GE, Ashraf GM, Elfil M. The neutrophil-to-lymphocyte ratio in Alzheimer's disease: Current understanding and potential applications. *J Neuroimmunol.* (2020) 349:577398. doi: 10.1016/j.jneuroim.2020.577398

51. Mortaz E, Alipoor SD, Adcock IM, Mumby S, Koenderman L. Update on neutrophil function in severe inflammation. *Front Immunol.* (2018) 9:2171. doi: 10.3389/fimmu.2018.02171

52. Holmes C, Cunningham C, Zotova E, Neurology DC. Proinflammatory cytokines, sickness behavior, and Alzheimer disease. *Neurology.* (2011) 77:212–8. doi: 10.1212/WNL.0b013e318225ae07

53. Cowburn AS, Deighton J, Walmsley SR, Chilvers ER. The survival effect of TNF-α in human neutrophils is mediated *via* NF-κB-dependent IL-8 release. *Eur J Immunol.* (2004) 34:1733–43. doi: 10.1002/eji.200425091

54. Schroeder JT. Basophils: Emerging roles in the pathogenesis of allergic disease. *Immunol Rev.* (2011) 242:144–60. doi: 10.1111/j.1600-065X.2011.01023.x

55. Siracusa MC, Comeau MR, Artis D. New insights into basophil biology: Initiators, regulators, and effectors of type 2 inflammation. *Ann N Y Acad Sci.* (2011) 1217:166–77. doi: 10.1111/j.1749-6632.2010.05918.x

56. Schroeder JT. Basophils beyond effector cells of allergic inflammation. *Adv Immunol.* (2009) 101:123–61.

57. Song C, Vandewoude M, Stevens W, De Clerck L, Van der Planken M, Whelan A, et al. Alterations in immune functions during normal aging and Alzheimer's disease. *Psychiatry Res.* (1999) 85:71–80. doi: 10.1016/S0165-1781(98)00130-9

58. Goussakov I, Miller MB, Stutzmann GENMDA-. Mediated Ca2+ Influx drives aberrant ryanodine receptor activation in dendrites of young Alzheimer's disease mice. *J Neurosci.* (2010) 30:12128–37. doi: 10.1523/JNEUROSCI.2474-10.2010

59. Lane H-Y, Lin C-H, Green MF, Hellemann G, Huang C-C, Chen P-W, et al. Add-on treatment of benzoate for schizophrenia. *JAMA Psychiatry.* (2013) 70:1267. doi: 10.1001/jamapsychiatry.2013.2159

60. Randolph C, Roberts JW, Tierney MC, Bravi D, Mouradian MM, Chase TN. D-Cycloserine Treatment of Alzheimer Disease. *Alzheimer Dis Assoc Disord.* (1994) 8:198–205. doi: 10.1097/00002093-199408030-00006

61. Tsai GE, Falk WE, Gunther J. A preliminary study of d-cycloserine treatment in Alzheimer's disease. *J Neuropsychiatry Clin Neurosci.* (1998) 10:224–6. doi: 10.1176/jnp.10.2.224

62. Chang C-H, Lane H-Y, Tseng P-T, Chen S-J, Liu C-Y, Lin C-H. Effect of N-methyl-D-aspartate-receptor-enhancing agents on cognition in patients with schizophrenia: A systematic review and meta-analysis of double-blind randomised controlled trials. *J Psychopharmacol.* (2019) 33:436–48. doi: 10.1177/0269881118822157

63. Yao L, Zhou Q. Enhancing NMDA Receptor Function: Recent Progress on Allosteric Modulators. *Neural Plasticity.* (2017) 2017:1–11. doi: 10.1155/2017/2875904

64. Hashimoto K, Fukushima T, Shimizu E, Okada S, Komatsu N, Okamura N, et al. Possible role of d-serine in the pathophysiology of Alzheimer's disease. *Prog Neuro Psychopharmacol Biol Psychiatry.* (2004) 28:385–8. doi: 10.1016/j.pnpbp.2003.11.009

65. Biemans EALM, Verhoeven-Duif NM, Gerrits J, Claassen JAHR, Kuiperij HB, Verbeek MM. CSF d-serine concentrations are similar in Alzheimer's disease, other dementias, and elderly controls. *Neurobiol Aging.* (2016) 42:213–6. doi: 10.1016/j.neurobiolaging.2016.03.017

66. Madeira C, Lourenco MV, Vargas-Lopes C, Suemoto CK, Brandão CO, Reis T, et al. D-serine levels in Alzheimer's disease: Implications for novel biomarker development. *Transl Psychiatry.* (2015) 5:e561–561. doi: 10.1038/tp.2015.52

67. Nuzzo T, Miroballo M, Casamassa A, Mancini A, Gaetani L, Nisticò R, et al. Cerebrospinal fluid and serum D-serine concentrations are unaltered across the whole clinical spectrum of Alzheimer's disease. *Biochim Biophys Acta Proteins Proteomics.* (2020) 1868:140537. doi: 10.1016/j.bbapap.2020.140537

68. Choi HK, Ford ES, Li C, Curhan G. Prevalence of the metabolic syndrome in patients with gout: The third national health and nutrition examination survey. *Arthritis Rheum.* (2007) 57:109–15. doi: 10.1002/art.22466

69. Raurich JM, Llompart-Pou JA, Rodríguez-Yago M, Ferreruela M, Royo C, Ayestarán I. Role of elevated aminotransferases in ICU patients with rhabdomyolysis. *Am Surg.* (2015) 81:1209–15. doi: 10.1177/000313481508101219

70. Mardinoglu A, Agren R, Kampf C, Asplund A, Uhlen M, Nielsen J. Genome-scale metabolic modelling of hepatocytes reveals serine deficiency in patients with non-alcoholic fatty liver disease. *Nat Commun.* (2014) 5:3083.

71. Dufour DR, Lott JA, Nolte FS, Gretch DR, Koff RS, Seeff LB. Diagnosis and monitoring of hepatic injury. II. Recommendations for use of laboratory tests in screening, diagnosis, and monitoring. *Clin Chem.* (2000) 46:2050–68. doi: 10.1093/clinchem/46.12.2050

72. Vekrellis K, Ye Z, Qiu WQ, Walsh D, Hartley D, Chesneau V, et al. Neurons regulate extracellular levels of amyloid beta-protein *via* proteolysis by insulin-degrading enzyme. *J Neurosci.* (2000) 20:1657–65. doi: 10.1523/JNEUROSCI.20-05-01657.2000

73. Prema A, Justin Thenmozhi A, Manivasagam T, Mohamed Essa M, Guillemin GJ. Fenugreek seed powder attenuated aluminum chloride-induced tau pathology, oxidative stress, and inflammation in a rat model of Alzheimer's disease. *J Alzheimers Dis.* (2017) 60:S209–20. doi: 10.3233/JAD-161103

74. Ricchelli F, Drago D, Filippi B, Tognon G, Zatta P. Aluminum-triggered structural modifications and aggregation of β-amyloids. *Cell Mol Life Sci.* (2005) 62:1724–33. doi: 10.1007/s00018-005-5141-0

75. Drago D, Folin M, Baiguera S, Tognon G, Ricchelli F, Zatta P. Comparative effects of Abeta(1-42)-Al complex from rat and human amyloid on rat endothelial

cell cultures. *J Alzheimers Dis.* (2007) 11:33–44. doi: 10.3233/JAD-2007-11107

76. Zaky A, Mohammad B, Moftah M, Kandeel KM, Bassiouny AR. Apurinic/apyrimidinic endonuclease 1 is a key modulator of aluminum-induced neuroinflammation. *BMC Neurosci.* (2013) 14:26. doi: 10.1186/1471-2202-14-26

77. Exley C. The aluminium-amyloid cascade hypothesis and Alzheimer's disease. *Sub Cell Biochem.* (2005) 38:225–34. doi: 10.1007/0-387-23226-5_11

78. Lukiw WJ. Gene expression profiling in fetal, aged, and Alzheimer hippocampus: A continuum of stress-related signaling. *Neurochem Res.* (2004) 29:1287–97. doi: 10.1023/B:NERE.0000023615.89699.63

79. Ravi SK, Narasingappa RB, Vincent B. Neuro-nutrients as anti-alzheimer's disease agents: A critical review. *Crit Rev Food Sci Nutr.* (2019) 59:2999–3018. doi: 10.1080/10408398.2018.1481012

Development of a time-resolved fluorescence microsphere Eu lateral flow test strip based on a molecularly imprinted electrospun nanofiber membrane for determination of fenvalerate in vegetables

Le Zhang[1], Yiliu Zheng[1], Hua Shao[1]*, Ming Xiao[2],
Jianchun Sun[3], Maojun Jin[1], Fen Jin[1], Jing Wang[1],
A. M. Abd El-Aty[4,5,6] and Yongxin She[1]*

[1]Institute of Quality Standards and Testing Technology for Agro-Products, Chinese Academy of
Agricultural Sciences, Beijing, China, [2]Academy of Agriculture and Forestry Sciences, Qinghai
University, Xining, China, [3]Inspection and Testing Center of Agricultural Products of Tibetan
Autonomous Region, Lhasa, China, [4]State Key Laboratory of Biobased Material and Green
Papermaking, Qilu University of Technology, Shandong Academy of Sciences, Jinan, China,
[5]Department of Pharmacology, Faculty of Veterinary Medicine, Cairo University, Giza, Egypt,
[6]Department of Medical Pharmacology, Medical Faculty, Ataturk University, Erzurum, Turkey

Fenvalerate residues in fruits and vegetables may result in biological immune system disorders. Current sensor detection methods are harsh due to the shortcomings of antibody preparation and preservation conditions. Therefore, developing a recognition material with strong specificity, good stability, and low cost is of practical significance in designing a sensitive, simple, and rapid method. This study used precipitation polymerization to synthesize molecularly imprinted polymers (MIPs). The MIP was prepared into a fiber membrane using the electrostatic spinning method. After that, the fenvalerate hapten-mouse IgG-Eu fluorescent probe was synthesized, and the side flow chromatography strip was constructed to determine fenvalerate in vegetables using the immunocompetition method. The results showed that the adsorption capacity of MIP to fenvalerate was 3.65, and the adsorption capacity on MIPFM (an electrospinning membrane containing the fenvalerate MIPs) was five times that of free MIP. The test strip showed good linearity with $R^2 = 0.9761$ within the range of 50 μg/L-1,000 μg/L. In conclusion, substituting fenvalerate monoclonal antibodies with a molecularly imprinted electrospinning membrane is ideal for rapid onsite detection of pyrethroids.

Introduction

Pyrethroid pesticides have the broadest spectrum of high efficiency, low residue, moderate toxicity, and are biodegradable in plants. It effectively prevents and controls the storage of insect pests and has become the preferred pesticide in today's agriculture (1, 2). Type II pyrethroid pesticides have good efficacy and stability and are widely used to protect crops against insects. The highest detection rate was reported in crops, followed by sediment, soil, and water. M-phenoxybenzoic acid (3 PBA) is a common metabolite of several pyrethroid insecticides (3). In addition, studies have shown that pyrethroids can trigger immune disorders, which may seriously impact the occurrence of immune-related diseases (4). Therefore, it is necessary to monitor pyrethroids in agri-products. Many countries and agencies have set tolerance or maximum residue limits (MRL) for pyrethroids based on the potential impact of a pesticide on humans, referred to as risk assessment. For instance, in the EU, the MRL of fenvalerate in vegetables ranged from 0.02 to 0.2 mg/kg. In the Codex Alimentarius (CAS), the MRL of fenvalerate in vegetables ranged from 0.05 to 3.0 mg/kg. In Japan, the MRL of fenvalerate in vegetables ranged from 0.05 to 3.0 mg/kg. In the Republic of Korea, the MRL in vegetables ranged from 0.05 to 10.0 mg/kg, whereas in China, the MRL in vegetables ranged from 0.05 to 10.0 mg/kg. As they are lipophilic, their absorption in the gastrointestinal and respiratory tracts is higher than on the skin. They are also transmitted directly and indirectly through the food chain and eventually threaten human health and life (5).

At present, pyrethroids are detected by various techniques, including chromatography (6–8), liquid chromatography-mass spectrometry (9–11), and immunological methods (12). Chromatography-mass spectrometry is mostly used as a confirmation method due to the separation power of chromatography combined with the high selectivity of mass spectrometry. It is a high-throughput hyphenated technique that can detect multiple analytes in a single run. However, the sample preparation is time-consuming, and the equipment is expensive and requires professional personnel to operate. Immunoassays (IAs) are bioanalytical techniques that measure enzymes and proteins quantitatively and qualitatively using a combination of antigens and antibodies. Conversely, the immunochromatographic assay is an analytical method that combines immunotechnology and chromatography using fluorescent substances or colloidal gold (13, 14) labels. It is widely used in various fields. However, pyrethroids are small molecules that do not trigger an immune response. Preparing antibodies in the mouse body and optimizing storage conditions increase the cost and necessitate the sacrifice of animals. Therefore, to meet the demand for large-scale assessments, it is necessary to establish a fast, sensitive, accurate, and low-cost onsite analysis to monitor food pyrethroids (15).

Molecularly imprinted polymers (MIPs) have an affinity for the predetermination and specific identification of a molecule in addition to their practicability. The polymer has a simple preparation process, low-cost, good mechanical and chemical stability, and long service life to satisfy the features of a specific recognition material with reasonable practicability (16–19). For instance, Azizollah Nezhadali et al. (17) prepared a selective molecularly imprinted polymer-based solid-phase extraction (MISPE) by bulk polymerization using fenvalerate as a template and polypyrrole (PPy) as a monomer. The detection and quantification limits of this method were 0.19 ng/g and 0.63 ng/g, respectively, with a relative standard deviation of 4.07%. The method is simple and utilizes the minimum solvent volume, replacing the traditional sample preparation. Furthermore, Wang et al. (20) established a highly selective and sensitive photochemical sensor, CdTe QDS-MIP, fixed on a paper-based working electrode to determine fenvalerate in fruits and vegetables. This method has higher photocurrent transfer efficiency and the advantages of simplicity, speed, and low cost compared with pure CdTe QDs. Moreover, Wang et al. (21) developed a method for the selective identification and detection of λ-cyhalothrin with 5-isothiocyanate (6) (FITC) and 3-aminopropyltriethoxysilane (APTS)/SiO2 combined with fluorescent MIP. This method eliminates the interfering substances in the sample and improves the detection limit. Due to its excellent properties, MIP has been used as a direct substitute for natural antibodies, receptors, and enzymes in submolecular biology (22). In this study, MIP was directly immobilized on a nitrocellulose (NC) membrane by streaking, and it flowed away with the solution. Therefore, a relatively fixed method is needed to firmly stabilize the MIP particles on the NC membrane. Electrospinning is a non-mechanical electrostatic technique that can spin nanofibers directly from the polymer solution (23). The obtained fiber has the advantages of a large specific surface area, high porosity, fast mass transfer rate, and easy separation (24–27). For instance, Xing et al. developed an atrazine (ATZ) molecularly imprinted nanofiber membrane based on electrospinning. The membrane has a large specific surface area, enhanced rebinding ability, and selective permeability of ATZ, as well as having strong practicability for separating ATZ in water samples (28). Furthermore, Ruggieri et al. synthesized MIPs using ATZ as a template and dispersed MIPs in an electrospinning solution dissolved in polystyrene to prepare a molecularly imprinted electrospun nanofiber membrane (MIM). The adsorption evaluation of ATZ, ATZ metabolites atalido-deisopropyl, carboxylin, linuron, atraton, and chlorpyrifos was carried out in distilled and river water. Compared with the adsorption capacity of MIP for these five pesticides, the adsorption capacity of MIM significantly increased (37). In addition, under low pesticide concentrations, the efficiency of commercial SPE was higher than that of the MIM prepared in this study; however, for

complex matrices and high concentrations, MIM can replace commercial products well.

In our previous study, we developed a test strip based on surface molecularly imprinted electrospun affinity membranes to detect triazophos residues in water. We prepared the test line on a nitrocellulose membrane using a molecularly imprinted electrospinning technique. Then, we synthesized a triazophos hepten-murine IgG/fluorescein isothiocyanate conjugate (THBu-IgG-FITC) to directly compete with the target triazophos on the molecularly imprinted binding sites (29). However, the Stokes shift of the ordinary fluorescent group was 1–100 nm, the fluorescence lifetime was short, and quenching was easy, for example, for fluorescence quantum dots (30, 31). In comparison, time-resolved fluorescence immunoassays used trivalent rare-earth ions—such as Eu (III), Tb (III), and Sm (III)—as markers. These ions can produce high-intensity fluorescence and decay for a long time. Accordingly, short-delay measurement and interference with natural fluorescence can be eliminated, significantly improving the method's sensitivity (32, 33). It should be noted that the preparation of antibodies for pyrethroids is complicated; therefore, few strips can be used for rapid onsite detection. It is worth noting that there is no literature on the combination of molecularly imprinted electrospun nanofiber membranes and time-resolved fluorescence microspheres Eu. Hence, this study established a rapid determination method using a biomimetic immunoassay based on molecularly imprinted recognition material for the rapid and sensitive detection of fenvalerate in Brussels sprouts, cucumbers, and eggplants. Herein, time-resolved fluorescent latex microspheres Eu were labeled with a conjugate of fenvalerate hapten-IgG (FH-IgG). It competed with the pyrethroid molecule in the sample to bind specific binding sites on the MIPs. The method was evaluated from the quantitative standard curve, detection limit, linear range, and actual examples by exploring the assembly of the biomimetic immunofluorescence strip. The findings were compared with the results of GC–MS/MS.

Experimental

Materials

Ethyl chrysanthemate (95%) and dowtherm A were secured from Macklin Biochemical Co., Ltd. (Shanghai, China). 2,2'-Azobisisobutyronitrile (AIBN) was acquired from Bailingwei Co., Ltd. (Beijing, China). Acrylamide (AA), ethylene glycol dimethacrylate (EGDMA), cellulose acetate (CA), dicyclohexylcarbodiimide (DCC), EDC, N-hydroxysuccinimide (NHS), and BSA were acquired from Sigma–Aldrich, St. Louis, MO, USA. Fenvalerate was obtained from Dr. Ehrenstorfer (GmbH, Germany). Goat anti-mouse IgG and mouse IgG dry powder were purchased from Solarbio

Technology Co., Ltd. (Beijing, China). Our laboratory provided fenvalerate haptens, whereas the NC membrane (NC95) was purchased from Sartorius Stedim in Germany. Glass fiber membrane RB45, absorbent paper SH27, and PVC base plate SMNF31-25 were obtained from Shanghai Jieyi Biotechnology Co., Ltd. (Shanghai, China). Sucrose, sodium chloride, sodium dihydrogen phosphate dihydrate, disodium hydrogen phosphate dodecahydrate, and Tween 20 were obtained from China National Medicines Corporation Ltd. (Beijing, China). Time-resolved fluorescent latex microspheres Eu (200 nm, wrapped by polystyrene) were obtained from Diibio Technology (Xiamen, China). Shanghai Yuanye Biotechnology Co., LTD supplied an MD3534-5 m dialysis bag. Deionized water was purified with a Milli-Q system (Millipore, Bedford, MA, USA). Acetone (purity $\geq$ 99.5%) was secured from Beijing Chemical Industry Group Co., Ltd., whereas HPLC-grade methanol (MeOH) was purchased from Fisher Scientific (Pittsburgh, PA, USA).

Molecularly imprinted polymers

Preparation of dual-template imprinted polymers

Molecularly imprinted polymers were prepared by precipitation polymerization (the brief process in Figure 1). Briefly, ethyl chrysanthemate (21.6 µL), 15.3 µL of dowtherm A and 43.236 mg of AA were dissolved in 50 mL of ACN in a round-bottomed flask and prepolymerized for 4 h in a water bath at room temperature. Then, 31.2 mg of AIBN and 282 µL of EGDMA were added separately to remove the oxygen from the solution by purging with nitrogen for 30 min and sealing. Afterward, the flask was placed in a water bath at 60 °C and shaken for 24 h at 150 rpm. After the polymerization reaction was completed, the mixture was centrifuged at 5,000 rpm for 5 min (Thermo Fisher Scientific, Waltham, MA, USA). Finally, the polymers were washed with methanol: acetic acid (*v/v*, 8:2) in a Soxhlet extractor until HPLC detected no template. The MIPs were washed several times with pure methanol, dried at 40°C, and stored at room temperature. Non-imprinted control polymers were the same as MIP conditions except without templates.

Binding experiments

According to the specific adsorption of MIPs, 20 mg of MIPs or NIPs and 1 mL of 40 mg/L fenvalerate were added to a centrifuge tube and oscillated for different times (0, 10, 20, 30, 60, 90, and 180 min) at room temperature. Next, the mixtures were centrifuged at 5,000 rpm for 3 min, and HPLC (Waters 2695 Alliance HPLC system with a 2489 UV detector, Waters Corporation, Milford, MA, USA) was used to determine the concentration at 235 nm for fenvalerate in the supernatant to

FIGURE 1
The synthesis process of MIP.
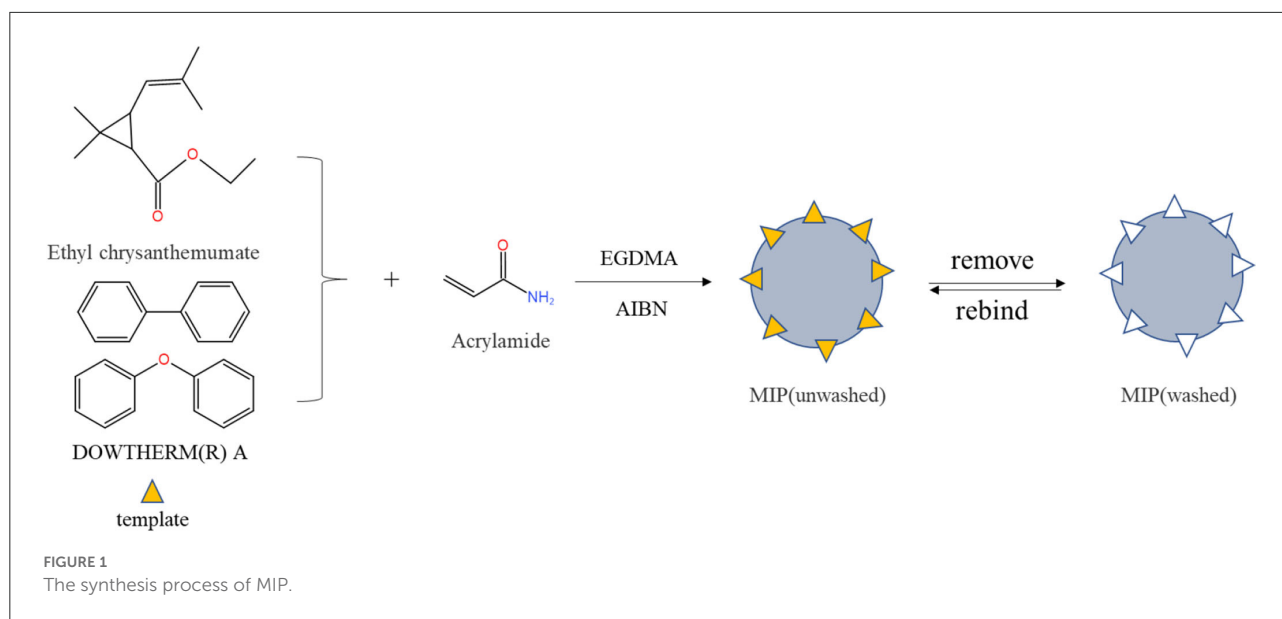
assay the saturation adsorption time. Afterward, 20 mg of MIPs or NIPs was weighed in a 2 mL centrifuge tube, and 1 mL of fenvalerate at different concentrations (40, 60, 80, 100, 150, and 200 mg/L) was added and shaken well for 90 min. Finally, the mixtures were centrifuged at 5,000 rpm for 3 min, and HPLC was used to determine the concentration in the supernatant to calculate the saturated absorption amount. The adsorption capacity Q (mg/g) of MIP to fenvalerate was calculated using formula (1). The maximum apparent capacity and binding site were determined by the Scatchard equation (2).

$$Q = (C_0 - C)\, V/m \tag{1}$$

$$\frac{Q}{C} = (Q_{\max} - Q)/k_d \tag{2}$$

where Q is the amount of MIP adsorbed on the target at equilibrium, C_0 is the initial concentration of fenvalerate, C represents the final concentration in the supernatant at equilibrium, and V is the volume of fenvalerate (mL), with m referring to the amount of MIP added. Qmax is the maximum apparent adsorption capacity, and k_d is the equilibrium dissociation constant.

Specificity of PyMIP

The specific selectivity of PyMIP was evaluated using different concentrations of fenvalerate and the structural analogs silafluofen, sulfadiazine, ethiprole, and buprofezin at concentrations between 0.5 and 20 mg/L. Then, 5 mg of PyMIP and NIP were accurately weighed, and a 1 mL standard solution of fenvalerate (F), thiazone (B), acetonitrile (E), and sulfadiazine (Su) gradient series (0.5, 1, 2, 3, 5, 10, and 20 mg/L) was added. The solution was oscillated at room temperature for

1 h, centrifuged, and the supernatant was taken. After filtration through a 0.22 μm microporous membrane, the concentration of the target substance in the supernatant was determined by HPLC, the adsorption capacity was determined, and the specificity of the polymer was evaluated.

Preparation of a molecularly imprinted test line on an NC membrane using electrospinning

Preparation of the electrospinning solution

A 15% electrospinning solution was prepared by adding 1.5 g of cellulose acetate (CA) to 12.7 mL of acetone and methanol (9:1, *v/v*). Then, the MIP dispersion solution and Tween-20 solution dissolved in methanol were added to the electrospinning solution. The solution was stirred at room temperature until the MIPs were evenly dispersed in the electrospinning solution (electrospinning solution: MIP dispersion solution: Tween-20, =1,000 μL:100 μL:10 μL, *v/v/v*) to obtain a uniform pyrethrin molecularly imprinted electrospinning solution.

Preparation of the T-line on the NC membrane by electrospinning

The laboratory electrospinning device was used to prepare nanofiber layers. The electrospinning solution was injected into a typical syringe, the 18-gauge needle was used as a nozzle, and the distance between the needle and the receiver was 16 cm. The spinning test was carried out under a voltage of 13 kV. At this point, the electrospinning membrane containing the fenvalerate

MIPs (MIESM) was formed on foil paper and then placed in an oven at 37°C for drying. After removing the paper, the film was cut into a shape similar to the test line (T-line) in the lateral flow test strips and stuck on scotch tape for later use.

Preparation of the immunochromatographic test strip

Synthesis of the FH-IgG conjugate

The synthetic method was moderately modified based upon previous work carried out by Yahui He as follows: 10 mg of fenvalerate hapten (FH), 4.6 mg of N-hydroxysuccinimide (NHS), and 8.24 mg of dicyclohexylcarbodiimide (DCC) were dissolved in a 5 mL glass bottle with 0.5 mL of anhydrous DMF. The reaction mixture was stirred overnight at room temperature and then centrifuged at 4,000 rpm for 1 min. The supernatant was collected and slowly added to 1.5 mL of PBS (0.01 mol/L) containing 4 mg of mouse IgG and stirred at room temperature for 3 h. All of the above solutions were transferred to a dialysis bag. Finally, the solution was dialyzed several times against 0.01 mol/L PBS solution (pH = 7.4) at 4 °C until the dialysate was clear. Afterward, the conjugate (FH-IgG) was freeze-dried in a freeze-dryer for 24 h, stored at −20 °C, and then set aside.

Time-resolved fluorescent microsphere-FH-IgG conjugates

A 100 μL time-resolved fluorescence microsphere Eu was added to 900 μL of labeled buffer (50 mM 2-morpholinoethanesulfonic acid (MES), pH = 6.0). To activate the carboxyl groups on the surface of time-resolved fluorescence microspheres Eu, 10 μL and 5 μL of 20 mg/mL NHS and EDC were added sequentially and mixed at room temperature for 20 min. After the solution was centrifuged at 9,000 rpm for 15 min and cleaned by MES several times, 0.5 mg of FH-IgG was added and kept at room temperature for 2 h. Afterward, 100 μL of 20 mg/mL BSA (dissolved in 0.05 M PBS buffer solution) was added to the solution and mixed at room temperature for 1 h. The obtained solution was centrifuged at 9,000 rpm for 15 min. The fluorescent microspheres were precipitated twice to remove the unbound antibodies. The fenvalerate hapten-IgG-fluorescent microsphere labeling complex (FH-IgG-Eu) was obtained and stored at 4°C for further experimental work.

Preparation and assembly of the immunochromatographic strip assay
Assemble biomimetic immunochromatographic strip test

The composition of the test strip is shown in Figure 2. The fluorescence was sprayed on the mat at a speed of 0.5 μL/mm by the injector and then dried in the oven at 37°C for further use.

Goat-mouse IgG was coated on a nitrocellulose (NC) membrane as a control (C) line by an HM3030 XYZ 3D membrane spraying instrument (Shanghai Jieyi Biotechnology Co., Ltd., Shanghai, China) at a proper jetting rate. The coated membrane and sample pad treated with blocking buffer were dried overnight at 37°C. Then, the NC membrane, sample pad, and absorbent were assembled on a fluorescent plastic backing and cut to 4 mm in length. Afterward, the electrostatic fiber membrane was removed from the foil paper and stuck on the sticker, and then the area of the MIP membrane was cut into pieces 2 mm in width, 4 mm in length, and then stuck 5 mm from the C-line as the T-line.

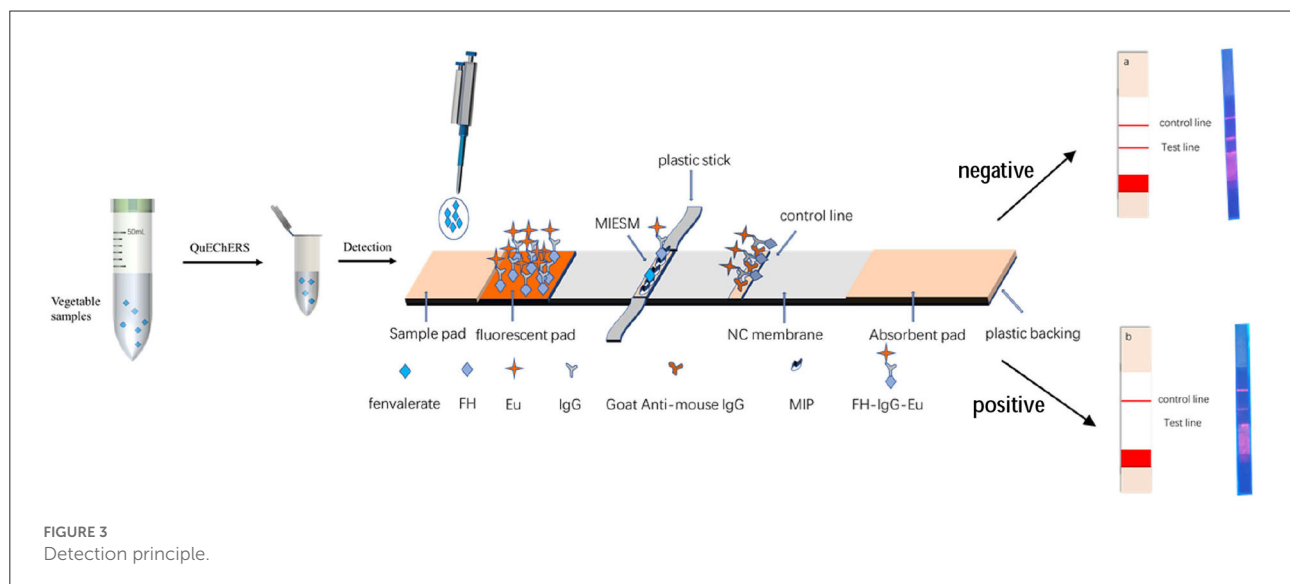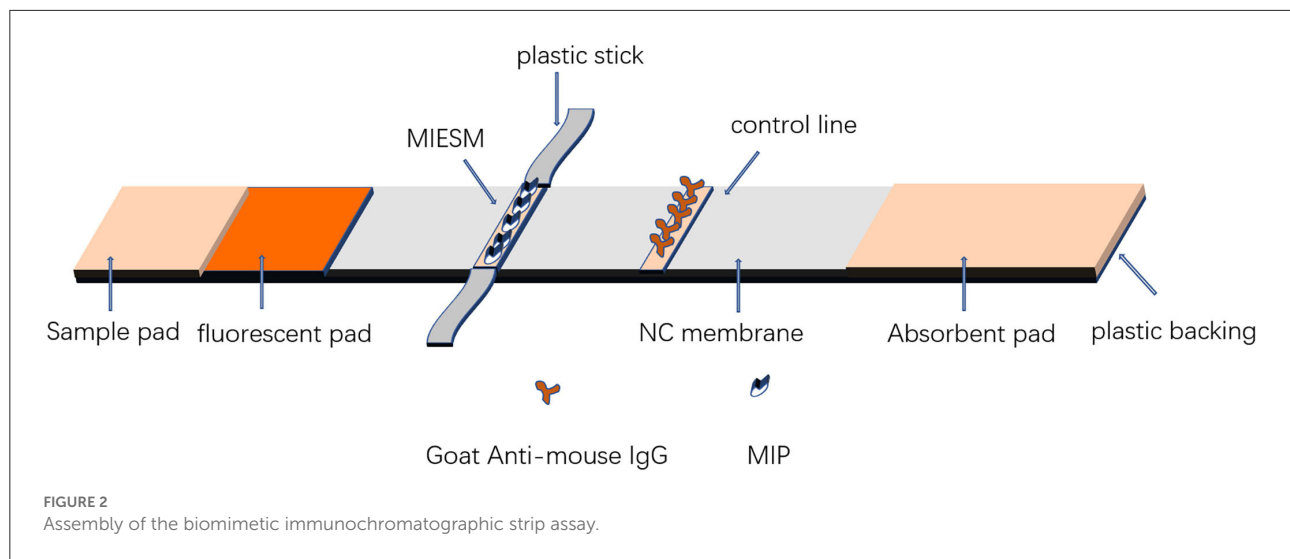### Detection principle of the immunochromatographic strip test

The MIP was fixed on the NC membrane by electrospinning (alternative to antibody) as the T-line and goat-mouse IgG as the C-line immobilized by the instrument and sprayed the FH-IgG-Eu solution onto a mat as a fluorescent mat. As shown in Figure 3, when fenvalerate was dripped onto the sample pad, it moved to the fluorescent mat, and the FH-IgG-Eu was dissolved in the buffer solution and flowed to the NC membrane together. The target fenvalerate and the FH in FH-IgG-Eu could compete for the binding site at the MIPs so that the fluorescence intensity of the T-line forms an inverse relationship with the concentration of fenvalerate. The remaining fluorescence probes are transported to the C-line and combined with secondary antibodies to effectively control the quality of the label flow strips. Finally, the immunofluorescence card reader (Beijing Qinbang Biology Co., LTD. Beijing, China) read T, C, and T/C values according to the intensity of T-line fluorescence and T/C value to be quantified.

Immunochromatographic strip optimization procedure
The fixation method of the T-line and the use of fluorescent microspheres

Because MIPFM replaces the T-line, its fixation needs to be optimized to do the T-line work normally and reduce agglomeration. Therefore, the following two methods were tested. One method involved not cutting the NC membrane directly to glue the MIPFM and fixing it on the NC membrane as a T-line. Another way required cutting the NC membrane and sticking the MIPFM with foil paper as a T-line.

Two methods were tested: one mixed the fluorescent probe and buffer solution and dropped it into the test (way 1), and the other used the fluorescent pad for the test (way 2). According to the calculation, the spraying amount of the fluorescent pad was approximately 2 μL/4 mm. Thus, 2 μL of fluorescent probes were added to 100 μL of buffer solution in the direct drip method.

FIGURE 2
Assembly of the biomimetic immunochromatographic strip assay.

FIGURE 3
Detection principle.

Optimization of the amount of MIP, FH-IgG, and fluorescence

Taking the FH-IgG labeling amount, fluorescent pad spraying amount, and MIP content in the T-line as three factors, we designed the test to fulfill the optimal test parameters of the strip. The secondary antibody concentration in the C-line was fixed at 2 mg/mL. As described in Section GC–MS/MS, the fluorescence immunocard reader was used to read the T/C values under the negative condition. At the same time, 100 μL of fenvalerate standard solution (500 μg/L) was dropped to compete with MIP binding sites as a positive control. Formula (3) was used to calculate the competitive inhibition rate. The optimum experimental conditions were selected as the appropriate T-line fluorescence intensity and the maximum rate of competitive inhibition. Each experiment was reproduced five

times, and the final results were expressed as an arithmetic mean.

$$\left(1 - \frac{B}{B_0}\right)^* 100\% \qquad (3)$$

where B is the T/C value under positive conditions and B_0 is the T/C value under negative conditions.

Optimization of the concentration of secondary antibodies

Sheep anti-mouse IgG at concentrations of 1, 2, 3, and 4 mg/mL was fixed on the NC membrane to assemble the strips. The optimal concentration of secondary antibodies was selected according to the competitive inhibition rate and the brightness of the lines on the strips.

Optimization of the buffer solution

The buffer solution was vital for the fluorescence microspheres on the NC membrane. The buffer solution affects whether fluorescence microspheres climb. In this experiment, eleven different buffer solutions were prepared to select the appropriate solution (Supplementary Table S1).

Optimization of the organic solvent tolerance of the immunochromatographic strip test

Because fenvalerate is insoluble in water, organic solvents were used for reconstitution. Herein, we tested acetonitrile, methanol, isopropanol, ethanol, ethyl acetate, acetone, and *n*-hexane. Furthermore, acetone and *n*-hexane can dissolve fenvalerate directly through GC/MS. Due to the limited IgG and NC membrane tolerance to organic solvents, it is necessary to optimize the addition amount. Thus, we set the amounts to 1, 5, 10, 15, and 20% for optimization.

Performance of the method

To estimate the performance of the strip, the buffer solution was used to dilute the fenvalerate standard (dissolved in acetonitrile) to concentrations of 0, 20, 50, 100, 200, 500, 800, and 1,000 μg/L, and 100 μL was added to the assembled strip. After 15 min of reaction in a dark environment, the values were read, and each concentration was repeated five times. The Log10 value of the concentration of fenvalerate standard solution was used as the X-axis, and the corresponding T/C value was used as the Y-axis. The T/C value decreased gradually with increasing concentrations of the standard solution. The IC50 and the limit of detection (LOD), defined as the fenvalerate concentration with 10% inhibition, were computed by the standard curve and used as reference standards of the sensitivity.

Sample preparation

Vegetables, including Brussels sprouts, cucumbers, and eggplants, were procured from local supermarkets in Beijing. The homogenates were pretreated with QuEChERS. A10 samples (accurate to 0.01 g) were weighed into a 50 mL centrifuge tube, and the fenvalerate standard was spiked at 100, 500, and 1,000 μg/L. After withstanding for 30 min, 10 mL of acetonitrile, 4 g of anhydrous magnesium sulfate, 1 g sodium chloride, 1 g sodium citrate, and 0.5 g disodium hydrogen citrate were added, shaken vigorously for 1 min, and centrifuged at 4,200 r/min for 5 min. A 3 mL supernatant was added to 450 mg of anhydrous magnesium sulfate and 150 mg of PSA, followed by vortex mixing for 1 min and centrifugation at 4,200 r/min for 5 min. The supernatant was filtered through microporous filtration membranes (0.22 μm) for analysis.

Test strip

First, 1 mL of supernatants were dried with nitrogen in a centrifuge tube, then 50 μL acetonitrile was added into that centrifuge tube for redissolution, after which a 1,950 μL buffer solution was also added into that centrifuge tube to diluent the solution for the strip determination. Measure 100 μL of the solution and drop it onto the strip for the test.

GC–MS/MS

0.5 mL of supernatants were dried with nitrogen in sample vials, and then 1 mL of *n*-hexane was added to the sample vial to redissolve fenvalerate for detection by GC–MS/MS (Shimadzu GCMS-TQ8040 gas mass spectrometry tandem mass spectrometry, Shimadzu, Japan). The capillary column was a DB-5MS chromatographic column (5% phenyl and 95% polysiloxane stationary phase, 30 m × 0.25 mm × 0.25 μm). The GC oven temperature program was as follows: 50°C was raised to 150°C at a rate of 25°C/min and then raised to 300°C at a rate of 35°C/min and held for 4 min.

Results and discussion

Characterization of MIPs and NIPs

Morphology of PyMIP and NIP

Scanning electron microscopy (SEM, SU8020, Hitachi, Japan) was used to characterize the synthesized molecularly imprinted polymers. As shown in Figure 4, the NIP was similar to the MIP, but the spheres were smoother, and the particle diameters of the MIP and NIP were approximately 1.3 μm. The surface area measurements of unwashed, washed MIP and NIP were performed and were 2.1170, 2.9272, and 0.8669 m^2/g, respectively. The BET areas of MIPs are 3.37 and 1.3 times higher than those of NIPs and MIPs without elution, respectively. From Figure 5, the pore volumes of MIPs are 6.1 and 2.3 times higher than those of NIPs and MIPs without elution, respectively. These results indicate that after eluting the templates, many mesopores of the templates are imprinted on MIPs. MIPs with more imprinted cavities and active sites would exhibit greater adsorption capacity and a greater number of combined target molecules than NIPs and MIPs without elution.

To further confirm the chemical bonds and functional groups of the MIP, the materials were characterized by FTIR spectrometry (Figure 6). The characteristic peaks of the unwashed MIP at wavelengths of 1,160 cm^{-1} and 1,260 cm^{-1} are higher than those of NIP and washed MIP, which might be attributed to the C-H in-plane bending vibration of the ester group of ethyl chrysanthemate and dowtherm A, respectively. Strong characteristic peaks at 1,730 cm^{-1} and 3,450 cm^{-1} are assigned to the stretching vibration of amide C=O and O-H or N-H of acrylamide, respectively. In sum, MIPs were synthesized successfully.
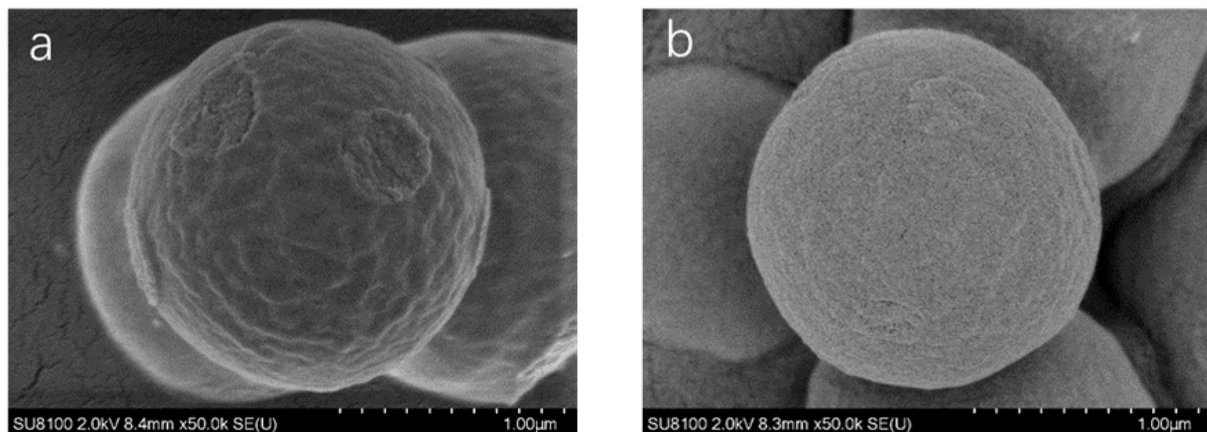
FIGURE 4
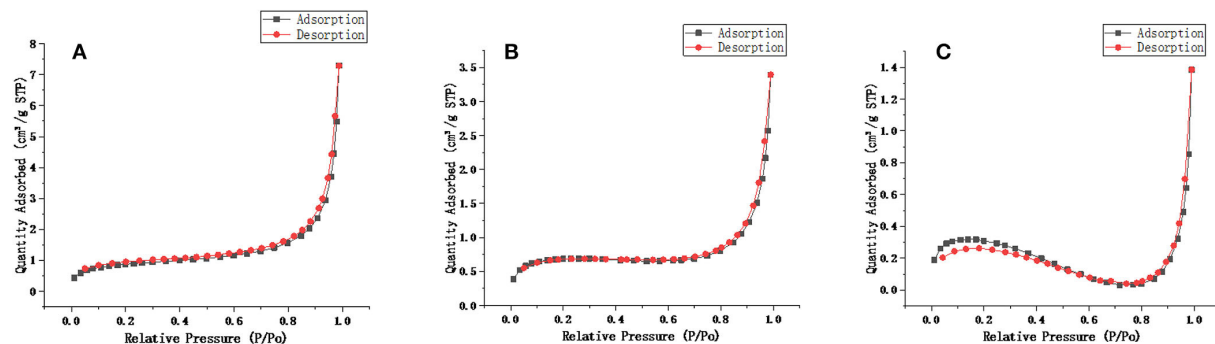Scanning electron micrographs of MIP **(a)** and NIP **(b)**.

FIGURE 5
Linear isotherm plot of **(A)** washed MIP. **(B)** Unwashed MIP. **(C)** NIP.

Adsorption and specific selectivity analysis of PyMIP

Through the dynamic and isothermal adsorption experiments of fenvalerate by MIP and NIP. Supplementary Figure S1A shows that the adsorption capacity of MIP and NIP concerning fenvalerate increases gradually with increasing time, and the saturation adsorption time was determined to be 90 min. Supplementary Figure S1B shows that the adsorption capacity of MIP and NIP increased with increasing fenvalerate concentration. MIP had a higher adsorption capacity for fenvalerate than NIP. Therefore, MIP has specific adsorption to fenvalerate. As shown in Supplementary Figure S1C, Q/C and Q were linearly related, suggesting that MIP had a single binding site per template molecule. According to formulas (1) and (2), Qmax is 3.65 mg/g, and Kd is 47.62 mg/L, which are higher than those in the literature (34). By comparing the experimental results with those in other literature (Table 1), we concluded that

the MIPs have a high adsorption capacity. The PyMIP exhibited specific adsorption of fenvalerate better than the other pesticides and had apparent selectivity for fenvalerate (Figure 7).

Characterization of MIP electrospun membranes

The electrospun membrane was obtained under 15% electrospinning solution mass concentration, an 18 G spinning needle, a 16 cm distance from the receiver, and 13 kV voltage. As shown in Supplementary Figure S2, the fiber diameter of the spinning membrane (MIPFM) under this condition is uniform.

Compared to the adsorption properties of MIPFM and MIP, the adsorption capacity of fenvalerate on MIPFM was five times
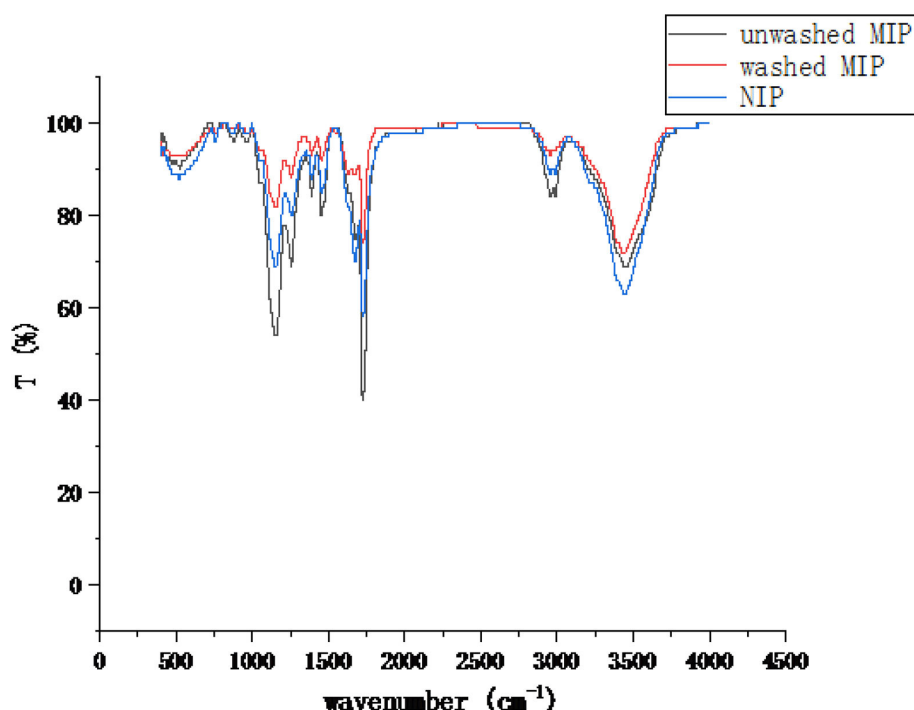
FIGURE 6
FTIR of unwashed MIP, washed NIP, and NIP.

TABLE 1 Comparison of MIPs with other literature.

Imprinting system	Synthetic method	Imprinting factor	Qmax µg/g	References
Ethyl chrysanthemate and dowtherma: MAA	precipitation polymerization	6.12	3650.0	This paper
Fenvalerate: Pyrrole	bulk polymerization	1.09	1084.4	(17)
Fenvalerate: MICOFs	Schiff reaction	4.60	9657.7	(35)
Fe_3O_4-NH_2@GO@MIP: 3-PBA	surface polymerization	1.78	91700.0	(36)
Phenyl ether-biphenyl eutectic: MAA	atom transfer radical polymerization	1.92	2300.0	(34)

that of free MIP, as shown in Supplementary Figure S3. This may be because MIPs wrapped in electrospinning solution are more dispersed, which fully exposes the adsorption site and improves the adsorption capacity of fenvalerate.

High-resolution mass spectral characterization of FH-IgG-Eu

By comparing the m/z values of the mouse antibody, fenvalerate hapten, and FH-IgG, the success of FH-IgG conjugation was confirmed, and the conjugation ratio was estimated. As shown in Supplementary Figure S4, the m/z value of antibody (b) was 71232.385, and the m/z value of the coupling between the two (c) was 81044.724. In addition, the molecular mass of fenvalerate hapten (a) was 499, and the m/z value of the connection between the two was higher than that of the antibody. Therefore, it was suggested that the antibody and fenvalerate hapten had linked successfully, and the connection ratio was 1:20.

Optimization of immunochromatographic strip parameters

The fixation of the T-line and the usage of fluorescent microspheres

In method 1, the MIPFM was stuck at the cutting point when the NC membrane was cut. The cutting point has much fluorescence, making the fluorescence at the C-line fragile
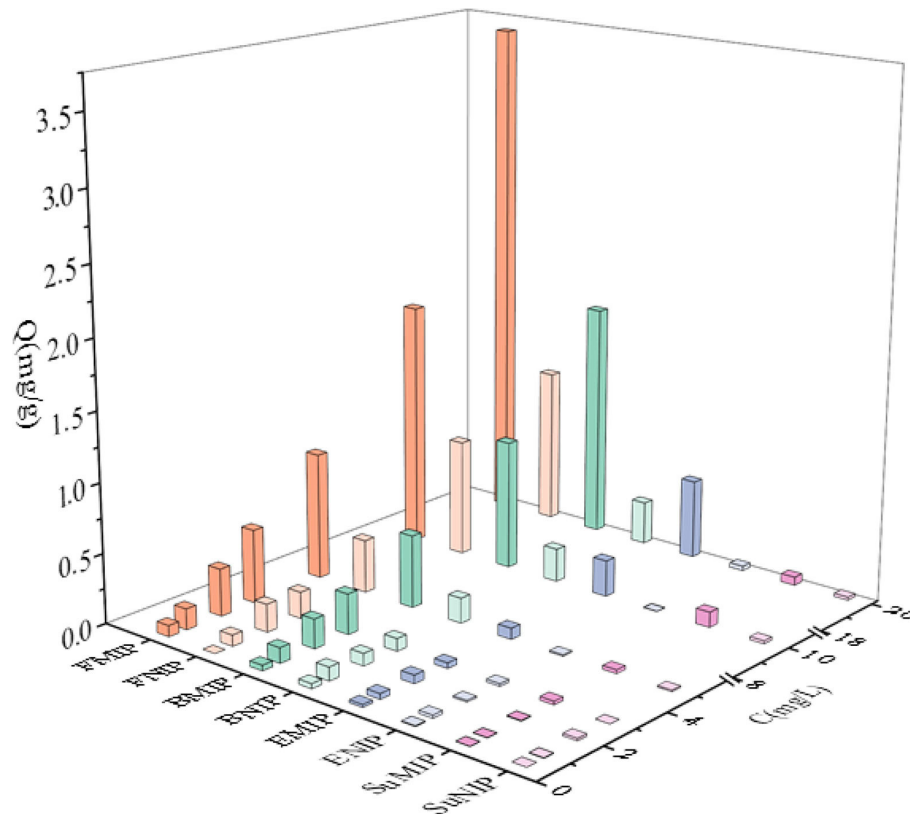
FIGURE 7
Special adsorption of PyMIP and NIP. FMIP, fenvalerate; MIP, BMIP: buprofezin; MIP, EMIP, ethiprole; MIP, and SuMIP, sulfadiazine MIP.

and in the T-line very strong but prone to false-negative results. However, method 2 could avoid the phenomenon of fluorescence agglomeration at the T-line. Thus, method 2 was selected for the subsequent experiments. The results showed that way 1 had a high background value when we dropped the fluorescent probe directly. However, the opposite result was observed in way 2, which used a fluorescence pad. When the buffer solution had been chromatographed, the background was spotless; therefore, we selected the second method to use a fluorescence pad for further experiments.

Optimization of the amount of MIP, FH-IgG, and fluorescence

The results showed that the fluorescence intensity of the T-line was strong. The inhibition rate was 78.2% when the FH-IgG labeling amount was 0.5 mg, the spraying amount of the fluorescence pad was 5 μL/cm, and the MIP amount of the T-line was 10 mg/mL. We also found that the FH-IgG labeling amount was 0.5 mg, with the spray amount of the fluorescent pad being more than 5 μL/cm. The T-line value was higher when the spraying amount was 5 μL/cm. However, due to the high cost

of FH-IgG, a spraying amount of fluorescence of 5 μL/cm was selected as the optimal experimental condition.

Optimization of the concentration of secondary antibodies

Under ultraviolet light, the color of the line is light or dark and can be misread. As shown in Supplementary Figure S5, when the secondary antibody concentration was 2 mg/mL, the competitive inhibition rate was 79.4%. The C-line had bright red fluorescence under the UV lamp. On the other hand, when the secondary antibody concentration was 1 mg/mL, the color of the C-line was relatively lighter and difficult to distinguish. Furthermore, when it was 3 and 4 mg/mL, the competitive inhibition rate was high; however, the color of the C-line was darker and considerably wider. The parallelism of reading values by card readers was substantially different. Therefore, 2 mg/mL was chosen as the optimal concentration of the C-line.

Optimization of the buffer solution

In this experiment, eleven different buffer solutions were prepared to select the most suitable one. When 0.02 molar (M)
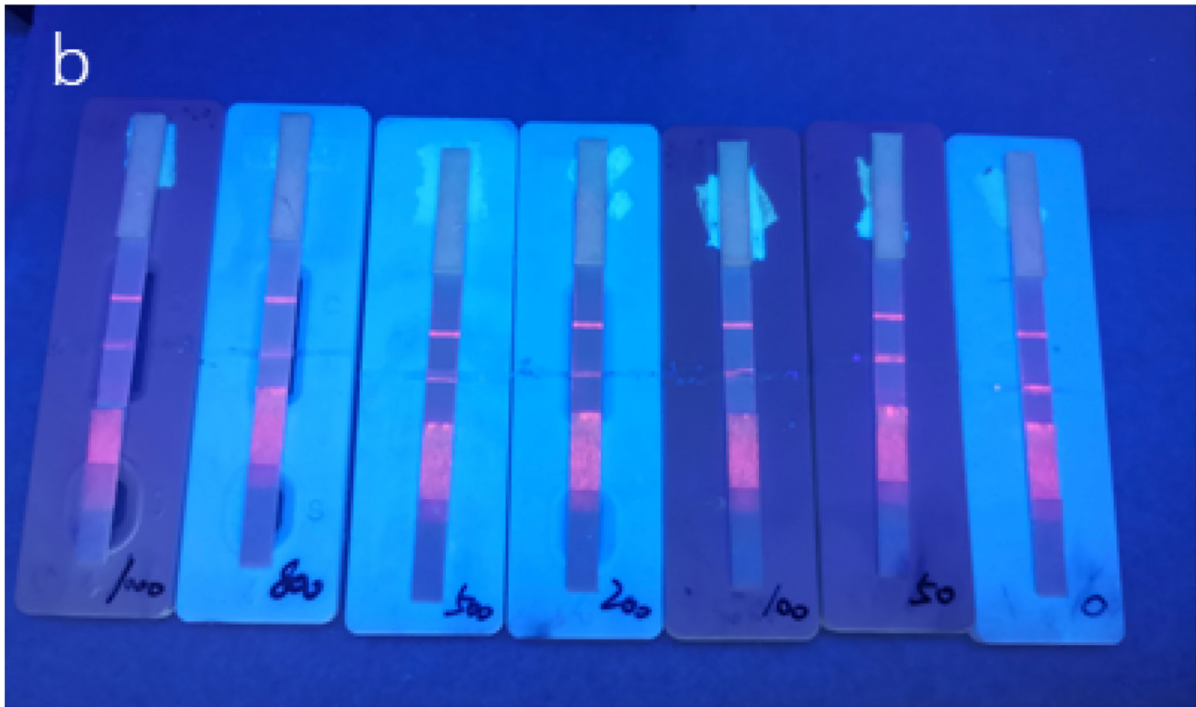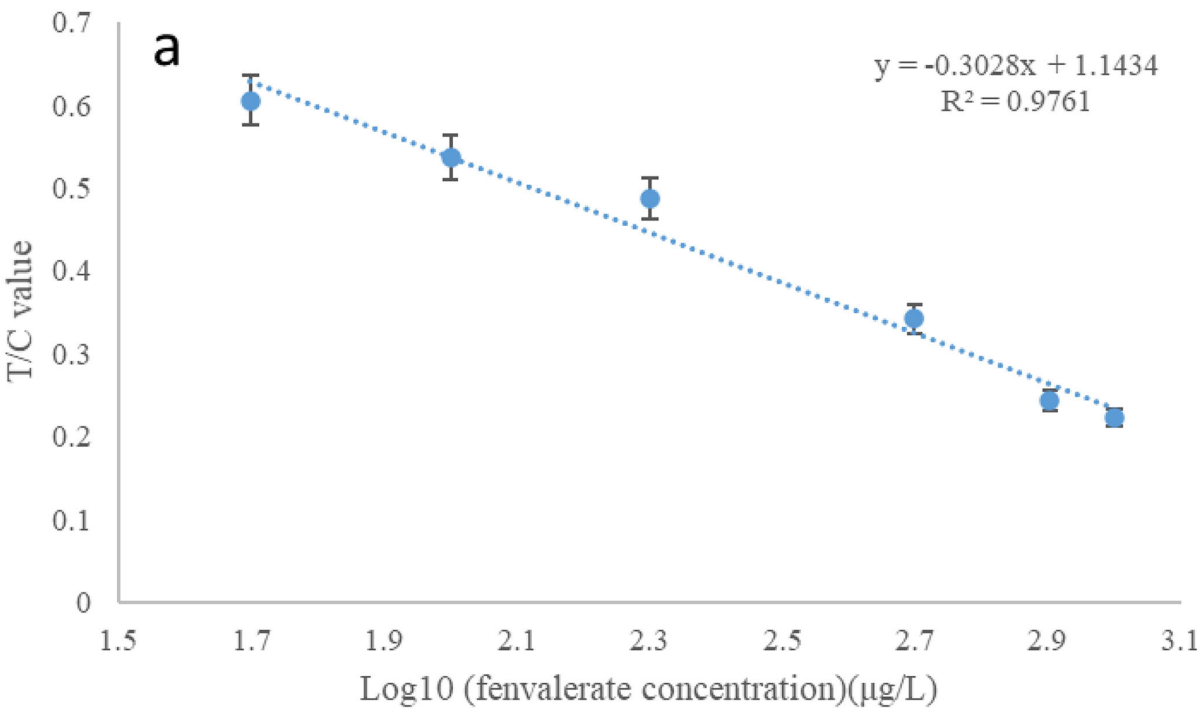
FIGURE 8
(a) Standard curve of fenvalerate measured by strip. (b) Different concentrations of fenvalerate (from right to left 0, 50, 100, 200, 500, 800, and 1,000 μg/L).

phosphate buffer (PB)+20% Tween-20 was used as a buffer solution, the brightness of the T- and C-lines was the best, and the edges of the T- and C-lines were smooth under UV; hence, it was used as a buffer solution. However, pyrethroids have low water solubility and are hydrophobic. We needed an organic reagent that could dissolve in water, so the influence of the organic reagent on the strip was determined when 5% acetonitrile was added to the buffer solution. Without adding Tween-20, we found that the brightness of the T- and C-lines was relatively shallow compared to that of Tween-20, even though there was no brightness on the T- and C-lines in many repeated experiments. When a certain amount of sucrose was added to the buffer solution, the brightness of the T- and C-lines was not changed significantly. Thus, the method without sucrose was chosen to simplify the experimental process. It must be noted that the addition of cations would have a particular influence on the charge balance of time-resolved fluorescence microspheres, so PB buffer was selected as the buffer solution. In conclusion, 0.02 m PB+20% Tween-20 was taken as the optimal buffer solution, and acetonitrile, the tolerable amount of organic solvent in the strip, was added to determine the analytes in the matrices. Then, the strip was measured by diluting the analytes with buffer solution.

Optimization of the organic solvent tolerance of the immunochromatographic strip test

The results showed that the darker the background color is, the more significant the impact on T and C read values when the competitive inhibition rate is higher than 60%. False-positive or false-negative results were judged when the background color was darker than the T-line. Therefore, acetonitrile was selected for further testing.

By comparing the amount of acetonitrile added in different ratios under a UV lamp, the brightness of the T and C lines gradually decreases with increasing acetonitrile content. The background of the strip was red, and the value read by the card reader of the strip was no longer accurate, resulting in incorrect interpretation. When the amount of acetonitrile was more than 5%, the edge of the T-line and C-line strips became no longer apparent. Hence, the highest organic solvent tolerance of the strip was 5%.

Method validation

Under the optimal conditions stated above, a time-resolved fluorescent strip was used to detect different concentrations of fenvalerate standard. The buffer solution was used to dilute a series of standard concentrations of 50, 100, 200, 500, 800, and 1,000 μg/L. The results are shown in Figure 8. The Log10 value of the concentration of fenvalerate standard solution was used as the X-axis, and the corresponding T/C value was used as the Y-axis. The T/C value decreased gradually with increasing

concentrations of the standard solution. The two are linear (y = −0.3028x+1.1434) with a coefficient of determination of R^2 = 0.9761 (Figure 8a). When the concentration of the standard solution was 50 μg/L (Figure 8b), the competitive inhibition rate was 61.4%, a value higher than 60%. Hence, 50 μg/L was considered the detection limit for fenvalerate, which was lower than the MRLs of fenvalerate in Brussels sprouts, cucumbers, and eggplants in the Chinese standard (GB2763-2021).

Analysis of fenvalerate in real samples

The developed method was evaluated by analyzing fenvalerate in Brussels sprouts, cucumbers, and eggplants. Different concentrations of fenvalerate at 100 μg/L, 500 μg/L, and 1,000 μg/L were added to the blank matrices, and sample pretreatment was carried out as described in Section *Sample preparation*. Each concentration level was tested at least three times using a strip of test paper. The recovery rates ranged from 68.7to 109.2%, with RSDs between 1.8 and 14.4%. This finding implies that the strip could detect fenvalerate. To further verify the applicability of this method, ten cabbage samples were tested, and none of the samples tested positive for fenvalerate residues. This finding was similar to the results of GC–MS/MS.

Conclusions

A lateral flow test strip was successfully designed based on molecularly imprinted and electrospun techniques to rapidly detect fenvalerate residues in vegetables. Unlike the traditional test strip for pesticide detection, our innovation lies in a molecularly imprinted electrostatic spinning film instead of a monoclonal antibody. The results were calculated using T/C values and target concentration curves using a fenvalerate hepten-IgG-Eu fluorescent probe competing with fenvalerate in the sample for specific recognition sites on MIPs. The method showed a good linear relationship in the 50–1,000 μg/mL concentration range, with a detection limit of 51.29 μg/mL. This is an attempt to reduce animal sacrifice and experimental costs, and the method is relatively simple and fast and can be used for rapid detection in the field.

Data availability statement

The original contributions presented in the study are included in the article/Supplementary material, further inquiries can be directed to the corresponding author/s.

Author contributions

LZ: data curation and writing-original draft. YZ: data curation and resources. HS: funding acquisition and writing-review and editing. MJ and FJ: supervision and validation. MX

and JS: review. JW: project administration. AMAE-A: writing-review and editing. YS: formal analysis, methodology, and writing-review and editing. All authors contributed to the article and approved the submitted version.

Conflict of interest

The authors declare that the research was conducted in the absence of any commercial or financial relationships that could be construed as a potential conflict of interest.

Publisher's note

Supplementary material

The Supplementary Material for this article can be found online at: https://www.frontiersin.org/articles/10.3389/fnut.2022.957745/full#supplementary-material

References

1. Asrorov AM, Matušíková I, Ziyavitdinov JF, Gregorová Z, Majerčíková V, Mamadrakhimov AA. Changes in soluble protein profile in cotton leaves indicate rubisco damage after treatment with sumi-alpha insecticide. *Agriculture (Pol'nohospodárstvo)*. (2020) 66:40–4. doi: 10.2478/agri-2020-0004

2. Hua N. Progress and trend of pyrethroid pesticides. *Pesticide Market News*. (2015) 3:29–26. doi: 10.13378/j.cnki.pmn.2015.02.019

3. Tang W, Wang D, Wang J, Wu Z Li, L, Huang M et al. Pyrethroid pesticide residues in the global environment: an overview. *Chemosphere*. (2018) 3:990–1007. doi: 10.1016/j.chemosphere.2017.10.115

4. Nagy K, Racz G, Matsumoto T, Adany R, Adam B. Evaluation of the genotoxicity of the pyrethroid insecticide phenothrin. *Mutat Res Genet Toxicol Environ Mutagen*. (2014) 770:1–5. doi: 10.1016/j.mrgentox.2014.05.001

5. Işıldar GY, Günal AÇ, Sahin D, Memmi BK, Dinçel AS. How potential endocrine disruptor deltamethrin effects antioxidant enzyme levels and total antioxidant status on model organisms. *Turkish J Biochem*. (2020) 45:415–21. doi: 10.1515/tjb-2019-0382

6. Qian H, Yang, Q., Qu, Y., Ju, Z., and Zhou, W. and Gao, H. Hydrophobic deep eutectic solvents based membrane emulsification-assisted liquid-phase microextraction method for determination of pyrethroids in tea beverages. *J Chromatogr A*. (2020) 1623, 461204. doi: 10.1016/j.chroma.2020.461204

7. Jia F, Wang W, Wang J, Yin J, Liu Y, Liu Z. New strategy to enhance the extraction efficiency of pyrethroid pesticides in fish samples using a modified QuEChERS (Quick, Easy, Cheap, Effective, Rugged and Safe) method. *Analytical Methods*. (2012) 4. doi: 10.1039/c2ay05681j

8. Sun P, Gao Y, Xu C, Lian Y. Determination of seven pyrethroid pesticide residues in vegetables by gas chromatography using carboxylated multi-walled carbon nanotubes as dispersion solid phase extraction sorbent. *Food Addit Contam Part A Chem Anal Control Expo Risk Assess*. (2017) 34:2164–2172. doi: 10.1080/19440049.2017.1382725

9. Petrarca MH, Ccanccapa-Cartagena A, Masiá A, Godoy HT, Picó Y. Comparison of green sample preparation techniques in the analysis of pyrethrins and pyrethroids in baby food by liquid chromatography-tandem mass spectrometry. *J Chromatogr A*. (2017) 1497, 28–37. doi: 10.1016/j.chroma.2017.03.065

10. Li W, Morgan MK, Graham SE, Starr JM. Measurement of pyrethroids and their environmental degradation products in fresh fruits and vegetables using a modification of the quick easy cheap effective rugged safe (QuEChERS) method. *Talanta*. (2016) 151:42–50. doi: 10.1016/j.talanta.2016.01.009

11. Jeong D, Kang JS, Kim KM, Baek SH, Choe S, Pyo J. Simultaneous determination of pyrethroids and their metabolites in human plasma using liquid chromatography tandem mass spectrometry. *Forensic Sci Int*. (2019) 302:109846. doi: 10.1016/j.forsciint.2019.06.004

12. Zhao Y, Ruan X, Song Y, Smith JN, Vasylieva N, Hammock BD, et al. Smartphone-based dual-channel immunochromatographic test strip with polymer quantum dot labels for simultaneous detection of cypermethrin and 3-phenoxybenzoic acid. *Anal Chem*. (2021) 93:13658–66. doi: 10.1021/acs.analchem.1c03085

13. Liu Y, Wu A, Hu J, Lin M, Wen M, Zhang X, et al. Detection of 3-phenoxybenzoic acid in river water with a colloidal gold-based lateral flow immunoassay. *Anal Biochem*. (2015) 483:7–11. doi: 10.1016/j.ab.2015.04.022

14. Kranthi KR, Davis M, Mayee CD, Russell DA, Shukla RM, Satija U, et al. Development of a colloidal-gold based lateral-flow immunoassay kit for 'quality-control' assessment of pyrethroid and endosulfan formulations in a novel single strip format. *Crop Protection*. (2009) 28:428–34. doi: 10.1016/j.cropro.2009.01.003

15. Zhang L, Zhao M, Xiao M, Im MH, Abd El-Aty AM, Shao H, et al. and She, Y. Recent advances in the recognition elements of sensors to detect pyrethroids in food: a review. *Biosensors*. (2022) 12:402. doi: 10.3390/bios12060402

16. Gong JL, Gong FC, Kuang Y, Zeng GM, Shen GL, Yu RQ. Capacitive chemical sensor for fenvalerate assay based on electropolymerized molecularly imprinted polymer as the sensitive layer. *Anal Bioanal Chem*. (2004) 379:302–7. doi: 10.1007/s00216-004-2568-3

17. Nezhadali A, Feizy J, Beheshti HR. A molecularly imprinted polymer for the selective extraction and determination of fenvalerate from food samples using high-performance liquid chromatography. *Food Analytical Methods*. (2014) 8:1225–37. doi: 10.1007/s12161-014-0004-7

18. Shi X, Liu J, Sun A, Li D, Chen J. Group-selective enrichment and determination of pyrethroid insecticides in aquaculture seawater via molecularly imprinted solid phase extraction coupled with gas chromatography-electron capture detection. *J Chromatogr A*. (2012) 1227:60–6. doi: 10.1016/j.chroma.2012.01.012

19. Chen Y, Xie Z, Zhang L, Hu X. Effective preparation of magnetic molecularly imprinted polymer nanoparticle for the rapid and selective extraction of cyfluthrin from honeysuckle. *J Biomater Sci Polym Ed*. (2020) 31:954–68. doi: 10.1080/09205063.2020.1731788

20. Wang Y, Zang D, Ge S, Ge L, Yu J, Yan M. A novel microfluidic origami photoelectrochemical sensor based on CdTe quantum dots modified molecularly imprinted polymer and its highly selective detection of S-fenvalerate. *Electrochimica Acta*. (2013)107:147–154. doi: 10.1016/j.electacta.2013.05.154

21. Wang J, Gao L, Han D, Pan J, Qiu H, Li H, et al. Optical detection of lambda-cyhalothrin by core-shell fluorescent molecularly imprinted polymers in Chinese spirits. *J Agric Food Chem.* (2015) 63:392–9. doi: 10.1021/jf5043823

22. Sergeyeva T, Yarynka D, Piletska E, Lynnik R, Zaporozhets O, Brovko O, et al. Fluorescent sensor systems based on nanostructured polymeric membranes for selective recognition of Aflatoxin B1. *Talanta.* (2017) 175:101–7. doi: 10.1016/j.talanta.2017.07.030

23. Ravandi SA, Sadrjahani M, Valipouri A, Dabirian F, Ko FK. Recently developed electrospinning methods: a review. *Textile Res J.* (2022) 26:9880. doi: 10.1177/00405175211069880

24. Bhardwaj N, Kundu SC. Electrospinning: a fascinating fiber fabrication technique. *Biotechnol Adv.* (2010) 28:325–47. doi: 10.1016/j.biotechadv.2010.01.004

25. Zhou Q, Lin X, Li B, Luo X. Fluoride adsorption from aqueous solution by aluminum alginate particles prepared via electrostatic spinning device. *Chem Engin J.* (2014). 256:306–315. doi: 10.1016/j.cej.2014.06.101

26. Criscenti G, De Maria C, Longoni A, Van Blitterswijk CA, Fernandes HA, Vozzi G, et al. Soft-molecular imprinted electrospun scaffolds to mimic specific biological tissues. *Biofabrication.* (2018) 10:045005. doi: 10.1088/1758-5090/aad48a

27. Demirkurt M, Olcer YA, Demir MM, Eroglu AE. Electrospun polystyrene fibers knitted around imprinted acrylate microspheres as sorbent for paraben derivatives. *Anal Chim Acta.* (2018) 1014:1–9. doi: 10.1016/j.aca.2018.02.016

28. Xing W, Ma Z, Wang C, Lu J, Gao J, Yu C, et al. Novel molecular organic framework composite molecularly imprinted nanofibrous membranes with a bioinspired viscid bead structure for selective recognition and separation of atrazine. *ACS Appl Mater Interfaces.* (2021) 13:28749–63. doi: 10.1021/acsami.1c02829

29. He Y, Hong S, Wang M, Wang J, Abd El-Aty AM, Hacimuftuoglu A, et al. Development of fluorescent lateral flow test strips based on an electrospun molecularly imprinted membrane for detection of triazophos residues in tap water. *New J Chem.* (2020) 44:026–36. doi: 10.1039/D0NJ00269K

30. Sabzehmeidani MM, Kazemzad M. Quantum dots based sensitive nanosensors for detection of antibiotics in natural products: A review. *Sci Total Environ.* (2022) 810:151997. doi: 10.1016/j.scitotenv.2021.151997

31. Zhou JW, Zou,XM, Song SH, Chen, GH. Quantum dots applied to methodology on detection of pesticide and veterinary drug residues. *J Agric Food.* (2018) *Chem* 66:1307–19. doi: 10.1021/acs.jafc.7b05119

32. Majdinasab M, Sheikh-Zeinoddin M, Soleimanian-Zad S, Li P, Zhang Q, Li X, et al. A reliable and sensitive time-resolved fluorescent immunochromatographic assay (TRFICA) for ochratoxin A in agro-products. *Food Control.* (2015) 47:126–34. doi: 10.1016/j.foodcont.2014.06.044

33. Liao T, Yuan F, Shi C, He CX, Li Z. Lanthanide chelate-encapsulated polystyrene nanoparticles for rapid and quantitative immunochromatographic assay of procalcitonin. *RSC Advances.* (2016) 6:103463–70. doi: 10.1039/C6RA23816E

34. Zhang M, He J, Shen Y, He W, Li Y, Zhao D, et al. Application of pseudo-template molecularly imprinted polymers by atom transfer radical polymerization to the solid-phase extraction of pyrethroids. *Talanta.* (2018) 178:1011–16. doi: 10.1016/j.talanta.2017.08.100

35. Ji W, Sun R, Geng Y, Liu W, Wang X. Rapid, low temperature synthesis of molecularly imprinted covalent organic frameworks for the highly selective extraction of cyano pyrethroids from plant samples. *Anal Chim Acta.* (2018) 1001:179–88. doi: 10.1016/j.aca.2017.12.001

36. Zhao Y, Du D, Li Q, Chen W, Li Q, Zhang Q, et al. Dummy-surface molecularly imprinted polymers based on magnetic graphene oxide for selective extraction and quantification of pyrethroids pesticides in fruit juices. *Microchem J.* (2020) 159:105411. doi: 10.1016/j.microc.2020.105411

37. Ruggieri F, D'archivio AA, Di Camillo D, Lozzi L, Maggi MA, Mercorio R, et al. Development of molecularly imprinted polymeric nanofibers by electrospinning and applications to pesticide adsorption. *J Sep Sci.* (2015) 38:1402–10.

Advantages of publishing in Frontiers

OPEN ACCESS
Articles are free to read for greatest visibility and readership

FAST PUBLICATION
Around 90 days from submission to decision

HIGH QUALITY PEER-REVIEW
Rigorous, collaborative, and constructive peer-review

TRANSPARENT PEER-REVIEW
Editors and reviewers acknowledged by name on published articles

Frontiers
Avenue du Tribunal-Fédéral 34
1005 Lausanne | Switzerland

Visit us: www.frontiersin.org
Contact us: frontiersin.org/about/contact

REPRODUCIBILITY OF RESEARCH
Support open data and methods to enhance research reproducibility

DIGITAL PUBLISHING
Articles designed for optimal readership across devices

FOLLOW US
@frontiersin

IMPACT METRICS
Advanced article metrics track visibility across digital media

EXTENSIVE PROMOTION
Marketing and promotion of impactful research

LOOP RESEARCH NETWORK
Our network increases your article's readership